Synthetic mimics of beta-sheets : design, synthesis and evaluation of their ability to modulate the aggregation of the beta-amyloid 1-42 peptide.

Nicolo Tonali

▶ **To cite this version:**

Nicolo Tonali. Synthetic mimics of beta-sheets : design, synthesis and evaluation of their ability to modulate the aggregation of the beta-amyloid 1-42 peptide.. Medicinal Chemistry. Université Paris-Saclay, 2016. English. NNT : 2016SACLS544 . tel-01933728

HAL Id: tel-01933728
https://theses.hal.science/tel-01933728

Submitted on 24 Nov 2018

HAL is a multi-disciplinary open access archive for the deposit and dissemination of scientific research documents, whether they are published or not. The documents may come from teaching and research institutions in France or abroad, or from public or private research centers.

L'archive ouverte pluridisciplinaire **HAL**, est destinée au dépôt et à la diffusion de documents scientifiques de niveau recherche, publiés ou non, émanant des établissements d'enseignement et de recherche français ou étrangers, des laboratoires publics ou privés.

NNT : 2016SACLS544

THESE DE DOCTORAT
DE
L'UNIVERSITE PARIS-SACLAY
PREPAREE A
"UNIVERSITE PARIS-SUD FACULTE DE PHARMACIE"

ECOLE DOCTORALE N° 569
Innovation thérapeutique : du fondamental à l'appliqué

Spécialité de doctorat : Chimie thérapeutique

Par

Nicolo Michele Tonali

Mimes synthétiques de feuillets bêta: conception, synthèse et évaluation de leur capacité à moduler l'agrégation du peptide bêta-amyloïde 1-42.

Thèse présentée et soutenue à Châtenay-Malabry, le 24 Novembre 2016 :

Composition du Jury :

M.	Aitken, David	Professeur, Université Paris-sud	Président
M.	Maillard, Ludovic	Maître de Conférences, Université de Montpellier	Rapporteur
M.	Guichard, Gilles	Directeur de recherche, Université de Bordeaux	Rapporteur
M.	Lequin, Olivier	Professeur, Université Pierre et Marie Curie	Examinateur
Mme	Ongeri, Sandrine	Professeur, Université Paris-sud	Directrice de thèse
Mme	Kaffy, Julia	Maître de Conférences , Université Paris-sud	Co-encadrante

Synthetic mimics of β-sheets: design, synthesis and evaluation of their ability to modulate the aggregation of the β-amyloid 1-42 peptide

Nicolo Tonali

Contents

List of Abbreviations

Aβ Amyloid β

AA Amino acid

Ac Acetyl

Ac2O Acetic anhydride

ACN Acetonitrile

AcOH Acetic acid

ADME Absorption, distribution, metabolism, and excretion

AICD Amyloid precursor protein intracellular domain

ApoE Apolipoprotein E

APP Amyloid precursor protein

APTS p-Toluenesulfonic acid

BACE β-secretase inhibitor

Bn Benzyl

Boc tert-butyloxycarbonyl

Boc2O Di-tert-butyl dicarbonate

BSBp β-sheet breaker peptide

C-PIB Pittsburgh compound B

CA Clan CA cysteine proteases

Cbz Carboxybenzyl

CD Circular dichroism

CD Clan CD cysteine proteases

CDI 1'-Carbonyldiimidazole

CE Capillary electrophoresis

CNS Central nervous system

COSY Correlation spectroscopy

COX Cyclooxygenase

CSD Chemical shift deviation

CTF C-terminal fragment

Cyclo Cyclohexane

DCM Dichloromethane

DFT Density functional theory

DIPEA N,N-Diisopropylethylamine

DMAP 4-Dimethylaminopyridine

DMF N,N-diméthylformamide

DMSO Dimethyl sulfoxide

EDC 1-Ethyl-3-(3-dimethylaminopropyl)carbodiimide

EGCG Epigallocatechin-3-gallate

EM Electron microscopy

eq. Equivalent

Et2O Diethyl ether

EtOAc Ethyl acetate

FDA Food and drug administration

Fmoc Fluorenylmethyloxycarbonyl

Fmoc-Osu Fmoc N-hydroxysuccinimide

For Formyl

FTIR Fourier transform infrared

HCl Hydrochloric acid

HFIP Hexafluoroisopropanol

HIV-1 PR Human Immunodeficiency Virus 1 protease

HMBC Heteronuclear multiple-bond correlation spectroscopy

HOAt 1-Hydroxy-7-azabenzotriazole

HOBt Hydroxybenzotriazole

HPLC High-performance liquid chromatography

HRMS High resolution mass spectrometry

HSQC Heteronuclear Single Quantum Coherence

I.D. Internal diameter

IDP Intrinsically disordered protein

iPrOH Isopropanol

IR Infrared

L-CPL Left-handed circularly polarised light

LC-MS Liquid chromatography-mass spectrometry

LDH Lactate dehydrogenase

LTD Long-term depression

LTP Long-term potentiation

M-TTR monomeric variant of transthyretin

MAP Microtubule associated protein

MCMM Monte Carlo Multiple Minima

Me Methyl

MeOH Methanol

MM Molecular modelling

MO Molecular orbital

MRI Magnetic resonance imaging

MW Molecular weight

NBO Natural Bond Orbital

NMDA N-methyl-D-aspartate receptor

NMM N-Methylmorpholine

NMR Nuclear magnetic resonance

NOESY Nuclear Overhauser effect spectroscopy

Nos Nosyl

NSAIDs Non-steroidal anti-inflammatory drugs

PDA Photodiode Array Detector

PET Positron emission tomography

PhSH Thiophenol

Py Pyridine

R-CPL Right-handed circularly polarised light

Rf Retardation factor

ROESY Rotating-frame nuclear Overhauser effect correlation spectroscopy

SAA Serum amyloid A

SAR Structure activity relationship

SDS-PAGE Sodium Dodecyl Sulphate-PolyAcrylamide Gel Electrophoresis

SREs Self-recognition elements

TDA Taylor dispersion analysis

TEA Triethylamine

TEM Transmission electron microscopy

THF Tetrahydrofuran

ThT Thioflavin T

TLC Thin-layer chromatography

TOCSY Total correlation spectroscopy

Tos Tosyl

UV Ultraviolet

Acknowledgement

First, I would like to thank my thesis supervisor Sandrine Ongeri to have always been present during these three years, for giving me the opportunity to grow scientifically. Thanks for your professionalism and for all the time you devoted to me to best perform my thesis but also thank you for the human support and for being too a big help in daily life on a personal level.

Thanks to Julia Kaffy for being an important co-supervisor and always being available to discuss and give good advice.

I want to thank the members of the jury who accepted to judge my work.

This thesis has been possible thanks to numerous collaborations with several laboratories, who have welcomed and formed me. I would like to thank all the members of these laboratories to be available to welcome me. I would especially like to thank Myriam Taverna, Dimitri and Nacéra (Protéines et Nanotechnologies Séparatives en Sciences, Institut Galien de Paris Sud, UMR-CNRS 8612, Université Paris Sud) for their invaluable support during my months, spent learning the capillary electrophoresis.

The laboratory of Maria Luisa Gelmi (DISFARM Sezione di Chimica Generale e Organica "A. Marchesini", Università Degli studi di Milano, Milano, Italy) welcomed me very well during my two months in visiting scholar.

Thanks to Carine Van Heijenoort (Dept Chimie et Biologie Structurales et Analytiques CNRS, ICSN Gif sur Yvette France) for allowing us to perform the conformational analysis by NMR in Gif sur Yvette.

Thanks to Olivier Lequin and Isabelle Correia for being a great support during the month spent to perform the conformational analysis by NMR on the azatide peptidomimetics. Thank you for your patience and for your expertise.

Thanks to Camille Dejean for the contribution to the various NMR analysis of the synthesized compounds and thanks to Karine Leblanc for your time that allowed me to analyze the purity and the mass of all the molecules synthesized in the course of this thesis.

During these three years I had the opportunity to meet and know people who have become part of my life. Jean Louis thanks for your continued support, for chats together and the many advice. Thanks to Jordi for your sympathy in the laboratory and for all the moments spent together.

Thank you so much Guillaume for all the help you have given me to create a well-paged manuscript but above all thanks very much for your professionalism and for your deep knowledge in all areas. Thank you for everything you taught me: I will always take with me.

Thanks to all the team members of the Molécules Fluorées et Chimie Medicinale laboratory: Benoit Crousse, Thierry Milcent , Tap Ha-Duong, Sophie, Marius, Jing, Linh, Alastair and Renjing. Thanks for all the good times we spent together.

Special thanks to Leila, Lucia and Yasmine with whom I spent some wonderful moments in the laboratory and some beautiful days in Paris and elsewhere.

Thanks to the two training students Viviana and Alexandre for having contributed to this thesis.

Thank Marianna for her work during the nine months of Erasmus and for contributing to this thesis work and also spending pleasant moments of leisure.

Many thanks to Faustine for all the wonderful moments spent together, for French lessons and cooking, for the various re-readings and all other moments to come.

Special thanks to Mr Yao, a good friend and the best colleague ever. Thanks for the many talks, for dinners, for all the moments that have characterized the past three years. We'll see you soon in China.

Thanks to all the wonderful people I met here in Paris, and that are now part of my second family: Betty, Irene e Andrea, Angela, Valentina, Manush, Giuliana, Elena, Sevérine e Cedric avec la petite Heléna et encore plus petite Apolline, Simona, Roberta, Eleonora e Guido insieme al piccolo che arriverà, Nathalie, Audrey, e Naf.

Thanks to all my close friends in Italy that always stand by me, and always do feel their affection: Angelika, Marta, Carolina, Arianna, Laura e Martina.

Thanks to Francesco for taking me on a daily basis in this wonderful adventure but especially for supporting me during these months of preparation.

Thanks to my beautiful Eizel for her affection and for her patience in listening to me repeat my talks.

And last but not least, I want to thank the people who most of all believe in me and I will always stand by. I want to thank my sister and my niece, and above all my parents, because they deserve all the joy that I have, dedicating this thesis to them.

Chapter 1

Introduction

In nature, proteins constitute a class of bio macromolecules which affect every feature that characterizes a living organism. They are responsible for most of the complex functions, for instance: enzymatic catalysis, transport and storage, coordinated motion, mechanical support, immune protection, generation and transmission of nerve impulses, cell growth control and differentiation.

In spite of these diverse biological functions, protein are linear polymers built on various combination of 20 amino acids. They differ only for the sequence in which the amino acids are assembled into polymeric chains. The secret of their functional diversity lies in the diversity of the three-dimensional structures that these building blocks can form, simply by being linked in different sequences. In fact, the amino acid sequence itself contains all the instructions needed for proper folding [1].

1.1 Three-dimensional structure of polypeptides and proteins

The late 30s of the twentieth century, Linus Pauling started a series of studies to determine the geometry of the peptide bond. One of his most important findings was that the peptide bond is planar. Thanks to this observation, a polypeptide chain can be divided into peptide units that go from one α-carbon to the next α-carbon (Figure 1.1). The reason for dividing the chain in this way is that all the atoms in such unit are fixed in a plane with the bond lengths and bond angles very nearly the same in all units in all proteins.

If we want to describe the geometry of a peptide bond, we can observe that the bond angles around the carbonyl group and the nitrogen measure at least 120°, due to the resonance of the not shared doublet of nitrogen with the carbonyl group. For the atoms of a peptide bond two configurations are allowed: one in which the two α-carbons are *cis* and another in which they are

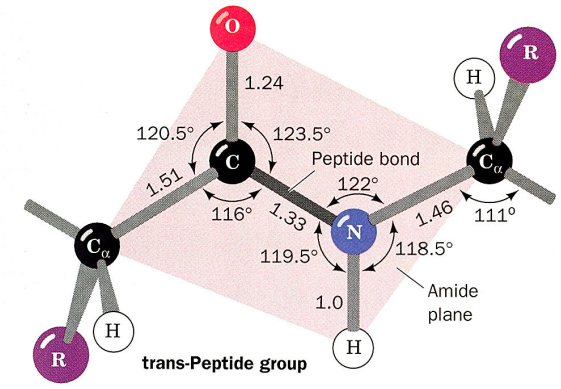

Figure 1.1: Geometry of a peptide bond (Voet D. and Voet J.G., Biochemistry. John Wiley and sons, New-York, 1990)

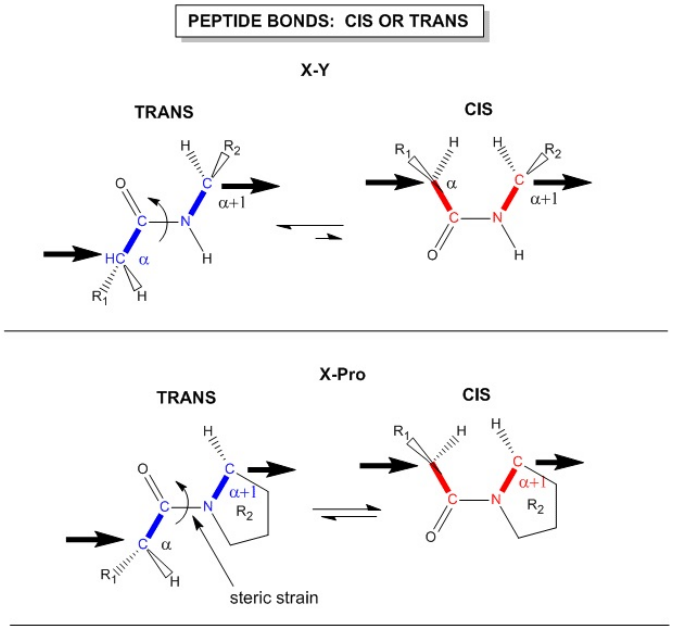

Figure 1.2: *cis* and *trans* configuration of a peptide bond (Jakubowski H., Biochemistry online, https://employees.csbsju.edu/hjakubowski/classes/ch331/protstructure/olunderstandconfo.html)

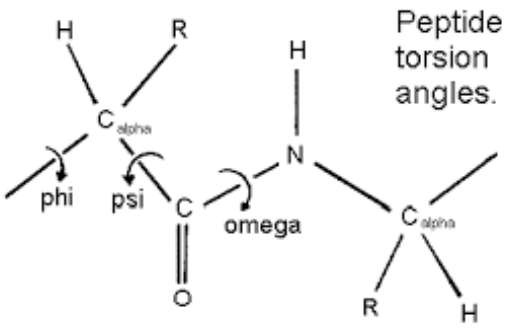

Figure 1.3: Torsional angles that characterize the skeleton of a peptide

trans. The s-*trans* configuration is the most favorable because the α-carbons that carry the bulky groups are farer than in s-*cis* configuration. Almost all the peptide bonds in natural proteins present a s-*trans* configuration, except for proline which shows a *cis* configuration in the most of the time (Figure 1.2).

1.1.1 Secondary structure

The secondary structure is related to the arrays (conformations) of amino acids in localized regions of a polypeptide or protein. The first studies about the conformations of peptides were carried out by Linus Pauling and Robert Corey from 1939. They assumed that in the most stable conformations all the six atoms of the repeating peptide unit, cited above (Figure 1.1), lay on the same plane and there are hydrogen bonds between the N-H of an amide bond and the carbonyl group of another peptide bond of the sequence. Pauling suggested that the most stable type of folding should be two: the α-helix and the antiparallel β-sheet. The X-ray crystallography demonstrated these predictions.

The main chain presents three covalent bonds for each amino acid. The α-carbon of an amino acid is linked to an amine function and a carbonyl function and the last one forms an amide bond with the amine function of the next amino acid. Since the peptide units are effectively rigid groups that are linked into a chain by covalent bond at the α-carbons, the only degrees of freedom they have are rotations around these bonds. Each unit can rotate around two such bonds: the C_α-CO (ψ) and the N-C_α (φ) bonds. The conformation of the skeleton of an amino acid can be described by the two torsional angles, φ and ψ (Figure 1.3). The different combinations of angles are correlated with the adopted secondary structure thanks to the Ramachandran plot [2]. In this plot, we can observe two main regions that correspond to the two energetically more stable conformations: the α-helix

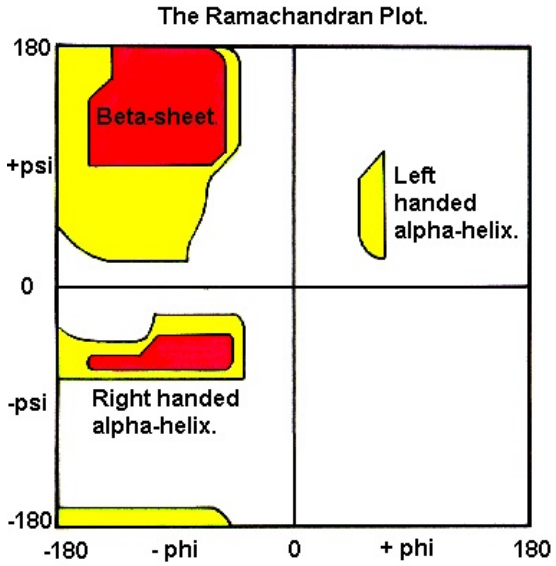

Figure 1.4: Ramachandran plot

and the β-sheet (Figure 1.4).

α-Helices The α-helix is a right-handed rod-like structure in which the inner part is formed by the coiled polypeptide main chain and the surface by the side chains projecting outwards in a helical arrangement. In natural proteins the torsion and dihedral angle values associated with α-helical conformations range from $-57°$ to $-70°$ for φ, and from $-35°$ to $-48°$ for ψ. The arrangement allows the carbonyl group of every peptide bond (i, acceptor) to establish a hydrogen bond with the N-H (donor) of an amide bond that is situated four amino acids farer ($i + 4$). These hydrogen bonds are straight, strong, and parallel to the long axis of the helix. The N-H of every amide bond points down, parallel to the helix axis, and the carbonyl points upper, always parallel to the helix axis. The regular α-helix has 3.6 residues per turn with each residue offset from the previous residue by 1.5 Å (translation per residual distance) (Figure 1.5).

The most frequently α-helix in proteins is the right handed helix, but a left-handed α-helix is also sterically possible. Since the side chains are too close to the main chain, this conformation is unstable and rarely present in natural polypeptides. A less common helical secondary structure is the 3_{10}-helix. Having three residues per turn, the carbonyl on residue i is hydrogen-bonded to the amide NH on residue $i + 3$, forming 10-membered repetitive rings.

Different side chains have been found to have weak but definite preferences

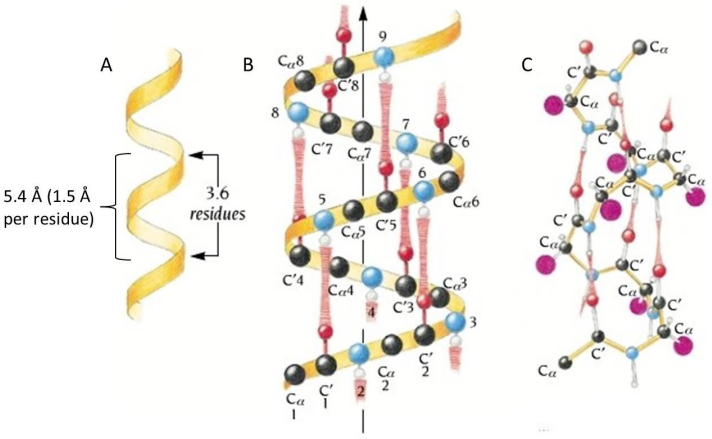

Figure 1.5: Exemple of a right handed α-helix. A) Idealized diagram of the path of the main chain in an α-helix; B) The same as A) but with approximate positions for main-chain atoms and hydrogen bonds included. The arrow denotes the direction from N-terminus to the C-terminus; C) Schematic diagram of an α-helix. Oxygen atoms are red, and N atoms are blue. Hydrogen bonds are red and striated. The side chains are represented as purple circles. (Branden C. and Tooze J., Introduction to protein structure, Garland Publishing, 1999)

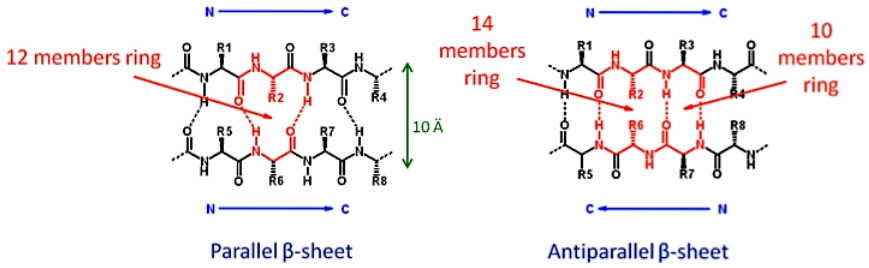

Figure 1.6: Schematic representation of parallel and antiparallel β-sheets

either for or against being in α-helices. Thus Ala, Glu, Leu and Met are good α-helix formers, while Pro, Gly, Tyr and Ser are very poor. Such preferences were central to all early attempts to predict secondary structure from amino acid sequence, but they are not strong enough to give accurate predictions.

Proline fits very well in the first turn of an α-helix, but it usually produces a significant bend if it is anywhere else in the helix.

β-Sheets The second most regular and recognizable secondary structural motif is the β-sheet. This structure is built up from a combination of several regions of the polypeptide chain, in contrast to the α-helix, which is built up from one continous region. The β-sheet consists of a long polypeptide chain with vicinal portions which develop in the same (parallel) or opposite (antiparallel) direction (Figure 1.6).

A poly-Gly can adopt an extended conformation with all the hydrogen bonds in the same plane. In this zig-zag conformation, the distance between the α-carbon of the amino acid i and the α-carbon of the amino acid $i+2$ is of 7.4 Å. This type of structure is called β-strand. The N-H and C=O bonds of the peptide skeleton are oriented almost perpendicularly to the poly-Gly backbone and can establish hydrogen bonds with other polypeptides, forming in this way a β-sheet. In a parallel β-sheet, there is a recurring hydrogen bond pathway, forming 12-membered cycle. On the contrary, in an antiparallel β-sheet the hydrogen bond pathway forms 10 or 14-membered rings alternately. This latter type of β-sheet is more stable because the hydrogen bond acceptors and the donors are oriented in a favorable way, allowing shorter bonds. The average distance between the polypeptide chains in both types is 4.8 Å [3].

When the associated polypeptides present amino acids with side chains, these last affect the global conformation and the β-sheet shows a torsion. In fact, the side chains are located perpendicularly to the amide bonds plane and alternately above or below the plane.

The stability of a β-sheet is due to both the hydrogen bonds between the

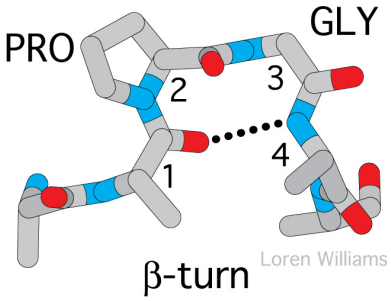

Figure 1.7: Schematic representation of a β-turns

amide functions and the interaction between the amino acid side chains of the two or more β-strands. These interactions can be established by polar amino acids (ionic interactions and hydrogen bonds), or by aromatic and aliphatic with branched chain amino acids (hydrophobic interactions). Otherwise the stability of a β-sheet increases with the number of β-strands [4]. Generally, the residues with high intrinsic β-sheet properties are $Val > Ile > Thr > Tyr > Trp > Phe > Leu$, whereas Cys, Met, Gln, Ser and Arg are more or less neutral to adopt β-sheet conformations.

Characteristic average values for the φ and ψ angles of β-strand residues in antiparallel β-sheet are $-139°$ and $135°$, respectively and about $-120°$, $115°$ in parallel sheets.

In nature, there are not so many short β-sheets and in the most of cases they are cyclical or stabilized by disulfide bridges. One of the physicochemical consequences of the β-sheet folding is the loss of solubility of the oligopeptides [5].

β-Turns Tight turns (also known as reverse turns, β-turns, β-bends, hairpin bends, 3_{10}-bends, kinks, widgets, etc.) are the first and most prevalent type of non-repetitive structure that has been recognized. A β-turn comprises four consecutive residues where the distance between the α-carbon of C_i and the α-carbon of C_{i+3} is less than 7 Å and where hydrogen bonds can form between the carbonyl oxygen of residue i and the N-H group 3 residues along the chain $(i + 3)$ (Figure 1.7).

Initially recognized in silk proteins by Geddes *et al.* and later defined stereo-chemically by Venkatachlam, β-turns are widespread in proteins and both linear and cyclic peptides, generally occurring on their surface. Turns tend to be on the solvent-exposed surface of proteins, because the hydrophilic residues are more likely to occur than hydrophobic residues, so Gly, Pro, Asn, Ser and Asp are particularly favorable amino acids involved in turns.

Turn Type	Dihedral angles (°)			
	ϕ_{i+1}	ψ_{i+1}	ϕ_{i+2}	ψ_{i+2}
I	-60	-30	-90	0
I'	60	30	90	0
II	-60	120	80	0
II'	60	-120	-80	0
IV	-61	10	-53	17
VIa1	-60	120	-90	0
VIa2	-120	120	-60	0
VIb	-135	135	-75	160
VIII	-60	-30	-120	120

Figure 1.8: Dihedral angles of different type of beta-turn

Pieces of non-repetitive structure have a particular succession of different φ and ψ values for each residues, so that the concept of residue position within the structure is more influential than in a repeating structure. According to the last revaluation of the β-turn classification, nine distinct structural types were suggested based on the φ and ψ torsion angles in residues $i+1$ and $i+2$ ("corner" residues). Venkatachlam proposed two main classes of four-residue β-turn, namely type I and II. The main difference among these two types is the relative orientation of the peptide bond between residues $i+1$ and $i+2$, which, consequently, modifies the side chain positions. Type I turns, the most prevalent in naturally occurring proteins, have approximately $\varphi_2 = -60°$, $\psi_2 = -30°$, $\varphi_3 = -90°$, $\psi_3 = 0°$, and present the $i+1$ and $i+2$ positions accommodated by L-residues; however proline preferentially fits the $i+2$ position. Type II turns have approximately $\varphi_2 = -60°$, $\psi_2 = 120°$, $\varphi_3 = 80°$, $\psi_3 = 0°$, and in this case the $i+1$ position is occupied by an L-residue (generally proline) and the $i+2$ favors a glycine, small polar L-residues, or a D-residue because of steric clash with a side chain in the L-configuration. Proline in the $i+1$ position is a strong sequence determinant for either a type I or II turn because of the restriction on the ϕ angle from the cyclic side chain.

Type I and III are identical for residue 2 and differ by only 30° in φ_3 and ψ_3. Type III actually has repeating φ and ψ values of $-60°$, $-30°$ and is identical with the 3_{10}-helix.

Type I' and II' are the mirror images of types I and II, with the inverse φ and ψ values and are energetically equivalent if residues of opposite chirality occupy corresponding sequence positions. This means that, for exemple, a D-Pro residue would be favored in position $i+1$ of a type I' turn or in position

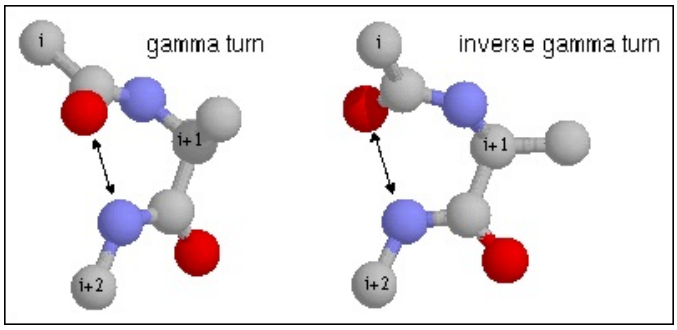

Figure 1.9: Schematic representation of classical and inverse gamma-turns

$i+2$ of a type II' turn. On the other hand, the intervening peptide bond (between residues $i+1$ and $i+2$) can adopt a *cis* conformation and still allow the turn to form an i to $i+3$ hydrogen bond and link two β-strands. The resulting turn is called a type VI turn. Type IV is essentially a miscellaneous category, which includes any example with two of the dihedral angles more than 40° away from ideal values for any of the other types (Figure 1.8).

γ-Turns The γ-turn consists of three consecutive residues with an intra-turn hydrogen bond formed between the main chain CO_i and $NH_i + 2$ and is the second most characterized and commonly found turn, after the β-turn. There are two types of γ-turns: inverse and classical which differ in that the main-chain atoms of the two forms are related by mirror symmetry. Of the two, classic ones are far less common and inverse γ-turns tend not to give rise to polypeptide chain reversal.

This kind of turn is characterized by the fact that the middle residue $(i+1)$ does not participate in H-bonding, while the first and the third ones can form the final and initial H-bonds of the antiparallel β-strands, resulting in a 7-membered hydrogen bond ring (Figure 1.9). The change in direction of the polypeptide chain caused by a γ-turn is reflected in the values of φ and ψ for the central residue. As a result of the size and conformational flexibility, Gly is a favoured residue in this position although other amino acids can be found.

β-Hairpins Large portions of most protein structures can be described as stretches of secondary structure joined by turns, which provide direction change and offset between sequence adjacent pieces of secondary structure. Tight turns work well as α-α and α-β joints, but their neatest application is a hairpin connection between adjacent antiparallel β-strands, where the hydrogen bond of the turn is also one of the β-sheet hydrogen bonds. It has often been suggested that turns can provide a decisive influence in directing

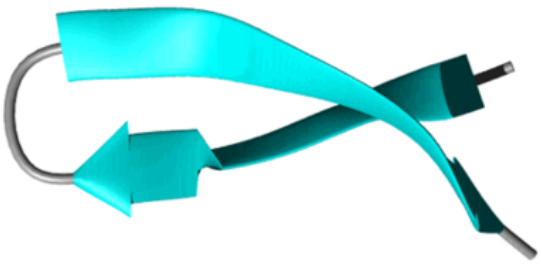

Figure 1.10: General conformation of a beta-hairpin

the process of protein folding to the native conformation.

The simplest units one can construct from β-strands and β-turns are β-hairpins. These occur widely in proteins and make up the fundamental building blocks of antiparallel β-sheet. This type of structure has been found in many naturally bioactive cyclic peptide such as Gramicidin S and the peptide hormones oxytocin and vasopressin. β-hairpins are stabilized by cross-strand interactions that may include aromatic-aromatic, charge-charge electrostatic, or hydrophobic packing interactions, disulfide bridges and hydrogen bonds.

The different β-hairpin motifs can be categorized according to the number of residues in the turn and the number of inter-strand hydrogen bonds between the residues flanking the turn. The most frequent β-turns used for the construction of β-hairpins are type II, followed by type III, while type I occurs rarely (Figure 1.10).

1.1.2 Tertiary structure

The tertiary structure regards the overall folding arrangement and the arrangement in space of all atoms of a single polypeptide chain. The secondary structure is correlated with the spatial distribution of neighbors amino acids on a polypeptide chain, while the tertiary structure is correlated to the three-dimensional distribution of all atoms of the chain. The most important factors that stabilize a tertiary structure are: the disulfide bridges, the hydrophobic interactions, the hydrogen bonds and the salt bridges. Proteins can contain in their conformation α-helix and β-sheet structures, but it's clear that there are different variations of the relative amounts of the two structures.

1.1.3 Quaternary structure

Most of the proteins with a molecular weight more than $50\,000\,\mathrm{g\,mol^{-1}}$ are presented as a combination of two or more polypeptide chains, linked in a non-covalent manner. The disposition of the single polypeptide chain in a multi-subunit complex is known as quaternary structure. The most important factor that stabilizes the aggregation of the single peptide units is the hydrophobicity. When the single polypeptides wrap in three-dimensional compact structures to expose the polar side chains to the aqueous environment and to shield the hydrophobic side chains from water, hydrophobic areas on the surface in contact with the water can form. These areas can be protected from water if two or more polypeptides are arranged in such a way that their hydrophobic regions are in contact.

Examples of proteins with quaternary structure include hemoglobin, DNA polymerase, and ion channels. The formation of the quaternary structure of a given protein is sometimes a necessary condition to exercise its specific biological function. The HIV-1 protease can only cleave the peptide bond if it is correctly assembled into a dimer. The hemoglobin molecule is an assembly of four globular protein subunits, each composed of a protein chain tightly associated with a non-protein heme group.

1.2 Alzheimer's disease

1.2.1 Amyloidosis and neurodegenerative disease

More than 20 degenerative disorders affecting the central nervous system or peripheral tissues and organs are associated with the deposition of proteins in the form of amyloid fibrils and plaques. Between these disorders, we can count Alzheimer's, Parkinson's and prion diseases, as well as type II diabetes and Huntington's chorea; these pathologies are of enormous importance in the context of present-day human health and welfare [6][7][8][9][10][11][12].

Amyloidosis is the generic word to name a group of diseases that are caused by the misfolding and extracellular accumulation of various proteins. The misfolded proteins form fibrillar deposit that present affinity with both Congo red and green birefringence under cross-polarized light, using polarization microscopy [13].

Biophysicists prefer a molecular-based definition because they assume that the same disease-related proteins form similar fibers in vitro and many other proteins form similar fibers when denaturated or during their physiological roles. So they decided to adopt a structure-related definition that describe the amyloid fibers as deposits that display the cross-β fiber diffraction pattern [8].

Amyloid fibrils are filamentous structures with a width of at least 10 nm and a length of 0.1–10 µm. A defining feature, originally detected by X-ray

fiber diffraction assay, is the presence of cross-β structure [10]. The most general characteristics about their structure are:

1. in all amyloid fibers, the repeating β-sheets are in parallel to the fibril axis and their β-strands are perpendicular to the axis;

2. the β-sheets can be parallel or antiparallel, or rather adjacent hydrogen-bonded β-strands within a sheet can run in the same or opposite direction;

3. the sheets are usually "in register", meaning that strands align with each other such that identical side chains are on top of one other along the fibril axis. In parallel sheets, identical side chains are separated by an interstrand distance of 4.8 Å (interstrand spacing) and in antiparallel sheets, they are separated by 9.6 Å (intersheet spacing).

Although we could determine the atomic structure of some amyloid spines, we are in absence of more detailed information about the full atomic structures for whole amyloid fibrils, because these latter are more complicated than the simple spine structures and show a great variety of structural complexity [8].

Amyloidosis can be hereditary or acquired, localized or systemic. Depending on these characteristics but also on the type of pathology they cause and the organ they affect, amyloid proteins can be classified in different categories. 27 different human proteins with amyloidogenic potential in vivo have been identified; at least 15 of these proteins cause systemic amyloidosis [9].

Neurodegenerative disease proteins often appear to be natively unfolded [14]. We can hypothesize that a stochastic event occurs and initiate the misfolding in a particular cell [15]. The aggregation can start, for exemple, by an increasing of protein concentration, caused by genetic dosage alterations. Early deposition of Aβ plaques occurs in individuals with Down's syndrome because these patients carry an extra copy of the APP locus on chromosome. The protein amount can be also increased by an altered transcription due to polymorphisms in promoter sites of disease-related genes. The altered primary structure owing to protein-coding mutations presumably makes the protein more prone to aggregate [16]. The aggregation can also be facilitated by covalent modifications: oxidative modifications of proteins (α-synuclein) and phosphorylation (tau protein). Finally, proteolytic cleavage may have a role in several of the neurodegenerative diseases, including Alzheimer's disease.

We can distinguish two categories of amyloidogenic proteins: the category 1 with proteins that initially adopt a well-defined, folded and three dimentional structure and need a partial loss of this well-defined structure to initiate their aggregation process [17], and category 2 with proteins that are intrinsically disordered and undergo thermodynamically linked aggregation

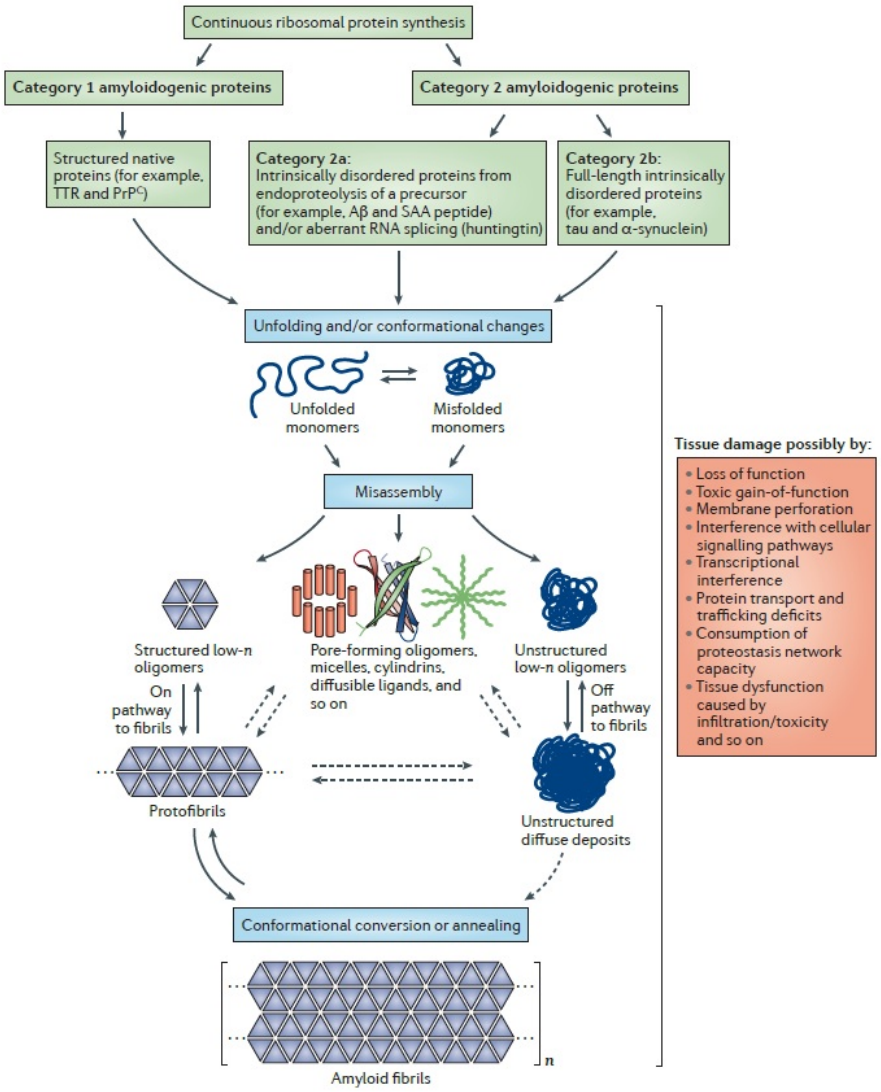

Figure 1.11: Classification of the amyloid proteins based on the different aggregation pathways [7]

and conformational changes, thus giving rise to more β-sheet-rich structures (Figure 1.11) [18].

For the category 1 proteins the conformation-change is the base of their aggregation; the same forces that drive the intramolecular protein folding (hydrogen bond formation and hydrophobic effect), also mediate intermolecular aggregation and amyloidogenesis when the misfolded protein is present at sufficient concentrations.

The category 2 proteins can be further divided into two subcategories: category 2a that comprises intrinsically disordered polypeptides resulting from the endoproteolysis of a precursor protein (Aβ-peptides, the SAA peptide and the huntington protein) and category 2b that includes polypeptides as full-length intrinsically disordered proteins that do not require endoproteolysis to aggregate (tau protein and α-synuclein) [19] [20]. These latter proteins aggregate intracellularly and the aggregation process depends on the concentration of proteins but also on the post-translational modifications, such as phosphorylation and nitrosylation at certain residues [21].

In literature, we can find three different mechanisms of protein aggregation, based on *in vivo* data and consistent with mathematical models of protein aggregation. In the first mechanism proteins aggregate starting from a nucleated polymerization; it is necessary that a high-energy, sparsely populated species is formed (*nucleus*) and can subsequently efficiently add monomers to form an aggregate that is more thermodinamically stable. Generally this *nucleus* implicates oligomeric species but also monomers and presents a cross-β-sheet structure or an alternative structure that may or may not later conformationally convert to a cross-β-sheet structure. The requirement for *nucleus* formation can be passed by adding *seeds* (often cross-β-sheet aggregates) of a particular protein, such as Aβ, to a solution of monomers of the same protein.

The second mechanism requires a nucleated conformational conversion; it means that there is an equilibrium between monomers and structurally heterogeneous oligomers that are generally, but not always, more stable than the monomers. Over time, the oligomers are converted into a *nucleus* and then into amyloid fibrils. This is the case, for example, of the aggregation process of the prion protein Sup35, which is initially unstructured in solution and then forms self-seeded amyloid fibers. Structurally fluid oligomeric complexes appear to be crucial intermediates in *de novo* amyloid *nucleus* formation. Rapid assembly ensues when these complexes conformationally convert upon association with *nuclei* [22].

The third mechanism is not a seedable process. In this case, the rate-limiting step is the formation of the aggregation-prone misfolded monomer from a natively folded protein. To have an efficient aggregation, it is not necessary to form a high-energy *nucleus* [7]. M-TTR(monomeric variant of transthyretin) aggregation, for example, is not accelerated by seeding, and the dependence of the reaction timecourse is first-order on the M-TTR

concentration, consistent with a nonnucleated process where each step is bimolecular and essentially irreversible. Amyloid formation by M-TTR under partially denaturing conditions is a downhill polymerization, in which the highest energy species is the native monomer [23].

As we could see, protein aggregation is a complex process, involving several kinds of intermediates and resulting in different kinds of fibers or amorphous aggregate. It remains unclear which step of the amyloid formation cascade is toxic, and this step may be different for the various amyloid diseases. In affected patient tissues, the protein aggregates are generally located extracellularly or intracellularly but recently different evidence showed that both intracellular and extracellular aggregates are present in nearly all of the aggregation-associated degenerative diseases [24][25][26]. So we can note that proteinopathy was once thought to result predominantly from extracellular aggregation but now more evidence suggest that there is an equilibrium of concentration between intracellular and extracellular amount of aggregates, and intracellular toxicity might also contribute to proteinopathy.

For the moment it remains unclear to what extent amyloid fibrils are by themselves the toxic entities, or if other forms of misassembled proteins contribute to the cytotoxicity. We know that amyloids disrupt tissue structure and organ function via simple mass action but currently smaller diffusible oligomers are considered the drivers of the degenerative pathology. This mass action mode of toxicity may well be the most important one for most systemic amyloidoses and for the amyloid associated with the cerebral vessels [27].

Because of their greater diffusion capability through the tissue and into various compartments , these such small aggregates are notably more toxic than amyloid fibrils [28] [29]. These diffusible oligomers could be formed either by fragmentation of fibrils into small pieces or from unsuccessful degradation of fibrils by the lysosome or proteasome, or independently.

In conclusion, in patients with amyloid disease, we can recognize extracellular and/or intracellular cross-β-sheet structures amyloid fibril deposits in tissues that represent the histopathological hallmarks for a diagnostic confirmation of disorders. The aggregation and accumulation of protein deposits can be considered the primary influence driving pathogenesis (*"amyloid hypothesis"*) [8]. The process of amyloidogenesis is dynamic: there is a constant flux of newly synthesized protein aggregating into a range of transient structures evolving over time.

Even with this incomplete knowledge of the aggregated structures, there are some currently developing therapeutic strategies with the aim to prevent active protein aggregation and/or remove the soluble oligomers, to ameliorate the toxic effects of aggregates and to limit the physiological function of the involved proteins (Figure 1.12). One strategy can be to enhance cellular defence mechanism by using drugs that modulate the chaperone levels or stimulate the proteasome activity. Other therapeutic intervention would

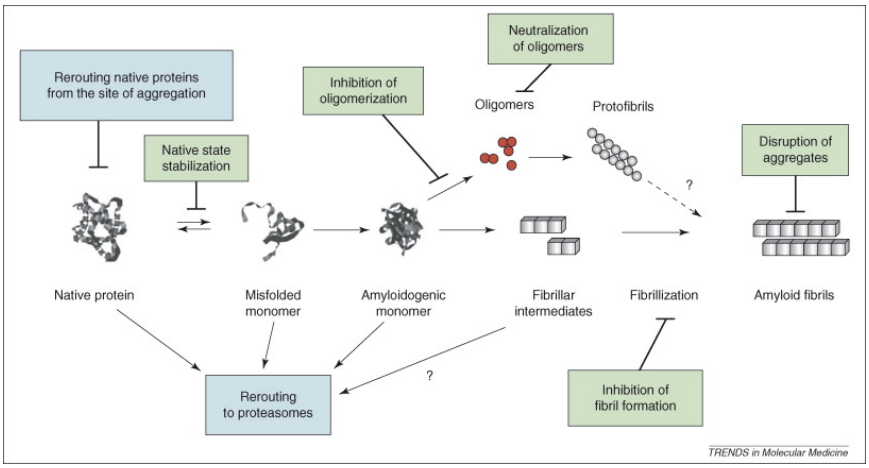

Figure 1.12: Currently developing therapeutic strategies in the field of amyloidosis

be to reduce the level of abnormal protein by using RNA interference with viral vectors to inactivate the mutant allele. About chemical interventions, one approach can be the stabilization of the structure of the soluble form of a protein, diminishing the rate to convert to the amyloid state. A second approach is the screening of small-molecule agents to inhibit fibril and oligomer formation. A third approach is to use the self-assembling property of amyloid fibers to poison the growth of amyloid fibers with peptides or to block the ends of fibrils. Finally, another approach could be the identification of specific pathogenic mechanisms for individual diseases and develop a targeted therapy (proteolytic cleavage, inhibition of the generation of amyloidogenic proteins or their precursors) [8] [10].

1.2.2 Physiopathology of Alzheimer's disease

Introduction In 1906, Alois Alzheimer presented interesting results obtained from the histological examination of one of his patient's brain at the 37^{th} meeting of the Society Of Southwest German Psychiatrics in Tübingen, Germany. The detailed analyses that were performed in psychiatric hospital in Munich, revealed the presence of abnormal protein deposits in the brain. The study conducted to the identification of neuritic plaques and neuro-fibrillary tangles, the defining neuropathological characteristics of the disease. Whereas plaques had been reported before, Alzheimer was the first to describe the tangle pathology and the intraneuronal fibrils, a deposition of a pathological metabolic substance.

Today, 100 years later, the presence of neurofibrillary tangles and amyloid deposits are still the disease-defining parameters [30]. We can consider

Alzheimer's disease as the most common form of dementia that causes memory loss in the elderly. Worldwide, nearly 44 million people have Alzheimer's or a related dementia; only 1- in 4 people with Alzheimer's disease have been diagnosed and this type of dementia is most common in Western Europe and the top cause for disabilities in later life. The global cost of caring for Alzheimer's patients is estimated to be $605 Billion in 2016, which is the equivalent to 1 % of the entire world's gross domestic product. The number of patients is expected to double by 2050 (alzheimers.net).

Diagnostics Alzheimer's is a progressive disease, where dementia symptoms gradually worsen over a number of years. In its early stages, memory loss is mild, but with late-stage Alzheimer's individuals lose the ability to carry on a conversation and respond to their environment. These symptoms are correlated and associated with a reduction of the volume in the gray matter (neurons) and of the thickness of the medial temporal lobe, and with the entorhinal cortex atrophy. The endorhinal cortex, together with the medial temporal lobe, is only a tiny fraction of the whole cerebral cortex, but a key interface because the functionning of their connections is essential for the formation of long-term memory.

Those with Alzheimer's live an average of eight years after their symptoms become noticeable to others, but survival can range from four to twenty years, depending on age and other health conditions. The most common early symptom is the difficulty remembering newly learned information because Alzheimer's changes typically begin in the part of the brain that affects learning. As Alzheimer's advances through the brain, it leads to increasingly severe symptoms, including disorientation, mood and behaviour changes; deepening confusion about events, time and place; unfounded suspicious about family, friends and professional caregivers.

For the moment, the only reliable diagnosis of the Alzheimer's disease is the *post mortem* identification of the two biomarkers of the disease: the amyloid plaques and the neurofibrillary tangles. The diagnosis by neuropsychological assays is mainly completed by imaging technique. Early longitudinal imaging studies based on computed tomogram techniques follow the reduction of the thickness of the medial temporal lobe. Modern magnetic resonance imaging (MRI) techniques not only allow to study the volume reduction in the gray matter but also the entorhinal cortex atrophy. In addition to the structural MRI techniques, positron-emission tomography (PET) studies measuring Aβ deposition with C- PIB (Pittsburgh compound B, a radioactive analog of thioflavin T) or other PET ligands and functional techniques such as glucose utilization and functional MRI (fMRI) are used today to follow the progress of the disease. However, these types of exams do not allow to put in evidence the specific injuries caused by the amyloid plaques and neurofibrillary tangles [31].

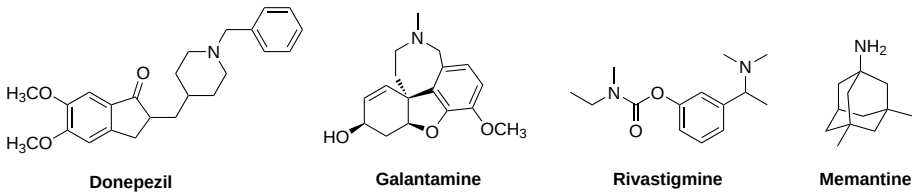

Figure 1.13: Chemical structures of the commercially available therapeutic agents for Alzheimer's disease

Therapeutic situation To date, the exactly cause of the Alzheimer's disease is not still known and so there is no effective treatment of the disease. The only available drugs that are approved by the Food and Drug Administration (FDA) are symptomatic; it means that these drugs are able to decrease the symptoms of the disease, that are principally psychological and behavioural. This approach is based on the cholinergic hypothesis, which proposes that Alzheimer's disease is caused by reduced synthesis of the neurotransmitter acetylcholine [32].

We can distinguish two type of drugs: cholinesterase inhibitors and memantine (antagonist of the NMDA receptor). Cholinesterase inhibitors have the aim to decrease the degradation of the acetylcholine and so to raise its amount available to nerve cells by preventing its breakdown in the brain. This neurotransmitter is implicated in the inter-neuronal communication at the level of synapses and its amount is diminished in Alzheimer's patients. There are three FDA-approved cholinesterase inhibitors in the market: *Donepezil*, *Galantamine* and *Rivastigmine* (Figure 1.13).

Memantine is an antagonist of the N-methyl-D-aspartate receptors (NMDA) with the aim to modulate the effects of the high pathological level of glutamate that can lead to a neuronal disfunctionality. The glutamate is a chemical messenger widely involved in brain functions. All these drugs showed to be used for the treatment of mild to moderate Alzheimer's disease with an efficacy for not more than 36 months and various side effects. These drugs could not treat the real cause of the disease.

1.2.3 The hypotheses of the cause of the disease

Other therapeutic approaches are contemplated and described in this thesis, based on the different hypotheses trying to explain the cause of the disease: *Tau hypothesis*, *Metal Ion hypothesis* and *Amyloid hypothesis* together with the *Oligomer hypothesis*. We decided to focus our attention to these latter and to get more in detail in the Aβ 1-42 peptide aggregation process and in the therapeutical targets to affect its oligomerisation and fibrillization.

Figure 1.14: Chemical structure of $LMTX^{TM}$

Tau hypothesis Tau is a neuronal microtubule associated protein (MAP) that is found mainly in the CNS in six different isoforms ranging between 352 and 441 amino acids. It consists of three major domains: an amino terminal projection domain, a carboxy terminal domain of microtubule-binding repeats and a short tail sequence. In healthy neurons, tau is present along the axons, where its role is to maintain axonal transport [33].

In pathological conditions, such as in Alzheimer's disease and other taupathies, tau becomes excessively phosphorylated. The phosphorylation decreases the affinity of tau for microtubules and redistributes tau from axons into dendrites and somata [34]. In the brain of Alzheimer's patients, tau aggregates intracellularly into stable insoluble fibrils which are the main constituent of neurofibrillary tangles.

The β-sheet structure formed by two hexapeptide motifs ($V^{275}QILNK^{280}$ and $V^{306}QILVYK^{311}$) is the driven force that starts the aggregation process (von Bergen 2000). The details of the structural transition during the aggregation are poorly understood and it remains unclear. Its deleterious effect is probably due to the loss of its physiological functions intracellularly as well as the gain of toxic function of its misfolded and aggregated form [35].

The processing therapeutical strategies adopted in this field can be grouped in four main categories:

- Diminishing the hyperphosphorylation. It means that the aim is to restore the equilibrium between the phosphatase and the kinase of the protein, by activating the phosphatases or by inhibiting the kinase [36]. The main downside of this approach is that these enzymes have different substrates and work in different organs. So there is the risk to alterate many different physiological functions;

- Stabilizing the microtubules. This strategy uses compounds that are able to stabilize the microtubules to fill in the deficiency and to restore the axonal transport. These compounds are derived from Taxol, passing the blood brain barrier; it's an anticancer agent, well known to stabilize the microtubules [37];

- Inhibiting the aggregation. This strategy has the aim of preventing the formation of the degenerative neurofibrillary tangles that are considered

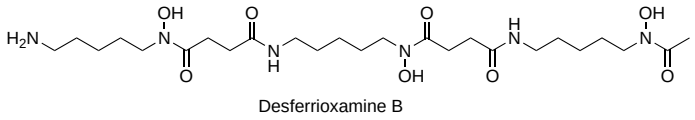

Figure 1.15: Chemical structure of Desferrioxamine B

responsible for the block of the axonal transport and for the cellular death. $LMTX^{TM}$ (Figure 1.14) is a a derivative of methylene blue that is actually on phase III as inhibitor of tau aggregation. This compound is able to stabilize the protein tau in its monomeric form by the oxydation of the cysteine residues [38]. It was demonstrated that the formation of intermolecular disulfide bonds promotes aggregation and that blocking the SH group, mutating Cys for Ala, or keeping tau in a reducing environment all inhibited assembly;

- Targeting Tau. This strategy adopts the immunotherapy to target hyperphosphorylated tau protein by using antibodies [39].

Metal Ion hypothesis The cellular homeostasis of biometals such as ionic copper, iron, and zinc is disrupted in Alzheimer's disease, though it remains unclear whether this is produced by or causes the changes in proteins. The metal ion hypothesis contributes substantially to the neuropathogenesis involved in Alzheimer's disease. The strong involvement in the Aβ aggregation and the toxicity of metals are demonstrated by the presence of high concentration of metal ions (Cu^{2+}, Zn^{2+}, Fe^{2+}) coordinated with the peptide in senile plaques. The dysregulation of the ion metal homeostatis in the brain, due to the sequestration of physiologically important metal ions by Aβ, can involve the ROS generation and cause synaptic breakdown, finally leading to neuronal cell death [40].

In this case, the therapeutical strategy is to disrupt the Aβ-metal interactions by using metal chelators, in order to reduce neurotoxicity initiated by the Aβ-metal complex and to renovate metal ion homeostasis in the brain [41]. Desferrioxamine B (Figure 1.15) was the first metal chelator that showed the capacity to enhance cognitive ability in a mouse model; unfortunately this compound presented a poor blood brain barrier permeability and fast *in vivo* degradation in combination with other adverse side effects. Recently, 8-hydroxyquinoline-based molecule [42] and 6-chlorotacrine, an AChE inhibitor derivatized with chelating agents[43] have met tremendous interest as metal chelators.

Amyloid and Oligomeric hypotheses Aβ peptide has been considered as the key component involved in the progression of Alzheimer's disease. Aβ

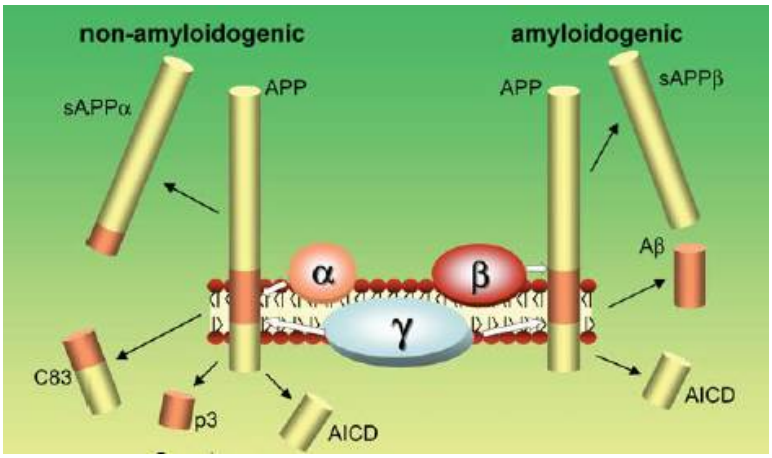

Figure 1.16: Amyloid β-protein generation by proteolytic processing of β-amyloid precursor protein [44]

presents physiological roles in maintaining a healthy nervous system in a concentration-dependent manner (picomolar concentration). Between its physiological roles we can count: neurogenesis, synaptic plasticity, memory formation, calcium homeostasis, metal sequestration and antioxidant properties. In particular it participates to the formation and differentiation of neurons, to the gliogenesis of neuronal stem cells and to the cell viability, exerting neuroprotective effects [44].

Aβ peptides structures Aβ peptides, with a sequence length ranging from 36-43 residues, are produced by the proteolytic cleavage of an integral membrane protein called APP (amyloid precursor protein). APP is composed by 695 amino acids and it belongs to the type 1 transmembrane glycoprotein family. It can be expressed on both intra- and extra-cellular membranes and it presents different physiological functions [45]. The cleavage of APP is realized in two steps and in two different pathways (Figure 1.16); in the case of non-amyloidogenic pathway, the α-secretase cleaves within the Aβ sequence resulting in the formation of the APPsα fragment and α-CTF. Then, the γ-secretase cleaves the α-CTF (α C-terminal fragment) releasing the so-called P3 peptide and AICD (amyloid precursor protein intracellular domain). In amyloidogenesis, APP is first cleaved by β-secretase producing APPsβ and β-CTF (β C-terminal fragment). Successively, γ-secretase on the transmembrane domain produces Aβ peptide and AICD [46].

Nearly 80 % of the Aβ in normal human brain constitutes of Aβ 1-40 but under the diseased condition excess Aβ 1-42 is produced and predominantly accumulated as amyloid plaques. The Aβ 1-42 has a remarkable propensity to self-aggregate at high concentration and demonstrates much more rapid

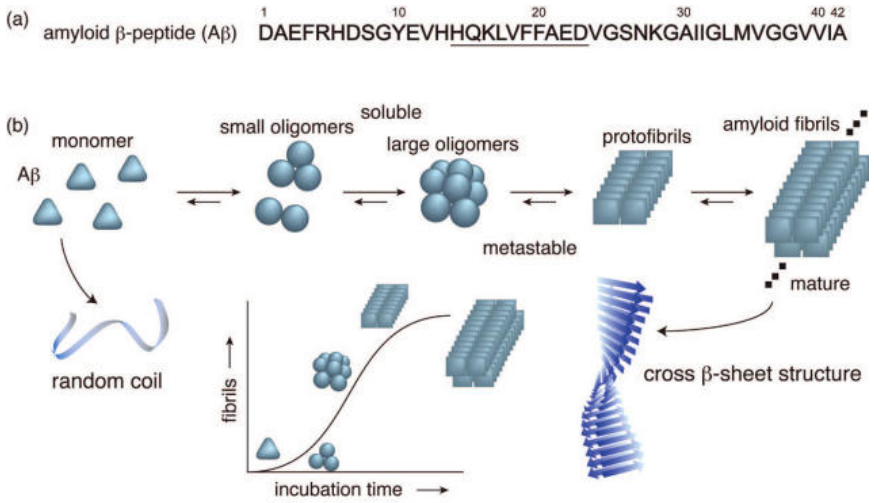

Figure 1.17: Schematic representation of the Aβ 1-42 aggregation process [51]

fibril formation *in vitro* [47][48]. In addition, studies in animal models demonstrated that Aβ 1-42 is mainly required for the formation of plaques. Overexpression of Aβ 1-42, in fact, showed to be able to develop the plaque toxicity, while overexpression of Aβ 1-40 did not [49].

To study the difference in aggregation behaviour of Aβ 1-40 and Aβ 1-42, random mutagenesis on positions 41 and 42 were performed and the results indicated that the hydrophobicity of residues at these positions plays a dominant role in promoting aggregation. So it is the hydrophobicity and β-sheet propensity of residues 41 and 42 that cause the enhanced amyloidogenicity of Aβ 1-42 relative to Aβ 1-40 [50].

The natively unfolded Aβ 1-42 peptide, a prominent member of the class of IDPs, shows low transformation into a partially folded state (β-sheet). Partially folded units associate with each other through hydrophobic interaction and hydrogen bonding to form paranucleus which then self-associate to form higher-order structures called protofibrils. Protofibrils are further self-assembled through the elongation phase to form long fibrillar aggregates [52][53][54](Figure 1.17).

By molecular dynamics simulation, it was proposed a model for the elongation mechanism. During elongation, it was observed that the N-terminal associates with the core Aβ fibril through intermolecular hydrogen bonding (β_1). Successively, a β-hairpin structure is formed by the association of the β_2 strand of the monomer with the β_1 strand through intramolecular hydrogen bonding; in this way the Aβ unit finally associates with the full Aβ fibril. In this mechanism, we can note that β-hairpin can be one of the

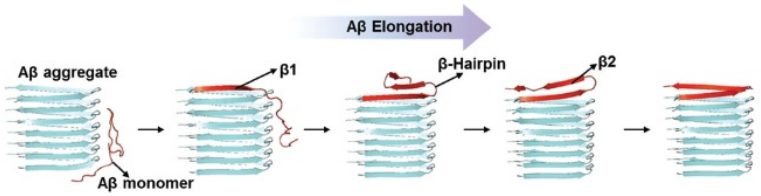

Figure 1.18: Schematic representation of the Aβ 1-42 elongation process [55]

possible targets for designing drugs, due to the fact that its stabilization enhances the aggregation rate [55] (Figure 1.18).

The relationship between low molecular weight toxic oligomers and the mature fibrils has remained elusive, with some studies suggesting that oligomers are generated predominantly as on-pathway intermediates in fibril formation and others indicating that these different species originate mainly from independent pathways.

A recent *in vitro* study, combining kinetics studies, selective radiolabelling experiments and cell viability assays demonstrated that once a small but critical concentration of amyloid fibrils has accumulated, the toxic oligomeric species are predominantly formed from monomeric peptide molecules through a fibril-catalyzed secondary nucleation reaction, rather than through a classical mechanism of homogeneous primary nucleation [52]. Initially, in the absence of fibrils, all oligomers have to be generated through primary pathways because secondary nucleation requires the presence of fibrils. Once the critical concentration of amyloid fibrils has formed, however, secondary nucleation will overtake primary nucleation as the major source of new oligomers and further proliferation becomes exponential in nature due to positive feedback.

Structural studies of amyloid fibrils are non-trivial. They are extremely insoluble and stable and therefore very difficult to work with by conventional methods. Aβ research has concentrated on the use of model peptides for structural studies, and this has led to an in-depth knowledge of the importance of various regions of Aβ. However, the information generated from these studies is complex because of the many different solvents and conditions used in different studies of amyloid fibril structure and assembly [56].

X-ray fibre diffraction, electron microscopy (EM), solid state NMR, Fourier transform infrared spectroscopy (FTIR) and circular dichroism (CD) have been used to examine amyloid structure. These techniques have yielded information about the morphology of amyloid fibrils formed *in vitro* from synthetic peptides homologous to the Aβ peptide. However, most of these

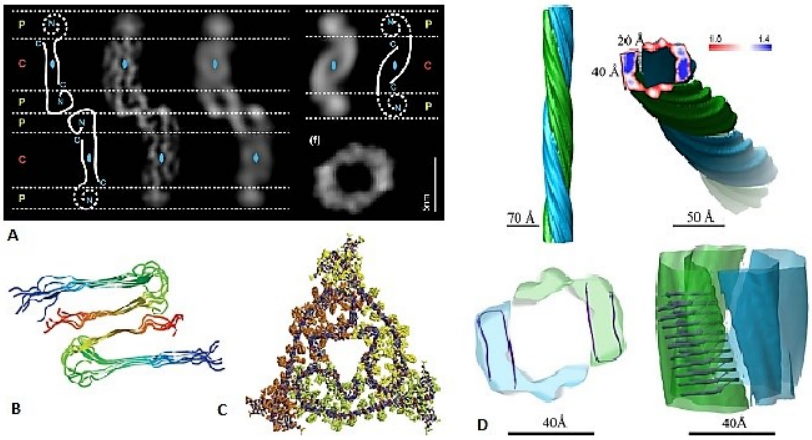

Figure 1.19: A) Cryo-EM cross-sections of different Aβ fibril morphologies and structural interpretations of the cross-section (on the left Aβ 1-40 and on the right Aβ 1-42) [57]; B) Structural model of Aβ 1-40 with two-fold symmetry about the fibril growth axis, from ssNMR and electron microscopy measurements; C) Structural model of Aβ 1-40 with three-fold symmetry about the fibril growth axis (fibrils seeded from Alzheimer's patient tissue) [58]; D) The cryoEM structure of Aβ 1-42 amyloid fibrils (the cross-section composed by two protofilaments, the atomic model and the particular of one protofilament) [59]

studies were conducted on peptide fragments of Aβ, and in particular on Aβ 1-40 peptide. We have yet to obtain an unambigous structure of the amyloid fibril and the structural transition from the disordered monomeric form to the aggregate one remains unclear [56].

The significant chemical similarities of the two Aβ 1-40 and Aβ 1-42 peptides might suggest that their conformational properties are also largely similar. Instead, near to the higher aggregation propensity for Aβ 1-42, there are inevitable differences associated with the additional two C-terminal residues. Reconstructions made by cryo-EM from the two peptides demonstrated differences in protofilament packing: while Aβ 1-42 fibrils showed either a single-protofilament arrangement or a two-protofilament assembly, the Aβ 1-40 reconstructions are differently structured; the cross-section of Aβ 1-40 fibrils consists of either two or three β-cross units (two- or three-fold symmetry), while there is only one molecule per protofilament unit length in Aβ 1-42 fibrils [60][57][61] (Figure 1.19).

By contrast, it has also been shown that the protofilaments of Aβ 1-40 and Aβ 1-42 fibrils are highly similar. Furthermore, there is evidence that fibrils formed by the two peptides differ, at least slightly, in the exact residues

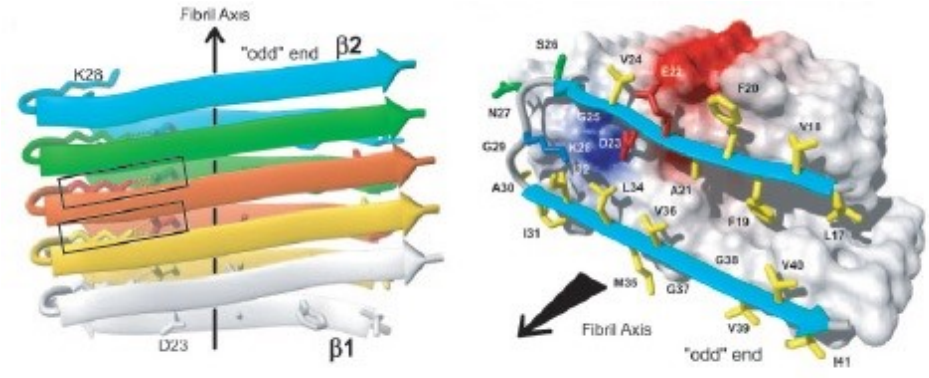

Figure 1.20: 3D structure of Aβ 1-42 fiber proposed by Lurhs [62]

that form the secondary structural elements [59].

The heterogeneity in Aβ monomer structure reflects itself in heterogeneous Aβ fibrils assembled *in vitro* as well as ones isolated from Alzheimer's disease brains. This makes the structural characterization complicate and full of results in inconsistency in suggested Aβ fibrils structures [35]. The structural variations, observed during conformational studies, demonstrate that Aβ peptides present a polymorphic nature at atomic resolution and that the structural and morphological dissimilarities depend on the method of preparation[59]. Therefore, studying the differences between the two Aβ peptides and their aggregation products can help to understand the pathological process involved in the fibril and plaque formation and to design structure-specific ligands or inhibitors of aggregation.

In comparison with the extensive studies of Aβ 1-40, not much is known about the structure of Aβ 1-42 fibrils [62][57][63][64], which are established to be more toxic [65] and possess different aggregation properties [66].

There are interesting results about the 3D structure of the fibrils comprising Aβ 1-42, obtained using hydrogen bonding constraints from quenched hydrogen-deuterium exchange NMR. It was observed that residues 1-17 are disordered and residues 18-42 form a β-strand-turn-β-strand motif that contains two intermolecular, parallel, β-sheets that are formed by residues 18-26 (β-1) and 31-42 (β-2). At least two molecules of Aβ 1-42 are required to achieve the repeating structure of a protofilament (Figure 1.20).

The side-chains of the odd-numbered residues of strand β-1 of the n^{th} molecule form contacts with the even-numbered residues of strand β-2 of the $(n-1)^{th}$ molecule [62]. The intersheet side-chain interactions observed in Aβ 1-42 are the intersheet contacts formed between residues F19/G38 and A21/V36 and a salt bridge between residues D23/K28. The fibrils are stabilized by intermolecular domain swapping-type side-chain interactions

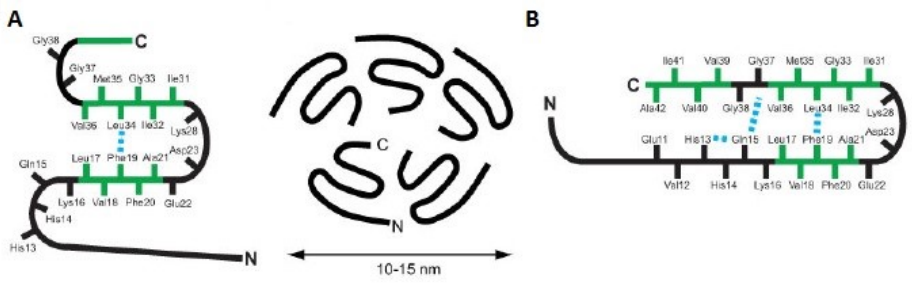

Figure 1.21: Molecular models of Aβ 1-42 oligomers (A) and fibrils (B) proposed by Ahmed [64]

(Figure 1.20).

More recently, Ahmed *et al.* showed that the neurotoxic oligomers formed during the aggregation process do not have the β-sheet structure characteristic of fibrils and that a structural conversion occurs during the passage from oligomers to fibrils [64]. In particular, they proposed two models for the structure and composition of Aβ 1-42 peptide: one for oligomers and another for fibrils (Figure 1.21).

Aβ 1-42 can form stable disc-shaped pentamers in which each monomer has a diameter of at least 5 nm and a height of 2 nm. The pentamers show discrete units surrounding a central axis. The hydrophobic C terminus of each monomer is oriented toward the center of the oligomer and the folded conformation is facilitated by the turns at His13-Gln15, Gly25-Gly29 and Gly37-Gly38, which allow the formation of the contact between Phe19 and Leu34 (Figure 1.21A).

For the fibrils, it was confirmed that the C-terminal hydrophobic sequence of the peptide folds into a β-turn-β conformation with molecular contacts between Phe19 and Leu34 and between Gln15 and Gly37. This model differs from the one proposed previously with respect to the specific side chain packing arrangement (Figure 1.21B).

Before this structural characterization, in a solution NMR study, Yu *et al.* [67] reported a dimeric structure for a soluble Aβ 1-42 species, called preglobulomer, which presented a mixed parallel and antiparallel β-sheet structure, different from fibrils which contain only parallel β-sheets. The preglobulomer presents two-β-strands: residues V18-D23 form one strand of an interchain antiparallel β-sheet connected by a β-hairpin (V24-N27) to the other intrachain strand K28-V40. Residues L34-V40 form an interchain in-register parallel β-sheet [67] (Figure 1.22).

The model presented by Ahmed is consistent with recent findings of Laganowsky *et al.* [68]. They performed conformational studies on a segment

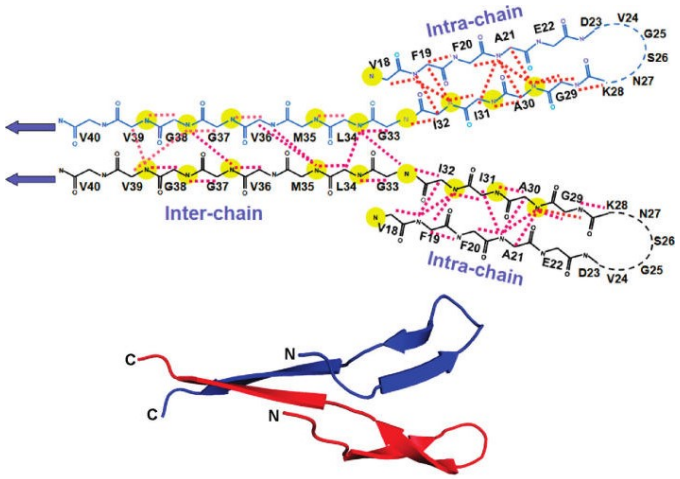

Figure 1.22: Structural model of a soluble Aβ 1-42 oligomer proposed by Yu [67]

of αB crystallin and they observed that this segment can form an oligomer composed of an antiparallel-β-sheet or a fibril composed of parallel-β-sheet.

NMR experiments on Aβ 1-42 oligomers conducted by Tay *et al.* [63] revealed that oligomers present β-strand secondary structure in which there are the same intermolecular proximities between F19 and I31 observed in fibrils. Unlike fibrils, oligomers are not characterized by in-register β-sheets and differ from them in schemes of intermolecular organisation. In this model, each molecule would contribute a single β-strand to two separate β-sheets. The β-sheets are arranged with a stagger such that closest proximities between F19 and I31 are between side chains on different molecules. The staggered β-strands may induce a β-sheet curvature that prevents the oligomer structures from extending into a fibrillar structure. This distinct intermolecular arrangement between oligomers and fibrils may explain why this oligomeric state appears off-pathway for monomer self-assembly to fibrils [63] (Figure 1.23).

The same research team has recently reported new solid-state NMR constraints on oligomers, confirming the existence of an antiparallel β-sheet formed by residues near the C-terminus, in which the V36 residue is in the closest possible proximity to V36 residues on adjacent molecules [69].

So we can ascertain that Aβ self-assembly processes can occur via multiple pathways to produce more than one possible fibril structure and there is no widely accepted structural model for Aβ oligomers. More structural knowledge is needed to explain how oligomers differ structurally from protofibrils and fibrils.

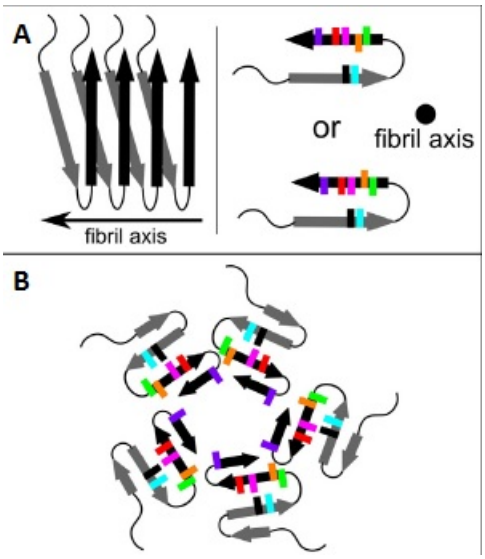

Figure 1.23: Schematic NMR models of Aβ fibrils (A) and oligomers (B) proposed by Tay [63]

Origin of Aβ toxicity Because the progression of Alzheimer's disease and its mechanism of toxicity are not very well understood, researchers have put forward various hypothesis about the Aβ toxicity. An accumulation of the peptide can induce oxidative stress: redox-active copper ions have been found accumulated in amyloid plaques and catalyse the production of ROS [70].

Aβ oligomers and not its insoluble aggregates are considered to be responsible for synaptic dysfunction with a mechanism that is not fully understood [71][72][73][29][74][75].

Aβ small aggregates can also interact with the cellular membrane, leading to pore formation and so causing the abnormal flow of ions, in and out of the neuronal cells [76].

Recently, the research team of Qu *et al.* showed that Aβ oligomers could inhibit telomerase activity both *in vitro* and *in vivo*, binding to the DNA-telomerase complex and blocking the elongation of telomeric DNA [77].

Finally the neuronal loss in Alzheimer's disease patients has been linked to the ability of Aβ to induce the process of programmed cell death (apoptosis) by activation of the signalling pathway that decreases the expression of cytochrome c oxidase subunit (COXIII) and inhibits COX activity leading to mitochondrial disfunction [78].

The amyloid hypothesis, however, is unable to clearly explain why some individuals with high histological plaque counts are cognitively normal. This observation brought to revise the amyloid hypothesis and to consider soluble

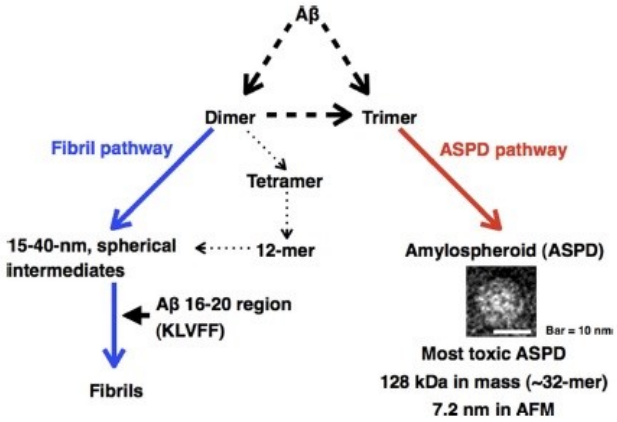

Figure 1.24: Two distinct Aβ assembly pathways, one leading to ASPDs (red) and the other to fibrils (blue) [53]

and neurotoxic Aβ aggregates the reason of the synaptic dysfunction and the initiators of the cascade of events that result in Alzheimer's disease (oligomer hypothesis).

As we have already described, toxic oligomers are predominantly generated from the monomeric peptide in a secondary nucleation reaction [52]. Because it is still unclear whether these originate from a linear process or a series of parallel processes involving different intermediates, Matsumura *et al.* [53] prepared highly toxic spherical Aβ assemblies (ASPDs) which were not fibril intermediates. The ASPD concentration was correlated with the pathological severity of the disease, demonstrating their pathological role. Thanks to these results, they provided two distinct assembly pathways, one leading to higly toxic spherical Aβ assemblies, existing *in vivo*, and the other to fibrils. The ASPD pathway requires the trimerization, while the pathway to fibrils begins with dimers, which further assemble into spherical intermediates. For this latter step, the Aβ 16-20 region is critical for intermediate conversion into fibrils, but not for ASPD formation [53] (Figure 1.24).

It remains uncertain if there is one species of oligomer that is responsible of the toxicity or whether multiple species are involved, because the aggregation process is dynamic and makes it extremely difficult to discern the sizes and the abundance of each oligomer present. Not all the oligomers are toxic or neurologically active and if we compare the toxic with the non-toxic oligomers, we can note that the toxicity increases with the extent of solvent exposure of two hydrophobic domains (aa 16-22 and 30-42), reflecting the importance of conformation in toxicity [79][29].

Ono *et al.* [29] demonstrated that the oligomerization process is accompanied by an increase in structural order (β-sheet content) and oligomer

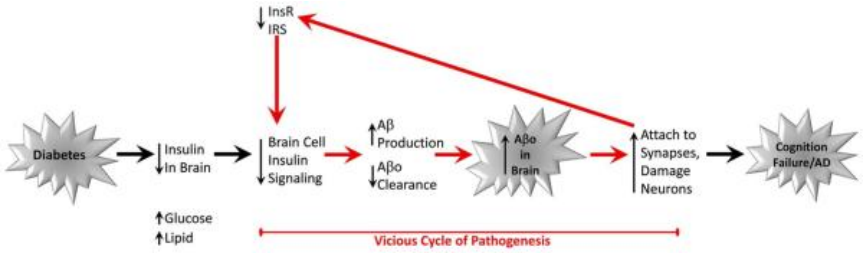

Figure 1.25: The vicious cycle that links Alzheimer's to diabetes [80]

secondary structure and order correlated directly with fibril nucleation activity. The monomer addition to dimeric and higher-order assemblies is associated with tertiary conformational changes producing relatively extended conformers. The toxicity of these assemblies correlates with the dependencies observed in the structural studies[29].

The same link between toxicity and oligomer size was also investigated by Cizas *et al.* [72]. They showed that small oligomeric forms of Aβ 1-42 are the most toxic species and induce rapid necrotic neuronal cell death, while oligomers with $n > 14$ do not cause significant cell death. The toxicity is probably due to the high capacity to bind to lipid membranes [72].

To compare the effect of Aβ oligomers and fibrils on the neuronal viability, several reseach teams developed different aggregation protocols in order to obtain different Aβ samples containing either soluble oligomers or fibrils with different size and shape and to correlate them with the neurotoxicity. In particular Dahlgren *et al.* reported that oligomers inhibit neuronal viability 10-fold more than fibrils and at least 40-fold more than unaggregated peptide [75].

The etiology of amyloid oligomer buildup may involve disparate factors and recently a developing area of investigation, that puts in relationship Aβ oligomers, diabetes and resistance to insuline signalling in the Alzheimer's disease brain, appears [81]. Aβ oligomers induce a dysfunctionality in the insulin signalling in neuronal cells by blocking trafficking of insulin receptors to dendritic membranes. So we can consider Alzheimer's disease as a Type 3 diabetes, because oligomers make neurons insulin-resistant. On the other side, the CNS insulin signalling is important to prevent the Aβ oligomers buildup and to block their neurotoxicity binding. This vicious cycle results in cognitive failure (Figure 1.26).

It's uncertain if oligomers accumulate and damage intracellularly or extracellularly. Measurements of oligomers in cerebrospinal fluid of Alzheimer's disease patients revealed the presence of oligomers extracellularly at very early stages of pathology but on the other hand intracellular oligomers were detected in animal models overproducting APP and Aβ [82][83]. Different

studies suggested that the accumulation and the clearance of Aβ are influenced by ApoE isoforms, which are secreted by astrocytes and plays a role in the receptor-mediated uptake of Aβ by neurons [84]. The fact, that antibodies directed against oligomers showed the ability to reduce oligomers and plaques and to improve memory function, supports the hypothesis of extracellular oligomers but also the idea that intracellular and extracellular oligomers pools are dynamically related. It was also demonstrated that intracellular accumulation of oligomers is upstream of tau pathology [85][86].

The Aβ oligomers have been shown to be able to alter synapse physiology and in particular to affect the maintenance of hippocampal LTP (long-term potentiation) which is the system able to repetitively stimulate synaptic circuits in order to induce synaptic plasticity. Soluble Aβ oligomers, extracted from the cerebral cortex of typical Alzheimer's disease patients, are able to inhibit LTP, enhance LTD (long-term depression) and reduce dendritic spine density in normal rodent hippocampus, impairing synapse structure and function [74]. These effects are due to the fact that oligomers are able to target both metabotropic glutamate receptors, required for the induction of LTD, and NMDA receptors, needed for spine loss, although these receptors are unlikely to be the sole effector targets of soluble Aβ oligomers.

Aβ oligomers bind only to particular neurons, at most half those present in hippocampal cultures. Less binding occurs in cortical cultures and little to non in cerebellar cultures [87]. Cell-specific binding correlates with toxic responses, as the stimulation of tau hyperphosphorylation by Aβ oligomers [88]. The exogenous Aβ oligomers accumulate at synapses and in particular at synapses spines and this specific binding is probably mediated by cell surface proteins that act as toxin receptors and are expressed only on certain cells [89][90].

A prominent alternative to the receptor hypothesis is that Aβ oligomers insert directly into the lipid bilayer and disrupt membranes as a pore [91]. Prangkio *et al.*[73] proposed a multivariate analyses of Aβ oligomer populations that demonstrates a connection between pore formation and cytotoxicity. The pore formation is one plausible mechanism for toxicity resulting in aberrant flux of Ca^{2+} ions and causing cell death. They found that tetramers to 13-mers contributed positively to pore formation and toxicity and within this range, the tetramer to hexamer populations showed the highest statistical significance. These oligomers have been also found in the brain of Alzheimer's disease patients [73].

Multiple strategies are being explored that target Aβ oligomers for therapeutics and all these efforts reflect a widely held belief that oligomers provide an unifying molecular basis for the cause, diagnosis ant treatment of Alzheimer's disease. Nonetheless, there is no consensus of agreement concerning the Aβ oligomers hypothesis [80].

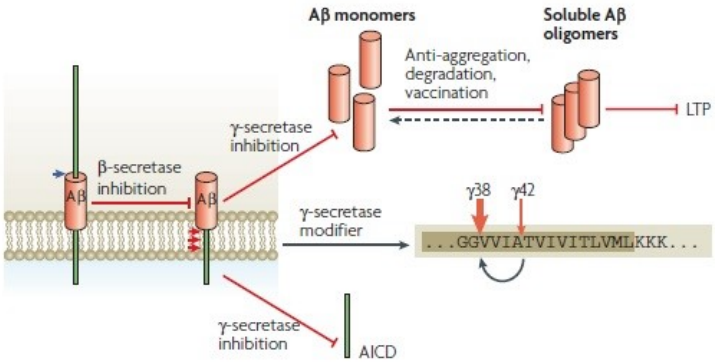

Figure 1.26: Therapeutic approaches targeting amyloid β-protein production and oligomerization [71]

1.3 Therapeutical strategies in development to target Aβ 1-42 peptide

The prominent role played by Aβ in Alzheimer's disease makes it an obvious therapeutic target. In this section, we discuss about the different approaches in development, targeting Aβ peptide, in particular its production, its aggregation and its homeostasis. In fact, starting from the amyloid and oligomer hypotheses, there are various strategies to prevent Aβ-induced toxicity. One is to inhibit either β- or γ-secretase in order to decrease the production of the peptide and so to lower its aggregation.

Another strategy is the immunotherapy, through either active Aβ peptide vaccination or passive infusion of anti-Aβ monoclonal antibodies with the goal to prevent the formation of Aβ oligomers and/or disrupt pre-existing oligomers.

In order to maintain a normal Aβ concentration in the brain (Aβ homeostatis), another therapeutical approach is to enhance the regulatory pathway involving apolipoprotein E or to increase the clearance by peptidase activity [58].

Finally, targeting Aβ aggregation by modulators is considered an effective therapeutic strategy (Figure 1.26). We can account as modulators of Aβ aggregation molecules that can:

- block β-sheet formation;
- prevent the fibrillogenesis;
- dissolve Aβ aggregates to non-toxic species;
- destabilize Aβ oligomers;

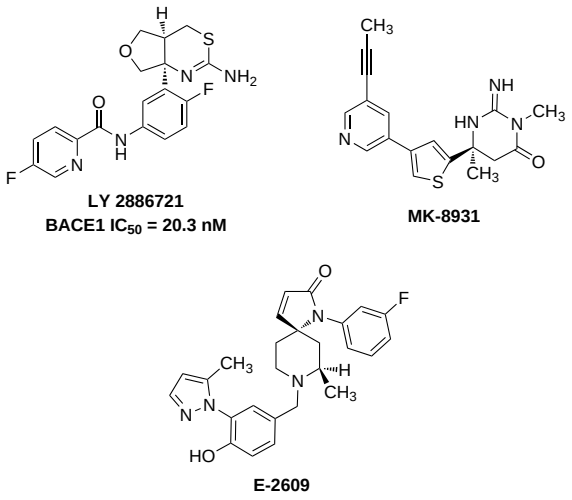

Figure 1.27: Examples of β-secretase inhibitors in clinical trials

- accelerate the conversion of Aβ oligomers to Aβ aggregates.

Below, after doing a brief rundown on the situation in therapeutic approaches that involve the production and homeostasis of Aβ and the immunotherapy, we will try to give a better insight about the aggregation modulators described in literature, in order to make the state of the art about the therapeutic approach that we wanted to develop in this thesis.

1.3.1 Enzyme inhibitors

In this part we focus our attention on enzyme inhibitors of β-secretase and γ-secretase which are involved in APP processing to produce Aβ.

β-Secretase inhibitors (BACE inhibitors) In recent times, LY2886721, MK-8931 (actually in phase II/III) and E-2609 (actually in phase II) (Figure 1.27) have completed phase I clinical trials and entered phase II trials. No single BACE1 inhibitor has currently passed phase II/III of clinical trials [92]. This is due to the lack of improvement of cognitive abilities [93] or to the development of side effects, as in the case of LY2886721 that was terminated due to liver abnormalities.

A series of molecules containing 4-bromophenyl piperazine coupled to a phenylimino-*2H*-chrome-3-carboxamide moiety were designed based on docking studies and molecule **1.1** (Figure 1.28) displayed remarkable inhibition properties [94].

Hunt *et all.* have designed a spirocyclin-based efficient and selective inhibitor **1.2** (Figure 1.28) [95] and similarly Thomas *et all.* have developed

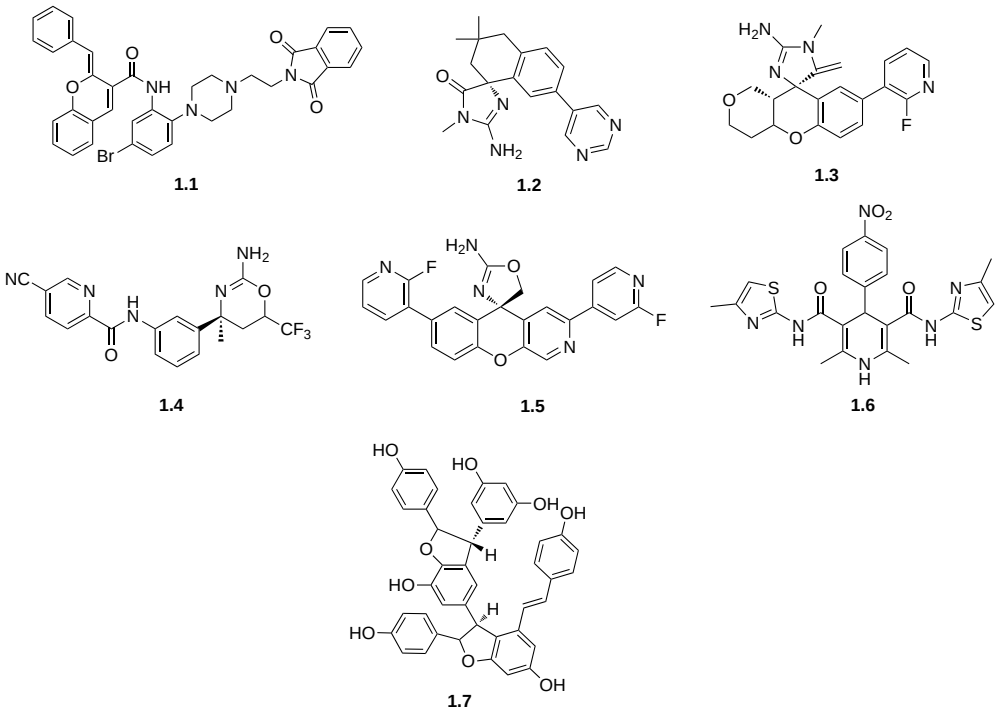

Figure 1.28: Examples of β-secretase inhibitors in the literature

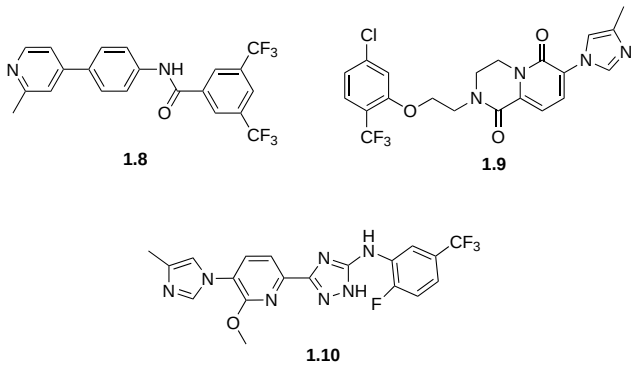

Figure 1.29: Examples of γ-secretase inhibitors in the literature

spirocyclic acyl guanidine based molecules with 2-fluoropyridine-3-yl as a substituent (molecule **1.3**, Figure 1.28). Both showed the ability to dicrease the Aβ levels in *in vivo* studies [96].

1,3-Oxazine (molecule **1.4**, Figure 1.28) is a moderate inhibitor and showed the ability to enhance the inhibition once derivatised with the fluorine moiety and even better with a CF_3 it improved its activity and its BBB crossing ability [97].

2-aminoxazoline xanthine is another promising inhibitor with the problem of cross-binding to hERG channels. So a substitution was performed to overcome this problem and to obtain an efficient molecule **1.5** (Figure 1.28) that showed reduced levels of Aβ *in vivo* [98].

Miri *et al.* designed a series of molecules based on 3,5-bis-*N*(aryl/eteroaryl) carbamoyl-4-aryl-1,4-dihydro pyridine to obtain an inhibitor (molecule **1.6**, Figure 1.28) with negligible calcium channel blocking affinity [99].

Finally, the natural product miyabenol C (molecule **1.7**, Figure 1.28), a resveratrol trimer, has showed selective and effective inhibition of the β-secretase [100].

γ-Secretase inhibitors To date, molecules that inhibit directly γ-secretases are not so much considered, due to the fact that they produce detrimental side effects as the enzyme is involved in many other critical functions like lymphocyte development and cell differentiation. Recently, in this field, researchers prefer to develop γ-secretase modulators that selectively modulate the APP cleaving site and prevent the production of neurotoxic Aβ peptide.

By structural optimisation of the γ-secretase modulator scaffold based on sulfonamide moiety, Wood *et al.* designed and synthesized molecule **1.8** (Figure 1.29) that showed improved cell potency, enhanced pharmacokinetics and drug methabolism and reduced the Aβ 1-42 production [101].

The introduction of pyridopiperazine-1,6-dione ring on a previously de-

signed γ-secretase inhibitor, performed by Pettersson *et al.*, allowed to obtain molecule **1.9** (Figure 1.29) with better ADME parameters and an efficient modulation of the enzyme, with reduction of Aβ 1-42 levels [102].

Finally, an efficient anilinotriazole (molecule **1.10**, Figure 1.29) was introduced after optimisation through a varying spacer link between the triazole ring and substituted aromatic ring and was shown to reduce Aβ levels both *in vitro* and *in vivo* [103] (Figure 1.29).

Recently, another approach in this field appeared with the aim to modulate γ-secretase instead of inhibiting. Certain non-steroidal anti-inflammatory drugs (NSAIDs) and their derivatives have been shown to shift the cleavage site of the enzyme from the rapidly aggregating 42-residue variant to the far less amyloidogenic 38-residue form.

1.3.2 Immunotherapy

Recent discovery efforts concern vaccines that target Aβ oligomers. The new and promising approach of immunoterapy is through either active Aβ-peptide vaccination [104] or passive infusion of anti-Aβ monoclonal antibodies [105]. An Aβ 1-42 vaccine, however, presented the development of a T-cell-mediated, autoimmune meningoencephalitis in 6 % of patients during the phase II trial and this led to cessation of dosing [106]. Despite this side effect, a portion of the patients, who subsequently developed anti-Aβ antibodies, seemed to have some slowing of their cognitive decline. So an alternative immunotherapeutic approach to avoid brain inflammation uses passive infusions of a monoclonal antibody.

Recently, Kraft *et al.* [107] reported a selective, high affinity humanized antibody engineered into an IgG2 (ACU-193) for Aβ oligomeric species. Although effective in model systems, ACU-193 has not been tested in humans. BAN-2401 is another humanized antibody that is now in phase II clinical trials [107].

Finally, Pradier *et al.* developed SAR228810, a humanized antibody engineered into IgG4. This antibody is able to bind higher molecular weight soluble Aβ oligomers and fibrils with high affinity over monomeric Aβ and lower soluble Aβ oligomers [108].

Actually, there are two IgG1 monoclonal antibodies in Phase III. Solanezumab is a humanized monoclonal antibody directed against the mid-domain of the Aβ peptide. It recognizes soluble monomeric, not fibrillar, Aβ. The other is Aducanumab, a fully human monoclonal antibody against a conformational epitope found on Aβ. It binds aggregated forms of Aβ, not monomer. In the brain, Aducanumab preferentially binds parenchymal over vascular amyloid.

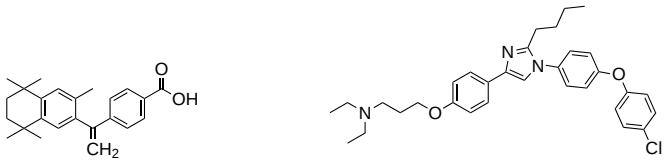

Bexarotene Azeliragon

Figure 1.30: Two therapeutic agents that modulate the homeostasis of Aβ peptide

1.3.3 Aβ homeostasis

The Aβ concentration in the normal brain is maintained by a regulatory pathway involving apolipoprotein E (apoE). In Alzheimer's disease patients, apoE/Aβ complex forming probability is reduced, thus increasing Aβ concentration in the brain. ApoE4, allele of apoE, is less lipidated in the disease and this lead to increase oligomeric Aβ levels, due to a reduced stability and lower levels of apoE/Aβ complex. So, probably, if the lipidation of apoE is increased, the concentration of Aβ is decreased. The apoE expression is transcriptionally regulated by peroxisome proliferator-activated receptor gamma (PPARγ) and liver X receptors (LXRs) which form heterodimers with retinoid X receptors (RXRs).

Landreth *et al.* observed that bexarotene, an anti-cancer agent, is able to behave as agonist for RXRs and so to over-express apoE and reduce Aβ levels [109]. Now bexarotene is in phase II clinical trials.

Other strategies with the aim to modulate the homeostasis of Aβ peptide in the brain include either the activation of the low-density lipoprotein receptor-related protein 1 (LRP-1) that is responsible for the outflow of Aβ or the inhibition of the receptors for advanced glycation endproducts (RAGE), located on the walls of blood vessels. These receptors are responsible for the passage of the peptide into the brain and for the activation of a signalling pathway that leads to apoptosis and inflammation. The inhibition of the link between Aβ and RAGE in mouse models showed the possibility to decrease the accumulation of Aβ in the brain and so its toxicity [110]. To date, Azeliragon, a RAGE inhibitor developed by Pfizer, is in phase III clinical trials (Figure 1.30).

Neprilysin (NEP) and neprilysin 2 (NEP2) are endopeptidases involved in the Aβ clearance by peptidase activity. A recent strategy involves virus transfection in order to increase the expression of these endopeptidases and so reduce the Aβ load in the brain [111].

Autophagy is the natural, destructive mechanism that disassembles, through a regulated process, unnecessary or dysfunctional cellular components. It was observed that in Alzheimer's disease there is a defective

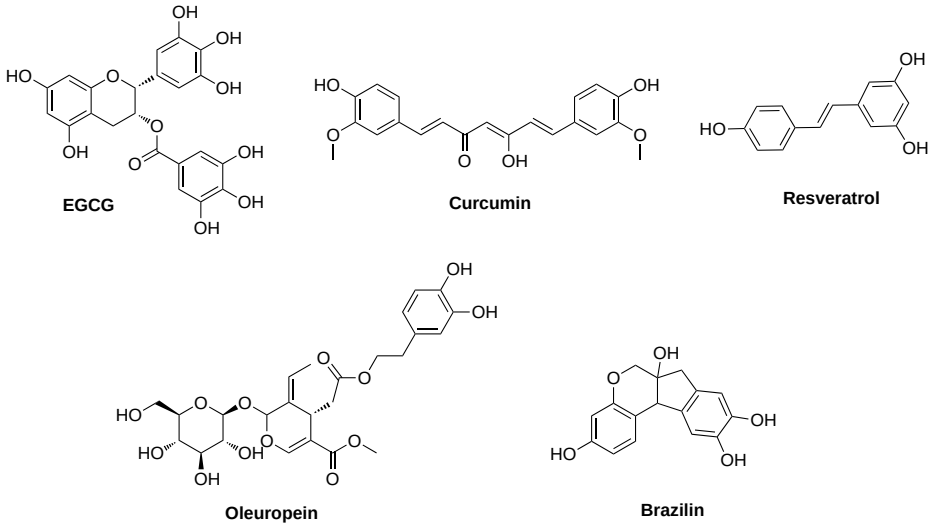

Figure 1.31: Polyphenols able to inhibit the Aβ aggregation process

delivery of autophagosomes to lysosomes and so a down-regulation of autophagy. Using small molecules that can upregulate the autophagy is a promising approach for the elimination of misfolded protein aggregates [112].

Other strategies aimed to promote the elimination of Aβ peptide, maintained in soluble forms. Thus Tramiprozate (3-amino-1-propane sulfonic acid) was developed with the aim to mimic glycosaminoglycans (GAG) and to keep Aβ peptides in a non-toxic form and promote its clearance. Indeed physiologically these elements of the extracellular matrix bind to soluble forms of Aβ peptide. Unfortunately these GAG mimics also cause the aggregation of the protein Tau. So the tests were halted in Phase III clinical developement [113].

1.3.4 Modulators of Aβ aggregation

In this part, we present a general overview about the discovery and design of compounds able to inhibit the protein self-assembly, through small drug-like molecules and peptide based inhibitors, such as β-sheet breaker (SRE mimics) and α-helix or β-hairpin foldamers.

Small molecules Small molecule inhibitors are low molecular weight organic compounds that bind with high affinity to biomacromolecules such as proteins, nucleic acids, or polysaccharides, altering their activity or function. Two types of small molecule inhibitors of the Aβ aggregation have been recognized: polyphenols and non-polyphenols [101].

Polyphenols comprise a large group of aromatic compounds containing

one or more phenolic hydroxyl groups. These natural compounds are often found in food or in herbal medicines, such as wine, tea bush, grape or coffee. Their well known antioxidant capacity may counteract oxidative stress induced by Aβ thus hampering neurodegeneration and modulating the vicious cycle between Aβ generation and oxidative stress [114]. Furthermore, these compounds may interact with aromatic residues in amyloidogenic proteins, being imposed between two aromatic residues, prevent the π-π stacking, and block the self-assembly process (Figure 1.31).

Epigallocatechin-3-gallate (EGCG) is a member of a family of plant-derived flavan-3-ols, and is the major polyphenolic compound of green tea. It has been demonstrated that EGCG is able to inhibit the fibrillization, to form large, spherical oligomers which seem to be off-pathway species, and to remodel Aβ mature fibrils into smaller, amorphous protein aggregates that are nontoxic to mammalian cells [115][116]. EGCG is now in phase III clinical trials.

Curcumin is the main constituent of the spice turmeric. *In vitro* curcumin inhibits fibril formation and destabilizes preformed fibrils, due to its Congo Red dye-like biphenolic structure [117]. Recently, Tooyama *et al.* performed structural modification in curcumin by introducing alkyl (propyl) ester and its corresponding acid at the C_4-position to obtain two analogues that demonstrated the ability to reduce insoluble Aβ deposits and so improve cognitive deficits in comparison with curcumin [118].

Resveratrol is a stilbene polyphenol which holds great promise as a therapeutic agent. This compound is able to prevent β-structural transitions, thereby reducing oligomers and protofibrils formation, and attenuating Aβ-induced cellular toxicity [119].

Oleuropein is one of the main phenolic components of olive oil. This polyphenol eliminates the appearance of early toxic oligomers favouring the formation of stable protofibrils, structurally different from the typical Aβ-sheet rich fibrils [120].

Brazilin is a natural product that showed its activity of inhibiting Aβ 1-42 aggregation and remodeling the aggregates to prevent them from acting as secondary nucleation centers. The mechanism of action of this molecule was studied by molecular docking studies that suggested the ability of brazilin to interfer with the intermolecular salt bridge of D23-K28 *via* hydrogen bonding [121].

The main issues about using polyphenols is that their bioavailability is in general low and some concerns still remain regarding their capacity to bypass the blood brain barrier.

Non-polyphenol inhibitors include small molecules like alkaloids, glycosides and phenazine, containing one or several aromatic rings, which are the key factors to the inhibitory effect (Figure 1.34). For exemple one molecule targeting the central core of Aβ peptide is RS-0406 (bis(3-hydroxyphenyl)pyridazine-3,6-diamine) and this molecule demonstrated to

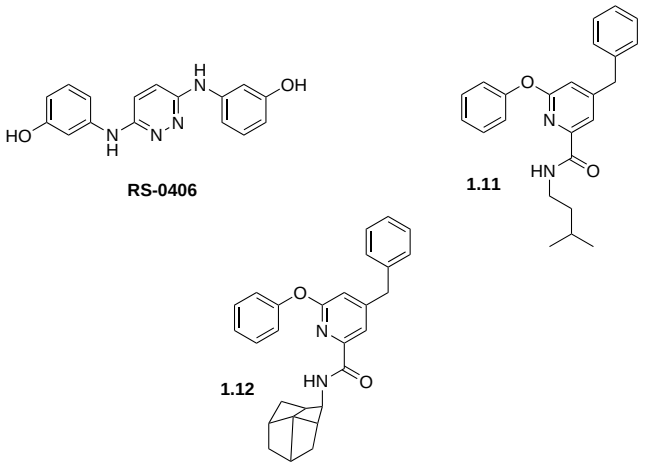

Figure 1.32: Non polyphenol inhibitors of the Aβ aggregation process

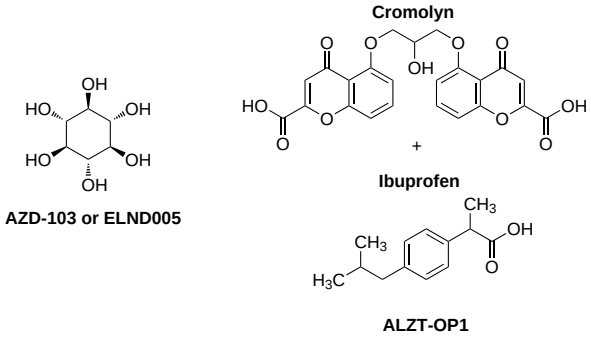

Figure 1.33: Non polyphenol inhibitors of the Aβ aggregation process in clinical trials

be able to inhibit the fibrillogenesis and to ameliorate the Aβ cytotoxicity [122]. Since melatonin and indole-3-propionic acid inhibit the formation of amyloid fibrils, several indole derivates have been tested as inhibitors of the Aβ aggregation.

Recently, Arai *et al.* reported two novel potential non-peptide small lead molecules with significant inhibitory properties against Aβ 1-42 aggregation. These compounds were designed through the use of structure-activity relationship data from cyclo-KLVFF peptide, in which the side chains of Leu2, Val3, Phe4 and Phe5 were identified as unique pharmacophore motifs responsible of the Aβ 1-42 peptide aggregation inhibition without the involvement of backbone amide bonds [123] (Molecules **1.11** and **1.12**; Figure 1.34).

Finally, we count a glycolipid-derive sugar, scyllo-inositol (AZD-103,

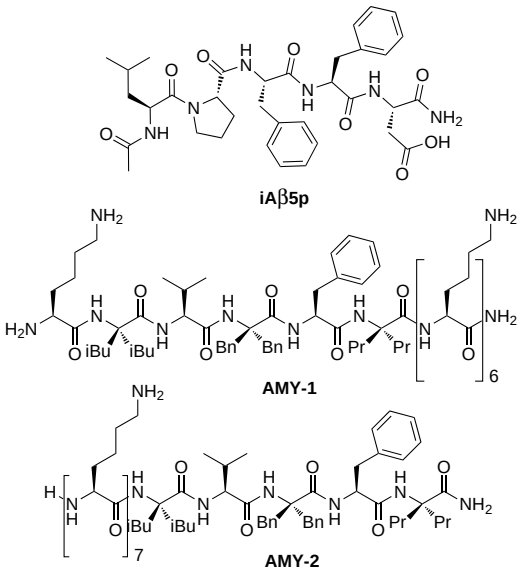

Figure 1.34: iAβ5 and two exemples of peptidomimetics with α-α-disubstituted amino acids

ELND005, Figure 1.33) that, to date, is in phase II clinical trials, targeting the lipid Aβ interaction and thus the aggregation process, and ALZT-OP1 (Figure 1.33) that is a combination of cromolyn (non-corticosteroid treatment of choice in the treatment of asthma) and ibuprofen and enters in phase III clinical trials as inhibitor of the aggregation process.

β-sheet breakers Therapeutic peptides offer several advantages over small organic molecules. The first advantage is that, often representing the smallest functional part of a protein, they offer greater efficacy, selectivity and specificity than small organic molecules. A second advantage is that the degradation products of peptides are amino acids, thus minimizing the risk of systemic toxicity and so the drug-drug interactions. Third, because of their short half-life, few peptides accumulate in tissues and the risk of complications caused by their metabolites is reduced.

The formation of amyloid fibrils by Aβ 1-42 peptide can be hindered by short synthetic peptides (β-sheet breakers, BSBp) homologous to the central hydrophobic region, modified by the substitution of some hydrophobic residues with hydrophilic ones [124]. β-sheet breakers are synthetic rationally-designed peptides specifically created to break β-sheets. The self-recognition sequence Aβ 16-20 (KLVFF), in the central region of the Aβ peptide, proved to be important in the aggregation process, because it binds β-sheets and initiates aggregation (nucleation site).

Tjernberg was the first to make use of a core section of Aβ as a structural starting point and showed that Aβ 16-20 was able to bind full-length peptide and thus prevent its assembly into fibrils [125]. Soto and co-workers successively designed a series of inhibitors containing Aβ amino acids 17-20 (LVFF), and then replaced the valine and the alanine with a proline and an aspartic acid respectively to obtained the so called iAβ5 (Figure 1.34); this synthetic peptide showed a number of interesting properties, in particular permeability accros the blood brain barrier and inhibition of the fibrillization [124].

Several iAβ5 derivates were designed in order to improve the solubility and the plasma half-life, and in particular one of them with a single N-methylation between Pro and Phe maintained the inhibitory activity and improved its stability in rat brain homogenates [126]. Methylation of the amide groups may prevent intermolecular hydrogen bonding and result in decreased aggregation and toxicity. In order to increase the resistance to proteolysis, the proline residue of iAβ5 was replaced with a set of synthetic non-proteinogenic amino acids [127] and in order to increase the solubilty, sulfonylamide derivates were synthesized, showing that polar substitution at the N- and C-terminal regions may increase the BSBp solubility. Good inhibitors have been designed and synthesized by combining the hydrophobic core sequence with a bulky hydrophobic or hydrophilic moiety, such as cholic acid or aminoethoxy ethoxyacetic acid units [128][129].

Finally, Acerra *et al.* proposed retro-inversal sequence of iAβ5, by substituting the L-amino acids for their D-counterparts and reversing the sequence. These modification led to a mimic that retains the same inhibitory aggregation qualities with increased protease resistance [130]. Mandal *et al.* introduced ortho-aminobenzoic acid in the structure of iAβ5 and they obtained a modulator for both inhibition and dissolution of Aβ aggregates [131].

Other modifications involved the N- and C- terminal of the core domain. In particular a variant of this sequence containing a polycationic disrupting region linked to the C terminus (KLVFFKKKKKK) was shown to increase the rate of fibril formation and cell viability, while the modification of the N terminus with a polycationic sequence (KKKKLVFF) and the introduction of anionic elements (KLVFFEEEKKK) was demonstrated to accelerate fibril formation but also to decrease toxicity, suggesting that the new fibrils were not toxic or no longer in equilibrium with the toxic intermediates [132][133].

A peptide corresponding to the Aβ 31-34 sequence when linked to a N-terminal propionyl group was shown to form fibers and was toxic to neuroblastoma cells. However, replacement of the propionyl group with an arginine resulted in a peptide which inhibited fibril formation and reduced toxicity of Aβ [134].

Another exemple of conformationally constrained peptides is the class of α-α-disubstituted amino acids that were incorporated in such a way that

one face of the peptide would be sterically blocked (Figure 1.34). Also in this case, it was observed that this type of inhibitors is able to change the secondary structure of the peptide to a predominantly β-sheet structure, which is consistent with the design of these inhibitors preferring a β-sheet-like conformation [135].

The Allsop's research group designed a retro-inverso peptide (RI-OR2) based on a previously described inhibitor of Aβ oligomer formation (OR2, H_2N-R-G-K-L-V-F-F-G-R-NH_2). Unlike OR2, RI-OR2 was highly stable to proteolysis and completely resisted breakdown in human plasma and brain extracts and showed to maintain the inhibition activity over the formation of soluble Aβ oligomers, in particular of Aβ 1-42 [136].

Another designed peptide LF, having sequence Ac-KQKLLLFLEE-NH2 [51], was demonstrated to form amyloid-like fibrils that efficiently coassemble with mature Aβ 1-42 fibrils and soluble oligomers of Aβ efficiently, thereby reducing the toxicity of Aβ to a mammalian cell. The team concludes the presentation of their work in the paper, by focusing on the problem that peptides and proteins cannot be directly used for constructing therapeutics agents against Alzheimer's disease. One of the major problem in drug development for Alzheimer's disease is the blood-brain barrier permeability. Peptide and protein mimetics based on Aβ structures during various misfolding states might lead to the identification of compounds with a therapeutic benefit in a range of amyloid disorders, including Alzheimer's disease [51].

Schrader *et al.* opened the way to the development of nonpeptidic inhibitors, by synthesizing dimeric to tetrameric aminopyrazole ligands (Figure 1.35) [137]. By combining natural and unnatural amino acids to improve the water solubility of these structure that are prone to self-aggregation via hydrogen bonds, he obtained ligands that for the first time allowed to gain detailed insight into the complexation of β-sheet ligands with model peptides taken directly from Aβ. Two classes of designed aminopyrazole hybrid ligands were shown to undergo a specific interaction with KKLVFF, the key fragment from the nucleation site of Aβ in water [137].

Another research team developed a series of substituted bisphenol A derivatives as β-amyloid peptide aggregation inhibitors. The same group, in a previous work, showed that Aβ undergoes α-helix/β-sheet intermediate during the conformational transition, and an Aβ aggregation inhibitor was discovered by targeting the intermediates (Molecule **1.13**, Figure 1.35). In a more recent paper they presented the structure optimization toward this compound and the discovery of a more effective inhibitor, which not only can suppress the aggregation of Aβ but also can dissolve the preformed fibrils [138].

Recently, a dipeptide containing an aspartyl derivate was presented by Nadimpally *et al.* as potential inhibitor. This molecule undergoes a chemical transformation under physiological conditions and this transformation generates the breaker element *in situ* (Figure 1.36) [139]. In particular,

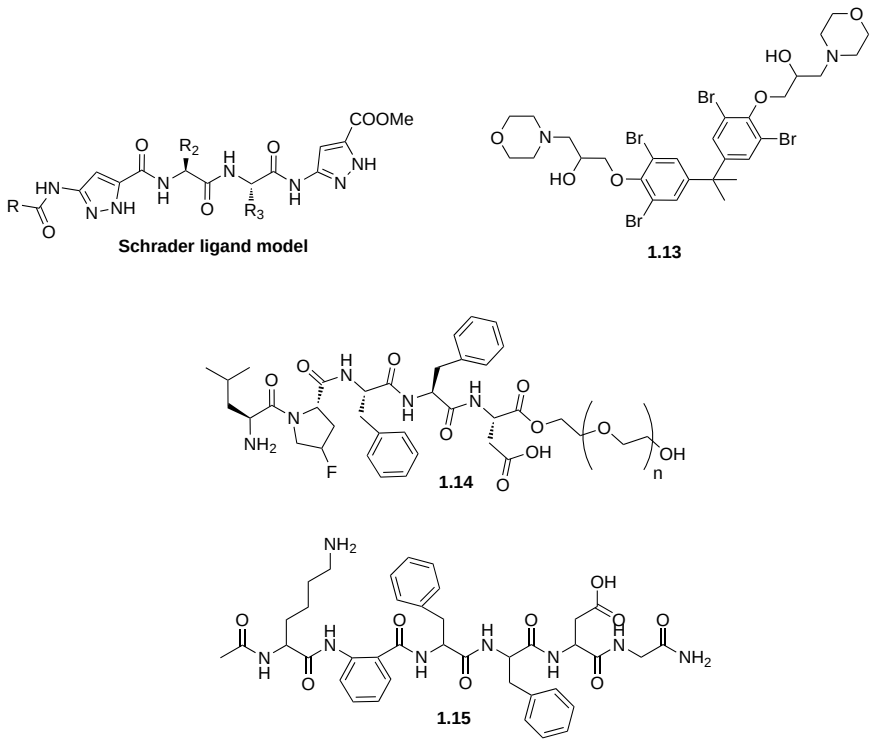

Figure 1.35: Exemples of peptidomimetic β-sheet breakers

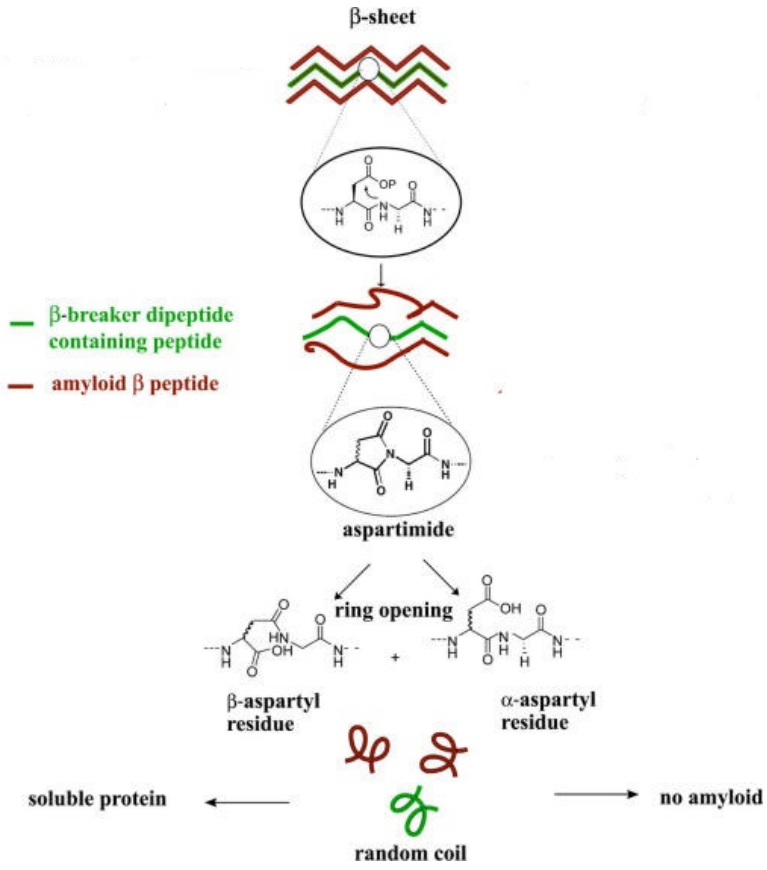

Figure 1.36: Concept of β-sheet disruption using β-breaker-dipeptide containing β-sheet breaker peptides [139]

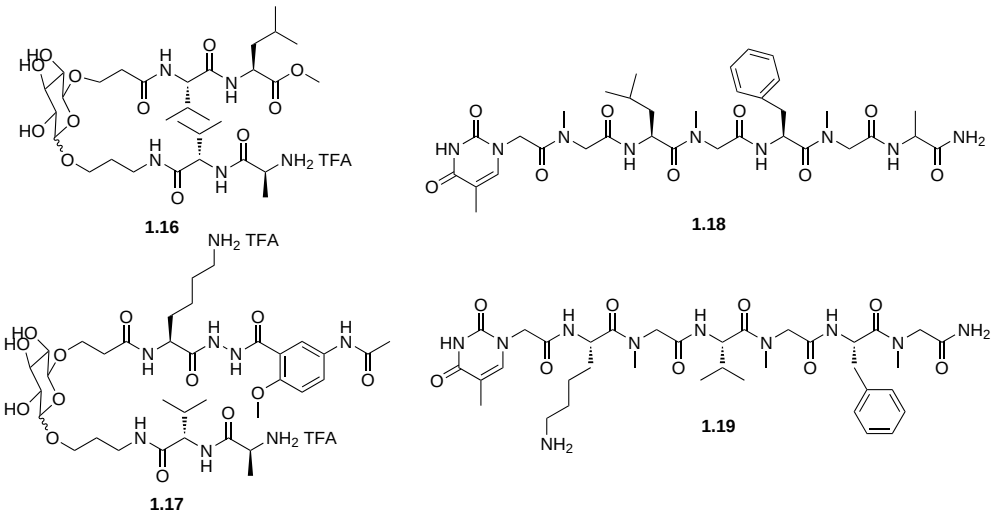

Figure 1.37: Exemples of other peptidomimetic β-sheet breakers

peptides containing a β-breaker dipeptide undergo a chemical conversion to aspartimide-containing peptides at physiological pH and generate a kink in the peptide backbone *in situ*. Formation of aspartimide, subsequent ring-opening and racemisation of Asp finally disrupt the native backbone of the breaker peptide.

Peptide inhibitors of Aβ aggregation have been generated by modifying the amino acids within or around SREs (self recognition elements). Of particular interest are those that include D-amino acid stereoisomers, as these peptides are more protease resistant. Kumar *et al.* created a peptide construct that targets the 17-21 SRE of Aβ, starting with Aβ 14-23 and introducing D-enantiomer(s) in place of L-phenylalanines at position 19 and/or 20 to stericaly interfere with π-stacking in the aggregate state. These peptidomimetics have showed that they can modulate Aβ 1-42 aggregation in favour of non-toxic oligomerization, possibly via alteration of oligomer surface binding sites and/or sequestration of Aβ 1-42 into large amorphous aggregates [140].

Fluorination of hydrophobic amino acids such as valine or phenylalanine in sequences that interfere with amyloid fibril formation has recently demonstrated to induce significantly a delay in the aggregation process. This is the effect of the interaction between the fluorinated amino acids and the hydrophobic residues of the peptide (Molecule **1.14**, Figure 1.35) [141].

Ashim *et al.* developed a novel class of conformationally restricted β-sheet breaker hybrid peptide comprised of a recognition motif of the target amyloidogenic peptide and anthranilic acid (Ant) as the breaker element (Molecule **1.15**, Figure 1.35) [131].

Our laboratory developed sugar-based pentapeptides of Ala-Val and Val-Leu with D-glycopyranosyl derivatives and small glycopeptidomimetics (Molecules **1.16** and **1.17**, Figure 1.37) that showed a good inhibition of protein-protein interactions mediating amyloid β-peptide oligomerization and fibrillization. In particular, we demonstrated that molecules delaying the aggregation can stabilize the monomeric peptide or promote the formation of soluble oligomeric species. On the contrary, molecules that accelerate the aggregation can prevent the presence of small toxic oligomers [142][143].

Finally, Rajasekhar *et al.* developed optimized peptidomimetics inhibitors based on KLVFFA. To enhance the binding affinities of inhibitors they incorporated multiple hydrogen bond donor-acceptor moieties (thymine/barbiturate) at the N-terminal to improve the inhibition efficiency and modified the backbone by introducing N-methylglycine at alternate positions to improve the blood serum stability. They obtained two new β-sheet breakers (**1.18** and **1.19**, Figure 1.37) that showed good activity in both inhibition and dissolution of Aβ 1-42 aggregates [144].

α-helices As we discussed above, there are several exemples of chemically diverse compounds that bind to an elongated form of the protein in a β-strand conformation and thereby exert their therapeutic effect. However, this approach could favor the formation of prefibrillar oligomeric species and they can act as aggregators. For this reason, another emerging alternative approach is to design helical coiled-coil-based inhibitor peptide in order to engage a coiled-coil-based amyloid-forming model peptide in a stable coiled-coil arrangement. In fact, initially, when generated from APP, Aβ admits a discordant α-helix with residues that have a high propensity for β-strand formation [145]. So one way to inhibit the aggregation process could be trapping Aβ in a state similar to its native α-helix structure.

Matsuzaki *et al.* designed α-helix analogue by simply cross-linking the Cys residues of A30C, G37C-Aβ 1-42 with 1,6-bismaleimidohexane. The analogue showed the ability to assume a weak α-helical conformation under conditions in which the wild type formed a β-sheet, indicating the cross-linking locally induced a helical conformation. This analogue is not only a model peptide to investigate the role of helical intermediates in fibrillization, but also an inhibitor of Aβ-induced cytotoxicity [146].

Using simple *de novo* designed model peptides, Brandeburg *et al.* showed that a coiled-coil-based amyloidogenic target peptide that shows α/β discordance, could become engaged in a stable helical arrangement in the presence of an idealized helical-coil model peptide as an alternative to adopting a β-sheet conformation and ultimately forming amyloid structures. Stabilizing the helical state would make the amyloid-forming sequence more susceptible to degradation by protease [147].

The same research team performed proteolysis studies that revealed dif-

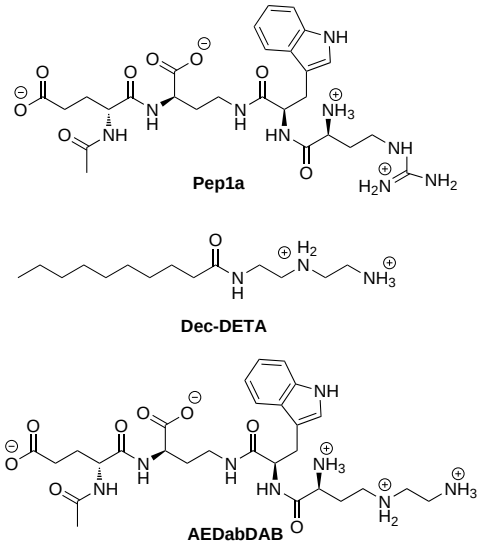

Figure 1.38: Chemical structure of Pep1, Dec-DETA and AEDabDAB: compounds that stabilize the Aβ 1-42 α-helix conformation

ferences in the degree of the dynamics of proteolytic degradation of the soluble and aggregated states of the model peptides. The amount of the unfolded state as well as the different conformation of the folded state influence the protease stability of peptides. A local rearrangement is necessary for the substrate to bind to the active site of the enzyme and this rearrangement is hypothesized to be relatively easy for helices but not for extended β-sheet structures, because in the latter case too many hydrogen bonds need to be broken [147].

In this type of therapeutic approach, we can distinguish molecules that are able to stabilize the α-helix conformation of the Aβ 1-42 peptide without forming a particular conformation, and molecules that are able to fold in α-helix manner and to present a good inhibition with this conformation.

Nerelius *et al.* were the first to design ligands able to bind and stabilize the 13-26 region of Aβ in an α-helical conformation, inspired by the postulated Aβ native structure. Pep1 and Dec-DETA affect Aβ helical content, polymerization and toxicity *in vitro* and *in vivo* (Figure 1.38). Successively, the effects of the two ligands (Dec-DETA and Peb1b) on the stability of the Aβ central helix were investigated by using MD simulations. It was quantitatively demonstrated that the stability of the Aβ central helix is increased by both ligands, and more effectively by Peb1b than by Dec-DETA, probably due to the fact that Peb1b has both basic and acid functional groups which can simultaneously bind to the acidic and basic residues of Aβ, whereas Dec-DETA has only the basic functional groups. An additional

reason would be that Peb1b includes a centrally placed aromatic ring which can interact with the Aβ middle non polar part [148][149].

In order to improve the interaction of the ligand with the helical conformation of the central part of Aβ, a novel Aβ targeting ligand AEDabDAB containing a new triamino acid, (2-aminoehtyl)-2,4-diamino butanoic (AEDab) acid, was developed (Figure 1.38). The new triamino acid carries an extra positive charge in the side chain and it is designed to be incorporated into a ligand AEDab-Dab where the AEDab replaces an arginine moiety in the previously developed ligand Peb1b. Molecular dynamics simulation of the stability of the Aβ central helix showed a further stabilization of the helical conformation and the evaluation studies demonstrated that the triamino acid resulted in an improved capability to prevent the Aβ 1-42 neurotoxicity [150].

Foldamers are artificial folded molecular architectures inspired by the structures and functions of biopolymers [151]. Classical foldamers consit of homogeneous backbones, for example oligomers assembled exclusively from monomers of a single class. Biotic foldamers are designed to mimic the structures, and, potentially, the biological properties of their natural counterparts and they are composed, for example, by N-substituted oligoglycine (peptoids), β-amino acids or their higher γ and δ homologues, or they present the replacement of the amide bonds by ureas, hydrazide or hydroxy amide functions. In contrast, abiotic foldamers with backbones and folding modes different from those of biopolymers have also emerged. Many of them are aromatic rich sequences [151].

In contrast to biopolymers, however, foldamer synthesis is not limited to homogeneous oligomers. It might be possible to mimic the secondary structure of proteines through foldamers by creating heterogeneous backbones that combine more than one type of constituent units. For example, sheet can be formed upon alternating turn and strand segments made of distinct backbones [151] [152].

The hypothesis to use foldamers to capture the Aβ oligomer aggregates and so for protein recognition and inhibition, emerged in this field when *in vitro* biophysical and biochemical tests indicated the tight binding between the foldamer conjugates and the Aβ oligomers. Foldamers may have the potential to improve on related protein therapeutics thanks to their medium size with large contact areas, their bottom-up designed modular chemical structure, their folding predictability, their resistence to hydrolysis and their tunable pharmacokinetic properties. In particular short helical β-peptide foldamers with designed secondary structures and side chain chemistry patterns were applied as potential recognition segments. The foldamer helices were synthesized by using β^3-amino acids with proteinogenic side chains, various diastereomers of alicyclic β-amino acids with 6- or 5- membered side chains and natural amino acids. The combination of the foldamer methodology with the fragment-based approach and the multivalent design

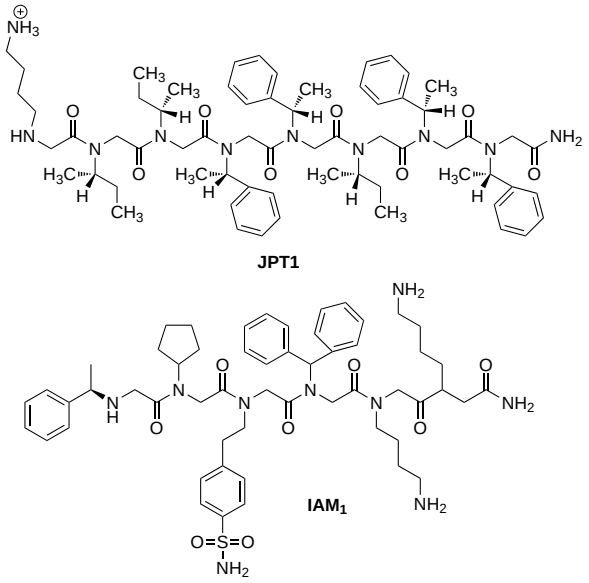

Figure 1.39: Two exemples of peptoids: JPT1 and IAM1

offered a pathway to unnatural molecules that are capable of specific molecular recognition, and resulted in an inhibitor that was able to interact with the target by its conformational structure as H14 helix [153].

Recently, poly-N-substituted glycines (peptoids) are emerging as a new class of peptidomimetics to mimic the peptide KLVFF, the nucleation site of Aβ 1-42 peptide. Peptoids are similar in structure to peptides, but with the side chain appended to the amide group rather than the α-carbon. This change leads to a lack of chirality and hydrogen bond donors, both of which are required for secondary structure formation. However, the inclusion of chiral side chains in the peptoid sequence leads to the formation of helical secondary structure. Generally peptoids that include chiral, aromatic side chains form polyproline type-I-like helices, stabilized by steric interactions rather than hydrogen bonds. The peptoid-based mimic of the peptide KLVFF called JPT1 (Figure 1.39) has been reported to modulate the aggregation of Aβ 1-40 by inducing the formation of a stable helical secondary structure that allows great interaction between the aromatic side chain and the cross β-sheet of Aβ [154].

Previously, Luo *et al.* used a combinatorial library to identify peptoids that bind to Aβ 1-40 and Aβ 1-42. The peptoid IAM1 (Figure 1.39) was shown to inhibit the aggregation of both peptides and its dimer (IAM)2 was shown to be more active in inhibiting the Aβ 1-42 peptide [155].

β-sheet mimics and β-hairpins To our knowledge, the use of small acyclic β-hairpins has been scarcely explored as β-sheet binders and inhibitors of aggregation.

In 2009, Teplow *et al.* demonstrated a 13-residue peptide hairpin, PP-Leu, as inhibitor, able to block the formation of the extendeed β-sheets necessary for Aβ fibril growth, to disrupt the structure of preformed fibrils and to potently inhibit Aβ oligomerization [156].

A new class of amyloid inhibitors was developed in 2011 by Andersen *et al.* that introduced hairpin peptides bearing cross-strand Trp-Trp and Tyr-Tyr pairs at non-H-bonded strand sites. These molecules showed the ability to modulate the aggregation of two unrelated amyloidogenic systems: human pancreatic amylin (hAM) and α-synuclein (α-syn), associated with type II diabetes and Parkinson's disease, respectively [157].

More recently, Hopping *et al.* presented trpzip peptides that among the smallest β-hairpin peptides are known to fold spontaneously without the use of disulfide-bonds or metal ions. The trpzip peptides are small, monomeric and extremely stable β-hairpins that have become valuable tools for studying protein folding. One type of these trpzip peptides (trpzip-3) showed to inhibit the aggregation in two very different amyloid systems: transthyretin (TTR:trpzip-3 1:20) and Aβ 1-42 (Aβ:trpzip-3 1:10) [158].

During the last twenty years, Nowick and co-workers developed the enourmous work in β-sheet mimics field. Their first paper, published in 1992, described an intramolecularly hydrogen-bonded oligourea molecular scaffold. This achievement represented one of the first examples of synthetic foldamers. Later on, the attachement of two peptide strands to an urea-based scaffold led to Nowick's first artificial β-sheet, which folded in chloroform solution to mimic the structure and H-bonding patter of a parallel β-sheet [159].

Nowick and co-workers also developed a series of molecular templates based on 5-amino-2-methoxybenzoic acid, and its hydrazide derivatives, to mimic and complement the hydrogen-bonding functionality of peptide strands and block unfilled hydrogen-bonding valences. The 2-methoxy group played the dual role of blocking the H-bond donor group and providing organization through intramolecular hydrogen bonding within these β-strand mimics. By combining the urea-based molecular scaffold with these β-strand mimics, a variety of artificial β-sheets were created, that folded into well-defined structures in chloroform and other organic solvents [160].

More recently, Nowick's group developed building blocks containing the amino acid ornithine and the so-called "Hao unit" to create a composite fragment that can be incorporated into peptides to induce folding and dimerization in organic solvents. The acronyme "Hao" was devised to reflect the three components by which it is formed: hydrazine, 5-amino-2-methoxybenzoic acid and oxalic acid. They prepared many different structures forming well-defined turns, with distinct NMR properties (NOEs, magnetic anisotropy, J-coupling) that indicate their folding. Combination of the Hao amino acid

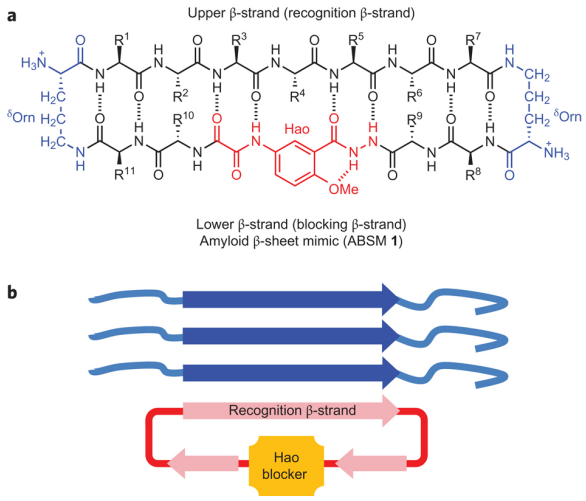

Figure 1.40: 54-membered macrocycle β-sheet mimic and its mechanism of action [162]

β-strand mimic with two ornithine β-turn mimics and α-amino acids results in cyclic modular β-sheets that present peptide β-strands along one edge [161].

So, they designed and prepared 54-membered macrocycle β-sheet mimics to display a variety of exposed heptapeptide β-strand sequences from different amyloid proteins so that these β-strands can recognize and bind their parent amyloid proteins and to antagonize their aggregation at the same time. Actually, they showed the good inhibitory activity of these well-defined β-sheets in the aggregation of amyloid protein in Alzheimer's disease. These amyloid β-sheet mimics (ABSMs) containing one hydrogen-bonding edge and one blocking edge are an effective design for inhibitors of amyloid aggregation (Figure 1.40)[162].

They developed also a series of macrocycles with suitable recognition strands and facial hydrophobicity that delay and suppress the onset of aggregation of AcPHF6, the tau 306-311 derived peptide. They observed a cooperative inhibition mechanism in which two molecules of the macrocycle bind simultaneously to the two β-sheet layers of tau model peptide [163].

Furthermore, they used these macrocycle peptides to explore oligomer structure. By incorporating a pentapeptide sequence from Aβ peptide into macrocycles, they limited the growth of the oligomers so that they may crystallize and cannot fibrillate. They determined the atomic structure and oligomers revealed tetrameric interfaces in which β-sheet dimers pair together, suggesting a common structure for amyloid oligomers and fibrils [164].

Finally, we cite the natural antibiotic gramicidine S that in a recent paper [165] demonstrated its ability to inhibit Aβ amyloid formation *in vitro* and to

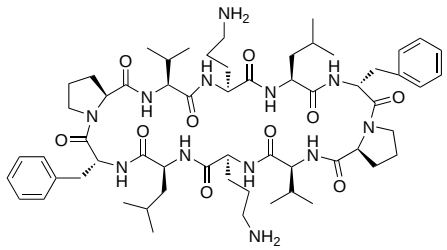

Gramicidine S

Figure 1.41: Chemical structure of Gramicidin S

dissolve amyloids that had formed in the absence of the antibiotic. In silico docking suggested that gramicidine S, a cyclic decapeptide that adopts a β-sheet conformation, binds to the Aβ peptide hairpin-stacked fibril through β-sheet interactions, probably explaining its inhibitory activity (Figure 1.39). The same research group identified an analogue with a potency that was four-times higher than that of the natural product [165].

1.4 General conception of the hairpin mimics design

The objective of this PhD thesis work is to design and synthesize new ligands of the Aβ 1-42 peptide in order to slow down or inhibit its aggregation process. Our strategy includes compounds that are able to recognize the nucleation site or the hydrophobic C-terminal sequences of the Aβ 1-42, by forming β-sheet secondary structure with the peptide target and so preventing its aggregation. However, contrary to the peptide or β-strand mimics, we will use β-sheet mimics (β-hairpins) that are able to form a β-sheet structure, once in contact with Aβ. We hope to develop this strategy in order to evaluate if the preorganization and the stability of the obtained β-sheet mimics will be able to inhibit more efficiently the aggregation of Aβ and to elucidate which stage of the oligomerization process is inhibited by these molecules. Based on the few recent published data on β-hairpin mimics, in particular on the macrocyclic structures of Nowick, we hypothesized that pre-structuring the peptidomimetic molecules might increase their affinity for Aβ peptide and thus increase their aggregation inhibitory activity.

As Aβ-aggregation is a dynamic and complex process, the use of flexible β-hairpins could be a strategy to obtain effective inhibitors. We hypothesize that flexible β-hairpins could adapt themselves in the interaction with the different Aβ 1-42 conformations present during the aggregation process, and in particular in the early stages of oligomerization.

For that purpose, our objective is to design and synthesize new β-hairpins able to structure themselves in a β-sheet manner or when they are in contact

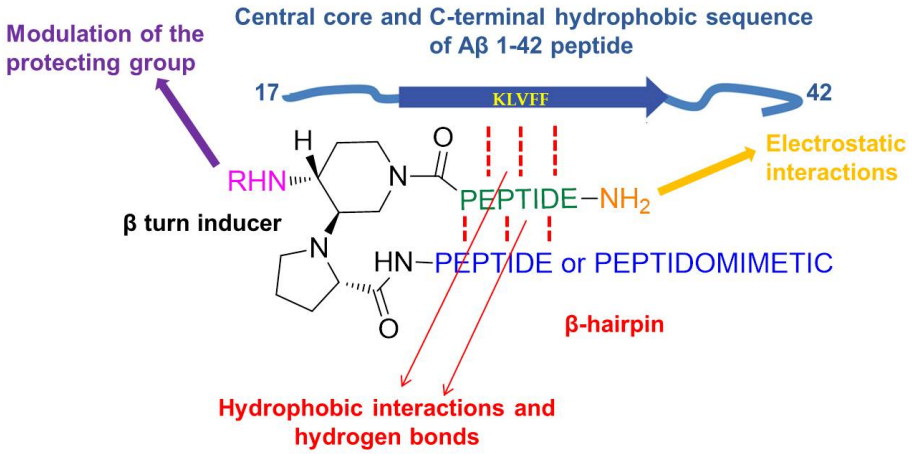

Figure 1.42: Schematic view of the interactions of designed inhibitors with the crucial sequence in Aβ 1-42 peptide

with the Aβ peptide (Figure 1.42). The design of β-sheet mimics represents a challenge for chemists, as we were able to realize thanks to our bibliographic research, because several problems are encountered during the preparation of these mimics:

- the design of a good scaffold able to induce the good folding of a peptide chain (Figure 1.42);
- the determination of the nature and the composition of the peptide strands or eventually the peptidomimetic sequences, that have to interact with the target in a β-sheet manner (Figure 1.42);
- the obtaining of compounds that are soluble in organic solvents and first of all in water or in a medium, compatible with the biological evaluations.

These compounds are also designed to provide electrostatic interactions with Aβ 1-42 and so to increase their affinity with the peptide (Figure 1.42). In particular they are conceived to establish electrostatic interactions with the two amino acids involved in the formation of the salt bridge (D23/K28) that stabilizes the β-strand-turn-β-strand unit in the Aβ 1-42 conformation (see the Aβ 1-42 structure proposed by Luhrs [62] and presented in section 1.2.3 of this chapter) (Figure 1.42) or with the C-terminal Ala42 that demonstrated to form a salt bridge with K28 and to be responsible of the triple parallel-β-sheet motif, as showed by Xiao *et al.* [166].

In conclusion, our objective is to meet the criteria above with the aim to obtain β-haipins that we will study by NMR, circular dichroism and

molecular modelling, in order to establish their secondary structure. These molecules will be tested to determine their activity and their ability to inhibit the oligomerization and fibrillization of Aβ 1-42 peptide. To our knowledge, the use of small acyclic β-hairpins has been very rarely explored as β-sheet binders and inhibitors of aggregation.

These compounds will be characterized by a β-turn inducer, based on a piperidine-pyrrolidine semi-rigid structure, able to fold the molecule in a β-hairpin manner and two rationally designed peptide or peptidomimetic sequences able to interact both with Aβ 1-42 peptide and between them, by establishing hydrophobic interactions and hydrogen bonds. The primary amine protecting group of the scaffold will be modulated in order to study the influence of the protecting group and of the free primary amine on the inhibitory activity of the compounds and on their solubility. Finally, the peptide and peptidomimetics arms will be conceived to be able to engage electrostatic interactions with Aβ 1-42, through the free N-terminal amine or the charged amino acid residues of the sequences (Figure 1.42).

Through this structure-activity relationship study, our aim is to understand what is needed to interact with Aβ 1-42 and to inhibit its aggregation process. We hypothesize that our β-hairpins might interact with the peptide by establishing β-sheet secondary structures with it and so stabilize its monomeric form, preventing the protein-protein interactions.

We decided to present this thesis work in four different parts, according to the different chemical nature of the designed molecules:

1. the first one includes the design, synthesis and evaluation of β-hairpins, based on the piperidine-pyrrolidine scaffold and bearing self-recognition peptide sequences, rationally designed according to the oligomer and fibril structure of Aβ 1-42 (Chapter 2) (Figure 1.43);

2. the second one includes the design, synthesis and evaluation of peptidomimetic β-hairpins, bearing either a dipeptide or tripeptide chain, a 5-acetamido-2-methoxybenzohydrazide peptidomimetic derivative unit and different protecting group on the free primary amine of the scaffold (Chapter 3) (Figure 1.43);

3. the third one includes the design and synthesis of a fluorinated peptidomimetic analogue of the benzohydrazide derivative unit and the conception of the corresponding β-hairpin analogue (Chapter 4) (Figure 1.43);

4. the fourth and last part includes the design, synthesis and conformational study of 2:1 [Aza/α]-tripeptide peptidomimetics and the conception of the corresponding β-hairpin analogues (Chapter 5) (Figure 1.43).

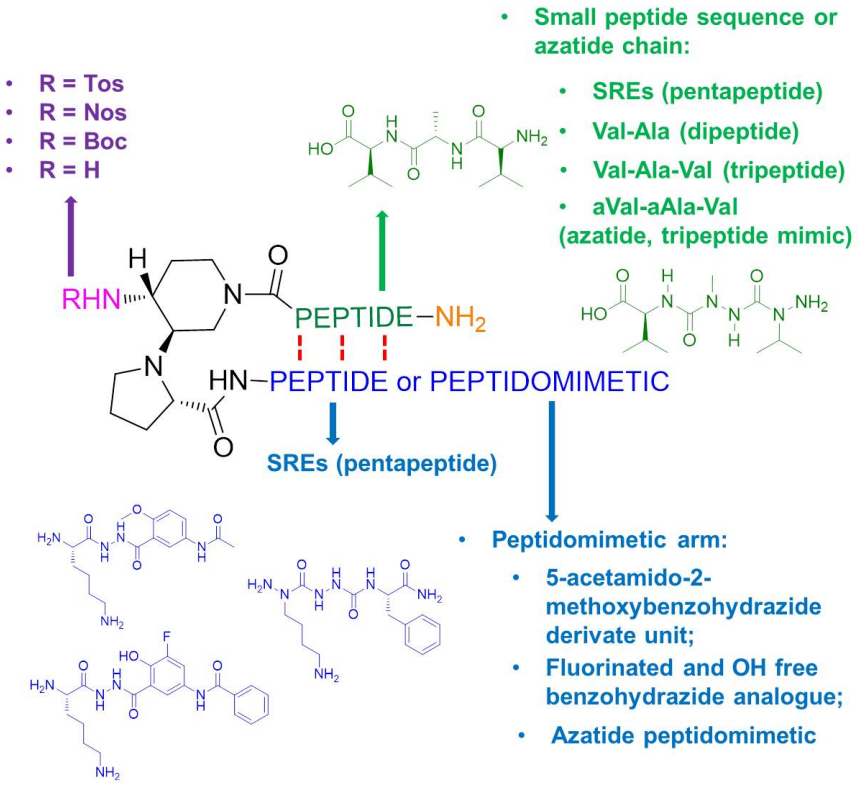

Figure 1.43: The pharmacomodulation of the designed β-hairpin mimics discussed in this thesis

Chapter 2

β-hairpin mimics containing the piperidine-pyrrolidine scaffold and rationally designed peptide sequences

In this chapter, we report the design, synthesis and conformational analysis of four β-hairpin mimics containing a piperidine-pyrrolidine scaffold and bearing two small recognition peptide sequences. These compounds demonstrated to be able to greatly delay the kinetics of Aβ 1-42 aggregation process. Therefore, we present, in the last part of the chapter, the results obtained by thioflavin-T fluorescence spectroscopy, transmission electron microscopy, capillary electrophoresis and cellular evaluation against Aβ 1-42 toxicity.

2.1 Design of the β-hairpin mimics

As we could ascertain in the first chapter, the aggregation process of Aβ peptide is dynamic and complex, because it involves different conformational and structural species that are in equilibrium between them and that influence each other. Despite this complex system, it can be possible to target the central or C-terminal hydrophobic region of the Aβ 1-42 peptide, in order to interact with it by mimicking the hydrogen bond network of a β-sheet and forming 10- or 14-membered cycle and by mimicking hydrophobic interactions [167][143][142]. Mimicking β-strands to antagonize β-sheet formation or recognition represent a new therapeutic strategy toward the prevention or treatment of diseases associated with β-sheet structures and, in particular for Alzheimer's disease, in which the protein aggregation process involves a secondary structure transition from unfolded/α-helix to β-sheet rich conformations.

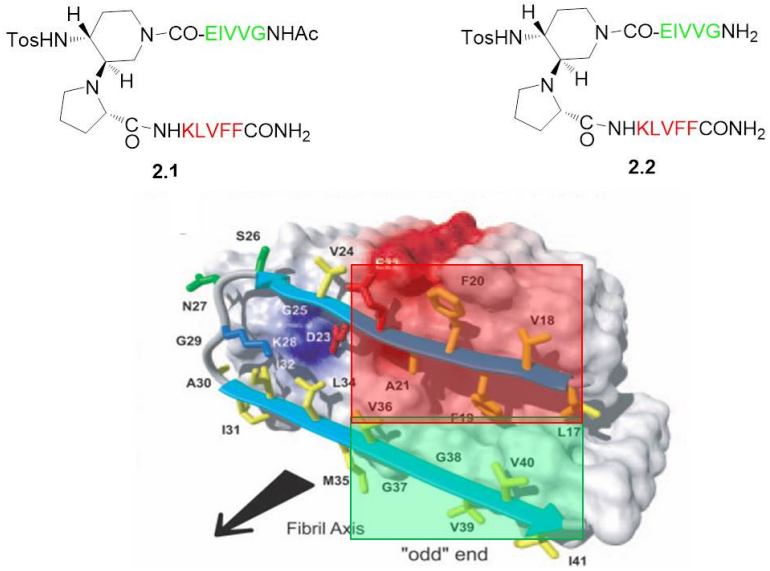

Figure 2.1: Structure of β-amyloid mimics **2.1** and **2.2** and 3D structure of Aβ 1-42 peptide presented by Luhrs in 2005 [62]

There are two possible ways to antagonize the β-sheet formation: inhibiting the formation of oligomers by stabilizing the non-toxic monomer or redirecting the aggregation cascade toward off-pathway species with reduced toxicity [167][143][142][29]. Between the many and various therapeutic strategies contemplated for the Aβ aggregation (see Chapter 1), we retained the approach that uses peptide ligands as a good strategy to selectively target the early stages of the oligomerization process [168][169].

With the aim to interfere with the oligomerization and fibrillization processes of Aβ 1-42, we decided to use β-hairpin mimics that present a certain flexibility to adapt themselves when in interaction with different Aβ 1-42 conformations present during the aggregation process, and in particular in the early stages of oligomerization. We hypothesized that this ability to fold in a β-hairpin manner, that mimics a two-strand β-sheet, might increase the affinity for the peptide target and thus increase the inhibitory activity.

For that purpose, we designed four acyclic β-hairpin mimics **2.1** and **2.2** (Figure 2.1) and **2.3** and **2.4** (Figure 2.2) based on a piperidine-pyrrolidine semi-rigid scaffold, that has been recently developed by our collaborators in Milan, to be a flexible β-turn inducer [170], and on different SREs (selective recognition elements of peptide sequences) of Aβ 1-42. In both cases, we chose to link the peptide sequence from residue 16 to residue 20 (KLVFF), that corresponds to the central region of the Aβ peptide, proved to be important in Aβ-Aβ interaction, because it binds β-sheets and initiates aggregation (nucleation site) [125]. A recently published study of co-crystallisation of

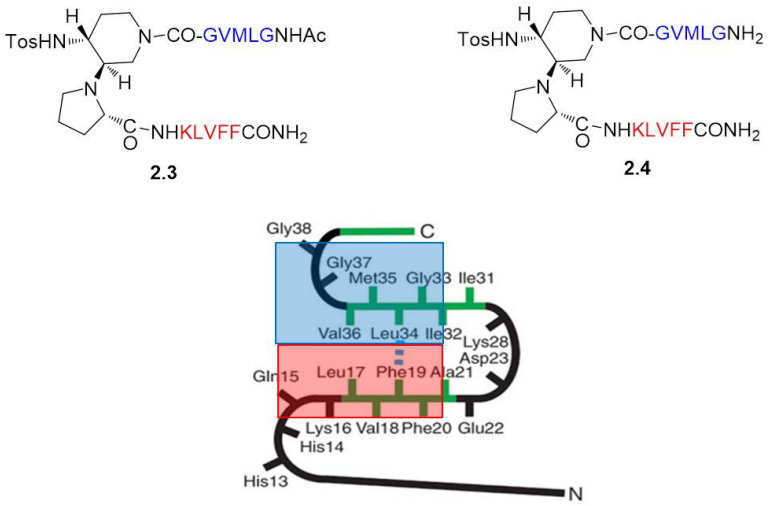

Figure 2.2: Structure of β-amyloid mimics **2.3** and **2.4** and the molecular model of Aβ 1-42 oligomers proposed by Ahmed in 2010 [64]

an Aβ 1-42 segment (residues 16–21) with the dye orange-G, the natural compound curcumin, and the Alzheimer's diagnostic compound DDNP demonstrated that the organic compounds were able to inhibit the aggregation process because they interacted with this nucleation site [171].

To choose the other peptide sequences, we were inspired by the 3D structure of Aβ 1-42 peptide presented by Luhrs in 2005 [62] and by the molecular model of Aβ 1-42 oligomers proposed by Ahmed in 2010 [64]. Our objective was to compare the conformation and the activity of two series of molecules: one that mimics the secondary structure of the Aβ 1-42 into fibers and one that mimics the β-sheet structure of Aβ into oligomers. So, in one case we linked to the scaffold the complementary sequence in front of KLVFF in the β-sheet conformation formed by the peptide in fiber morphology (42-AIVVG-38) with the replacement of the alanine by glutamic acid in order to possibly engage an ionic interaction with the facing lysine residue, thus stabilizing the β-hairpin structure (compounds **2.1** and **2.2**, Figure 2.1).

In the other case, we linked to the scaffold the complementary hydrophobic sequence (37-GVMLG-33), facing the nucleation site in the β-sheet structure of Aβ 1-42 peptide into the more flexible oligomeric structure, presented by Ahmed (Figure 2.2).

Finally, the N-terminal amino acid was either acetylated (Molecules **2.1** and **2.3**) or not (Molecules **2.2** and **2.4**), in order to evaluate the capacity of the compounds to engage electrostatic interactions with acidic residues of Aβ and thus to prevent the formation of the peptide β-sheet that initiate

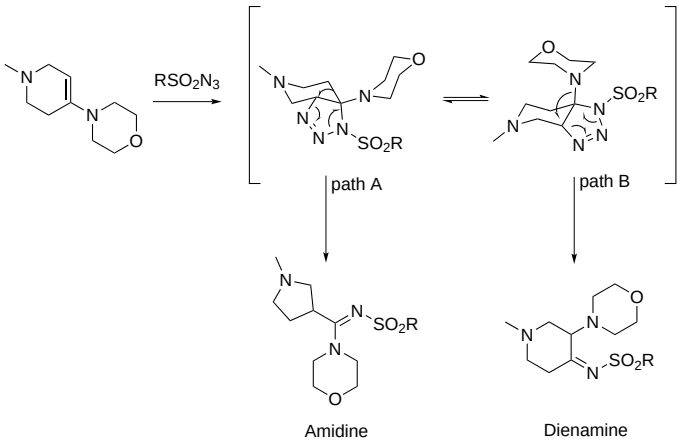

Figure 2.3: Proposed concerted mechanism

the aggregation cascade (Figures 2.1 and 2.2). As we saw in the introduction (pages 37-38), ionic interactions seem to stabilize the β-sheet conformations. In particular a salt bridge between Lys28 and Asp23 was found in fibers and oligomers structures proposed by Luhrs [62] and Ahmed [64] respectively, as well as between Lys28 and Ala42 by Xiao [166].

2.2 Synthesis of the piperidine-pyrrolidine scaffold

The synthesis of the β-turn inducer was conceived by a general study of the cycloaddition reaction between azides and enamines to obtain a triazoline ring. The evolution of the triazoline is governed by the type of azide and by the carbonyl group from which the enamine is formed. The reaction is conducted as a multicomponent reaction that allows to obtain the desired products in one step, by reacting the carbonyl group (aldehyde or ketone), the amine (primary or secondary) with a dehydrating agent, as molecular sieves, and the azide. As a result of the triazoline rearrangement, it's possible to obtain different products depending on the reaction conditions and the nature of the starting materials. Generally, this reaction leads to the formation of amidines. The discovery of the scaffold comes from the study of the synthesis of triazolines that lead to transformation products different from amidine.

Recently, the research team of the University of Milan, with which we collaborate, published a study that describes the different stages associated to the transformation of the triazoline [172]. In particular, they studied the results obtained by the cycloaddition reaction between the sulphonylazide and the enamine formed by 1-alkyl-piperidin-4-one and an amine. The results were compared with those acquired by the reaction with the enamine of the cyclohexanone. In the case of the enamine of 1-alkyl-piperidin-4-one, the

main product is the dienamine and only few traces of amidine were detected (Figure 2.3).

They observed that the triazolidine undergoes a reaction of ring opening with concerted mechanism and can evolve in two pathways:

- transposition of the alkyl substituent and ring contraction, leading to the amidine (pathway A, Figure 2.3);
- migration of the amine, obtaining the imine that transposes spontaneously in dienamine (pathway B, Figure 2.3).

These transformations are both accompanied by a loss of molecular nitrogen. The favored pathway is the one associated with the lower energy transformation and, in particular for the 1-alkyl-piperidin-4-one, the energy associated to the migration of the amine is lower than that associated to the transposition of the alkyl substituent. Instead, when the cyclohexanone is employed, the lower energy is associated to the transposition of the alkyl group and in this case the amidine is the main product.

With the aim to obtain interesting building blocks, useful for the preparation of peptidomimetic β-turn inducers, the research team decided to investigate the same reaction by using proline methyl ester as the amine. This choice was justified by the fact that the reaction intermediate is more stable to hydrolysis and that proline is known to be a β-turn inducer in secondary structure of proteins and peptides.

The multicomponent reaction between 1-benzyl-piperidin-4-one, proline methyester and tosyl azide has been developed through the following procedure, developed by our colleagues in Milan [170].

One equivalent of proline methyl ester hydrochloride was suspended in dichloroethane and the free secondary amine was obtained by adding an equimolar amount of triethylamine. One equivalent of 1-benzyl-piperidin-4-one is subsequently added, followed by the addition of molecular sieves and a catalytic amount of indium trichloride (10 %). After 1 hour, one equivalent of tosyl azide is added and the reaction can be considered finished after at least 45 minutes (checking the disappearance of the azide by TLC). Because the produced dienamine is instable and tending to degrade, the best way to isolate the final compound is subjecting the crude to reduction with sodium triacetoxy borohydride in order to obtain a more stable diamine compound that, after work up, is easily crystallized in methanol. The reduction of the double bond creates two new asymmetric carbons and so, theoretically, four diastereomers: two with the hydrogens in *trans* conformation and the other two with the hydrogens in *cis* conformation [170].

The major product of the reducing reaction is the diastereomer with the configuration 4R, 3R, S (**2.5**) and this product can be easily isolated from the crude by crystallization in methanol. The yield obtained after this crystallization is not so high (15 %) but it allows to isolate the product with

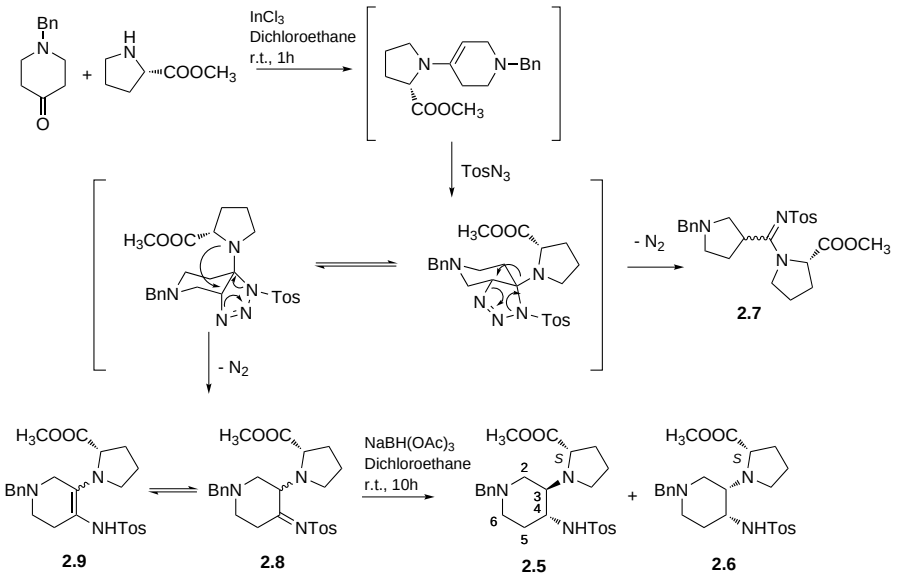

Figure 2.4: Mechanism of the multicomponent reaction of compound (**2.5**)

high purity and selectivity. The analysis of the supernatant, conducted by analytical HPLC, revealed the presence of three other products. One of these was found to be still the major diastereomer and the other two were the minor isomer (4R, 3S, S, **2.6**) and the amidine (**2.7**). Thus, the two isolated stereoisomers showed the same stereochemistry at C4, differing only for the configuration of the stereocenter C3 (Figure 2.4).

To explain the stereochemical outcome of the reduction, insights on the reaction mechanism were acquired. It is assumed that the reaction takes place by insertion of the hydride on the carbon atom substituted with the NH-Tosyl. It is possible that this position is the one most electron-poor both because of the effect of withdrawing electron tosyl group and because of the possible tautomeric forms present in solution. Between tautomers **2.8** and **2.9** (Figure 2.5), the imine **2.8** is the most reactive toward hydrides, as the negative charge deriving from the nucleophilic attack can be delocalized on the more electronegative sulfonamide group, while on **2.9** it would be delocalized on carbon. It was observed by theoretical analyses of chemical reactions and DFT calculations that the hydride only attacks at the *Re* face, thus leading to the R configuration of C4. This is probably due to the fact that the carboxyl group of the proline, masking the face *Si*, guides the hydride attack on the *Re* face.

The variability at C3 should instead depend on the thermodynamic stability of the two possible diasteroisomeric intermediate imides, which are in equilibrium due to the tautomerization between **2.8** and **2.9** (Figure

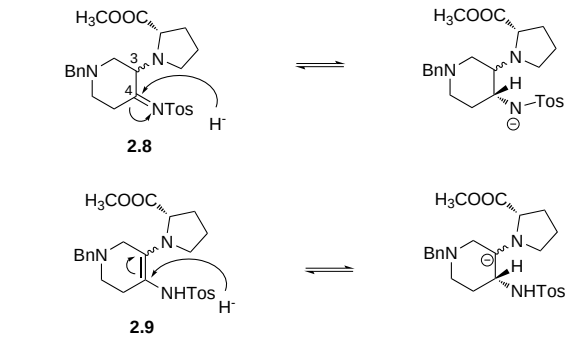

Figure 2.5: Hypothesized mechanism for hydride attack on tautomers **2.8** and **2.9**

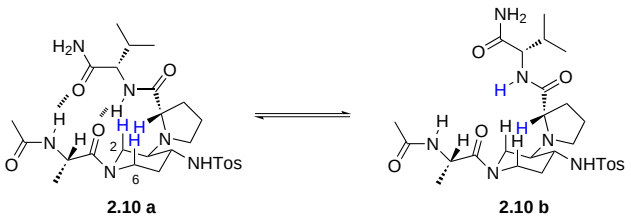

Figure 2.6: Schematic representation of the conformers of compound **2.10** supported by NOE experiments (in blue the protons that showed spatial proximities (NOEs) distincly in the two conformations)

2.5). Diastereoselection was observed to be dependent from the difference in energy between the two transition states obtained from the axial or equatorial attack of the hydride on C4. The axial attack of the hydride is the most favored because in the axial transition state the bulky substituents at C3 and C4 are both in equatorial position and there is a stabilization by electrostatic interactions between the Na^+ ion and the partially negative charged sulfonamide nitrogen, the proline nitrogen, the carbonyl group and the SO_2 oxygen. Conversely, in the equatorial transition state, the two substituents at C3 and C4 are both axial, and less stabilizing interactions are found between the Na^+ ion and electron-rich groups.

From the crystal structure, it was evidenced that the carboxylic group of proline and the benzyl substituent on the piperidine ring were oriented in the same direction. This observation conducted to the hypothesis that this scaffold could act as β-turn inducer. So, the peptidomimetic compound **2.10** (Figure 2.6) was obtained by coupling the carboxylic group of proline with the amino acid valine and the secondary amine of the piperidine ring with the amino acid alanine. Peptidomimetic **2.10** was conformationally studied

by NMR and it was showed that it was present in solution as a mixture of two conformers in 1:1 *ratio* [170].

In the first isomer, NH-Val and NH-acetyl were involved in medium-weak hydrogen bond, while none of the amide protons of the other isomer showed low temperature coefficients. In the NOESY experiments, both conformers showed spatial proximity between the α-hydrogen of alanine and two hydrogens in position C2 and C6. On the contrary, Overhauser effect between the α-hydrogen of proline and two hydrogens in position C2 and C6 were present only for the hydrogen bonded conformer (β-turn conformation), while for the other only spatial proximity between the α-hydrogen of proline and NH-Val was found, showing a more extended conformation (Figure 2.6) [170].

Normally, conformationally constrained β-turn mimics are prepared by employing heterocyclic and carbocyclic systems, able to reduce the conformational freedom of the peptide backbone, locking it in the cyclic system. One of the limitations of this approach is that it does not take into account possible interactions between the functional groups of the side chains, which are important both for folding and for the biological interaction. The effect to have two conformations in equilibium with one that is able to stabilize a β-turn conformation, shows the opportunity to create new β-hairpin mimics with the ability to establish both interactions between the side chains of the amino acids and a stiffening of the backbone, which both allow to obtain molecules that better interact with the biological target [173].

2.3 Synthesis of β-hairpins

Compounds **2.1** and **2.3** were prepared by solid phase peptide synthesis, using the Fmoc strategy. In order to use the piperidine-pyrrolidine scaffold for the peptide solid-phase synthesis, it was necessary to arrange it with compatible protective groups.

Thus, the Fmoc-protected compound **2.13** was synthesized in solution starting from the known compound **2.5** [170]. Hydrogenolysis of **2.5** was performed in toluene with an equivalent amount of 10 % Pd/C to afford free amino compound **2.11** in 99 % of yield. The ester function was hydrolyzed in acidic condition (HCl 6M) at 110 °C, yielding compound **2.12** (99 %). Finally, the Fmoc group was introduced using Fmoc-OSu, in the presence of DIPEA in a MeOH/ACN (4:1) solution mixture affording compound **2.13** in 72 % yield (Figure 2.7).

Peptide KLVFF was synthesized on Rink-amide resin (0.72 loading) using standard conditions (AA/HOBt/HBTU/DIPEA, 5:5:5:10) [174]; 1 h coupling and then 20 % piperidine in DMF for Fmoc cleavage. Peptidomimetics **2.16** and **2.17** were prepared by performing the coupling of compound **2.13** (1.5 eq.) on the peptide growing chain linked to rink-amide resin using HBTU

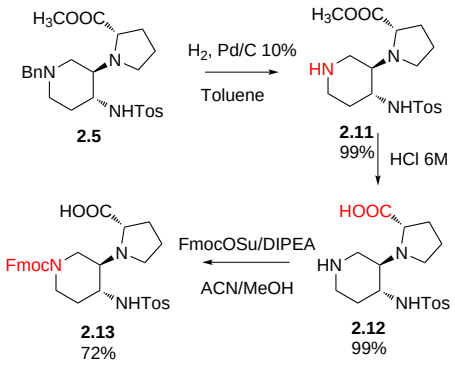

Figure 2.7: Synthesis of Fmoc-protected scaffold **2.13**

(1.5 eq.) and HOBt (1.5 eq.) and DIPEA (3 eq.), and standing the mixture under shaking overnight. The other peptide chain was elongated by step by step addition of the five amino acids using the same coupling conditions described above. Finally peptidomimetics **2.2** and **2.4** were achieved after resin cleavage using the reagent K (trifluoroacetic acid/phenol/water/thioanisol/1,2-ethanedithiol; 82.5:5:5:5:2.5) for 180 min [175] (Figure 2.8).

Instead, to obtain compounds **2.1** and **2.3**, at the final step of the peptide solid-phase synthesis, before resin cleavage, the intermediates were acetylated on resin using acetic anhydride (10 eq.) and DIPEA (10 eq.) (Figure 2.8).

In order to evaluate the efficacy of the β-sheet mimics with respect to a truncated derivate or the single arms, we also prepared compound **2.15** (Figure 2.8), containing the scaffold and only the Aβ 16-20 sequence (KLVFF), and compounds **2.18** (Ac-GLMVG-$CONH_2$), **2.19** (Ac-GVVIE-$CONH_2$), **2.20** (Ac-KLVFF-$CONH_2$), corresponding to the different SREs, introduced in the β-hairpin mimics.

The SREs were synthesized by the same peptide solid-phase synthesis described above and compound **2.14** was acetylated and cleaved to afford compound **2.15** (Figure 2.8).

2.4 Conformational studies

In this section, I present the results obtained from the conformational studies by Circular Dichroism (CD) and NMR, conducted on the two acetylated compounds **2.1** and **2.3**. These conformational studies were performed by our collaborators at the Università degli Studi di Milano.

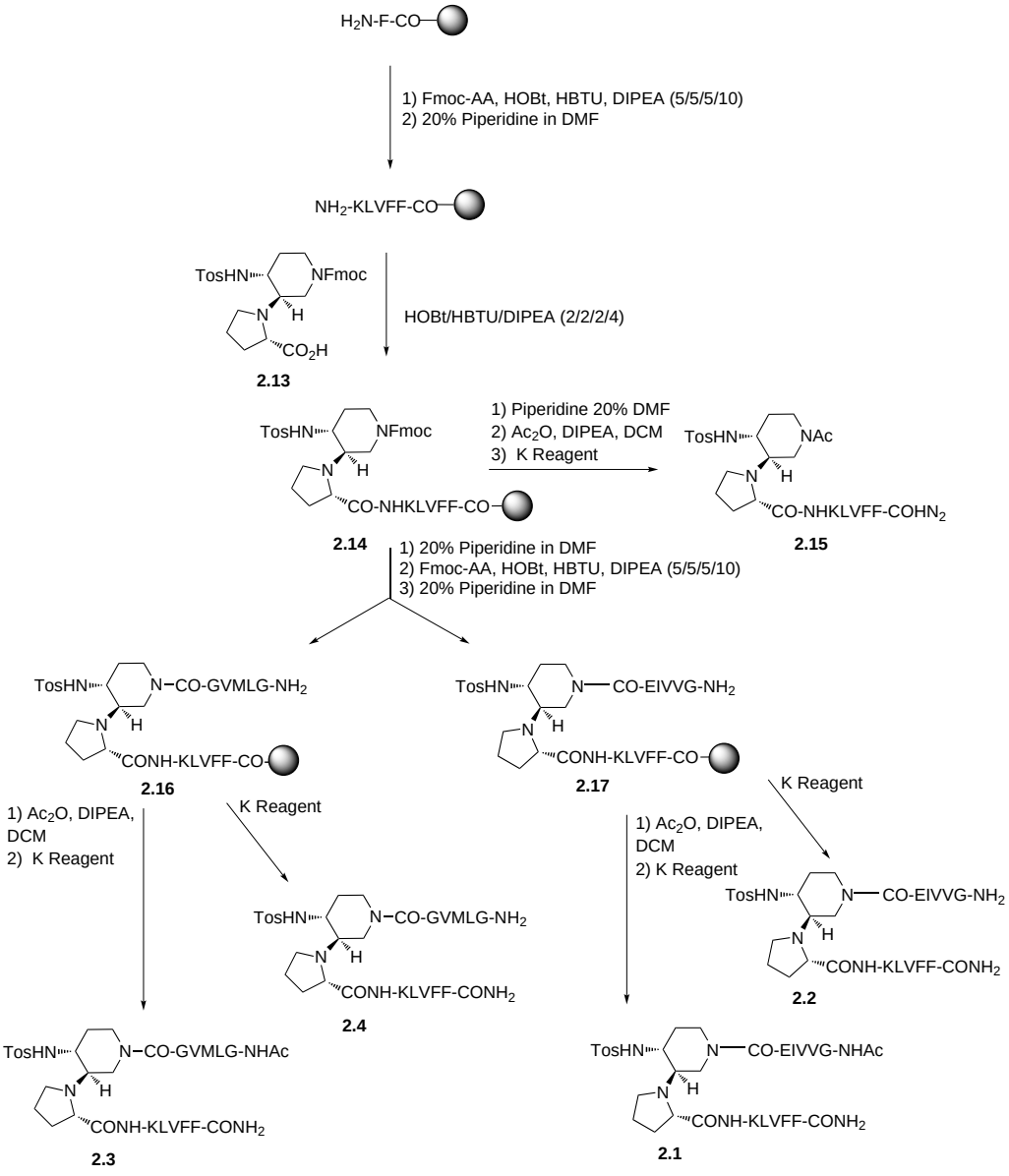

Figure 2.8: Synthesis of **2.1**, **2.2**, **2.3**, **2.4** and **2.15**

2.4.1 Circular Dichroism (CD)

Circular dichroism (CD) is the difference in the absorption of left-handed circularly polarised light (L-CPL) and right-handed circularly polarised light (R-CPL) and occurs when a molecule contains one or more chiral chromophores (light-absorbing groups). A CD signal can be positive or negative, depending on whether L-CPL is absorbed to a greater extent than R-CPL (CD signal positive) or to a lesser extent (CD signal negative). CD spectrometers measure alternately the absorption of L- and R-CPL, usually at a frequency of 50 kHz, and then calculate the circular dichroism signal.

The study of biological molecules is the main application of the technique. A large subset of the use of CD in biochemistry is in the understanding of the higher order structures of chiral macromolecules such as proteins. The CD spectrum of a protein is not a sum of the CD spectra of the individual residues but is grealy influenced by the 3-dimension structure of the macromolecule itself. Each structure has a specific CD signature, and this can be used to identify structural elements and to follow changes in the structure of chiral macromolecules.

This technique can be used for different applications and studies, in particular:

- the secondary structure prediction of a protein;
- dynamic changes in the structure of a protein;
- the comparison between two macromolecules or the same molecule under different conditions and determination of the presence or not of a similar structure.

As we mentioned above, CD is an excellent method of determining the secondary structure of proteins. When the chromophores of the amides of the polypeptide backbone of proteins are aligned in arrays, their optical transitions are shifted or split into multiple transitions due to exciton interactions. The result is that different structural elements have characteristic CD spectra. For exemple, α-helical proteins have negative bands at 222 nm and 208 nm and a positive band at 193 nm. Proteins with well-defined antiparallel β-sheets have negative bands at 218 nm and positive bands at 195 nm, while disordered proteins have very low ellipticity above 210 nm and negative bands near 195 nm [176].

In order to study the eventual ability of compounds **2.1** and **2.3** to establish a β-hairpin conformation, we collected CD spectra of both molecules in MeOH (50 µmol m^{-3}, 1.5 ml) at 25 °C.

So, as we can see in Figure 2.9, compound **2.3** showed a negative band at 195 nm indicating that in solution this peptidomimetic did not assume a preferred, single conformation. On the contrary, the spectrum of **2.1** was

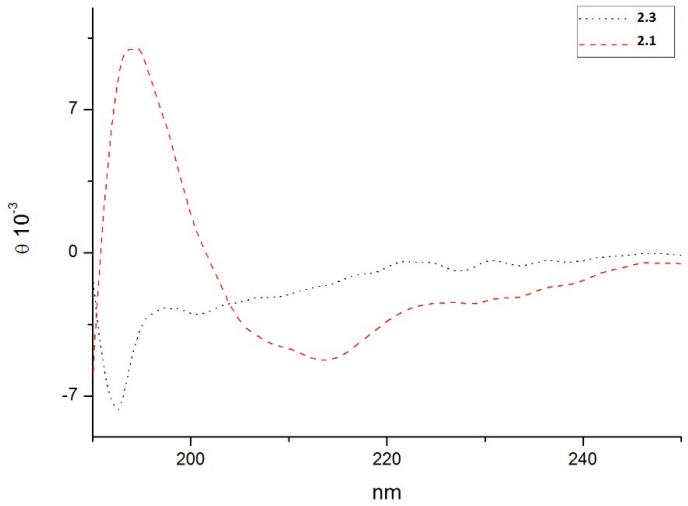

Figure 2.9: CD spectra of **2.1** and **2.3**

characterized by a strong positive Cotton Effect at around 195 nm, and a negative band at around 215 nm, typical of β-sheet structure.

From these results, we could start to draw some preliminary conclusions, by observing that the compound with the complementary sequence into oligomers does not seem able to adopt a privileged conformation and so looks flexible. Instead, compound **2.1** with the complementary sequence into fibers and the replacement of the Ala with glutamic acid, demonstrated its ability to adopt a stable β-hairpin conformation.

2.4.2 Nuclear Magnetic Resonance (NMR)

In the past 10 years, nuclear magnetic resonance (NMR) spectroscopy has proved itself as a potentially powerful alternative to X-ray crystallography for the determination of macromolecular three-dimensional structure. NMR has the advantage over crystallographic techniques in that experiments are performed in aqueous solution as opposed to a crystal lattice and also it's possible to study proteins that are dynamic macromolecules whose structure can change overtime in solution.

It is possible to determine the secondary structures of a protein using NMR techniques without determining the three-dimensional structure. Unlike secondary structure determinations by CD and IR which provide overall secondary structure content, using NMR parameters, secondary structures are localized to specific segments of the polypeptide chain.

Resonance	alpha helical	beta-sheet
Hα	upfield (-0.38)	downfield (+0.38)
Hβ	0	-0.1
HN	upfield (-0.19)	downfield (+0.29)
Cα	downfield (+2.6)	upfield (-1.4)
Cβ	upfield (-0.4)	downfield (+2.2)
CO	downfield (+1.7)	upfield (-1.4)
N	upfield (-1.7)	downfield (+1.2)

Table 2.1: Average secondary structure shifts relative to random coil values [178]

Structural information from NMR experiments comes primarily from through-bond (scalar or *J coupling*) or through space (the nuclear Overhauser effect (*NOE*) magnetization transfer between pairs of protons.

The three-bond coupling constant depends on the dihedral angle defined by rotation around the middle bond in the coupling system. One particularly important application of the coupling constant is as a mesure of the coupling constant between the H^{α} and the H^{N} in the peptide backbone. This coupling depends on the ϕ-angle in the peptide bond. The Karplus curve shows the correlation between the coupling between H^{α} and the H^{N} and the ϕ-angle. It is seen that coupling constants are around 4 Hz for peptide segments in α-helices where the ϕ-angle is around $-60°$, and it is between 8 Hz and 12 Hz for peptide segments in β-structures, where the ϕ-angle is in the $-120°$ range [177].

The other major source of structural information comes from through space dipole-dipole coupling between two protons called the *NOE*. The intensity of a NOE is proportional to the inverse of the sixth power of the distance separating the two protons and is usually observed if two protons are separated by < 5 Å. Thus the NOE is a sensitive probe of short intramolecular distances. The cross relaxation rate and the related nuclear Overhauser effect can be used to estimate distances between two nuclei in a protein molecule. Extended conformations (e.g., beta strands) are characterized by short sequential, d-H^{α}NH, distances. The formation of sheets also results in short distances between protons on adjacent strands (e.g., d-$H^{\alpha}H^{\alpha}$ and d-H^{α}NH).

Correlations between chemical shift tendencies and secondary structures have been identified. The α-proton of all 20 naturally occurring amino acids has been shown to have a strong correlation with secondary structure. Wishart *et al.* have produced a simple method for secondary structure determination by analysing the difference between the α-proton chemical shift for each residue and that reported for the same residue type in a random coil conformation [178]. Helical segments have groupings of α-protons whose chemical shifts are consistently less than the random coil values whereas

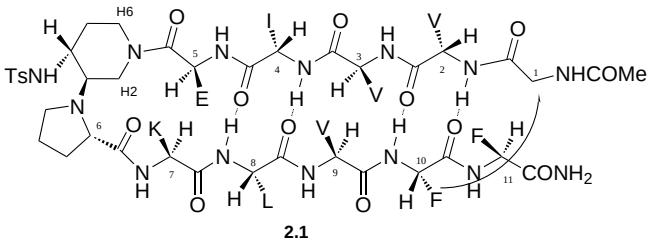

2.1

Figure 2.10: Structure of compound **2.1**

β-strands had values consistently greater. For the determination of the secondary structure type, also ^{13}CO, $^{13}C^{\alpha}$ and $^{13}C^{\beta}$ of the peptide backbone can be used. Chemical shift deviations (CSD) are defined as the differences between experimental chemical shifts and corresponding random coil values. In the table 2.1, we can observe the average secondary structure shifts relative to random coil values.

The regular hydrogen-bonded secondary structures protect amide protons involved in them as evidenced by their significantly reduced amide proton exchange rates with the solvent. Hydrogen exchange can be studied by NMR spectroscopy. By replacing water with deuterium oxide, for example, the exchange process will lead to the replacement of hydrogen with deuterium. ^{1}H-NMR can study the exchange process, since the hydrogen giving rice to a ^{1}H NMR signal is exchanged by deuterium, which is not observable by NMR at the ^{1}H NMR frequency. By recording the hydrogen exchange rates the stability of the individual hydrogen bonds can be measured.

Finally, to provide other information on the network of hydrogen bonds and their relative stabilities, it's possible to examine the temperature dependence of amide proton chemical shifts. Amide protons that are engaged in intramolecular hydrogen bonds typically exhibit small temperature dependence ($\Delta\delta_{NH}/\Delta$T > -4.5 ppb K^{-1}) in aqueous and alcoholic solvents, while those that are not intramolecularly hydrogen-bonded usually exhibit largely negative values of their temperature coefficients [152]. To distinguish the intra- and inter-molecular hydrogen bonds and to investigate whether the stabilization of a particular conformation could result from intermolecular association at high concentration, it's possible to perform the NMR analyses at different concentration (generally one more concentrated and the other more diluted) and observe if there are no significant changes in chemical shifts and linewidths, ruling out the possibility of aggregation in the more concentrated solution.

So, the different behaviour of **2.1** and **2.3** was confirmed by ^{1}H NMR experiments (500 MHz, CD_3OH, 4 mM).

^{1}H NMR spectrum of compound **2.1** showed a good dispersion of the

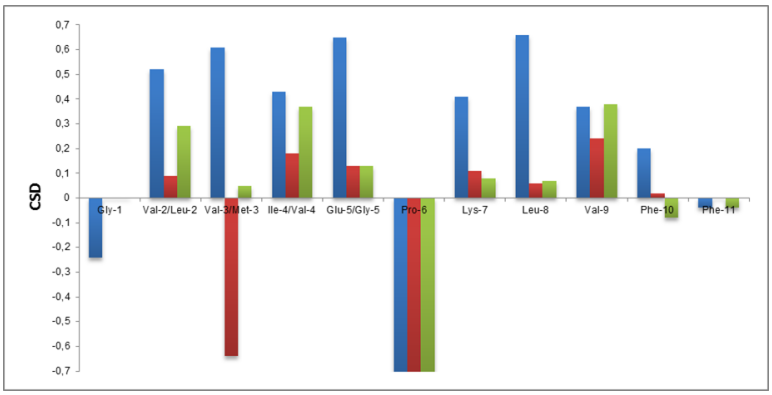

Figure 2.11: Plot of difference between H_α chemical shift values in the random coil and the values determined experimentally for **2.3a** (red), **2.3b** (green) and **2.1** (blue)

NH chemical shifts indicating the presence of a single conformation (Figure 2.10). NOESY and ROESY experiments on compound **2.1** evidenced strong CH/NH(i,i+1) ROEs and the formation of a turn in the region containing the scaffold. Spatial proximity between the piperidine moiety of scaffold (H-2 and H-6) with both the α proton of Pro-6 and Glu-5 was observed.

A cross-strand NOE was detected between CHGly-1 and the phenyl ring of Phe-10. However, no other no ambiguous NOEs were observed between cross-strand residues due to peaks overlapping among them or overlapped with the solvent signals.

The profiles of $\Delta\delta_{H\alpha}$ conformational shift values ($\Delta\delta$ observed - $\Delta\delta$ random coil) as well as a deviation of more than 0.1 ppm from random coil for several successive residues exhibited by peptide **2.1**, are consistent with those of the target β-stranded antiparallel β-sheet (Figure 2.11) [178]. Furthermore the separation of resonances of the two α protons of Gly-1 indicates a β-hairpin structure as reported in the literature [179].

A further confirmation is given by $^3J_{NH/CH}$ coupling constant distributions that are commonly used for identifying secondary structure in the NMR structure determination. Values higher than 8 Hz characterize a β-strand, as observed for **2.1** peptide. Positive difference between $^3J_{NH/CH}$ values in the random coil and the values determined experimentally were found. As an exception, Glu-5 is characterized by a lower J value that is justified by a sharp change in backbone direction indicative of a β-turn (Figure 2.12) [180].

NMR characterization of **2.3** has been more complex but the chemical shifts of two main isomers (2:1 ratio), named **2.3a** and **2.3b** were assigned. The presence of two conformers of **2.3** is proved by several negative NH/NH ROEs. This observation indicates a dynamic equilibrium between different conformers [181]. Interestingly, a strong intrastrand ROE was found between

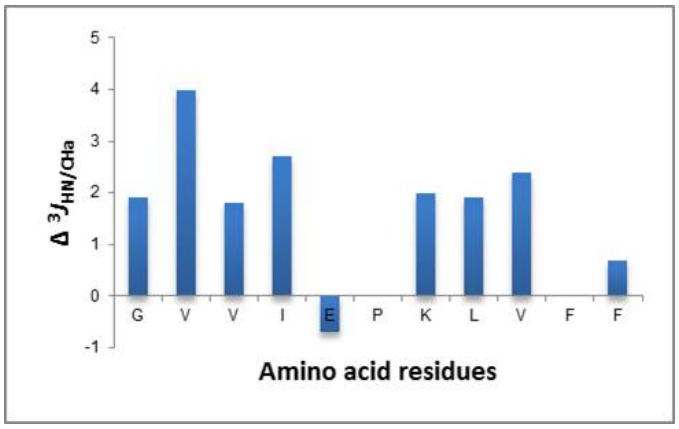

Figure 2.12: Plot of difference between $^3J_{NH/CH}$ values in the random coil and values determined experimentally for **2.1** [178]

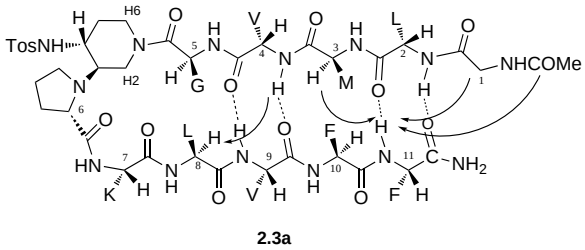

Figure 2.13: Structure of compound **2.3a**

NHVal-4 of **2.3b** and CHVal-4 of **2.3a** one, suggesting that Val-4 is probably involved in the dynamic switch between the two isomers.

ROESY experiments confirmed the presence of a turn structure in both **2.3a** and **2.3b** isomers. Spatial proximity was indeed observed between the piperidine moiety of the scaffold (H-2 and H-6) with both proline and Gly-5, confirming the reported data for model sequences.

A complete set of CH/NH(*i*, *i+1*) ROEs is present for isomer **2.3a** (except for Val-4/Met-3 and Leu-2/Gly-1) (Figure 2.13). CH/NH interstrand ROEs between NHVal-4/CHLeu-8, NHPhe-11 with both CHGly-1 and MeCO and NHPhe-11/CHMet-3 are present. The last ROE is of particular relevance to demonstrate that the β-hairpin of **2.3a** is characterized by a different hydrogen bond network with respect to **2.3b** minor isomer.

The presence of a β-hairpin structure is further confirmed by positive $\Delta\delta_{H\alpha}$ shift values (Figure 2.11). These values are smaller with respect to **2.3b** and **2.1** indicating that the hairpin conformation of **2.3a** is not very stable. Only Met-3 is characterized by a negative $\Delta\delta_{H\alpha}$ value. This is

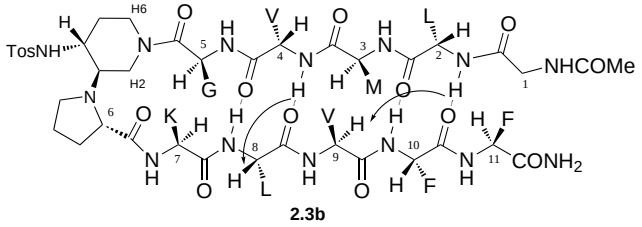

Figure 2.14: Structure of compound **2.3b**

probably due to the anisotropic effect of the aromatic ring of Phe-11 [182], that faces Met-3, as demontrated by Roesy experiment.

The minor conformer **2.3b** (Figure 2.13) showed higher $\Delta\delta_{H\alpha}$ values with respect to those of **2.3a**. Of relevance, the positive value of methionine indicates its different sterical environment. A complete set of CH/NH(*i*, *i+1*) ROEs are present, except for NHVal-9 and CHLeu-8. Interstrand ROEs were found between NHVal-4/CHLeu-8, NHPhe-11/MeCO and NHLeu-2/CHVal-9, indicating the formation of a β-hairpin characterized by the same H-bond network proposed for **2.1**.

2.5 Evaluation of β-hairpin ability to inhibit Aβ 1-42 aggregation

The synthesized final products were all tested to investigate their influence on Aβ 1-42 aggregation kinetics. The ability of compounds to inhibit amyloid fibrils formation was first examined by a thioflavin T (ThT) fluorescence assay. The effect of the more promising compounds (from ThT assay) were then evaluated by transmission electron microscopy (TEM) analyses in order to validate the results of ThT and by capillary electrophoresis (CE) in order to study the effect on the early oligomerization process.

The inhibitors were, finally, investigated to determine their ability to reduce the toxicity of aggregated Aβ 1-42 towards SH-SY5Y neuroblastoma cells.

2.5.1 Thioflavin T fluorescence spectroscopy (ThT)

ThT is one of the most commonly used optical probes to follow the Aβ 1-42 aggregation process in real time. This molecule is positively charged and presents an aniline type core and a benzothiazole type fragment. The molecular rotor allows benzothiazole nuclei and benzylamine to rotate freely in solution around the C-C single common bond. In this case, the rapid rotations quench the excited states generated by photon excitation. On the contrary, when the ThT is inserted into the β-sheet amyloid assemblies,

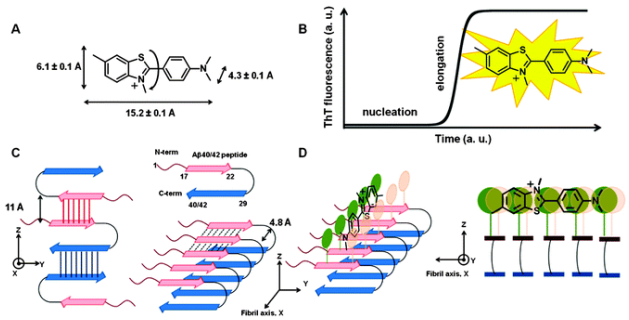

Figure 2.15: (A) ThT dye with its specific dimensions. (B) Sigmoid ThT fluorescence curve observed for the formation of amyloid fibrillar aggregates containing β-sheets. (C) Scheme of Aβ peptide; β-sheets interactions along the z axis involve side chains of the amino-acids residues (left) while β-sheets interaction along the x axis (fibril axis) involves H-bond between backbone CO and NH groups (right). (D) Scheme of ThT interaction within the fibrils along the fibril axis (left) and perpendicular to it (right). Green and orange circles stand for hydrophobic residues (such as Phe, Leu, Val from the central hydrophobic core of Aβ peptide) able to interact with aromatic rings of the ThT.

the molecular rotor is then immobilized, preserving the excited state and allowing a multiplication of fluorescence quantum yield by 1,000 (Figure 2.15) [183] [184].

Different studies hypothesized that the interaction between ThT and the Aβ 1-42 fibers is made at the hydrophobic core of the peptide, at the hydrophobic sequence 16-20 (KLVFF) by π-stacking type interactions with the aromatic residues (Phe) [185].

So, ThT fluorescence assay can be used to follow *in vitro* the fibrillization process of Aβ peptide. In fact, the association of ThT with the amyloid fibrils leads to a modification of its fluorescence properties, which results in the appearance of an excitation maximum at 450 nm associated to an emission maximum of 485 nm.

The Aβ peptide aggregation in amyloid fibers is a process with different stages. Each of these steps enables the formation of species with specific properties. The β-sheet of the fibers are necessary to the appearance of the fluorescence. We can describe three different stages, following over time the kinetics of the aggregation by spectroscopy.

1. A latency or nucleation step: the peptide, in its monomeric form, begins to structure and to assemble into oligomeric species, not sufficiently structured in β-sheet manner to bind ThT (no fluorescence observed).

2. An ascendant or elongation step: the fibrillar assemblies grow and

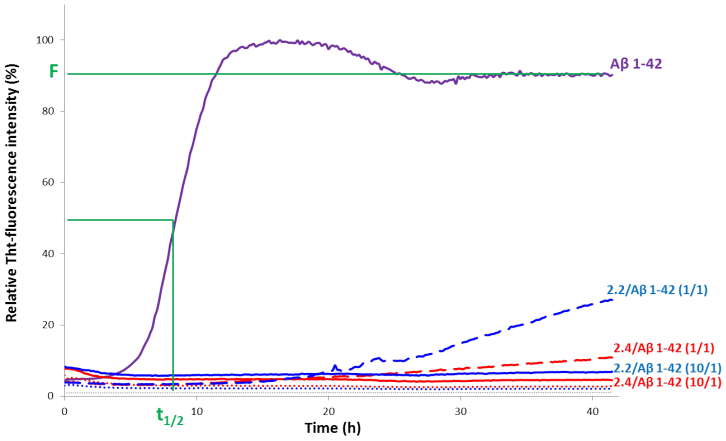

Figure 2.16: Representative curves of ThT fluorescence assays over time showing Aβ 1-42 aggregation in the absence (purple curve) and in the presence of compound **2.2** (blue curves) and **2.4** (red curves) at ratio 10/1 and 1/1. The control curves are represented in dotted curves

begin to be increasingly β-sheet rich; this results in an abrupt increase in fluorescence.

3. A plateau step: the fluorescence reaches its maximal level when fibers are completely formed.

The fluorescence curve for Aβ 1-42 at a concentration of 10 µM follows the typical sigmoidal pattern with a lag phase of 8-9 hours followed by an elongation phase and a final plateau reached after 15-18 hours (Figure 2.16, purple curve). Two parameters are derived from the ThT curves of Aβ alone and Aβ in the presence of the evaluated compound: one is $t_{1/2}$ which is defined as the time at which the half maximal ThT fluorescence is observed and gives insight on the rate of the aggregation process; the other is the fluorescence intensity (F) at the plateau which is assumed to be dependent on the amount of fibrillar material formed.

Compounds **2.2** and **2.4** resulted the most promising inhibitors of Aβ 1-42 aggregation. As we can see in Figure 2.16, they totally suppressed Aβ 1-42 aggregation at compound/Aβ 1-42 ratio of 10/1 and still dramatically delayed Aβ 1-42 aggregation at 1/1 ratio.

Both acetylated derivatives **2.1** and **2.3** retained this activity, but to a lesser extent (Figure 2.17). This result supports our hypothesis on the importance to establish an ionic interaction with acidic residues of Aβ 1-42 to have a better inhibitory activity.

If we compare the two peptide sequences, chosen to be complementary to KLVFF, we notice that the series containing the facing sequence GVMLG

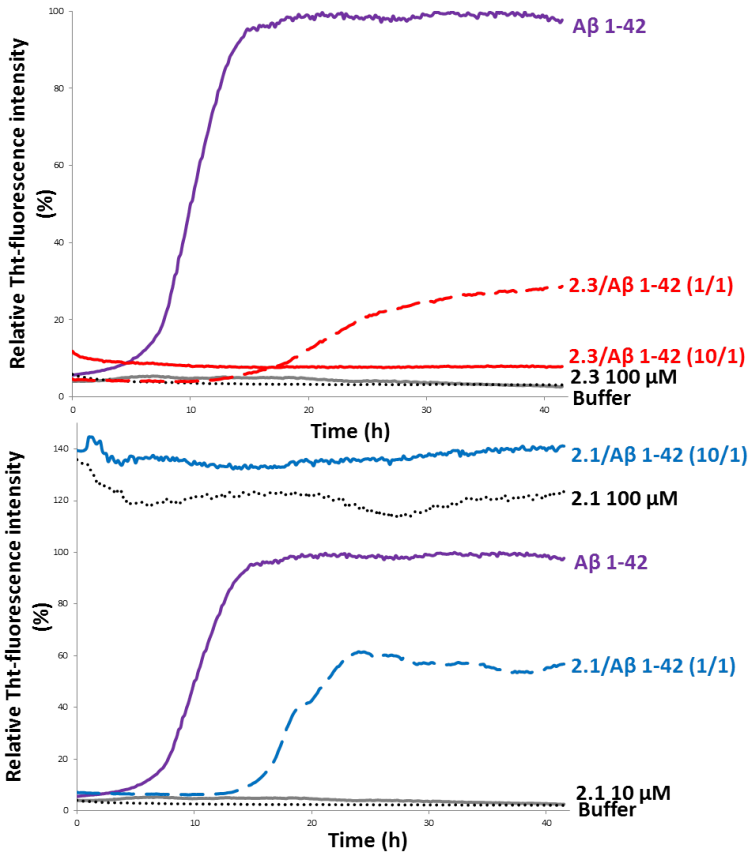

Figure 2.17: Representative curves of ThT fluorescence assays over time showing Aβ 1-42 aggregation in the absence (purple curve) and in the presence of compound **2.1** (blue curves) and **2.3** (red curves) at ratio 10/1 and 1/1. The control curves (compound alone) are represented in dotted curves

Compounds (Compound/Aβ ratio)	$t_{1/2}$ extension	Change of fluorescence intensity at the plateau (%)
2.1 (10/1)	Sat [a]	Sat [a]
2.1 (1/1)	1.76±0.11	−41±7%
2.3 (10/1)	NA	−97±1%
2.3 (1/1)	2.06±0.12	−71±2%
2.2 (10/1)	NA	−95±1%
2.2 (1/1)	>3.56±0.12	−73±3%
2.4 (10/1)	NA	−97±1%
2.4 (1/1)	NA	−90±2%
2.15 (10/1)	NA	−97±1%
2.15 (1/1)	3.05±0.07	−70±4%
2.18 (10/1)	1.31±0.09	−26±4%
2.18 (1/1) (Ac-GLMVG-$CONH_2$)	1.18±0.01	ne
2.19 (10/1)	ne	−19±11%
2.19 (1/1) (Ac-GVVIE-$CONH_2$)	ne	−21±3%
2.20 (10/1)	2.72±0.07	−46±2%
2.20 (1/1) (Ac-KLVFF-$CONH_2$)	1.17±0.01	ne

Figure 2.18: Effects of compounds on A1-42 fibrillization assessed by ThT-fluorescence spectroscopy at 10/1 and 1/1 compound/Aβ ratios and compared to the values obtained for Aβ 1-42 alone ($t_{1/2}$ and F) analysed at the same concentration. ne = no effect, NA = no aggregation, parameters are expressed as mean ± SE, n=3-6

of the oligomers exerts a slightly superior inhibitory activity, highlighted at a low ratio 1/1, in comparison to the series containing EIVVG, the mimic of the facing sequence into fibers.

Combining the results obtained by conformational studies and by ThT fluorescence assay, we can assert that the choice of a peptide sequence that can induce the formation of a dynamic mixture of β-hairpin architectures, resulted in a complete inhibition of the aggregation, with respect to a more structurally organized system.

As we said before, in order to evaluate the efficacy of β-hairpins molecules with respect to a truncated derivative with just one peptide arm and to the single peptide arms, we also evaluated compound **2.15** and the different SREs **2.18** (Ac-GLMVG-$CONH_2$), **2.19** (Ac-GVVIE-$CONH_2$), **2.20** (Ac-KLVFF-$CONH_2$), used for the peptidomimetics (Figure 2.18).

No activity was observed for the three isolated pentapeptide sequences. As already described in literature [125] [128] [186][187], the pentapeptide **2.20** (Ac-KLVFF-$CONH_2$) delayed the Aβ 1-42 aggregation at ratio 10/1, however in much less extent than our compounds, and exerted no activity at ratio 1/1. The **2.15** intermediate resulted to be more active than **2.20** (Ac-KLVFF-$CONH_2$). These results highlighted that the piperidine-pyrrolidine scaffold and the pentapeptide Ac-KLVFF-$CONH_2$ are both crucial

for the activity, but the whole β-hairpin construct is necessary to strongly delay the Aβ 1-42 aggregation kinetics.

2.5.2 Transmission electron microscopy (TEM)

Transmission electron microscopy uses high energy electrons (up to 300 kV accelerating voltage) which are accelerated to nearly the speed of light. The electron beam behaves like a wavefront with wavelength about a million times shorter than light waves. When an electron beam asses through a thin-section specimen of a material, electrons are scattered. A sophysticated system of electromagnetic lenses focuses the scattered electrons into an image or a diffraction pattern, or a nano-analytical spectrum, depending on the mode of operation. It's possible to observe objects to the order of a few angstrom. The possibility for high magnifications has made the TEM a valuable tool in both medical, biological and materials research.

In order to evaluate the activity of synthesized compounds on the fibrillization of Aβ 1-42 peptide, the ThT fluorescence assay was first employed but the reduction or the increase of the final fluorescence intensity of Aβ 1-42 induced by the peptidomimetics should not necessarily be interpreted quantitatively in terms of the amount of fibrillar material formed. Changes in the binding constant or the quantum yield of the dye and binding of the dye to aggregated synthetic molecules might also affect the fluorescence intensity. Thus, it is important to assay any potential inhibitor or accelerator by an independent method. TEM analyses can be performed to complement the ThT assay and validate the obtained results [167]. Furthermore, TEM analyses gives insight about the nature of the fibers and the aggregates in the presence of an inhibitory compound and allows to compare their morphology with the Aβ 1-42 alone. It allows to observe if the fibers are thinner or thicker, more or less dense, longer or shorter, with a different morphology, such as, for example, more globular, than the peptide control.

In practice, the samples to be tested are adsorbed on a metal grid covered with a thin carbon film. A solution containing uranyl acetate, the contrast agent, is added to the grid for a few seconds and then absorbed. The biological sample appears lighter than its surroundings, in a negative staining. The observation of the fibril formation over time in absence and in presence of a compound allows to follow the morphological evolution of the fibers formed during the process.

TEM analyses were performed on the most promising **2.2**, **2.3** and **2.4** compounds (Figure 2.19). Images were recorded at 20 hours and 42 hours of fibrillization kinetics with sample containing 10 µM of each compound corresponding to the 1/1 ratio. Differences were observed in quantity and morphology of aggregates formed in presence of these compounds.

Already at 20 hours it was possible to note the presence of some fibers in the peptide control. At the end of aggregation (42h), a very dense network

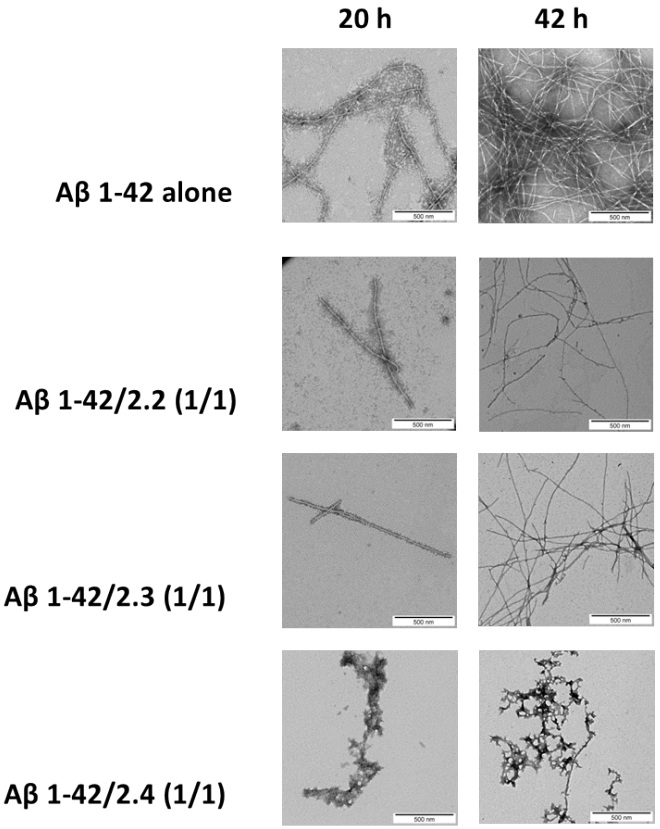

Figure 2.19: Effects of derivatives **2.2**, **2.3** and **2.4** on fibril formation of Aβ 1-42 visualized by TEM

of fibers, displaying a typical morphology, was observed for the peptide alone. In the samples containing **2.3**, the network of fibers was significantly less dense after 20h and 42h than in the control experiments and the fibers displayed the same morphology.

In sample containing **2.4**, we mainly observed globular aggregates after 20h and 42h, indicating that the aggregation pathway could be different from the one observed for Aβ 1-42 alone.

In sample containing **2.2**, the network of fibers was significantly less dense after 20h and 42h and the fibers displayed the same morphology as the control experiment.

These results confirmed the ThT fluorescence data, indicating that compounds **2.2**, **2.3** and **2.4** dramatically slowed down the aggregation of Aβ 1-42 and efficiently reduced the amount of typical amyloid fibrils. At the same time, we obtained more information about the morphology of the species formed after 42 h in the presence of the inhibitors.

2.5.3 Capillary electrophoresis (CE)

Capillary electrophoresis (CE) is a powerful technique for electrophoretic separation of molecules of varying sizes within a capillary of small internal diameter (20–100 µm). Because of its intrinsic qualities (high efficiency and resolution, rapid analysis and low consumption of sample) it is of particular interest for the analysis of proteins or peptides. Its principle is based on the migration of species in solution, subjected to an electric field. A potential difference of up to 30 kV is applied to the ends of a fused silica capillary. Migration of the analytes introduced into the capillary is the resultant of the electrophoretic migration, characteristic of each compound in a given electrolyte, and electroosmotic flow.

The capillary is filled with an electrolyte at constant pH and ionic strength. The voltage is applied after injection of the analyte into the capillary. The separation is then governed by the charge-to-hydrodynamic radius ratio, more often assimilated to charge-to-mass ratio. More the ratio of the species is elevated, more their mobility will increase. The buffer pH plays a preponderant role, because it determines the ionisation state of the polypeptides in terms of their isoelectric point (pI), but also the magnitude of the electroosmotic flow. If the electroosmotic flow is bigger in absolute value than the electrophoretic mobility of anions, the CE allows to separate simultaneously species with different and opposite charge, despite the direction of the electrophoretic migration is opposite.

Recently, our laboratory proposed an improved method by CE to monitor *in vitro* over time the crucial early steps of the oligomerization process of Aβ 1-42 peptide and to analyze the effect of drugs on these first stages [143][188]. Using this method, the disappearance of the monomer as well as the progressive formation of oligomeric soluble species during the self-

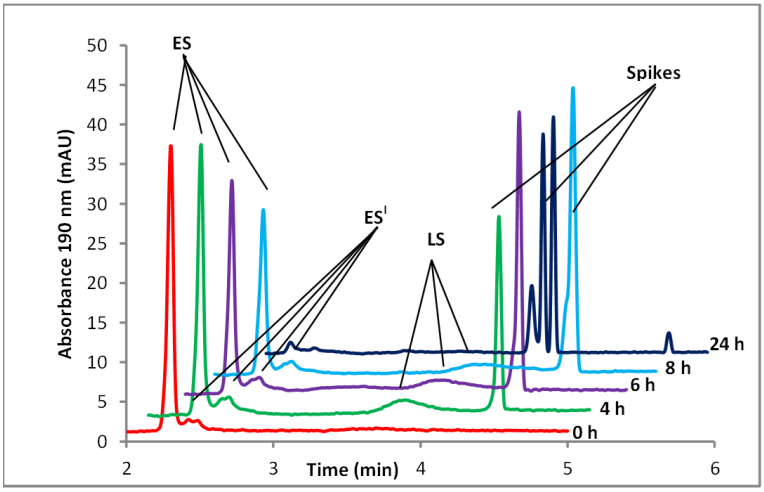

Figure 2.20: Electrophoretic profile of Aβ 1-42 peptide (100 µM) at 0 h (red), 4 h (green), 6 h (purple), 8 h (light blue) and 24 h (blue) in phosphate buffer 20 mM and DMSO (2.5 %). The monomeric species at 2.3 min decreases dramatically overtime.

assembly process can be monitored and quantified over time. We focused our attention on three kinds of species: the monomer (peak ES), different small metastable oligomers grouped under peak ES' and transient species formed later and which correspond to species larger than dodecamers and still soluble (peak LS).

Centrifugation of the peptide sample using filters with different cut off indicated that ES contains species with a molecular mass under 50 kDa while peak LS was mainly constituted by larger species (>50 kDa, monomer has a molecular mass around 4.5 kDa) [188]. The hydrodynamic radius of the species present at the initial kinetics step was estimated around 1.8 nm by Taylor Dispersion Analysis (TDA) while SDS-PAGE analyses showed the predominance of the monomer. So, taken together the TDA, SDS-PAGE and CE kinetics results strongly suggest that ES peak is mainly constitued by the monomeric form of the peptide. Dimitri *et al.* demonstrated that the optimized sample preparation combined with the improved CE method allows the monitoring of the monomer self-assembly at its earlier stages [188].

I first followed the aggregation kinetics of Aβ 1-42 peptide alone. It showed that over time the monomer ES peak decreased in favor of the oligomers peaks ES' and LS, and that poorly soluble and aggregated species, defined as spikes, started to appear after 4 h due to the self-aggregation (Figure 2.20). The monomeric species decreased dramatically and were not detectable after 24 h of kinetics, while only spikes were present in the kinetics profile.

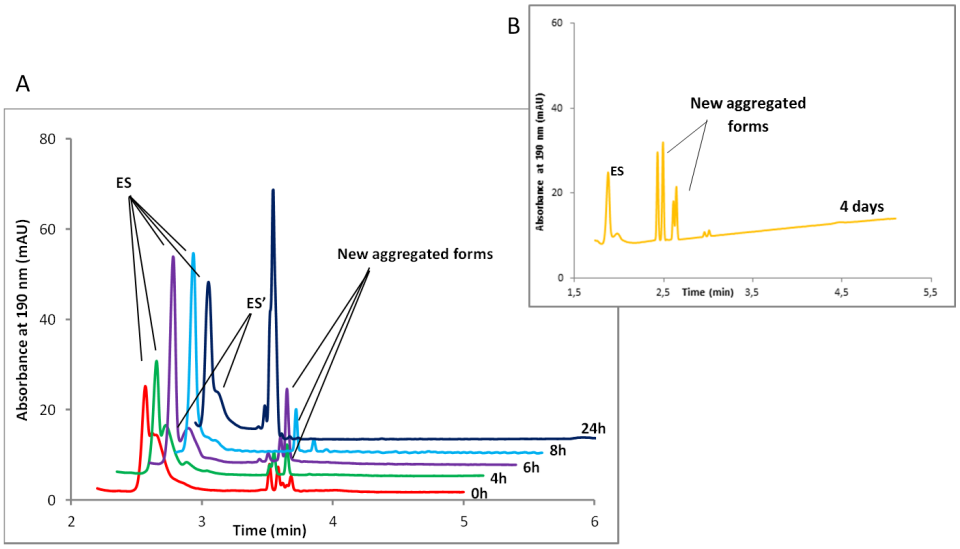

Figure 2.21: Electrophoretic profile of Aβ 1-42 peptide (100 µM) in the presence of **2.4** (1/1 ratio) at A) 0 h (red), 4 h (green), 6 h (purple), 8 h (light blue), 24 h (blue) and B) after 4 days in phosphate buffer 20 mM and DMSO (2.7 %)

In order to study the activity of compounds **2.2** and **2.4** on small soluble oligomer formation and in particular on the crucial early steps involved in the formation of the neurotoxic oligomers, I followed the aggregation kinetics of Aβ 1-42 peptide in the presence of **2.2** and **2.4** by capillary electrophoresis. The two compounds were chosen because they displayed the most promising activity on Aβ 1-42 aggregation in ThT fluorescence assays.

In the presence of **2.4** at 1/1 ratio, the aggregation kinetics of Aβ 1-42 peptide was greatly modified (Figure 2.21A). Noteworthy, the monomeric species (peak ES) was dramatically stabilized. More precisely, up to 4h, the monomer (ES) quantity was lower and the metastable species ES' were in larger amount than in the control experiment. Then, the monomer peak increased between 4 and 8 h and remained stable until 24 h. Indeed, the larger aggregated species LS were not detected over the kinetics but new aggregated forms of Aβ 1-42 between ES' and LS migration time were observed on each electrophoretic profile. These new aggregated forms of Aβ 1-42 were not due to **2.4** degradation or self-aggregation, as its electrophoretic profile was stable over time (Figure 2.22).

They were probably aggregated forms with a different morphology than the spikes observed in the peptide control. This observation is in accordance with the TEM images where globular aggregates were observed after 20 h and 42 h instead of the classical dense network of fibers (Figure 2.19). In ThT

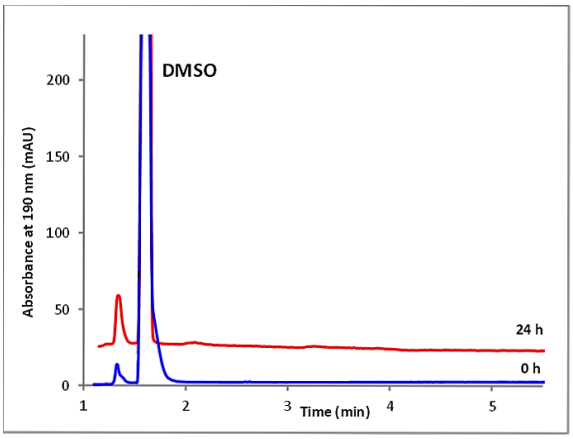

Figure 2.22: Electrophoretic profile of **2.4** alone at 0 h (blue) and 24 h (red) in phosphate buffer 20 mM and DMSO (2.7 %)

assays, no fluorescence was detected, indicating that the globular species were not characterized by a highly ordered β-structures (Figure 2.16).

From these results, we hypothesized that **2.4** was able to induce metastable species at the beginning of the kinetics which gave back to the monomeric state. 86 % of the monomer remained after 24 h in the presence of **2.4**, while it was not detectable in the control peptide sample (Figure 2.23). Remarkably, the presence of the monomer was maintained even after 4 days (Figure 2.21B).

So, we can conclude that **2.4** is able to prevent the formation of soluble oligomers described as toxic of Aβ 1-42 peptide and to maintain the presence of the non-toxic monomer over time.

The electrophoretic profile of Aβ 1-42 in the presence of **2.2** (1/1 ratio) was very different from the one observed in the presence of compound **2.4** (Figure 2.24). The species present over the kinetics were similar to the species observed with Aβ 1-42 peptide alone in the first electrophoretic profiles (0-6 h). We observed a classical but slower kinetics with a decreasing of the monomeric peak over time, together with an increasing of ES' and LS peaks and the appearance of spikes. However, LS peak grew up less than in the profile of Aβ alone. After 8 h of kinetics the electrophoretic behaviour changed: the soluble large species (LS) disappeared and new aggregated forms transiently appeared. These last were not anymore detectable after 24 h. Also in this case, the presence of new aggregated forms between the ES' and LS migration time was not due to **2.2** degradation or self-aggregation, as its electrophoretic profile was stable over time (Figure 2.25).

80 % of the monomer remained after 24 h in the presence of **2.2**, while it was not detectable in the control peptide sample (Figure 2.23). Remarkably,

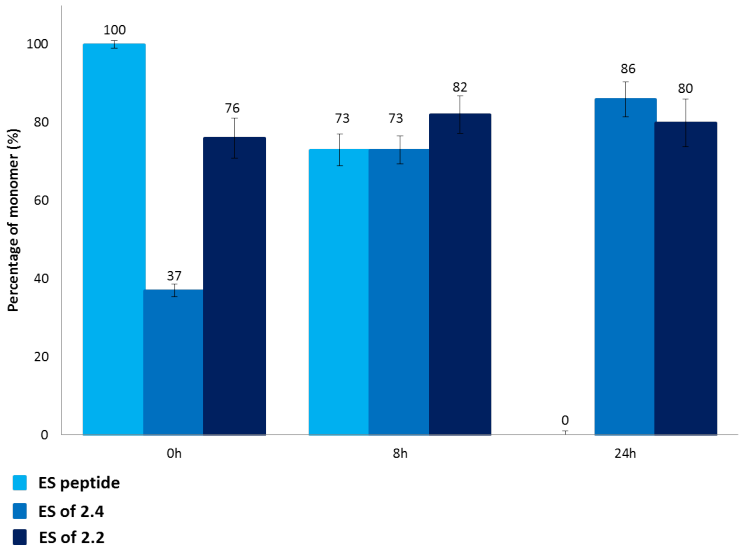

Figure 2.23: Peak area of the monomer in **2.2** and **2.4** profiles at 0, 8 and 24 h related to the peak area of Aβ 1-42 peptide at time 0

the presence of the monomer was maintained even after 8 days (Figure 2.24).

This result was also in accordance with the TEM images where we observed a much less dense network of fibers at 20 h and 42 h, however with the typical morphology.

So, we can conclude that **2.2** is able to dramatically delay the oligomerization process and to decrease the fibers amount, by maintaining over time the presence of the non-toxic monomer.

2.5.4 Cell viability assay

The inhibitors were investigated to determine their ability to reduce the toxicity of aggregated Aβ 1-42 to SH-SY5Y neuroblastoma cells. The cell viability assay was performed in partnership with the Lancaster University, Division of Biomedical and Life Sciences, Faculty of Health and Medicine.

The addition of all compounds, with the exception of **2.2**, showed a protective effect on cell survival (MTS assay, Figure 2.26) and membrane damage (LDH membrane integrity assay, Figure 2.27) in the presence of cytotoxic 5 µM Aβ 1-42. Remarkably, this protective effect was seen at equimolar amounts of inhibitor to Aβ 1-42 and was still significant at a very low ratio of 0.1/1 (inhibitor/Aβ1-42) in the MTS assay.

Both **2.1** and **2.4** showed a slight negative effect on cell viability when incubated with cells alone, although this was negated when Aβ was present.

This protective effect is more marked than that observed with molecules

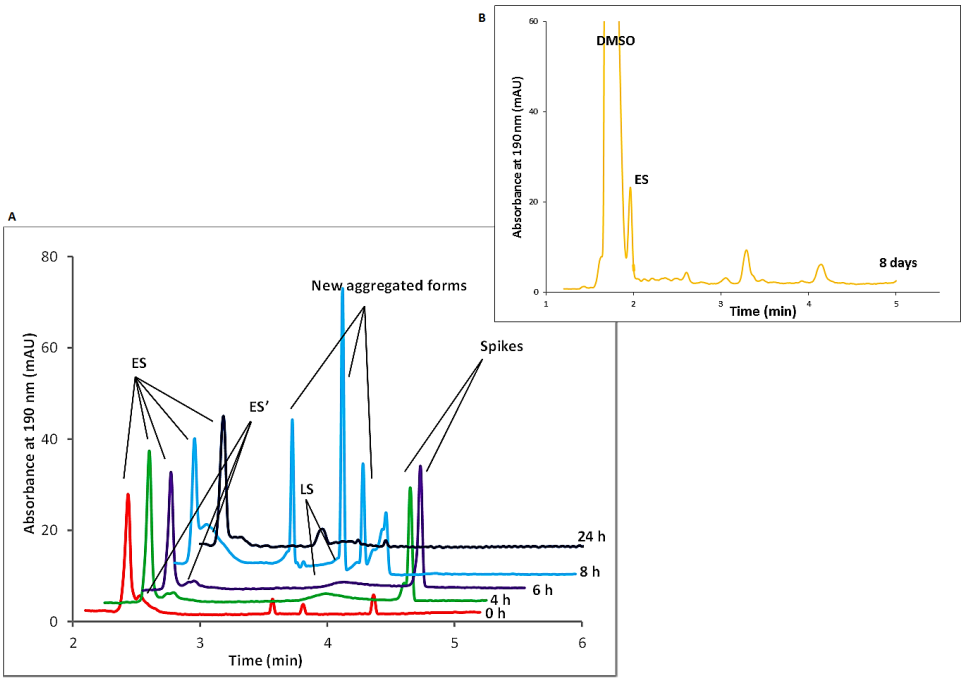

Figure 2.24: Electrophoretic profile of Aβ 1-42 peptide (100 µM) in the presence of **2.2** (1/1 ratio) at A) 0 h (red), 4 h (green), 6 h (purple), 8 h (light blue), 24 h (blue) and B) after 4 days in phosphate buffer 20 mM and DMSO (2.7 %)

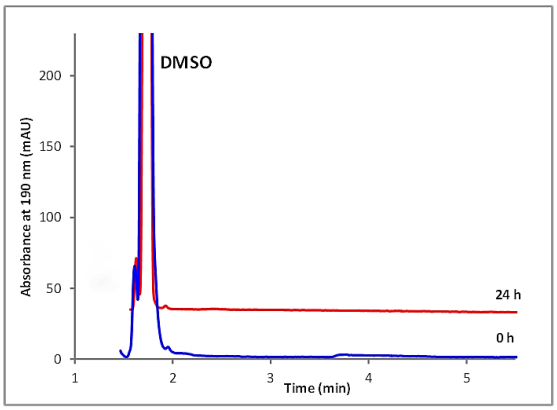

Figure 2.25: Electrophoretic profile of **2.2** alone at 0 h (blue) and 24 h (red) in phosphate buffer 20 mM and DMSO (2.7 %)

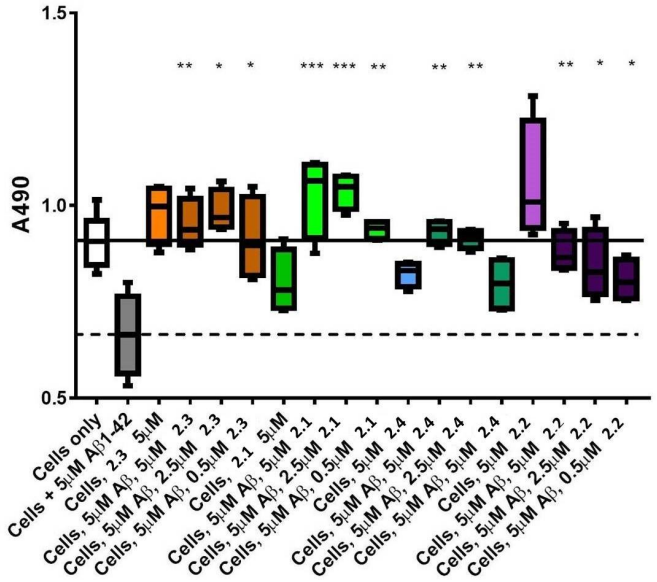

Figure 2.26: Cell viability assay results. The solid line represents the absorbance value seen for cells incubated without Aβ (white box) and the dotted line that seen for cells incubated with 5 µM Aβ (grey box). A statistically significant difference between A treated cells with and without inhibitor is indicated by */**/*** corresponding to p>0.05/0.01/0.001. n=4 for each condition

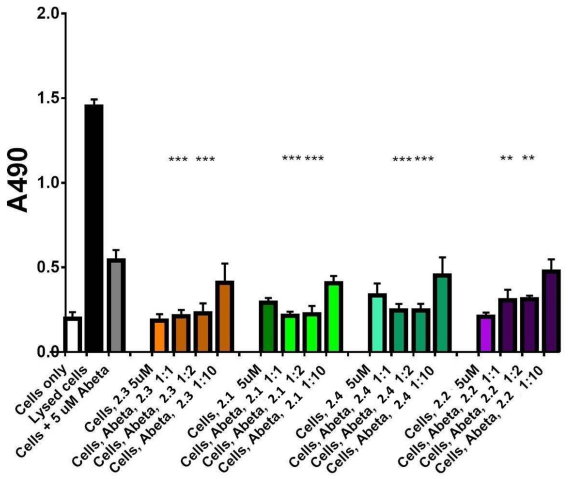

Figure 2.27: LDH based cell toxicity test. Statistical analysis was performed using a Student's t test comparing the results for cells exposed to 5 µM Aβ 1-42 with and without inhibitor where ** = p<0.01 and *** = p<0.001.

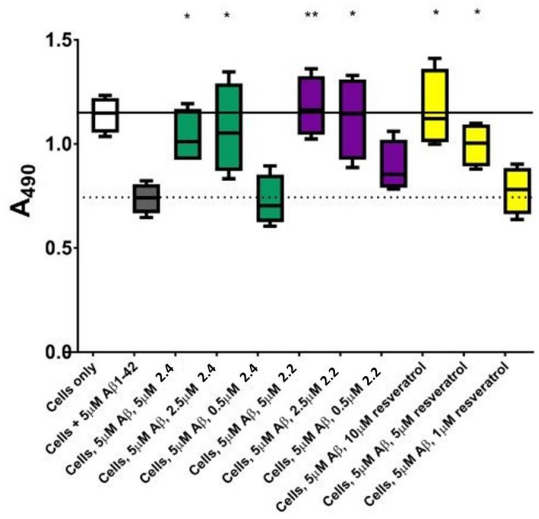

Figure 2.28: Cell viability assay results of resveratrol compared to **2.2** and **2.4**. The solid line represents the mean absorbance value seen for cells incubated without Aβ 1-42 (white box) and the dotted line seen for cells incubated with 5 µM Aβ 1-42 (grey box). A statistically significant difference between Aβ 1-42 treated cells with and without inhibitor is indicated by */**/*** corresponding to p>0.05/0.01/0.001. n=4 for each condition

which have undergone clinical trials [189] [190] [191] or other molecules recently described as efficient reducers of Aβ 1-42 toxicity [192]. In particular, in the literature, resveratrol was reported to protect SH-SY5Y neuroblastoma cells from Aβ 1-42 toxicity at 10:1 and 2:1 (resveratrol:Aβ 1-42) *ratios* [189], scyllo-inositol was demonstrated to protect PC-12 cells at 10:1 *ratio* (scyllo-inositol:Aβ 1-42) [190], and (-)-epigallocatechin-3-gallate protected murine neuro-2a neuroblastoma cells at 1:1 *ratio* (epigallocatechin-3-gallate:Aβ 1-42) [191]. In our hands, and comparable to published data [189], resveratrol efficiently protected SH-SY5Y neuroblastoma cells only at a *ratio* of 2:1 (resveratrol:Aβ 1-42). A stoichiometric *ratio* 1:1 was less efficient than a substoichiometric *ratio* of **2.2** and **2.4** (0.5:1 compound:Aβ 1-42) (Figure 2.28).

2.6 Conclusion

In this chapter, we described new β-hairpin mimics designed on oligomeric and fibril structures of Aβ 1-42 peptide and containing a piperidine-pyrrolidine β-turn inducer. The presence of two small recognition sequences able to engage both hydrophobic and ionic interactions with Aβ 1-42, increased dramatically the inhibitory effect on the fibrillization process. Furthermore, the presence of the semi-rigid piperidine-pyrrolidine scaffold, which makes possible a dynamic equilibrium between different architectures, leads to the obtainement of **2.4** compound able to totally inhibit the formation of amyloid fibrils and to greatly modify the oligomerisation process.

With these compounds, we put in evidence the importance of rationally designed peptide sequences to have selectivity for the target, the significance of a β-turn inducer in order to fold the molecule in a β-hairpin manner, able to better interact with the target peptide, and the relevance of hydrophilic groups that can form ionic interactions with the target peptide and prevent the formation of its β-sheet structure during the aggregation process.

Thanks to these observations, the following objective was to take inspiration from this study to design new peptidomimetics with the aim to decrease the peptidic character of the molecules and to increase their hydrosolubility, in order to obtain compounds more resistant to proteolysis and bioavailable. This will be the topic for the next chapters of this thesis.

Chapter 3

β-hairpin mimics containing the piperidine-pyrrolidine scaffold and the 5-acetamido-2-methoxy-benzohydrazide peptidomimetic derivative unit

In this chapter, we report the design, synthesis and conformational analysis of nine β-hairpin mimics containing the piperidine-pyrrolidine scaffold and bearing a 5-acetamido-2-methoxybenzohydrazide peptidomimetic derivative unit. We described the structure-activity relationship of these β-hairpin mimics by showing the results obtained by Th-T fluorescence assays. We obtained a compound that demonstrated the ability to greatly delay and inhibit the kinetics of Aβ 1-42 aggregation process. We also present, in the last part of the chapter, the conformational studies conducted on two of these compounds by NMR spectroscopy.

3.1 Design of the β-hairpin mimics

3.1.1 Previous results in the laboratory

As we could see in the previous chapter, Aβ-1-42 amyloid related peptidomimetics, built on the piperidine-pyrrolidine semi rigid scaffold and bearing two small recognition peptide sequences, demonstrated to be able to

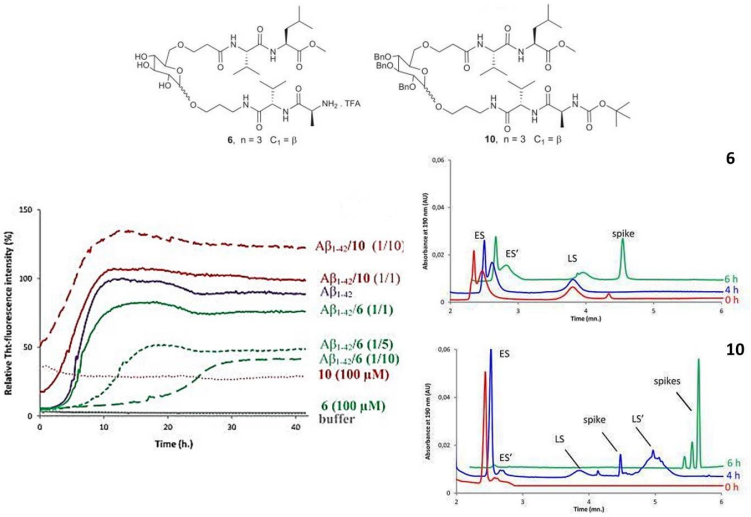

Figure 3.1: ThT fluorescence assays and electrophoretic profiles of two glycopeptides developed by our laboratory, that showed the ability to inhibit or accelerate the Aβ 1-42 aggregation process and to stabilize or prevent the presence of small soluble toxic oligomers, respectively [143]

greatly delay the kinetic of Aβ-1-42 aggregation process and to preserve the monomer species. However, these compounds still present a strong peptide character that could make them sensitive to proteolytic attack.

So, starting from these observations, we decided to maintain the same piperidine-pyrrolidine semi rigid scaffold, which largely demonstrated its ability to induce β-hairpin structures, and to substitute one pentapeptide sequence by a peptidomimetic arm and the second pentapeptide sequence by shorter peptide chains, in order to further decrease the number of potential sites for proteolytic attack.

Recently, our group has developed potential ligands of β-amyloid peptide which could modulate the aggregation of Aβ peptides involved in Alzheimer's disease. A novel class of glycopeptides, based on two hydrophobic dipeptides (Ala-Val and Val-Leu) linked to a hydrophilic D-glucopyranosyl scaffold through aminoalkyl and carboxyethyl linkers in C1 and C6 positions, respectively, were designed to combine the targeting of the hydrophobic recognition interfaces with an original hydrophilic sugar β-breakage strategy. These peptidomimetics dramatically slow down the aggregation of Aβ 1-40 even at low ratios of inhibitors, alter the morphology of Aβ species and efficiently reduce the amount of typical amyloid fibrils [167].

The most effective molecules were also evaluated by a recently developed capillary electrophoresis method, providing *in vitro* monitoring of the crucial, very early stages of the self-assembly process. The technique provided that

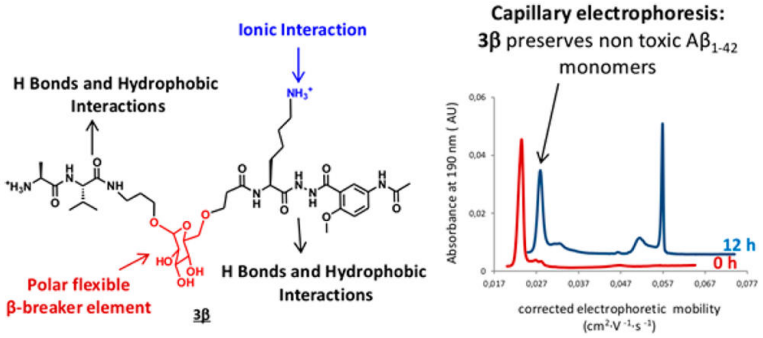

Figure 3.2: Structure of the sugar-based peptidomimetic that combines hydrophobic moieties, hydrogen bond donors and acceptors, ammonium groups and a hydrophilic β-sheet breaker element; on the right the electrophoretic profile of Aβ 1-42 peptide in the presence of this compound [142]

inhibitors of Aβ 1-42 aggregation, as detected by Th-T fluorescence assay and TEM, show no effect or can stabilize soluble oligomeric species. On the contrary, accelerating Aβ 1-42 aggregation was demonstrated to prevent the presence of small soluble oligomers described as toxic, by accelerating the disappearance of all soluble species visible in the control profile (Figure 3.1) [143].

Pharmacomodulations of these compounds allowed the discovery of sugar-based peptidomimetics able to inhibit both Aβ 1-42 early oligomerization and fibrillization [142]. It has been demonstrated that these molecules interact with soluble oligomers in order to maintain the presence of non-toxic monomers and to prevent fibrillization (Figure 3.1). For these molecules, it was decided to replace the C-terminal Leu of the previous sugar-based compounds by the 5-amino-2-methoxybenzhydrazide unit, which is a part of the β-strand mimic (Hao unit) reported by Nowick and co-workers [162] [193]. The introduction of a 5-amino-2-methoxybenzhydrazide unit into a β-strand mimic was also shown by our group to be extremely effective in the prevention of protein-protein interactions involving intermolecular β-sheets of HIV-1 protease in order to inhibit its dimerization [194] [195].

Nowick and co-workers showed that the Hao unit (Hydrazide, 5-amino-2-methoxybenzoic acid and Oxalic acid) allows to establish hydrogen bonds between the two β-strands of a 10- or 14-membered macrocycle in order to form an antiparallel β-sheet (see Chapter 1, paragraph 1.2.3). In fact the Hao unit is a tripeptide mimic and it participates to the macrocycle structuration by forming appropriate H-bonds. But the Hao unit doesn't admit the formation of an appropriate hydrogen bond network required for the prosecution of the β-sheet formation and also the necessary π-stacking interactions to recognize the nucleation site on the lower face. So, the Hao

unit is able to perturb the oligomerization process [162] [193].

We adapted this strategy by using the Hao unit without the oxalic acid and by incorporating it in a smaller peptidomimetic arm that we coupled to the sugar moiety. In a first generation, the Val residue was kept and linked to the 5-acetamido-2-methoxybenzohydrazide unit. Next, the valine residue was replaced by a Lys residue, to further provide these molecules with the possibility of engaging electrostatic interactions with Aβ 1-42, in order to increase their affinity for Aβ 1-42. The presence of the amine of the side chain of the Lys residue proved to be beneficial for the inhibitory activity in comparison with the Val residue (Figure 3.1) [142].

Thanks to these results, we decided to design new β-hairpin mimics. Our objective is to design molecules which are druggable, namely small molecules (MW around 800) with a good hydrophobicity/hydrophilicity balance and resistant to proteolytic degradation.

3.1.2 β-hairpin mimics based on the Tosyl scaffold and the 5-amino-2-methoxybenzhydrazide unit

Our design towards a stable β-hairpin mimic, which could interact and eventually act as β-binder and aggregation inhibitor, involved assembling the piperidine-pyrrolidine semi rigid scaffold mentioned previously, the 5-amino-2-methoxybenzhydrazide peptidomimetic strand with a Lys residue to stabilize the formation of β-sheets and finally a suitable and small peptide sequence for binding to the aggregating protein.

Indeed, with the view to increase the affinity of this series of hairpin mimics towards Aβ 1-42, we provided to these molecules the possibility to also engage electrostatic interactions with the peptide. For this purpose, the N-terminal residue and the amine of the Lys side chain were deprotected in all the final molecules in order to promote ionic interactions with acidic residues of Aβ 1-42.

In a first attempt, we designed and synthesized two β-hairpin mimics, both composed by the same piperidine-pyrrolidine scaffold, as in compounds **2.1**-**2.4** in chapter 2, protected on the C4 primary amine by a tosyl protective group, and by the 5-amino-2-methoxybenzhydrazide peptidomimetic strand linked to a Lys residue. In one case, we decided to maintain the dipeptide sequence Val-Ala which had already demonstrated in the glycopeptidomimetic series its capacity to provide the recognition with the Aβ 1-42 peptide (Molecule **3.1**) (Figure 3.3). On the other case, we decided to lengthen of an amino acid the peptide chain, because we thought that the β-hairpin mimic could be stabilized, given the fact that the 5-amino-2-methoxybenzhydrazide unit is a tripeptide mimic (Molecule **3.2**) (Figure 3.3).

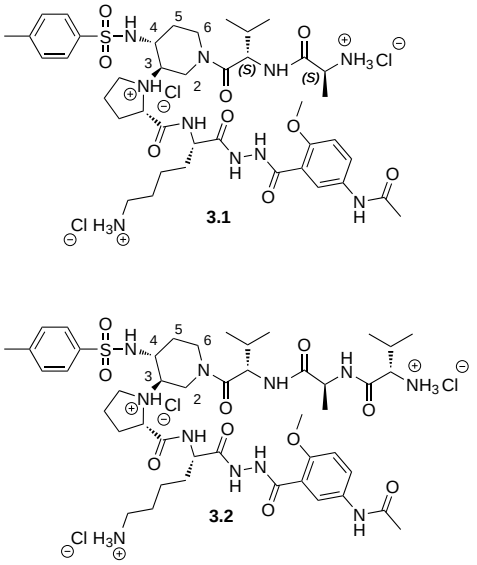

Figure 3.3: Structure of the two tosylated β-hairpin mimics **3.1** and **3.2** bearing the 5-amino-2-methoxybenzhydrazide unit

3.1.3 Modulation of the protective group of the β-turn scaffold

We thought that, by tuning the type of sulphonylazide used in the multicomponent reaction for the synthesis of the scaffold, it could be possible to obtain β-sheet mimetic decorated with different functionality, such as fluorophore (e.g dansyl) to perform localization studies, hydrophilic chain to improve the solubility, or cell penetreting sequences (e.g Tat from HIV or polyArg) to increase biovailability. So, we performed a new synthetic pathway to obtain another type of scaffold with orthogonal protecting groups which allowed to operate some structure-activity relationship studies around the most promising compound in the tosyl series.

We designed and synthesized the β-hairpin mimic analogue of compound **3.1** composed by the same peptidomimetic sequence and the same dipeptide chain (Molecule **3.3**) (Figure 3.4). Instead of the tosyl protecting group, the piperidine-pyrrolidine scaffold was protected by a *tert*-butyloxycarbonyl protecting group which allowed to compare the inhibitory activity with its tosyl counterpart and to provide information about the role of the type of protecting group used for the C4 primary amine of the scaffold.

Furthermore, by using an easier removable protecting group, we had the possibility to cleave it and to study the activity of the totally deprotected analogue (Molecule **3.4**) (Figure 3.4). The possibility to obtain a free primary amine gives the advantage to increase the water solubility of the molecule and

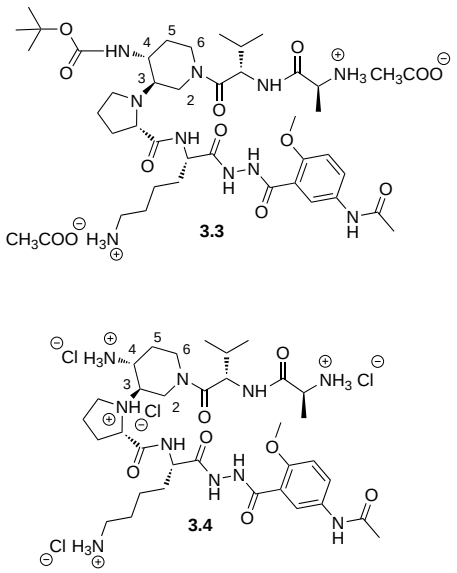

Figure 3.4: Structure of the two β-hairpin mimics **3.3** and **3.4** with and without the Boc protecting group

also to further functionalize it with cell penetreting sequences or fluorophore.

Finally, considering that we needed to pass through a piperidine-pyrrolidine scaffold protected by a nosyl group to obtain the Boc protected one, we decided to perform the synthesis of the β-hairpin mimic analogue of compound **3.1** composed by the 5-amino-2-methoxybenzhydrazide peptidomimetic strand, the dipeptide Val-Ala sequence and the nosyl protected scaffold. After cleavage of the N-terminal residue and the amine of the Lys side chain, we obtained compound **3.5** (Figure 3.5) that gave the opportunity to study the effect of replacing a methyl group by a primary aromatic amine on the inhibitory activity.

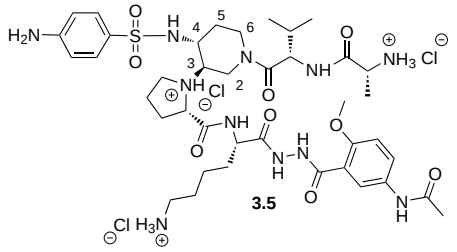

Figure 3.5: Structure of the β-hairpin mimic **3.5**

3.2 Synthesis of the β-hairpin mimics

3.2.1 Synthesis of compounds 3.1 and 3.2

For the synthesis of the β-hairpin mimics **3.1** and **3.2**, we performed the synthesis of the tosyl protected piperidine-pyrrolidine scaffold by following the same synthetic approach, already described in Chapter 2 (Figure 2.7, page 75).

Once obtained the scaffold, it was necessary to adapt it to an orthogonal liquid-phase peptide synthesis with the 5-amino-2-methoxybenzhydrazide peptidomimetic arm, composed by a Lys residue, bearing a CbZ protecting group on the side chain.

Hydrogenolysis of compound **2.5** and the following hydrolysis of the methyl ester were performed using the protocol described in Chapter 2 (Figure 2.7). To afford a scaffold suitable for a peptide synthesis with a Boc strategy, we tried to protect the secondary amide of the piperidine ring by a *tert*-butyloxycarbonyl protecting group. We performed the reaction in different conditions, by changing the amine (TEA or a 10 % solution of sodium carbonate) or the solvent (MeOH, dioxane, dioxane/water), but we never succeeded to improve the yield, more than 47 %. As a better result was obtained in the case of a Fmoc protection (72 % yield, see Chapter 2), we finally decided to keep the same scaffold **2.13** even for the liquid-phase peptide synthesis.

The coupling reaction between the β-strand **3.6** and compound **2.13** provided the desired product using different coupling agents: DMTMM in the presence of NMM and EDC in the presence of HOBt and DIPEA allowed to obtain compound **3.7** with a poor yield of 18 % and 43 %, respectively.

Satisfactory results were obtained with HATU and HOAt that are the common coupling reagents for sterically hindered systems. Product **3.7** was obtained in 88 % yield, performing the coupling in DMF with 1.1 eq. of HATU and HOAt and 6.0 eq. of collidine and letting the reaction stirring overnight at room temperature (Figure 3.6).

The construction of the lower peptide arm was then performed via solution peptide synthesis using Boc protected amino acids. In each coupling step, the Boc protected amino acid was introduced using HATU and HOAt (2.0 eq.) in DMF, leading to the formation of the expected compound in satisfactory yields. The first amino acid (Val) was introduced after the Fmoc cleavage of product **3.7**, providing compound **3.8** in 60 % yield. After cleavage of the Boc protecting group of compound **3.8**, the second amino acid (Ala) was coupled and the first totally protected β-hairpin mimic **3.9** was obtained in 83 % yield (Figure 3.6). After purification by column chromatography on silica gel, **3.9** was used for the evaluation as aggregation inhibitor.

By using the same synthetic approach (Boc cleavage/amino acid coupling) we continued our synthesis to obtain the second β-hairpin mimic **3.10**, in 57 %

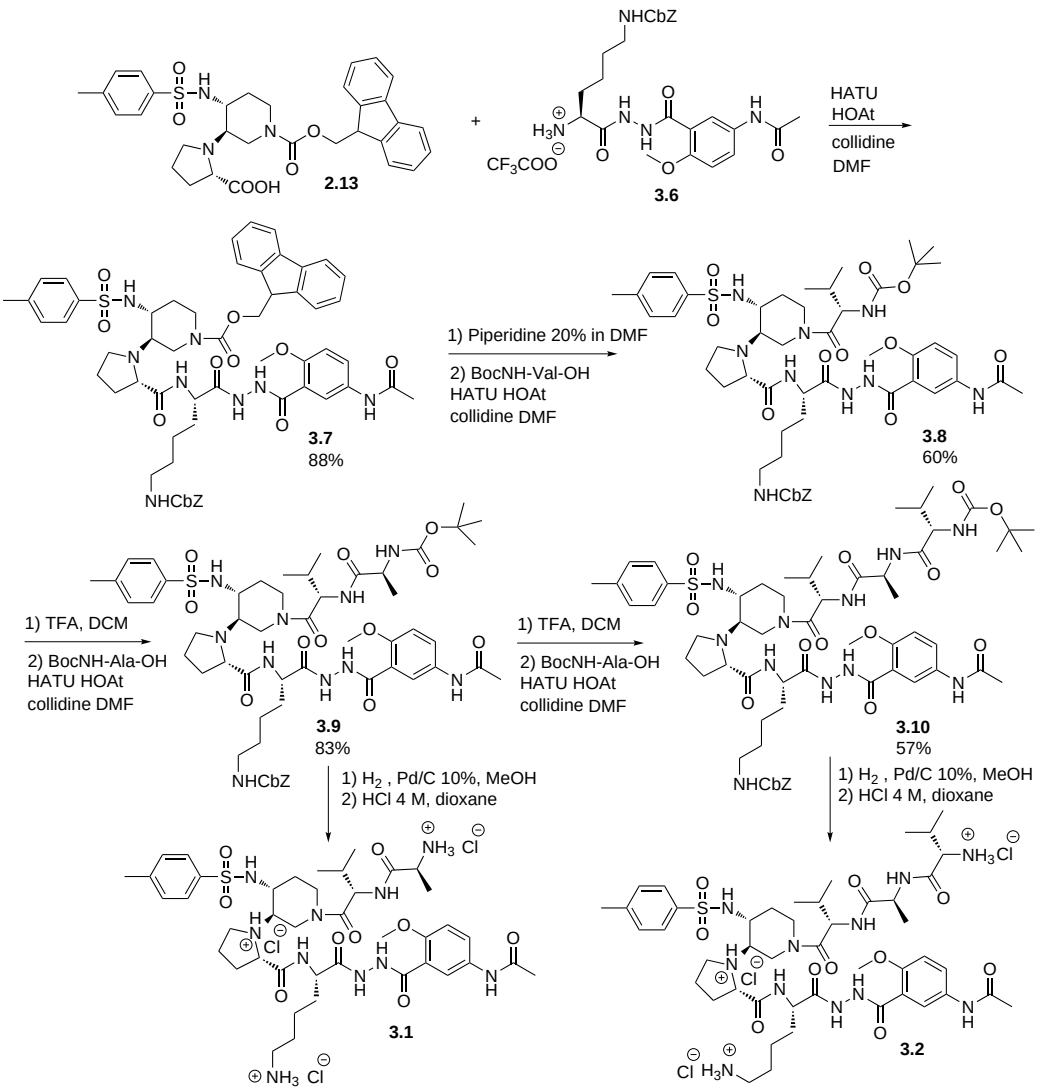

Figure 3.6: Synthetic scheme of the totally protected β-hairpin mimics **3.9** and **3.10**

yield (Figure 3.6). After purification by column chromatography on silica gel, compound **3.10** was used for the evaluation as aggregation inhibitor.

The two final hairpins were then deprotected: the Cbz protecting group was cleaved first by hydrogenolysis using Pd/C and hydrogen in MeOH, and then after filtration the resulting product was subjected to Boc cleavage in presence of HCl 4 M in dioxane. The cleavage of the two protecting groups gave the deprotected compounds **3.1** and **3.2** which, after purification by crystallization in MeOH and diethyl ether or iPrOH and di-isopropyl ether, were used for the evaluation as aggregation inhibitors and also for the conformational NMR study, discussed later (see the evaluation section of this chapter).

3.2.2 Trials of Tosyl cleavage of scaffold 2.5

In order to obtain a scaffold bearing an amino group in position 4 more easily functionalizable (Boc, Nosyl, free amine, etc.), we first tried to find the appropriate conditions to remove directly the tosyl group of the scaffold **2.5**.

In a first attempt, we tried to reproduce the conditions described by Tammadon *et al.* [196] that propose an efficient protocol for the desulfonylation of amines using CsF-Celite as catalyst. Although they reported that the dissociation of desorbed water in the presence of basic fluoride anion led to the production of HO^- whose attack to the SO group of sulfonamide led to the cleavage of this bond, we didn't obtain the desired deprotected scaffold but only its counterpart without the methyl ester.

We observed the same result by using the method for N-detosylation using cesium carbonate described by Bajwa *et al.* [197]. We followed the representative procedure that uses a mixture of THF and MeOH at room temperature with 3.0 eq. of cesium carbonate.

Due to the stability of sulfonamide bond, its removal needs harsh basic conditions which are incompatible with the other present functional groups in the molecule, as we could see in our case for the ester funtion. So, we decided to turn towards acidic conditions variously described in literature.

Katagiri *et al.* [198] used the tosyl moiety as an amine protecting group for the synthesis of optically pure α-trifluoromethyl-α-amino acids. They presented a detosylation procedure, by using concentrated sulfuric acid, and they demonstrated the absence of racemization during the cleavage reaction. When we tried to reproduce this method on our scaffold **2.5**, we surprisingly recovered the undamaged starting material.

Finally, we tried the deprotection conditions described by Lupi *et al.* [199]. They performed the detosylation by reaction with 40 % HBr-AcOH in the presence of phenol as bromide scavanger, to avoid aromatic bromination of the products. Also in this case we only recovered our scaffold **2.5**, without any traces of deprotected molecule.

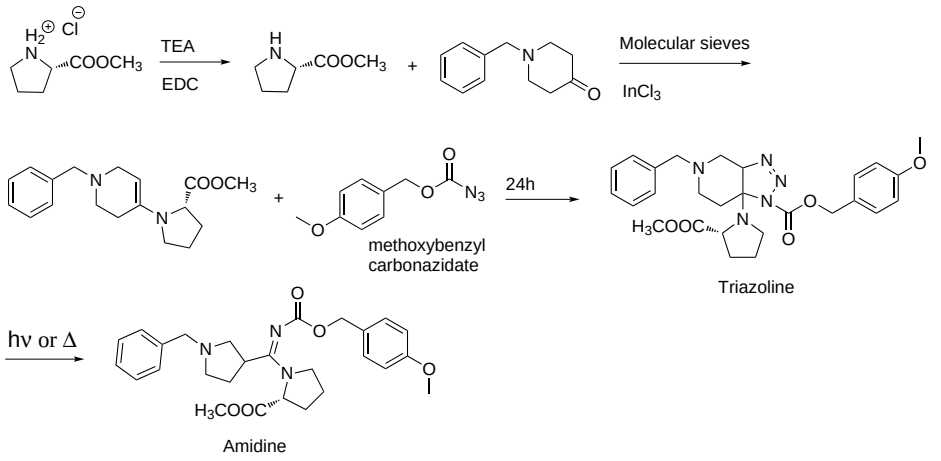

Figure 3.7: The synthetic pathway of the cycloaddition between the 4-methoxybenzyl carbonazidate and the proline enamine

3.2.3 Synthesis of the Nosyl scaffold 3.11

As a result of these unsatisfactory results and the difficulty of removing the tosyl group, it became necessary to synthesize a new scaffold, by trying with different types of azides to obtain a primary amine protecting group different from tosyl. To achieve this objective, I spent two months as a visiting scholar at the University of Milan, to learn the scaffold synthesis and to develop a new synthetic pathway.

As we have already explained in Chapter 2 (Paragraph 2.2), the evolution of the triazoline, during the cycloaddition reaction between azides and enamines, is governed by the type of azide and by the carbonyl group from which the enamine is formed. Maintaining the proline and the benzyl piperidinone as substrates for the formation of the enamine, the different behaviour, that we expected from the reaction by changing the type of azide, was totally attributable to the azide.

We first tried to observe if the cycloaddition was possible with the 4-methoxybenzyl carbonazidate, as a model of an azide produced from a carbamate, in order to achieve a scaffold with a carbamate protecting group, easy to remove from the primary amine. In this case, the triazoline ring obtained from the cycloaddition reaction between the 4-methoxybenzyl carbonazidate and the proline enamine resulted to be stable during the reaction conditions. This type of triazoline didn't show the typical behaviour of ring opening with concerted mechanism which we encountered for the triazoline ring, obtained from the tosyl azide. We successively tried to open this triazoline ring both by warming and by photochemistry but we were not able to isolate the good product, due to the formation of the amidine as

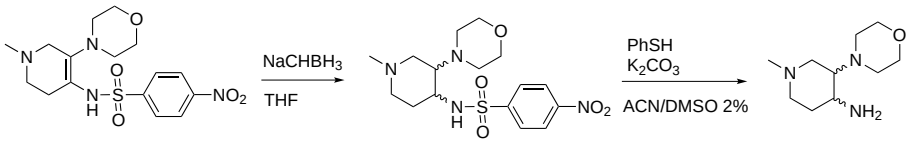

Figure 3.8: Attempts of Nosyl cleavage on a model compound

main compound and other products of degradation (Figure 3.7).

In literature, 2- and 4-nitrobenzensulfonamides are known as exceptionally versatile means for protection of amines. In particular, the resulting primary nosylamide adducts can be cleaved under mild conditions to provide the corresponding primary amines [200][201][202][203][204][205][206][207]. We used, in a first attempt, a model easily available in the laboratory, to check if the cleavage conditions described in literature were compatible with our type of substrates (Figure 3.8). We used the stable dienamine product obtained from the rearrangement of the triazoline ring formed by the enamine, obtained from the 1-methyl-piperidin-4-one and the morpholine, and the p-nitrophenylsulfonyl azide. The corresponding dienamine was reduced with sodium cyanoborohydride in THF. The diastereomeric mixture was then reacted with thiophenol (1.2 eq.) and potassium carbonate (3.0 eq.) in DMF, in order to cleave the 4-nitrobenzensulfonyl group. In these conditions, we didn't obtaine the desired product but we only recovered the starting material.

In literature, attempts of deprotection of the primary nosylamides employing the Fukuyama conditions [200] resulted in sluggish reaction rates and incomplete reactions. Maligres *et al.* observed that replacement of DMF with acetonitrile as the solvent results in complete deprotection within 24 h at 50 °C and the addition of 2 % DMSO to the acetonitrile shortens the reaction time [201]. So, we tried again the cleavage reaction on the same substrate with these conditions and we achieved the good deprotected compound (Figure 3.8).

Thanks to these positive results we decided to develop a new synthetic pathway for obtaining the scaffold by starting from the 4-nitrobenzensulfonyl azide. Compared to the analogue with the 2,4-dinitrobenzensulfonyl azide, the mono-nitro analogue gives the possibility to evit the too much strong reactivity of the azide that can affect the development of the reaction towards byproducts.

The multicomponent reaction between 1-benzyl-piperidin-4-one and nosyl azide has been developed through the following procedure (Figure 3.9). One equivalent of proline methyl ester hydrochloride was suspended in dichloroethane (this solvent was better than chloroform or THF) and the free secondary amine was obtained by adding an equimolar amount of TEA.

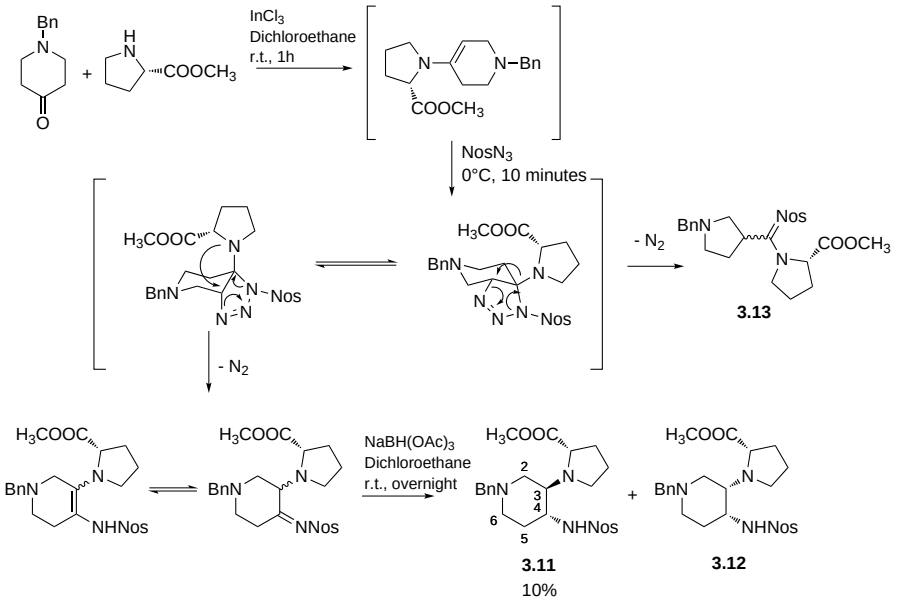

Figure 3.9: Mechanism of the multicomponent reaction to obtain the nosyl scaffold **3.11**

One equivalent of 1-benzyl-piperidin-4-one was subsequently added, followed by molecular sieves and a catalytic amount of indium trichloride (10 %). After 1 hour, one equivalent of nosyl azide, suspended in dichloroethane, was added dropwise during 10 minutes, to the reaction mixture cooled at 0 °C. The reaction was considered finished after one hour at room temperature (monitoring by TLC the disappearance of the azide). Because, also in this case, the produced dienamine was instable and tending to degradation, the best way to isolate the final compound was subjecting the crude to reduction with triacetoxy borohydride that showed a different reactivity compared to sodium cyanoborohydride both in terms of yield and distribution of diastereomers.

After processing, the nosyl scaffold **3.11** was isolated by column chromatography and successively the fraction containing the good diastereomer (3R, 4R, S) was further purified by precipitating the 4-nitrobenzensulfonyl amide impurity by reverse crystallization in DCM/Cyclohexane, to afford the pure compound **3.11** in 10 % yield.

The analysis of every fractions of the column revealed a similar profile to that obtained with the tosyl scaffold, in terms of diastereomers and byproducts, formed during the ring rearrangement and the reduction step:

- Spot 1: Impurity (8 % of total crude);
- Spot 2: Scaffold isomer *trans* (3R, 4R, S) **3.11** with impurity (40 % of

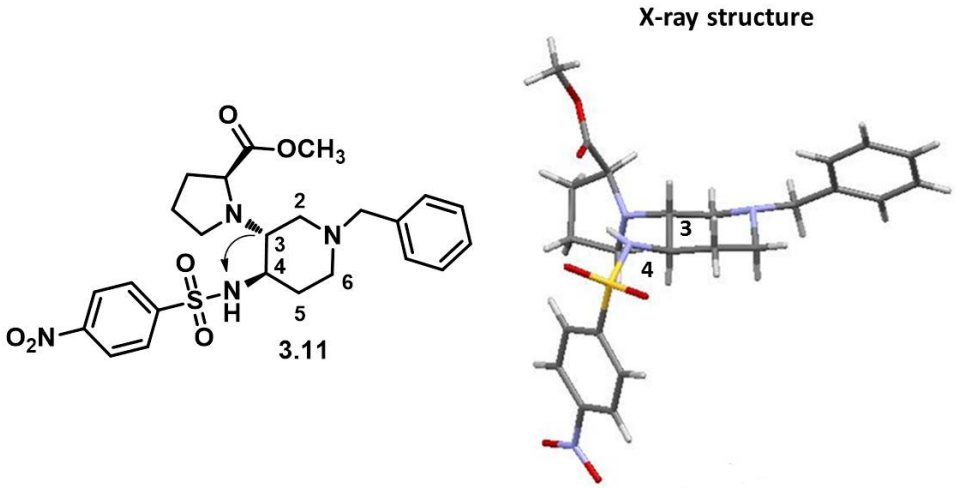

Figure 3.10: The assigned NOE observed by NMR analysis and X ray structure of the nosyl scaffold **3.11** to determine the stereochemistry

total crude);

- Spot 3: Scaffold isomer *trans* (3R, 4S, S) **3.12** (26 % of total crude);
- Spot 4: mixture of the minor isomers *trans* (3S, 4S, S) and *cis* (3S, 4R, S)(18 % of total crude);
- Spot 5: Amidine **3.13** (8 % of total crude).

This similar distribution of the different products obtained from the multicomponent reaction was confirmed by the HPLC analysis of the crude. The second spot revealed the presence of two compounds: 32 % corresponded to the scaffold isomer *trans* (3R, 4R, S) and 18 % to the 4-nitrobenzensulfonyl amide impurity. This observation suggested the necessity to perform the reverse crystallization, as mentioned above.

To confirm the good stereochemistry of compound **3.11** we performed both NMR analysis and X-ray crystallography (Figure 3.10). The proton in position C3 showed the same coupling constants observed in the tosyl analogue (2.60 ppm, td, $J = 10.6$ Hz, 3.7 Hz) and a Nuclear Overhauser Effect (NOE) with the proton sulfonyl amide, suggesting a *trans* configuration of the Pro and NHNos substituents on the piperidine ring (Figure 3.10).

X-ray analysis confirmed the *trans* configuration of the substituents, indicating a R configuration of both C3 and C4 stereocenters and the S configuration of Pro (Figure 3.10).

Once obtained compound **3.11**, the next objective was to see if the same conditions of deprotection, used on the model compound (Figure 3.8), worked

Entry	Reactive	Solvent	Temperature	Time	Yield
1	PhSH and K_2CO_3	ACN and 2% DMSO	50°C	7h and overnight	Starting material
2	$HSCH_2COOH$ and LiOH	DMF	rt to 70°C	overnight	Starting material
3	PhSH and K_2CO_3	ACN and 2% DMSO	Ultrasonic conditions	3 h	Starting material
4	PhSH and K_2CO_3	ACN and 2% DMSO	Microwaves (110°C)	1 h	η=63%

Table 3.1: Synthetic trials for the Nosyl cleavage of the scaffold **3.11**

well also in this nosyl scaffold **3.11**. Upon treatment with thiophenol and potassium carbonate in acetonitrile and 2 % DMSO at 50 °C didn't afford the deprotected compound. Also by using ultrasonic conditions or the other Fukuyama reagents, such as thioglycolic acid, lithium hydroxyde in DMF at room temperature or at 70 °C, we didn't obtain the desired product but we always recovered the starting material (Table 3.1).

To remove the nosyl group, it was necessary to perform the reaction with microwaves at 110 °C for 1 hour. However, during the deprotection of the nosyl group under microwaves we observed the formation of a cyclised byproduct, due to the reaction between the free primary amine of the piperidine ring and the methyl ester of the proline. This byproduct reduces the global yield of the cleavage to 63 %.

3.2.4 Synthesis of compound 3.5

Once established that it was possible to remove the nosyl group of the scaffold, the next objective was to synthesize the β-hairpin analogue of compound **3.1** with the removable nosyl group.

Also in this case, it was necessary to adapt the scaffold to an orthogonal liquid-phase peptide synthesis with the 5-amino-2-methoxybenzhydrazide peptidomimetic arm, linked to a Lys residue, bearing a CbZ protecting group on the side chain.

However, in this case, instead of subjecting the scaffold **3.11** to hydrogenolysis in the presence of a nitro group easily reducible, we decided to reproduce the carbamate exchange procedure, already described by Philippe *et al.* [208]. The reaction plans to exchange the benzyl group by a large excess of fluorenylmethyloxycarbonyl chloride (5.0 eq.) in THF, affording compound **3.14** in 57 % yield (Figure 3.11).

The ester function was successively hydrolyzed in acidic condition (HCl 6 M) at 110 °C, yielding compound **3.15** (100 %) (Figure 3.11).

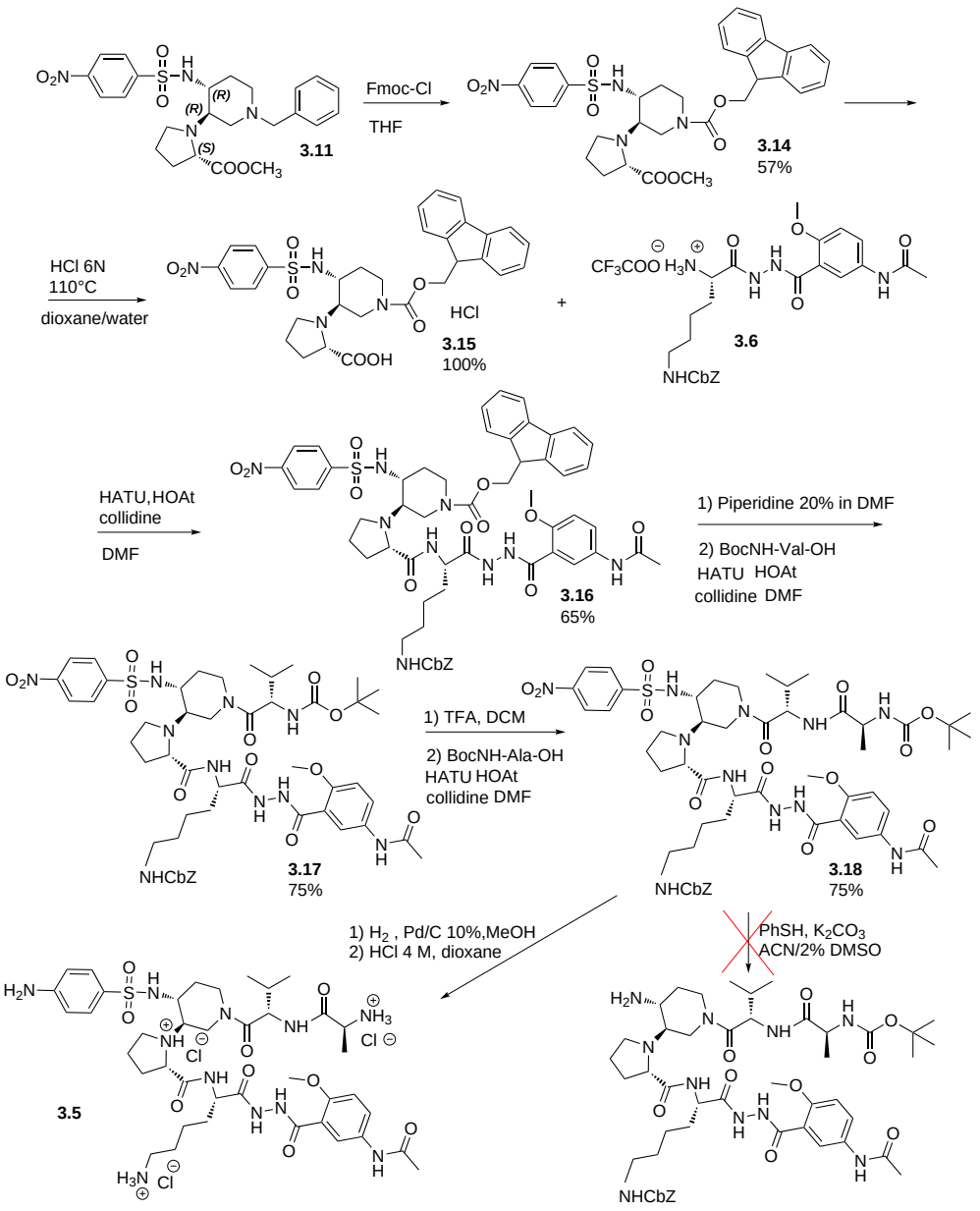

Figure 3.11: Synthetic scheme of compound **3.5**

The coupling reaction between the β-strand mimic **3.6** and compound **3.15** provided the desired product using HATU and HOAt, the common coupling reagents for sterically hindered systems, in DMF in the presence of collidine. The coupling product **3.16** was obtained in 65 % yield (Figure 3.11).

The construction of the upper peptide arm was then performed via solution phase peptide synthesis using Boc protected amino acids, as already described for compounds **3.1** and **3.2**. In each coupling step, the Boc protected amino acid was introduced using HATU and HOAt (2.0 eq.) in DMF, leading to the formation of the expected compound in high yields. The first amino acid (Val) was introduced after the Fmoc cleavage of product **3.16**, providing compound **3.17** in 75 % yield. After cleavage of the Boc group of compound **3.17**, the second amino acid (Ala) was coupled and the totally protected β-hairpin mimic **3.18** was obtained in 75 % yield (Figure 3.11).

Once obtained compound **3.18**, we tried the deprotection of the nosyl group by using the procedure described in the previous paragraph. Upon treatment with thiophenol (3.0 eq.) and potassium carbonate (4.0 eq.) in acetonitrile and 2 % DMSO with microwaves at 110° for 1 hour, we observed the degradation of compound **3.18**. By warming at 70–80° instead of using microwaves, even after four days, we didn't afford the deprotected compound but we only recovered intact the starting material.

So, we discovered that the deprotection conditions of the nosyl scaffold were not compatible with the structure of the final β-hairpin compound **3.18**.

However, the Cbz protecting group of **3.18** was cleaved first by hydrogenolysis using Pd/C and hydrogen in MeOH. The hydrogenolysis reduced also the nitro group of the nosyl group. After filtration the resulting product was subjected to Boc cleavage in the presence of HCl 4 M in dioxane. The cleavage of the two protecting groups and the reduction of the nitro function of the nosyl group afforded the deprotected compound **3.5** which, after purification by crystallization in MeOH and diethyl ether, was used for the evaluation of its aggregation inhibitory activity.

3.2.5 Synthesis of the Boc scaffold 3.20

As we saw in the previous paragraph, the conditions necessary for the removal of the nosyl group are too strong for a deprotection at the last step of the synthesis of a β-hairpin mimic. From this evidence, we perceived the need to provide the deprotection directly on the scaffold and subsequently to carry out the protection with an orthogonal easier to remove protecting group, such as the *tert*-butyloxycarbonyl group.

However, during the deprotection of the nosyl group under microwaves we observed the formation of a cyclised byproduct, due to the reaction

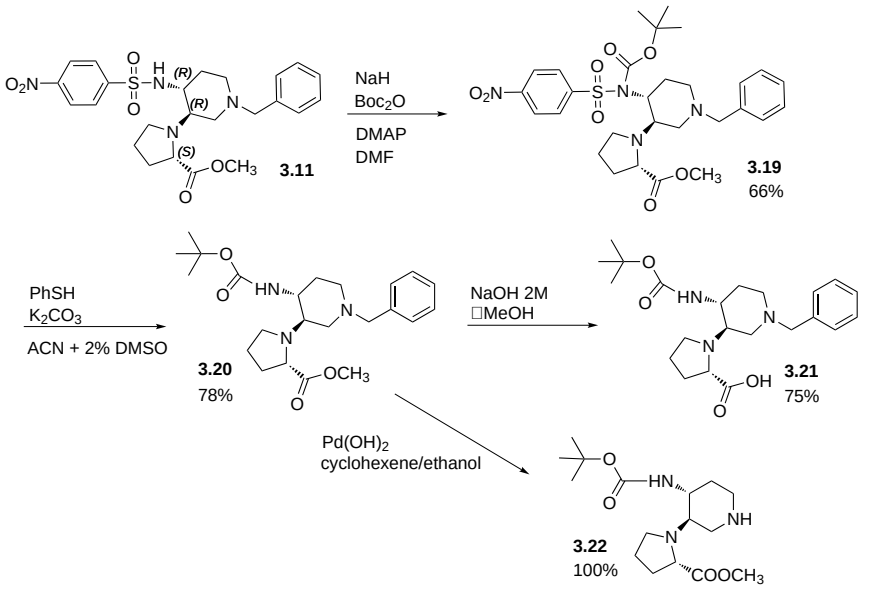

Figure 3.12: Synthetic scheme of the Boc scaffolds **3.21** and **3.22**

between the free primary amine of the piperidine ring and the methyl ester of the proline. This byproduct, together with a loss of material during the purification step and a poor reproducibility, makes this reaction one limiting step for the overall yield of the synthesis of β-hairpin mimics.

In literature, we found that the prior conversion of the nosylamides to the Boc-nosylimide derivate activates the nosyl group towards attack and cleavage by thiophenol [201], probably making easier the deprotection, without the aid of microwaves. So, we first tried to react the nosyl scaffold **3.10** with the di-*tert*-butyl dicarbonate in DMF in the presence of DMAP, but we didn't obtain the corresponding Boc-nosylimide derivate. By adding 1.1 eq. of sodium hydride to the solution of scaffold in DMF and successively 1.1 eq. of di-*tert*-butyl dicarbonate and DMAP and letting the reaction mixture stirring overnight, we succeeded to obtain the Boc intermediate compound **3.19** in 66 % yield (Figure 3.12).

The nosyl group of compound **3.19** could be cleaved under mild condition, with thiophenol (1.5 eq.) and potassium carbonate (3.0 eq.) in acetonitrile and 2 % DMSO and by warming at 70 °C, to afford compound **3.20**. The yield of the reaction resulted much more better (78 %) compared to the reaction without the addition of DMSO to the reaction mixture (35 %) (Figure 3.12).

Thanks to these two steps, we managed to get a new scaffold with three perfectly orthogonal protecting groups: a Boc group which can be easily cleaved in acidic conditions, a benzyl group that can be removed by hydrogenolysis and finally a methyl ester that can be hydrolyzed in basic

conditions.

Compound **3.20** was hydrolyzed by using 2.5 eq. of NaOH 2 M in MeOH at reflux overnight, to afford the free acid scaffold **3.21** in 75 % yield (Figure 3.12).

As we saw in paragraph, the classical hydrogenolysis procedure of **3.20** with hydrogen and Pd/C 10 % didn't allow to obtain the free secondary amine of the scaffold. We got a great result of deprotection when we employed the transfer hydrogenation method described by Kende *et al.* [209]. Catalytic transfer hydrogenation has been successfully applied for removal of the benzyl group, using cyclohexene as the hydrogen donor. We performed the reaction with the Pearlman's catalyst (20 % $Pd(OH)_2$/C) and cyclohexene in ethanol (1/1 volume), by stirring overnight at reflux. We obtained the deprotected compound **3.22** in quantitative yield (Figure 3.12).

3.2.6 Synthesis of compounds 3.3 and 3.4

For the synthesis of compound **3.3** and **3.4**, we decided to begin from the upper dipeptide arm, in order to develop a synthetic pathway that would allow to maintain the dipeptide sequence and vary the type of peptidomimetic arm.

The construction of the upper peptide arm was performed via solution peptide synthesis. For each coupling step, we used HATU and HOAt (2.0 eq.) as coupling reagents and collidine (6.0 eq.) as base. The first amino acid (Val) was coupled to compound **3.22**, providing the product **3.23** in 58 % yield. After cleavage of the Fmoc group of **3.23** with a solution of 20 % piperidine in DMF, the second amino acid (Ala) was coupled using the same coupling procedure, to afford compound **3.24** in 69 % yield (Figure 3.13).

The saponification of compound **3.24** with 5.0 eq. of NaOH 2 M in MeOH at 60 °C for 2 hours afforded product **3.25** in 92 % yield (Figure 3.13).

The coupling reaction between the β-strand mimic **3.6** and compound **3.25**, by using HATU and HOAt, didn't provide the desired final product. Satisfactory results were obtained when we used the triazine-based reagent DMTMM (1.1 eq.) in the presence of NMM (4.0 eq.) in DMF. In this way, the coupling product **3.23** was obtained in 61 % yield (Figure 3.13).

The final β-hairpin compound **3.26** was deprotected with the classical procedure described for the previous β-hairpin mimics. The two Cbz protecting groups were cleaved by hydrogenolysis using Pd/C 10 % and hydrogen in MeOH, to afford the first final compound **3.3** with the Boc protected group. Compound **3.3** was prepared as an acetate salt which, after purification by crystallization in MeOH and diethyl ether, was used for the evaluation of its aggregation inhibitory activity.

Finally, product **3.3** was subjected to Boc cleavage in the presence of HCl 4 M in dioxane to afford the other final compound **3.4**, completely deprotected. The tetrahydrochloride salt of compound **3.4** was purified by crystallization

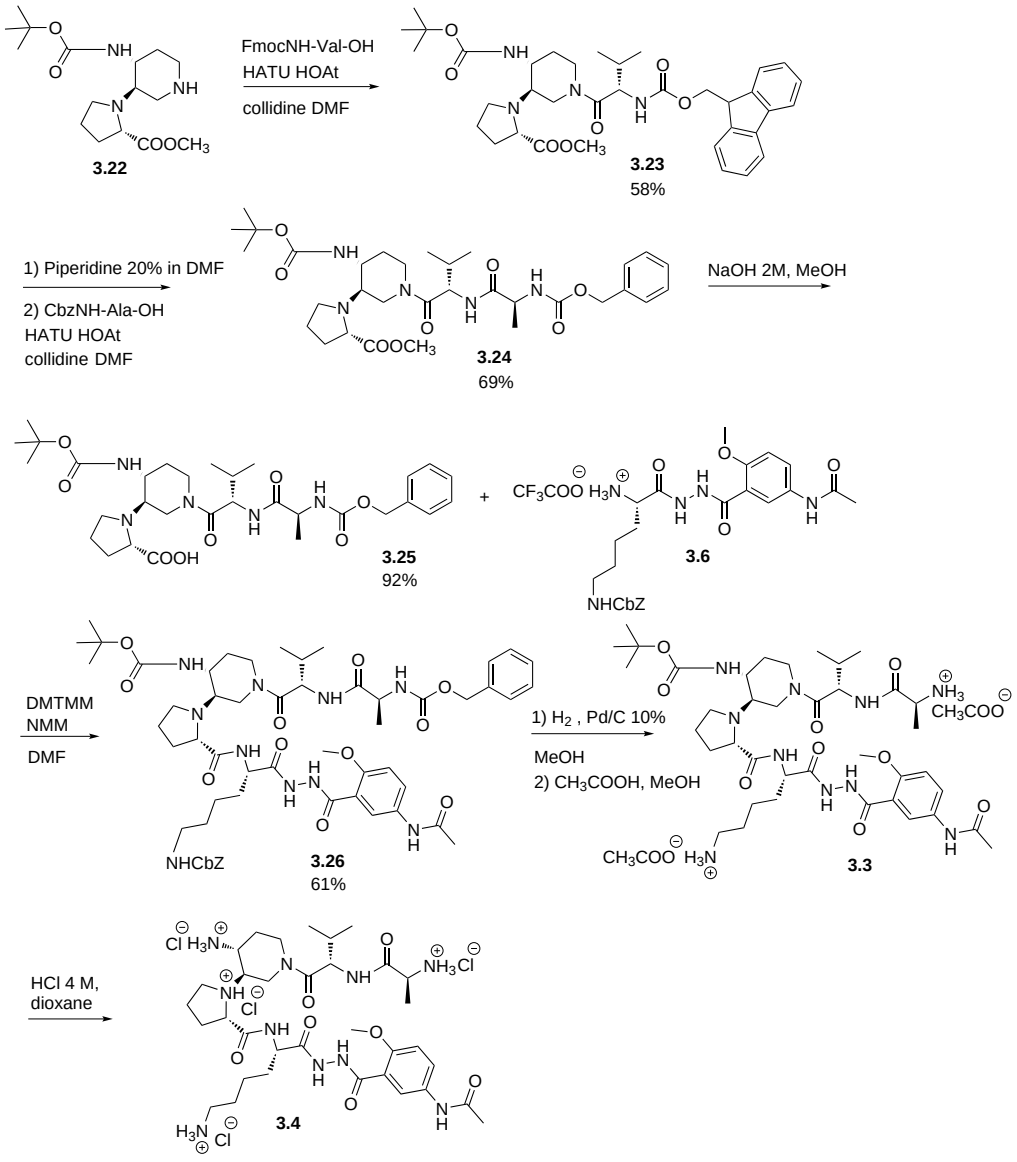

Figure 3.13: Synthetic scheme of the β-hairpin mimics **3.3** and **3.4**

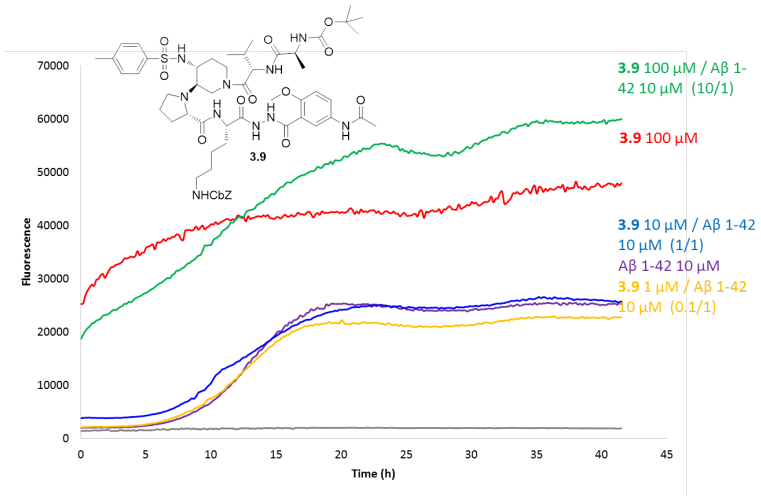

Figure 3.14: Representative ThT curves of protected hairpin **3.9**

in MeOH and diethyl ether and used for the evaluation of its aggregation inhibitory activity.

3.3 Evaluation of the β-hairpin mimics

The compounds synthesized in this chapter were tested using the Thioflavin T (ThT) fluorescence assay to validate their ability to inhibit the Aβ 1-42 peptide aggregation. All types of compounds were investigated: fully protected final products, partially deprotected intermediates and totally deprotected structures at different *ratios*.

We report in this part a brief description of structure-activity relationship (SAR) of synthesized compounds and Aβ 1-42 peptide. The parameters that we used to evaluate the activity of the molecules are the same already described in Chapter 2 (paragraph 2.5.1): the time at which the half maximal ThT fluorescence is observed and the fluorescence intensity at the plateau. The first parameter gives insight on the rate of the aggregation process and the second one is assumed to be dependent on the amount of fibrillar material formed.

Compounds 3.9, 3.27 and 3.1 The complete β-hairpin **3.9**, bearing the N-Boc terminal protected dipeptide Val-Ala and the N$_\zeta$-Cbz-Lys seems to self-aggregate at a concentration of 100 µM, forming organized structures able to bind ThT dye in control experiments (see the red curve, Figure 3.14). We cannot say anything about the activity at the 10:1 (**3.9**:Aβ 1-42) *ratio*, due to this self-aggregation process. At the other two lower *ratios* (1:1 and

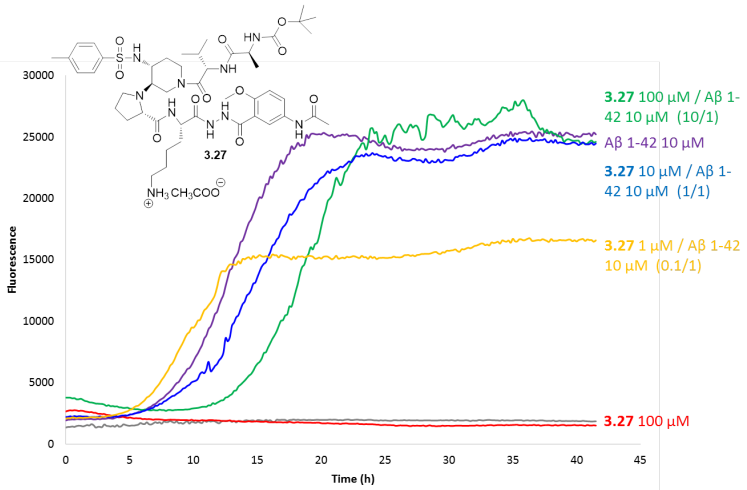

Figure 3.15: Representative ThT curves of partially deprotected hairpin **3.27**

0.1:1) compound **3.9** does not significantly affect the aggregation process.

The intermediate compound **3.27**, deriving from the hydrogenolysis of **3.9**, demonstrated the ability to slightly slow down the kinetics of aggregation of Aβ 1-42 peptide at 10:1 (**3.27**:Aβ 1-42) *ratio* (see the green curve, Figure 3.15). It increases the half-time by a factor of 1.59 with no effect on the fluorescence plateau. At the same time we observed a concentration dependence of the activity, because the same compound at 1:1 (**3.27**:Aβ 1-42) *ratio* is able to increase the half-time by a factor of 1.23 with no effect on the fluorescence plateau. The same compound at 0.1:1 *ratio* displays no effect.

Once the Boc moiety was cleaved, the fluorescence result became different from the protected compound, as we expected, revealing a more significant activity of the designed β-hairpin **3.1**. At the 10:1 (**3.1**:Aβ 1-42) *ratio* (see the green curve, Figures 3.16), the Aβ 1-42 fibrillization is inhibited. Compound **3.1** increases the half-time by a factor of 1.76 and decreases the fluorescence plateau of 66 %. The same compound at 1:1 (**3.1**:Aβ 1-42) *ratio* (see the blue curve, Figures 3.16) is still able to increase the half-time by a factor of 1.36 with a decreasing effect on the fluorescence plateau of 38 %. At 0.1:1 *ratio* (see the yellow curve, Figures 3.16), it displays only an effect on the fluorescence plateau with a value comparable to the previous *ratio*.

We also tried to evaluate the inhibitory activity at an intermediate *ratio* in order to see the effect of compound **3.1** on the kinetics profile of Aβ 1-42 at a concentration of less than 100 µM. As we can see in Figure 3.17, compound **3.1** at a 5:1 (compound:Aβ 1-42) *ratio* is already able to significantly delay the aggregation process of the peptide: we observed an increasing of the half-time by a factor of 1.28 with a decreasing effect on the fluorescence plateau of 27 %.

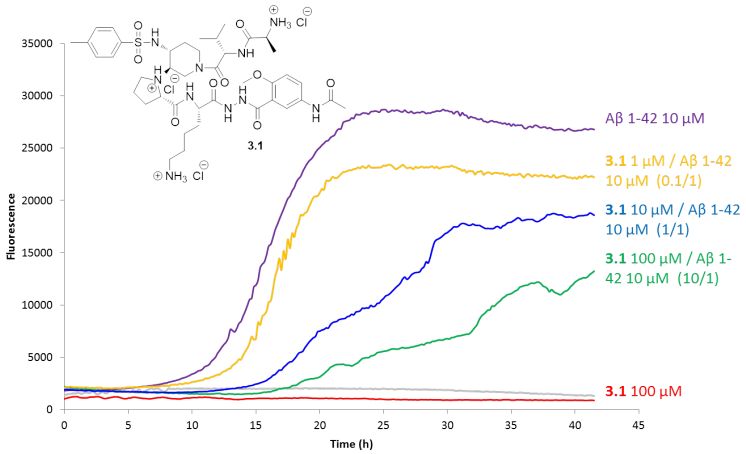

Figure 3.16: Representative ThT curves of totally deprotected hairpin **3.1**

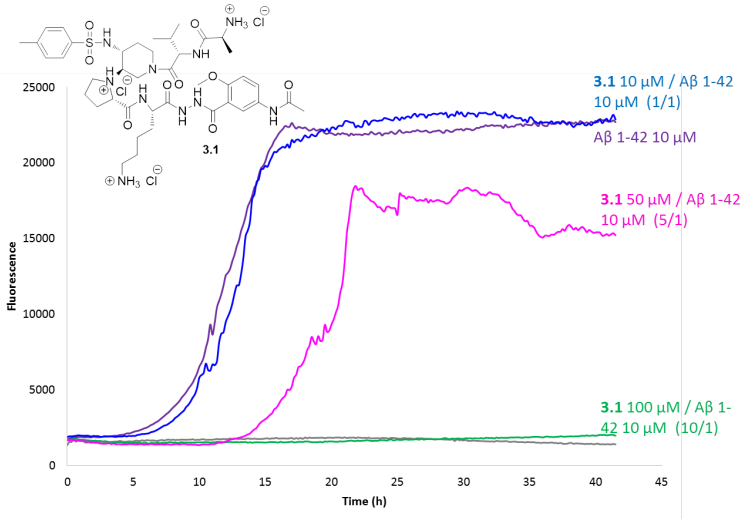

Figure 3.17: Representative ThT curves of deprotected hairpin **3.1** at 5:1 (compound:peptide) *ratio*

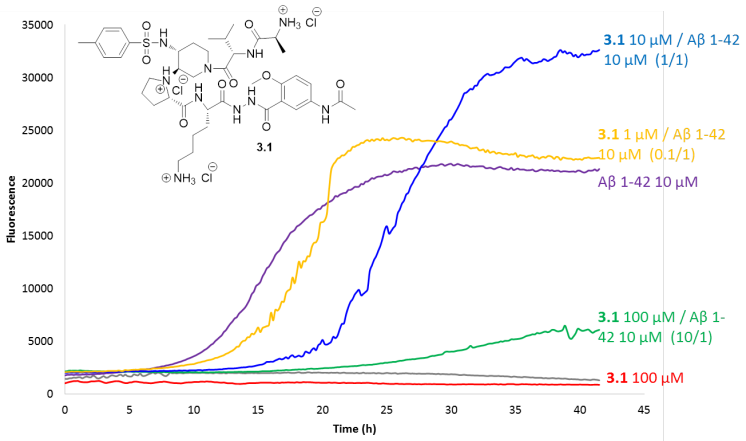

Figure 3.18: Representative ThT curves of totally deprotected hairpin **3.1** in water

Taking into account the solubility of the compound **3.1** in water, we decided to perform the analysis in an aqueous environment in order to get as close as possible to the physiological conditions. As we can see from Figure 3.18, compound **3.1** is able to maintain its activity even in water. We can observe that at the 10:1 (**3.1**:Aβ 1-42) *ratio* increases the half-time by a factor of 1.96 and decreases the fluorescence plateau of 81 %. The same compound at 1:1 (**3.1**:Aβ 1-42) *ratio* increases the half-time by a factor of 1.65 with an increasing effect on the fluorescence plateau of 43 %. At 0.1:1 *ratio*, compound **3.1** displays no effect.

So, thanks to these results, we can conclude that compound **3.1** is the most promising molecule which demonstrated its ability to inhibit the aggregation process of Aβ 1-42 peptide. Compared to the other two partially and totally protected analogues, we can notice that the possibility to engage electrostatic interactions with the peptide is an important feature to increase the affinity of the β-hairpin mimic towards Aβ 1-42.

However, if we compared the activity of compound **3.1** with that of the β-hairpin mimics, bearing the rationally designed peptide sequences, described in Chapter 2, we can notice a decrease in activity which we can explain as a consequence of the replacement of the peptide sequences. Probably, the rationally peptide sequences that we chose for the peptide β-hairpin mimics are important for the affinity and the interaction with the Aβ 1-42 peptide. On the contrary, the peptidomimetic and the dipeptide arms of compound **3.1** reduce the affinity and so the inhibitory activity.

This molecule, showing intermediate characteristics between the series of glycopeptidomimetics and that of peptide compounds, described in Chapter 2, has been proved to maintain a discrete activity together with characteristics

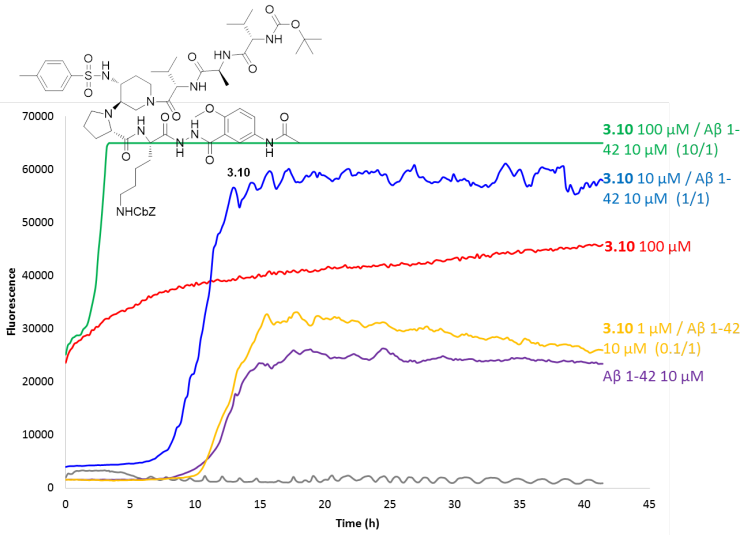

Figure 3.19: Representative ThT curves of protected hairpin **3.10**

of stability, lower molecular weight and solubility in water, that make it a good pharmaceutical candidate.

We are in front of a molecule that could have a higher stability against protease: more investigation about its enzymatic stability and its cell toxicity could bring much more information, useful to better compare it with the peptide analogues. If the tests will provide positive results, the loss of activity would be rewarded by a greater stability, a lower molecular weight and a hydrophilicity/ hydrophobicity balance, comparable to peptide analogues, that allows a good solubility in water without losing the hydrophobic character needed to pass through the blood brain membrane and to establish hydrophobic interactions. We established a similar hydrophilicity/hydrophobicity balance between the peptide analogues **2.2** and **2.4** and compound **3.1**, by comparing the LC-MS retention times, calculated with the same analytical conditions (XBridge C18, water + 0.1 % formic acid/acetonitrile gradient 5–100 % in 20 minutes). Compound **3.1** showed a retention time of 10.08 min, while the peptide analogues **2.2** and **2.4** displayed a retention time of 12.39 min and 12.62, respectively.

Compounds 3.10 and 3.2 The β-hairpin **3.10**, bearing the N-Boc terminal protected tripeptide Val-Ala-Val and the N_ζ-Cbz-Lys seems to self-aggregate at a concentration of 100 µM, forming organized structures able to bind ThT dye in control experiments (see the red curve, Figure 3.19). We cannot say anything about the activity at the 10:1 and 1:1 (**3.10**:Aβ 1-42) *ratios*, due to this self-aggregation process. On the other hand, at the

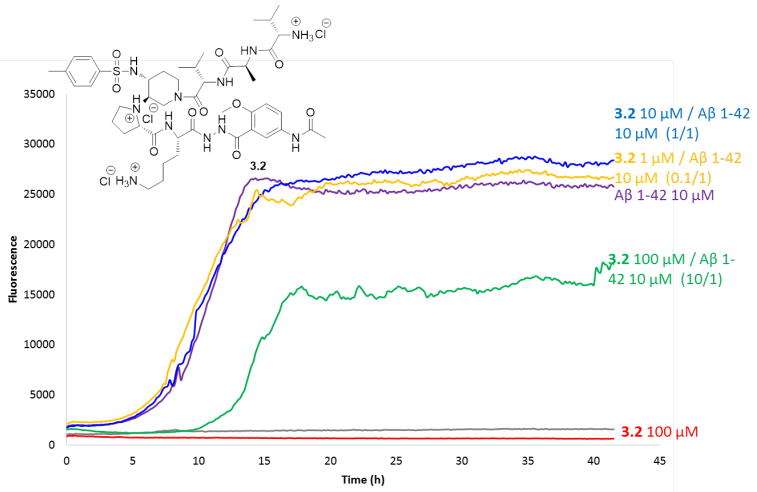

Figure 3.20: Representative ThT curves of totally deprotected hairpin **3.2**

lower 0.1:1 *ratio*, compound **3.10** does not significantly affect the aggregation process.

Once all the protecting groups were cleaved, compound **3.2** is slightly active at 10:1 *ratio* (Figure 3.20), with an increasing of the half-time by a factor of 1.30 and a decreasing effect on the fluorescence plateau of 32 %. Compound **3.2** is completely inactive at the other lower *ratios*.

Also in this case, having regard to the solubility of compound **3.2** in water, the ThT assay was performed in acqueous medium. The results were confirmed with a slight activity at 10:1 *ratio* (increasing of the half-time by a factor of 1.58 and decreasing effect on the fluorescence plateau of 35 %) (Figure 3.21) and no effect at the other lower *ratios*.

This result showed that the simple elongation of the peptide chain of an amino acid can affect the activity of our molecule, probably due to an influence on the structural conformation of the molecule itself (see conformational studies of this chapter).

Compounds 3.26, 3.3 and 3.4 The protected β-hairpin **3.26**, bearing the N-Cbz terminal protected dipeptide Val-Ala, the N_ζ-Cbz-Lys and the Boc protecting group on the scaffold, seems to self-aggregate at a concentration of 100 µM, forming organized structures able to bind ThT dye in control experiments (see the red curve, Figure 3.20). We cannot say anything about the activity at the 10:1 (compound:Aβ 1-42) *ratio*, due to this self-aggregation process. At the other two *ratios* (1:1 and 0.1:1) compound **3.26** does not significantly affect the aggregation process. Compound **3.26** behaves in the same way of the tosyl analogues **3.9** and **3.10**.

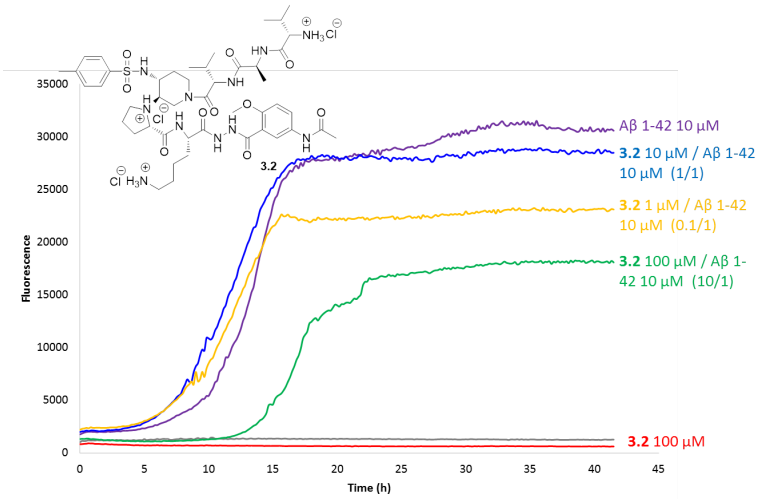

Figure 3.21: Representative ThT curves of totally deprotected hairpin **3.2** in water

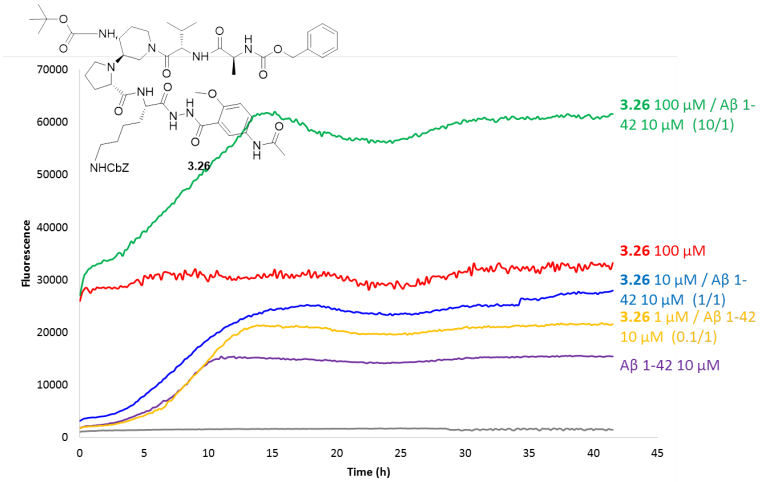

Figure 3.22: Representative ThT curves of protected hairpin **3.26**

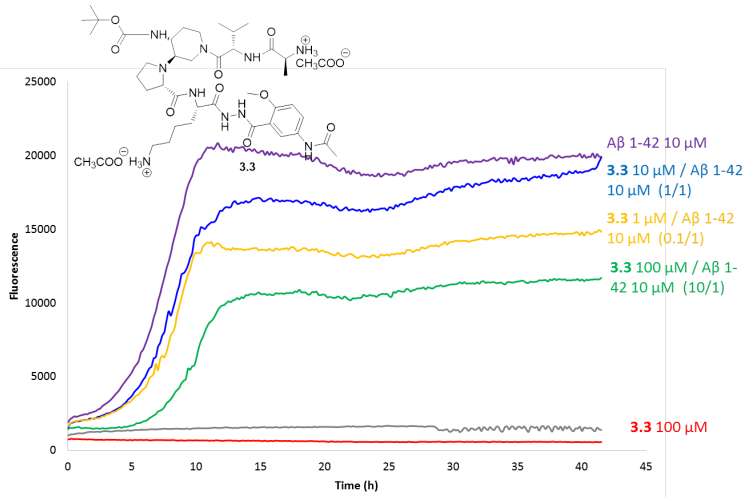

Figure 3.23: Representative ThT curves of deprotected hairpin **3.3** with the Boc on the primary amine

Surprisingly, when we cleaved the two protecting Cbz groups of compound **3.26** in order to establish ionic interactions with the Aβ 1-42 peptide, we noticed that the analogue **3.3** with the Boc scaffold was no longer able to inhibit the aggregation process at the same *ratio*, as compound **3.1** (Figure 3.23). Compound **3.3** is slightly active at 10:1 *ratio* (Figure 3.23), with an increasing of the half-time by a factor of 1.29 and a decreasing effect on the fluorescence plateau of 43 %. At 1:1 *ratio*, it is still able to increase the half-time by a factor of 1.13, but without effect on the fluorescence plateau. No activity was observed at the lower 0.1:1 *ratio*.

This result demonstrated that the simple replacement of the tosyl group by a Boc can affect the activity of the molecule. Probably, the tosyl group is important to establish other hydrophobic interactions, such as π-stacking, that increase the affinity of the molecule for Aβ 1-42 peptide.

The same result was obtained, when we cleaved the Boc protecting group of the scaffold. Compound **3.4** demonstrated to be completely inactive at all *ratios* (Figure 3.24). We observed only a very slight activity at 10:1 *ratio*, at which compound **3.4** is able to increase the half-time by a factor of 0.90 and to decrease the fluorescence plateau of 18 %.

Surprisingly, the tosyl group demonstrated to be important for the inhibitory activity, probably thanks to its ability to perform π-stacking interactions. Our objective was to see if we were able to maintain the activity without this protecting group which is very difficult to remove and so, probably, extremely stable from a metabolic point of view. The aim was also to have the possibility to functionalize the free primary amine of

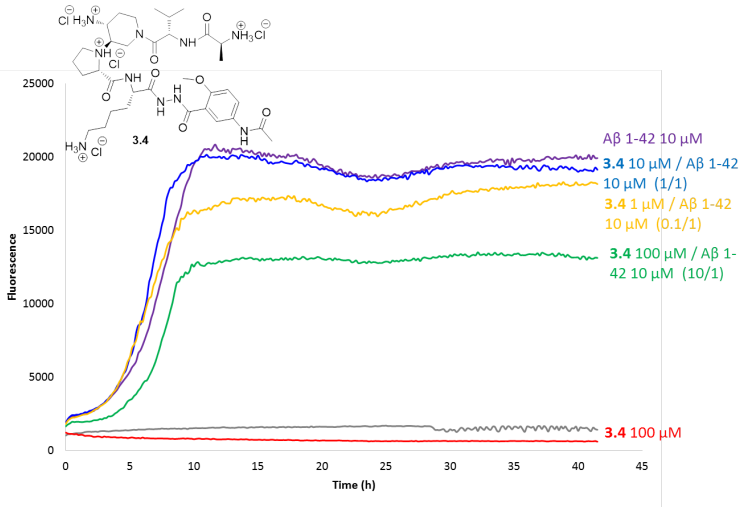

Figure 3.24: Representative ThT curves of totally deprotected hairpin **3.4**

the piperidine ring with a chromophore to perform localization studies or a cell penetrating sequence to increase the bioavailability. Due to the lack of time, we could not achieve this latter objective. Between the perspectives it remains to try to see if through a chromophore, generally characterized by aromatic rings, it is possible to restore the activity, by maintaining the ability to perform hydrophobic interactions but at the same time allowing to make localization studies.

Since in the glycopeptidomimetic series we had shown that the presence of the hydrophilic sugar, considered as a β-sheet breaker element, was important to prevent the cross-β-sheet elongation of Aβ 1-42, we were led to think that compound **3.4** could act in the same way, due to the presence of a protonated and polar primary amine together with the protonated nitrogen of the proline residue, which could make the scaffold an hydrophilic β-sheet breaker element. The absence of activity well demonstrated that this scaffold, as it was conceived, acts as a β-turn inducer instead of as a β-sheet breaker.

Compound 3.5 We decided to evaluate the deprotected β-hairpin **3.5** bearing a p-aminobenzensulfonamide, in order to study the effect on the inhibitory activity of the replacement of the methyl group of the aromatic ring by a primary amine. Compound **3.5** maintained an inhibitory activity however to a 10:1 (**3.5**:Aβ 1-42) *ratio*: we observed an increasing of the half-time by a factor of 1.53 and a decreasing of 46 % of the fluorescence plateau (Figure 3.25). Compared to compound **3.1**, for which we observed a significant and more pronounced inhibititon activity at the same *ratio*, we can notice that **3.5** is less active. This result demonstrated that compound

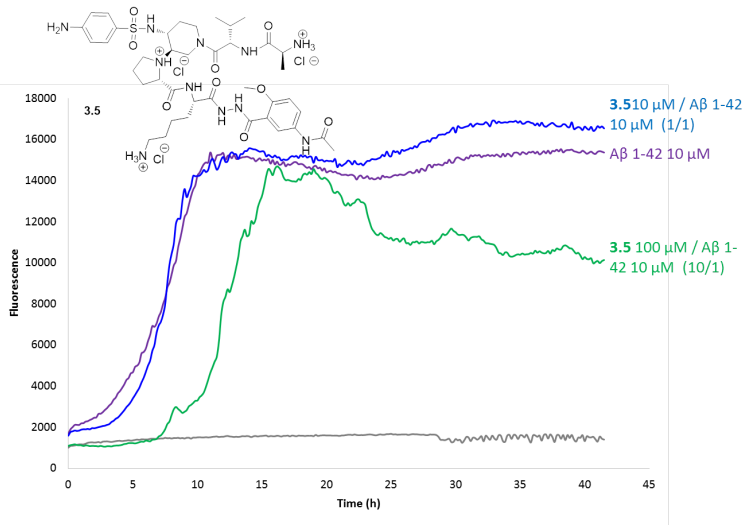

Figure 3.25: Representative ThT curves of deprotected hairpin **3.5**

3.5 has still the possibility to establish hydrophobic interactions, such as π-stacking, but the presence of a polar group on the aromatic ring destabilizes this interaction and so affect the inhibitory activity of the molecule.

3.4 Conformational analysis of the β-hairpin mimics 3.1 and 3.2

In this section, we report the conformational studies of compounds **3.1** and **3.2**. The analysis were conducted in a protic solvent, which is more challenging for intramolecular hydrogen bond formation in comparison with aprotic organic solvents such as chloroform. We used water in order to study the conformation of our molecules in a medium that is the closest as possible to the physiological conditions. Through these studies, we tried to identify the possible reason for the marked difference in activity between the two compounds.

Compound 3.1 Proton NMR spectra were recorded on a spectrometer operating at 600 MHz, equipped with a cryoprobe (ICSN, Institut de Chimie des Substances Naturelles, Gif-sur-Yvette). ^{1}H and ^{13}C resonances were completely assigned using 1D ^{1}H WATERGATE, 2D ^{1}H-^{1}H TOCSY (duration 30 ms or 100 ms), 2D ^{1}H-^{1}H ROESY (200 ms mixing time), 2D ^{1}H-^{13}C HSQC and 2D ^{1}H-^{13}C HMBC spectra, recorded at 278 K and 298 K. ^{1}H and ^{13}C chemical shifts were calibrated using the solvent residual peak (H_2O/D_2O, δ ^{1}H 4.80 ppm). The chemical shifts deviations were calculated

Residue	δ NH (ppm)	δ H_α (ppm)	δ H_β (ppm)	δ other protons (ppm)	δ CO (ppm)	δ C_α (ppm)	δ C_β (ppm)	δ other carbons (ppm)
Ala	7.93 (7.89)	3.89	1.25 (1.18)	/	170.6 (170.4)	48.6	16.5 (16.4)	/
Val	8.45 (8.47)	4.40	1.75 (1.80)	0.62/0.63 (0.71/0.67)	171.5	54.9	29.4 (29.6)	18.3/16.5 (17.8/17.3)
Pro	/	3.55 (3.50)	2.34, 1.95	γ 1.88, 1.73 δ 3.72, 2.93	164.9	51.5 (52.4)	30.1	γ 23.9 δ 43.8
Lys	9.00 (8.92)	4.30 (4.33)	1.77	γ 1.35 δ 1.54 ε 2.83 NH_2 7.42	171.9	52.5 (52.3)	30.3	γ 21.8 δ 26.3 ε 39.1
NH_c-NH_b	10.37, 10.18	/	/	/	/	/	/	/
Amb	9.70 (H_a)	/	/	H_3 6.99 (7.08) H_4 7.35 H_6 7.66 OCH_3 3.76 (3.69)	166.4	/	/	C_1 118.5, C_2 155.1, C_3 112.7, C_4 128.4, C_5 129.8, C_6 124.8 OCH_3 55.9 (55.7)
Acetyl	/	/	/	CH_3 1.96	172.9	/	/	CH_3 22.3
Tosyl	7.76	/	/	CH (Ar) 7.61, 7.27 CH_3 2.22	/	/	/	CH (Ar) 146.6, 135.6, 130.1, 126.5 CH_3 20.5
Piperidine ring	/	/	/	CH_2(2) 4.02, 2.38 CH (3) 2.64 CH (4) 2.79 CH_2(5) 1.22, 1.05 CH_2(6) 4.09, 3.32	/	/	/	CH_2(2) 41.1 CH (3) 31.1 CH (4) 36.7 CH_2(5) 30.1 CH_2(6) 43.9

Table 3.2: ^1H-NMR and ^{13}C-NMR chemical shifts of compound **3.1** in water at 278 K; in brackets the chemical shifts of the minor conformer

Residue	δ NH (ppm)	δ H_α (ppm)	δ H_β (ppm)	δ other protons (ppm)	δ CO (ppm)	δ C_α (ppm)	δ C_β (ppm)	δ other carbons (ppm)
Ala	8.06	4.11	1.46 (1.37)	/	170.7	48.8	16.5 (16.6)	/
Val	8.52 (8.56)	4.60	1.94 (2.02)	0.82/0.83 (0.92/0.87)	171.3	55.1	29.7 (29.9)	18.5/16.7 (18.0/17.4)
Pro	/	3.72 (3.67)	2.50, 2.11	γ 2.06, 1.90 δ 3.93, 3.15	164.9	52.1 (53.0)	30.4	γ 24.1 δ 44.1
Lys	9.09 (9.00)	4.52 (4.56)	1.98	γ 1.53 δ 1.76 ε 3.04 NH_2 7.56	171.9	52.2 (52.1)	30.1	γ 21.8 δ 26.4 ε 39.3
NH_c-NH_b	10.42, 10.31	/	/	/	/	/	/	/
Amb	9.70 (H_a)	/	/	H_3 7.22 (7.29) H_4 7.57 (7.67) H_6 7.88 (7.85) OCH_3 3.96 (3.89)	166.5	/	/	C_1 118.7, C_2 155.1, C_3 112.9 (113.1), C_4 128.4 (126.6), C_5 130.2, C_6 124.7 (124.9) OCH_3 56.3 (56.1)
Acetyl	/	/	/	CH_3 2.18 (2.11)	173.1	/	/	CH_3 22.5 (22.7)
Tosyl	7.95	/	/	CH (Ar) 7.84, 7.47 CH_3 2.44	/	/	/	CH (Ar) 145.6, 135.6, 130.2, 126.7 CH_3 20.6
Piperidine ring	/	/	/	CH (1) 2.85 CH (2) 3.01 CH_2(3) 1.63, 1.48 CH_2(4) 4.23, 3.48 CH_2(6) 4.22, 2.60	/	/	/	CH_2(2) 41.4 CH (3) 31.4 CH (4) 37.0 CH_2(5) 30.4 CH_2(6) 44.2

Table 3.3: ^1H-NMR and ^{13}C-NMR chemical shifts of compound **3.1** in water at 298 K; in brackets the chemical shifts of the minor conformer

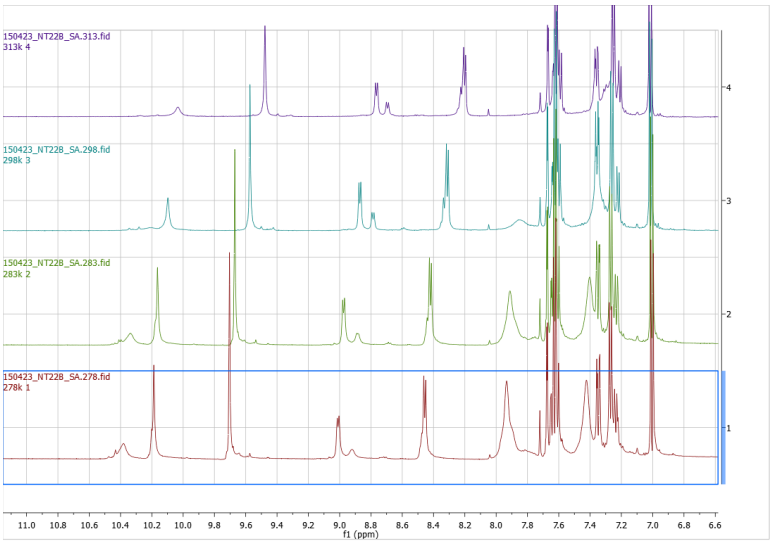

Figure 3.26: 1D ^1H spectra of compound **3.1** at different temperature from 278 K to 313 K

as the differences between observed chemical shifts and random coil values reported by Wishart *et al.* [178]. Vicinal coupling constants were extracted from 1D ^1H spectrum and from 2D ^1H-^1H COSY at 278 K and 298 K. The observed proton and carbon chemical shifts are displayed in Table 3.2 and Table 3.3.

As we can see from the data of Table 3.2, compound **3.1** is present in solution as a mixture of two conformers in 3:1 *ratio*. The dynamic equilibrium between the two conformers was confirmed by the occurance of splitting for some protons: the α-protons of Pro and Lys, the amide protons of Lys and Val and the side chain protons of Val and Ala. However, no negative NH/NH ROEs were detected.

By recording the spectra at different temperatures (Figure 3.26), we noticed that the hydrazide proton NH(b) at higher temperature showed a broad signal and NH(c) was broadened beyond detection, while cooling the sample down to 278 K gave rise to peak sharpening of hydrazide protons and in particular the NH(c) proton could be observed (the numbering of the NH protons is indicated in Figure 3.27). We were not able to get the coalescence between the two forms. Even at 313 K, we detected the splitting of the amide protons of Lys and Val residues and at lower temperature the multiplicity of the amide proton of Lys, corresponding to the minor isomer, became not detectable. The *ratio* between the two conformations remained constant in all the range of temperatures.

To study the eventually presence of intramolecular hydrogen-bonded protons, we examined the temperature dependence of amide proton chemical

Residue	$\Delta\delta/\Delta T$ (ppb K^{-1})
Lys NH	- 6.93
Val NH	- 7.33
NH_a	- 6.33
NH_b	- 4.47
NH_c	- 9.08

Table 3.4: Temperature coefficients for the amide protons of **3.1** major conformer in water

Residue	$\Delta\delta/\Delta T$ (ppb K^{-1})
Lys NH	- 6.33
Val NH	- 6.87

Table 3.5: Temperature coefficients for the Lys and Val amide protons of **3.1** minor conformer in water

shifts, as it can provide information on the network of hydrogen bonds and their relative stabilities.

None of the amide protons of the major isomer showed low temperature coefficients, except for the NH(b) proton that presented the smallest variation and demonstrated to be hydrogen bonded with the methoxy group of the aromatic unit, as already presented by Nowick for the Hao motif (Table 3.4). However, all the other temperature coefficients tended to be slightly higher than expected. In both conformers the temperature coefficients of the Lys and Val amide proton fell within intermediate values, suggesting a partial engagement in intramolecular hydrogen bonds (Table 3.5).

We are probably faced with a dynamic equilibrium between two different β-hairpin conformations, characterized by a weak network of hydrogen bonds that determines the formation of two conformers, one more compact than the other. The intermediate values of the temperature coefficients indicate that these hydrogen bonds are weak and allow the amide protons to exchange quite easily with the solvent: their temperature dependence is more evident at higher temperatures. Hydrogen bonding not only causes a resonance shift to lower field, as we can see for the Lys and Val amide protons in both

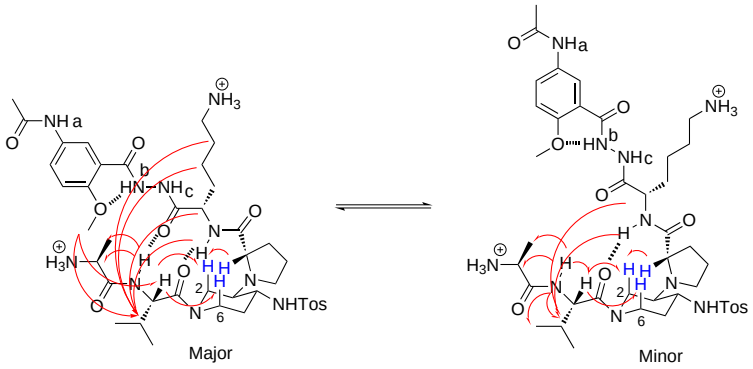

Figure 3.27: Chemical structures of the two conformers of compound **3.1** showing the assigned ROEs by red flashes and the hypothesized hydrogen bonds

conformations, but also decreases the rate of intermolecular proton exchange and allows the exchangeable protons to remain bonded for a sufficient time to exert their spin coupling influence, as we can always observe for the Lys and Val amide protons in the major conformer.

In the ROESY experiments at 278 K, both conformers showed spatial proximity between the α-hydrogen of Val and the two hydrogens in position C2 and C6 of the piperidine ring (Figure 3.27) and an overhauser effect between the α-hydrogen of Pro and the hydrogen in position C2, suggesting that a β-turn conformation was present in both conformers.

We also observed long-range ROEs between the dipeptide and the peptidomimetic arm. The amide proton and the α-hydrogen of Lys were able to see the β-hydrogen of Val in both conformations but only in the major isomer the protons of the Lys side chain and the β-hydrogen of Val faced together and the methoxy group of the benzohydrazide motif made contact with the α-and β-hydrogens of Val. These latter ROEs were not detected for the minor isomer, suggesting that the difference between the two conformers was the proximity of the benzohydrazide motif to the dipeptide sequence. In the major isomer we could notice a more compact β-hairpin conformation, while in the minor isomer we observed a more open structure. This difference is probably due to the rotation around the single NH-NH bond of the diformyl hydrazine motif in the peptidomimetic arm.

Strong sequential and medium intraresidual ROEs, which are characteristic of an extended backbone conformations, were detected for the dipeptide sequence.

By recording the conformational studies at 298 K, we obtained the same long-range ROEs observed at 278 K and the same differences between the two conformers.

Major conformer

AA	δ NH$^{\alpha}$ random coil	δ NH$^{\alpha}$ experimental	Δ NH	$^{3}J_{HN/H\alpha}$ random coil	$^{3}J_{HN/H\alpha}$ experimental	Δ *J*	δ H$^{\alpha}$ random coil	δ H$^{\alpha}$ experimental	Δ H$^{\alpha}$
Val	8.03	8.45	+ 0.42	7.7	7.6	- 0.1	4.12	4.40	+ 0.28
Ala	8.24	7.93	- 0.31	5.8	8.4	+ 2.3	4.32	3.89	- 0.43
Lys	8.29	9.00	+ 0.71	7.1	7.3	+ 0.2	4.32	4.30	- 0.02
Pro	/	/	/	/	/	/	4.42	3.55	- 0.87

AA	δ CH$^{\alpha}$ random coil	δ CH$^{\alpha}$ experimental	Δ CH$^{\alpha}$	δ C=O random coil	δ C=O experimental	Δ C=O
Val	62.2	54.9	- 7.3	176.3	171.5	- 4.8
Ala	52.5	48.6	- 3.9	177.8	170.6	- 7.2
Lys	56.2	52.5	- 3.7	176.6	171.9	- 4.7
Pro	63.3	52.5	- 10.8	177.3	164.9	- 12.4

Minor conformer

AA	δ NH$^{\alpha}$ random coil	δ NH$^{\alpha}$ experimental	Δ NH	$^{3}J_{HN/H\alpha}$ random coil	$^{3}J_{HN/H\alpha}$ experimental	Δ *J*	δ H$^{\alpha}$ random coil	δ H$^{\alpha}$ experimental	Δ H$^{\alpha}$
Val	8.03	8.47	+ 0.44	7.7	9.0 Hz	+ 1.3	4.12	4.40	+ 0.28
Ala	8.24	7.89	- 0.35	5.8	10.8 Hz	+ 5.0	4.32	3.89	- 0.43
Lys	8.29	8.92	+ 0.63	7.1	12.0 Hz	+ 4.9	4.32	4.33	+ 0.01
Pro	/	/	/	/	/	/	4.42	3.50	- 0.82

AA	δ CH$^{\alpha}$ random coil	δ CH$^{\alpha}$ experimental	Δ CH$^{\alpha}$	δ C=O random coil	δ C=O experimental	Δ C=O
Val	62.2	54.9	- 7.3	176.3	171.5	- 4.8
Ala	52.5	48.6	- 3.9	177.8	170.4	- 7.4
Lys	56.2	52.3	- 3.9	176.6	171.9	- 4.7
Pro	63.3	52.4	- 10.9	177.3	164.9	- 12.4

Table 3.6: Chemical shift deviations (CSD) of aliphatic residues and coupling constants for NH protons at 278 K of the two conformers of compound **3.1** in water

Major conformer

AA	δ NH$^{\alpha}$ random coil	δ NH$^{\alpha}$ experimental	Δ NH	$^{3}J_{HN/H\alpha}$ random coil	$^{3}J_{HN/H\alpha}$ experimental	Δ *J*	δ H$^{\alpha}$ random coil	δ H$^{\alpha}$ experimental	Δ H$^{\alpha}$
Val	8.03	8.52	+ 0.49	7.7	7.8	+ 0.1	4.12	4.60	+ 0.48
Ala	8.24	8.06	- 0.18	5.8	/	/	4.32	4.11	- 0.21
Lys	8.29	9.09	+ 0.80	7.1	7.5	+ 0.4	4.32	4.52	+ 0.20
Pro	/	/	/	/	/	/	4.42	3.72	- 0.70

AA	δ CH$^{\alpha}$ random coil	δ CH$^{\alpha}$ experimental	Δ CH$^{\alpha}$	δ C=O random coil	δ C=O experimental	Δ C=O
Val	62.2	55.1	- 7.1	176.3	170.7	- 5.6
Ala	52.5	48.8	- 3.7	177.8	171.3	- 6.5
Lys	56.2	52.2	- 4.0	176.6	171.9	- 4.7
Pro	63.3	52.1	- 11.2	177.3	164.9	- 12.4

Minor conformer

AA	δ NH$^{\alpha}$ random coil	δ NH$^{\alpha}$ experimental	Δ NH	$^{3}J_{HN/H\alpha}$ random coil	$^{3}J_{HN/H\alpha}$ experimental	Δ *J*	δ H$^{\alpha}$ random coil	δ H$^{\alpha}$ experimental	Δ H$^{\alpha}$
Val	8.03	8.56	+ 0.49	7.7	11.5	+ 3.8	4.12	4.60	+ 0.48
Ala	8.24	8.06	- 0.18	5.8	/	/	4.32	4.11	- 0.21
Lys	8.29	9.00	+ 0.71	7.1	8.0	+ 0.9	4.32	4.56	+ 0.24
Pro	/	/	/	/	/	/	4.42	3.67	- 0.75

AA	δ CH$^{\alpha}$ random coil	δ CH$^{\alpha}$ experimental	Δ CH$^{\alpha}$	δ C=O random coil	δ C=O experimental	Δ C=O
Val	62.2	55.1	- 7.1	176.3	170.7	- 5.6
Ala	52.5	48.8	- 3.7	177.8	171.3	- 6.5
Lys	56.2	52.1	- 3.9	176.6	171.9	- 4.7
Pro	63.3	53.0	- 10.3	177.3	164.9	- 12.4

Table 3.7: Chemical shift deviations (CSD) of aliphatic residues and coupling constants for NH protons at 298K of the two conformers of compound **3.1** in water

The vicinal $J_{NH-H\alpha}$ coupling constant also yields direct information on the main chain φ dihedral angle, through the Karplus relationship. For the major folded isomer, the coupling constants exhibited values between 7.4 Hz and 8.7 Hz and positive difference between $J_{NH-H\alpha}$ values in the random coil and the values determined experimentally were found, reflecting φ angle values around $-120°$, as expected for extended conformation (Figure 3.6 and Figure 3.7) [177].

Interestingly, for the minor conformation, the $J_{NH-H\alpha}$ value for the Val, Ala and Lys residues resulted higher than in the major conformer, suggesting a more extended conformation of the dipeptide sequence. We hypothesized that in the major β-hairpin conformer an adaptation of the peptide chain to the peptidomimetic, due to an increased interaction, occurs. This is proved by the interaction between the side chain of the Lys residue and that of the Val, which was not observed in the minor conformer. When the conformation is more open, the fact of not having this interaction is reflected in a greater extension.

Chemical shift deviations (CSD) are defined as the difference between experimental chemical shifts and corresponding random coil values and are considered good descriptors of backbone conformational space for each residue. We calculated the CSD for all the natural amino acids present in the molecule (Table 3.6 and Table 3.7) and we observed that, for both the conformers, the α-carbon and the carbonyl group were upfield shifted (negative CSD), indicating that an extended conformation for the peptide and peptidomimetic arms predominate. The negative values of the α-hydrogen of Pro indicated the turn region of the molecule, while the negative values for the amide proton and the α-hydrogen of Ala suggested some flexibility at the N-terminal amine of the molecule. The other two amino acids Val and Lys, more implicated in the β-hairpin structure, were characterized by downfield shifted α-hydrogens and amide protons (positive CSD).

Compound 3.2 Proton NMR spectra were recorded on a spectrometer operating at 800 MHz, equipped with a cryoprobe (ICSN, Institut de Chimie des Substances Naturelles, Gif-sur-Yvette). ^1H and ^{13}C resonances were completely assigned using 1D ^1H WATERGATE, 2D ^1H-^1H TOCSY (duration 30 ms or 100 ms), 2D ^1H-^1H ROESY (300 ms mixing time), 2D ^1H-^{13}C HSQC and 2D ^1H-^{13}C HMBC spectra, recorded at 283 K. ^1H and ^{13}C chemical shifts were calibrated using the solvent residual peak (H_2O/D_2O, δ ^1H 4.80 ppm). The chemical shifts deviations were calculated as the differences between observed chemical shifts and random coil values reported by Wishart *et al.* [178]. Vicinal coupling constants were extracted from 1D ^1H spectrum and from 2D ^1H-^1H COSY at 283 K. The observed proton and carbon chemical shifts are displayed in Table 3.8.

As we can see from the data of Table 3.8, compound **3.2** is present in

Residue	δ NH (ppm)	δ H_α (ppm)	δ H_β (ppm)	δ other protons (ppm)	δ CO (ppm)	δ C_α (ppm)	δ C_β (ppm)	δ other carbons (ppm)
Val1	7.82	3.49	1.91	0.73/0.63	169.0	58.3	29.9	17.3/16.6
Ala	8.46 (8.41)	4.12 (4.07)	1.05 (1.19)	/	170.1	49.3 (49.6)	16. 3 (16.5)	/
Val2	8.18 (8.09)	4.25 (4.33)	1.67 (1.72)	0.57/0.54 (0.64/0.59)	171.6	54.6 (54.7)	29.8 (30.1)	18.4/16.9 (18.0/17.3)
Pro	/	3.47 (3.41)	2.26, 1.71	γ 1.81, 1.65 δ 3.64, 2.83	170.8	51.5 (52.6)	30.1	γ 23.8 δ 43.6
Lys	8.89 (8.87)	4.24	1.72	γ 1.28 δ 1.49 ε 2.76 NH_2 7.33	171.8	52.4	30.1	γ 21.9 δ 26.3 ε 39.2
NH_c-NH_b	10.27, 10.09	/	/	/	/	/	/	/
Amb	9.59 (H_a)	/	/	H_3 6.92 H_4 7.27 H_6 7.59 OCH_3 3.69 (3.64)	166.3	/	/	C_1 118.4, C_2 155.1, C_3 112.7, C_4 128.4, C_5 129.8, C_6 124.7 OCH_3 56.0 (55.8)
Acetyl	/	/	/	CH_3 1.88	172.9	/	/	CH_3 22.5
Tosyl	7.79	/	/	CH (Ar) 7.54, 7.18 CH_3 2.15	/	/	/	CH (Ar) 145.3, 135.3, 130.1, 126.6 CH_3 20.6
Piperidine ring	/	/	/	CH (1) 2.77 CH (2) 3.83 CH_2(3) 1.30, 1.19 CH_2(4) 3.92, 2.29 CH_2(6) 4.34, 2.84	/	/	/	CH_2(2) 39.1 CH (3) 46.8 CH (4) 48.9 CH_2(5) 30.1 CH_2(6) 40.9

Table 3.8: ^1H-NMR and ^{13}C-NMR chemical shifts of compound **3.2** in water at 283 K; in brackets the chemical shifts of the minor conformer

solution as a mixture of two conformers in 4:1 *ratio*. The dynamic equilibrium between the two conformers was confirmed the occurence of splitting for some protons: the α-protons of Pro, Val2 and Ala, the amide protons of Lys, Val2 and Ala and the side chain protons of Val2 and Ala. However, no negative NH/NH ROEs were detected.

By recording the spectra at different temperature (Figure 3.28), we noticed a similar behaviour to compound **3.1**: the hydrazide proton NH(b) at higher temperature showed a broad signal and NH(c) was broadened beyond detection, while cooling the sample down to 278 K gave rise to peak sharpening of hydrazide protons and in particular the NH(c) proton could be observed. We were not able, also in this case, to get the coalescence between the two forms. The *ratio* between the two conformations didn't change with the temperature and the profile of the amide proton signals remained roughly unchanged.

We examined the temperature dependence of amide proton chemical shifts, as it can provide information on the network of hydrogen bonds and their relative stabilities. As we can see in the Table 3.9, none of the amide protons showed low temperature coefficients, except for the NH(b), always engaged in the hydrogen bond with the methoxy group. The profile of temperature coefficients between the two isomers showed to be similar (Table 3.10). Only the Lys and Ala amide protons falls within intermediate values, indicating a partial engagement in intramolecular hydrogen bonds.

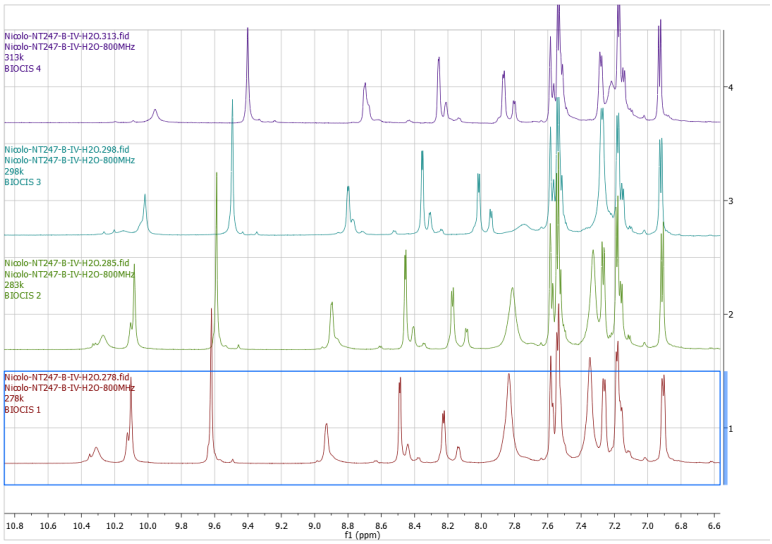

Figure 3.28: 1D ^{1}H spectra of compound **3.2** at different temperature from 278 K to 313 K

Residue	$\Delta\delta/\Delta T$ (ppb K^{-1})
Lys NH	- 6.47
Val(2) NH	- 10.33
Ala NH	- 6.60
NH_a	- 6.33
NH_b	- 4.00
NH_c	- 8.00

Table 3.9: Temperature coefficients for the amide protons of **3.2** major conformer in water

Residue	$\Delta\delta/\Delta T$ (ppb K^{-1})
Lys NH	- 6.33
Val(2) NH	- 9.40
Ala NH	- 6.60

Table 3.10: Temperature coefficients for the Lys and Val amide protons of **3.2** minor conformer in water

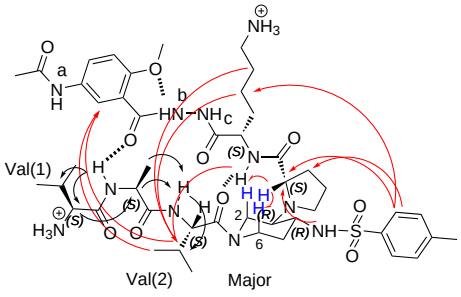

Figure 3.29: Chemical structures of the major conformer of compound **3.2** showing the assigned long-range ROEs by red flashes and intraresidual ROEs by black flashes, and the hypothesized hydrogen bonds

In the ROESY experiments we were able to detect some spatial proximities for the major conformer, while we didn't notice unambigous ROEs between cross-strand residues in the minor one, due to peaks overlapping among them or with the solvent signals (Figure 3.29). The major conformer showed an Overhauser effect between the α-hydrogen of Pro and the hydrogens in position C2 and C6 of the piperidine ring, suggesting that a β-turn conformation was present. However, we couldn't detect a spatial proximity between the α-hydrogen of Val and the two hydrogens in position C2 and C6, as we observed for the major conformer of compound **3.1**.

We also discovered interesting ROEs between the 5-acetamido-2-methoxy-benzohydrazide peptidomimetic derivate unit and the tripeptide sequence Val-Ala-Val. In particular the amide proton of Lys and the protons of the Lys side chain were able to see the β-hydrogen of Val(2). Furthermore one aromatic proton of the benzohydrazide motif made contact with the β-and γ-hydrogens of the Val(2) residue. Surprisingly we noticed the spatial proximity between the α-proton of Pro and the aromatic and the sulphonamide protons of the tosyl group and a long-range ROE between the Lys side chain protons and the tosyl aromatic moiety, suggesting that the tosyl protecting group folded and approached the two arms of the β-hairpin structure.

Strong sequential and medium intraresidual ROEs, which are characteristic of an extended backbone conformations, were detected for the tripeptide sequence.

The difference with respect to the β-hairpin structure of compound **3.1** is how the benzohydrazide motif made contact with the tripeptide. In this case we hypothesized that the two protons involved in the weak hydrogen bonds were the amide protons of the Lys and Ala residues. In particular, the hydrogen bond that engaged the amide proton of Ala changed the position of the benzohydrazide unit. So that the side available for the recognition and interaction with Aβ 1-42 was already occupied in the interaction with the tripeptide sequence.

The evidence of this change was the different ROEs of the Val residue with the peptidomimetic arm: in compound **3.1** we observed the ROEs with the methoxy group of the benzohydrazide unit, while in compound **3.2** the Overhauser effect was seen with the aromatic proton in *meta* position with respect to the methoxy group. The two β-hairpin structures differ for the orientation of the side part of the peptidomimetic arm that might be responsible for the minimization of the edge-to-edge aggregation with the Aβ 1-42 peptide (see discussion below).

The vicinal $J_{NH-H\alpha}$ coupling constant also yields direct information on the main chain ϕ dihedral angle, through the Karplus relationship. For both conformers, the coupling constants were slightly greater with respect to the J values of an unfolded peptide and were indicative of φ angle values around $-120°$, as expected for a β-strand conformation (Figure 3.11). Positive difference between $J_{NH-H\alpha}$ values in the random coil and the values

Major conformer

AA	δ NH$^{\alpha}$ random coil	δ NH$^{\alpha}$ experimental	Δ NH	$^{3}J_{HN/H\alpha}$ random coil	$^{3}J_{HN/H\alpha}$ experimental	Δ *J*	δ H$^{\alpha}$ random coil	δ H$^{\alpha}$ experimental	Δ H$^{\alpha}$
Val	8.03	8.18	+ 0.15	7.7	8.3	+ 0.6	4.12	4.25	+ 0.13
Ala	8.24	8.46	+ 0.22	5.8	6.1	+ 0.3	4.32	4.12	- 0.20
Lys	8.03	7.82	- 0.21	7.7	bp	/	4.12	3.49	- 0.63
Pro	8.29	8.89	+ 0.60	7.1	7.5	+ 0.4	4.32	4.24	- 0.08

AA	δ CH$^{\alpha}$ random coil	δ CH$^{\alpha}$ experimental	Δ CH$^{\alpha}$	δ C=O random coil	δ C=O experimental	Δ C=O
Val	62.2	54.62	- 7.58	176.3	171.64	- 4.66
Ala	52.5	49.31	- 3.19	177.8	174.06	- 3.74
Lys	62.2	58.3	- 3.90	176.3	168.97	- 7.33
Pro	56.2	52.4	- 3.80	176.6	171.84	- 4.76

Minor conformer

AA	δ NH$^{\alpha}$ random coil	δ NH$^{\alpha}$ experimental	Δ NH	$^{3}J_{HN/H\alpha}$ random coil	$^{3}J_{HN/H\alpha}$ experimental	Δ *J*	δ H$^{\alpha}$ random coil	δ H$^{\alpha}$ experimental	Δ H$^{\alpha}$
Val	8.03	8.09	+ 0.06	7.7	8.4	+ 0.7	4.12	4.33	+ 0.21
Ala	8.24	8.41	+ 0.17	5.8	6.7	+ 0.9	4.32	4.07	- 0.25
Lys	8.03	7.82	- 0.21	7.7	bp	/	4.12	3.49	- 0.63
Pro	8.29	8.87	+ 0.58	7.1	/	/	4.32	4.24	- 0.08

AA	δ CH$^{\alpha}$ random coil	δ CH$^{\alpha}$ experimental	Δ CH$^{\alpha}$	δ C=O random coil	δ C=O experimental	Δ C=O
Val	62.2	54.7	- 7.50	176.3	171.64	- 4.66
Ala	52.5	49.6	- 2.90	177.8	174.06	- 3.74
Lys	62.2	58.3	- 3.90	176.3	168.97	- 7.33
Pro	56.2	52.5	- 3.90	176.6	171.84	- 4.76

Table 3.11: Chemical shift deviations (CSD) of aliphatic residues and coupling constants for NH protons at 283K of the two conformers of compound **3.2** in water

determined experimentally were found in both conformations. However, as for the major conformer of compound **3.1**, the values are slightly higher, suggesting that also in this case the two sequences are quite extended because of an adaptation due to the interaction.

Chemical shift deviations (CSD) are defined as the difference between experimental chemical shifts and corresponding random coil values and are considered good descriptors of backbone conformational space for each residue. We calculated the CSD for all the natural amino acids present in the molecule (Figure 3.11) and we observed that, for both the isomers, the α-carbon and the carbonyl group were upfield shifted (negative CSD), indicating that an extended conformation for the peptide and peptidomimetic arms predominate. The negative values of the α-hydrogen of Pro indicated the turn region of the molecule, while the negative values for the amide proton of Val-1 suggested some flexibility at the N-terminal amine of the molecule. All the other amide protons were weakly downfield shifted but, except for the Val-2 residue, all the other α-hydrogens resulted upfield shifted. Altogether this analysis suggests a lightness preference for a β-strand conformation.

Discussion In the light of the results obtained from the conformational NMR study, we can make some hyphothesis about the reason for the large difference of activity between the two compounds **3.1** and **3.2**. We can suggest that the activity of compound **3.1** might be linked to its ability to behave as a flexible β-hairpin structure. The fact that compound **3.1**

is not completely well organized in a preferential conformation could be an advantage, compared to a rigid β-sheet structure, to better establish hydrophobic and ionic interactions with the Aβ 1-42 peptide. Our molecule could well fit the target peptide thanks to its flexibility and, once in contact with the Aβ 1-42, could inhibit the aggregation process, by preventing another peptide to approach, probably through the peptidomimetic sequence that blocks the edge-to-edge aggregation or through a destabilization of the interactions between the various peptide monomers.

On the other hand, compound **3.2** loses the inhibitory activity: the presence of an additional Val residue in the peptide sequence reinforces the β-hairpin conformation but promotes a change of the position of the benzohydrazide unit so that the side normally used for the recognition and interaction with Aβ 1-42 is already engaged in the interaction with the tripeptide sequence. The side that remains exposed to the target peptide is the one which doesn't admit the formation of an appropriate hydrogen bond network. This is probably the reason why compound **3.2** has no affinity for Aβ 1-42 peptide and doesn't inhibit its aggregation process.

Compared to the peptide counterparts **2.1**, **2.2**, **2.3** and **2.4** described in Chapter 2, compound **3.1** is less active, especially at *ratio* 1:1, where we didn't observe any inhibitory activity. This is probably due to a different affinity for the Aβ 1-42 peptide: in the peptide analogues we have peptide sequences rationally designed to interact with the Aβ 1-42 and inspired by the 3D structure of Aβ into fibers and oligomers, while in compound **3.1** we have a peptidomimetic arm and a dipeptide that have been shown to maintain the interaction with the target peptide but not sufficiently to inhibit the aggregation also at *ratio* 1:1. Other modulation studies of the peptide sequence and peptidomimetic arm could lead to an improvement in the affinity towards Aβ 1-42 and so to a better inhibitory activity, comparable to the peptide analogues.

3.5 Conclusions

In this chapter we reported the synthesis and the evaluation of nine β-sheet mimics based on a 5-acetamido-2-methoxybenzohydrazide peptidomimetic derivate unit. The ThT fluorescence spectroscopy conducted on these compounds allowed us to get some information about the inhibitory activity and to correlate the ability to prevent or delay the aggregation process of these compounds with the length of the peptide chain and the type of protecting group on the primary amine of the scaffold. Furthermore, we could investigate the impact of protected or deprotected amines on the inhibition process and the importance of the possibility to establish ionic interaction to improve the affinity and the activity.

In particular, all the protected compounds (**3.9**, **3.10**, and **3.26**) were

inactive and showed a propensity to self aggregate. The cleavage of the CbZ protecting group on the side chain amine of Lys residue (compound **3.27**) is not necessary to observe the inhibitory activity. We observed a good inhibition when also the N-terminal amine resulted deprotected (compound **3.1**).

The importance of the tosyl protecting group was confirmed by the loss of activity observed for the Boc-protected analogue (compound **3.3**) and the totally deprotected compound **3.4**. This result led us to rule out the hypothesis that our most promising compound **3.1** behaves as a β-sheet breaker, as we deduced for the glycopeptidomimetics series.

The presence of a p-aminobenzensulfonyl group (compound **3.5**) restores slightly the activity compared to the Boc-analogue even the presence of the polar amino group on the aromatic moiety, however, dramatically decreases the inhibitory activity compared to the methyl group. This probably means that a hydrophobic interaction between the tosyl group and the target peptide is important for the affinity of the compound.

Finally, the ThT fluorescence results together with the NMR conformational studies conducted on compounds **3.1** and **3.2** suggest that the possibility to form a flexible β-hairpin structure might increase the affinity for Aβ 1-42 peptide and thus increase the aggregation inhibitory activity or could make the molecule more able to disrupt the conformation of the Aβ 1-42 peptide which is responsible for the aggregation process.

Compared to the peptide counterparts, we noticed that the activity of our compounds might be linked to their ability to behave as flexible β-hairpin structures and to the possibility to establish ionic interactions with the Asp23 or Ala42 of the Aβ 1-42 peptide. Rationally designed sequences are important for the affinity with the target peptide and hydrophobic amino acids are necessary to establish hydrophobic interactions either with the nucleation site or the C-terminus.

As we have already said, the rationally peptide sequences that we chose for the peptide β-hairpin mimics are, probably, important for the affinity and the interaction with the Aβ 1-42, because the amino acids that composed them are well recognized by the target peptide and the length of the peptide chain is appropriate to have more interactions. On the contrary, the peptidomimetic and the short dipeptide arms of compound **3.1** reduce the affinity and so the inhibitory activity.

On the other hand, compound **3.1** could have a higher stability against protease: more investigation about its enzymatic stability and its cell toxicity could bring much more information, useful to better compare it with the peptide analogues. The loss of activity would be rewarded by a greater stability, a lower molecular weight and a hydrophilicity/ hydrophobicity balance, comparable to peptide analogues, that allows a good solubility in water without losing the hydrophobic character needed to pass through the blood brain membrane and to establish hydrophobic interactions.

Before drawing definitive conclusions, other analyses are needed and would allow us to better understand both the inhibitory activity of compound **3.1** and its stability and protection against Aβ 1-42 cell toxicity. They are in perspectives a study on the oligomerization inhibitory activity through capillary electrophoresis, an investigation on the ability to withstand enzymatic cleavage by a plasma stubility assay and, finally, an analysis of the protection against Aβ 1-42 cell toxicity.

In conclusion, this structure-activity study allowed us to confirm that for the inhibitory activity of the Aβ 1-42 aggregation process, we need:

- a flexible scaffold that acts as β-turn nucleator;
- a peptidomimetic arm that decreases the peptide character of the compound;
- a peptide chain that is able to interact with the peptidomimetic sequence in order to stabilize the β-hairpin structure;
- a flexible β-hairpin structure characterized by two β-strands composed by hydrophobic amino acids that are able to establish hydrophobic interactions with the target peptide;
- an aromatic moiety that can establish hydrophobic interactions and increase the affinity for the peptide;
- a free terminal amine and a Lys residue to establish ionic interactions with the C-terminal carboxylate or the aspartic acid in position 23 of the Aβ 1-42 peptide sequence.

Chapter 4

β-hairpin mimic containing the piperidine-pyrrolidine scaffold and a fluorinated peptidomimetic derivate unit

In this chapter, we report the design and synthesis of a β-hairpin mimic containing the piperidine-pyrrolidine scaffold and bearing a fluorinated 5-benzamido-2-hydroxybenzohydrazide peptidomimetic derivate unit. In particular, we present a new synthetic pathway, developed to prepare a fluorinated analogue of the peptidomimetic arm **3.6**, discussed in Chapter 3. The objective was to study the pharmacomodulation properties of a fluorine and its effect on the conformational preference and the inhibitory activity of our β-hairpin mimic.

4.1 Design of the fluorinated β-hairpin mimic

4.1.1 The importance of fluorine in bioorganic and medicinal chemistry

Over the last 25 years, the number of fluorine containing drugs and biomolecules has increased significantly. The ever-growing knowledge of how fluorine substitution can modulate the physicochemical and biochemical properties of lead compounds has been a source of inspiration for scientists to develop novel fluorinated biomolecules and drugs. At present, hundreds of fluorinated drugs exist; in fact they account for more than 20 % of all pharmaceuticals [210].

Fluorine is a small atom, the smallest of the halogens, with a van der Waals radius of 1.47 Å which is only 20 % larger than that of hydrogen and much smaller than those of other halogens [211]. Fluorine is the most

electronegative element in the periodic table, with a value of 3.98 on the Pauling electronegativity scale. It has a very low polarizability.

The C-F bond length in CH_3-F is 1.38 Å, which is 0.29 Å longer than the methane's C-H bond, but 0.40 Å and 0.55 Å shorter than the C-Cl and C-Br bonds, respectively. Because of this similarity in size to hydrogen, it has been shown that microorganisms or enzymes often do not recognize the difference between a natural substrate and its analogue wherein a C-H bond of the substrate is replaced with a C-F bond (mimic effect of fluorine for hydrogen).

Fluorine and oxygen are nearly isosteric from a structural point of view and the bond length of C-F (1.39 Å) is close to the bond length of C-O (1.43 Å) [210]. Replacement of hydroxyl group with fluorine is therefore possible without adding excessive steric strain [212]. Fluoromethylene C=CHF and difluoromethylene $C=CF_2$ groups have been used as bioisosters of the peptide bond [213].

The incorporation of fluorine into a drug achieves the simultaneous modulation of electronic, lipophilic and steric parameters, and all of these properties can influence both the pharmacokinetic and pharmacodynamic properties of drugs [214]. The size and electronegativity of fluorine as well as the length and the strength of C-F bond are the key factors related to fluorine substitution and its outcome.

Due to its strong electron withdrawing nature, fluorine substitution has a profound impact on acidity and basicity of the neighbouring functional groups via inductive effect. When fluorine and/or fluorine-containing groups are incorporated into bioactive compounds, these substituents will exert strong effects on the binding affinity for the receptors or target enzymes, biological activities, and pharmacokinetics. Depending on the position of fluorine substitution, pKa shifts of several log units can be observed. Generally, alcools, carboxylic acids, heterocycles and phenols become more acidic with adjacent fluorine substitution. Often a change in pKa has a major impact on the pharmacokinetics of the molecule and its binding affinity.

The absorption and distribution of a drug molecule *in vivo* are controlled by its balance of lipophilicity and hydrophilicity as well as ionization. Enhanced lipophilicity together with change in amine pKa often leads to increase in blood-brain barrier (BBB) permeability or binding free energy through favorable position between the polar aqueous solution and the less-polar binding site. It is generally conceived that incorporation of fluorine or fluorinated groups increases the lipophilicity of organic compounds, especially aromatic compounds.

Fluorine can share three sets of lone-pair electrons with electron-deficient atoms intramolecularly or intermolecularly, in particular with a relatively acidic hydrogen bound to a heteroatom. In addition, its strongly electron-withdrawing property increases the acidity of proximate functional groups such as alchool and amine, making them better hydrogen bond donor.

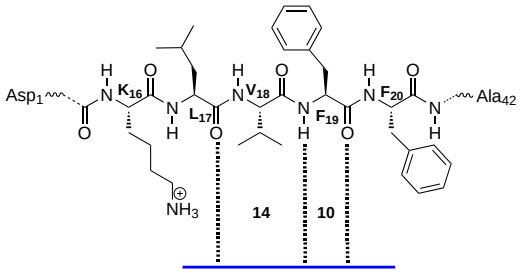

Figure 4.1: The KLVFF sequence of Aβ 1-42 peptide and the hydrogen bond network of an antiparallel β-sheet formed with a general compound designed to interact with the nucleation site

It has recently been shown that the polar C-F bond-protein interactions play a critical role in the stabilization of fluorine-containing drugs and their target proteins [215]. A large number of exemples for the polar C-F bond-protein interactions include those between a C-F bond and polar functional groups such as carbonyl and guanidinium ion moieties in the protein side chains, indicating the C-F bond unit as a poor-hydrogen bond acceptor.

Since the H_3C-F bond is stronger than that of H_3C-H, the replacement of a specific C-H bond with a C-F bond can effectively block metabolic processes via hydroxylation of C-H bonds. Strategic incorporation of fluorine into metabolism site has been widely used to prevent deactivation of biologically active substances *in vivo* [216].

On the basis of these considerations, we decided to synthesize the β-strand analogue of the 5-acetamido-2-methoxybenzohydrazide peptidomimetic derivate unit, containing fluorine and a free adjacent hydroxyl group, in order to study the pharmacomodulation properties of fluorine in the most promising compound **3.1**, described in the Chapter 3.

4.1.2 Design of the fluorinated β-strand peptidomimetic

The design of the fluorinated β-strand peptidomimetic takes part of a project that had already been carried out in our laboratory by Dimitri Brinet and Leila Vahdati (both PhD thesis, Université Paris Sud, 2015). The objective of this project was to synthesize peptidomimetic compounds, designed to interact with the central sequence of the Aβ 1-42 peptide (KLVFF), the nucleation site, and to modulate the oligomerization process.

Some research groups synthesized, as we have already seen in Chapter 1, peptide sequences designed to establish a β-sheet structure, once in contact with the nucleation site of the Aβ 1-42, and able to inhibit the aggregation process (Figure 4.1). Our approach was to conceive and synthesize new original mimetics of the nucleation site and to evaluate their influence on the

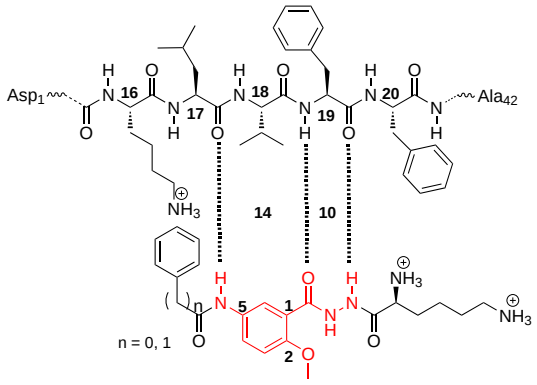

Figure 4.2: The Dimitri Brinet's mimic of the K(LV)F sequence, represented with the possible interactions with the central region of the target peptide

oligomerization process which constitutes the early step of the aggregation process of Aβ.

These peptidomimetics would interact with the central region of the peptide by respecting the network of hydrogen bonds in a β-sheet conformation and by alternately forming 10 and 14-membered rings (Figure 4.1). These β-strand mimics, designed in the laboratory, rely on different previous works [194][167][142][143][195] and those of Nowick, who incorpores the unnatural amino acid Hao in β-sheet mimics [162][193][217][218].

We adapted the Nowick's strategy by depriving the Hao motif of its oxalic acid and designing and synthesizing simple peptidomimetics with a lower molecular weight than that of the macrocycles. These characteristics together with the diminished peptide character allow access to better and more bioavailable drug candidates.

In Dimitri Brinet's thesis, the objective has been to make a mimic of the K(LV)F sequence, as KLVFF has been reported as able to prevent the fibrillization of Aβ (see Chapter 1, section 1.3.4). On either side of the 5-acetamido-2-methoxybenzohydrazide, that mimics a dipeptide, the following motifs have been coupled:

- a Lys residue, that is an amino acid commonly found in the β-sheets (Figure 4.2);
- a phenyl or benzyl carbonyl group to mimic the Phe side chain, that is another hydrophobic amino acid commonly found in the β-sheets and able to establish hydrophobic interactions (Figure 4.2).

Between all the compounds evaluated by ThT fluorescence assay, DBT 067 showed the ability to totally inhibit the aggregation process of Aβ 1-42 peptide at *ratio* 1:10 (peptide/compound) and also a significant decreasing

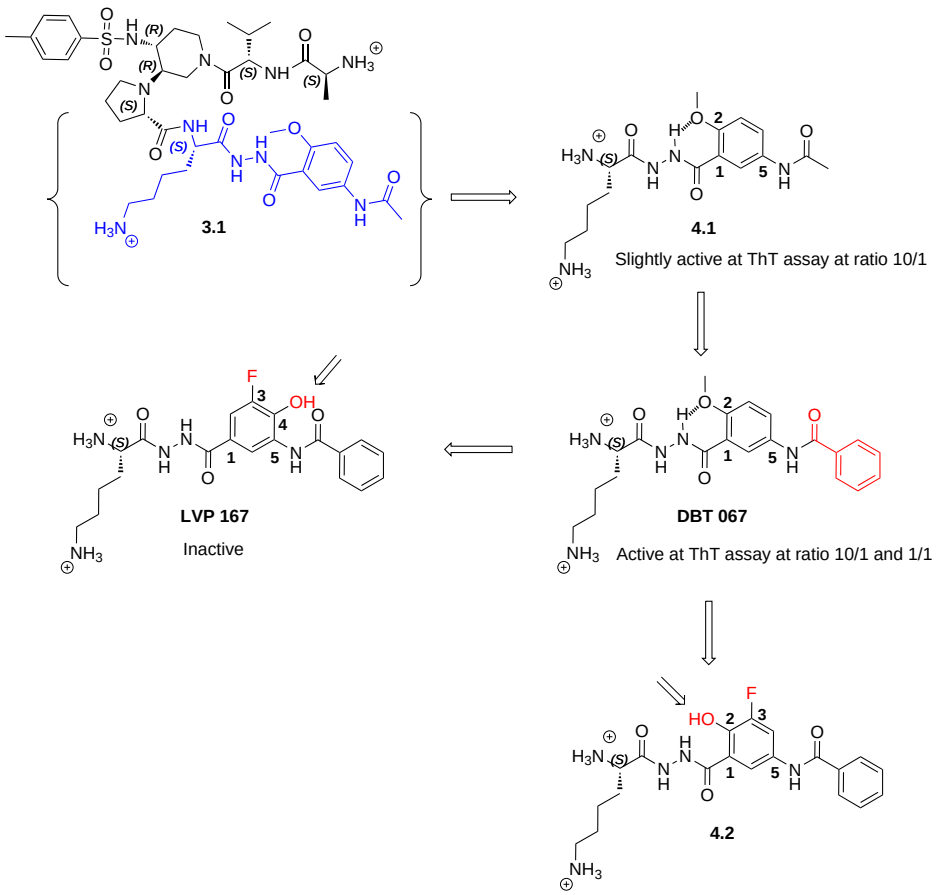

Figure 4.3: Design of the fluorinated 5-benzamido-2-hydroxybenzohydrazide peptidomimetic **4.2**

effect of the fluorescence intensity at *ratio* 1:1 (see the evaluation section 4.3 of Chapter 4).

If we compare the activity of DBT 067 with that of compound **4.1**, the totally deprotected peptidomimetic arm that was used for the synthesis of the β-hairpin mimics described in Chapter 3 (for example compound **3.1**, figure 4.3), we can observe that a phenyl carbonyl group instead of an acetyl one allows to improve the activity and to obtain a significant effect even at a lower *ratio* (Figure 4.3). This first difference justified the choice of the phenyl carbonyl group for the design of the fluorinated compound **4.2**.

In Leila Vahdati's thesis, the synthesis of a first peptidomimetic analogue containing fluorine and a free adjacent OH was presented. Compound LVP 167 was tested by ThT fluorescence assay to study its effect on the aggregation process of Aβ 1-42 peptide but it demonstrated to be completely inactive (Figure 4.3) (see the evaluation section 4.3 of Chapter 4). In this case, the

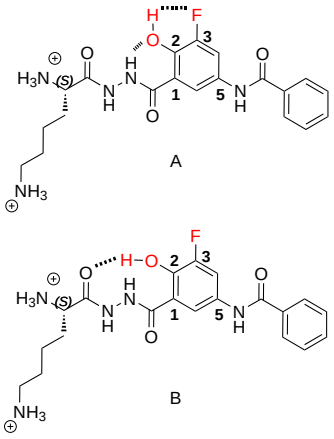

Figure 4.4: Hypothesized intramolecular hydrogen bond network of the fluorinated 5-benzamido-2-hydroxybenzohydrazide peptidomimetic **4.2**

hydroxyl group was in *ortho* position related to the fluorine (third position) and in the fourth position of the benzohydrazide motif, so not at the same one than the methoxy group in the 5-acetamido-2-methoxybenzohydrazide derivate unit.

So, my objective was to develop a new synthetic pathway in order to obtain compound **4.2**, composed by the benzohydrazide motif containing a fluorine in position 3 and a hydroxyl group at the same position 2 than the methoxy one in the peptidomimetic arm **4.1** (Figure 4.3). This derivate unit was coupled on one side with a Lys residue and on the other side with a phenyl carbonyl group.

The first hypothesis was to check if the presence of a more polar hydroxyl group could be able to maintain the activity of compound DBT 067, increasing at the same time the solubility of the peptidomimetic arm. The presence of the fluorine in *otho* position with respect to the hydroxyl group was dictated by the desire to increase the acidity of the phenol group, and then to increase its ability to establish hydrogen bonds with the water molecules and thereby increase the water solubility of the compound.

The second hypothesis was to study the effect of the hydroxyl group position in the benzohydrazide derivate unit. We thought that the loss of activity of compound LVP 167 was essentially due to the wrong position of the hydroxyl group and, as a consequence, the impossibility to establish the intramolecular hydrogen bond with the hydrazine NH.

The third hypothesis was to evaluate the effect of the replacement of a hydrogen bond acceptor as a methoxy group by a hydrogen bond donor as the hydroxyl group. The fluorine atom close to the free hydroxyl group makes its proton more acidic and so more inclined to establish hydrogen bonds, as

donor. The replacement of a methoxy group by a hydroxyl one could be reflected in a behavioural change of the peptidomimetic arm. In this case we may face to the possibility to create another type of intramolecular hydrogen bond netwotk (Figure 4.4) that could lead to another way to interact with the peptide and inhibit its aggregation.

The hydroxyl group, as hydrogen bond donor, might interact, in fact, either with the carbonyl group of the Lys residue (case B, Figure 4.4) or with the neighbouring fluorine atom (case A, Figure 4.4) and affect the peptidomimetic corformational preference [219] or behave as a simple polar β-sheet breaker.

4.1.3 Design of the fluorinated β-hairpin

Taking compound **3.1** as the most promising candidate of the β-hairpin series, we wanted to develop a new synthetic pathway that allows to change the type of peptidomimetic arm of the β-hairpin structure, by maintaining the same tosyl scaffold and the same dipeptide sequence, in order to make some structure-activity investigation, and to study the pharmacomodulation of different peptidomimetic β-strands.

In the previous synthetic pathway, described in chapter 3 (Figure 3.11), we performed before the coupling with the peptidomimetic arm and further the synthesis of the di- or tripeptide.

So, the first objective was to synthesize the intermediate **4.4** (Figure 4.5) composed by the tosyl scaffold and the dipeptide Val-Ala and a free carboxylic acid necessary to perform the coupling reaction with the amine function of any type of peptidomimetic.

Finally, the second objective was to find the best conditions to couple the peptidomimetic arm **4.5** and to finally obtain the fluorinated β-hairpin compound **4.3** (Figure 4.5). The aim was to study the influence of this new fluorinated peptidomimetic unit both on the inhibitory activity and on the structuring in a β-hairpin conformation.

4.2 Synthesis of the fluorinated β-hairpin mimic

This section will be divided into two parts: the first one that will highlight the synthesis of the fluorinated peptidomimetic arm **4.5** necessary for the final coupling reaction in the synthesis of the β-hairpin mimic, and the second one that will show the new synthetic pathway for obtaining the other precursor **4.4**, composed by the tosyl scaffold and the dipeptide sequence, ready for the final coupling.

4.2.1 Synthesis of the fluorinated β-strand peptidomimetic

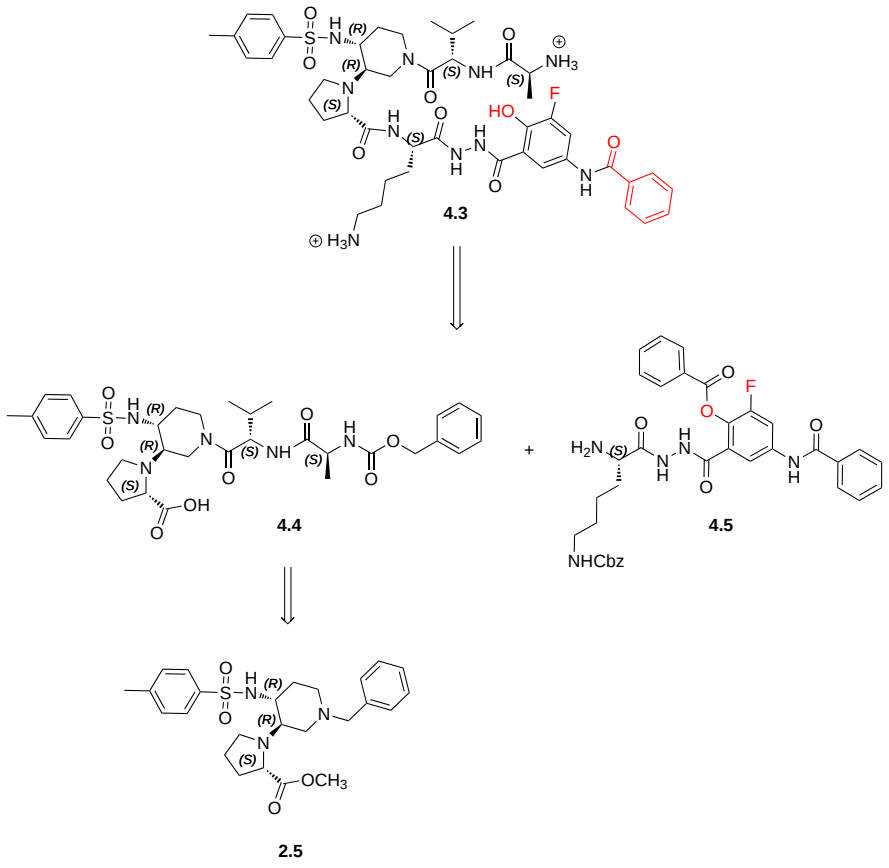

Figure 4.5: Retrosynthetic approach for obtaining the fluorinated β-hairpin compound **4.3**

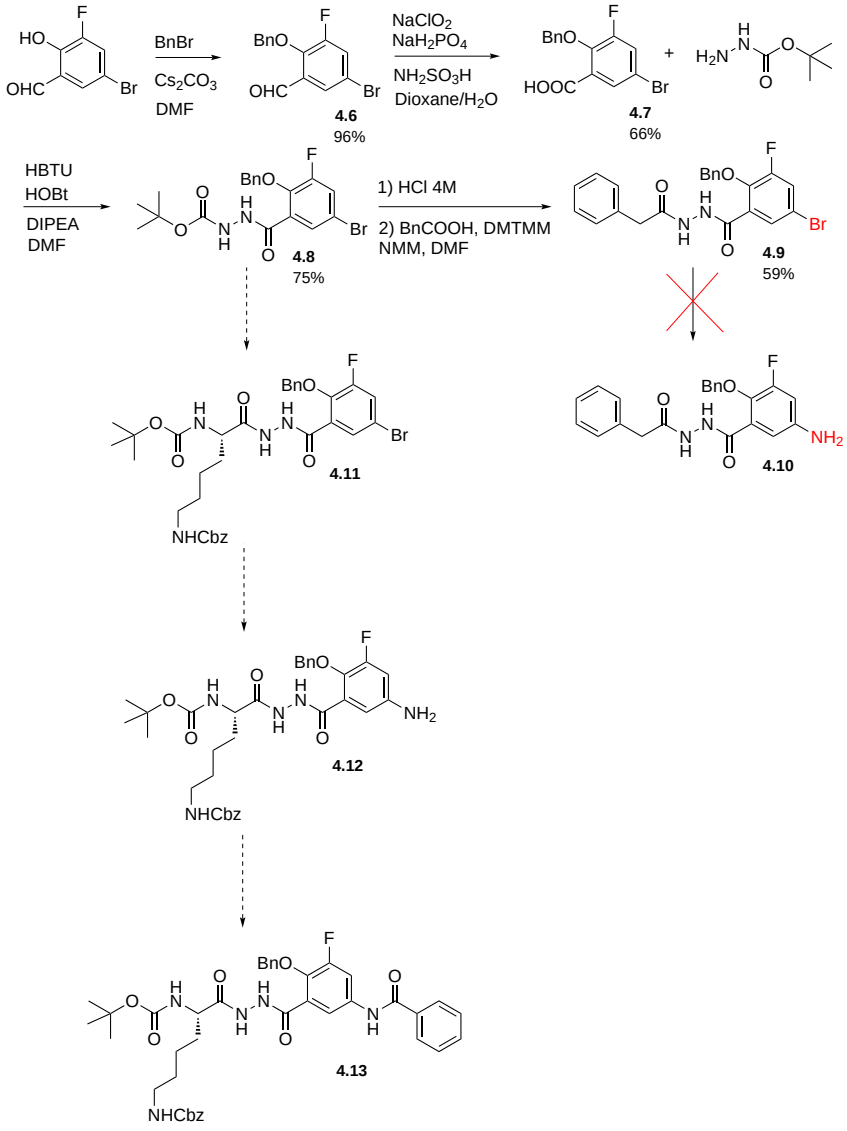

Figure 4.6: First synthetic pathway of fluorinated β-strand peptidomimetic **4.13**

First synthetic strategy When I embarked on this synthesis, we decided to use the new synthetic scheme developed in our laboratory (Figure 4.6) which started from the benzylation reaction of the hydroxyl group of the commercially available 5-bromo-3-fluorosalicylaldehyde to obtain the intermediate **4.6**, followed by the oxidation of the aldehyde group to the carboxylic acid, to afford compound **4.7**. This building block was then coupled with the *tert*-butyl carbazate, forming **4.8**, which was our key intermediate for the synthesis of the final product **4.13**.

While the Boc-cleavage of compound **4.8** and the following coupling reaction with benzoic acid had already been put in place, suggesting the possibility to couple the Lys residue (**4.11**), on the other side the access to the primary aniline from the aryl bromide of **4.9** had not yet been explored. So, my first objective was to investigate which conditions should allow us to obtain the primary aniline (**4.12**) and successively complete the synthesis of the final compound **4.13**, by the coupling reaction of **4.12** with benzoic anhydride or benzoyl chloride (Figure 4.6).

Since intermediate **4.9** was already available in the laboratory and synthesized in parallel by a Master's student, I started my research with this compound to find the necessary conditions for the substitution of the bromine with an amino group.

First, we chose to introduce the amino group directly using the benzophenone imine as a surrogate for ammonia in a Pd-catalyzed amination. This reagent is commercially available and allows an easy deprotection of the amino function under mild conditions. We followed the procedure described by Gelmi *et al.* [220] and successfully tested in our laboratory [221]. So, compound **4.9** and benzophenone imine were subjected to the Buchwald-Hartwig reaction. The intermediate formed during this step was not isolated but hydrolyzed immediately using MeOH in the presence of AcONa and NH_2OH hydrochloride. We recovered the starting material (Entry **1**, Table 4.1). An attempt to perform this amination on compound **4.6** was also unsuccessful and only byproducts of degradation were observed.

More recently, Messaoudi *et al.* demonstrated the efficiency of a practical Copper-catalyzed method in the synthesis of various anilines [222]. The reaction conditions involve the use of copper powder as the catalyst, ethanol as the solvent in the presence of pipecolinic acid as the ligand and ascorbic acid as the additive. In this case, the amine source is the sodium azide and, although there is no clear experimental evidence, they suppose that the reaction preceeds by a nitrene thermolysis mechanism that coverts the nitrene into aniline by hydrogen abstraction. However, this procedure didn't allow us to isolate compound **4.10** and also in this case we only recovered starting material (Entry **2**, Table 4.1). The reaction was tried also using both **4.8** and **4.6**, but was not successful too.

Having regard to the possibility to access to primary anilines by passing through a direct transformation from aryl halide into aryl azide, we tried

Entry	Conditions	Temperature	Time	Result
1	a) Benzophenone imine (1.5 eq.), $Pd(Oac)_2$ (10% mol), Xantphos (20% mol), K_2CO_3 (20 eq.), dry dioxane b) $NH_2OH.HCl$ (3.1 eq.) $NaOAc.3H_2O$, MeOH	a) 110° C b) rt	a) 15 h b) 6 h	Recovered starting material
2	Cu(0) powder (10% mol), Pipecolinic acid (30% mol), Ascorbic acid (20% mol), NaN_3 (2.2 eq.), EtOH	100° C	3 h	Recovered starting material
3	Cu_2O (40% mol), NaN_3 (2.0 eq.) , TBAP (10% mol), EtOH/EG 7:3	95° C	2 h	Degradation
4	Cu_2O (40% mol), NaN_3 (2.0 eq.) , TBAP (10% mol), DMF/EG 7:3	95° C	2 h	Degradation
5	CuI (1.0 eq.), NaN_3 (2.0 eq.) , Proline (1.3 eq.), DMSO	100° C	3 h	Other more polar produc
6	Cu_2O (1.0 eq.), NaN_3 (2.0 eq.) , Proline (1.3 eq.), DMSO	100° C	3 h	Other more polar product
7	Pinacol diborane (1.5 eq.), $Pd(PPh_3)_4$ (10% mol), NaOAc (6.0 eq.), DMF	90°C	4 days	Other more polar product
8	Pinacol diborane (1.5 eq.), $Pd_2(dba)_3$ (0.1 eq.), Xantphos (0.25 eq.), KOAc (6.0 eq.), Dioxane	80°C	4 days	Recovered starting material

Table 4.1: The different reaction conditions to obtain compound **4.10** from the brominated precursor **4.9**

to study if we could isolate the aryl azide of our substrate to successively transform it in primary aniline. Hajipour *et al.* introduced an efficient catalytic system based on Cu_2O/tetraethylammonium prolinate (TEAP), for the reaction of aryl halides with sodium azide in the mixed solvent EtOH/ethylene glycol (EG) (7/3), which provided a variety of aromatic azides [223]. Quaternary ammonium salts have been highly successful in enhancing the reactivity and selectivity of metal-catalyzed organic reactions and the research team developed a new system composed by metal nanoparticles of Cu_2O stabilized by quaternary salts that act as phase-transfer catalysts to facilitate the migration of reactants in the reaction mixture.

We tried this procedure in two different solvent media (EtOH/EG 7/3 and DMF/EG 7/3) and with tetrabutylammonium prolinate (TBAP) instead of TEAP, but we didn't succeed, probably because of the limitation of this type of transformation with electron-poor aryl halides (Entry **3** and **4**, Table 4.1).

Given the difficulty of access to the azide formation on our substrate, we decided to come back to the classical method of synthesis of primary aryl amines through a copper-assisted aromatic substitution reaction with sodium azide. Markiewicz *et al.* reported that this reaction is indeed of wide scope for conversion of aryl halides into amines , and that the same copper-based conditions also affect reduction of aryl azides into the amines [224]. They showed that, contrary to earlier suggestions, the formation of amines may not be due to thermal decomposition of azide but rather to its role as a reducing agent in a transformation that is catalyzed by copper. This reaction leads to a complete consumption of starting material only when polar solvents are used and when proline and CuI or Cu_2O are employed as ligand and catalyst, respectively. Unfortunately, with both types of copper source we couldn't obtain the desired product but we only observed the formation of a byproduct, difficult to purify and to isolate, probably because of the formation of a complex with the metal (Entry **5** and **6**, Table 4.1).

We found in literature that diversely substituted anilines were prepared by treatment of functionalized arylboronic acids with a common, inexpensive source of electrophilic nitrogen (H_2N-OSO_3H, hydroxylamine-O-sulphonic acid HSA) under basic aqueous conditions. Even moderately electron-poor substrates are well tolerated under the room temperature conditions and sterically hindered substrates appear to be equally effective compared to unhindered ones [225].

So, I first tried to obtain the corresponding arylboronic acid of compound **4.9**. Tetraalkoxydiboron compounds could be coupled with aromatic halides in the presence of catalytic amounts of $PdCl_2$(dppf) to afford arylboronic esters. The palladium-catalyzed cross-coupling reaction of aromatic and heteroaromatic halides or triflates with tetraalkoxyboron compounds to give arylboronic and heteroarylboronic esters is referred to as the Miyaura boration. The first step of the Miyaura boration is the oxidative addition of the

$Pd^{(0)}$-complex into the C-X bond of the aryl halide. Next, a transmetallation takes place, the exact mechanism of which depends on the nature of the substrate, and finally the reductive elimination affords the product.

First, we tried to reproduce the conditions reported by Miyashita *et al.* [226], through a $Pd^{(0)}$-catalyzed coupling reaction between compound **4.9** and the pinacol diborane, in the presence of $Pd(PPh_3)_4$ as catalyst and NaOAc as a base in DMF. In this case, after 4 days of reaction, we observed the formation of a byproduct more polar than the starting material which we were not able to characterize, probably beacause of a thermal decomposition (Entry **7**, Table 4.1).

We decided to follow the protocol described by Voth *et al.* [225], in which the catalyst employed is the $Pd_2(dba)_3$ in the presence of the ligand Xantphos in dioxane, in order to see if the lack of activity was due to the type of catalyst or to our substrate. Unfortunatly, we recovered the starting material **4.9**, suggesting that probably our aryl halide substrate is highly electron-deficient, due to the fluorine atom, and this can explain the impossibility to have access to the primary aniline by passing through a boronic acid (Entry **8**, Table 4.1).

Second synthetic strategy Since we could not replace the bromine substituent with an amino group, we decided to change strategy, starting from another commercially available compound, the 3-fluorosalicylaldehyde (Figure 4.7). In this case we carried out a nitration reaction to introduce the precursor group of the amino function, subsequently obtainable by reduction.

The reaction of aromatic nitration performed in sulphuric acid in the presence of ammonium nitrate at 0 °C, was regioselective in *meta* position relating to the aldehyde function. The intermediate **4.14** was obtained in a very good yield (98 %). Benzylation of **4.14** with benzyl bromide in the presence of cesium carbonate as a base gave compound **4.15** in a moderate yield (61 %). The next step included the oxidation of the aldehyde group of **4.15** by a Pinnick oxidation to obtain the carboxylic acid compound **4.16** in 95 % yield (Figure 4.7).

The coupling reaction between compound **4.16** and the *tert*-butyl carbazate in the presence of HBTU, HOBt and DIPEA allowed to obtain the intermediate **4.17** in a satisfactory yield (64 %) (Figure 4.7). During this coupling, the order of addition of the reagents was extremely decisive outcome on the result of the reaction. In fact we observed that the yield was higher when the *tert*-butyl carbazate, the coupling reactives and the base were added once all together to the stirred solution of compound **4.16**, cooled at 0 °C. If this procedure was not followed, we observed the formation of a byproduct, due to the decomposition of compound **4.16**, which greatly decreased the yield of the reaction.

After the Boc cleavage, the coupling reaction of **4.16** with Boc-NH-

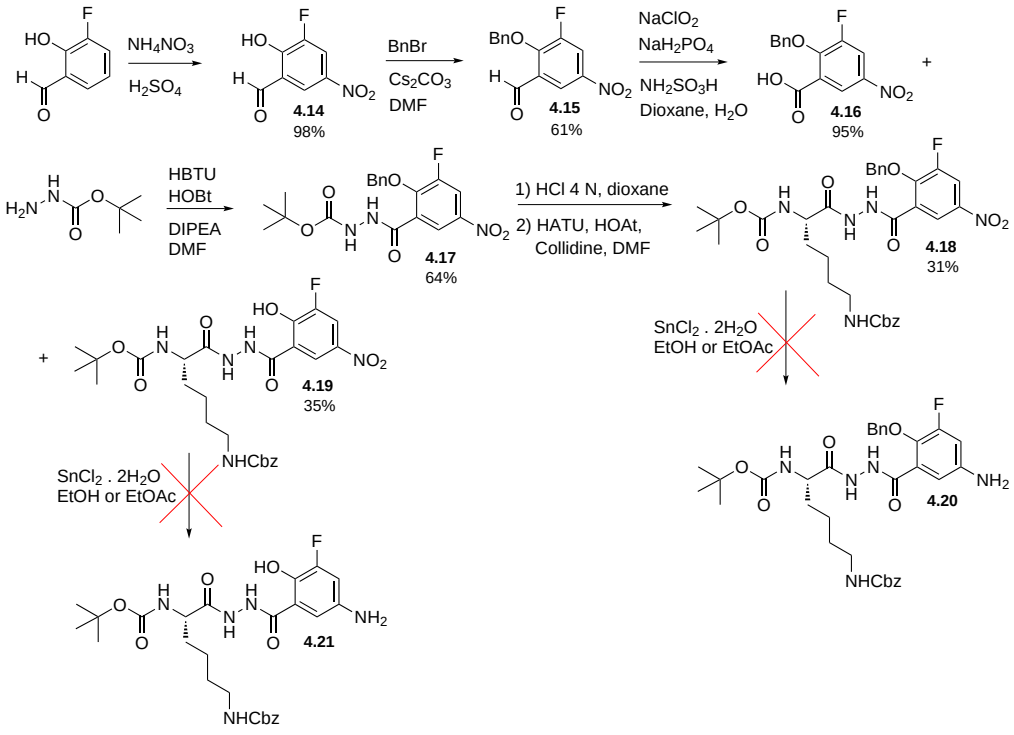

Figure 4.7: Second synthetic pathway of the fluorinated β-strand peptidomimetic

Lys(Z)-OH was performed with HATU and HOAt in the presence of collidine or with DMTMM in the presence of NMM. Despite the use of two different systems of coupling reagents, we surprisingly observed the same reaction trend. The global coupling yield was around 60 % but we obtained a mixture of two compounds: the desired product **4.18** and the debenzylated analogue **4.19**, in 1:1 *ratio* (Figure 4.7). We supposed that the basic conditions were strong enough to promote a nucleophilic aromatic substitution, since the electron-withdrawing effect of the fluorine makes the carbon more electrophile.

At this point of the synthesis, we decided to continue on both intermediates in parallel and tried to reduce the nitro group. Bellamy *et al.* described a selective reduction of aromatic nitro compounds with stannous chloride in non acidic and non aqueous medium, where other reducible or acid sensitive groups, such as the O-benzyl or Cbz, remain unaffected [227]. So, we performed this procedure on our intermediates **4.18** and **4.19** in EtOAc or EtOH at 70 °C, but we noticed the formation of a mixture of products that were not very easy to purify. The purification step and the isolation of the products resulted even more difficult for compound **4.21**, due to its higher polarity.

Third synthetic strategy Since the coupling reaction between the deprotected compound **4.17** and the Lys residue led to the formation of two separate products **4.18** and **4.19** and since the subsequent reduction of the nitro group further lowered the yields of the synthesis, we decided to perform a catalytic hydrogenation directly on the intermediate **4.17**. We were conscious to sacrifice the benzyl protecting group of the aromatic hydroxyl function, and by this way, we obtained compound **4.22** in quantitative yield and with a satisfactory degree of purity, directly without further purification (Figure 4.8).

The benzoylation of compound **4.22** with an excess of benzoyl chloride in the presence of pyridine as a base and solvent allowed to obtain the intermediate **4.23** in 95 % yield, with the advantage to both correctly functionalize the amino group and protect the hydroxy group, as a benzoyl ester. This would allow to avoid undesired reactions during the subsequent coupling reaction with the lysine (Figure 4.8).

After the Boc cleavage of compound **4.23**, the coupling reaction with the Boc-NH-Lys(Z)-OH was performed with DMTMM and NMM in DMF and afforded the desired product **4.24** in 45 % yield (Figure 4.8).

The Boc cleavage of compound **4.24** with HCl 4 mol dm^{-3} in dioxane allowed to obtain the intermediate **4.5**, necessary for the coupling reaction with compound **4.4** (Figure 4.5).

As we needed also the totally deprotected molecule for the study of its inhibitory activity by ThT fluorescence assay, the Cbz group was removed by hydrogenolysis. We tried successively to hydrolyze the ester in basic

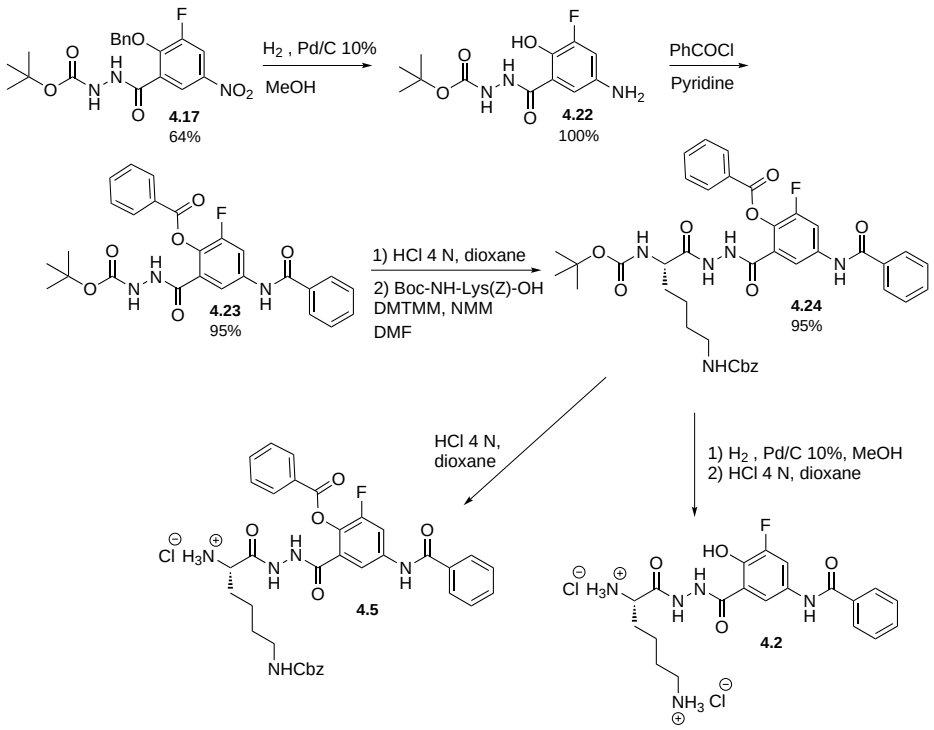

Figure 4.8: Third synthetic pathway for the synthesis of the fluorinated β-strand peptidomimetic **4.24**

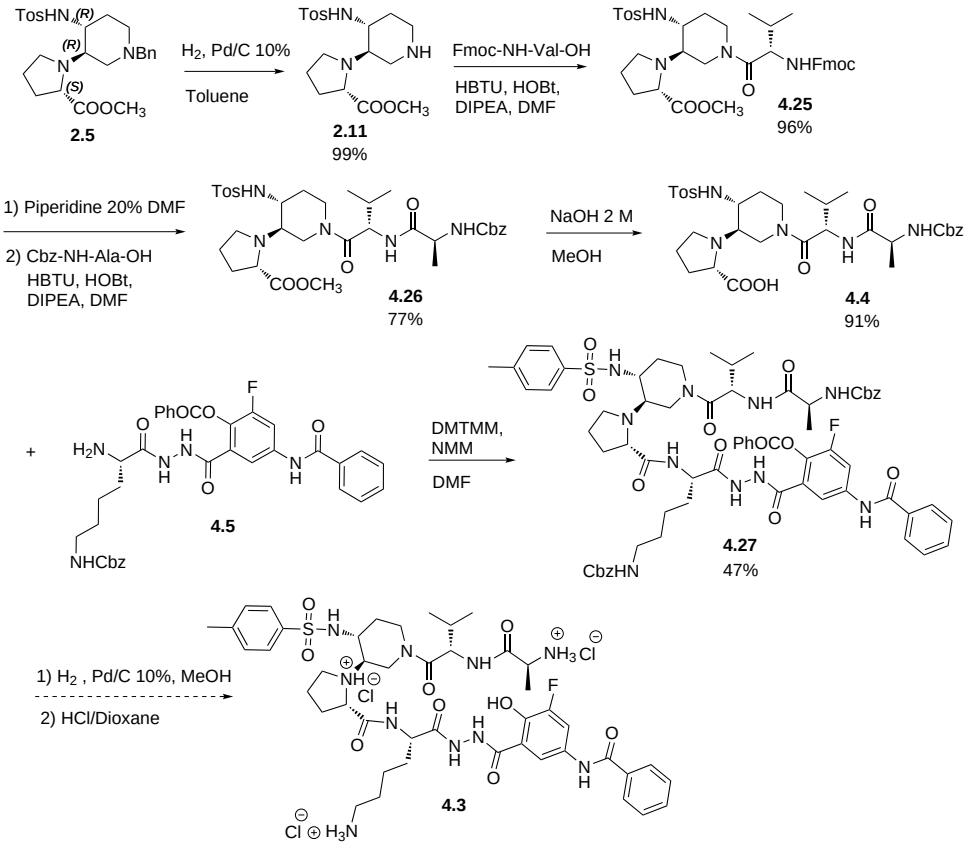

Figure 4.9: Synthetic scheme for the synthesis of compound **4.4** and the fluorinated β-hairpin **4.3**

conditions with NaOH or LiOH but in both cases we assisted to a degradation of our compound, resulting in a byproduct with the free hydroxy group but without the Lys residue. So we decided to keep the ester group and to perform, immediately after the hydrogenolysis, the Boc cleavage in acidic conditions using HCl 4 mol dm^{-3} in dioxane. These two steps together allowed also to hydrolyze the benzoyl ester that protected the hydroxy group, resulting to compound **4.2** as a hydrochloride salt (Figure 4.5).

4.2.2 Synthesis of compound 4.4 and of the fluorinated β-hairpin 4.3

Compound **4.4**, consisting of the tosyl scaffold and the dipeptide sequence Val-Ala, was synthesized according to the classical peptide synthesis procedure in solution.

Hydrogenolysis of **2.5** was performed in toluene with an equivalent amount

of 10 % Pd/C to afford the free amino compound **2.11** in 99 % of yield. The first Fmoc protected amino acid Val was introduced using HBTU and HOBt in DMF in the presence of DIPEA, providing compound **4.25** in 96 % yield (Figure 4.9).

After cleavage of the Fmoc group of **4.25** with a solution of 20 % piperidine in DMF, the second amino acid (Cbz-NH-Ala-OH) was coupled using the same coupling procedure, to afford compound **4.26** in 77 % yield (Figure 4.9).

The saponification of compound **4.26** with NaOH 2 mol dm^{-3} in MeOH at 60 °C afforded the key intermediate **4.4** in 91 % yield (Figure 4.9).

The coupling reaction between the fluorinated β-strand **4.5** and compound **4.4** was performed with the triazine-based reagent DMTMM in the presence of NMM in DMF. In this way, the final β-hairpin compound **4.27** was obtained in very good yield (91 %) (Figure 4.9).

The cleavage of the two Cbz groups in compound **4.27** by hydrogenolysis and the formation of the corresponding chloride salt will afford the final compound **4.3**, which will be used for the evaluation of its aggregation inhibitory activity (Figure 4.9). Unfortunately, due to the lack of time, this deprotection has not been yet performed.

4.3 Evaluation of the fluorinated β-strand 4.2 by ThT fluorescence assay

In this section, we report the evaluation of the inhibitory activity of compound **4.2** by ThT fluorescence assay. The results are compared to the β-strand peptidomimetics, based on the same benzohydrazide motif, which were previously designed and synthesized in our laboratory (see Figure 4.3, in this Chapter) and from which the design of **4.2** was inspired.

As we can see from Figure 4.10, compound **4.1** showed a slight activity at *ratio* 10:1 (compound:Aβ 1-42), while it demonstrated to be completely inactive at lower *ratios*. The results suggested that the β-strand peptidomimetic arm alone is not able to inhibit the aggregation process of Aβ 1-42 peptide and a complete β-hairpin structure is therefore important in modulating the aggregation kinetics. Compound **4.1** displayed a retarding effect on the $t_{1/2}$ by a factor of 1.07 and a small effect on the fluorescence plateau with a decrease of 44 % at *ratio* 10:1.

The replacement of the acetyl group of **4.1** by a benzoyl one demonstrated to increase the activity of the β-strand peptidomimetic arm. Compound DBT 067, at the *ratio* 10:1 (compound:Aβ 1-42), delayed significantly the kinetics of fibrillization (green curve, Figure 4.11): $t_{1/2}$ was increased by a factor 1.69 and the final fluorescence was decreased by 60 %. At the *ratio* 1:1 and 0.1:1 no effect was observed on the $t_{1/2}$ but we noticed a similar decreasing effect of the plateau by 46 % and 40 %, respectively.

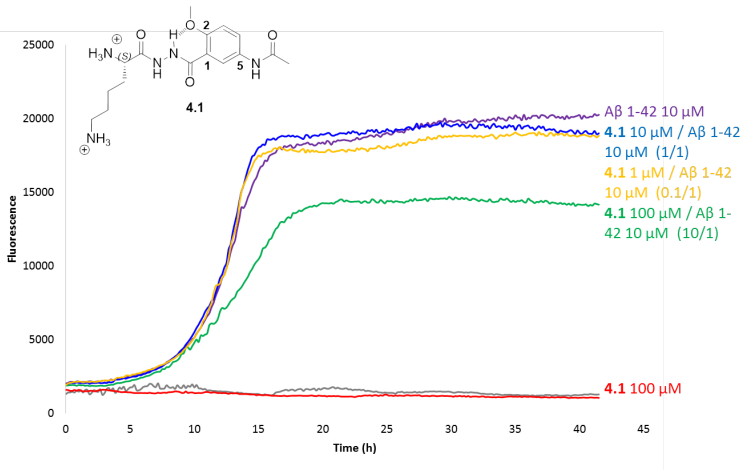

Figure 4.10: ThT curves of β-strand **4.1**

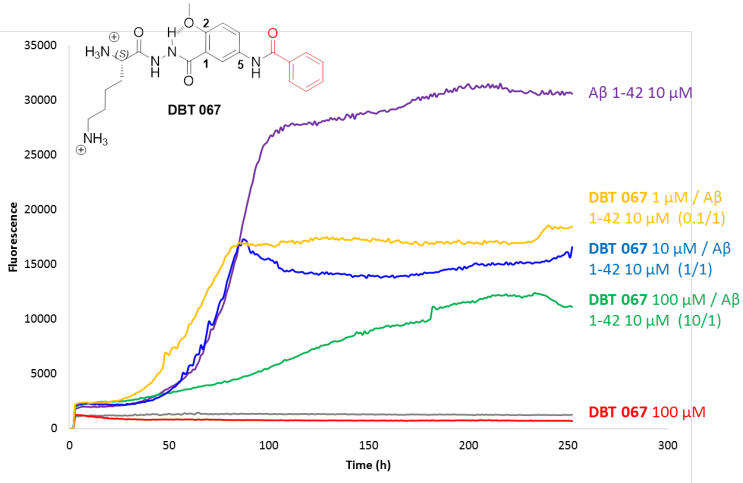

Figure 4.11: ThT curves of β-strand DBT 067

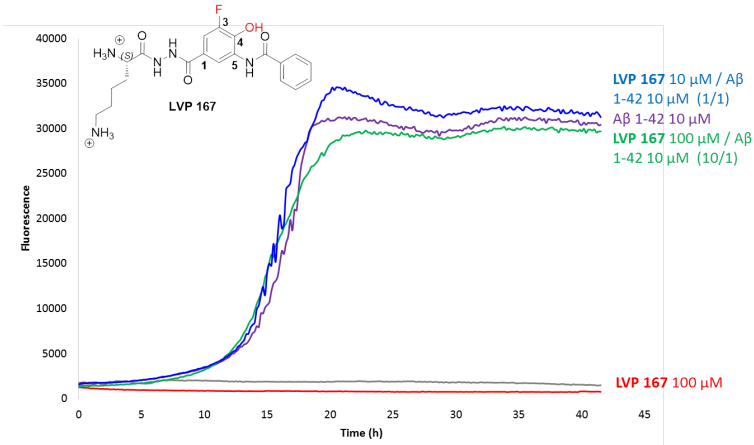

Figure 4.12: ThT curves of β-strand LVP 167

These results justified the choice of the benzoyl group for the design of the fluorinated compound **4.2**.

The absence of effect on the kinetics of the Aβ 1-42 aggregation of the totally deprotected compound LVP 167 (Figure 4.12), which corresponds to the analogue of compound DBT 067 with a fluorine substituent in position 3 of the benzohydrazide motif and an hydroxyl group in position 4, suggested that the free hydroxyl group in the wrong position related to the methoxy one in the two previous β-strand peptidomimetics might be sufficient to lose the activity of the molecule or that the replacement of a hydrogen bond acceptor by a donor one could affect the inhibition activity.

To better elucidate if the reason of the lack of activity was essentially due to the wrong position or to the presence of a more polar and hydrogen bond donor substituent, we tested compound **4.2** and interestingly we observed a recovery of the inhibitory activity of the β-strand peptidomimetic. In particular, as we can observe in Figure 4.13, compound **4.2**, at the *ratio* 10:1 (compound:Aβ 1-42), delayed significantly the kinetics of fibrillization (green curve): $t_{1/2}$ was increased by a factor 1.16 and the final fluorescence was decreased by 63 %. These results confirmed that the position of the hydroxyl group is important for the inhibition activity and that the presence of a hydrogen bond donor instead of an acceptor one doesn't affect the activity.

At lower *ratios* we noticed a concentration dependent inhibitory activity with respect to the decrease of the final plateau by 28 % at 1:1 *ratio* and 11 % at 0.1:1 *ratio*. However, the effect on the $t_{1/2}$ resulted not significant.

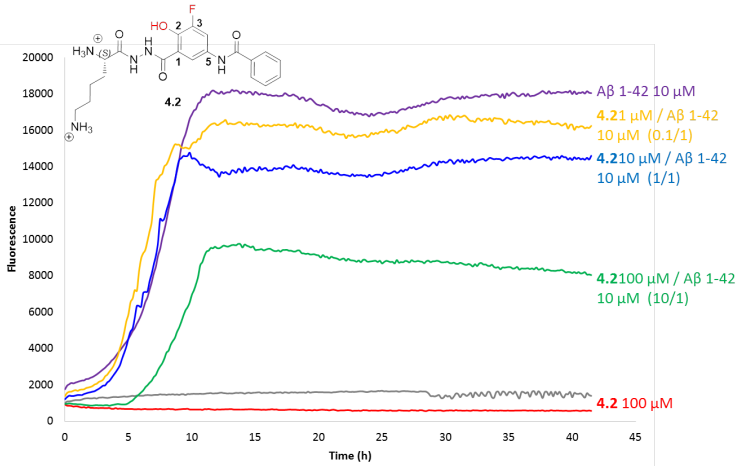

Figure 4.13: ThT curves of β-strand **4.2**

4.4 Conclusions and perspectives

In this chapter we reported the design and the developement of the synthesis of a new fluorinated peptidomimetic based on the 5-acetamido-2-methoxybenzohydrazide derivate unit. We proved the possibility to perform the coupling reaction between this peptidomimetic arm and a β-turn inducer bearing a dipeptide sequence.

We observed that this new β-strand mimic is able at *ratio* 10:1 (compound / Aβ 1-42) to delay the kinetic of the Aβ 1-42 aggregation process. Compared to the previous peptidomimetic based on the 5-acetamido-2-methoxybenzohydrazide motif we obtained a compound that demonstrated to have a better inhibitory activity alone, thus suggesting the possibility of improving the activity of our most promising β-hairpin compound **3.1**.

This fluorinated peptidomimetic arm, although it has shown a slightly inferior inhibition activity compared to compound DBT 067, offers in addition the possibility to exploit the fluorine atom to undertake more extensive conformational studies, as well as the contribution of all the advantages of fluorine on lipophilicity, pKa, intermolecular interactions, molecular conformation and stability.

In perspective, we want to perform the cleavage of the two Cbz groups in compound **4.27** by hydrogenolysis and the acidic hydrolysis of the benzoyl ester group, in order to afford the final compound **4.3** (Figure 4.9), which will be used for the evaluation of its aggregation inhibitory activity by ThT fluorescence assay and for its conformational analyzes by NMR.

Chapter 5

β-hairpin mimics containing the piperidine-pyrrolidine scaffold and azatide β-strand peptidomimetics

In this chapter, we report the design, synthesis and evaluation of a β-hairpin mimic analogue in which the 5-acetamido-2-methoxybenzohydrazide derivate unit has been replaced by another type of peptidomimetic, called azatide. Together with the synthesis of this peptidomimetic, we present here the synthesis of other 2:1 [Aza/α]-tripeptides (peptidomimetic sequences composed by three elements: two aza-amino acid residues and a natural amino acid), which were designed and synthesized in order to study in a general manner the conformational preference of this type of peptide mimetic, composed by two α-aza-amino acids linked to a natural amino acid. The aim was to better understand if this type of peptidomimetics could adopt an extended conformation (β-strand) when employed in a β-hairpin structure. Here, we present the results obtained by NMR analyses, X-ray crystallography and molecular modelling.

5.1 Design of the azatide peptidomimetics and the β-hairpin mimics

5.1.1 State of the art

In the field of peptidomimetic foldamers, our laboratory research focuses on the design and synthesis of conformationally constrained compounds that mimic or induce specific secondary structural features of peptides and proteins. In particular, as it's possible to see in the previous chapters, we are interested in acyclic β-hairpin mimics where a β-turn inducer is linked

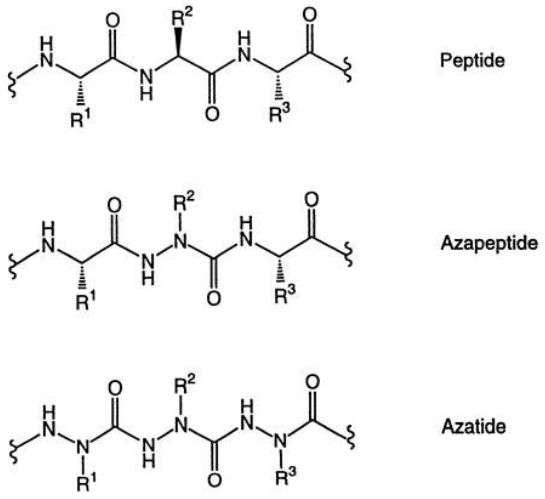

Figure 5.1: Comparison of a peptide, azapeptide and azatide (Han1996)

to peptidomimetic and/or peptide arms. These molecules are designed to disrupt the protein-protein interactions by reproducing the hydrogen bond pattern found in the antiparallel β-sheet formed during the Aβ 1-42 aggregation process.

In order to decrease the number of potential sites for proteolytic attack of our β-hairpin mimics, we designed peptidomimetic arms that are able to form interacting β-strands. In biological, chemical and pharmaceutical areas modified peptides and mimetics offer interesting advantages over physiologically active peptide. Beside increasing efficiency and selectivity of natural peptides, this class of compounds known as peptidomimetics may decrease side effects, improving oral bioavailability and prolonging the pharmacological activity by hindering enzymatic degradation within the organism [228]. The peptidomimetic research continues to inspire medicinal chemists for seeking either potential drugs or pharmacological tools to investigate how the secondary structure can affect the activity [229]. This knowledge can be useful to modulate the activity of the studied target proteins and peptides.

The modification of peptides to peptidomimetics has included peptide side chain modifications, amino acid extentions, deletions, substitutions, and, most recently, backbone modifications. The most common manipulation involving the α-carbon atom of peptides is the inversion of stereochemistry to yield D-amino acids. Azapeptides, however, are peptides in which one (or more) of the α-carbon(s) has been replaced by a trivalent nitrogen atom. This transformation results in a loss of asymmetry associated with the α-carbon and yields a structure that can be considered intermediate in configuration

between D- and L- amino acids (Figure 5.1) [230].

Aza-amino acid residues impart special conformational properties to the parent peptide structure[231] due to the loss of stereogenicity and reduction of flexibility. So, the incorporated aza-amino acid could adopt the proper pharmacophore orientation for activity and selectivity, by confering also resistance towards proteolytic degradation. Replacement of an α-carbon by a nitrogen in a peptide results in an additional possibility for the formation of hydrogen bonds [232] and was also found to affect the acidity of the neighbouring amide N-H bonds. The presence of an aza-amino acid residue may increase the biological activity and/or improve the pharmacokinetic properties of the parent peptide [232]. In particular, the replacement of the α-carbon by a nitrogen in a biologically active peptide will doubtless affect its absorption, transport, distribution, enzyme or receptor binding, and metabolic stability in the organism.

Application of azapeptides in the study of biologically active peptides has had significant success. For example, azapeptides have exhibited longer duration of action to natural peptides, presumably because of increased resistance to proteases and because ureas are generally more chemically stable than amides [233].

Azapeptide analogues of peptide hormones have been synthesized, including thyrotropin-releasing hormone (TRH)[234], bovine angiotensin II [235], oxytocin [236], eledoisin [237], enkephalin [238], and luliberin (LHRH) [239]. Containing only one aza-amino acid residue in the peptide sequence, these aza-analogues of biologically active peptides exhibited improved pharmacological properties relative to their parent peptide, such as increased duration of action, potency, and/or selectivity.

Aza-amino acids have also been employed as components of serine [240] [241] and cysteine [242] [243] [244] [245] protease inhibitors exhibiting competitive, reversible, and irreversible mechanism-based inhibitory activity. Also in this case, we have only exemples of azapeptides composed by only one aza-amino residue inserted at various positions within the peptide sequence.

One product of aza analogue series of the ovulation-inducing hormone luliberin was introduced into the pharmaceutical market as a drug for treating carcinoma of the prostate (Zoladex).

More recently, benzotriazole-mediated synthesis of aza-peptides, containing one aza-amino acid residue, has been developed and led to the preparation of azatripeptides and tetrapeptides that could be valuable building blocks for the synthesis of longer or cyclic azapeptides. By adopting this novel protocol, an aza-leu-enkephalin analogue was synthesized [246].

An azapeptide analogue of hexarelin, a growth hormone releasing peptide, exhibited a characteristic β-turn conformation and a slightly higher CD36 binding affinity relative to parent hormone. In this case the aza-amino acid residue was introduced in the middle of the peptide sequence. This analogue was prepared by submonomer solid-phase synthesis that offered a powerful

means for making azapeptides, for studying structure-activity relationships with target receptors [247].

A similar approach was followed by Proulx *et al.*. They developed a copper-catalyzed N-arylation of semicarbazones for the synthesis of aza-arylglycine-containing aza-peptides, based on the hexapeptide sequence of Growth Hormone Releasing Peptide-6 (GHRP-6). CD spectroscopy indicated the propensity for the aza-peptides, containing aza-arylglycines at the Trp position of GHRP-6 sequence, to adopt β-turn conformation [248].

Aza-aminoacyl-L-proline dipeptides were employed to prepare azapeptide derivatives to target the prostaglandine-F2α receptor and always with the aim to improve the pharmacokinetic properties of the corresponding peptide counterparts. The addition of different side chains to the single aza-amino acid residue has provided a set of analogues exhibiting varying degrees of biological activity, probably due to the effects on ligand conformation and interactions with the receptor, caused by the various substituents employed [249]. Once again the azapeptides have proven their versatility, their effectiveness and their use as peptidomimetics, stable toward the proteolysis.

A new series of azapeptide inhibitors of cathepsins B and K, structurally based upon inhibitory sites of cystatins and characterized by an aGly residue in the midldle of the hexapeptide sequence, proved to be more potent inhibitors of cathepsin B in comparison with cathepsin K. The research team proposed the idea that the conformational flexibility of the bonds in the vicinity of azaamino acid residue is probably responsible for good inhibitory properties of azapeptides toward cysteine proteases. They presented the strong evidence that the inhibitor belonging to the investigated class of peptidomimetic substances can adopt the conformation which facilitates possible interactions between its residues and amino acids forming the appropriate binding sites of cystein proteases [250].

An exemple of this evidence was presented by Bailey *et al.* [251]. They successfully identified a new series of potent NS3 serine protease inhibitors that incorporate an aza-amino-acyl fragment. Transferred NOE experiments, performed on one of these compounds, have shown that the azapeptide binds in an extended conformation, similar to that observed for the inhibitor series previously reported by the same group.

Boeglin *et al.* reported the synthesis and evaluation of aza-analogues of the potent melanocortin receptor agonist Ac-His-D-Phe-Arg-Trp-NH_2. Aza amino acids were inserted one by one along the peptide sequence to probe the importance of local configuration and turn conformation on the biology of this tetrapeptide. Although systematic substitution of Phe and Arg residues by aza-amino acids led to a significant loss of activity relative to the parent peptide, substitution at C-terminal residue gave analogues equipotent to the parent peptide. This study demonstrated that the recognition of a ligand by a receptor is particularly sensitive to modifications of configuration and conformation that the substitutions with aza-amino acids impart to the

parent peptide [252].

In an effort to obtain greater potency and selectivity for inhibitors of caspases, the research group of Powers elaborated two novel classes of irreversible protease inhibitors for clan CD cysteine proteases without cross reactivity with the clan CA proteases. This was possible by elaborating aza-peptide Michael acceptors and aza-peptide epoxides that allowed to elucidate the structural determinants for the preference and discrimination at the binding site [253] [254].

Aza-peptides were also used to design new anticonvulsivant agents that provided moderate-to-excellent protection against MES(maximal electroshock)-induced seizures in mice and rats [255] and to prepare a new class of cysteine proteinase inhibitor for hepatitis A virus and human rhinovirus 3C enzymes which showed potent, irreversible inhibitory activity with IC_{50}'s in the low micromolar range [256].

5.1.2 Objectives

This bibliographic overview showed how the azapeptide domain is not deeply explored and limited to a narrow field of application; in particular it is not yet explored their role in protein-protein interactions. Most of the azapeptides that are reported in literature presented the substitution of just one amino acid with an aza-residue, and only one exemple [238] of a complete azatide oligomer was reported several years ago. At the same time, we can notice that azapeptides proved themselves to be drug-worthy in the clinical setting and that the recent discoveries around aza-peptide domain resulted in a steady increase in the number of azapeptides being generated. This result is due to the structural diversity of the side chains attached to the substituted hydrazines, as precursors of aza-amino acid residues. The aza-peptide field looks very rich for the harvest of innovation in the future [257].

Thanks to these observations, we decided to design and synthesize three new azatide-type peptidomimetics and use them in the synthesis of β-hairpin mimics in order to make structure-activity relationship studies. In particular we designed an aza-peptide mimetic of the 5-acetamido-2-methoxybenzohydrazide derivate unit **3.6** which previously demonstrated to be active in the most promising compound **3.1**. This peptidomimetic is composed by two aza-amino acid residues (aLys and aGly) coupled to the natural amino acid L-Phenylalanine amide (Molecule **5.1**) (Figure 5.2). This sequence has been chosen to provide both ionic interactions by the free amine on the aLys side chain and hydrophobic interactions by the aromatic side chain of the Phe. As we could see in the previous chapters 3 and 4, the amino acid Lys is important to break the salt bridge between D23 and K28 or K28 and A42 in the β-sheet structure of Aβ 1-42 peptide during the conformational change that leads to the aggregation process. On the other hand, it's also important to maintain a certain hydrophobicity to interact with either the nucleation

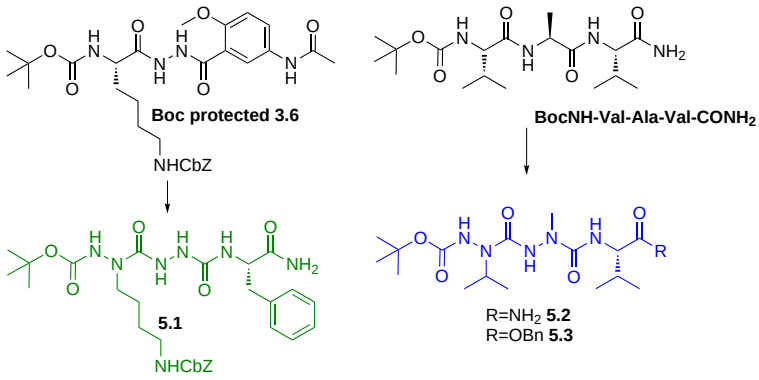

Figure 5.2: Structure of the three new azatide-type peptidomimetics **5.1**, **5.2** and **5.3**

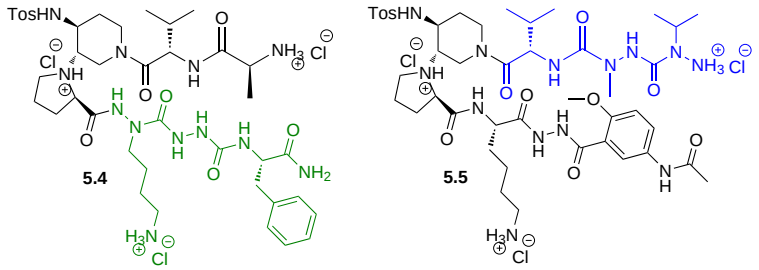

Figure 5.3: Structure of the two β-hairpin mimics **5.4** and **5.5** composed by either the azatide **5.1** or the azatide **5.3** alternatively

site or the C-terminus of the peptide, both composed by hydrophobic amino acids.

The other two azatide chains are designed to mimic a natural tripeptide sequence that has been used in the conception of the previous β-hairpin mimics, described in the third chapter. We decided to synthesized the 2:1 [Aza/α]-tripeptide sequence aVal-aAla-Val-$CONH_2$ (Molecule **5.2**) (Figure 5.2), composed by two aza-amino acids aVal and aAla and one natural amino acid L-Valine amide, to provide structural studies and to observe if this azatide could adopt an extended conformation (β-strand) alone or when employed in a β-hairpin structure, and the 2:1 [Aza/α]-tripeptide sequence aVal-aAla-Val-COOBn (Molecule **5.3**) (Figure 5.2), composed by two aza-amino acids aVal and aAla and one natural amino acid L-Valine benzyl ester, in order to make the coupling reaction with the secondary amine of the piperidine cycle of the scaffold and so replace the natural di- or tripeptide sequence, already used in the molecules discussed in the third chapter.

So, once the synthesis of the azapeptide sequences was finished, the objec-

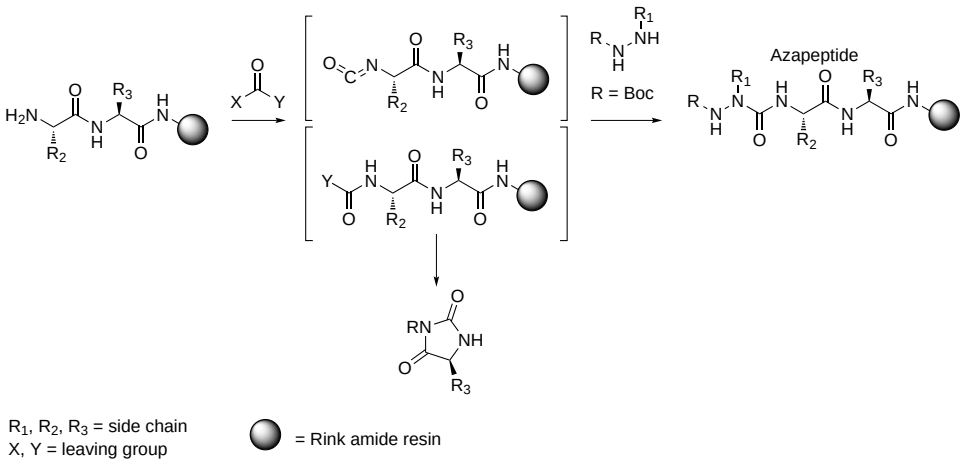

Figure 5.4: The azapeptide synthesis approach mediated by the activation of the peptide N-terminus

tive was to incorporate either the azatide **5.1** or the azatide **5.3** alternatively to the tosyl scaffold in order to synthesize two different β-hairpin analogues of **3.1**, by replacing on one hand the 5-acetamido-2-methoxybenzohydrazide derivate unit (Molecule **5.4**) and on the other the dipeptide sequence Val-Ala (Molecule **5.5**) (Figure 5.3).

5.2 Synthesis of the azatide peptidomimetics

Azapeptide synthesis has traditionally involved a combination of hydrazine chemistry and peptide synthesis in order to substitute a nitrogen atom for the α-carbon of one or more amino acids in the sequence.

Azapeptides have been typically synthesized by way of two general approaches: the activation of the peptide N-terminus (Figure 5.4), as an isocyanate or active carbamate, followed by coupling to the hydrazide, and the activation of the hydrazide moiety (Figure 5.5), which is usually in the form of N-alkyl carbazate [230] [258] [259][233] [260] [232].

The synthesis of azapeptides, that provides the activation of the N-terminus of a growing peptide before the hydrazine acylation, needs the formation of a reactive isocyanate or active carbamate intermediate. Generally, in the activation step, it's typical to use *bis*-(2,4-dinitrophenyl) carbonate and carbonyldiimidazole (CDI) as carbonyl donors. The major drawback of this methodology is competitive formation of the hydantoin byproduct, generated by the intramolecular nucleophilic attack at the activated isocyanate or its equivalent by the secondary amide nitrogen of the preceding amino acid residue (Figure 5.4).

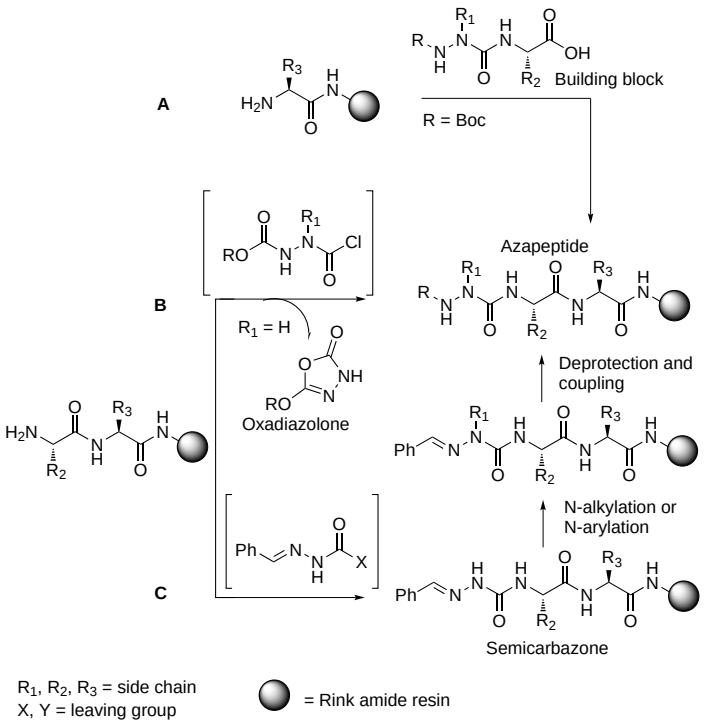

Figure 5.5: The azapeptide synthesis approach mediated by the activation of the hydrazide moiety

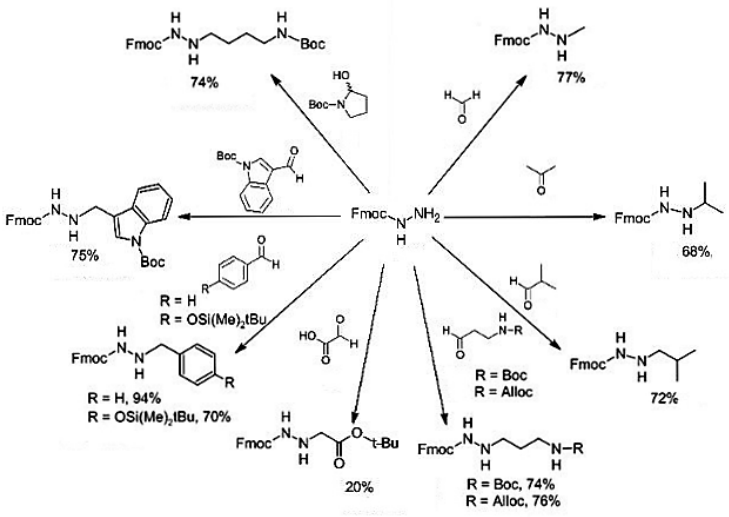

Figure 5.6: Exemples of N-alkyl carbazate precursors for aza-amino acid residues, protected by a fluoren-9-ylmethyl carbazate

To circumvent the formation of hydantoin byproduct, it's possible to activate the N-protected aza-di- or tripeptides (building blocks) and successively couple to the amine terminus of a growing peptide. The *in situ* activation of amino esters with phosgene produces an amino isocyanate that can be coupled to an N-protected substituted hydrazine, to finally obtain a building block that can be used for peptide solid phase synthesis. The drawback with this approach is the reduced activity of the aza-amino acid residue relative to a natural amino acid counterpart for the subsequent coupling reaction for the elongation of the azapeptide sequence (Figure 5.5, pathway A).

An *aza-amino acid scanning* is a systematic sequential replacement of amino acid residues by their aza-counterparts to prepare a library of azapeptides for studying the effects on backbone conformation and activity. To provide this sequential synthesis, it was necessary to develop a systematic method for obtaining different azapeptides in good yield. So, N-alkyl carbazate building blocks were empoyed: their activation by various coupling agents is followed by solid-phase deprotection of the hydrazine terminus and elongation of the peptide sequence. The most used coupling agents include bis(pentafluorophenyl) carbonate, triphosgene, phosgene and CDI (Figure 5.5, pathway B).

N-alkyl carbazate precursors for aza-amino acid residues possessing a variety of side chains have been synthesized for conducted structure-activity relationship studies of biological active peptides (Figure 5.6). They have

Entry	T	Acid catalysis	Hydrazone isolation	Yield
1	r.t.	AcOH (0,9 eq.)	yes	-
2	r.t	APTS (0,1 eq.)	no	49%

Table 5.1: Synthetic trials for the synthesis of the aLys precursor **5.8**

been synthesized by carbazate condensation with an appropriate aldehyde of ketone, followed by reduction using either catalytic hydrogenation or hydride addition. Direct alkykation of N-protected hydrazine with reactive alkyl halides has also been used to install certain chains.

More recently, Sabatino *et al.* proposed another synthetic pathway to prepare azapeptides: the submonomer azapeptide synthesis. This approach applies the Schiff-base amine protection for the modification of glycine esters and amides at the α-carbon. Hydrazone protection is perceived to allow installation of various side chains by alkylation of an aza-glycine residue at the N-terminus of a resin-bound peptide. This submonomer approach consists of acylation of a resin-bound peptide with a hydrazone-derived activated alkylidene carbazate, regioselective deprotonation and alkylation of the semicarbazone and chemoselective semicarbazone deprotection [261] (Figure 5.5, pathway C).

Our synthesis of N'-substituted Boc hydrazines was designed according to the literature procedures for the synthesis of Boc, Fmoc and CbZ substituted hydrazines [230] [260] [232].

aLys-aGly-Phe-CONH2, 5.1 For the synthesis of the azapeptide analogue of the 5-acetamido-2-methoxybenzohydrazide derivate unit **5.1** (Figure 5.7), it was necessary to prepare the N-alkyl carbazate precursor of the aLys. Following the procedure described by Boeglin and Freeman [260] [232], I first prepared the orthogonal protection of the free amine of the 4-aminobutyraldehyde diethylacetal by using benzyl chloroformate in DCM in the presence of TEA. The reaction afforded the desired product **5.6** in 58 % yield. The Cbz-protected 4-aminobutyraldehyde diethylacetal was successively hydrolyzed to afford the cyclized aldehyde **5.7**, necessary for the next alkylation step of the tert-butyl carbazate. The hydrolysis was conducted in a mixture of AcOH and water (2:1) overnight, to afford compound **5.7** as N-carboxybenzyl 2-hydroxypyrrolidine (94 %).

Finally, the protected hydrazine for the synthesis of aLys was made by condensation of tert-butyloxycarbonyl carbazate with compound **5.7** in the presence of APTS. The corresponding hydrazone, used without further purification, was treated with sodium cyanoborohydride under mild acidic

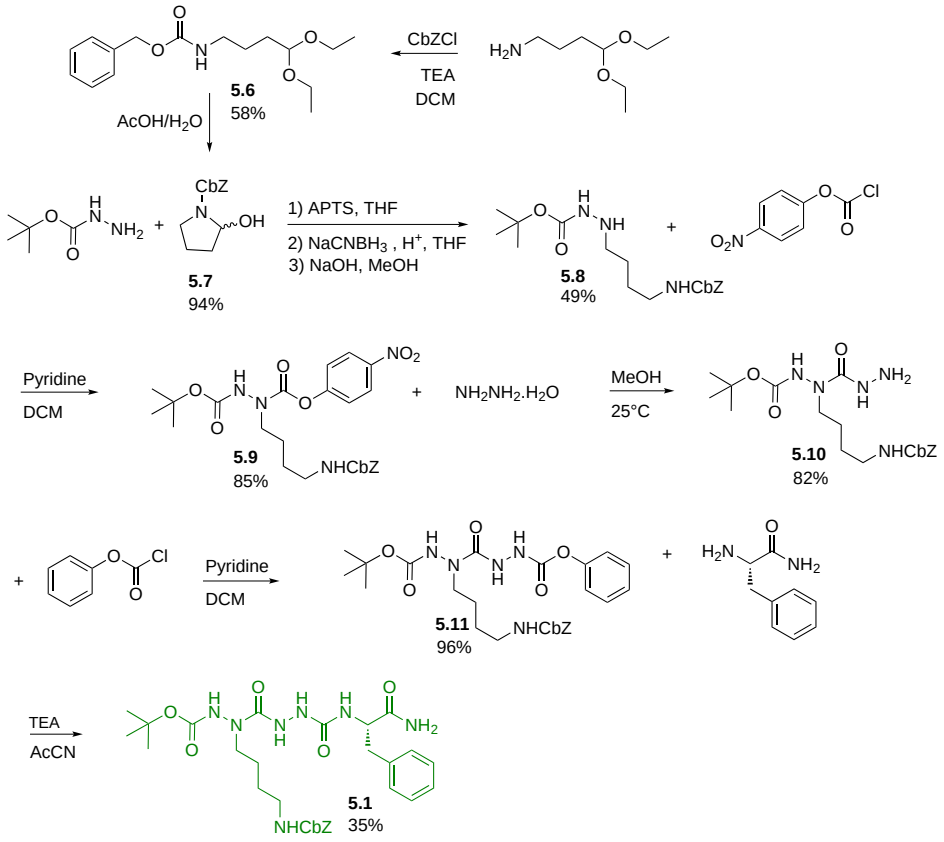

Figure 5.7: Synthetic scheme of compound **5.1**

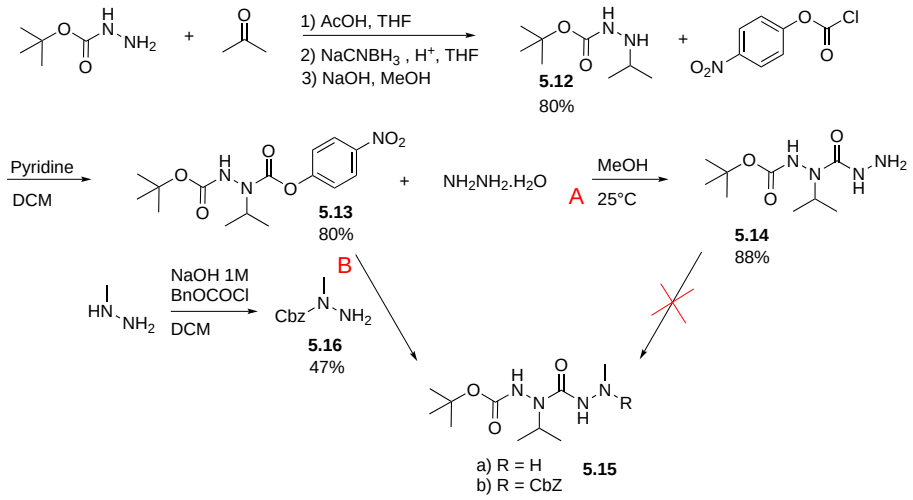

Figure 5.8: First synthetic scheme of compound **5.2**

conditions overnight. By making the reaction twice, I realized that the reaction works better when the corresponding hydrazone is not isolated and when APTS (0.1 eq.) is used instead of AcOH (0.9 eq.) during the formation of the hydrazone (Table 5.1). The obtained BH_2CN adduct was subsequently hydrolized with aqueous sodium hydroxide in methanol to give the desired product **5.8** (49 %).

The carbazate **5.8** was then activated by the 4-nitrophenyl chloroformate in DCM and pyridine to afford compound **5.9** with 85 % yield. Due to the instability of compound **5.9** during the column chromatography conditions and a satisfactory purity after whashing treatment, this activated intermediate was used without further purification for the next coupling reaction.

Compound **5.9** was let to react with hydrazine monohydrate in methanol overnight to afford the di-azatide aLys-aGly precursor **5.10** in 82 % of yield.

The activation of the carbazate **5.10** was performed once with 4-nitrophenyl chloroformate, producing a compound not so stable and too much reactive for the subsequent coupling reaction, and the other time with phenyl chloroformate. In this last case, the reaction, conducted in THF and pyridine, afforded the stable, easy to isolate and pure compound **5.11** with 96 % of yield. I realized that, when the carbonylhydrazine is not substituted, it's better to activate it with a milder chloroformate.

The final coupling reaction with the L-phenylalanine amide was performed in acetonitrile in the presence of TEA, leaving the reaction stirring for three days. After column chromatography purification, compound **5.1** was obtained with a low yied of 35 %.

Entry	T	Acid catalysis	Hydrazone isolation	Yield
1	r.t	AcOH (0,9 eq.)	yes	26%
2	25°C	AcOH (0,9 eq.)	no	72%

Table 5.2: Synthetic trials for the synthesis of the aVal precursor **5.12**

aVal-aAla-Val-CONH2, 5.2 For the synthesis of the azapeptide analogue of the tripeptide sequence Val-Ala-Val, it was necessary first to prepare the N-alkyl carbazate precursor of aVal [232]. N-isopropyl tert-butyl carbazate as precursor of aVal residue was synthesized by condensation of tert-butyl carbazate with acetone in THF that readily gave the corresponding Boc hydrazone, which was reduced without further purification. Reduction was performed with sodium cyanoborohydride under mild acidic conditions achieved by acetic acid. The obtained BH_2CN adduct was subsequently hydrolyzed with aqueous sodium hydroxide in methanol to give the desired N-substituted Boc hydrazine **5.12** (80 %) (Figure 5.8).

Also in this case, I performed the synthesis of the aVal precursor by changing conditions in order to improve the yield of the reaction. The formation of the hydrazone didn't occur without a catalytic amounts of AcOH (0.9 eq.) and the yield was better when the hydrazone was not isolated by column chromatography and when the temperature was controlled by a vertex system at 25 °C (Table 5.2).

The first synthetic pathway (Pathway A) (Figure 5.8), that we adopted to prepare the di-azatide aVal-aAla, planed the activation of the N-isopropyl tert-butyl carbazate and the coupling with the hydrazine hydrate, in order to obtain the di-azatide aVal-aGly **5.15** that would be alkylated with a methyl in a second moment.

First, I tried to find the best conditions to activate the N-isopropyl tert-butyl carbazate and successively to react it with hydrazine. When I employed the phenyl chloroformate, I needed more drastic conditions to perform the coupling with hydrazine, probably due to a non-sufficient activation of the N-alkyl carbazate. The reaction conditions were never reproducible on a large scale and provided problems for purification of compound **5.14** (Table 5.3).

So, I decided to employ the 4-nitrophenyl chloroformate as coupling agent and the yield of the reaction was increased. The possibility to perform the reaction in methanol and to use only 6.0 eq. of hydrazine without the need to use elevated temperatures, allowed to obtain compound **5.14**, easy to isolate by column chromatography (88 %) (Table 5.4).

Once the diazatide precursor aVal-aGly **5.14** was obtained, the next step

Entry	T	Solvent	Eq. of hydrazine	Time	Yield
1	Reflux (60° C)	MeOH	15	3h and then overnight	sm
2	Reflux (101°C)	Dioxane	10	overnight	42% (not pure)
3	Reflux (101°C)	Dioxane	10	4h	32% (not pure) 26% (pure)
4	60° C	Dioxane	6	overnight	89 % (not pure)

Table 5.3: Synthetic trials for the synthesis of the aVal-aGly **5.14** by activation with phenyl chloroformate

Entry	T	Solvent	Eq. Hydrazine	Time	Yield
1	r.t.	Dioxane	4.0	10h	66%
2	25°C	Dioxane	6,0	overnight	73%
3	25°C	MeOH	6,0	overnight	88%

Table 5.4: Synthetic trials for the synthesis of the aVal-aGly **5.14** by activation with 4-nitrophenyl chloroformate

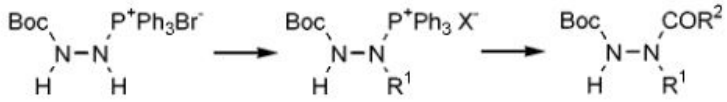

Figure 5.9: The combination of *tert*-butoxycarbonyl and triphenylphosphonium protecting groups in the synthesis of substituted hydrazines proposed by Tsubrik *et al.* [262]

Entry	Reaction condition	Results
1 (Tried on the tert-butyl carbazate as model)	Ph_3PBr_2, TEA, toluene, r.t. nBuLi, THF, 0°C, CH_3I NaOH, DCM and water	No product, only starting material
2 (with isolation of hydrazone intermediate)	Formaldehyde, EtOH, reflux, o.n. $NaCNBH_3$, AcOH, THF, o.n. EtOH, reflux	No product, only starting material
3 (with isolation of hydrazone intermediate)	Formaldehyde, MeOH, reflux, o.n. $NaCNBH_3$, AcOH, THF, o.n. EtOH, reflux	No product
4 (one pot reaction)	Formaldehyde, AcOH, THF, o.n. $NaCNBH_3$, APTS, THF NaOH, MeOH	Crude NMR and Mass spectra showed the product.
5 (one pot reaction)	Formaldehyde, AcOH, THF, o.n. $NaCNBH_3$, APTS, THF, o.n. NaOH, MeOH	Not reproducible in large scale, recuperated starting material
6	CH_3I, HFIP, 60°C, 24h	Recuperated starting material
7	Formaldehyde, AcOH, THF, 3h $NaCNBH_3$, APTS, THF, o.n. NaOH, MeOH	Yield = 23%

Table 5.5: Synthetic trials for the synthesis of the aVal-aAla precursor **5.15a**

was the methylation of the carbazate in order to introduce the methyl side chain of the aAla residue and obtain compound **5.15a**.

I first tried to reproduce the conditions described by Tsubrik *et al.* [262] that reported the simultaneous use of triphenylphosphonium and other protecting group for the systematic synthesis of multisubstitued hydrazines (Figure 5.9). They developed a new reagent containing a combination of Boc and triphenylphosphine groups. This reagent can be easily synthesized from commercially available tert-butyl carbazate and triphenylphosphine dibromide. By the action of 1.0 eq. of BuLi, a phosphinimine is produced; successively, without isolation, the following alkylation is carried out as a one-pot synthesis by using alkyl halide. The triphenylphosphonium moiety can be easily cleaved within 2-3 minutes at room temperature with sodium hydroxide 2 M in DCM.

By using the tert-butyl carbazate (Entry **1**, Table 5.5), unfortunately, I didn't obtain the N-methyl tert-butyl carbazate and so I decided not to reproduce these conditions with the precious intermediate **5.14**.

I tried, then, to investigate the best conditions by using the same procedure that I performed to prepare the aVal precursor (Entries **2** and **3**, Table 5.5). It involved the condensation of intermediate **5.14** with the appropriate formaldehyde to give the hydrazone that was reduced by hydride addition. I followed the procedure proposed by Boeglin *et al.* [260] by preparing the hydrazone in ethanol or methanol at reflux and by performing, after isolation or without isolation of the hydrazone, the reduction step with sodium cyanoborohydride under mild acidic conditions achieved by acetic acid but I didn't obtain the desired product **5.15a**.

I tried also the conditions proposed by Freeman *et al.* [232] by performing a one-pot reaction in THF with acetic acid to promote the formation of the hydrazone and with APTS for the following reduction step with sodium cyanoborohydride. In this case, I obtained the desired product with just 23 % of yield, but unfortunately the reaction was not reproducible in large scale and a significant amount of starting material was recuperated (Entries **4**, **5** and **7**, Table 5.5).

Recently, Lebleu *et al.*[263] described a very simple method for the direct N-monomethylation of primary amines in HFIP. The key point of this method rests on the original role of HFIP that avoids overmethylation by the selective deactivation of secondary and tertiary amines through hydrogen bonding. I tried to follow the same condition with methyl iodide as a source of methyl but I didn't succeed (Entry **6**, Table 5.5).

Due to the difficulties to achieve the methylation of the intermediate **5.14**, we decided to change the synthetic strategy and to prepare individually the two aza-amino acid residues and then to perform the coupling reaction between them in solution phase (Pathway B), (Figure 5.8).

N-methyl tert-butyl carbazate as precursor of aza-Ala residue **5.16** was synthesized by selectively protection of the secondary amine function of N-methyl hydrazine with benzyl chloroformate in DCM (Molecule **5.16**, 47 %) [264].

At this point, I activated the N-isopropyl tert-butyl carbazate with the 4-nitrophenyl chloroformate and I performed the coupling reaction with the CbZ-protected N-methyl hydrazine both in methanol and DCM, with or without DMAP, but I didn't obtain the di-azatide compound **5.15b** (Table 5.6).

Finally, I decided to reverse the direction of the coupling reaction, by activating the CbZ-protected N-methyl hydrazine **5.16** to obtain **5.17** (93 % and successively complete the coupling by adding the N-isopropyl tert-butyl carbazate **5.12** (Figure 5.10). Only by activating the aAla precursor with 4-nitrophenyl chloroformate and by operating with an amount of DMAP at room temperature in DCM, it was possible to obtain the desired di-azatide

Entry	Solvent	Temperature	Time	Base	Yield
1	MeOH	25°C	Overnight	-	No product
2	DCM	rt	30' rt 40°C reflux	DMAP	No product

Table 5.6: Synthetic trials for the synthesis of compound **5.15b**, by activating the aVal residue and successively coupling the aAla residue

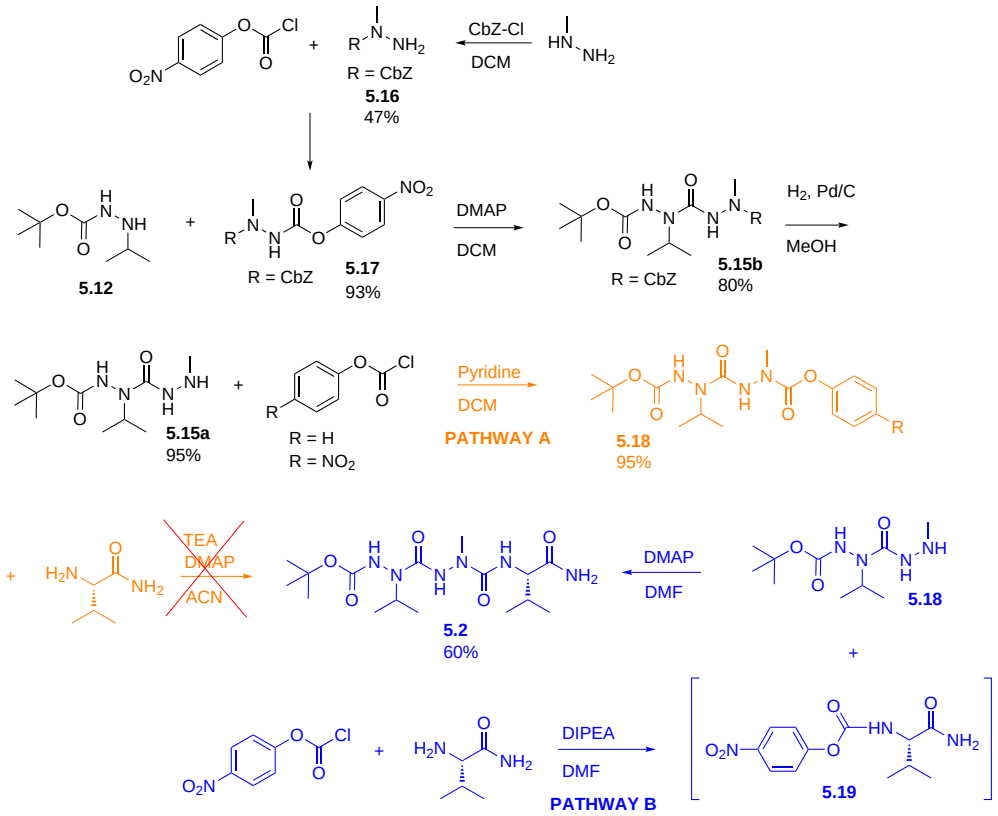

Figure 5.10: Second synthetic scheme of compound **5.2**

Entry	Carbonyl donor	Temperature	Time	Base	Solvent	Yield
1	Phenyl chloroformate	rt	Overnight	DMAP	DCM	No product
2	p-NO_2 phenyl chloroformate	rt	Overnight	DMAP	DCM	80%

Table 5.7: Synthetic trials for the synthesis of compound **5.15b**, by activating the aAla residue and successively coupling the aVal residue

chain aVal-aAla **5.15b** in 80 % of yield (Table 5.7).

Thanks to the orthogonally protective groups, we cleaved the CbZ group by hydrogenolysis in the presence of 20 % Pd/C in MeOH to achieve the intermediate **5.15a** (95 %) with the free secondary amine function for the next coupling reaction with L-valinamide.

Activation of intermediate **5.15a** with either phenyl chloroformate or 4-nitrophenyl chloroformate and coupling of the activated compound **5.18** with L-valinamide hydrochloride in the presence or not of DMAP in acetonitrile and TEA didn't afford the final compound **5.2** (Figure 5.10, pathway A).

So, to couple the diazatide moiety to a natural amino acid, we designed the activation of the free primary amine of valinamide by using 4-nitro phenyl chloroformate in order to generate *in situ* the activated complex **5.19**. This latter was not isolated but on the contrary immediately reacted, by adding the diazatide oligomer **5.15a** in DMF in the presence of DMAP, to complete the synthesis of the 2:1 [Aza/α]-tripeptide **5.2** (aVal-aAla-Val-CONH2) in 60 % yield (Figure 5.10, pathway B).

aVal-aAla-Val-COOBn, 5.3 For the synthesis of the azapeptide analogue of the tripeptide sequence Val-Ala-Val with the ester instead of the amide at the C-terminus, we followed the same synthetic pathway of compound **5.2** but instead of using the valinamide for the last coupling reaction, we used the valine benzyl ester to obtain the final compound **5.3** in 66 % yield (Figure 5.11).

5.3 Conformational studies

In this section, we present the results obtained from the conformational analyses by X-ray cristallography, NMR and molecular modeling, conducted on the three compounds **5.1**, **5.2** and **5.3**. Our objective was to investigate the conformational preference of a 2:1 [Aza/α]-tripeptide sequence in solution compared to a natural tripeptide. In particular, our interest was to get more

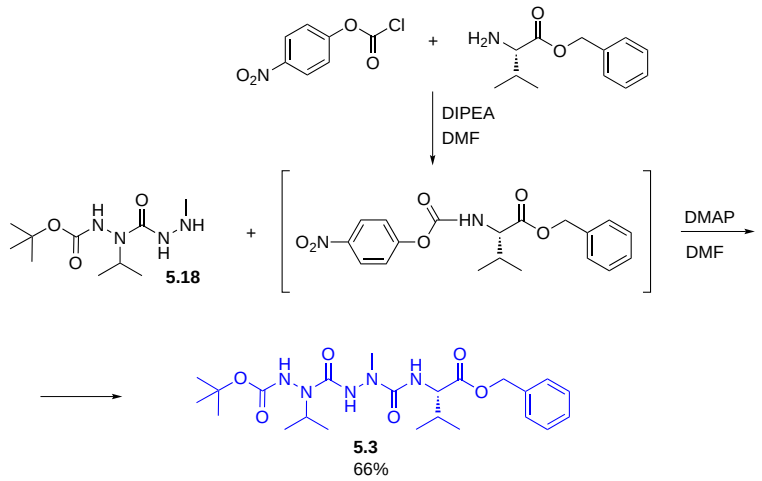

Figure 5.11: Synthetic scheme of compound **5.3**

in detail in the conformational studies of azatide chains, due to the lack in literature of a deep understanding about their role in a peptide sequence, and also to observe if this type of peptidomimetics could be able to adopt a β-strand conformation when employed in a β-hairpin structure.

In a previous work conducted in the laboratory [265], it was demonstrated that carbonylhydrazide-based molecular tongs inhibit wild-type and mutated HIV-1 protease dimerization. It was showed that the presence in the molecular tongs arms of carbonylhydrazide (CONHNHCO) peptidomimetic fragment that have perpendicular hydrogen bonding properties led to a noticeable increase of the inhibitory activity. Molecular modeling was used to build several complexes that might be formed between the molecular tongs and the HIV-1 protease monomer and they were used to correlate inhibitory activity with structural characteristics. The designed carbonylhydrazide peptidomimetics, having the sequence aGly-aGly-Val-$CONH_2$, showed an extended conformation compatible with the formation of a β-sheet structure. Also after minimization, the carbonylhydrazide peptidomimetic arms maintained the extended conformation and the postulated β-sheet structure was not disrupted. However, no conformational studies of the molecular tongs (without the presence of the target protease) have been conducted.

Starting from these observations, we were interested to know if the presence of side chains on the α-nitrogen of the 2:1 [Aza/α]-tripeptide could affect the extended conformation that we observed with aGly-aGly-Val-$CONH_2$ and if the fact to be bounded or not to the target protein could play a determinant role on the conformational preference of an azapeptide.

So, here I begin to present a general overview on the conformational properties of azapeptides and successively I will report our findings from

X-ray crystallography, NMR and molecular modeling, respectively.

Studying the 3D molecular structure of peptides and peptidomimetics is important because their specifically adopted conformation is the driving force for the binding to an acceptor molecule. Stabilization of particular conformation features by the introduction of geometrical constraints may be of major interest for the establishment of structure-activity relationships, view that the substitution of nitrogen for the α-carbon leads to significant changes in the structure and dynamics of the peptide backbone and to reduced flexibility [257] [259].

5.3.1 State of the art

Introduction of an α-nitrogen atom generates two structural elements: hydrazine, whose conformation is described by the peptide torsion angle ϕ, and urea constituent, where the peptide rotation angle ψ indicates the various conformation possibilities [231]. In order to understand the conformation of azapeptide, several model systems have been examined.

Computational analysis of 1,2-diformylhydrazine indicated that the stable structures of the molecule are non-planar at nitrogen and show twisted conformation around the N-N bond (φ dihedral angle) [266]. The tendency of the molecule to destabilize the planar structures is a typical feature of the hydrazine derivates and was ascribed to the antibonding effect of the four π electrons in the planar conformation. The twisted structure of 1,2-diformylhydrazine is the preferred conformation but the planar conformation is destabilized by $55\,\mathrm{kJ\,mol^{-1}}$ with respect to the twisted conformation. In fact, the π-electron-withdrawing properties of the formyl group contribute to delocalize partly the nitrogen atom lone pair onto the carbonyl group and consequentely to reduce the destabilization of the planar form with respect to the hydrazine molecule itself. The formyl group helps to stabilize the planar structure by delocalizing the nitrogen atom lone pair onto the carbonyl system and with the hydrogen bonds formation contributes to stabilize the planar structure in accordance with the crystal molecule. The presence of two methyl groups instead of two formyl groups makes the energy difference between the two twisted and planar conformation greater, demonstrating that a weak π-electron donor group such as methyl can increase the barrier of planarity of hydrazine derivates [266].

Calculations which have been used to determine the minimum energy structures of 1,2-diformylhydrazine and its N-substituted derivatives show that the global minimum is the non planar structure in which nitrogen lone pairs are perpendicular to one other. However the energy barrier required for (Z,Z)-diformylhydrazine to adopt a planar structure is very low (Figure 5.12). When the nitrogen are substituted, the hydrogen, that form intramolecular hydrogen bonds, are lost and the planar structure becomes less stable relative to the twister rotamer [267].

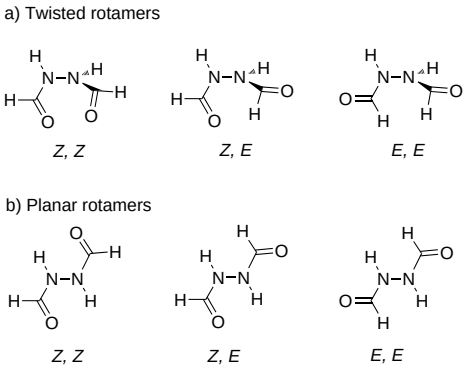

Figure 5.12: Rotamers of 1,2-diformylhydrazine

In order to get general information on the consequences of the introduction of aza-amino acids into peptide sequence, Thormann *et al.* systematically examined the conformation of several model compounds for azapeptides (1,2-diformylhydrazine, hydrazine, diamide analogues of peptides as For-AzaXaa-NH_2, Ac-AzaXaa-NHMe with AzaXaa=AzaGly and AzaAla and finally triamide analogues as Ac-AzaXaa-L-Ala-NHMe and Ac-L-Ala-AzaXaa-NHMe, with AzaXaa=AzaGly and AzaAla) on the basis of *ab initio* MO theory at various approximation levels. This study leaded to a characteristic conformer pattern which excluded the possibility of β-sheet conformation, but indicated a high potency for the formation of helix and β-turn structures. On the basis of the results obtained for hydrazine and 1,2-diformylhydrazine and the well-known planar structure for urea, typical torsion angle values of $\pm$70–95° for ϕ and about 180° or, alternatively, 0° for ψ could be expected in azapeptides [231].

The aza-amino acid residue may be better considered as having a configurationally labile α-center, which may invert between two mirror image nitrogen pyramids passing through a planar structure. Although rapid inversion may be expected at room temperature, a particular chiral nitrogen pyramid may be preferred contingent on peptide sequence. For exemple, the nitrogen at the α-position may, in principle, participate in hydrogen bonds, which could favor a preferred geometry [231] [268].

A natural bond orbital (NBO) analysis was performed to evaluate the origin of rotational barrier in azapeptides that have the possibility to show different conformation in solution or solid state in case that the repulsion energy between nitrogen lone pairs is not large enough. The barrier energy in the rotation of the N-N bond is composed of structural energy (bond and lone pair energies), steric repulsion energies and delocalization energy. The pyramidalization of nitrogen atoms leads to decrease structural energy changes and increase the total exchange repulsion and delocalization energies.

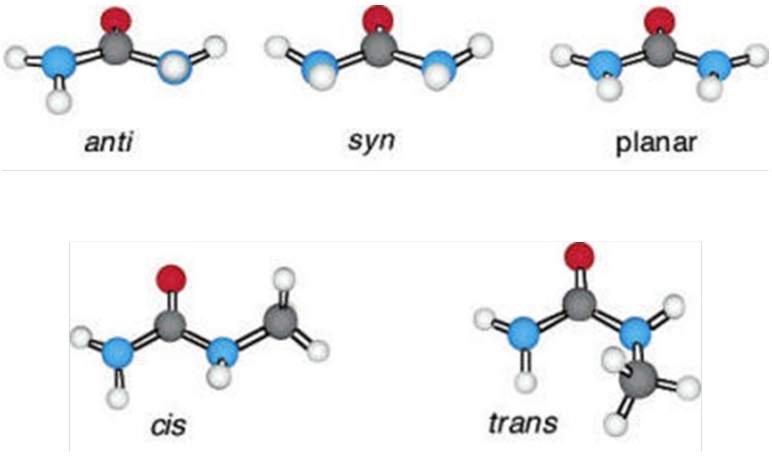

Figure 5.13: Urea and alkylurea geometries

The intramolecular hydrogen bonding energy could be important term in forming planar conformation, as found in crystal structure, but is not dominant energy term to lower the barrier in comparison to the amide resonance and total exchange repulsion [269].

As we said, the other structural element in the aza-peptide structure that can influence the various conformation possibilities is the urea constituent. The conformational analysis and rotational barriers of alkyl- and phenyl-substituted urea derivatives have been explored by Bryantsev *et al.* [270] and the results establish that in contrast to urea, for which both *anti* and *syn* equilibrium conformations exist (Figure 5.13), *syn* forms of mono-alkylureas are not stationary points and the *cis* configurations are more stable than *trans* configurations (Figure 5.13).

Semetey *et al.* demonstrated that in ureidopeptide derivatives, the urea moiety classically assumes the *all-trans* planar conformation in the crystal state but it is able to adopt a stable *cis-trans* conformation in low polar solvent, which can be further stabilized by an intramolecular hydrogen bond [271] (Figure 5.14).

In literature, we can find some exemples of model compounds containing different aza-amino acid residues which have been investigated by computational, crystallographic and spectroscopic approaches. Most of these studies were conducted on azapeptide models (tri- or tetrapeptide) in which only one natural amino acid was replaced by an aza-amino residue or on dipeptide building blocks composed by a natural amino acid linked to an aza one. Close to a few examples of structural studies conducted by NMR and X-ray crystallography, we ascertained a greater interest in theoretical studies with an NBO approach to give an overview of how the aza amino acids might act in a peptide sequence. However, an overview of the preferred conformations

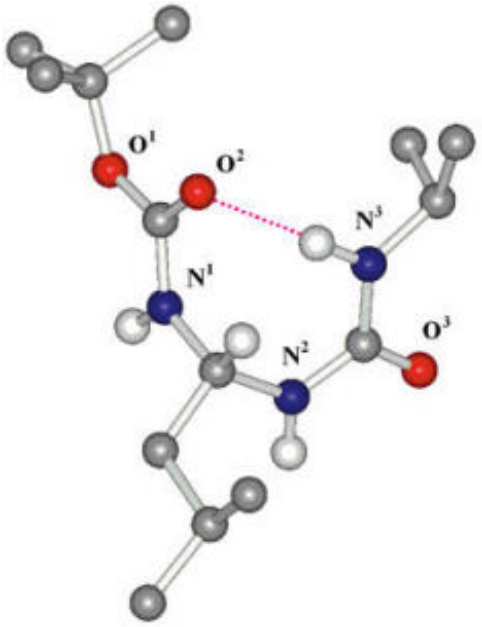

Figure 5.14: The urea moiety in a single-residue ureidopeptide assuming a *cis-trans* conformation [271]

of sequences composed by two or more aza amino acids (azatide) is still far from clear and comprehensive.

Studies of model peptides containing various aza-amino acids using *ab initio* calculations and NMR spectroscopy, indicated that the preferred backbone conformations of aza-amino acids (azaAla, azaGly, azaLeu, azaPhe) in peptides are similar regardless of the side chain functional groups brought by the nitrogen, and the preferred conformations for these residues are limited to the range of stereochemically allowed dihedral angle ($\phi = \pm 90° \pm 30°$, $\psi = 0° \pm 30°$ or $180° \pm 30°$) unlike the amino acid residues. These dihedral angles values appeared to be the β-turn motif for the $i+2$ residue [272].

In order to investigate the role of aza-amino acid in the peptide structure and the influence of the change of chain length by the addition of an aza-amino acid in azapeptide, Lee *et al.* employed *ab initio* MO theory to calculate the backbone dihedral angle of the most stable conformer for For-Ala-aAla-NH_2 in comparison with that of the azapaptide model, For-aAla-NH_2. The theoretical results were successively compared with the solution conformation of two azapeptides, Boc-Ala-Phe-azaLeu-Ala-OMe and Boc-Phe-azaLeu-Ala-OMe, by using IR, NMR and restrained molecular dynamics.

They demonstrated with *ab initio* calculation that the βII-turn was the lowest energy conformation of For-Ala-aAla-NH_2 and they verified that the incorporation of an additional amino acid in the designed di-azapeptide

would not influence the backbone dihedral angles of the azaamino acid, in azapeptides with the stable β-turn structure. This implies that the intercalation of an azaamino acid residue in tripeptide or tetrapeptide induces the βII-turn conformation, and the increase of chain length by the addition of an amino acid in azapeptide constituents would not disrupt the backbone dihedral angle pattern. Therefore, these findings suggest that aza-amino acids could be utilized in designing new peptidomimetics adopting β-turn scaffold [268].

A similar approach was followed in the investigation of another model compound, Ac-aPhe-NHMe: its theoretical conformation, performed by *ab initio* calculation, was compared with that of Ac-Phe-NHMe to investigate the influence of the Phe group in the structure of the azapeptide. Also in this case it was demonstrated that the incorporation of aPhe residue in designed azapeptide would not perturb the backbone dihedral angles of azapeptide occurring at the stable β-turn structure. The solution structure of the designed azapeptides, including azaPhe residue and varying the natural amino acid immediately preceding the aza residue, clearly indicated that the intercalation of azaPhe residue in synthetic tripeptide provides the stable βII-turn conformation [273].

A more recent work has shown the experimental evidence that the azapeptide building blocks, used for the *ab initio* calculation, led to a β-turn conformation. Abbas *et al.* described the preparation of a 2:1 [α/aza]-oligomer precursors (Boc-aXaa-Xbb-OMe) that can be used as building blocks for introduction into biologically active peptides. Conformational studies showed that these building blocks with an amino acid further led to β-turn folded structure [274].

Successively, Zhou *et al.* investigated the role of an aza-amino acid residue in the oligomer structure obtained by oligomerization of an α/aza/α pseudotripeptide. The NMR, FTIR, restrained molecular dynamics and X-ray diffraction analyses show that 2:1 [α/aza]-oligomers are able to adopt a $i+2$ hydrogen-bonded helical conformation [275].

So, we can observe that a limit to these studies is to consider the individual building block and its structure as a predictor of the azapeptide final conformation. As we could see from the last exemple, the building block provided a β-turn conformation but on the other side its oligomer counterpart showed an helical conformation. This suggested us that the effective role of the aza-amino acid in a peptide sequence is not yet completely explored, in particular for peptidomimetics characterized by more than one aza-amino acid residue in the sequence. The information that we can receive from the literature is not yet able to respond to the conformational requirements for azapeptide compounds composed by more than one aza amino acid and for azatide oligomers composed by only aza-amino acids.

Only Han *et al.* reported an efficient method for both solution and soluble polymer syntheses of a biopolymer mimetic consisting of α-aza amino acids

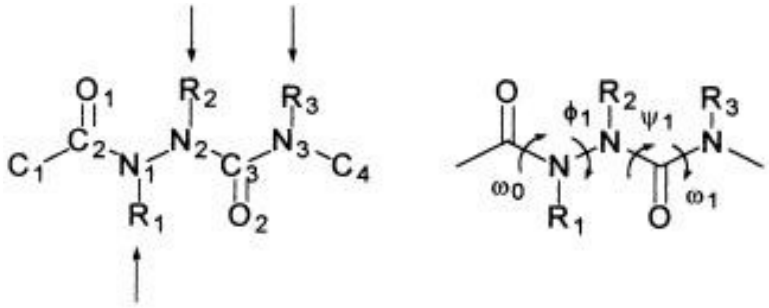

Figure 5.15: General chemical structure and torsion angles for N-methyl azapeptide derivatives [276]

in a repetitive manner to form what we term an azatide oligomer. This is the first azatide oligomer sequence synthesized. However, they didn't afford an X-ray structure of the pure azapeptide, so the exact bioactive conformation of this peptide remained shrouded. They just reported in the paper that simple unsubstituted diacyl hydrazines (i.e., glycine azatides) contain a dihedral (ϕ) angle of ca.$-175°$, while N-substituted ones (i.e., all other azatides) possess a dihedral (ϕ) angle of ca. $-110°$. Taken as a whole, these data suggest that this type of peptidomimetics should adopt a more extended conformation within the critical glycine region [230] [243].

Another theoretical study of conformational properties of N-methyl azapeptide derivatives (general formula Ac-azaXaa-NHMe, where azaXaa=azaGly or azaAla) was conducted in order to study the structural perturbation by methyl group substitution in three N-positions of an aza-amino acid (Figure 5.15) [276]. N-methyl groups, depending on their positions, were found to affect the orientation of the amide group in the lowest energy conformations, the pyramidality of the N2 atom, and the bond length in azapeptide derivatives.

The methyl groups at the N1 and N2 position demonstrated to restrict the energetically allowed ϕ and ψ dihedral angles of the aza-amino acid with respect to the Ac-aGly-NHMe, without perturbing much the structure, whereas the additional N-methyl group on the N3 atom significantly changed the backbone torsion angles. The β-strand regions (ϕ and ψ around 180°) were destabilized by N-methylation [276].

The rotational barrier of N1-N2 bond (ϕ) and N2-C3 bond (ψ) could give insight into the preferred conformation or rigidity of azapeptides. The rotational barrier of N1-N2 bond (ϕ) depends on the orientation of the acetyl amide group and the number of methyl groups bound to azapeptide derivatives, in particular the methyl groups at N1 and N2 position increase the rotational barriers due to steric hindrance. Methyl groups at the N3

position would not affect the rotational barriers of the N1-N2 bond.

The average rotational barrier for the N2-C3 bond (ψ) is relatively higher when an additional methyl group at N3 is present. The rotational barrier of the N1-N2 and N2-C3 bonds are sufficiently large to restrict the free rotation [276].

In addition to the backbone dihedral angles, another characteristic structural difference in N-methyl azapeptide is the pyramidalization of the N2 position. A methyl group bound to the N2 enhances the planarity of the α-nitrogen atom and pyramidalization of the N2 atom decreases the amide conjugation between N2 and C3=O and increases the N2-C3 bond length, indicating that N2-methyl group can stabilize the urea-type amide resonance structure of azapeptide derivatives [276].

More recently, it was demonstrated that methylation of the peptide bond in model azadipeptides leads to the *E* configuration of the CO-NMe and hence to atropisomerism due to a restricted rotation around the N-N axis [277] [278]. Atropisomerism is a source of chirality that has been increasingly recognized as a concept in drug developement, since chirality of small molecules results in different pharmacological effects of the distinct enantiomers. The author considered azadipeptide amides to be atropochiral molecules with a hindered single-bond rotation. Diastereotopicity was applied as a sensor of chirality to reveal atropisomerism which originates from a restricted rotation around the N-N bond [277].

X-ray cristallographic analyses have been performed on simple aza-amino acid model systems, short azapeptides, as well as all azapeptide renin inhibitor [279][280][281][282][283][284]. Among these few exemples of azapeptides for which X-ray data are available, the majority possess proline or aza-proline residues, which may favor the observed turn conformation. In general, X-ray structures of aza-peptides showed an α-N-CO bond which is longer (0.3–0.6 Å) than a peptide amide bond and shorter (0.11–0.14 Å) than the usual distance of the peptide α-C-CO bond [257].

Recently, Zhang *et al.* demonstrated by CD and molecular dynamics, that the addition of an extra H-bond donor in collagen, through the substitution of glycine with aza-glycine, may increase the number of interfacial cross-strand H-bonds and can lead to a hyperstable collagen triple helix [285].

In this scenario, with a lack of information about the structural conformation of a di-azatide peptidomimetic, linked to a natural amino acid, we decided to perform some conformational analyses on the three different synthesized peptidomimetics **5.1**, **5.2** and **5.3**. In particular, we have tried to compare the results obtained with different techniques in order to find a correlation between the peptidomimetic sequence (the type of side chains and the position of the aza-amino acid residue) and its conformational preference. Our interest was to know how the α-nitrogen and the side chain, eventually linked to it, could influence and affect the conformation with respect to a natural peptide. Together with experimental information, taken from

NMR spectroscopy and X-ray crystallography, we performed computational analysis by molecular modelling.

5.3.2 General procedures for the conformational analyses

To get information concerning the conformational behaviour of a 2:1 [Aza/α]-tripeptide, we decided to perform 2D-NMR analysis and deduce some structural information from through-bond (scalar or *J coupling*) or through space (Nuclear Overhauser Effect, *NOE*) magnetization transfer between pairs of protons.

Proton NMR spectra were recorded on a spectrometer operating at 400 MHz (at Chatenay-Malabry, BioCIS) or 500 MHz (at UPMC, in collaboration with Pr. O. Lequin and Dr. I. Correia, UMR 7203). ^{1}H and ^{13}C resonances were completely assigned using 1D ^{1}H, 2D ^{1}H-^{1}H COSY, 2D ^{1}H-^{1}H ROESY, 2D ^{1}H-^{13}C HSQC and 2D ^{1}H-^{13}C HMBC spectra. ^{1}H and ^{13}C chemical shifts were calibrated using the solvent residual peak (DMSO-d_6, δ ^{1}H 2.50 ppm, δ ^{13}C 39.51; DMF-d_7, δ ^{1}H 2.92 ppm, 2.75 ppm and 8.03 ppm, δ ^{13}C 34.89, 29.76 and 39.51; CD_3OH, δ ^{1}H 3.31 ppm, δ ^{13}C 49.5 ppm).

A first structural information was deduced from through space dipole-dipole coupling correlations (ROEs): extended conformations are characterized by short sequential and medium intraresidual distances, while folded structures are identified by numerous long-range ROEs involving both backbone and sidechain protons.

To provide information on the network of hydrogen bonds and their relative stabilities, it's possible to examine the temperature dependence of amide proton chemical shifts. Amide protons that are engaged in intramolecular hydrogen bonds typically exhibit small temperature dependence ($\Delta\delta_{NH}/\Delta$T $>$ -4.5 ppb K^{-1}) in aqueous and alcoholic solvents, while those that are not intramolecularly hydrogen-bonded usually exhibit large negative values of their temperature coefficients [152].

The temperature gradients of the amide proton chemical shifts were derived from the 1D ^{1}H spectra recorded between 258 K and 313 K.

One particularly important application of the coupling constant is as a measure of the coupling between the H^{α} and the H^{N} in the peptide backbone. This coupling depends on the ϕ-angle in the peptide bond. The Karplus curve shows the correlation between the coupling between H^{α} and the H^{N} and the ϕ-angle. It is seen that coupling constant is around 4 Hz for peptide segments in α-helices where the ϕ-angle is around $-60°$, and it is between 8 Hz and 12 Hz for peptide segments in β-structures, where the ϕ-angle is in the $-120°$ range [177].

Vicinal coupling constants were extracted from 1D ^{1}H spectrum at the temperature of the 2D-NMR analysis.

Correlations between chemical shift tendencies and secondary structures

have also been considered. Chemical shift deviations (CSD) are defined as the difference between experimental chemical shifts and corresponding random coil values and are considered good descriptors of backbone conformational space for each residue. The chemical shifts deviations were calculated as the differences between observed chemical shifts and random coil values reported by Wishart *et al.* [178].

Molecular mechanic studies were performed using Macro-Model from the Schrodinger software suite (MacroModel, version 10.2, Schrodinger, LLC, New York, NY, 2013). An arbitrary initial conformation of the compound was energy-minimized using the conjugate gradient method with the OPLS-2005 force field and GBSA as an implicit water solvation model. The convergence criterion was set to $0.05\,\mathrm{kJ\,mol^{-1}\,\AA^{-1}}$ on the energy gradient.

An unconstrained conformational search was then performed starting from this structure and using the MCMM (Monte Carlo Multiple Minima) method with the same force field, the solvation model and the convergence criterion. 100000 conformations were generated, energy-minimized and deduplicated [152].

For the clustering of these results we used the centroid linkage method with a 0.66 Å merge distance threshold [152].

5.3.3 Structural constituents of a 2:1 [Aza/α]-tripeptide

In order to better understand the structural elements that we will consider to perform the conformational analyses of the azapeptide peptidomimetics, we found necessary to make a brief and comprehensive as possible overview of the definitions of the structural constituents of our azapeptides.

First, we call 2:1 [Aza/α]-tripeptide a peptidomimetic sequence composed by three elements: two aza-amino acid residues and a natural amino acid. In this sequence, we can recognize two diformylhydrazine motifs (green parts in Figure 5.16) and two urea constituents (blue parts in Figure 5.16).

The conformation of the hydrazine elements can be described by the peptide torsion angle φ that we define as the dihedral angle between two intersecting planes defined by the four heavy atoms C(O), N(H), N(R) or C(R), C(O). On the other hand, the various conformation possibilities of the urea constituent are indicated by the ψ peptide rotation angle that we define as the dihedral angle between two intersecting planes defined by the four heavy atoms N(H), N(R) or C(R), C(O), N(H) (Figure 5.16).

The dihedral angle associated with the peptide group (defined by the four atoms N(R), C(O), N(H), N(R) or C(R)) is denoted ω ; $\omega = 0°$ for the *cis* isomer (synperiplanar conformation) and $\omega = 180°$ for the *trans* isomer (antiperiplanar conformation). In the first case the N-H bond is oriented in a direction opposed to that of the carbonyl and in the second one in the same direction to that of the carbonyl (Figure 5.16).

The urea constituent can exhibit two *trans* amide bonds, so that both N-R

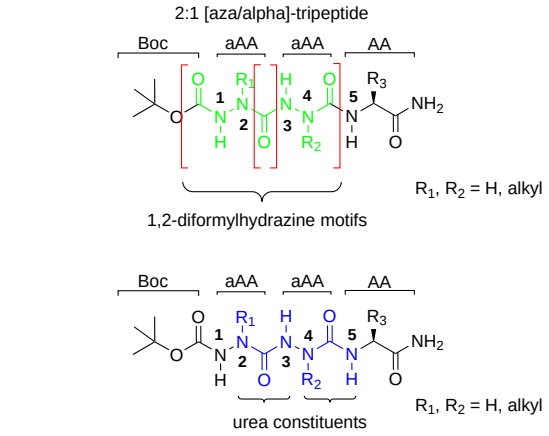

Figure 5.16: Structural constituents of a 2:1 [Aza/α]-tripeptide

Residue	δ NH (ppm)	δ H_α (ppm)	δ H_β (ppm)	δ other protons (ppm)	δ CO (ppm)	δ C_α (ppm)	δ C_β (ppm)	δ other carbons (ppm)
a-Lys (i)	9.14	/	3.35	H_γ 1.43 H_δ 1.42 H_ε 3.00 NH_ζ 7.10	158,6	/	47.8	C_γ 24.0 C_δ 26.6 C_ε 40.1
a-Gly (i + 1)	7.75	8.65 (NH)	/	/	155.0	/	/	/
Phe (i + 2)	6.18 (J=8.3 Hz)	4.26	3.06, 2.76	Ar: 7.23, 7.17	173.7	54.4	37.8	Ar: 138.1, 129.1, 128.0, 126.1

Table 5.8: Chemical shifts for protons and carbons of **5.1**

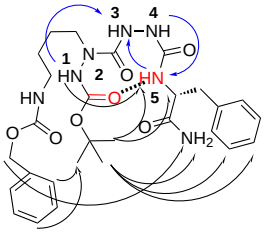

Figure 5.17: Schematic representation of **5.1** conformational structure; in blue arrows the ROEs, confirming the presence of a β-turn and in black arrows the long-range ROEs

and N-H bonds are oriented in a direction opposed to that of the carbonyl (all-*trans* planar conformation *Z,Z*), or one *cis* amide bond and the other *trans*, so that the N-R bond is oriented in the same direction of the carbonyl and the N-H bond in a direction opposed to that of the carbonyl (*cis-trans* conformation *E,Z*) (Figure 5.16).

5.3.4 Conformational analyses of compound 5.1

NMR studies Proton NMR spectra of compound **5.1** were recorded on a spectrometer operating at 400 MHz, equiped with a MicroProbe, at 298 K. Compound **5.1** was dissolved at a concentration of 0.23 M in 35 µL of DMSO-d_6. The observed proton and carbon chemical shifts are displayed in Table 5.8.

A number of sequential $d_{NN}(i, i+1)$ ROEs were observed in the whole segment, which indicate that the molecule adopts a folded conformation. In particular, we observed a strong ROE between the NH(5)-Phe and the

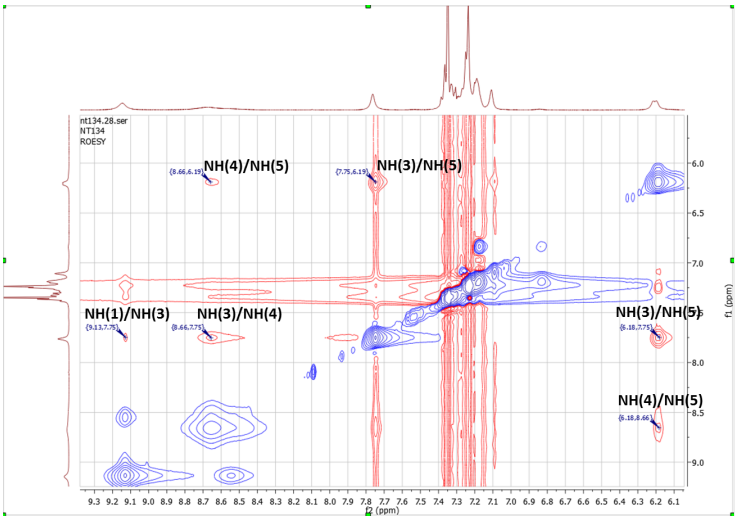

Figure 5.18: The assigned ROEs of **5.1**, confirming the presence of a β-turn

NH(3) of aGly (Figure 5.17) and a medium ROE with the α-nitrogen proton NH(4) of aGly. These two latter indicate that the azatide adopts a βII-turn structure. However the presence of a weak ROE between the NH(3) of aGly and the proton amide NH(1) of aLys suggests that the azapeptide has also the possibility to form a βI-turn structure, although we are unable to determine the relative *ratio* between the two structures (Figure 5.18) [268] [273].

We observed numerous long-range ROEs between the two N- and C-terminus of the diazapeptide. The Boc protective group of aLys and the α-hydrogen, the amide proton and the side chain of Phe face together and the two side chains of the aLys and Phe make contact among them (Figure 5.19).

The urea-type Phe NH(5) of the azatide **5.1**, resonating at 6.18 ppm, seems to be involved in intramolecular hydrogen bonding since the hydrogen-bonded urea-type NH resonates at 5.62 ppm in chloroform [268] [273]. We supposed that the intramolecular hydrogen bond, that stabilizes the folded structure, involves the PheNH(5) and the (Boc)CO groups (Figure 5.17).

We examined the temperature dependence of amide proton chemical shifts as it can provide information on the network of hydrogen bonds and their relative stabilities. The amide protons of Phe exhibited the smallest variation ($\Delta\delta_{NH}/\Delta$T = -2.5 ppb K^{-1}), demonstrating the engagement in an hydrogen bond. On the contrary, the other amide protons had higher coefficients and exposed to the solvent (Table 5.9).

The coupling constant of the natural amino acid in the sequence exhibited a value of 8.3 Hz, reflecting a ϕ angle value around $-120°$, as expected for

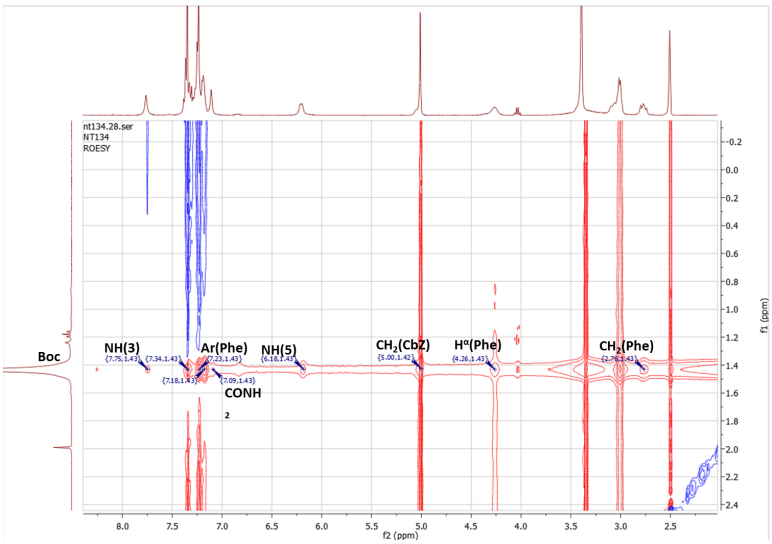

Figure 5.19: The assigned ROEs of **5.1**, confirming the contact between the N- and C-terminus

Residue	$\Delta\delta/\Delta T$ (ppb K^{-1})
a-Lys NH(1)	- 5.5
a-Gly NH(3)	- 5.0
a-Gly NH(4)	- 7.5
$CONH_2$	- 6.0
Phe NH(5)	- 2.5

Table 5.9: Temperature coefficients for the amide protons of **5.1** in DMSO

Residue	NH (ppm)	H^{α} (ppm)	C^{α} (ppm)	CO (ppm)
Phe	- 2.12	- 0.36	- 3.3	- 2.1

Table 5.10: Chemical shift deviations (CSD) of Phe residue of compound **5.1** in DMSO

β-strand conformation [177]. However, the Karplus correlation reflects a dihedral ϕ angle that takes into account the two coupled protons and not the heavy atoms of the backbone. So, it provides an information that doesn't clearly reflect the backbone trend and the dihedral angle values that are used as descriptors of a βturn conformation.

Finally, we calculated the CSD for the natural amino acid and we observed that the carbonyl group and the α-carbon were upfield as the amide proton and the α-hydrogen (Table 5.10). These negative CSD values are in agreement with a folded region that involves the Phe residue in the sequence.

MM studies Molecular mechanic studies were performed on compound **5.1** and other two analogues: one exhibiting only aGly residue in the middle together with natural Lys and Phe amino acids, on the left and on the right respectively (BocNH-Lys-aGly-Phe-$CONH_2$), and one presenting all three aza-amino acid residues (BocNH-aLys-aGly-aPhe-$CONH_2$).

For compound **5.1**, clustering yielded 286 representative conformations within a sliding energy window of 16.112 kJ mol^{-1}. Most of them exhibited an extended conformation, in particular in the central region, corresponding to the diformylhydrazine motif. In all the extended structures, the urea constituent assumed the classical *all-trans* planar conformation. All the amide bonds were trans-planar, except for the Boc that showed an equilibrium between *cis* and *trans* isomers. Although the αNH(4)-CO bond of the aGly residue was present in a *Z* conformation for only the extended structures, on the contrary the RN(2)-CO bond of the aLys residue showed an *E* configuration for all the type of conformations (Table 5.11).

The first two structures at the lowest energy (-778.029 kJ mol^{-1} and -777.349 kJ mol^{-1} respectively) were extended (Entries **1** and **2**) (Figure 5.20). The β-turn motif with the hydrogen bond between the Boc carbonyl group and the proton amide of Phe was detected at the third (-776.717 kJ mol^{-1}) and 32^{nd} (-770.197 kJ mol^{-1}) position (Entries **3** and **32**) (Figure 5.20).

The calculated distances between the amide protons, that characterize the βI/βII-turn motif of the third entry, were consistent with the experimentally observed ROEs for both conformations (less than 5.0 Å).

The backbone dihedral angles for the two lowest energy β-turn conformations were found to be the dihedral angles that appear in the βI-turn

Entries	Relative Potential Energy (kcal/mol)	Peptide bonds	Urea type bonds	φ angles	ψ angles	Distance (Å)
1	1.161	*cis, trans, trans*	*E, Z*	φ_1= 83.5 φ_2= 167.6 φ_3= 81.0	ψ_1= -9.3 ψ_2= -175.2 ψ_3= -19.8	a) 2.92 b) 4.21 c) 2.20
2	1.324	*cis, trans, trans*	*E, Z*	φ_1= -84.8 φ_2= -158.1 φ_3= -82.1	ψ_1= 2.9 ψ_2= 173.9 ψ_3= -18.8	a) 2.71 b) 4.24 c) 2.21
3	1.475	*trans, trans, trans*	*E, E*	φ_1= 64.8 φ_2= 82.5 φ_3= -87.4	ψ_1= 2.4 ψ_2= 10.2 ψ_3= -18.7	a) 3.18 b) 2.30 c) 3.43
16	2.400	*trans, trans, trans*	*E, E*	φ_1= 87.5 φ_2= -75.7 φ_3= -77.8	ψ_1= 13.4 ψ_2= -5.9 ψ_3= -14.1	a) 2.50 b) 2.92 c) 3.40
32	3.035	*trans, trans, trans*	*E, E*	φ_1= 66.4 φ_2= 100.4 φ_3= -89.0	ψ_1= 5.9 ψ_2= 2.0 ψ_3= -11.8	a) 2.96 b) 2.29 c) 3.44

Table 5.11: Selected representative entries of **5.1**: structure and energy data. Distances a) between NH(1) and NH(3), b) between NH(3) and NH(5) and c) between NH(4) and NH(5)

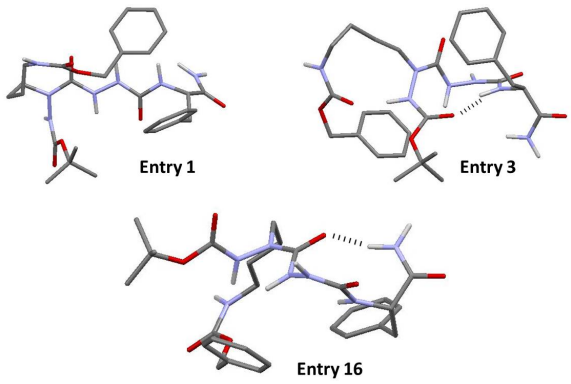

Figure 5.20: Selected representative entries of compound **5.1**

Entries	Relative Potential Energy (kcal/mol)	Peptide bonds	Urea type bonds	φ angles	ψ angles	Distance (Å)
1	0.381	*cis, trans, trans*	*E, Z, E*	φ_1= -85.5 φ_2= -136.3 φ_3= -87.9	ψ_1= 5.3 ψ_2= 169.9 ψ_3= -2.4	a) 2.89 b) 4.35 c) 2.33
2/13	0.434/ 2.092	*trans, trans, trans*	*E, E, E*	φ_1= -83.6 φ_2= 74.9 φ_3= 89.8	ψ_1= -14.1 ψ_2= 9.1 ψ_3= 2.0	a) 2.54 b) 2.96/4.58 c) 3.56
30/31	2.881/ 2.900	*trans, trans, trans*	*E, E, E*	φ_1= 75.5 φ_2= 86.7 φ_3= 102.3	ψ_1= 3.6 ψ_2= 17.3 ψ_3= 0.6	a) 3.00 b) 4.36 c) 2.32

Figure 5.21: Selected representative entries of aLys-aGly-aPhe: structure and energy data. Distances a) between NH(1) and NH(3), b) between NH(3) and NH(5) and c) between NH(4) and NH(5)

motif for the $(i+2)$ and $(i+3)$ residues ($\varphi_2 = \pm 60°$, $\psi_2 = \pm 30°$, $\varphi_3 = \pm 90°$, $\psi_3 = 0°$).

Between all the representatives entries, another conformation was observed with the *E* configuration of the urea-type NH(4)-CO bond of the aGly, but without the dihedral angle values and the H-bond typical of the folded β-turn structure. This conformation presented a H-bond between the carbonyl group of the aLys residue and one of the two hydrogens of the primary C-terminal amide (Entries **16**) (Figure 5.20). It was interesting to notice that in this double turn conformation the dihedral angle φ_2 was negative compared to the folded structure. A rotation of 180° around φ_2 allows the possibility to destabilize the folded β-turn conformation and to establish another H-bond that changes the conformational preference of the azapeptide.

In the analogue with only one aza-amino acid (aGly), in the middle of the azapeptide chain, we obtained 446 representative entries within a sliding energy window of 22.724 kJ mol^{-1}. In this case we observed a less rigid sequence, with the possibility to explore different conformations. We found again different extended structures, mixed with folded ones. All the amide bond were *trans*-planar and we observed again the equilibrium between the *E* and *Z* conformations of the urea-type NH(4)-CO bond of the aGly, which gets to β-turn or double turn structures in the first case and extended in the second one.

On the contrary, the effect to have all three aza-amino acid residues makes the sequence more rigid with only 308 representatives entries within a sliding energy window of 19.376 kJ mol^{-1}. The number of conformations is lower compared to the mono-azapeptide but higher than the di-azapeptide. We could notice that the folded β-turn conformation (Entries **30/31**) is less

stable with respect to the mono- and di-azapeptide and a more extended or double turn conformation is preferred (Entries **2/13**). In particular, we always observed the *E* and *Z* isomerization of the urea-type NH(4)-CO bond of the aGly, conducing to the same results discussed above. However, for the complete azatide sequence, we noticed that the interchange between the two different conformations was not completely correlated to the rotation around the φ_2 dihedral angle. We observed that both negative and positive values of φ_2 dihedral angle are able to lead to double turn or β-turn conformation. The difference has been found in the combination of the other φ dihedral angles related to φ_2: a β-turn conformation prefers an accordance of signs between the first and second dihedral angle; on the contrary a double turn conformation is favored when there is an accordance of signs between the second and third dihedral angles (Figure 5.21).

Generally, in the folded structure we noticed a value of φ_2 around 80–100° and a value of φ_1 around 70°. Instead, in the more extended and double turn conformation, we observed the preference for a value of φ_2 around 75° and a value of φ_1 around 80–85°.

It seems that the lack of a stereocenter allows to obtain both conformations with various combinations of dihedral angles and that precisely the presence of a nitrogen instead of an α-carbon influences the difficult rotation around the dihedral angle φ_2. This difficult rotation is probably responsible of the two different conformations when the urea-type motif is in its *E* conformation. It seems that, when a natural amino acid is present in the sequence and brings flexibility, the value and the sign of the φ_2 dihedral angle may be correlated to the two different conformations, but not in the case of a pure azatide.

5.3.5 Conformational analyses of the Val-Ala-Val tripeptide analogues

Compound 5.2 Also for compound **5.2** (aVal-aAla-Val-$CONH_2$), we decided to perform 2D-NMR analysis and deduce some structural information from through-bond (scalar or *J coupling*) or through space (Nuclear Overhauser Effect, *NOE*) magnetization transfer between pairs of protons. In parallel we performed an unconstrained conformational search using the MCMM (Monte Carlo Multiple Minima) method. Finally, the results attained by these two techniques were compared with the structure obtained by X-ray crystallography.

NMR studies in DMF-d_7 Proton NMR spectra were recorded on a spectrometer operating at 400 MHz in DMF-d_7 at 258 K. Compound **5.2** was dissolved at a concentration of 27.6 mM in 750 µL of DMF-d_7. The observed proton and carbon chemical shifts are displayed in Table 5.12.

Residue	δ NH (ppm)	δ H_α (ppm)	δ H_β (ppm)	δ other protons (ppm)	δ CO (ppm)	δ C_α (ppm)	δ C_β (ppm)	δ other carbons (ppm)
a-Val (i)	9.65/ 9.45	/	4.58/ 4.52	H_γ 1.09/ 1.03	156.52/ 155.41	/	48.02/ 48.26	C_γ 18.32/ 19.26
a-Ala (i + 1)	9.98/ 9.56	/	3.01/ 2.95	/	158.49	/	35.5	/
Val (i + 2)	6.43 (J=8.5 Hz)/ 6.39 (J=9.0 Hz)	4.07	2.33/ 2.19	H_γ 0.97/ 0.92	174.23	59.35	28.84/ 28.95	C_γ 18.84/ 16.43
NH_2	7.18, 7.42/ 7.29, 7.38	/	/	/	/	/	/	/
Boc	1.44/ 1.41	/	/	/	155.79/ 156.21	80.18	/	/

Table 5.12: Chemical shifts for protons and carbons of **5.2** in DMF at 258 K

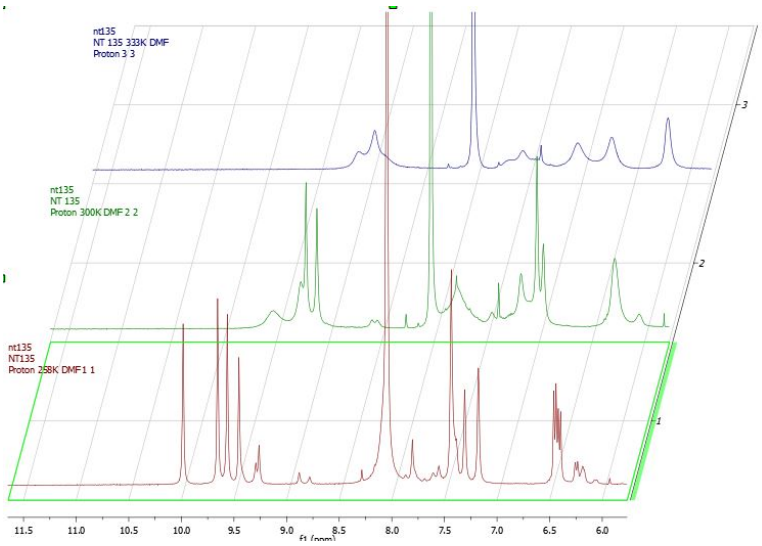

Figure 5.22: 1D ^1H spectra of compound **5.2** at different temperature from 258 K to 333 K

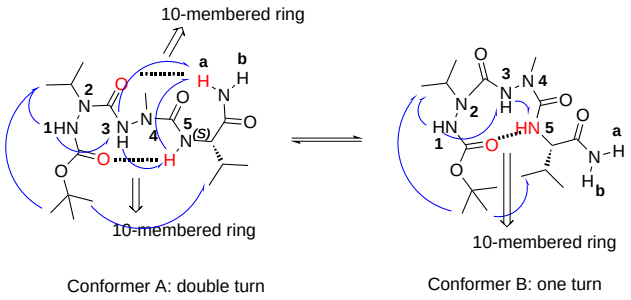

Figure 5.23: Schematic representation of **5.2** conformational structures; in blue arrows the ROEs and in red the atoms involved in hydrogen bonds

As we can see from the data of Figure 5.22, compound **5.2** is present in solution as a mixture of two conformers in 1:1 *ratio*. We observed an unexpected occurrence of splitting for all the amide protons and also for the side chains protons of aVal and aAla and the methyl protons of the Boc protective group, indicating a dynamic equilibrium between at least two conformers. This equilibrium was confirmed by the presence of different negative NH/NH ROEs (exchange peaks), in particular for the amide protons of the two aza-amino acid residues. By recording the spectra at different temperatures, we observed the classic line broadening and coalescence phenomenon: at 258 K we observed all fine peaks for each mobile proton and, increasing the temperature, we were able to observe the coalescence at 333 K (Figure 5.22).

Together with this equilibium, we remarked the presence of other small peaks correlating with other conformers. Probably, these peaks correspond to the minority forms of each conformer due to the *cis* and *trans* isomerization of the Boc protective group.

The analysis of $^{1}H_{\alpha}$-$^{1}H_{N}$ ROE correlations revealed strong sequential and medium intraresidual ROEs in both conformers. We didn't observe long-range ROEs between the two N- and C-terminus, indicating the presence of a classical βI-turn conformation as we saw for compound **5.1**. The only long-range ROE was observed between the *tert*-butyl of the Boc and the *iso*-propyl of the Val residue, suggesting the presence of a folded conformation in both conformers.

We observed a ROE between the NH(5)-Val and the NH(3) of aAla (Figure 5.23) and a weak ROE between the NH(3) of aAla and the proton amide NH(1) of aVal suggests that the azapeptide has the possibility to form a β-turn structure.

The absence of ROE correlations of the urea-type NH(3) and NH(5) with the *iso*-propyl and the methyl groups respectively, demonstrated the *cis-trans* conformation of the urea-type motif in the aza-amino acid residues.

Residue	$\Delta\delta/\Delta T$ (ppb K^{-1})
a-Val NH(1)	- 8.5
a-Ala NH(3)	- 9.0
Val NH(5)	- 3.0
H_a	- 3.0
H_b	- 10.0

Table 5.13: Temperature coefficients for the amide protons of **5.2** conformer A in DMF

Residue	$\Delta\delta/\Delta T$ (ppb K^{-1})
a-Val NH(1)	- 7.0
a-Ala NH(3)	- 8.0
Val NH(5)	- 1.0
H_a	- 8.0
H_b	- 5.5

Table 5.14: Temperature coefficients for the amide protons of **5.2** conformer B in DMF

The difference between the two conformers was the presence of two medium ROEs in conformer A that we didn't detect in the other conformer B: one between the Val proton amide NH(5) and one of the two protons of the terminal primary amide and the second between the NH(3) and always the same proton of the terminal primary amide (Figure 5.23). This finding suggested the presence of an equilibrium between two conformations that differed for the spatial proximity of the N-terminal amide to the aVal residue. In one conformer this proximity showed to be more pronounced than in the other.

In both conformations, the amide protons of aVal NH(1) and aAla NH(3) residues exhibited the strongest variations of the temperature coefficients, as expected for solvent-exposed groups. In contrast one of the two protons of the C-terminal primary amide (H_a) and the Val proton amide NH(5)

Residue	NH (ppm)	H_α (ppm)	C_α (ppm)	CO (ppm)
Val	- 1.6	- 0.05	- 2.85	- 2.07

Table 5.15: Chemical shift deviations (CSD) of Val residue of compound **5.2** in DMF

showed the smallest variations for one (conformer A) of the two conformers. The other conformer (conformer B) presented only the Val proton amide NH(5) with a small temperature dependence. All together this analysis suggests an engagement in intramolecular hydrogen bonds and is indicative of an equilibrium between two conformational structures that share the same hydrogen bond involving the Val proton amide NH(5) and that differ among them for the presence or not of a hydrogen bond involving one of the two protons of the primary terminal amide (Figure 5.13, Figure 5.14).

The vicinal $J_{NH-H\alpha}$ coupling constant also yields direct information on the main chain ϕ dihedral angle, through the Karplus relationship. The coupling constant of the natural amino acid in the sequence exhibited in both isomers large values (8.5 Hz and 9.0 Hz), reflecting a ϕ angle value around $-120°$, as expected for β-strand conformation [177].

We calculated the CSD for the natural amino acid (Table 5.15) and we observed that the proton amide and the α-proton were upfield shifted as in α-helix structure. On the other hand, the carbonyl group and the α-carbon were found to be upfield shifted as in the β-sheet conformation. These values are in accordance with the evidence of the hydrogen bond between one of the two primary amide protons of the Val and the carbonyl group of the aVal residue, that determines a folding of the azapeptide C-terminus.

NMR studies in CD_3OH The 2D-NMR analysis was conducted also in CD_3OH, in order to get as close as possible, by using a polar protic solvent, to an aqueous environment and with characteristics suitable as a biological medium. Furthermore, a protic solvent is more challenging for intramolecular hydrogen bond formation in comparison with aprotic organic solvents.

Proton NMR spectra were recorded on a spectrometer operating at 500 MHz (at UPMC, in collaboration with Pr. O. Lequin and Dr. I. Correia, UMR 7203). Compound **5.2** was dissolved at a concentration of 28.6 mM in 600 µL of CD_3OH The observed proton and carbon chemical shifts are displayed in Table 5.16.

The analysis in CD_3OH confirmed the dynamic equilibrium between at least two major conformations with the presence of the minor forms of each conformer due to the *cis* and *trans* isomerization of the Boc protective group.

The analysis of $^1H_\alpha$-^1H_N ROE correlations revealed the same intraresid-

Residue[a]	δ HN (ppm)	δH^{α} (ppm)	δH^{β} (ppm)	δ Other protons (ppm)
Boc-Carbamate	-	-	-	CH_3 1.52 (a) CH_3 1.51 (b)
aVal[1]	9.26 (a) 9.16 (b)		4.55 (a) 4.54 (b)	γ CH_3 1.12, γ′ CH_3 1.08 (a) γ CH_3 1.11, γ′ CH_3 1.04 (b)
aAla[2]	9.65 (a) 9.35 (b)	-	3.07 (a) 3.08 (b)	
Val[3]	6.55 (a) 6.52 (b)	4.08 (a) 3.98 (b)	2.33 (a) 2.17 (b)	γ CH_3 0.987, γ′ CH_3 0.98 (a) γ CH_3 0.990, γ′ CH_3 0,98 (b)
NH_E	7.35 (a) 7.19 (b)		-	
NH_Z	7.39 (a) 7.54 (b)		-	

Residue[a]	δ CO (ppm)	δC^{α} (ppm)	δC^{β} (ppm)	δ Other carbons (ppm)
Boc-Carbamate	157.7 (a) 157.8 (b)	-	-	Cq 82.4, CH_3 28.4 (a) Cq 82.3, CH_3 28.5 (b)
aVal[1]	158.6 (a) 158.0 (b)	-	50.3 (a) 50.0 (b)	γ CH_3 19.8, γ′ CH_3 19.1 (a) γ CH_3 20.1, γ′ CH_3 19.1 (b)
aAla[2]	161.0 (a) 160.6 (b)	-	36.8 (a) 36.5 (b)	- -
Val[3]	178.2 (a) 177.8 (b)	61.3 (a) 61.5 (b)	30.5 (a) 31.1 (b)	γ CH_3 17.3, γ′ CH_3 19.8 (a) γ CH_3 18.3, γ′ CH_3 19,9 (b)

Table 5.16: Chemical shifts for protons and carbons of **5.2** in CD_3OH at 273 K

Residue	ΔδHN/ΔT (ppb/K)	*$J_{HN\text{-}H\alpha}$ (Hz)
aVal[1]	-7.29 (a) -7.07 (b)	-
aAla[2]	-6.55 (a) -6.76 (b)	-
Val[3]	-2.60 (a) -2.28 (b)	9,0 (a) 8.4 (b)
NH_b	-8.42 (a) -7.27 (b)	-
NH_a	-3.28 (a) -6.19 (b)	-

Table 5.17: NMR conformational parameters for **5.2** in CD_3OH

ual ROEs pathway previously described in DMF. We confirmed the equilibrium between two conformations that differ for the spatial proximity of the N-terminal amide to the aVal residue. In one conformer this proximity showed to be more pronounced than in the other, creating two 10-membered cycles thanks to the possibility to establish two hydrogen bonds, one between the carbonyl group of Boc and the proton amide NH(5) of Val and the other between the carbonyl group of aVal and the terminal primary amide (H_a).

The amide proton NH(5) of the Val residue showed the smallest variation of the temperature coefficient for both the conformers (Table 5.17), suggesting that the first 10-membered cycle with the hydrogen bond between the carbonyl group of Boc and the proton amide of Val is stable and common to both conformations.

On the contrary, the smallest variation for one (H_a) of the two protons of the C-terminal primary amide (Table 5.17) was observed for only one conformer, demonstrating that the dynamic equilibrium is created by the less stable second 10-membered cycle with the hydrogen bond between the carbonyl group of aVal and the terminal primary amide.

The coupling constanct at 247.5 K of the natural amino acid in the sequence exhibited in both isomers large values (9.0 Hz and 8.4 Hz) (Table 5.17), reflecting a φ angle value around $-120°$, as expected for β-strand conformation [177] (in our case for the presence of a C-terminal primary amide the CSD should be corrected).

Finally, we observed that the proton amide and the α-proton of the natural Val residue were upfield shifted (-1.48 and -0.04, respectively) with respect to the random coil chemical shift values and the carbonyl group was downfield shifted (+ 1.9) as in α-helix structure.

MM studies Molecular modeling studies were performed using the same procedure described above for compound **5.1**. These studies were conducted on compound **5.2** and other four analogues:

- the azapeptide aVal-aGly-Val, to analyze the influence of the side chain

Entries	Relative Potential Energy (kcal/mol)	Peptide bonds	Urea type bonds	φ angles	ψ angles	Distance (Å)
1	0.395	*cis, trans, trans*	*E, E*	φ_1= 80.9 φ_2= -75.5 φ_3= -72.1	ψ_1= 5.4 ψ_2= -5.6 ψ_3= -17.5	a) 2.72 b) 2.67 c) /
2	0.900	*trans, trans, trans*	*E, E*	φ_1= -79.3 φ_2= -73.2 φ_3= -70.0	ψ_1= -2.2 ψ_2= -4.4 ψ_3= -19.3	a) 2.76 b) 2.67 c) /
3	1.059	*cis, trans, trans*	*E, E*	φ_1= -90.7 φ_2= -77.4 φ_3= -74.3	ψ_1= 1.0 ψ_2= -5.0 ψ_3= 17.2	a) 2.46 b) 2.76 c) /
4	1.323	*trans, trans, trans*	*E, E*	φ_1= 79.7 φ_2= -74.6 φ_3= -72.4	ψ_1= 6.5 ψ_2= -5.8 ψ_3= -17.3	a) 2.70 b) 2.66 c) /
5	1.438	*cis, trans, trans*	*E, E*	φ_1= -79.7 φ_2= 83.0 φ_3= -82.4	ψ_1= -6.1 ψ_2= 7.3 ψ_3= -15.4	a) 2.72 b) 2.49 c) /
6	2.211	*trans, trans, trans*	*E, E*	φ_1= -80.3 φ_2= 81.4 φ_3= -83.1	ψ_1= -6.5 ψ_2= 7.5 ψ_3= -14.8	a) 2.72 b) 2.44 c) /
7	2.378	*trans, trans, trans*	*E, E*	φ_1= 85.5 φ_2= 82.7 φ_3= -79.2	ψ_1= -0.2 ψ_2= 8.5 ψ_3= -17.6	a) 2.68 b) 2.57 c) /
8	2.961	*cis, trans, trans*	*E, E*	φ_1= 94.8 φ_2= 84.6 φ_3= -90.8	ψ_1= -8.9 ψ_2= 0.3 ψ_3= -10.6	a) 2.58 b) 2.74 c) /

Table 5.18: Selected representative entries of **5.2**: structure and energy data. Distances a) between NH(1) and NH(3), b) between NH(3) and NH(5) and c) between NH(4) and NH(5)

(methyl) of the central aza-amino acid in **5.1** on the conformational preference;

- the azapeptide Val-aAla-Val, to compare the conformational behaviour of a di-azapeptide with its counterpart formed by a single central aza-amino acid;
- the azatide aVal-aAla-aVal, to observe the effect of a complete azatide chain on the conformation;
- the natural tripeptide Val-Ala-Val, to compare the conformation of **5.1** with the natural counterpart.

For compound **5.2**, clustering yielded 17 representative conformations within a sliding energy window of 19.332 kJ mol^{-1}. All the 17 entries showed

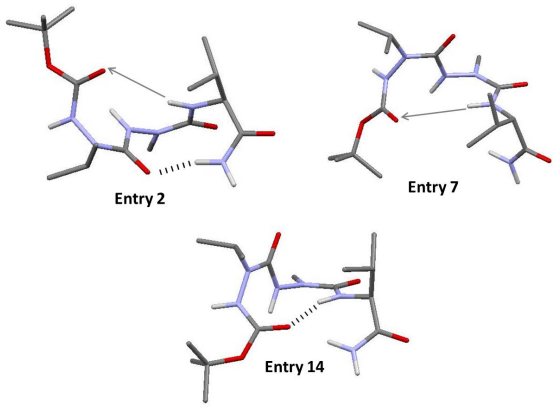

Figure 5.24: Selected representative entries of **5.2**

trans-planar amide bond, except for the Boc that showed an equilibrium between *cis* and *trans* isomers. Both the urea-type RN(2)-CO and RN(4)-CO bond presented only the *E* isomerization, confirming that the presence of a side chain on the α-nitrogen leads to a *cis* conformation of the RN-CO bond (Table 5.18).

The first four structures (Entries **1**-**4**), at the lowest relative potential energy, showed a quite folded conformation, with a hydrogen bond between the carbonyl group of the aVal residue and one of the two hydrogens of the primary C-terminal amide. We called this type of conformation double turn unit because of the presence of two possible 10-membered rings: one generated by the H-bond between the carbonyl group of the aVal and the C-terminal primary amide (H_a) and the other by the possible H-bond that may be established by the proximity of the carbonyl group of Boc and the proton amide NH(5) of Val.

The following other four conformations (Entries **5**-**8**) were not characterized by the presence of the hydrogen bond and revealed almost the same dihedral angle backbone profile, except for the φ_2 dihedral angle (aAla residue). We noticed that the value of this angle was negative (around $-75°$) when there was the characteristic hydrogen bond, and positive (around $85°$) when it was not present. We can hypothesize that a rotation of at least $180°$ around φ_2 allows the possibility to establish or not a H-bond between the carbonyl group of the aVal and the C-terminal primary amide (H_a) (Figure 5.24). On the other hand, the possibility to establish a H-bond between the carbonyl group of Boc and the NH(5) of Val can be observed for both conformations and in particular when the φ_1 dihedral angle assumes a value around $80°$ with a sign in accordance with that of φ_2 and in the presence of the all *trans* amide bonds, including the Boc (Entries **2** and **7**).

The absence of a hydrogen bond between the Boc carbonyl group and

Entries	Relative Potential Energy (kcal/mol)	Peptide bonds	Urea type bonds	φ angles	ψ angles	Distance (Å)
1	0.107	*cis, trans, trans*	*E, Z*	φ_1= 78.8 φ_2= 147.2 φ_3= -77.0	ψ_1= 5.5 ψ_2= -169.2 ψ_3= -19.1	a) 2.74 b) 4.23 c) 2.23
3	1.137	*trans, trans, trans*	*E, Z*	φ_1= -81.1 φ_2= -172.2 φ_3= -79.7	ψ_1= -3.6 ψ_2= -178.5 ψ_3= -17.0	a) 2.71 b) 4.24 c) 2.23
4	1.496	*cis, trans, trans*	*E, E*	φ_1= -89.7 φ_2= -77.9 φ_3= -76.0	ψ_1= -1.3 ψ_2= -7.8 ψ_3= -14.6	a) 2.43 b) 2.80 c) 3.38
9	2.639	*trans, trans, trans*	*E, E*	φ_1= 70.8 φ_2= 85.7 φ_3= -82.5	ψ_1= 4.2 ψ_2= 5.4 ψ_3= -31.4	a) 2.93 b) 2.38 c) 3.43

Table 5.19: Selected representative entries of aVal-aGly-Val: structure and energy data. Distances a) between NH(1) and NH(3), b) between NH(3) and NH(5) and c) between NH(4) and NH(5)

the Val proton amide can be explained by the fact that this method has the limitation of not considering the possible pyrimidalization of the nitrogen atom which can eventually affect the backbone profile and slightly modify the dihedral angle values. We hypothesize that the pyramidalization is the driving force that allows the N-terminal Boc and the NH Val to get close enough to make the H-bond possible.

We found a classical βI-turn-like conformation only in the 14^{th} and last positions, suggesting that the βI-turn structure is less stable and representative (Relative Potential Energy of 4.686 kJ mol^{-1} and 5.020 kJ mol^{-1}, respectively).

In the di-azatide analogue with the aGly in place of aAla (aVal-aGly-

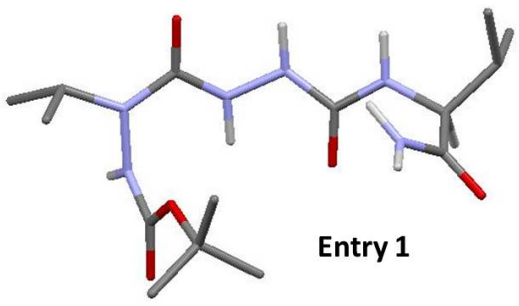

Figure 5.25: Selected representative entry of aVal-aGly-Val

Val), we obtained 20 representative conformations within a sliding energy window of 19.709 kJ mol^{-1}. In this case the preferred conformation was the extended one (Entries **1** and **3**): although the first urea-type bond RN(2)-CO presented only the *E* conformation due to the presence of the alkyl substituent on the nitrogen, the other urea-type bond RN(3)-CO showed also the *Z* conformation because of the absence of the side chain. All the entries, presenting in the central region the urea constituent with the classical *all-trans* planar conformation (not found in compound **5.2**), were characterized by a more extended structure and by larger dihedral φ_2 angle values (Table 5.19 and Figure 5.25).

Other entries (Entry **4**, for exemple) showed a *cis-trans* conformation even for the second urea constituent (*E* configuration of the NH(4)-CO bond). In this case, we observed the possibility to establish an hydrogen bond between the carbonyl group of the aVal residue and one of the two hydrogens of the primary C-terminal amide. Also in this case, as in compound **5.2**, we found the interesting correlation between the negative and positive sign of the φ_2 dihedral angle value and the double turn conformational structure with or without the hydrogen-bond, respectively (Table 5.19).

All the amide bonds were found to be *trans*-planar, except for the Boc that showed the *cis* and *trans* isomerizarion.

The classical βI-turn conformation (Entry **9**), with the hydrogen bond between the Boc carbonyl group and the proton amide of Val (both φ_1 and φ_2 with positive values) was found to be energetically more stable than in compound **5.2**. This is probably due to the effect of the side chain on the α-nitrogen that makes the azatide backbone more rigid and less willing to rotate around the φ_2 dihedral angle and to induce the formation of the one and only hydrogen bond that stabilizes the βI-turn conformation. So we can suggest that the presence of the side chain on the α-nitrogen of the second aza-amino acid residue makes the βI-turn conformation less probable compared to the situation with the aGly residue.

In the analogue with only one aza-amino acid (aAla) (Val-aAla-Val), in the middle of the azatide chain, we obtained 21 representative entries within a sliding energy window of 14.377 kJ mol^{-1}. We observed the same behaviour that we met in the analysis of compound Lys-aGly-Phe, with the exception of the *E* and *Z* isomerization of the urea constituent. All the amide bonds were *trans*-planar, except for the Boc that showed the *cis* and *trans* isomerizarion and the NR(4)-CO bond of the aAla residue always remained in its *E* configuration. We observed both the conformation with the hydrogen bond between the carbonyl group of the first Val residue and one of the two hydrogens of the primary C-terminal amide (Entry **1**) and the βI-turn structure with the hydrogen bond between the Boc carbonyl group and the proton amide of the third Val residue (Entry **8**). In this case, however, the βI-turn structure was already present in the first eight entries at a more stable energetically level and the double turn conformation, even

Entries	Relative Potential Energy (kcal/mol)	Peptide bonds	Urea type bonds	φ angles	ψ angles	Distance (Å)
1	1.529	*cis, trans, trans*	*E*	φ_1= -139.2 φ_2= -80.0 φ_3= -81.3	ψ_1= 153.4 ψ_2= -4.9 ψ_3= -11.6	a) 4.47 b) 2.65 c) /
8	3.125	*trans, trans, trans*	*E*	φ_1= -53.0 φ_2= 86.4 φ_3= -129.0	ψ_1= 130.1 ψ_2= -2.4 ψ_3= -48.7	a) 4.73 b) 2.56 c) /

Table 5.20: Selected representative entries of Val-aAla-Val: structure and energy data. Distances a) between NH(1) and NH(3), b) between NH(3) and NH(5) and c) between NH(4) and NH(5)

if it was represented, showed to be less stable. So, the presence of only one aza-amino acid residue in the middle of the tripeptide sequence makes the βI-turn structure more stable and representative (Table 5.20).

We still noticed that the effect to have all aza-amino acid residues makes the azatide more rigid with only 16 representatives entries within a sliding energy window of 15.751 kJ mol^{-1}. Surprisingly we found the folded classical βI-turn structure as the most energetically favored (Entry **1**). Switching to a sequence consisting of only aza-amino acids seems to lead to the less stable energy conformation found in the di-azapeptide analogue. However, the energy difference between the βI-turn and the double turn conformation was not so large, indicating a favorable exchange among them. All the amide bonds were *trans*-planar, except always for the Boc that showed the *cis* and *trans* isomerizarion, and the NR-CO bond of all aza-amino acid residues presented an *E* configuration (Table 5.21).

We observed that the combination of the other φ dihedral angles related to φ_2 was responsible of the conformational preference: generally the double turn conformation was detected when φ_2 showed a value around $-75°$ and there was an accordance of signs for all dihedral angles (Entries **3** and **5**), while the βI-turn conformation was favored when φ_2 presented a value around $\pm 85°$ and there was an accordance of signs for the first and second dihedral angles (Entries **1**). The value of φ_1 demonstrated to be considerable for establishing the H-bond between the carbonyl group of Boc and the NH-Val in the double turn conformation: a value around $\pm 80°$ induced a more open conformation and a value of at least $\pm 70°$ allowed the formation of the 10-membered ring structure (Table 5.21). The double turn conformation without the characteristic H-bonds was also detected when the φ_2 presented a value around 80° but there was no sign accordance with φ_1 dihedral angle (Entry **7**).

To conclude, the lack of a natural amino acid in the third position of an

Entries	Relative Potential Energy (kcal/mol)	Peptide bonds	Urea type bonds	φ angles	ψ angles	Distance (Å)
1	0.000	*trans, trans, trans*	*E, E, E*	φ_1= 70.4 φ_2= 81.2 φ_3= -86.1	ψ_1= 8.4 ψ_2= 7.4 ψ_3= -6.2	a) 2.85 b) 2.46 c) /
3	0.135	*cis, trans, trans*	*E, E, E*	φ_1= -82.0 φ_2= -74.6 φ_3= -83.5	ψ_1= -6.6 ψ_2= -13.3 ψ_3= -4.4	a) 2.69 b) 2.77 c) /
6	1.176	*trans, trans, trans*	*E, E, E*	φ_1= -68.5 φ_2= -75.1 φ_3= -82.2	ψ_1= -9.0 ψ_2= -10.4 ψ_3= -4.0	a) 2.89 b) 2.56 c) /
7	1.718	*cis, trans, trans*	*E, E, E*	φ_1= -80.0 φ_2= 82.3 φ_3= -84.0	ψ_1= -5.5 ψ_2= 11.4 ψ_3= -7.9	a) 2.72 b) 2.60 c) /

Table 5.21: Selected representative entries of aVal-aAla-aVal: structure and energy data. Distances a) between NH(1) and NH(3), b) between NH(3) and NH(5) and c) between NH(4) and NH(5)

azatide chain seems to allow the formation of all the types of conformations, that we encountered for compound **5.2**, with various combinations of positive and negative dihedral angles. We discovered that a double turn conformation is favored when φ_2 has a value around $-75°$, admitting the H-bond between the carbonyl group of aVal and the amide proton of Val, while a value around 85° favors either a βI-turn conformation or a double turn structure without the hydrogen bond involving the C-terminal primary amide. The possibility to observe a H-bond becomes more likely when there is accordance of signs between the dihedral angles.

So, the presence of a natural amino acid in the third position of an azapeptide sequence allows to make less stable the classical βI-turn conformation and to create an equilibrium between two different types of double turn structures that differ for the value and sign of the φ_2 dihedral angle. This difference has an influence on the formation of the hydrogen bond that stabilizes the 10-membered ring structure, formed by the hydrogen bond between the carbonyl group of aVal and the amide proton of Val.

X-ray studies Compund **5.2** was crystallized in methanol, by putting the clear solution in a saturated chamber of diethyl ether and letting the sample to crystallize during two weaks. On the obtained crystal, we performed X-ray spectroscopy (at the Plateforme DRX Institut Parisien de Chimie Moléculaire - UMR 8232) in order to characterize the molecular structure. We observed that this compound is present in the unit cell as a dimer with intermolecular hydrogen bonds between the protons of the primary amide of one molecule and the carbonyl group of the aVal residue of another

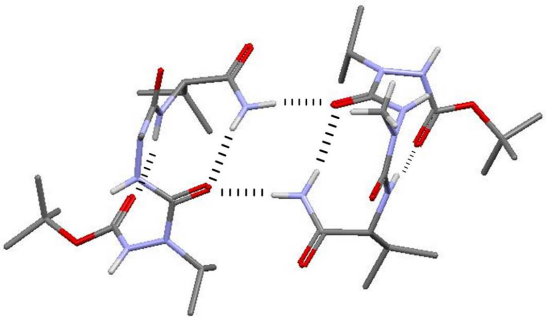

Peptide bonds	Urea type bonds	φ angles	ψ angles	Distance (Å)
trans, trans, trans	*E, E*	φ_1= 62.3 φ_2= 78.9 φ_3= 66.6	ψ_1= 21.9 ψ_2= 7.6 ψ_3= 28.0	a) 2.80 b) 2.84 c) /
trans, trans, trans	*E, E*	φ_1= 61.2 φ_2= 76.8 φ_3= 63.0	ψ_1= 16.3 ψ_2= 5.1 ψ_3= 18.4	a) 2.78 b) 2.90 c) /

Figure 5.26: Crystallography structure of compound **5.2** and the corresponding mesured dihedral angles

molecule. Also intramolecular hydrogen bonds are present: one involving again the primary amide protons and the carbonyl group of aVal, and the other involving the Boc carbonyl group and the proton amide of the Val residue (Figure 5.26).

We mesured the dihedral angles φ and ψ of the backbone of both monomers and we observed a similar conformational sequence between the two structures. All the amide bonds were *trans*-planar and the NR-CO bond of all aza-amino acid residues presented an E configuration (Figure 5.26).

The similar values of the dihedral angles and the presence of the hydrogen bond between one of the two protons of the C-terminal primary amide of Val and the carbonyl group of the aVal residue induced us to think that the structure that we found by molecular modelling analysis was almost the same. We superimposed the two sequences and we validated the similarity between the crystal conformation and the second entry of the molecular mechanic study (Entry **2**, Table 5.18).

The only difference that we observed was a slight dissimilarity of the N-terminal trend, which in the crystal allows the carbonyl group of the Boc to approach to the amide proton of Val and establish the H-bond, necessary to create the other 10-membered ring of the double turn conformation. This difference, as we have already said, is a consequence of the conformational search study limitation of not considering the effect of the pyramidalization of the nitrogen atom. We supposed that this dissimilarity of approximately 20° of the molecular modelling representative entry related

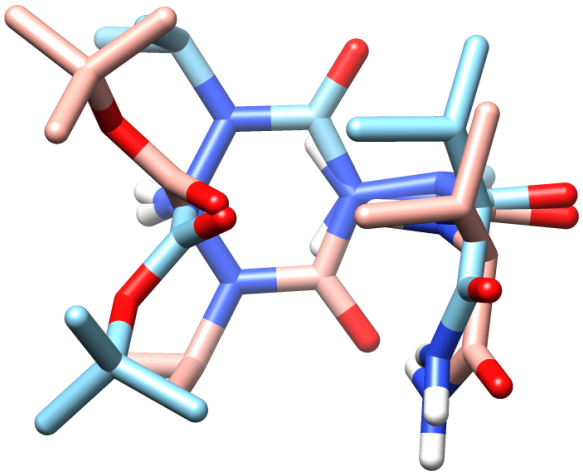

Figure 5.27: Superimposition of calculated conformations **2** and **7** of compound **5.2** at the B3LYP/6-31G* level in DMF, showing the quasi-symmetric relationship between the two

to the crystal conformation would have to be attributed to this phenomenon of pyramidalization.

DFT analysis The geometry of representative conformations **2** and **7** of compound **5.2** found by Monte-Carlo search using molecular mechanics were refined using DFT (at the B3LYP/6-31G* level) with solvation models for dimethylformamide, methanol as well as water for extrapolation purposes. The conformation extracted from X-ray structure was also subjected to geometry optimisations under the same conditions. During this process, geometry of conformation **2** and that of crystal structure converged exactly to yield the same conformation. The conformations obtained were also almost independent of the solvent model used during the calculation, and the free energy difference found between **2** and **7** did not exceed 0.6 kcal/mol, indicating that the co-existence of both conformations was likely.

Comparison of conformations **2** and **7** after DFT optimisation shows that they differ mostly by the opposite orientations of the NH(1)-NR(2)-CO-NH(3) fragment relatively to a pseudo-cycle (itself remaining unchanged) involving the quasi-hydrogen bond between the Boc carbonyl group and the proton amide of Val (Figure 5.27).

The dihedral angle values and the hydrogen bond network of the double β-turn structure induced us to think that this type of peptidomimetic could bring to an α-helix structure. In order to anticipate on what structure could exhibit a molecule possessing the sequence aVal-aAla-Val repeated twice in water, we built a model of compound **5.21** (Figure 5.28) by duplicating

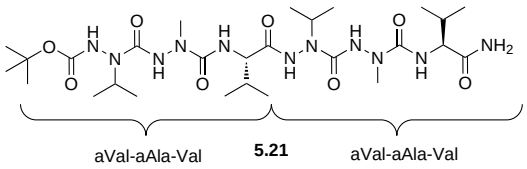

Figure 5.28: Compound **5.21**

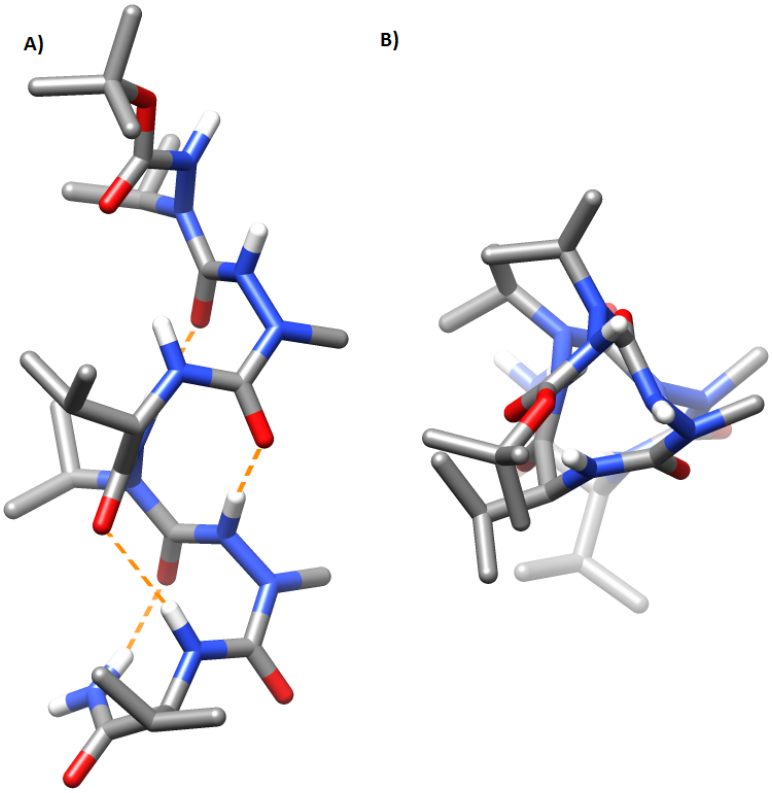

Figure 5.29: A possible conformation of compound **5.21** calculated at the B3LYP/6-31G* level in water. A) side view; B) top view

Residue[a]	δ HN (ppm)	δH^{α} (ppm)	δH^{β} (ppm)	δ Other protons (ppm)
Boc-Carbamate	-	-	-	CH_3 1.44
Val[1]	6.62 (d)	3.87	2.03	γ CH_3 0.95, γ′ CH_3 0.91
Ala[2]	8.18 (d)	4.41 (q)	1.36	
Val[3]	7.86 (d)	4.17 (dd)	2.07	γ CH_3 0.96, γ′ CH_3 0.95
NH_E	7.04 (s)	-	-	
NH_Z	7.60 (s)	-	-	

Residue[a]	δ CO (ppm)	δC^{α} (ppm)	δC^{β} (ppm)	δ Other carbons (ppm)
Boc-Carbamate	158.0	-	-	Cq 80.5, CH_3 28.6
Val[1]	174.3	61.4	32.0	γ CH_3 19.74, γ′ CH_3 18.2
Ala[2]	174.7	50.4	17.9	-
Val[3]	176.1	59.8	31.8	- γ CH_3 19.69, γ′ CH_3 18.3

Table 5.22: Chemical shifts for protons and carbons of the tripeptide Val-Ala-Val-$CONH_2$ in CD_3OH at 292.8 K

conformation **2**, assembling fragments thereof, and optimising the result at the same DFT level. The conformation obtained could be assigned to some sort of 3_{10}-helix (Figure 5.29). Further *in silico* investigation remains necessary though, in order to more accurately predict the most stable structure that such a molecule could possess. Other MM conformational studies are required to check if this structure corresponds to the more populated and stable one and, certainly, more information might be obtained from experimentally NMR studies with the synthesized compound.

Natural tripeptide Val-Ala-Val-$CONH_2$ In order to compare the conformational preference of the 2:1 [Aza/α]-tripeptide **5.2** with its natural counterpart, we decided to synthesize the tripeptide Val-Ala-Val by a classical liquid phase coupling protocol with HBTU and HOBt (see the experimental part for the synthesis and characterization of each intermediate). Once synthesized, we performed a 2D-NMR analysis to deduce some structural information and an unconstrained conformational search using the MCMM method.

NMR studies in CD_3OH Proton NMR spectra were recorded on a spectrometer operating at 500 MHz (at UPMC, in collaboration with Pr. O. Lequin and Dr. I. Correia, UMR 7203) in CD_3OH at 292.8 K. The tripeptide Val-Ala-Val-$CONH_2$ was dissolved at a concentration of 4.0 mM. The observed proton and carbon chemical shifts are displayed in Table 5.22.

The 1D-^{1}H spectra of a sample of freshly dissolved tripeptide Val-Ala-Val-$CONH_2$ recorded in methanol at 0.4 mM and 4.0 mM concentrations at 292.8 K are

characterized by sharp line widths and concentration-independent chemical shifts suggesting the presence of a monomeric form. However the presence of weak shoulders on the 1D-^{13}C of the 4.0 mM solution observed for α-carbon signals of the Val1, Val3 and Ala2 residues suggested the presence of minority species. This assumption was confirmed by the formation of aggregates in the saturated solution incubated for 30 days at room temperature. The 1D-^{1}H and 1D-^{13}C spectra recorded did not show any variation in comparison to the fresh solution, suggesting that the formed aggregates are not soluble in methanol and coexist with a monomeric form.

However, supplementary peaks were observed on the 1D-^{13}C spectrum for a saturated solution (1.6 mg in 0.6 mL methanol) after 30 days in incubation at 0 °C. At least four different peaks characterized by different linewidths of the resonance were observed for each α-carbon and carbonyl group of the residues Ala and Val in about 40 %, 25 %, 25 % and 10 % proportions. The resonances of major species have the same chemical shift than that of the monomeric form although the resonances of the minority species are down shielded, suggesting a more extended conformation for the tripeptide due to a reorganization of the side chains in soluble oligomers.

Weak additional resonances could be detected on low-temperature 1D-^{1}H spectra of freshly sample corresponding to a second set of chemical shifts. This minor species, representing around 10 %, turns out to be in equilibrium with the major form as exchange peaks were observed on 2D spectrum Roesy between the NH protons of two forms, especially for the amide proton signals of residues Val1, Val3 and one of the two protons of the C-terminal primary amide. The origin of this exchange phenomenom could be due to the presence of *cis*- and *trans*-rotamers of the Boc group. The *trans* is more stable as supported by detection of about 90 % on the low temperature NMR spectra. The *cis*-rotamer was difficult to identify at room temperature since its signals broaden because of the rotation around the CO-N bond, causing their lines to blend into the baseline.

The analysis of $^{1}H_{\alpha}$-$^{1}H_{N}$ ROE correlations revealed strong sequential and medium intraresidual $^{1}H_{\alpha}$-$^{1}H_{N}$ ROEs, which are characteristic of extended backbone conformations.

We next examimated the temperature dependence of amide proton chemical shifts as it can provide information on the network of hydrogen bonds and their stabilities. The amide proton of Ala residue, both amide protons of Val1 and Val3 residues and the free NH_2 C-terminal primary amide protons exhibit strong variations expected for solvent-exposed groups (Table 5.23).

The coupling constants of the Val1 and Val3 residues exhibited large values (8.7 Hz and 8.6 Hz) (Table 5.23) reflecting a φ angle values around $-120°$, as expected for extended conformation. The coupling constant (6.6 Hz) (Table 5.23) of Ala2 residue was also characteristic of extended or random coil structures. This assumption is also supported by the values of the coupling constants $^{3}J_{\alpha-\beta}$ (about 7.0 Hz) (Table 5.23) of side chains indicating that

Residue	ΔδHN/ΔT (ppb/K)	$^3J_{HN\text{-}H\alpha}$ (Hz)	$^3J_{H\alpha\text{-}H\beta}$ (Hz)
Val[1]	-8.54	8.7	7.0
Ala[2]	-7.72	6.6	7.0
Val[3]	-8.41	8.6	6.8
NH_b	-7.09	-	-
NH_a	-8.29	-	-

Table 5.23: NMR conformational parameters for the tripeptide Val-Ala-Val-$CONH_2$ in CD_3OH

Entries	Relative Potential Energy (kcal/mol)	Peptide bonds	φ angles	ψ angles	Distance (Å)
1	0.604	*trans, trans, trans*	φ_1= -59.3 φ_2= 68.0 φ_3= -83.4	ψ_1= 125.3 ψ_2= 16.3 ψ_3= 8.1	a) 4.55 b) 2.66 c) 3.02
2	0.874	*trans, trans, trans*	φ_1= -67.0 φ_2= -81.7 φ_3= -76.1	ψ_1= 156.3 ψ_2= -15.2 ψ_3= -38.3	a) 4.66 b) 2.48 c) 3.43
7	3.556	*trans, trans, trans*	φ_1= -135.0 φ_2= -138.5 φ_3= 78.5	ψ_1= 160.3 ψ_2= 24.0 ψ_3= -44.9	a) 4.41 b) 2.20 c) 2.92

Table 5.24: Selected representative entries of Val-Ala-Val: structure and energy data. Distances a) between NH(1) and NH(3), b) between NH(3) and NH(5) and c) between CH(4) and NH(5)

the conformations about the C_α-C_β bond of the side chains are disordered.

Finally, the CSD must be corrected by the presence of a N-terminal carbamate group and a free C-terminal primary amide in our case. Hence, the CSD of Ala2 was alone considered here. Ala2 residue is characterized by downfield shifted H^α proton (positive CSD value +0.1 ppm) and upfield shifted α-carbon and carbonyl group (negative CSD value -2.1 ppm and -3.1 ppm, respectively), indicating that extended conformation predominates.

MM studies About the conformational studies by molecular modelling conducted on the natural tripeptide Val-Ala-Val, clustering yielded 14 representative conformations within a sliding energy window of 17.928 kJ mol^{-1}. All the 14 entries showed *trans*-planar amide bond, except for the Boc *cis* and *trans* isomerization (Table 5.24).

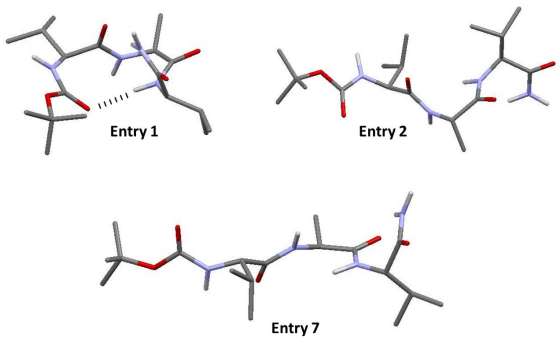

Figure 5.30: Selected representative entries of the natural tripeptide Val-Ala-Val

The first low energy entry presented a folded conformation with the typical dihedral angles and proton amide distances of a βI-turn structure (Entry **1**). Among the fourteen entries, this was the only βI-turn structure observed. All the other conformations showed extended or semi-folded structures. In particular we detected an average value of φ_2 dihedral angle (Ala residue) around $\pm 140°$ when we observed the typical extended β-sheet conformation (Entry **7**), and around $\pm 80°$, when we noticed the similar backbone conformation (Entry **2**) of compound **5.2** (Figure 5.30) when it's not characterized by the hydrogen bond established between the carbonyl group of the first residue and the C-terminal primary amide. We didn't observe the double-turn conformation as in compound **5.2**.

Some of the structures showed a H-bond between one of the two C-terminal primary amide protons and the carbonyl group of the Val residue in the first position of the peptide sequence, making the φ_3 dihedral angle less than $-139°$ and so moving the tripeptide from a perfectly extended structure.

In conclusion, we can assert that the presence of aza-amino acid residues seems to increase the rigidity of the diazapeptide sequence and to improve the formation of intramolecular hydrogen bonds that become possible thanks to the limited range of stereochemically allowed dihedral angles. Despite the replacement of the α-carbon by a nitrogen, the global conformational shape and the side chain functional groups disposition seem to be similar to the peptide counterpart: the diazatide chain is able to adopt structural conformations that the peptide counterpart is already able to embrace, destabilizing the βI-turn conformation. However, the natural tripeptide is able to adopt a more extended conformation than compound **5.2** and didn't show the double-turn conformation that characterizes compound **5.2**. The βI-turn conformation becomes more stable in the presence of only one aza-amino acid in the middle of the azapeptide sequence. This observation suggests

Residue	δ NH (ppm)	δ H_α (ppm)	δ H_β (ppm)	δ other protons (ppm)	δ CO (ppm)	δ C_α (ppm)	δ C_β (ppm)	δ other carbons (ppm)
a-Val (i)	9.12/ 9.01	/	4.56	H_γ 1.13	154.9/ 155.1	/	47.3	C_γ 17.6
a-Ala (i + 1)	9.24/ 9.19	/	3.04	/	157.4	/	36.2	/
Val (i + 2)	6.48 (J=8.2 Hz)/ 6.31 (J=7.8 Hz)	4.25	2.14	H_γ 0.95	171.6	59.35	29.5	C_γ 16.7
Boc	1.47	/	/	/	155.3	79.3	/	/
OBn	/	5.21 (CH_2)	7.39, 7.46 (Ar)	/	/	64.7 (CH_2)	127.1, 127.5, 135.5 (Ar)	/

Table 5.25: Chemical shifts for protons and carbons of **5.3** in DMF at 303 K

that the diazapeptide is an important structural element to destabilize the βI-turn conformation.

Compound 5.3

NMR studies Proton NMR spectra were recorded on a spectrometer operating with a MicroProbe at 400 MHz at 258 K. Compound **5.3** was dissolved at a concentration of 0.30 M in 35 µL of DMF-d_7. The observed proton and carbon chemical shifts are displayed ind in Table 5.25.

As we can see from the data of Figure 5.31, compound **5.3** is present in solution as a mixture of two conformers in 3:2 *ratio*. We observed an unexpected occurrence of splitting for all the amide protons but not for the side chains protons of the residues. The dynamic equilibrium between the two conformers was confirmed by the presence of different negative NH/NH ROEs, in particular for the amide protons of the two aza-amino acid residues, and also by a strong NOE between the aAla amide protons of one isomer with the Val amide proton of the second isomer, suggesting that aAla is probably involved in the dynamic switch between the two isomers.

By recording the spectra at different temperatures, we observed the classical line broadening and coalescence phenomenon: at 293 K we observed

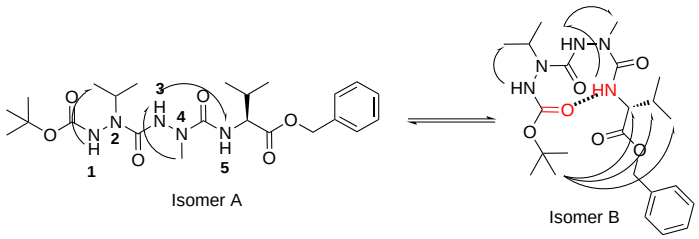

Figure 5.31: Schematic representation of **5.3** conformational structure; in black arrows the assigned ROEs

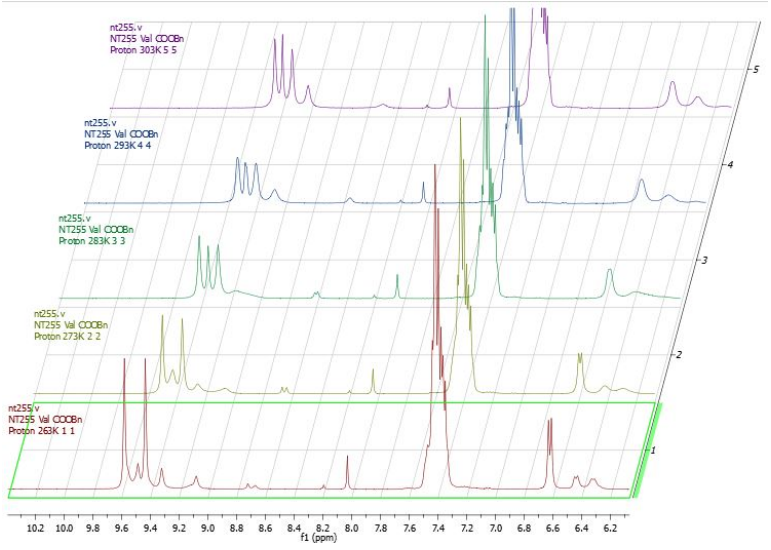

Figure 5.32: 1D ^1H spectra of compound **5.3** at different temperature from 263 K to 303 K

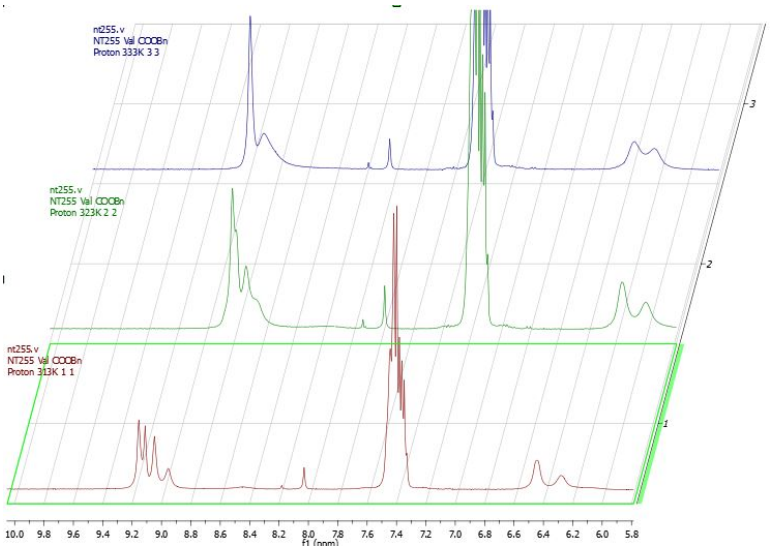

Figure 5.33: 1D ^1H spectra of compound **5.3** at different temperature from 313 K to 333 K

all fine peaks for each mobile proton and, increasing the temperature, we were able to observe the coalescence at 333 K (Figure 5.32). When we decreased the temperature, however, we observed that the peaks of one isomer became more and more fine and those of the other one more and more flattened. Furthermore, we noticed a changement of the *ratio* between the two isomers, becoming in favor of the more deshielded form (Figure 5.33). This means that at low temperature the exchange is so slow that we are able to observe mostly one of the two isomers, due to the fact that the other one is not observable at the analysis time scale.

The analysis of $^1H_\alpha$-^1H_N NOE correlations revealed strong sequential and medium intraresidual ROEs, which are characteristic of an extended backbone conformations. We also observed in the minor conformer weak long-range ROEs between the methyl protons of the Boc protective group with the α-, β- and γ-proton of Val, indicating the presence of a β-turn conformation (Figure 5.34). This means that, in solution, compound **5.3** is present as a mixture of two conformations: one more extended and the other with a more stable β-turn motif. The more extended conformation is the major conformer.

We examined the temperature dependence of amide proton chemical shifts as it can provide information on the network of hydrogen bonds and their relative stabilities. The amide protons of aVal and aAla residues exhibited the strongest variations, as expected for solvent-exposed groups. In contrast the Val proton amide showed the smallest variations for both conformers

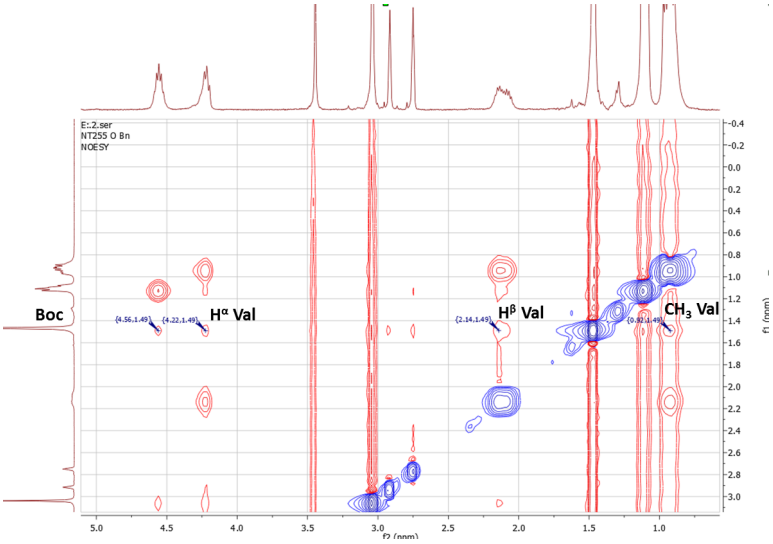

Figure 5.34: The assigned ROEs of **5.3**, confirming the presence of the β-turn minor isomer B

Residue	$\Delta\delta/\Delta T$ (ppb K^{-1})
a-Val NH(1)	- 7.5
a-Ala NH(3)	- 9.0
Val NH(5)	- 4.0

Table 5.26: Temperature coefficients for the amide protons of **5.3** isomer A in DMF

Residue	$\Delta\delta/\Delta T$ (ppb K^{-1})
a-Val NH(1)	- 8.0
a-Ala NH(3)	- 5.5
Val NH(5)	- 2.5

Table 5.27: Temperature coefficients for the amide protons of **5.3** isomer B in DMF

Residue	NH (ppm)	H_α (ppm)	C_α (ppm)	CO (ppm)
Val	- 1.55	+ 0.13	- 4.70	- 4.00

Table 5.28: Chemical shift deviations (CSD) of Val residue of compound **5.3** in DMF

(Table 5.26 and Table 5.27), but more accentuated for the minor one. This observation suggests an engagement in a stronger intramolecular hydrogen bond of the Val proton amide in one of the two conformers and is indicative of an equilibrium between two conformational structures that differ among them for the possibility to establish a more or less strong hydrogen bond.

If we observed the 1D ^1H spectrum, recorded in DMSO-d_6 at 300 K, we clearly noticed a stabilization of the more extended conformation, compared to the structure in DMF-d_7, due to the breaking of the hydrogen bond that destabilizes the β-turn structure.

The coupling constant in DMF-d_7 of the natural amino acid in the sequence exhibited at 303 K for the major isomer a large values (8.2 Hz), reflecting a ϕ angle value around $-120°$, as expected for β-strand conformation, and for the other minor isomer a smaller value (7.8 Hz), as expected for the folded structures [177].

We calculated the CSD for the only one natural amino acid and we observed that the proton amide was upfield shifted and the α-proton was downfield shifted. For the carbons, we found that the α-carbon and the carbonyl group were downfield shifted, suggesting a more extended structure (β-strand) (Table 5.28).

NMR studies in CD_3OH Proton NMR spectra were recorded on a spectrometer operating at 500 MHz (at UPMC, in collaboration with Pr. O. Lequin and Dr. I. Correia, UMR 7203). Compound **5.3** was dissolved at a concentration of 28.6 mM in 600 µL of CD_3OH The observed proton and carbon chemical shifts are displayed in Table 5.29.

The amide proton of the Val residue showed the smallest variation of the temperature coefficient for both conformers (Table 5.30), suggesting that a 10-membered cycle with the hydrogen bond between the carbonyl group of Boc and the proton amide of Val can be formed in both conformations. On the contrary, all the other amide protons exhibited strong variations (Table 5.30) as expected for solvent-exposed groups.

We are facing to an equilibrium between two secondary structures that present a similar 10-membered cycle observed for compound **5.2**. In this case, without the possibility to establish another hydrogen bond between the carbony group of the aVal residue and the C-terminal primary amide, the

Residue[a]	δ HN (ppm)	δH^{α} (ppm)	δH^{β} (ppm)	δ Other protons (ppm)
Boc-Carbamate	-	-	-	CH_3 1.49 (a) CH_3 1.50 (b)
aVal[1]	9.13 (a) 9.08 (b)		4.53 (a, b)	γ CH_3 1.11, γ□ CH_3 1.06 (a, b)
aAla[2]	9.43 (a) 9.38 (b)	-	3.08 (a) 3.07 (b)	
Val[3]	6.71 (a, b)	4.12 (a, b)	2.18 (a) 2.11 (b)	γ CH_3 0.96, γ' CH_3 0.93 (a) γ CH_3 0.93, γ' CH_3 0,89 (b)
OBz				CH_2 (5.17, 5.10), Bz 7,4 (a, b)

Residue[a]	δ CO (ppm)	δC^{α} (ppm)	δC^{β} (ppm)	δ Other carbons (ppm)
Boc-Carbamate	157.6 (a) 157.7 (b)	-	-	Cq 82.2, CH_3 28.5 (a) Cq 82.0, CH_3 28.4 (b)
aVal[1]	158.02(a) 157.97 (b)	-	49.9 (a, b)	γ CH_3 20.1, γ' CH_3 19.06 (a, b)
aAla[2]	160.7 (a) 160.6 (b)	-	36.3 (a, b)	- -
Val[3]	174.0 (a, b)	60.9 (a) 60.8 (b)	31.4 (a) 31.9 (b)	γ CH_3 18.6, γ' CH_3 19.6 (a) γ CH_3 19.13, γ' CH_3 19.4 (b)
O-Benzyl				CH_2 67.4, Bz (137.2, 129.36, 129.40, 129.2)

Table 5.29: Chemical shifts for protons and carbons of **5.3** in CD_3OH at 273 K

Residue	ΔdHN/ΔT (ppb/K)	*JHN-Hα (Hz)
aVal[1]	-7.03 (a) -6.92 (b)	-
aAla[2]	-7.75 (a) -7.69 (b)	-
Val[3]	-3,94 (a, b)	8.8 (a, b)

Table 5.30: NMR conformational parameters for **5.3** in CD_3OH

Entries	Relative Potential Energy (kcal/mol)	Peptide bonds	Urea type bonds	φ angles	ψ angles	Distance (Å)
1	1.038	*trans, trans, trans*	*E, E*	φ_1= 71.0 φ_2= 82.9 φ_3= -71.0	ψ_1= 5.4 ψ_2= 6.0 ψ_3= -54.7	a) 2.90 b) 2.38 c) /
2	1.465	*cis, trans, trans*	*E, E*	φ_1= -89.0 φ_2= -88.0 φ_3= -92.5	ψ_1= 124.6 ψ_2= -12.6 ψ_3= -62.5	a) 2.62 b) 2.48 c) /
3	1.826	*trans, trans, trans*	*E, E*	φ_1= -80.7 φ_2= 83.6 φ_3= -130.9	ψ_1= -6.1 ψ_2= 5.7 ψ_3= -43.3	a) 2.72 b) 2.40 c) /

Table 5.31: Selected representative entries of **5.3**: structure and energy data. Distances a) between NH(1) and NH(3), b) between NH(3) and NH(5) and c) between NH(4) and NH(5)

C-terminal Val residue is more flexible and cannot stabilize the double tight β-turn conformation. So, we observed a major conformation that recalls the second conformer of compound **5.2**, together with a minor structure with the characteristics of a classical β-turn.

The coupling constant at 251 K of the only one amino acid in the sequence exhibited in both isomers a large value (8.8 Hz) (Table 5.30), reflecting a φ angle value around $-120°$, as expected for β-strand conformation [177].

Finally, we observed that the proton amide of the natural Val residue was upfield shifted (-1.32) with respect to the random coil chemical shift values and in the same way the carbonyl group and the α-carbon demonstrated to be upfield shifted (- 2.3 and - 1.3, respectively). The proton CSD values indicated mainly an α-helix conformation, while the carbon chemical shift deviations showed a more extended one.

MM studies About the conformational studies conducted by molecular modelling on compound **5.3**, clustering yielded 40 representative conformations within a sliding energy window of 16.583 kJ mol^{-1}. All the 40 entries showed *trans*-planar amide bond, except for the Boc that showed an equilibrium between *cis* and *trans* isomers. Both the urea-type RN(2)-CO and RN(4)-CO bonds presented only the *E* isomerization, confirming again that the presence of a side chain on the α-nitrogen leads to a *cis* conformation of the RN-CO bond.

We found basically two types of representative conformations: one with the hydrogen bond between the Boc carbonyl group and the amide proton of Val, leading to a βI-turn conformation (Entry **1**, Table 5.31), and one without hydrogen bond and with a shape similar to the structure of compound **5.2** (Entries **2** and **3**, Table 5.31). This latter (Figure 5.35) is the most

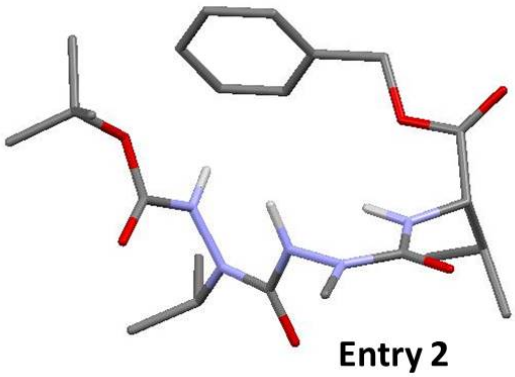

Figure 5.35: Selected representative entry of compound **5.3**

representative conformation, even if the entry with the lowest energy is the β-turn form.

Also in this case, the φ_2 dihedral angle seems to play an important role in determining the preferential conformation. A negative value destabilizes the βI-turn conformation, while a positive value can define both a well-established βI-turn structure and a less folded one, similar to **5.2**. In this latter case, it becomes very considerable the φ_1 dihedral angle related to φ_2: a negative φ_1 destabilizes the formation of the hydrogen bond and so leads to a more open conformation, while a positive φ_1 allows the formation of the βI-turn motif (Table 5.31).

If we compare the results obtained by the conformational research conducted on the two compounds **5.2** and **5.3**, we can conclude that the effect of a C-terminal primary amide is very important for the conformation of the azapeptide sequence. In particular, the presence of the primary amide can limit the equilibrium between only two conformers: the possibility to form or not the hydrogen bond between one of the two protons and the carbonyl group of the aVal residue and so to create the double turn structure is probably linked to the difficult rotation around the φ_2 dihedral angle and, even if the molecule passes through a positive dihedral angle that favors the folded structure becomes less probable and so less representative, favoring a structure that resembles the one with the typical hydrogen bond involving the primary amide. When we removed the primary amide and we replaced it by an ester, we can find again the βI-turn structure as an energetically favored conformation, due to the absence of possibility to form the H-bond.

The effect to have two aza-amino acid residues makes the sequence stiff enough to create this equilibrium that can allow to stabilize the double turn structure, compared to an azapeptide with only one aza-amino acid in the middle that is able to explore more different conformations, but not so rigid

as a pure azatide structure to limit the range of stereochemically allowed dihedral angles that favor the βI-turn conformation.

In any case, we proved that the presence of an aza-amino acid residue in the middle of an azapeptide sequence is not directely correlated with the formation of a βI-turn conformation, but rather an aza-amino acid can affect a peptide sequence by developing different conformations on the basis of its position in the sequence, the side chains of the amino acids linked to it, the type of the side chain bearing by the α-nitrogen and the number of aza-amino acids residues.

5.3.6 Conformational analyses of aGly-aGly-Val-$CONH_2$

In a previous work, we demonstrated by molecular modeling that the designed aGly-aGly-Val diazapeptide arm, into molecular tongs based on a rigid naphthalene scaffold, had an extended conformation compatible with the formation of a β-sheet. This observation was conducted on the complex between our molecular tongs and the HIV-1 PR monomer. We observed that the original hydrogen bonding properties made this peptidomimetic good modulator of protein-protein interactions involving β-sheet structures [265].

Starting from this observation, we decided to synthesize again the same peptidomimetic arm aGly-aGly-Val (see [265] for the synthesis details) in order to analyze by NMR its conformational structure alone in a protic solvent. The aim was to compare the structure of a diazapeptide without side chains on the α-nitrogen with compound **5.2** and to confirm the results obtained by molecular modelling with the peptidomimetic incorporated in a molecular tong in contact with the protease monomer.

NMR studies in CD_3OH Proton NMR spectra were recorded on a spectrometer operating at 500 MHz (at UPMC, in collaboration with Pr. O. Lequin and Dr. I. Correia, UMR 7203). Compound aGly-aGly-Val-$CONH_2$ was dissolved at a concentration of 40 mM in 600 µL of CD_3OH The observed proton and carbon chemical shifts are displayed in Table 5.32.

All the amide protons exhibited strong temperature coefficient variations (Table 5.33) as expected for solvent-exposed groups, and no hydrogen bonded.

We are facing to an equilibrium between different conformations (at least four) but the identification of their structure resulted difficult because of their broadened signals. The aGly-aGly-Val-$CONH_2$ compound exhibited in solution a more flexible behavior without a privileged conformation. Other ROEs experiments at low temperature (for exemple at 200 K) are in progress with the aim to better establish the exact conformation.

The coupling constant at 251 K of the natural amino acid Val in the sequence could not be measured because of the broad peak and so no information about the main chain φ dihedral angle could be extrapolated by the vicinal $^3J_{NH-H\alpha}$ constant.

Residue[a]	δ HN (ppm)	δH^{α} (ppm)	δH^{β} (ppm)	δ Other protons (ppm)
Boc-Carbamate	-	-	-	CH_3 1.47
aGly[1]	8.56	8.51	-	
aGly[2]	7,91	8.51	-	
Val[3]	6,47	4.11 (a) 4.10 (b)	2.16	γ CH_3 0.99, γ' CH_3 0,95
NH_E	7.62		-	
NH_Z	7.09		-	

Residue[a]	δ CO (ppm)	δC^{α} (ppm)	δC^{β} (ppm)	δ Other carbons (ppm)
Boc-Carbamate	158.3	-	-	Cq 81.9, CH_3 28.4
aGly[1]	160.9 (broad)	-	-	-
aGly[2]	161.3 (broad)	-	-	-
Val[3]	177.3 (a) 177.2 (b)	60.3 (a) 60.27 (b)	31.6	- γ CH_3 19.7, γ' CH_3 17.9

Table 5.32: Chemical shifts for protons and carbons of aGly-aGly-Val-$CONH_2$ in CD_3OH at 292.8 K

Residue	DdHN/DT (ppb/K)	*JHN-Ha (Hz)
aGly[1]	-9.4	broad
aGly[2]	-6.30	broad
Val[3]	-4.25	broad
NH_b	-8.64	s
NH_a	-6.12	broad

Table 5.33: NMR conformational parameters for aGly-aGly-Val-$CONH_2$ in CD_3OH

Entries	Relative Potential Energy (kcal/mol)	Peptide bonds	Urea type bonds	φ angles	ψ angles	Distance (Å)
1	0.000	*trans, trans, trans*	*Z, Z*	φ_1= -178.9 φ_2= 179.6 φ_3= -79.8	ψ_1= 179.8 ψ_2= -179.7 ψ_3= -16.9	a) 4.38 b) 4.24 c) 2.22
2	1.446	*cis, trans, trans*	*Z, E*	φ_1= -109.7 φ_2= 92.4 φ_3= -76.8	ψ_1= 175.3 ψ_2= 14.1 ψ_3= -18.1	a) 4.40 b) 2.35 c) 3.39
6	2.813	*trans, cis, trans*	*Z, E*	φ_1= 145.1 φ_2= -88.3 φ_3= -84.8	ψ_1= -165.7 ψ_2= 1.4 ψ_3= -14.0	a) 4.54 b) 2.51 c) 3.26
9	2.904	*trans, cis, trans*	*Z, Z*	φ_1= -178.0 φ_2= -95.4 φ_3= 179.8	ψ_1= 179.6 ψ_2= -178.9 ψ_3= -16.8	a) 4.52 b) 4.26 c) 2.20
10	2.951	*trans, trans, trans*	*E, Z*	φ_1= -92.4 φ_2= -173.8 φ_3= -79.9	ψ_1= -4.0 ψ_2= 178.8 ψ_3= -16.8	a) 2.62 b) 4.24 c) 2.23
26	4.619	*trans, trans, trans*	*E, E*	φ_1= 93.1 φ_2= -75.6 φ_3= -75.0	ψ_1= 5.9 ψ_2= -8.1 ψ_3= -14.7	a) 2.60 b) 2.73 c) 3.38

Table 5.34: Selected representative entries of aGly-aGly-Val: structure and energy data. Distances a) between NH(1) and NH(3), b) between NH(3) and NH(5) and c) between NH(4) and NH(5)

Finally, we observed that the proton amide of the natural Val residue was upfield shifted (-1.56) with respect to the random coil chemical shift values, while the α-proton showed a comparable value to a disordered structure. The α-carbon chemical shift resulted downfield shifted while the carbonyl one was upfield shifted. All together these results suggest a flexible structure without a privileged conformation.

MM studies About the conformational studies by molecular modelling conducted on the diazatide aGly-aGly-Val, clustering yielded 25 representative conformations within a sliding energy window of 20.67 kJ mol^{-1}. Most of them exhibited an extended conformation. In all the extended structures, the urea constituents assumed the classical *all-trans* planar conformation. All the amide bonds were *trans*-planar, except for the Boc and also for the second amide bond CO-NH(3): both exibited an equilibrium between *cis* and *trans* isomers. The Boc isomerization was found not to affect the global conformational structure of the diazapeptide sequence, as we could notice for the *cis* and *trans* amide bond CO-NH(3) between the two aGly residues. For both the aGly residues we detected an *E* conformation of the urea-type

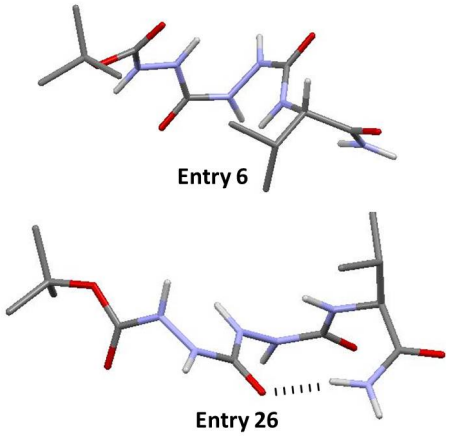

Figure 5.36: Selected representative entries of aGly-aGly-Val

NH(2)-CO and NH(4)-CO bonds, together with the *Z* conformation (Table 5.34).

If we exclude the isomerization of Boc and we take into account the *cis* and *trans* isomerization of the second peptide bond CO-NH(3) and the two *E* and *Z* conformations of the urea-type NH(2)-CO and NH(4)-CO bonds of the aGly residues, we could have in totally eight conformational possibilities. If we check all the 25 representative entries that we obtained, we discovered only six types of conformations. The combination between the *cis* CO-NH(3) peptide bond and the *E* configuration of the first urea-type NH(2)-CO bond is not allowed, thus excluding two conformational possibilities. Every representative entries for the other conformations are listed in Table 5.34.

Generally the *E* configuration of the first urea-type NH(2)-CO bond allows to obtain the similar values of φ_1 and ψ_1 dihedral angles observed when we had a side chain on the α-nitrogen of the aza-amino acid residue. In the same way the *E* configuration of the second urea-type NH(4)-CO bond lets φ_2 and ψ_2 dihedral angles close in value to the sequence with the side chains on the α-nitrogen.

The combination of all *trans* planar amide bonds and the *E* configuration of both urea-type NH(2)-CO and NH(4)-CO bonds allows to form the conformation with the hydrogen bond between one of the two C-terminal primary amide protons and the carbonyl group of the first aza-amino acid residue (Entry **26**) (Figure 5.36), as we saw for compound **5.2**. In this structure, we noticed a similar dihedral angle combination as in compound **5.2**. On the contrary, in absence of the characteristic hydrogen bond, the same combination of all *trans* planar amide bonds and the *E* configuration of both urea-type NH(2)-CO and NH(4)-CO bonds creates a dihedral angle

Compound	Preferential conformations
5.1 (BocNH-aLys-aGly-Val-$CONH_2$)	βI-turn (NMR, MM)
BocNH-Lys-aGly-Val-$CONH_2$	βI-turn/extended (MM)
BocNH-aLys-aGly-aVal-$CONH_2$	Double-turn/extended (MM)
5.2 (BocNH-aVal-aAla-Val-$CONH_2$)	Double-turn (2 conformations) (NMR, MM, X-Ray)
BocNH-aVal-aGly-Val-$CONH_2$	Extended (MM)
BocNH-Val-aAla-Val-$CONH_2$	Double-turn/βI-turn (MM)
BocNH-aVal-aAla-aVal-$CONH_2$	βI-turn (MM)
BocNH-Val-Ala-Val-$CONH_2$	Extended (NMR, MM)
5.3 (BocNH-aVal-aAla-Val-COOBn)	Double-turn (without the second hydrogen bond)/βI-turn (NMR, MM)
BocNH-aGly-aGly-Val-$CONH_2$	Extended (NMR, MM)

Table 5.35: Summary of the preferential conformations from experimental NMR conformational analyses and/or molecular modelling (MM)

composition not so similar to compound **5.2**. It seems that the hydrogen bond is important for the preferential conformation of compound **5.2**.

On the other hand, a similar dihedral angle composition to compound **5.2** without hydrogen bond was found for the combination of the *cis* second peptide bond CO-NH(3) and the *E* configuration of the second urea-type NH(4)-CO bond (Entry **6**) (Figure 5.36). This observation suggests that, when there is not the characteristic hydrogen bond that affects the dihedral angle composition, the side chain on the α-nitrogen of the second residue seems to create the effect of a *cis* second peptide bond on the conformational sequence, allowing a similar conformation but without the characteristic hydrogen bond, as we saw for the second isomer of **5.2**.

5.4 Conclusion and perspectives

As we can deduce from the results obtained by NMR and molecular modeling (Table 5.35), a 2:1 [Aza/α]-tripeptide sequence is not able to adopt an extended conformation but we cannot exclude that a β-strand conformation might be established when this type of tripeptide sequence is employed in a β-hairpin structure and interacts with a target peptide through hydrogen

bonds or hydrophobic interactions. It's for this reason that the next step will be to incorporate a 2:1 [Aza/α]-tripeptide in a β-hairpin, to study it facing to a target peptide and to observe if it is able to maintain its structure or if it adapts itself in order to establish protein-protein like interactions. In fact, the hydrogen-bonding properties of a 2:1 [Aza/α]-tripeptide has not yet, to our knowledge, been exploited in the design of the inhibition of protein-protein interactions.

If we compared the conformational behavior of a 2:1 [Aza/α]-tripeptide with amino acid side chains on the α nitrogen with respect to a similar sequence but without side chains (aGly-aGly-Val), we can notice that the fact to have substituted the nitrogen atom confers to the tripeptide analogue a more rigid character, limiting the range of stereochemically allowed dihedral angles.

Unlike the corresponding natural tripeptide, which resulted to be preferentially extended, a 2:1 [Aza/α]-tripeptide has been shown to have the tendency to confer on the peptide sequence a 10-membered β-turn conformation, with a hydrogen bond between the carbonyl group of residue i and the amide proton of residue $i + 3$.

The fact of having employed a C-terminal primary amide, mimicking the possible presence of an amide bond with a fourth residue, has allowed us to observe that a 2:1 [Aza/α]-tripeptide is able to impart to the backbone the possibility of establishing two 10-membered cycles with a further i-$i + 3$ hydrogen bond. This observation led to think that this pseudo-helix conformation could lead to the formation of a 3_{10}-helix structure and by DFT studies we demonstrated that the sequence aVal-aAla-Val repeated twice can adopt a conformation that could be assigned to some sort of 3_{10}-helix.

Finally, we observed that this type of double tight β-turn is possible thanks to the presence of two aza-amino acids, other than aGly, and of a natural amino acid. By molecular modelling conformational studies, we showed that, if on the one hand, the side chains on the α nitrogen allow certain dihedral angles that lead to the formation of a pseudo-helix structure, on the other the third natural amino acid allows a a degree of flexibility, necessary to establish the formation of the second 10-membered β-turn.

In perspectives, the aim is to synthesize the aVal-aAla-Val dimer **5.21** and to perform conformational analyses by NMR and X-ray spectroscopy in order to be able to determine with accuracy the 3_{10}-helix structure.

General conclusion

This PhD thesis work had the aim to design and synthesize new ligands of the Aβ 1-42 peptide in order to slow down or inhibit its aggregation process.

To meet this objective, we developed different synthetic pathways in order to obtain a diversified group of acyclic β-hairpin mimics, that allowed us to perform structure-activity relationship studies and to understand what is needed to interact with Aβ 1-42 and inhibit its aggregation process. Together with the conception and the synthesis, we carried out various physico-chemical assays to study the effect of our compounds on the oligomerization and fibrillization of Aβ 1-42 peptide. Thanks to the conformational analyses conducted by NMR and MM, we had also the possibility to examine the preferential conformations of our molecules and correlate them with their inhibitory activity.

In Chapter 2, we saw that the β-hairpin mimics, designed on oligomeric and fibril structure of Aβ and containing a piperidine-pyrrolidine β-turn inducer, were able to engage both hydrophobic and ionic interactions with the target peptide. The presence of two small recognition sequences, taken from the central core and the C-terminus of Aβ 1-42, proved to be important for the interaction and the affinity with the peptide. With these compounds, we put in evidence the importance of rationally designed sequences to have selectivity, the significance of a β-turn inducer able to fold the molecule in a β-hairpin manner and the relevance of amine groups that can form ionic interactions with the peptide.

The presence of a semi-rigid scaffold demonstrated to allow a dynamic equilibrium between different architectures and to obtain a compound (**2.4**) able to totally inhibit the formation of amyloid fibrils. The flexibility resulted to be an important characteristic to have a better inhibitory activity, compared to a more rigid β-hairpin structure.

In Chapter 3, we could investigate the inhibitory activity of nine β-sheet mimics with more druggable characteristics: a decreased peptide character, a lower molecular weight and a good hydrosolubility. We could correlate the ability to prevent or delay the aggregation process of these compounds with the length of the peptide chain and the type of protecting group on the primary amine of the scaffold. Furthermore, we could examine the impact of protected and deprotected amines on the inhibition process and

the importance of the possibility to establish ionic interactions to improve the affinity and the activity.

With this study, we demonstrated that, in order to have a good inhibitory activity, we need: 1) a flexible scaffold that allows to obtain a flexible β-hairpin structure; 2) a peptidomimetic arm that decreases the peptide character of the molecule and is able to establish hydrophobic interactions and hydrogen bond with Aβ; 3) a free terminal amine and a Lys residue to establish ionic interactions; 4) an aromatic moiety on the scaffold that can establish hydrophobic interactions.

It still remains to be discovered with which amino acids of Aβ, our compounds are able to establish ionic interactions. It could be interesting to deepen where in the Aβ peptide sequence our compounds are able to interact and how they act as inhibitor of the aggregation process.

In Chapter 4, we reported the design and the synthetic developement of a new fluorinated peptidomimetic. The objective was to incorporate it in a β-hairpin mimic and to investigate the possibility to exploit the fluorine atom to undertake more extensive conformational studies, as well as the contribution of all the advantages of fluorine on lipophilicity, pKa, intermolecular interactions, molecular conformation and stability. For the moment, we developped an efficient synthesis of the fluorinated peptidomimetic and we demonstrated that the single peptidomimetic has a better inhibitory activity compared to that we used in the previous structure-activity relationship studies (Chapter 3). This better activity justifies the interest of incorporating this fluorinated analogue in our most promising β-hairpin inhibitor **3.1**.

Finally, in Chapter 5, we presented the design and synthesis of another type of peptidomimetic arm based on a 2:1 [aza/α]-tripeptide sequence. Also in this case, we had not the possibility to study the role of this peptidomimetic in a β-hairpin structure but the conformational analyses that we performed by NMR, molecular modelling and X-ray spectroscopy demonstrated the possibility to achieve interesting conformations with this type of peptidomimetic unit.

We showed that a 2:1 [aza/α]-tripeptide is able to impart to the backbone the possibility of establishing two 10-membered cycles with a i-i + 3 hydrogen bond network. Preliminary results by DFT on a dimer of this peptidomimetic sequence demonstrated the possibility to explore other type of conformations rather than the β-strands, as the 3_{10}-helix structure.

The next step will be to incorporate a 2:1 [Aza/α]-tripeptide in a β-hairpin, to study it facing to a target peptide and to observe if it is able to maintain its structure or if it adapts itself in order to establish protein-protein like interactions.

Chapter 6

Experimental part

General experimental methods Usual solvents were purchased from commercial sources, dried and distilled by standard procedures. Pure compounds were obtained after liquid chromatography using Merch silical gel 60 (40–63 µm). TLC analyses were performed on silica gel 60 F_{250} (0.26 mm thickness) plates. The plates were visualized with UV light ($\lambda = 254$ nm) or revealed with a 4 % solution of phosphomolybdic acid in ethanol. NMR spectra were recorded on an ultrafield Bruker AVANCE 300 (^{1}H, 300 MHz, ^{13}C, 75 MHz) or on a Bruker AVANCE 400 (^{1}H, 400 MHz, ^{13}C, 100 MHz). Chemical shifts δ are in ppm and the following abbreviations are used: singlet (s), doublet (d), doublet of doublet (dd), triplet (t), quintuplet (qt), multiplet (m), broad multiplet (bm) and broad singlet (bs). Mass spectra were obtained using a Bruker Esquire electrospray ionization apparatus. HRMS were obtained using a TOF LCT Premier apparatus (Waters), with an electrospray ionization source. The purity of compounds was determined by HPLC using a WATERS gradient system (pump + controller E 600, UV detector PDA 2996, autosampler 717) and a column C18 (3.5 µm, 100 nm X 2.1 mm). Melting points were determined on a Kofler melting point apparatus. Element analyses (C, H, and N) were performed on a PerkinElmer CHN, Analyzer 2400 at the Microanalyses Service of the Faculty of Pharmacy at Chatenay-Malabry (BioCIS, France).

Fluorescence-detected ThT binding assay Thioflavin T was obtained from Sigma. Aβ 1-42 was purchased from American Peptide. The peptide was dissolved in an aqueous 1 % ammonia solution to a concentration of 1 mM and then, just prior to use, was diluted to 0.2 mM with 10 mM Tris-HCl, 100 mM NaCl buffer (pH 7.4). Stock solutions of β-hairpin mimics were dissolved in DMSO with the final concentration kept constant at 0.5 % (v/v).

Thioflavin-T fluorescence was measured to evaluate the development of Aβ 1-42 fibrils over time using a fluorescence plate reader (Fluostar Optima, BMG labtech) with standard 96-wells black microtiter plates. Experiments

were started by adding the peptide (final Aβ 1-42 concentration equal to 10 µM) into a mixture containing 40 µM Thioflavin T in 10 mM Tris-HCl, 100 mM NaCl buffer (pH 7.4) with and without the tested compounds at different concentrations (100 µM, 50 µM, 10 µM and 1 µM) at room temperature. The Th-T fluorescence intensity of each sample (performed in duplicate or triplicate) was recorded with 440 nm/485 nm nm excitation/emission filters set for 42 hours performing a double orbital shaking of 10 s before the first cycle. The fluorescence assays were performed between 2 and 4 times on different days, with two different batches of peptide. The ability of compounds to inhibit Aβ 1-42 aggregation was assessed considering both the time of the half-life of aggregation ($t_{1/2}$) and the intensity of the experimental fluorescence plateau (F). The extension of $t_{1/2}$ is defined as the experimental $t_{1/2}$ in the presence of the tested compound relative to the one obtained without the compound and is evaluated as the following ratio: $t_{1/2}$(Aβ+compound) / $t_{1/2}$(Aβ). The change of fluorescence intensity at the plateau decrease of the experimental plateau is defined as the intensity of experimental fluorescence plateau observed with the tested compound relative to the value obtained without the compound and is evaluated as the following percentage : (FAβ+compound − FAβ)/ FAβ x 100). A decrease is indicated with a (-) and an increase with a (+).

Transmission Electron Microscopy Samples were prepared under the same conditions as in the ThT-fluorescence assay. Aliquots of Aβ 1-42 (10 µM in 10 mM Tris-HCl, 100 mM NaCl buffer, pH 7.4 in the presence and absence of the tested compounds) were adsorbed onto 300-mesh carbon grids for 2 min, washed and dried. The samples were negatively stained for 45 s. on 2 % uranyl acetate in water. After draining off the excess of staining solution and drying, images were obtained using a ZEISS 912 Omega electron microscope operating at an accelerating voltage of 80 kV.

Capillary Electrophoresis (CE) - Sample preparation: The commercial Aβ 1-42 was dissolved upon reception in 0.16 % NH_4OH (at 2 mg mL^{-1}) for 10 minutes at 20 °C, followed by an immediate lyophilisation and a storage at −20 °C as pretreatment. - CE: CE experiments were carried out with a PA800 ProteomeLab instrument (Beckman Coulter Inc., Brea, CA, USA) equipped with a diode array detector. UV Detection was performed at 190 nm. The prepared sample (as previously described) was dissolved in 20 mM phosphate buffer pH 7.4 containing DMSO (control or stock solutions of compounds dissolved in DMSO) at 2.5 % (v/v) and the final peptide concentration at 100 µM regardless the peptide/compound *ratio*. For the CE separation of Aβ oligomers, fused silica capillary 80 cm (10.2 cm to the detector) and 50 mm I.D. were used. The background electrolyte was a 80 mM phosphate buffer, pH 7.4. The separation was carried out under −30 kV at 20 °C. The sample

was injected from the outlet by hydrodynamic injection at 3.44 kPa for 10 s. After each run, the capillary was rinsed for 5 min with water, 1 min with SDS 50 mM, 5 min with NaOH 1 M and equilibrated with running buffer for 5 min.

Cell Toxicity SH-SY5Y neuroblastoma cells were grown in low serum Optimem (Life Technologies) for 24 hours at 37 °C, 5 % CO_2 in a 96 well plate at 20000 cells per well. Aβ 1-42 was dissolved in a PBS at 50 µM concentration in the presence of 1, 5, 10 and 50 µM of compounds for 24 h at room temperature, along with a control incubation with no inhibitor. After the 24 h period, media were removed from the cells and replaced with Optimem containing the preincubated Aβ 1-42 plus inhibitor diluted one in ten (5 µM Aβ final concentration) in quadruplicate. The cells were incubated for a further 24 h as before, and the cell viability (MTS assay) and cell proliferation (LDH assay) were assessed using the CellT iter 96 Aqueous One Solution Cell Proliferation Assay (Promega) and CytoTox 96 Non-Radioactive Cytotoxicity Assay (Promega), respectively. The assays were repeated twice, and representative samples are shown.

NMR spectroscopy NMR experiments were recorded on different spectrometers: compounds **2.1** and **2.3** with a spectrometer operating at 500 MHz, compound **3.1** with a spectrometer operating at 600 MHz equiped with a cryoprobe, compound **3.2** with a spectrometer operating at 800 MHz equiped with a cryorobe, compound **5.1** with a spectrometer operating at 400 MHz equiped with a microrobe and compounds **5.2**, **5.3**, Boc-aGly-aGly-Val-$CONH_2$ and Boc-Val-Ala-Val-$CONH_2$ with a spectrometer operating at 500 MHz. ^1H and ^{13}C resonances were completely assigned using 1D ^1H, 2D ^1H-^1H COSY, 2D ^1H-^1H ROESY, ^1H-^1H NOESY, ^1H-^1H TOCSY, 2D ^1H-^{13}C HSQC and 2D ^1H-^{13}C HMBC spectra. ^1H and ^{13}C chemical shifts were calibrated using the solvent residual peak (DMSO-d_6, δ ^1H 2.50 ppm, δ ^{13}C 39.51; DMF-d_7, δ ^1H 2.92 ppm, 2.75 ppm and 8.03 ppm, δ ^{13}C 34.89, 29.76 and 39.51; CD_3OH, δ ^1H 3.31 ppm, δ ^{13}C 49.5 ppm; H_20/D_20, δ ^1H 4.80 ppm). The chemical shifts deviations were calculated as the differences between observed chemical shifts and random coil values reported by Wishart *et al.* [178]. Vicinal coupling constants were extracted from 1D ^1H spectrum or from 2D ^1H-^1H COSY. The temperature gradients of the amide proton chemical shifts were derived from 1D ^1H spectra recorded between 5 °C and 40 °C or between −15 °C and 40 °C, according to the solvent.

Computational methods Molecular mechanic studies were performed using Macro-Model from the Schrodinger software suite (MacroModel, version 10.2, Schrodinger, LLC, New York, NY, 2013). An arbitrary initial conformation of the compound was energy-minimized using the conjugate

gradient method with the OPLS-2005 force field [286] and GBSA as an implicit water solvation model [287]. The convergence criterion was set to $0.05\,\mathrm{kJ\,mol^{-1}\,\AA^{-1}}$ on the energy gradient.

An unconstrained conformational search was then performed starting from this structure and using the MCMM (Monte Carlo Multiple Minima) method [288] with the same force field, the solvation model and the convergence criterion. 100000 conformations were generated, energy-minimized and deduplicated [152].

For the clustering of these results we used the centroid linkage method with a 0.66 Å merge distance threshold [152] (as suggested by the Kelley penalty function) [289].

Structures of Entries **2** and **7** of compound **5.2** (see Chapter 5) were fully optimized in vacuum and without constraint using DFT method [290] [291] with the hybrid Becke3LYP functional [292] [293] and the 6-31G* base [294] as implemented in Gaussian 09 software package [295]. Vibrational analysis within the harmonic approximation was performed at the same level of theory upon geometrical optimization convergence and local minima were characterized by the absence of imaginary frequency. PCM model was used to take into account solvation [296].

(S)-methyl 1-((3R,4R)-1-benzyl-4-(4-methylphenylsulfonamido)piperidin-3-yl)pyrrolidine-2-carboxylate (**2.5**)

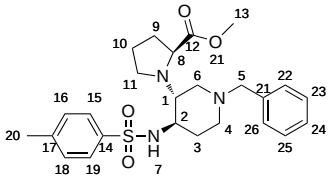

To a suspension of proline methyl ester hydrochloride (4.0 g, 24.0 mmol, 1.0 eq.) in 1,2 dichloroethane (40 mL) was added TEA (3.36 mL, 24.0 mmol, 1.0 eq.). After 15 min, under nitrogen atmosphere, 4-benzylpiperidone (4.2 mL, 24.0 mmol, 1.0 eq.) and molecular sieves (3 Å) were added to the solution. After 30 min, a catalytic amount of $InCl_3$ (0.53 g, 2.4 mmol, 0.1 eq.) was added, and stirring was continued for 45 min. At this moment, the reaction mixture was cooled at 10°C, and a solution of Tosyl azide (4.76 g, 24.0 mmol, 1.0 eq.) in 1,2 dichloroethane (20 mL) was introduced. After 45 min at room temperature, $(AcO)_3BHNa$ (25.4 g, 120.0 mmol, 5.0 eq.) was added and the mixture was allowed under stirring overnight at room temperature. The reaction was then successively filtered, washed with water (3 X 30 mL), and dried over Na_2SO_4. After removing the solvent under vacuum, the residue obtained was crystallized with MeOH giving first pure compound **2.5** (1.32 g, 2.79 mmol, Yield 12 %). Then, purification by column chromatography on silica gel of the mother liquor of the crystallization, using Cyclo/EtOAc 1:1 as eluent, afforded a further amount of **2.5**. The global yield of compound **2.5** was finally 15 % (1.67 g, 3.54 mmol).

Molecular weight = 471.61 g mol^{-1}

R_f = 0.65 (DCM/MeOH 20:1)

HRMS: Calcd. for $[C_{25}H_{33}N_3O_4S + H]^+$: M/z 472.2270, found: 472.2262

^{1}H NMR (MeOD, 400 MHz): δ 7.77 (2H, d, J = 8.2 Hz, H15, H19); 7.46, 7.44 (5H, m, H22, H23, H24, H25, H26); 7.40 (2H, d, J = 8.0 Hz, H16, H18); 4.19, 4,07 (2H, m, H5); 3.74 (3H, s, H13); 3.53 (1H, m, H8); 3.29 (1H, m, H6); 3.01 (1H, m, H2); 3.21 (1H, m, H4); 2.87 (1H, m, H1); 2.83 (1H, m, H6); 2.74 (1H, m, H4); 2.46 (1H, m, H3); 2.43 (3H, s, H20); 2.33 (2H, m, H11); 2.05 (1H, m, H9); 1.82 (1H, m, H9); 1.70 (1H, m, H3); 1.55, 1.33 (2H, m, H10) ppm

^{13}C NMR (MeOD, 100 MHz): δ 77.9 (C12); 145.8 (C21); 145.2 (C17); 138.1 (C14); 131.9, 130.9, 130.2 (C22, C23, C24, C25, C26); 130.9 (C16, C18); 128.4 (C15, C19); 63.0 (C8); 62.3 (C5); 58.1 (C1); 52.9 (C13); 52.8 (C2); 51.7 (C6); 51.3 (C4); 45.5 (C11); 31.7 (C3); 30.8 (C9); 25.3 (C10); 21.4 (C20) ppm

Melting point = 177–179 °C

IR: 3197 (N-H stretch); 2988, 2938, 2901 (C-H stretch); 1737 (C=O stretch); 1340, 1320 (CH3 bend); 1199, 1161, 1149 (C-N stretch, C-C(O)-C stretch) cm^{-1}

Elemental analysis: Calcd. for $C_{25}H_{33}N_3O_4S$: C 63.67, H 7.05, N 8.91; found: C 63.61, H 6.71, N 8.85

(S)-methyl-1-((3R,4R)-4-(4-methylphenylsulfonamido)piperidin-3-yl)pyrrolidine-2-carboxylate (**2.11**)

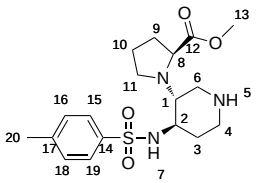

Compound **2.5** (500 mg, 1.06 mmol, 1.0 eq.) was dissolved in toluene (10 mL) and 10 % Pd/C (226 mg, 2.12 mmol, 2.0 eq.) was added. The reaction was stirred at 30°C under hydrogen atmosphere for 6 h. The solution was filtered through a pad of Celite and the filtrate was evaporated under vacuum affording compound **2.11** as a white solid (444.7 mg, 1.06 mmol, Yield 100 %).

Molecular weight = 381.17 g mol^{-1}

$R_f = 0.20$ (DCM/MeOH 20:1)

HRMS: Calcd. for $[C_{18}H_{27}N_3O_4S + H]^+$: M/z 382.1801, found: 382.1801

^{1}H NMR ($CDCl_3$, 300 MHz): δ 7.76 (2H, d, J = 7.6 Hz, H15, H19); 7.26 (2H, d, J = 7.6 Hz, H16, H18); 6.79 (1H, bp, NH7); 3.74 (3H, s, H13); 3.45 (2H, m, H8, NH5); 2.97 (2H, m, H2, H4); 2.74 (2H, m, H6); 2.49 (6H, m, H1, H4, H11, H20); 2.24 (1H, m, H11); 1.99 (1H, m, H9); 1.77 (2H, m, H3, H9); 1.39 (3H, m, H3, H10) ppm

^{13}C NMR ($CDCl_3$, 75 MHz): δ 176.3 (C12); 143.0 (C17); 137.5 (C14); 129.9 (C16, C18); 127.4 (C15, C19); 62.3 (C1); 59.9 (C8); 54.2 (C2); 52.6 (C13); 45.1 (C4); 44.9 (C6); 44.3 (C3); 35.3 (C9); 30.0 (C11); 24.6 (C10); 21.7 (C20) ppm

Melting point = 122–124 °C

IR: 3206 (N-H stretch); 2951-2849 (C-H stretch); 1727 (C=O stretch); 1669 (N-H bend); 1438 (C=C stretch); 1209-1161 (C-N stretch) cm^{-1}

(S)-1-((3R,4R)-4-(4-methylphenylsulfonamido)piperidin-3-yl)pyrrolidine-2-carboxylic acid (**2.12**)

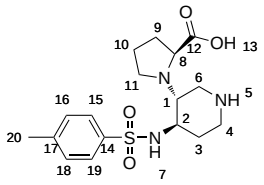

Compound **2.11** (324 mg, 0.85 mmol, 1.0 eq.) was dissolved in 6 M aqueous HCl (6.5 mL) and heated at 110° C under stirring. After 4 h, the solvent was removed, and the oily residue obtained was precipitated from acetone to give compound **2.12** as a white solid (341.6 mg, 0.85 mmol, Yield 100 %).

Molecular weight = 367.16 g mol^{-1}

$R_f = 0$ (DCM/MeOH/NH_4OH 90:10:0.2)

HRMS: Calcd. for $[C_{17}H_{25}N_3O_4S + H]^+$: M/z 368.1644, found: 368.1646

^{1}H NMR (MeOD, 300 MHz): δ 7.86 (2H, d, J = 8.1 Hz, H15, H19); 7.45 (2H, d, J = 8.1 Hz, H16, H18); 4.70 (1H, t, J = 8.5 Hz, H8); 3.88 (4H, m, H2, H4, H6); 3.60 (1H, m, H6); 3.48 (1H, td, J = 12.3 Hz, H1); 3.04 (1H, t, J = 11.9 Hz, H11); 2.58 (1H, dt, J = 15.2, 7.2 Hz, H3); 2.45 (3H, s, H20); 2.32 (1H, dt, J = 15.1, 7.8 Hz, H9); 2.13 (2H, m, H9, H11); 1.78 (1H, m, H3); 1.47 (1H, m, H10); 1.29 (1H, m, H10) ppm

^{13}C NMR (MeOD, 75 MHz): δ 171.6 (C12); 145.8 (C14); 138.8 (C17); 131.3 (C16, C18); 128.3 (C15, C19); 66.1 (C8); 61.2 (C1); 51.4 (C2); 51.1 (C11); 43.8 (C4); 42.0 (C6); 29.4 (C9); 28.8 (C3); 24.4 (C10); 21.5 (C20) ppm

Melting point = 191–193 °C

IR: 3376 (N-H stretch); 2985-2793 (C-H stretch, O-H stretch); 1725 (C=O stretch); 1630-1597 (N-H bend); 1450-1400 (O-H bend); 1327 (C-O stretch); 1160 (C-N stretch) cm^{-1}

(S)-1-((3R,4R)-1-(((9H-fluoren-9-yl)methoxy)carbonyl)-4-(4-methylphenylsulfonamido)piperidin-3-yl)pyrrolidine-2-carboxylic acid (**2.13**)

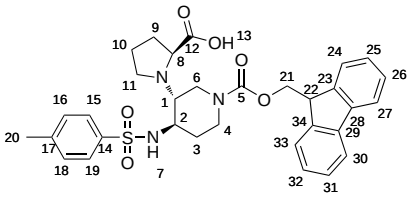

Compound **2.12** (312.3 mg, 0.85 mmol, 1.0 eq.) was dissolved in CH_3CN/MeOH (4:1, 8.5 mL). Fmoc-OSu (315.4 mg, 0.94 mmol, 1.1 eq.) and DIPEA (296 µL, 1.7 mmol, 2.0 eq.) were added to the solution. The reaction was left under stirring for 3 h. After the solvent was removed under vacuum, the crude residue was resuspended in DCM (30 mL) and the organic phase washed successively with water (3 X 30 mL), dried over Na_2SO_4 and evaporated under vacuum. The crude residue obtained was precipitated with EtOAc/Hexane affording compound **2.13** as a white solid (308.1, 0.52 mmol, Yield 61 %).

Molecular weight = 589.70 g mol^{-1}

R_f = 0.60 (DCM/MeOH 10:1)

HRMS: Calcd. for $[C_{32}H_{35}N_3O_6S + H]^+$: M/z 590.2325, found: 590.2321; Calcd. for $[C_{32}H_{35}N_3O_6S + Na]^+$: M/z 612.2144, found: 612.2140

^{1}H NMR (MeOD, 300 MHz): δ 7.79 (4H, m, H15, H19, H27, H30); 7.56 (2H, m, H24, H33); 7.35 (6H, m, H16, H18, H25, H26, H31, H32); 4.70 (1H, m, H8); 4.55 (2H, dd, J = 10.5, 4.9 Hz, H21); 4.20 (1H, t, J = 4.9 Hz, H22); 3.60 (2H, m, H2, H4); 3.30 (2H, m, H6); 2.84 (4H, m, H1, H4, H9, H11); 2.42 (3H, s, H20); 2.03 (2H, m, H9, H11); 1.61 (2H, m, H3); 1.16 (2H, m, H10) ppm

^{13}C NMR (MeOD, 75 MHz): δ 166.8 (C12); 157.0 (C5); 145.1 (C14); 142.7 (C28, C29); 138.7 (C23, C34); 135.1 (C17); 128.9 (C26, C31); 128.3 (C25, C32); 130.9 (C16, C18); 128.4 (C15, C19); 125.7 (C24, C33); 121.0 (C27, C30); 64.0 (C21); 61.8 (C8); 55.8 (C1); 53.4 (C2); 43.8 (C6); 42.8 (C4); 39.4 (C22); 32.6 (C11); 31.0 (C9); 28.3 (C3); 25.5 (C10); 21.5 (C20) ppm

Melting point = 134–136 °C

IR: 2951-2872 (C-H stretch, O-H stretch); 1698 (C=O stretch); 1599 (N-H bend); 1476-1448 (O-H bend); 1335-1317 (C-O stretch) cm^{-1}

(S)-6-(2-(5-acetamido-2-methoxybenzoyl)hydrazinyl)-5-((S)-1-((3R,4R)-1-((S)--2-((S)-2-ammoniopropanamido)-3-methylbutanoyl)-4-(4-methylphenylsulfonamido)-piperidin-3-yl)pyrrolidine-2-carboxamido)-6-oxohexan-1-aminium chloride (**3.1**)

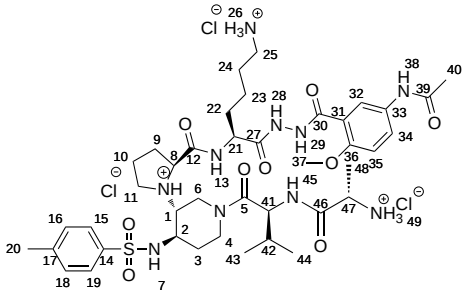

Compound **3.27** (40.0 mg, 0.039 mmol, 1.0 eq.) was dissolved in dioxane (2.0 mL) and a 4 N solution of HCl in dioxane (0.293 mL, 30.0 eq.) was successively added. The reaction was kept 2 hours under stirring at room temperature. After this time, product **3.1** was isolated as hydrochloride salt by precipitation in diethyl ether. The crude product was purified by crystallography in MeOH and diethyl ether to afford the pure compound **3.1** as a white powder (19.0 mg, 0.019 mmol, Yield 50 %).

Molecular weight = 980.44 g mol^{-1}

$R_f = 0$ (EtOAc/MeOH 95:5)

HRMS: Calcd. for $[C_{41}H_{62}N_{10}O_9S + H]^+$: M/z 871.4500, found: 871.4497; Calcd. for $[C_{41}H_{62}N_{10}O_9S + Na]^+$: M/z 893.4320, found: 893.4316

^{1}H NMR (H_2O/ D_2O, 600 MHz): δ (298K) 10.42 (1H, bp, NH28); 10.31 (1H, bp, NH29); 9.79 (1H, s, NH38); 9.09 (1H, bp, NH13); 8.52 (1H, bp, NH45); 8.06 (3H, bp, NH49); 7.95 (1H, bp, NH7); 7.88 (1H, s, H32); 7.84 (2H, m, H15, H19); 7.57 (1H, m, H34); 7.56 (3H, bp, NH26); 7.47 (2H, m, H16, H18); 7.22 (1H, m, H35); 4.60 (1H, m, H41); 4.52 (1H, m, H21); 4.23 (1H, m, H4); 4.22 (1H, m, H6); 4.11 (1H, m, H47); 3.96 (3H, s, H37); 3.93 (1H, m, H11); 3.72 (1H, m, H8); 3.48 (1H, m, H4); 3.15 (1H, m, H11); 3.04 (2H, m, H25); 3.01 (1H, m, H2); 2.85 (1H, m, H1); 2.60 (1H, m, H6); 2.50 (1H, m, H9); 2.44 (3H, s, H20); 2.18 (3H, s, H40); 2.11 (1H, m, H9); 2.06 (1H, m, H10); 1.98 (2H, m, H22); 1.94 (1H, m, H42); 1.90 (1H, m, H10); 1.76 (2H, m, H24); 1.63 (1H, m, H3); 1.53 (2H, m, H23); 1.48 (1H, m, H3); 1.46 (3H, d, H48); 0.82-0.83 (6H, m, H43, H44) ppm

^{13}C NMR (H_2O/ D_2O, 133 MHz): δ (298K) 173.1 (C39); 171.9 (C27); 171.3 (C5); 170.7 (C46); 166.5 (C30); 164.9 (C12); 155.1 (C36); 145.6 (C17); 135.6 (C14); 130.2 (C33); 130.2 (C16, C18); 128.4 (C34); 126.7 (C15, C19); 124.7 (C32); 118.7 (C31); 112.9 (C35); 56.3 (C37); 55.1 (C41); 52.2 (C21); 52.1 (C8); 48.8 (C47); 44.2 (C4); 44.1 (C11); 41.4 (C6); 39.3 (C25); 37.0 (C2); 31.4 (C1); 30.3 (C3); 30.2 (C9); 30.1 (C22); 29.7 (C42); 26.4 (C24);

24.1 (C10); 22.5 (C40); 21.8 (C23); 20.6 (C20); 18.5, 16.7 (C43, C44); 16.5 (C48) ppm

Melting point = 221–223 °C

IR: 3194 (N-H stretch); 2926 (C-H stretch); 1652 (C=O stretch); 1546-1493-1457 (N-H bend); 1252 (C-N stretch); 1157 (S=O stretch) cm^{-1}

HPLC purity (XBridge C18, 3.5 µm, H_2O + 0.2 % form. ac./ACN, gradient 5–100 % in 20 min): t_R = 10.08 min, 100 %

(S)-6-(2-(5-acetamido-2-methoxybenzoyl)hydrazinyl)-5-((S)-1-((3R,4R)-1-((S)--2-((S)-2-((S)-2-ammonio-3-methylbutanamido)propanamido)-3-methylbutanoyl)--4-(4-methylphenylsulfonamido)piperidin-3-yl)pyrrolidine-2-carboxamido)-6-oxohexan--1-aminium chloride (**3.2**)

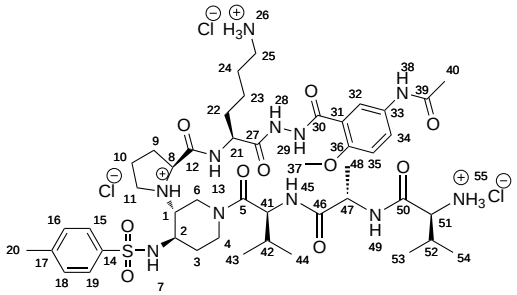

Compound textbf3.10 (50.0 mg, 0.042 mmol, 1.0 eq.) was dissolved in MeOH (4.0 mL) and 10 % Pd/C (10 mg) was added. The reaction was kept 2 hours under stirring in hydrogen atmosphere at room temperature. The catalyst was then removed over a celite pad and the solvent evaporated under vacuum. Successively, the resulting product was dissolved in dioxane (2.0 mL) and a 4 N solution of HCl in dioxane (0.311 mL, 30.0 eq.) was added. The reaction was kept 2 hours under stirring at room temperature. After this time, product textbf3.1 was isolated as hydrochloride salt by precipitation in diethyl ether. The crude was purified by crystallization in MeOH and diethyl ether to afford the pure compound textbf3.1 as a white powder (9.0 mg, 0.008 mmol, Yield 19 %).

Molecular weight = 1079.57 g mol^{-1}

R_f = 0 (EtOAc/MeOH 95:5)

HRMS: Calcd. for $[C_{46}H_{71}N_{11}O_{10}S+H]^+$: M/z 970.5184, found: 970.5181

^{1}H NMR (H_2O/ D_2O, 800 MHz): δ (283 K) 10.27 (1H, bp, NH28); 10.09 (1H, bp, NH29); 9.59 (1H, s, NH38); 8.89 (1H, bp, NH13); 8.46 (1H, bp, NH49); 8.18 (1H, bp, NH45); 7.82 (3H, bp, NH55); 7.79 (1H, bp, NH7); 7.59 (1H, s, H32); 7.54 (2H, m, H15, H19); 7.33 (3H, bp, NH26); 7.27 (1H, m, H34); 7.18 (2H, m, H16, H18); 6.92 (1H, m, H35); 4.34 (1H, m, H6); 4.25 (1H, m, H41); 4.24 (1H, m, H21); 4.12 (1H, m, H47); 3.92 (1H, m, H4); 3.83 (1H, m, H2); 3.69 (3H, s, H37); 3.64 (1H, m, H11); 3.49 (1H, m, H51); 3.47

(1H, m, H8); 2.84 (1H, m, H6); 2.83 (1H, m, H11); 2.77 (1H, m, H1); 2.76 (2H, m, H25); 2.29 (1H, m, H4); 2.26 (1H, m, H9); 2.15 (3H, s, H20); 1.91 (1H, m, H52); 1.88 (3H, s, H40); 1.81 (1H, m, H10); 1.71 (1H, m, H9); 1.70 (2H, m, H22); 1.67 (1H, m, H42); 1.65 (1H, m, H10); 1.49 (2H, m, H24); 1.30 (1H, m, H3); 1.28 (2H, m, H23); 1.19 (1H, m, H3); 1.05 (3H, d, H48); 0.73-0.71 (6H, m, H53, H54); 0.57-0.54 (6H, m, H43, H44) ppm

^{13}C NMR (H_2O/ D_2O, 200 MHz): δ (283 K) 174.1 (C46); 172.9 (C39); 171.8 (C27); 171.6 (C5); 170.8 (C12); 169.0 (C50); 166.3 (C30); 155.1 (C36); 145.3 (C14); 135.3 (C17); 130.1 (C16, C18); 129.8 (C33); 128.4 (C34); 126.6 (C15, C19); 124.7 (C32); 118.4 (C31); 112.7 (C35); 58.3 (C51); 56.0 (C37); 54.6 (C41); 52.4 (C21); 51.7 (C8); 49.3 (C47); 48.9 (C2); 46.8 (C1); 43.6 (C11); 40.9 (C4); 39.2 (C25); 39.1 (C6); 30.1 (C3); 30.1 (C22); 29.9 (C9); 29.9 (C52); 29.7 (C42); 26.3 (C24); 23.8 (C10); 22.4 (C40); 21.9 (C23); 20.6 (C20); 18.4, 16.9 (C43, C44); 17.5, 16.6 (C53, C54); 16.3 (C48) ppm

Melting point = 229–231 °C

IR: 3194 (N-H stretch); 2966 (C-H stretch); 1652 (C=O stretch); 1539-1494-1456 (N-H bend); 1250 (C-N stretch); 1161 (S=O stretch) cm^{-1}

HPLC purity (XBridge C18, 3.5 µm, H_2O + 0.1 % form. ac./ACN, gradient 5–100 % in 20 min): t_R = 10.47 min, 92 %

tert-butyl ((3R,4R)-3-((S)-2-(((S)-1-(2-(5-acetamido-2-methoxybenzoyl)hydrazinyl)-6-amino-1-oxohexan-2-yl)carbamoyl)pyrrolidin-1-yl)-1-((S)-2-((S)-2-aminopropanamido)-3-methylbutanoyl)piperidin-4-yl)carbamate (**3.3**)

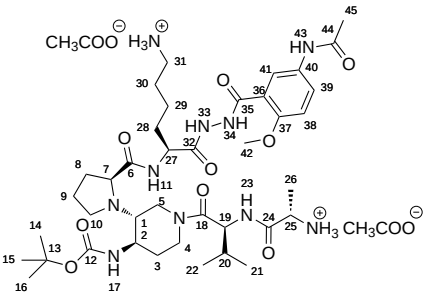

Compound **3.26** (63.0 mg, 0.06 mmol, 1.0 eq.) was dissolved in MeOH (4.0 mL) and 10 % Pd/C (x mg) was added. The reaction was kept 2 hours under stirring in hydrogen atmosphere at room temperature. The catalyst was then removed over a celite pad and the solvent evaporated under vacuum. The crude was diluted in a minimum amount of MeOH and 2.0 eq. of acetic acid were added. Product **3.3** was isolated as acetate salt by precipitation in diethyl ether. The crude product was purified by crystallography in MeOH and diethyl ether to afford the pure compound **3.3** as a white powder (25.0 mg, 0.03 mmol, Yield 50 %).

Molecular weight = 997.14 g mol^{-1}

$R_f = 0$ (EtOAc/MeOH 9:1)

HRMS: Calcd. for $[C_{39}H_{64}N_{10}O_9 + H]^+$: M/z 817.4936, found: 817.4939

^{1}H NMR (DMSO – d_6, 400 MHz): δ (NH17 not detected); (NH_3 Lys not detected); 10.80 (1H, bp, NH33); 10.72 (1H, bp, NH34); 10.03 (1H, s, NH43); 8.34 (1H, bp, NH11); 7.96 (1H, s, H41); 7.74 (1H, m, H39); 7.70 (1H, bp, NH23); 6.72 (3H, bp, NH_3 Ala); 7.10 (1H, m, H38); 4.55 (1H, m, H19); 4.52 (1H, m, H27); 3.85 (3H, s, H42); 3.67 (1H, m, H25); 3.33 (1H, m, H7); 3.32 (1H, m, H1); 2.73 (2H, m, H31); 2.21 (1H, m, H1); 2.01 (3H, s, H45); 1.88 (1H, m, H20); 1.81 (2H, m, H28); 1.58 (2H, m, H29); 1.23 (2H, m, H30); 4.43, 3.00 (2H, m, H5); 3.97, 3.10 (2H, m, H4); 1.69, 1.54 (2H, m, H3); 3.07, 2.65 (2H, m, H10); 2.22, 1.69 (2H, m, H8); 1.25 (2H, m, H9); 1.36 (9H, s, H14, H15, H16); 1.20 (3H, s, H26); 0.80, 0.70 (6H, m, H21, H22) ppm

^{13}C NMR (DMSO – d_6, 100 MHz): δ 174.8 (C6); 172.4 (C18); 171.4 (C24); 169.2 (C32); 168.2 (C44); 163.5 (C35); 155.2 (C12); 152.8 (C37); 129.2 (C40); 123.8 (C39); 121.6 (C41); 120.6 (C36); 112.2 (C38); 78.3 (C13); 70.4 (C7); 62.4 (C1); 58.8 (C2); 55.9 (C42); 52.9 (C19); 49.2 (C27); 48.5 (C25); 45.4 (C10); 44.2 (C4); 38.3 (C31); 38.2 (C5); 31.5 (C28); 30.4 (C8); 29.9 (C20); 28.2 (C29); 27.8 (C14, C15, C16); 25.9 (C30); 24.1 (C3); 23.3 (C45); 21.8 (C9); 19.1, 17.6 (C21, C22); 18.6 (C26) ppm

HPLC purity (XBridge C18, 3.5 µm, H_2O + 0.1 % form. ac./ACN, gradient 5–100 % in 20 min): t_R = 9.13 min, 86 %

(S)-N-((S)-1-(2-(5-acetamido-2-methoxybenzoyl)hydrazinyl)-6-amino-1-oxohexan--2-yl)-1-((3R,4R)-4-amino-1-((S)-2-((S)-2-aminopropanamido)-3-methylbutanoyl)-piperidin-3-yl)pyrrolidine-2-carboxamide (**3.4**)

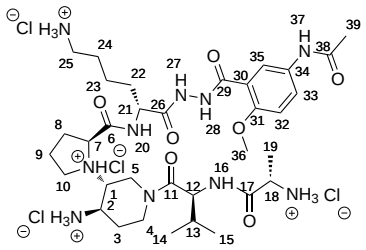

Compound **3.3** (20.0 mg, 0.02 mmol, 1.0 eq.) was dissolved in dioxane (2.0 mL) and a 4 N solution of HCl in dioxane (0.15 mL, 30.0 eq.) was successively added. The reaction was kept 2 hours under stirring at room temperature. After this time, product **3.4** was isolated as hydrochloride salt by precipitation in diethyl ether. The crude product was purified by crystallography in MeOH and diethyl ether to afford the pure compound **3.4** as a white powder (12.0 mg, 0.014 mmol, Yield 70 %).

Molecular weight = 862.72 g mol^{-1}

$R_f = 0$ (EtOAc/MeOH 9:1)

HRMS: Calcd. for $[C_{34}H_{56}N_{10}O_7 + H]^+$: M/z 717.4412, found: 717.4409

^{1}H NMR (DMSO–d_6, 400 MHz): δ 10.60 (1H, s, NH27); 10.20 (1H, s, NH37); 10.00 (1H, s, NH28); 8.03 (1H, s, H35); 8.97 (3H, bp, NH_3 scaff.); 8.51 (1H, bp, NH1-); 8.32 (3H, bp, NH_3 Ala); 8.30 (1H, bp, NH20); 8.25 (1H, bp, NH+ Pro); 8.05 (3H, bp, NH_3 Lys); 7.71 (1H, m, H33); 7.09 (1H, d, J=8.8 Hz, H32); 4.52 (1H, m, H12); 4.46 (1H, m, H21); 4.43 (1H, m, H5); 4.08 (1H, m, H4); 3.89 (1H, m, H7); 3.87 (3H, s, H36); 3.35 (1H, m, H18); 3.39 (1H, m, H1); 3.09 (1H, m, H4); 3.06 (1H, m, H10); 2.73 (2H, m, H25); 2.70 (1H, m, H5); 2.69 (1H, m, H10); 2.48 (1H, m, H2); 2.09 (1H, m, H8); 2.03 (3H, m, H39); 1.90 (1H, m, H13); 1.83 (1H, m, H3); 1.79 (2H, m, H22); 1.72 (1H, m, H8); 1.70 (1H, m, H3); 1.59 (2H, m, H23); 1.36 (2H, m, H9); 1.22 (2H, m, H24); 1.05 (3H, m, H19); 0.84, 0.78 (6H, m, H14, H15) ppm

^{13}C NMR (DMSO–d_6, 100 MHz): δ 171.3 (C6); 171.1 (C26); 170.0 (C17); 169.7 (C11); 163.8 (C38); 163.7 (C29); 153.0 (C31); 132.9 (C34); 123.5 (C33); 121.1 (C35); 120.8 (C30); 112.2 (C32); 64.1 (C1); 58.2 (C2); 55.9 (C36); 53.4 (C12); 50.4 (C21); 49.7 (C18); 47.5 (C7); 44.3 (C10); 42.8 (C4); 38.1 (C25); 37.9 (C5); 30.8 (C22); 30.5 (C8); 29.4 (C13); 28.4 (C24); 25.9 (C23); 24.1 (C3); 23.4 (C39); 22.0 (C9); 19.0, 17.7 (C14, C15); 14.7 (C19) ppm

Melting point = 226–228 °C

IR: 3235 (N-H stretch); 2967 (C-H stretch); 1634 (C=O stretch); 1547-1494 (N-H bend); 1252 (C-N stretch) cm^{-1}

HPLC purity (XBridge C18, 3.5 µm, H_2O + 0.1 % form. ac./ACN, gradient 1–60 % in 20 min): t_R = 7.75 min, 85 %

(S)-benzyl tert-butyl (6-(2-(5-acetamido-2-methoxybenzoyl)hydrazinyl)-6-oxohexane-1,5-diyl)dicarbamate (**NT05**)

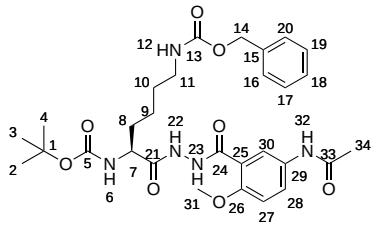

Bannwarth L. et al., Heterocycles 2009, 77, 445-460; Vidu A. et al., Chem Med Chem 2010, 5, 1899-1906

Compound **KFP24** (1.64 g, 4.3 mmol, 1.0 eq;) and Boc-NH-Lys(Z)-OH (1.96 g, 5.16 mmol, 1.2 eq.) were dissolved in DMF (10 mL). At this moment, DIPEA (7.5 mL, 43 mmol, 10.0 eq.), HBTU (1.96 g, 5.16 mmol, 1.2 eq.) and HOBt (0.70 g, 5.16 mmol, 1.2 eq.) were successively added to the reaction mixture. After stirring under argon atmosphere at room temperature for 24 h, DMF was evaporated under vacuum and the residue was taken up with EtOAc. The organic phase was successively washed with 10 % aqueous citric

acid solution, water, 10 % aqueous K_2CO_3 solution, brine, dried over Na_2SO_4, filtered. After evaporation of the solvent under vacuum, the resulting crude obtained was purified by column chromatography on silica gel using EtOAc 100 % as eluent to afford compound **NT05** (1.79 g, 3.13 mmol) as a white solid. Yield 73 %.

Molecular weight = 585.65 g mol^{-1}

$R_f = 0.40$ (EtOAc)

HRMS: Calcd. for $[C_{29}H_{39}N_5O_8 + Na]^+$: M/z 608.2696, found: 608.2712

^{1}H NMR ($CDCl_3$, 400 MHz): δ 11.88 (1H, bp, H22); 11.31 (1H, bp, H23); 8.79 (1H, bp, H32); 8.43 (1H, d, J = 7.8 Hz, H30); 7.99 (1H, bp, H28); 7.30 (5H, m, H16, H17, H18, H19, H20); 6.97 (1H, d, J = 9.2 Hz, H27); 5.65 (1H, d, J = 8.3 Hz, H6); 5.04 (2H, s, H14); 4.92 (1H, m, H7); 4.77 (1H, m, NH12); 4.02 (3H, s, H31); 3.04 (2H, m, H11); 2.20 (3H, s, H34); 1.78 (2H, m, H8); 1.46 (9H, s, H2, H3, H4); 1.38 (4H, m, H9, H10) ppm

^{13}C NMR ($CDCl_3$, 100 MHz): δ 169.2 (C21); 166.5 (C33); 158.8 (C24); 156.5 (C13); 155.7 (C5); 153.7 (C26); 136.7 (C15); 133.3 (C29); 128.6, 128.2 (C16, C17, C18, C19, C20); 126.2 (C28); 122.6 (C30); 117.9 (C25); 112.3 (C27); 80.0 (C1); 66.7 (C14); 56.7 (C31); 52.2 (C7); 40.9 (C11); 34.2 (C8); 29.7 (C10); 28.6 (C2, C3, C4); 24.6 (C34); 22.1 (C9) ppm

Melting point = 103–105 °C

IR: 3303 (N-H stretch); 2934 (C-H stretch); 1672, 1631 (C=O stretch); 1527, 1493 (N-H bend); 1247 (C-O-C stretch) cm^{-1}

HPLC purity (SUNFIRE C18, 3.5 µm, H_2O + 0.1 % form. ac./ACN, gradient 5–100 % in 20 min): t_R = 19.42 min, 96 %

(S)-1-(2-(5-acetamido-2-methoxybenzoyl)hydrazinyl)-6-(((benzyloxy)carbonyl)-amino)-1-oxohexan-2-aminium 2,2,2-trifluoroacetate (**3.6**)

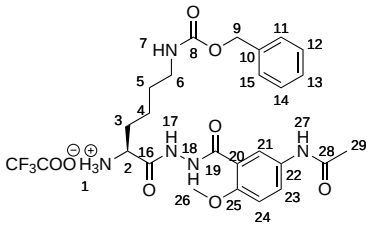

To a solution of the N-Boc-protected compound **NT05** (590 mg, 1.01 mmol, 1.0 eq.) in dry DCM (6.0 mL) was added TFA (3.0 mL) at 0°C. The reaction was stirred at room temperature for 3 hours. The solvent was evaporated, toluene (2x) was added followed by evaporation, and then ether was added and again evaporated to afford the corresponding TFA salt **36** (553 mg, 0.94 mmol) as a white solid. Yield 93 %.

Molecular weight = 599.56 g mol^{-1}

$R_f = 0$ (EtOAc)

^{1}H NMR (DMSO – d_6, 300 MHz): δ 10.90 (1H, s, H18); 10.14 (2H, m, H17, H29); 8.51 (3H, bp, H1); 8.16 (1H, bp, H7); 7.98 (1H, d, J = 2.4 Hz, H21); 7.77 (1H, dd, J = 8.8, 2.2 Hz, H23); 7.33 (5H, m, H11, H12, H13, H14, H15); 7.11 (1H, d, J = 9.0 Hz, H27); 4.99 (2H, s, H9); 3.80 (4H, m, H2, H26); 3.05 (2H, m, H6); 2.02 (3H, s, H29); 1.86 (2H, m, H3); 1.37 (4H, m, H4, H5) ppm

This product was already characterized in previous laboratory publications.

Bannwarth L. et al., Heterocycles 2009, 77, 445-460 Vidu A. et al., Chem Med Chem 2010, 5, 1899-1906

(3R,4R)-(9H-fluoren-9-yl)methyl 3-((S)-2-((((S)-1-(2-(5-acetamido-2-methoxybenzoyl)hydrazinyl)-6-(((benzyloxy)carbonyl)amino)-1-oxohexan-2-yl)oxy)carbonyl)pyrrolidin-1-yl)-4-(4-methylphenylsulfonamido)piperidine-1-carboxylate (**3.7**)

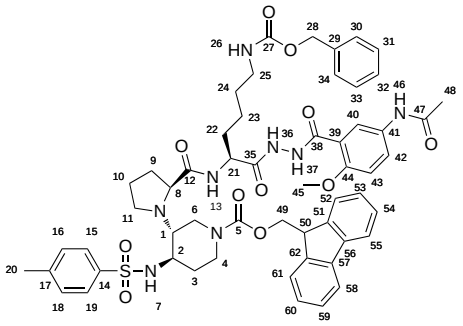

Compound **3.6** (452 mg, 0.93 mmol, 1.2 eq.) was dissolved in DMF (5.0 mL) under a nitrogen atmosphere and collidine (0.6 mL, 4.62 mmol, 6.0 eq) was added. This solution was let aside and meanwhile, compound **2.13** (454 mg, 0.77 mmol, 1.0 eq.) was dissolved in DMF (10.0 mL) under a nitrogen atmosphere and the solution was cooled to 0°C. A this moment, HATU (322 mg, 0.85 mmol, 1.1 eq.) and HOAt (115 mg, 0.85 mmol, 1.1 eq.) were then added at 0°C. The reaction was let stirring at 0°C for 1 h. Finally, the previous solution of compound **3.6** was added dropwise. The reaction was stirred at room temperature overnight. After concentration of the solvent under vacuum, the residue was taken up with EtOAc, washed successively with water, saturated aqueous $NaHCO_3$, brine, dried over Na_2SO_4 and the solvent evaporated under reduced pressure. The crude product obtained was purified by column chromatography on silica gel using EtOAc 100 % to EtOAc/MeOH 95:5 as eluent to afford compound **3.7** as a white solid (713 mg, 0.67 mmol, Yield 88 %).

Molecular weight = 1057.22 g mol^{-1}

$R_f = 0.60$ (EtOAc/MeOH 90:10)

HRMS: Calcd. for $[C_{56}H_{64}N_8O_{11}S+Na]^+$: M/z 1079.4313, found: 1079.4354

^{1}H NMR (DMSO – d_6, 400 MHz): δ 10.56 (1H, bp, NH36); 10.08 (1H, bp, NH37); 9.95 (1H, s, NH46); 8.19 (1H, bp, NH13); 8.01 (1H, s, H40); 7.84 (2H, m, H55, H58); 7.77 (1H, m, H42); 7.72 (2H, d, J = 7.9 Hz, H15, H19); 7.56 (2H, m, H52, H61); 7.56 (1H, bp, NH7); 7.35 (2H, m, H54, H59); 7.37 (2H, m, H16, H18); 7.34 (5H, m, H30, H31, H32, H33, H34); 7.30 (2H, m, H53, H60); 7.20 (1H, bp, NH26); 7.11 (1H, m, H43); 5.00 (2H, s, H28); 4.54 (1H, m, H21); 4.36 (2H, m, H49); 4.24 (1H, m, H50); 3.86 (1H, m, H4); 3.84 (3H, s, H45); 3.83 (1H, m, H8); 3.57 (1H, m, H6); 3.21 (1H, m, H2); 3.00 (2H, m, H25); 2.79 (1H, m, H6); 2.48 (1H, m, H4); 2.36 (3H, s, H20); 2.23 (1H, m, H1); 2.03 (3H, s, H48); 2.01 (1H, m, H11); 1.83 (1H, m, H9); 1.73 (2H, m, H22); 1.72 (1H, m, H9); 1.69 (1H, m, H11); 1.64 (1H, m, H3); 1.57 (1H, m, H10); 1.45 (2H, m, H24); 1.43 (1H, m, H10); 1.35 (2H, m, H23); 1.06 (1H, m, H3) ppm

^{13}C NMR (DMSO – d_6, 400 MHz): δ 170.8 (C35); 168.4 (C47); 163.7 (C36); 156.5 (C27); 154.5 (C5); 153.2 (C12); 152.8 (C44); 143.8 (C51, C62); 142.6 (C17); 140.8 (C56, C57); 138.7 (C14); 137.3 (C29); 132.7 (C41); 129.6 (C16, C18); 128.3 (C54, C59); 128.2 (C30, C31, C32, C33, C34); 127.1 (C53, C60); 126.5 (C15, C19); 124.8 (C52, C61); 123.7 (C42); 121.4 (C40); 120.7 (C39); 120.1 (C55, C58); 112.5 (C43); 66.9 (C49); 65.1 (C28); 58.9 (C1); 56.5 (C8); 56.1 (C45); 53.4 (C2); 50.3 (C21); 47.1 (C50); 44.9 (C4); 41.9 (C6); 40.1 (C25); 32.8 (C3); 32.3 (C9); 32.0 (C22); 30.9 (C11); 29.2 (C24); 24.7 (C10); 23.8 (C48); 23.2 (C23); 20.9 (C20) ppm

Melting point = 113–115 °C

IR: 3294 (N-H stretch); 2943 (C-H stretch); 1656, 1610 (C=O stretch); 1521-1450 (N-H bend) cm^{-1}

Compound (**3.8**)

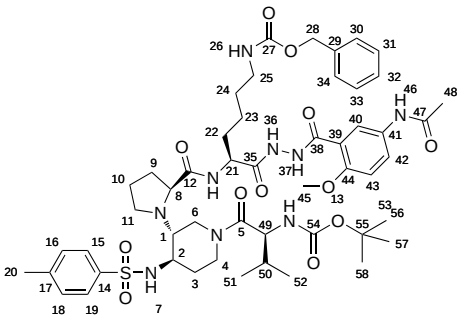

The N-Fmoc protected compound **3.7** (682 mg, 0.64 mmol, 1.0 eq.) was dissolved in a 20 % solution of piperidine in DMF (10 mL) and the reaction mixture was let stirring at room temperature for 2 h. The solvent

was evaporated to afford the deprotected amine that was used for the next coupling reaction without any further purification. The Boc-NH-Val-OH (278 mg, 1.28 mmol, 2.0 eq.) was dissolved in DMF (10.0 mL) under a nitrogen atmosphere and the solution was cooled to 0°C. A this moment, HOAt (174 mg, 1.28 mmol, 2.0 eq.) and HATU (487 mg, 1.28 mmol, 2.0 eq.) were then added. The solution was stirred at 0°C between 30 min and 1h and then the solution of the previous N-Fmoc deprotected compound **3.7** and collidine (0.34 mL, 2.56 mmol, 4.0 eq.) in DMF (5.0 mL) was added. The reaction was stirred at room temperature overnight. After concentration of the solvent under vacuum, the residue obtained was taken up with EtOAc, washed successively with water, saturated aqueous $NaHCO_3$, brine, dried over Na_2SO_4 and the solvent evaporated under reduced pressure. The crude product obtained was purified by column chromatography on silica gel using EtOAc 100 %, then EtOAc/MeOH 95:5 as eluent to afford compound **3.6** as a white solid (400 mg, 0.39 mmol, Yield 60 %).

Molecular weight = 1034.23 g mol^{-1}

R_f = 0.55 (EtOAc/MeOH 90:10)

HRMS: Calcd. for $[C_{51}H_{71}N_9O_{12}S+H]^+$: M/z 1034.5021, found: 1034.5016

^{1}H NMR (DMSO – d_6, 400 MHz): δ 10.55 (1H, bp, NH36); 10.04 (1H, bp, NH37); 9.95 (1H, s, NH46); 8.21 (1H, bp, NH13); 8.00 (1H, s, H40); 7.77 (1H, m, H42); 7.73 (2H, d, J = 7.8 Hz, H15, H19); 7.57 (1H, bp, NH7); 7.38 (2H, m, H16, H18); 7.36-7.34 (5H, m, H30, H31, H32, H33, H34); 7.21 (1H, bp, NH26); 7.12 (1H, m, H43); 6.70 (1H, s, NH53); 5.01 (2H, s, H28); 4.52 (1H, m, H21); 4.32 (1H, m, H6); 4.11 (1H, m, H49); 3.88 (1H, m, H4); 3.86 (3H, s, H45); 3.37 (1H, m, H8); 3.29 (1H, m, H2); 3.00 (2H, m, H25); 2.95 (1H, m, H4); 2.64 (1H, m, H6); 2.36 (3H, s, H20); 2.21 (1H, m, H1); 2.02 (3H, s, H48); 2.02 (1H, m, H11); 1.89-1.70 (2H, m, H22); 1.85 (1H, m, H3); 1.82 (1H, m, H50); 1.80 (1H, m, H9); 1.70 (1H, m, H9); 1.66 (1H, m, H11); 1.58 (1H, m, H10); 1.45 (2H, m, H24); 1.40 (1H, m, H10); 1.35 (2H, m, H23); 1.33 (9H, s, H56, H57, H58); 1.25 (1H, m, H3); 0.79-0.72 (6H, m, H51, H52) ppm

^{13}C NMR (DMSO – d_6, 400 MHz): δ 175.7 (C12); 169.9 (C35); 168.0 (C47); 163.1 (C36); 162.1 (C5); 156.5 (C54); 156.1 (C27); 152.8 (C44); 142.6 (C17); 138.4 (C14); 137.3 (C29); 132.7 (C41); 129.6 (C16, C18); 128.3-127.7-126.6 (C30, C31, C32, C33, C34); 126.0 (C15, C19); 123.3 (C42); 121.5 (C40); 120.9 (C39); 112.5 (C43); 77.1 (C55); 65.1 (C28); 62.6 (C8); 58.0 (C1); 55.8 (C45); 54.7 (C49); 52.8 (C2); 50.0 (C21); 42.4 (C4); 39.9 (C25); 39.2 (C6); 32.8 (C3); 31.8 (C22); 31.6 (C9); 29.8 (C11); 29.5 (C50); 28.5 (C24); 28.1 (C56, C57, C58);23.6 (C10); 23.8 (C48); 22.3 (C23); 20.9 (C20); 19.1-17.8 (C51, C52) ppm

Melting point = 151–153 °C

IR: 3280 (N-H stretch); 2938-2870 (C-H stretch); 1652 (C=O stretch);

1520-1454 (N-H bend) cm^{-1}

Compound (**3.9**)

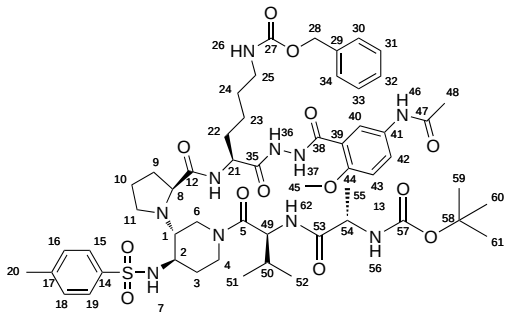

To a solution of the N-Boc protected compound **3.8** (256 mg, 0.25 mmol, 1.0 eq.) in DCM (5.0 mL) was added TFA (0.56 mL, 7.5 mmol, 30.0 eq.) then the reaction mixture was let stirring at room temperature for 2 h. The solvent was evaporated, toluene (2 x 10 mL) was added followed by evaporation, and then ether was added and evaporated to afford the corresponding TFA salt that was used for the next coupling reaction without any further purification. Boc-NH-Ala-OH (95 mg, 0.5 mmol, 2.0 eq.) was dissolved in DMF (5.0 mL) under a nitrogen atmosphere and the solution was cooled to 0°C. At this moment, HOAt (68 mg, 0.5 mmol, 2.0 eq.) and HATU (190 mg, 0.5 mmol, 2.0 eq.) were then added. The solution was stirred at 0°C between 30 min and 1h and then the solution of the previous TFA salt and collidine (0.13 mL, 1.0 mmol, 4.0 eq.) in DMF (5.0 mL) was added. The reaction was stirred at room temperature overnight. After concentration of the solvent under vacuum, the residue obtained was taken up with EtOAc, washed successively with water, saturated aqueous $NaHCO_3$, brine, dried over Na_2SO_4 and the solvent evaporated under reduced pressure. The crude product obtained was purified by column chromatography on silica gel using EtOAc 100 % then EtOAc/MeOH 95:5 as eluent to afford compound **3.9** as a white solid (228 mg, 0.21 mmol, Yield 83 %).

Molecular weight = 1105.31 g mol^{-1}

$R_f = 0.25$ (EtOAc/MeOH 95:5)

HRMS: Calcd. for $[C_{54}H_{76}N_{10}O_{13}S+H]^+$: M/z 1105.5392, found: 1105.5410; Calcd. for $[C_{54}H_{76}N_{10}O_{13}S + Na]^+$: M/z 1127.5212, found: 1127.5217

^{1}H NMR (DMSO – d_6, 400 MHz): δ 10.58 (1H, bp, NH36); 10.06 (1H, bp, NH37); 9.95 (1H, s, NH46); 8.22/7.75 (1H, bp, NH13); 8.01 (1H, s, H40); 7.76 (1H, m, H42); 7.74 (2H, m, H15, H19); 7.63 (1H, bp, NH62); 7.58 (1H, bp, NH7); 7.37 (2H, m, H16, H18); 7.34-7.29 (5H, m, H30, H31, H32, H33, H34); 7.21 (1H, bp, NH26); 7.12 (1H, m, H43); 6.95 (1H, bp, NH56); 5.00 (2H, s, H28); 4.52 (1H, m, H21); 4.48 (1H, m, H49); 4.33 (1H, m, H6); 3.95

(1H, m, H54); 3.86 (1H, m, H4); 3.85 (3H, s, H45); 3.37 (1H, m, H8); 3.29 (1H, m, H2); 3.00 (2H, m, H25); 2.98 (1H, m, H4); 2.65 (1H, m, H6); 2.36 (3H, s, H20); 2.24 (1H, m, H1); 2.04 (1H, m, H11); 2.03 (3H, s, H48); 1.85 (3H, m, H3, H9, H50); 1.81-1.71 (2H, m, H22); 1.67 (1H, m, H11); 1.59 (1H, m, H10); 1.44 (2H, m, H24); 1.43 (1H, m, H10); 1.34 (2H, m, H23); 1.35 (9H, s, H59, H60, H61); 1.28 (1H, m, H9); 1.26 (1H, m, H3); 1.12 (3H, s, H55); 0.74-0.72 (6H, m, H51, H52) ppm

^{13}C NMR (DMSO – d_6, 400 MHz): δ 174.5 (C12); 172.5 (C54); 170.5 (C35); 169.3 (C5); 168.0 (C47); 163.1 (C38); 156.1 (C27); 155.0 (C57); 152.8 (C44); 142.7 (C17); 138.5 (C14); 137.3 (C29); 132.7 (C41); 129.6 (C16, C18); 128.3, 127.7, 126.6 (C30, C31, C32, C33, C34); 126.9 (C15, C19); 123.7 (C42); 121.5 (C40); 120.6 (C39); 112.5 (C43); 78.1 (C58); 65.1 (C28); 62.9 (C8); 58.4 (C1); 56.2 (C45); 53.2 (C2); 52.8 (C49); 50.4 (C21); 49.8 (C54); 43.8 (C4); 40.3 (C25); 39.9 (C6); 33.7 (C3); 33.6 (C9); 31.8 (C22); 30.7 (C11); 30.2 (C50); 29.9 (C24); 28.2 (C59, C60, C61); 24.5 (C10); 23.8 (C48); 22.7 (C23); 20.9 (C20); 19.4, 17.5 (C51, C52); 17.9 (C55) ppm

Melting point = 149–151 °C

IR: 3298 (N-H stretch); 2932 (C-H stretch); 1652-1626 (C=O stretch); 1518-1455 (N-H bend) cm^{-1}

Elemental analysis: Calcd. for $C_{54}H_{76}N_{10}O_{13}S \cdot 1.0\,H_2O$: C 57.77, H 7.02, N 12.48; found: C 57.79, H 7.03, N 12.03

HPLC purity (SUNFIRE C18, 3.5 µm, H_2O + 0.2 % form. ac./ACN, gradient 5–100 % in 20 min): t_R = 17.83 min, 99 %

Compound (**3.10**)

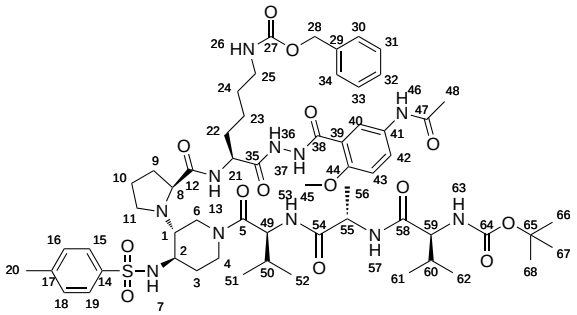

To a solution of the N-Boc protected compound **3.9** (228 mg, 0.21 mmol, 1.0 eq.) in DCM (5.0 mL) was added TFA (0.46 mL, 6.19 mmol, 30.0 eq.) and the reaction mixture was let stirring at room temperature for 2 h. The solvent was evaporated, toluene (2 x 10 mL) was added followed by evaporation, and then ether was added and evaporated to afford the corresponding TFA salt that was used for the next coupling reaction without any further purification. Boc-NH-Val-OH (91 mg, 0.42 mmol, 2.0 eq.) was dissolved in DMF (5.0 mL) under a nitrogen atmosphere and the solution was cooled to 0°C. At this

moment, HOAt (57 mg, 0.42 mmol, 2.0 eq.) and HATU (160 mg, 0.42 mmol, 2.0 eq.) were then added. The solution was stirred at 0°C between 30 min and 1h and then the solution of the previous TFA salt and collidine (0.11 mL, 0.84 mmol, 4.0 eq.) in DMF (5.0 mL) was added. The reaction was stirred at room temperature overnight. After concentration of the solvent under vacuum, the residue obtained was taken up with EtOAc, washed successively with water, saturated aqueous $NaHCO_3$, brine, dried over Na_2SO_4 and the solvent evaporated under reduced pressure. The crude product obtained was purified by column chromatography on silica gel using EtOAc 100 % then EtOAc/MeOH 95:5 as eluent to afford compound **3.10** as a white solid (144 mg, 0.12 mmol, Yield 57 %).

Molecular weight = 1204.44 g mol^{-1}

$R_f = 0.40$ (EtOAc/MeOH 95:5)

HRMS: Calcd. for $[C_{59}H_{85}N_{11}O_{14}S+H]^+$: M/z 1204.6076, found: 1204.6078; Calcd. for $[C_{59}H_{85}N_{11}O_{14}S + Na]^+$: M/z 1226.5896, found: 1226.5890

^{1}H NMR (DMSO – d_6, 400 MHz): δ 10.56 (1H, bp, NH36); 10.05 (1H, bp, NH37); 9.95 (1H, s, NH46); 8.23 (1H, bp, NH13); 8.00 (1H, s, H40); 7.87 (1H, bp, NH57); 7.86 (1H, bp, NH53); 7.76 (1H, m, H42); 7.74 (2H, m, H15, H19); 7.68 (1H, bp, NH7); 7.37 (2H, m, H16, H18); 7.36-7.34-7.16 (5H, m, H30, H31, H32, H33, H34); 7.20 (1H, bp, NH26); 7.12 (1H, m, H43); 6.67 (1H, bp, NH63); 5.01 (2H, s, H28); 4.52 (1H, m, H21); 4.44 (1H, m, H49); 4.30 (1H, m, H6); 4.34 (1H, m, H55); 3.79 (1H, m, H59); 3.87 (1H, m, H4); 3.85 (3H, s, H45); 3.38 (1H, m, H8); 3.29 (1H, m, H2); 3.00 (2H, m, H25); 2.96 (1H, m, H4); 2.65 (1H, m, H6); 2.36 (3H, s, H20); 2.24 (1H, m, H1); 2.05 (1H, m, H11); 2.03 (3H, s, H48); 1.91 (2H, m, H50, H60); 1.84 (2H, m, H3, H9); 1.69 (2H, m, H22); 1.65 (1H, m, H11); 1.59 (1H, m, H10); 1.43-1.23 (2H, m, H24); 1.43 (1H, m, H10); 1.36 (2H, m, H23); 1.36 (9H, s, H59, H60, H61); 1.26 (2H, m, H3, H9); 1.13 (3H, s, H55); 0.83-0.77 (6H, m, H61, H62); 0.77-0.73 (6H, m, H51, H52) ppm

^{13}C NMR (DMSO – d_6, 400 MHz): δ 174.2 (C12); 171.8 (C54); 170.9 (C58); 170.5 (C35); 169.4 (C5); 168.0 (C47); 163.3 (C38); 156.1 (C27); 155.4 (C64); 152.8 (C44); 142.6 (C17); 138.6 (C14); 137.3 (C29); 132.7 (C41); 129.6 (C16, C18); 128.3, 127.7, 126.5 (C30, C31, C32, C33, C34); 126.6 (C15, C19); 123.7 (C42); 121.5 (C40); 120.6 (C39); 112.5 (C43); 78.0 (C65); 65.1 (C28); 63.3 (C8); 59.4 (C59); 58.9 (C1); 56.2 (C45); 53.6 (C2); 53.2 (C49); 50.3 (C21); 47.9 (C55); 43.8 (C4); 40.5 (C25); 40.0 (C6); 33.7 (C3); 33.7 (C9); 32.1 (C22); 30.8 (C11); 30.4 (C60); 30.0 (C50); 29.0 (C24); 28.1 (C66, C67, C68); 24.7 (C10); 23.8 (C48); 23.2 (C23); 20.9 (C20); 19.4, 17.9 (C61, C62); 19.2, 17.7 (C51, C52); 18.3 (C56) ppm

Melting point = 153–155 °C

HPLC purity (XBridge C18, 3.5 µm, H_2O + 0.2 % form. ac./ACN, gradient 5–100 % in 20 min): t_R = 17.60 min, 90 %

(S)-methyl 1-((3R,4R)-1-benzyl-4-(4-nitrophenylsulfonamido)piperidin-3-yl)-pyrrolidine-2-carboxylate (**3.11**)

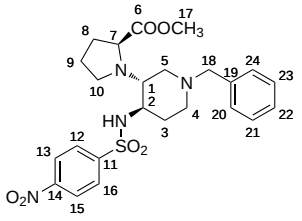

To a suspension of proline methyl ester hydrochloride (2.9 g, 17.4 mmol, 1.0 eq.) in 1,2 dichloroethane (40 mL) was added TEA (2.42 mL, 17.4 mmol, 1.0 eq.). After 15 min, under nitrogen atmosphere, 4-benzylpiperidone (3.23 mL, 17.4 mmol, 1.0 eq.) and molecular sieves were added to the solution. After 30 min, a catalytic amount of $InCl_3$ (0.39 g, 1.74 mmol, 0.1 eq.) wad added, and stirring was continued for 45 min. The reaction mixture was cooled at 0°C, and a solution of nosyl azide (3.97 g, 17.4 mmol, 1.0 eq.) in 1,2 dichloroethane (20 mL) was added. After 45 min at room temperature, $(AcO)_3BHNa$ (9.2 g, 43.5 mmol, 2.5 eq.) was added to the crude that was allowed to stir overnight at room temperature. The reaction was successively filtered, washed with water (3 X 30 mL), and dried with Na_2SO_4, and concentrated under vacuum. Purification by flash column chromatography on silica gel (c-Hex/EtOAc 6:4) afforded the good but not completed pure diastereoisomer (R,R,S). The impurity was then precipitated in DCM and finally removed by crystallization using AcOEt/c-Hex. The evaporation of the mother water afforded the title compound as a pale yellow solid (0.85 g, 1.68 mmol, Yield 10 %).

Molecular weight = 502.58 g mol^{-1}

R_f = 0.40 (Cyclo/EtOAc 1:1)

HRMS: Calcd. for $[C_{24}H_{30}N_4O_6S + H]^+$: M/z 503.1964, found: 503.1969

^{1}H NMR (Acetone–d_6, 400 MHz): δ 8.44 (2H, d, J = 8.9 Hz, H12, H16); 8.16 (2H, d, J = 8.9 Hz, H13, H15); 7.27, 7.22 (5H, m, H20, H21, H22, H23, H24); 7.27 (1H, NH); 3.75 (3H, s, , H17); 3.53, 3.50, 3.43 (3H, m, H7, H18); 2.92, 2.84, 2.73 (3H, m, H5, H2, H4); 2.59 (1H, td, , J = 10.7, 3.9 Hz, H1); 2.39, 2.30 (2H, m, H10, H3); 2.04, 1.97, 1.91, 1.78 (4H, m, H5, H8, H4, H8); 1.75, 1.55, 1.49, 1.31 (4H, m, H10, H3, H9, H9) ppm

^{13}C NMR (Acetone–d_6, 100 MHz): δ 177.6 (C6); 151.0 (C14); 147.4 (C11); 139.5 (C19); 129.6 (C12, C16); 129.5 (C20, C21, C23, C24); 127.45 (C22); 124.5 (C13, C15); 63.0 (C18); 62.5 (C7); 59.4 (C1); 54.5 (C2); 52.5 (C5); 52.4 (C17); 51.8 (C4); 44.9 (C10); 34.1 (C3); 29.9 (C8); 24.7 (C9) ppm

Melting point = 75–77 °C

IR: 3168 (N-H stretch); 2953-2820 (C-H stretch); 1723 (C=O stretch); 1527 (-NO2 aromatic); 1347 (-NO2 aromatic) cm^{-1}

(S)-methyl 1-((3R,4R)-1-benzyl-4-(N-(tert-butoxycarbonyl)-4-nitrophenylsulfonamido)piperidin-3-yl)pyrrolidine-2-carboxylate (**3.19**)

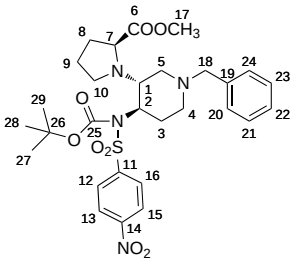

To a solution of compound **3.11** (854 mg, 1.7 mmol, 1.0 eq.) in DMF (30 mL) was added NaH 60 % in mineral oil (75.0 mg, 1.87 mmol, 1.1 eq.). After the reaction color turned from yellow to dark orange, Boc_2O (928 mg, 4.25 mmol, 2.5 eq.) and DMAP (519 mg, 4.25 mmol, 2.5 eq.) were added to the reaction mixture that was let stirring overnight at room temperature under argon atmosphere. The solvent was evaporated under vacuum and the resulting residue was dissolved in EtOAc and successively washed with water, saturated $NaHCO_3$ and brine, dried over Na_2SO_4, filtered and concentrated under vacuum. The crude product obtained was purified by column chromatography on silica gel using c-Hex/EtOAc 7:3 as eluent to afford compound **3.19** as a pale yellow solid (673 mg, 1.12 mmol, Yield 66 %).

Molecular weight = 602.70 g mol^{-1}

$R_f = 0.50$ (Cyclo/EtOAc 7:3)

HRMS: Calcd. for $[C_{29}H_{38}N_4O_8S + H]^+$: M/z 603.2489, found: 603.2496

^{1}H NMR (Acetone–d_6, 400 MHz): δ 8.63 (2H, d, J = 8.9 Hz, H12, H16); 8.42 (2H, d, J = 8.9 Hz, H13, H15); 7.35, 7.25 (5H, m, H20, H21, H22, H23, H24); 4.43 (1H, td, , J = 11.6, 4.6 Hz, H2); 3.92 (1H, t, J = 9.0 Hz, H1); 3.62 (3H, s, H17); 3.60, 3.53 (3H, m, H7, H18); 3.16 (1H, d, J = 9.0 Hz, H5); 3.05 (1H, m, H10); 2.91, 2.88 (2H, m, H10, H4); 2.63 (1H, qd, J = 12.2, 4.3 Hz, H3); 2.21 (1H, t, J = 10.7 Hz, H5); 2.07, 2.00, 1.86 (3H, m, H4, H8); 1.86, 1.82, 1.78 (3H, m, H9, H3, H9); 1.24 (9H, s, H27, H28, H29) ppm

^{13}C NMR (Acetone–d_6, 100 MHz): δ 176.4 (C6); 151.2 (C14); 150.8 (C25); 149.4 (C11); 139.9 (C19); 129.8 (C12, C16); 129.7 (C20, C24); 129.2 (C21, C23); 128.0 (C22); 125.1 (C13, C15); 85.6 (C26); 63.2 (C18); 62.8 (C7); 59.7 (C2); 57.1 (C1); 53.7 (C4); 52.8 (C5); 52.2 (C17); 46.6 (C10); 31.1 (C8); 31.0 (C3); 28.1 (C27, C28, C29); 25.7 (C9) ppm

Melting point = 61–63 °C

IR: 3026-2953-2820 (C-H stretch); 1737 (C=O stretch); 1531 (-NO2 aromatic); 1347 (-NO2 aromatic) cm^{-1}

(S)-methyl 1-((3R,4R)-1-benzyl-4-((tert-butoxycarbonyl)amino)piperidin-3-yl)pyrrolidine-2-carboxylate (**3.20**)

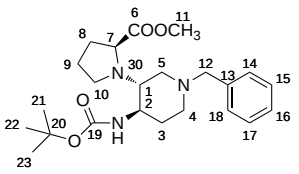

To a stirred solution of compound **3.19** (644 mg, 1.07 mmol, 1.0 eq.) in CH_3CN (15 mL) and 2 % of DMSO (0.3 mL) under nitrogen was added potassium carbonate (444 mg, 3.21 mmol, 3.0 eq.), followed by thiophenol (165 µL, 1.61 mmol, 1.5 eq.). The reaction was stirred at 70° C overnight. CH_3CN was removed under vacuum and the crude was dissolved in EtOAc, washed with saturated $NaHCO_3$, dried over Na_2SO_4 filtered and concentrated under vacuum. The resulting residue was purified by column chromatography on a silica gel using c-Hex/EtOAc 6:4 as eluent to yield compound **3.20** as a pale yellow oil (348 mg, 0.83 mmol, Yield 78 %).

Molecular weight = 417.54 g mol^{-1}

$R_f = 0.50$ (Cyclo/EtOAc 6:4)

HRMS: Calcd. for $[C_{23}H_{35}N_3O_4 + H]^+$: M/z 418.2706, found: 418.2712

^{1}H NMR (Acetone–d_6, 400 MHz): δ 7.45, 7.31, 7.24 (5H, m, H14, H15, H16, H17, H18); 5.98 (1H, bp, NH); 3.69 (3H, s, H11); 3.59, 3.56, 3.50 (3H, m, H12, H7, H12); 3.28 (1H, m, H2); 2.96, 2.94, 2.76, 2.75, 2.71 (5H, m, H4, H10, H10, H4, H1); 2.23 (2H, m, H3); 2.08, 1.97, 1.86, 1.71 (6H, m, H5, H8, H9); 1.40 (9H, s, H21, H22, H23) ppm

^{13}C NMR (Acetone–d_6, 100 MHz): δ 176.1 (C6); 155.8 (C19); 139.3 (C13); 129.5, 128.8, 127.6 (C14, C15, C16, C17, C18); 78.3 (C20); 63.2 (C12); 61.8 (C7); 59.5 (C1); 52.4 (C5); 52.2 (C4); 51.9 (C11); 51.8 (C2); 46.2 (C10); 32.4 (C3); 29.9 (C8); 28.4 (C21, C22, C23); 24.9 (C9) ppm

IR: 2927 (C-H stretch); 1737-1708 (C=O stretch); 1495-1453 (C=C stretch); 1241-1170 (C-C(O)-C stretch) cm^{-1}

(S)-methyl 1-((3R,4R)-4-((tert-butoxycarbonyl)amino)piperidin-3-yl)pyrrolidine-2-carboxylate (**3.22**)

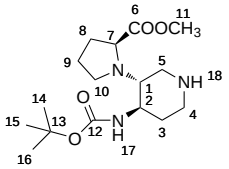

Compound **3.20** (330 mg, 0.79 mmol, 1.0 eq.) was dissolved in 8 mL of absolute ethanol. A gentle stream of nitrogen was passed through the

reaction mixture and agitation was starting. At this moment, an equal weight (330 mg) of Pearlman's catalyst (20 % $Pd(OH)_2/C$) was added followed by the addition of cyclohexene (8 mL) in order to obtain a ratio 1:1 between the two solvents. The reaction was let under stirring overnight at 70°C. The mixture then was filtered on a pad of Celite, washed several times with MeOH and concentrated under vacuum to obtain **3.22** in quantitative yield.

Molecular weight = 327.42 g mol^{-1}

$R_f = 0$ (Cyclo/EtOAc 6:4)

HRMS: Calcd. for $[C_{16}H_{29}N_3O_4 + H]^+$: M/z 328.2236, found: 328.2234

^{1}H NMR (Acetone–d_6, 400 MHz): δ 6.03 (1H, bp, NH17); 3.68 (3H, s, H11); 3.67 (1H, m, H7); 3.37 (1H, m, H2); 3.10 (1H, t, J = 9.0 Hz, H5); 2.95 (3H, m, H4, H10, NH18); 2.76, 2.64, 2.64, 2.56 (4H, m, H10, H1, H5, H4); 2.28 (1H, dt, J = 17.1, 8.6 Hz, H3); 2.09, 1.87, 1.72 (4H, m, H8, H9); 1.42 (9H, s, H14, H15, H16); 1.30 (1H, m, H3) ppm

^{13}C NMR (Acetone–d_6, 100 MHz): δ 176.2 (C6); 156.4 (C12); 78.5 (C13); 61.9 (C7); 60.1 (C1); 52.0 (C2); 46.1 (C10); 45.1 (C4); 44.6 (C5); 33.8 (C3); 31.9 (C11); 30.1 (C8); 28.5 (C14, C15, C16); 25.0 (C9) ppm

IR: 3342 (N-H stretch); 2975 (C-H stretch); 1702 (C=O stretch); 1504 (N-H bend); 1240-1165 (C-C(O)-C stretch) cm^{-1}

(S)-methyl 1-((3R,4R)-1-((S)-2-((((9H-fluoren-9-yl)methoxy)carbonyl)amino)-3-methylbutanoyl)-4-((tert-butoxycarbonyl)amino)piperidin-3-yl)pyrrolidine-2-carboxylate (**3.23**)

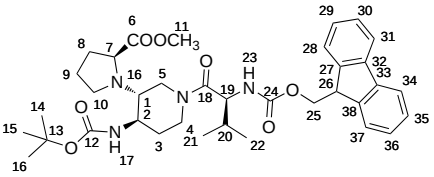

The Boc-NH-Val-OH (543 mg, 1.6 mmol, 2.0 eq.) was dissolved in DMF (5.0 mL) under a nitrogen atmosphere and the solution was cooled at 0° C. Then HOAt (218 mg, 1.6 mmol, 2.0 eq.) and HATU (608 mg, 1.6 mmol, 2.0 eq.) were successively added. The solution was stirred at 0°C for 30 min to 1h and at this moment a solution of **3.22** (264 mg, 0.8 mmol, 1.0 eq.) and collidine (0.64 mL, 4.8 mmol, 6.0 eq.) in DMF (4.0 mL) was added. The crude obtained was purified by column chromatography on a silica gel using c-Hex/EtOAc 6:4 as eluent to afford compound **3.23** as a white solid (296 mg, 0.46 mmol, Yield 58 %).

Molecular weight = 648.79 g mol^{-1}

$R_f = 0.40$ (Cyclo/EtOAc 6:4)

HRMS: Calcd. for $[C_{36}H_{48}N_4O_7 + H]^+$: M/z 649.3601, found: 649.3597

^{1}H NMR (DMSO – d_6, 400 MHz): δ 7.88 (2H, m, H31, H34); 7.74 (2H, m, H28, H37); 7.51 (1H, bp, NH23); 7.41 (2H, m, H30, H35); 7.32 (2H, m, H29, H36); 6.45 (1H, bp, NH17); 4.31 (1H, m, H5); 4.25 (2H, m, H25); 4.23 (1H, m, H19); 4.21 (1H, m, H26); 4.07 (1H, m, H4); 3.64 (1H, m, H7); 3.81 (1H, m, H2); 3.61 (3H, s, H11); 3.07 (1H, m, H4); 2.96 (1H, m, H10); 2.78 (1H, m, H10); 2.57 (1H, m, H5); 2.47 (1H, m, H1); 2.04 (2H, m, H3); 1.98 (1H, m, H20); 1.78 (2H, m, H8); 1.65 (2H, m, H9); 1.38 (9H, s, H14, H15, H16); 0.88, 0.83 (6H, m, H21, H22) ppm

^{13}C NMR (DMSO – d_6, 100 MHz): δ 175.1 (C6); 169.9 (C18); 156.1 (C24); 155.2 (C12); 143.8 (C27, C38); 140.7 (C32, C33); 127.6 (C30, C35); 127.0 (C29, C36); 125.3 (C28, C37); 120.0 (C31, C34); 77.5 (C13); 65.7 (C25); 60.1 (C7); 59.7 (C2); 59.3 (C1); 55.4 (C19); 51.5 (C11); 46.7 (C26); 47.1 (C10); 44.2 (C4); 39.9 (C5); 31.1 (C3); 29.8 (C20); 29.1 (C8); 28.2 (C14, C15, C16); 23.7 (C9); 19.5, 18.1 (C21, C22) ppm

Melting point = 104–106 °C

IR: 3324 (N-H stretch); 2967 (C-H stretch); 1707-1632 (C=O stretch); 1506 (N-H bend); 1219-1166 (C-C(O)-C stretch) cm^{-1}

(S)-methyl 1-((3R,4R)-1-((S)-2-((S)-2-(((benzyloxy)carbonyl)amino)propanamido)-3-methylbutanoyl)-4-((tert-butoxycarbonyl)amino)piperidin-3-yl)pyrrolidine-2-carboxylate (**3.24**)

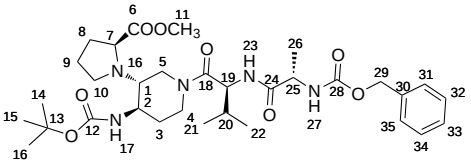

The N-protected compound **3.23** (253 mg, 0.39 mmol, 1.0 eq.) was dissolved in a 20 % solution of piperidine in DMF (10 mL) and the reaction mixture was let stirring at room temperature for 2 h. The solvent was evaporated under vacuum to give the Fmoc deprotected amine that was used for the next coupling reaction without any further purification.

The CbZ-NH-Ala-OH (174 mg, 0.78 mmol, 2.0 eq.) was dissolved in DMF (5.0 mL) under a nitrogen atmosphere and the solution was cooled at 0° C. Then, HOAt (106 mg, 0.78 mmol, 2.0 eq.) and HATU (297 mg, 0.78 mmol, 2.0 eq.) were added. The solution was stirred at 0°C for 30 min to 1h and at this moment, a solution of the previous Fmoc deprotected compound **3.23** and collidine (0.31 mL, 2.34 mmol, 6.0 eq.) in DMF (4.0 mL) were added. After stirring overnight at room temperature, the solvent was evaporated under vacuum. The resulting residue was taken up with EtOAc and successively washed with water, saturated $NaHCO_3$, brine, dried over Na_2SO_4, filtered and concentrated under vacuum. The crude obtained was purified by column chromatography on a silica gel using c-Hex/EtOAc

4:6 as eluent to afford compound **3.24** as a white solid (170 mg, 0.27 mmol, Yield 69 %).

Molecular weight = 631.76 g mol^{-1}

R_f = 0.50 (Cyclo/EtOAc 4:6)

HRMS: Calcd. for $[C_{32}H_{49}N_5O_8 + H]^+$: M/z 632.3659, found: 632.3663

^{1}H NMR (DMSO – d_6, 400 MHz): δ 7.82 (1H, bp, NH23); 7.42 (1H, bp, NH27); 7.34, 7.32, 7.30 (5H, m, H31, H32, H33, H34, H35); 6.49 (1H, bp, NH17); 5.01 (2H, s, H29); 4.54 (1H, m, H19); 4.28 (1H, m, H5); 4.09 (1H, m, H25); 3.83 (1H, m, H4); 3.82 (1H, m, H1); 3.65 (1H, m, H7); 3.60 (3H, s, H11); 3.11 (1H, m, H4); 2.95 (1H, m, H10); 2.78 (1H, m, H10); 2.57 (1H, m, H5); 2.45 (1H, m, H2); 2.01 (2H, m, H3, H8); 1.93 (1H, m, H20); 1.80 (1H, m, H8); 1.67 (2H, m, H9); 1.38 (9H, s, H14, H15, H16); 1.29 (1H, m, H3); 1.18 (3H, s, H26); 0.82, 0.81 (6H, m, H21, H22) ppm

^{13}C NMR (DMSO – d_6, 100 MHz): δ 175.5 (C6); 172.2 (C24); 169.3 (C18); 156.7 (C12); 155.5 (C28); 137.0 (C30); 128.3, 128.0, 127.8 (C31, C32, C33, C34, C35); 77.7 (C13); 65.4 (C29); 60.2 (C7); 59.9 (C1); 59.0 (C2); 53.0 (C19); 51.5 (C11); 50.1 (C25); 46.8 (C10); 42.7 (C4); 39.9 (C6); 30.8 (C3); 30.3 (C20); 29.1 (C8); 28.2 (C14, C15, C16); 23.5 (C9); 18.1, 17.7 (C21, C22); 18.0 (C26) ppm

Melting point = 97–99 °C

IR: 3306 (N-H stretch); 2970 (C-H stretch); 1708-1624 (C=O stretch); 1504-1453 (N-H bend); 1221-1167 (C-C(O)-C stretch) cm^{-1}

(S)-1-((3R,4R)-1-((S)-2-((S)-2-(((benzyloxy)carbonyl)amino)propanamido)-3-methylbutanoyl)-4-((tert-butoxycarbonyl)amino)piperidin-3-yl)pyrrolidine-2--carboxylic acid (**3.25**)

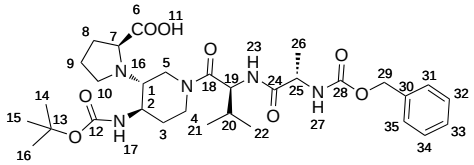

Compound **3.24** (150 mg, 0.24 mmol, 1.0 eq.) was dissolved in MeOH (8.0 mL) and NaOH 2 M (0.6 mL, 1.2 mmol, 5.0 eq.) was added dropwise to the solution. The reaction was stirred at 60° C for 2 h. The solvent was evaporated and the solid obtained was solubilized in water. The mixture was acidified with 10 % solution of $KHSO_4$ until pH = 2-3. A part of the product was extracted from the water phase with EtOAc and an another part of the desired compound was recuperated by solving an solid residue of the water phase with MeOH. The two combined organic phases were dried over Na_2SO_4 and concentrated under vacuum to yield compound **3.25** as a white solid (137 mg, 0.22 mmol, Yield 92 %).

Molecular weight = 617.73 g mol^{-1}

$R_f = 0$ (Cyclo/EtOAc 4:6)

HRMS: Calcd. for $[C_{31}H_{47}N_5O_8 + H]^+$: M/z 618.3503, found: 618.3514; Calcd. for $[C_{31}H_{47}N_5O_8 + Na]^+$: M/z 640.3322, found: 640.3322

^{1}H NMR (DMSO – d_6, 400 MHz): δ 8.31 (1H, bp, OH11); 7.87 (1H, bp, NH23); 7.44 (1H, bp, NH27); 7.35, 7.31, 7.22 (5H, m, H31, H32, H33, H34, H35); 6.80 (1H, bp, NH17); 5.02 (2H, s, H29); 4.55 (1H, m, H19); 4.28 (1H, m, H5); 4.09 (1H, m, H25); 3.84 (1H, m, H4); 3.81 (1H, m, H1); 3.57 (1H, m, H7); 3.13 (1H, m, H4); 3.04 (1H, m, H10); 2.82 (1H, m, H10); 2.56 (1H, m, H5); 2.49 (1H, m, H2); 2.06 (1H, m, H8); 1.91 (1H, m, H20); 1.83 (1H, m, H8); 1.71 (1H, m, H3); 1.62 (1H, m, H3); 1.38 (9H, s, H14, H15, H16); 1.24 (2H, m, H9); 1.18 (3H, s, H26); 0.82, 0.76 (6H, m, H21, H22) ppm

^{13}C NMR (DMSO – d_6, 100 MHz): δ 178.7 (C6); 172.1 (C24); 169.4 (C18); 156.5 (C12); 155.5 (C28); 136.9 (C30); 127.8, 127.4, 126.4 (C31, C32, C33, C34, C35); 77.7 (C13); 65.0 (C29); 61.4 (C7); 61.0 (C1); 59.6 (C2); 52.7 (C19); 49.6 (C25); 46.9 (C10); 42.8 (C4); 39.8 (C6); 29.8 (C20); 29.6 (C8); 27.9 (C14, C15, C16); 28.6 (C9); 23.8 (C3); 19.2, 17.4 (C21, C22); 17.9 (C26) ppm

Melting point = 129–131 °C

IR: 3310 (N-H stretch; O-H stretch); 2967 (C-H stretch); 1702-1627 (C=O stretch); 1547-1453 (N-H bend; O-H bend); 1225-1160 (C-C(O)-C stretch) cm^{-1}

Compound (**3.26**)

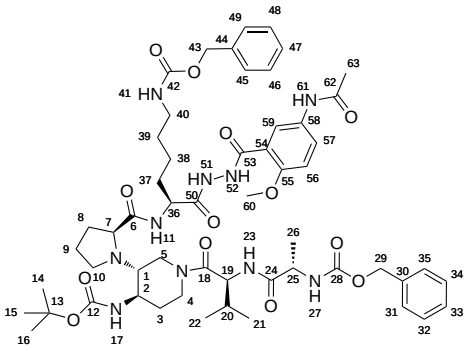

Compound **3.6** (132 mg, 0.22 mmol, 1.2 eq.) was dissolved in DMF (5.0 mL) under a nitrogen atmosphere then NMM (80 µL, 0.72 mmol, 4.0 eq.) was added. During this time, compound **3.25** (108 mg, 0.18 mmol, 1.0 eq.) was dissolved in DMF (5.0 mL) under a nitrogen atmosphere and cooled at 0° C. DMTMM (55 mg, 0.20 mmol, 1.1 eq.) was then added at 0°C. To this mixture the previous solution of compound **3.6** was added dropwise. After stirring overnight at room temperature, the solvent was evaporated under

vacuum. The resulting residue was taken up with EtOAc and successively washed with water, saturated $NaHCO_3$, brine, dried over Na_2SO_4, filtered and concentrated under vacuum. The crude residue obtained was purified by column chromatography on a silica gel using EtOAc 100 % to EtOAc/MeOH 95:5 then 90:10 as eluent to afford compound **3.26** as a white solid (114 mg, 0.11 mmol, Yield 61 %).

Molecular weight = 1085.25 g mol^{-1}

$R_f = 0.50$ (EtOAc/MeOH 9:1)

HRMS: Calcd. for $[C_{55}H_{76}N_{10}O_{13}+H]^+$: M/z 1085.5672, found: 1085.5688

^{1}H NMR (DMSO – d_6, 400 MHz): δ 10.64 (1H, bp, NH52); 10.03 (1H, bp, NH51); 9.96 (1H, s, NH61); 8.01 (1H, s, H59); 7.77 (1H, m, H57); 7.77 (1H, bp, NH23); 7.67 (1H, bp, NH11); 7.41 (1H, bp, NH27); 7.21 (1H, bp, NH41); 7.30-7.34 (10H, m, H31, H32, H33, H34, H35, H45, H46, H47, H48, H49); 7.11 (1H, m, H56); 6.84 (1H, bp, NH17); 5.00 (4H, s, H29, H43); 4.55 (1H, m, H36); 4.51 (1H, m, H19); 4.10 (1H, m, H25); 3.84 (3H, s, H60); 3.78 (1H, m, H7); 3.63 (1H, m, H2); 3.31 (1H, m, H1); 2.99 (2H, m, H40); 2.07, 1.70 (2H, m, H37); 1.44, 1.22 (2H, m, H39); 1.33 (2H, m, H38); 2.02 (3H, s, H63); 4.43, 2.63 (2H, m, H5); 3.97, 3.09 (2H, m, H4); 1.82, 1.66 (2H, m, H3); 4.38, 2.59 (2H, m, H10); 1.95, 1.35 (2H, m, H8); 1.69, 1.53 (2H, m, H9); 1.86 (1H, m, H20); 1.37 (9H, s, H14, H15, H16); 1.14 (3H, s, H26); 0.75, 0.66 (6H, m, H21, H22) ppm

^{13}C NMR (DMSO – d_6, 100 MHz): δ 172.4 (C6); 172.2 (C24); 171.9 (C18); 169.4 (C50); 162.5 (C53); 156.2 (C42); 155.7 (C28); 155.3 (C12); 152.9 (C55); 137.3 (C44); 137.1 (C30); 132.8 (C58); 128.4, 127.7, 127.3 (C31, C32, C33, C34, C35, C45, C46, C47, C48, C49); 123.9 (C57); 121.6 (C59); 120.4 (C54); 112.6 (C56); 78.4 (C13); 65.4 (C29, C43); 62.4 (C1); 61.2 (C2); 55.8 (C60); 53.2 (C19); 52.8 (C19); 50.1 (C7); 49.3 (C36); 49.6 (C25); 43.7 (C4); 40.3 (C10); 39.9 (C40); 39.1 (C5); 32.6 (C8); 32.0 (C3); 30.0 (C37); 29.7 (C20); 28.7 (C39); 23.4 (C63); 27.7 (C14, C15, C16); 24.3 (C9); 22.7 (C38); 19.1, 17.1 (C21, C22); 17.8 (C26) ppm

Melting point = 130–132 °C

IR: 3297 (N-H stretch); 2935-2870 (C-H stretch); 1658-1625 (C=O stretch); 1520-1455 (N-H bend); 1245 (C-O-C stretch) cm^{-1}

HPLC purity (XBridge C18, 3.5 µm, H_2O + 0.1 % form. ac./ACN, gradient 5–100 % in 20 min): t_R = 16.38 min, 94 %

(S)-6-(2-(5-acetamido-2-methoxybenzoyl)hydrazinyl)-5-((S)-1-((3R,4R)-1-((S)-
-2-((S)-2-((tert-butoxycarbonyl)amino)propanamido)-3-methylbutanoyl)-4-(4-methyl-
phenylsulfonamido)piperidin-3-yl)pyrrolidine-2-carboxamido)-6-oxohexan-1-aminium
acetate (**3.27**)

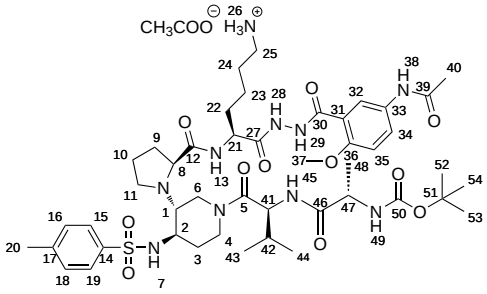

Compound **3.10** (64.0 mg, 0.058 mmol, 1.0 eq.) was dissolved in MeOH (4.0 mL) and 10 % Pd/C (13 mg) was added. The reaction was kept 2 hours under stirring in hydrogen atmosphere at room temperature. The catalyst was then removed over a celite pad and the solvent evaporated under vacuum. The crude was diluted in a minimum amount of MeOH and 1.0 eq. of acetic acid were added. Product **3.27** was isolated as acetate salt by precipitation in diethyl ether. The crude product was purified by crystallography in MeOH and diethyl ether to afford the pure compound **3.27** as a white powder (52.0 mg, 0.050 mmol, Yield 87 %).

Molecular weight = 1031.23 g mol^{-1}

$R_f = 0$ (EtOAc/MeOH 95:5)

HRMS: Calcd. for $[C_{46}H_{70}N_{10}O_{11}S+H]^+$: M/z 971.5025, found: 971.5021; Calcd. for $[C_{46}H_{70}N_{10}O_{11}S+Na]^+$: M/z 993.4844, found: 993.4814

^{1}H NMR (DMSO – d_6, 400 MHz): δ nd NH28; ns NH29; nd (3H, bp, NH26); 10.00 (1H, s, NH38); 8.27 (1H, bp, NH13); 8.18 (1H, bp, NH7); 7.65 (1H, bp, NH45); 6.95 (1H, bp, NH49); 8.05 (1H, s, H32); 7.74 (3H, m, H15, H19, H34); 7.35 (2H, m, H16, H18); 7.11 (1H, m, H35); 4.48 (1H, m, H21); 4.46 (1H, m, H41); 4.33 (1H, m, H6); 3.82 (1H, m, H4); 3.94 (1H, m, H47); 3.85 (3H, s, H37); 3.30 (1H, m, H2); 3.34 (1H, m, H8); 2.95 (1H, m, H4); 2.74 (2H, m, H25); 2.64 (1H, m, H6); 2.36 (3H, s, H20); 2.23 (1H, m, H1); 2.04 (1H, m, H11); 2.02 (3H, s, H40); 1.83 (1H, m, H42); 1.80 (1H, m, H9); 1.78 (1H, m, H3); 1.75 (2H, m, H22); 1.65 (1H, m, H11); 1.60 (1H, m, H10); 1.56 (2H, m, H24); 1.43 (1H, m, H10); 1.38 (2H, m, H23); 1.35 (9H, m, H52, H53, H54); 1.27 (1H, m, H3); 1.10 (3H, s, H48); 1.07 (1H, m, H9); 0.80-0.70 (6H, m, H43, H44) ppm

^{13}C NMR (DMSO – d_6, 400 MHz): δ 174.2 (C12); 173.0 (C5); 172.5 (C46); 169.2 (C27); 168.0 (C39); 162.3 (C30); 155.1 (C50); 152.8 (C36); 142.6 (C17); 138.9 (C14); 132.7 (C33); 129.6 (C16, C18); 126.5 (C15, C19); 123.6 (C34); 121.6 (C32); 120.7 (C31); 112.4 (C35); 78.1 (C51); 62.9 (C8); 58.5 (C1); 56.2

(C37); 53.2 (C2); 52.8 (C41); 50.5 (C21); 49.8 (C47); 43.4 (C4); 39.3 (C6); 38.9 (C25); 33.1 (C3); 31.8 (C9); 31.6 (C22); 30.3 (C11); 30.3 (C42); 28.2 (C52, C53, C54); 27.4 (C24); 24.2 (C10); 23.8 (C40); 22.4 (C23); 20.9 (C20); 19.4, 17.7 (C43, C44); 17.9 (C48) ppm

HPLC purity (SUNFIRE C18, 3.5 µm, H_2O + 0.2 % form. ac./ACN, gradient 5–100 % in 20 min): t_R = 11.12 min, 82 %

Compound (**3.5**)

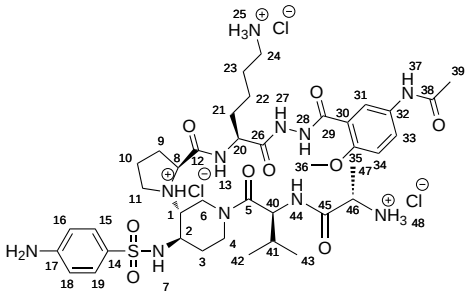

Compound **3.18** (25.0 mg, 0.022 mmol, 1.0 eq.) was dissolved in MeOH (4.0 mL) and 10 % Pd/C (5.0 mg) was added. The reaction was kept 2 hours under stirring in hydrogen atmosphere at room temperature. The catalyst was then removed over a celite pad and the solvent evaporated under vacuum. Successively, the resulting product was dissolved in dioxane (2.0 mL) and a 4 N solution of HCl in dioxane (0.17 mL, 30.0 eq.) was added. The reaction was kept 2 hours under stirring at room temperature. After this time, product **3.5** was isolated as hydrochloride salt by precipitation in diethyl ether. The crude was purified by crystallization in MeOH and diethyl ether to afford the pure compound **3.18** as a light yellow powder (13.0 mg, 0.013 mmol, Yield 60 %).

Molecular weight = 981.43 g mol^{-1}

R_f = 0 (EtOAc/MeOH 95:5)

HRMS: Calcd. for $[C_{40}H_{62}N_{11}O_9S + H]^+$: M/z 872.4453, found: 872.4440

^{1}H NMR (DMSO – d_6, 400 MHz): δ 10.50 (1H, bp, NH28); 10.20 (1H, bp, NH37); 9.96 (1H, s, NH27); 9.22 (1H, bp, NH13); 8.69 (1H, bp, NH44); 8.30 (3H, bp, NH48); 8.22 (3H, bp, NH25); 8.02 (1H, bp, NH7); 8.00 (1H, s, H31); 7.75 (1H, m, H33); 7.61 (2H, m, H15, H19); 7.10 (1H, m, H34); 6.86 (2H, m, H16, H18); 4.59 (1H, m, H8); 4.48 (1H, m, H20); 4.46 (1H, m, H40); 4.44 (1H, m, H6); 4.19 (2H, m, NH2); 3.97 (1H, m, H46); 3.86 (1H, m, H4); 3.84 (3H, s, H36); 3.66 (1H, m, H2); 3.15 (1H, m, H6); 3.12 (1H, m, H1); 3.09 (1H, m, H4); 2.79 (2H, m, H24); 2.06 (1H, m, H11); 2.02 (3H, s, H39); 1.89 (1H, m, H41); 1.20 (1H, m, H11); 1.79 (2H, m, H21); 2.49 (1H, m, H9); 1.37 (1H, m, H3); 2.10 (1H, m, H9); 2.05 (1H, m, H10); 1.63 (2H, m, H23); 1.80 (1H,

m, H10); 1.47 (2H, m, H22); 1.28 (1H, m, H3); 1.30 (3H, s, H47); 0.87-0.82 (6H, m, H42, H43) ppm

^{13}C NMR (DMSO – d_6, 100 MHz): δ 169.9 (C12); 169.5 (C5); 169.6 (C45); 169.4 (C26); 168.3 (C38); 163.6 (C30); 152.8 (C35); 149.9 (C17); 132.7 (C32); 128.6 (C15, C19); 128.2 (C14); 123.6 (C33); 121.4 (C31); 120.9 (C30); 115.1 (C16, C18); 112.4 (C34); 64.8 (C8); 61.5 (C1); 56.3 (C36); 53.8 (C40); 51.9 (C20); 50.5 (C2); 47.5 (C46); 42.6 (C4); 38.3 (C6); 38.1 (C24); 31.0 (C21); 29.7 (C9); 29.6 (C3); 29.4 (C41); 29.3 (C11); 26.1 (C23); 23.8 (C39); 23.0 (C10); 22.0 (C22); 19.5, 18.1 (C42, C43); 17.3 (C47) ppm

Melting point = 233–235 °C

IR: 3220 (N-H stretch); 2970 (C-H stretch); 1636 (C=O stretch); 1546-1494 (N-H bend); 1304-1254 (aryl and alkyl C-N stretch) cm^{-1}

HPLC purity (SUNFIRE C18, 3.5 µm, H_2O + 0.1 % form. ac./ACN, gradient 5–100 % in 20 min): t_R = 17.31 min, 97 %

(3R,4R)-(9H-fluoren-9-yl)methyl 3-((S)-2-(methoxycarbonyl)pyrrolidin-1-yl)--4-(4-nitrophenylsulfonamido)piperidine-1-carboxylate (**3.14**)

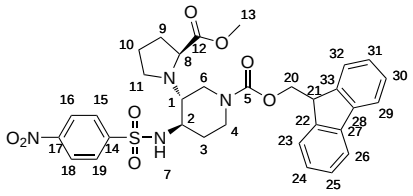

To a solution of compound **3.11** in anhydrous THF cooled to 0° C and under inert atmosphere was added fluorenylmethyl chloroformate (970 mg, 3.75 mmol, 5.0 eq.). The resulting mixture was allowed to warm to room temperature and was stirred for one day. Then, an aqueous solution of $NaHCO_3$ was added and product 1 was extracted with diethyl ether. The organic layer was dried over $MgSO_4$, filtered and concentrated under vacuum. The resulting oil was then purified by chromatography on silica gel using Cyclo/EtOAc 7:3 as eluent to afford product **3.14** as a pale yellow solid (273 mg, 0.43 mmol, Yield 57 %).

Molecular weight = 634.70 g mol^{-1}

R_f = 0.20 (Cyclo/AcOEt 7:3)

HRMS: Calcd. for $[C_{32}H_{34}N_4O_8S + H]^+$: M/z 635.2176, found: 635.2170; Calcd. for $[C_{32}H_{34}N_4O_8S + Na]^+$: M/z 657.1995, found: 657.1987

^{1}H NMR (DMSO – d_6, 400 MHz): δ 8.40 (2H, d, J = 8.0 Hz, H15, H19); 8.08 (2H, d, J = 8.0 Hz, H16, H18); 7.86 (2H, d, J = 7.3 Hz, H26, H29); 7.60 (3H, m, H23, H32, NH7); 7.40 (2H, t, J = 7.3 Hz, H25, H30); 7.31 (2H, m, H24, H31); 4.41, 4.25 (3H, m, H20, H21); 3.69 (3H, s, , H13); 3.60, 3.53 (3H, m, H4, H6, H1); 3.07, 2.86 (3H, m, H8, H4, H6); 2.35, 2.32, 1.97, 1.93, 1.91,

1.90, 1.74 (7H, m, H11, H2, H3, H3, H9, H11, H9); 1.49, 1.29 (2H, m, H10) ppm

^{13}C NMR (DMSO – d_6, 100 MHz): δ 175.6 (C12); 154.1 (C5); 149.6 (C14); 146.1 (C17); 143.8 (C27, C28); 140.8 (C22, C33); 128.3 (C16, C18); 127.5 (C25, C30); 127.0 (C24, C31); 124.8 (C23, C32); 124.5 (C15, C19); 120.0 (C26, C29); 66.4 (C20); 61.4 (C1); 58.3 (C2); 52.4 (C8); 52.0 (C13); 46.7 (C21); 45.5 (C11); 41.4 (C4); 40.9 (C6); 31.6 (C3); 29.3 (C9); 23.9 (C11) ppm

Melting point = 108–110 °C

IR: 3161 (N-H stretch); 2953-2868 (C-H stretch); 1697 (C=O stretch); 1528 (-NO2 aromatic); 1476-1435 (N-H bend); 1348 (-NO2 aromatic) cm^{-1}

(S)-1-((3R,4R)-1-(((9H-fluoren-9-yl)methoxy)carbonyl)-4-(4-nitrophenylsulfonamido)piperidin-3-yl)pyrrolidine-2-carboxylic acid (**3.15**)

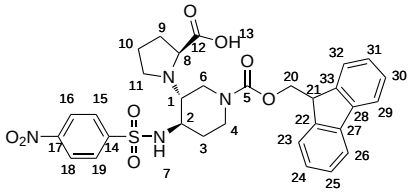

Compound **3.14** (237 mg, 0.37 mmol, 1.0 eq.) was dissolved in dioxane (10.0 mL) and 6 M HCl solution (5.0 mL) was added. The reaction mixture was heated at 110° C under stirring. After 4 h, the solvent was removed, and after adding acetone to the oily residue compound **3.15** precipitated in the form of a white solid (260 mg, 0.37 mmol, Yield 100 %).

Molecular weight = 620.67 g mol^{-1}

$R_f = 0$ (Cyclo/AcOEt 7:3)

HRMS: Calcd. for $[C_{31}H_{32}N_4O_8S + H]^+$: M/z 621.2019, found: 621.2012; Calcd. for $[C_{31}H_{32}N_4O_8S + Na]^+$: M/z 643.1839, found: 643.1825

^{1}H NMR (DMSO – d_6, 400 MHz): δ 8.69 (1H, bp, NH7); 8.46 (2H, d, J = 8.1 Hz, H15, H19); 8.13 (2H, d, J = 8.1 Hz, H16, H18); 7.88 (2H, dd, J = 8.3 Hz, H26, H29); 7.59 (2H, d, J = 6.7 Hz, H23, H32); 7.41 (2H, m, H25, H30); 7.32 (2H, m, H24, H31); 4.37, 4.27 (3H, m, H20, H21); 3.84 (1H, bp, , OH); 3.74 (1H, m, H8); 3.71 (2H, m, H11); 3.68 (2H, m, H6); 3.47 (2H, m, H4); 3.17 (1H, m, H2); 2.51 (1H, m, H1); 2.32 (2H, m, H9); 2.08 (2H, m, H3); 1.81 (2H, m, H10) ppm

^{13}C NMR (DMSO – d_6, 100 MHz): δ 154.1 (C5); 145.2 (C12); 149.8 (C14); 146.2 (C17); 143.7 (C27, C28); 140.7 (C22, C33); 128.2 (C16, C18); 127.7 (C25, C30); 127.1 (C24, C31); 124.9 (C23, C32); 124.8 (C15, C19); 120.1 (C26, C29); 72.2 (C4); 70.1 (C6); 66.9 (C20); 52.2 (C8); 48.6 (C2); 46.6 (C21); 43.6 (C11); 34.1 (C1); 28.6 (C3); 28.3 (C9); 22.9 (C11) ppm

Melting point = 151–153 °C

IR: 2954, 2867 (O-H stretch, C-H stretch); 1692 (C=O stretch); 1528 (-NO2 aromatic); 1477-1401 (N-H bend, O-H bend); 1347 (-NO2 aromatic); 1235 (C-O stretch) cm^{-1}

(3R,4R)-(9H-fluoren-9-yl)methyl 3-((S)-2-(((S)-1-(2-(5-acetamido-2-methoxybenzoyl)hydrazinyl)-6-(((benzyloxy)carbonyl)amino)-1-oxohexan-2-yl)carbamoyl)-pyrrolidin-1-yl)-4-(4-nitrophenylsulfonamido)piperidine-1-carboxylate (**3.16**)

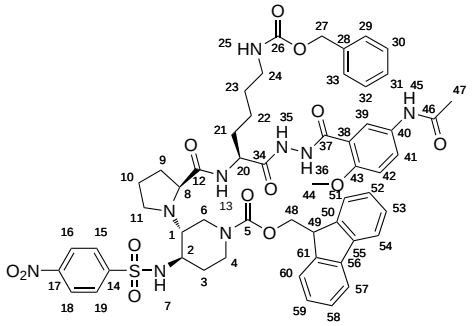

Compound **3.6** (246 mg, 0.41 mmol, 1.2 eq.) was dissolved in DMF (5.0 mL) under a nitrogen atmosphere and collidine (0.27 mL, 2.04 mmol, 6.0 eq) was added. This solution was let aside. At this moment, compound **3.15** (235 mg, 0.34 mmol, 1.0 eq.) was dissolved in DMF (10.0 mL) under a nitrogen atmosphere and the solution was cooled at 0°C. HATU (142 mg, 0.37 mmol, 1.1 eq.) and HOAt (51 mg, 0.37 mmol, 1.1 eq.) were then added. The reaction was let stirring at 0°C for 1 h. Finally, the previous solution of compound **3.6** was added dropwise. After stirring over the weekend at room temperature, the solvent was evaporated under vacuum. The resulting residue was taken up with EtOAc and successively washed with water, saturated $NaHCO_3$, brine, dried over Na_2SO_4, filtered and concentrated under vacuum. The crude residue obtained was purified by column chromatography on silica gel using EtOAc 100 % to EtOAc/MeOH 95:5 as eluent to afford compound **3.16** as a pale yellow solid (239 mg, 0.22 mmol, Yield 65 %).

Molecular weight = 1088.19 g mol^{-1}

R_f = 0.50 (EtOAc/MeOH 95:5)

HRMS: Calcd. for $[C_{55}H_{61}N_9O_{13}S+H]^+$: M/z 1088.4188, found: 1088.4180; Calcd. for $[C_{55}H_{61}N_9O_{13}S + Na]^+$: M/z 1110.4007, found: 1110.4021

^{1}H NMR (DMSO – d_6, 400 MHz): δ 10.56 (1H, bp, NH35); 10.08 (1H, bp, NH36); 9.95 (1H, s, NH45); 8.36 (2H, d, J = 8.8 Hz, H15, H19); 8.26 (1H, bp, NH13); 8.09 (2H, d, J = 8.8 Hz, H16, H18); 8.01 (1H, s, H39); 7.88 (2H, m, H54, H57); 7.83 (2H, m, H51, H60); 7.73 (1H, m, H41); 7.42 (2H, m, H53, H58); 7.36-7.34 (5H, m, H29, H30, H31, H32, H33); 7.34 (2H, m, H52, H59); 7.24 (1H, bp, NH25); 7.13 (1H, m, H42); 6.28 (1H, bp, NH7); 5.00 (2H, s,

H27); 4.54 (1H, m, H20); 4.35 (2H, m, H48); 4.21 (1H, m, H49); 3.85 (3H, s, H44); 3.38 (1H, m, H8); 3.20 (1H, m, H2); 3.01 (2H, m, H24); 2.94 (1H, m, H6); 2.70 (1H, m, H4); 2.46 (1H, m, H6); 2.37 (1H, m, H1); 2.33 (1H, m, H4); 2.02 (3H, s, H47); 2.00 (1H, m, H11); 1.85 (1H, m, H9); 1.83-1.74 (2H, m, H21); 1.76 (1H, m, H9); 1.67 (1H, m, H11); 1.65 (1H, m, H3); 1.59 (1H, m, H10); 1.44-1.23 (2H, m, H23); 1.42 (1H, m, H10); 1.32 (2H, m, H22); 1.22 (1H, m, H3) ppm

^{13}C NMR (DMSO – d_6, 100 MHz): δ 174.6 (C12); 171.1 (C34); 168.1 (C46); 165.7 (C5); 163.4 (C35); 156.2 (C26); 152.8 (C43); 149.4 (C17); 147.6 (C14); 139.7 (C50, C61); 137.8 (C55, C56); 137.3 (C28); 132.7 (C40); 129.2 (C52, C59); 127.9 (C16, C18); 127.9 (C53, C58); 127.7-127.3 (C29, C30, C31, C32, C33); 124.4 (C15, C19); 123.5 (C41); 121.5 (C54, C57); 121.3 (C39); 120.4 (C51, C60); 120.1 (C38); 112.6 (C42); 69.4 (C27); 66.8 (C48); 63.2 (C8); 59.6 (C44); 59.6 (C1); 54.5 (C2); 50.7 (C20); 47.0 (C49); 44.7 (C4); 44.3 (C6); 40.1 (C24); 34.6 (C3); 32.4 (C9); 32.0 (C21); 30.5 (C11); 29.0 (C23); 24.5 (C10); 23.8 (C47); 22.8 (C22) ppm

Melting point = 142–144 °C

IR: 3298 (N-H stretch); 2934 (C-H stretch); 1693 (C=O stretch); 1528 (-NO2 aromatic); 1477-1449 (N-H bend); 1347 (-NO2 aromatic) cm^{-1}

Compound (**3.17**)

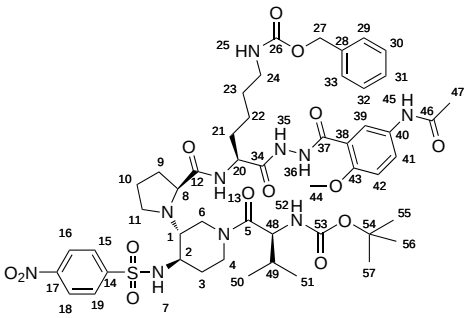

The Fmoc protected compound **3.16** (209 mg, 0.19 mmol, 1.0 eq.) was dissolved in a 65 % solution of piperidine in DMF (10 mL) and the reaction mixture was let stirring at room temperature for 2 h. After evaporation of the solvent under vacuum, the Fmoc deprotected amine was used for the next coupling reaction without any further purification.

Boc-NH-Val-OH (83 mg, 0.38 mmol, 2.0 eq.) was dissolved in DMF (10.0 mL) under a nitrogen atmosphere and the solution was cooled at 0°C. At this moment, HOAt (52 mg, 0.38 mmol, 2.0 eq.) and HATU (145 mg, 0.38 mmol, 2.0 eq.) were added at the same time. The solution was stirred at 0° C between 30 min and 1h and solution of the previous deprotected compound **3.16** and collidine (0.15 mL, 1.14 mmol, 6.0 eq.) in DMF (5.0 mL) was immediately added. After stirring at room temperature overnight, the

solvent was evaporated under vacuum. The resulting residue was taken up with EtOAc and successively washed with water, saturated $NaHCO_3$, brine, dried over Na_2SO_4, filtered and concentrated under vacuum. The resulting crude product was purified by column chromatography on silica gel using EtOAc 100 % then EtOAc/MeOH 95:5 as eluent to afford compound **3.17** (152 mg, 0.14 mmol, Yield 75 %) as a pale yellow solid.

Molecular weight = $1065.20\,\mathrm{g\,mol^{-1}}$

$R_f = 0.60$ (EtOAc/MeOH 90:10)

HRMS: Calcd. for $[C_{50}H_{68}N_{10}O_{14}S{+}H]^+$: M/z 1065.4715, found: 1065.4714; Calcd. for $[C_{50}H_{68}N_{10}O_{14}S + Na]^+$: M/z 1087.4535, found: 1087.4546

^{1}H NMR (DMSO – d_6, 400 MHz): δ 10.54 (1H, bp, NH35); 10.06 (1H, bp, NH36); 9.95 (1H, s, NH45); 8.38 (2H, d, J = 8.7 Hz, H15, H19); 8.25 (1H, bp, NH13); 8.12 (2H, d, J = 8.7 Hz, H16, H18); 8.03 (1H, s, H39); 7.72 (1H, m, H41); 7.36-7.34 (5H, m, H29, H30, H31, H32, H33); 7.21 (1H, bp, NH25); 7.12 (1H, m, H42); 6.72 (1H, s, NH52); 6.28 (1H, bp, NH7); 4.99 (2H, s, H27); 4.51 (1H, m, H20); 4.32 (1H, m, H6); 4.09 (1H, m, H48); 3.85 (1H, m, H4); 3.84 (3H, s, H44); 3.39 (1H, m, H8); 3.38 (1H, m, H2); 2.99 (2H, m, H24); 2.98 (1H, m, H4); 2.66 (1H, m, H6); 2.27 (1H, m, H1); 2.05 (1H, m, H11); 2.02 (3H, s, H47); 1.90 (1H, m, H49); 1.82-1.71 (2H, m, H21); 1.82 (1H, m, H9); 1.77 (1H, m, H3); 1.71 (1H, m, H9); 1.68 (1H, m, H11); 1.60 (1H, m, H10); 1.44 (2H, m, H23); 1.40 (1H, m, H10); 1.32 (2H, m, H22); 1.33 (9H, s, H55, H56, H57); 1.28 (1H, m, H3); 0.79-0.72 (6H, m, H50, H51) ppm

^{13}C NMR (DMSO – d_6, 100 MHz): δ 173.6 (C12); 172.1 (C5); 170.1 (C34); 168.0 (C46); 164.0 (C35); 156.8 (C26); 156.1 (C53); 153.4 (C43); 150.0 (C17); 147.6 (C14); 137.4 (C28); 133.3 (C40); 127.7 (C16, C18); 128.3-127.7-126.6 (C29, C30, C31, C32, C33); 124.5 (C15, C19); 123.9 (C38); 123.3 (C41); 121.1 (C38); 112.0 (C42); 78.0 (C54); 65.1 (C27); 62.7 (C8); 58.6 (C1); 56.2 (C44); 55.0 (C48); 53.5 (C2); 50.1 (C20); 43.3 (C4); 40.1 (C24); 39.8 (C6); 33.0 (C3); 31.9 (C21); 31.7 (C9); 30.4 (C11); 28.7 (C23); 28.1 (C55, C56, C57); 24.2 (C10); 23.8 (C47); 22.7 (C22); 21.1 (C49); 19.4-18.0 (C50, C51) ppm

Melting point = 146–148 °C

IR: 3296 (N-H stretch); 2939 (C-H stretch); 1684 (C=O stretch); 1527 (-NO2 aromatic); 1477-1450 (N-H bend); 1348 (-NO2 aromatic) $\mathrm{cm^{-1}}$

Compound (**3.18**)

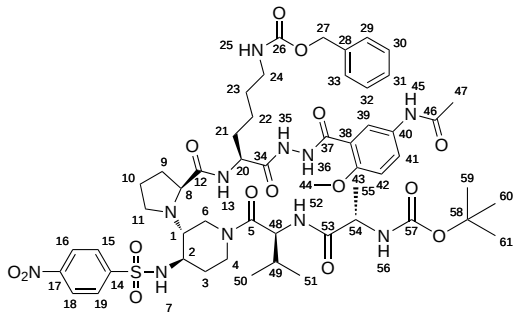

To a solution of the N-Boc protected compound **3.17** (125 mg, 0.12 mmol, 1.0 eq.) in DCM (8.0 mL) was added TFA (0.45 mL, 6.0 mmol, 50.0 eq.) and the reaction mixture was let stirring at room temperature for 2 h. The solvent was evaporated, then toluene (2 x 10 mL) was added followed by evaporation, and then ether was added and evaporated to afford the corresponding TFA salt that was used for the next coupling reaction without any further purification.

Boc-NH-Ala-OH (46 mg, 0.24 mmol, 2.0 eq.) was dissolved in DMF (5.0 mL) under a nitrogen atmosphere and the solution was cooled at 0°C. At this moment, HOAt (33 mg, 0.24 mmol, 2.0 eq.) and HATU (92 mg, 0.24 mmol, 2.0 eq.) were then added at the same time. The solution was stirred between 30 min and 1h at 0°C and the solution of the previous TFA salt and collidine (0.10 mL, 0.72 mmol, 6.0 eq.) in DMF (5.0 mL) was immediatly added. After stirring at room temperature overnight, the solvent was evaporated under vacuum. The resulting residue was taken up with EtOAc and successively washed with water, saturated $NaHCO_3$, brine, dried over Na_2SO_4, filtered and concentrated under vacuum. The crude product was purified by column chromatography on silica gel using EtOAc 100 % to EtOAc/MeOH 95:5 as eluent to yield compound **3.18** as a pale yellow solid (100 mg, 0.09 mmol, Yield 75 %).

Molecular weight = 1136.28 g mol^{-1}

$R_f = 0.55$ (EtOAc/MeOH 95:5)

HRMS: Calcd. for $[C_{53}H_{73}N_{11}O_{15}S+H]^+$: M/z 1136.5087, found: 1136.5095

^{1}H NMR (DMSO – d_6, 400 MHz): δ 10.54 (1H, bp, NH35); 10.05 (1H, bp, NH36); 9.94 (1H, s, NH45); 8.40 (2H, d, J = 8.5 Hz, H15, H19); 8.24 (1H, bp, NH13); 8.11 (2H, d, J = 8.5 Hz, H16, H18); 8.09 (1H, bp, NH7); 8.04 (1H, s, H39); 7.71 (1H, m, H41); 7.63 (1H, bp, NH52); 7.34 (5H, m, H29, H30, H31, H32, H33); 7.22 (1H, bp, NH25); 7.12 (1H, m, H42); 6.95 (1H, bp, NH56); 5.00 (2H, s, H27); 4.51 (1H, m, H20); 4.46 (1H, m, H48); 4.32 (1H, m, H6); 3.95 (1H, m, H54); 3.85 (1H, m, H4); 3.85 (3H, s, H44); 3.69 (1H,

m, H6); 3.39 (1H, m, H2); 3.38 (1H, m, H8); 3.01 (2H, m, H24); 2.96 (1H, m, H4); 2.30 (1H, m, H1); 2.04 (1H, m, H11); 2.02 (3H, s, H47); 1.90/1.83 (1H, m, H49); 1.85 (1H, m, H11); 1.82-1.69 (2H, m, H21); 1.81 (1H, m, H9); 1.80 (1H, m, H3); 1.68 (1H, m, H9); 1.62 (1H, m, H10); 1.43 (2H, m, H23); 1.42 (1H, m, H10); 1.33 (2H, m, H22); 1.36 (9H, s, H59, H60, H61); 1.29 (1H, m, H3); 1.10 (3H, s, H55); 0.77-0.72 (6H, m, H50, H51) ppm

^{13}C NMR (DMSO – d_6, 100 MHz): δ 174.6 (C12); 172.7 (C53); 172.3 (C5); 170.7 (C34); 169.6 (C57); 168.3 (C46); 163.8 (C37); 156.1 (C26); 153.1 (C43); 149.5 (C17); 147.4 (C14); 137.3 (C28); 132.7 (C40); 127.9 (C29, C30, C31, C32, C33); 127.8 (C16, C18); 124.5 (C15, C19); 123.4 (C41); 121.4 (C39); 120.6 (C38); 112.5 (C42); 78.4 (C58); 65.1 (C27); 63.1 (C8); 58.5 (C1); 56.2 (C44); 53.4 (C2); 52.6 (C48); 50.2 (C20); 49.6 (C54); 43.3 (C4); 40.1 (C24); 39.5 (C6); 33.0 (C3); 31.9 (C9); 31.6 (C21); 30.3 (C11); 30.2 (C49); 28.9 (C23); 28.1 (C59, C60, C61); 24.2 (C10); 23.8 (C47); 22.7 (C22); 19.2, 17.5 (C50, C51); 17.8 (C55) ppm

Melting point = 148–150 °C

IR: 3297 (N-H stretch); 2933 (C-H stretch); 1653 (C=O stretch); 1527 (-NO2 aromatic); 1494-1454 (N-H bend); 1348 (-NO2 aromatic) cm^{-1}

Elemental analysis: Calcd. for $C_{53}H_{73}N_{11}O_{15}S \cdot 1.5\,H_2O$: C 54.72, H 6.60, N 13.25; found: C 54.70, H 6.25, N 12.41

HPLC purity (SUNFIRE C18, 3.5 µm, H_2O + 0.2 % form. ac./ACN, gradient 5–100 % in 20 min): t_R = 17.68 min, 100 %

(S)-6-(2-(5-acetamido-2-methoxybenzoyl)hydrazinyl)-6-oxohexane-1,5-diaminium chloride (**4.1**)

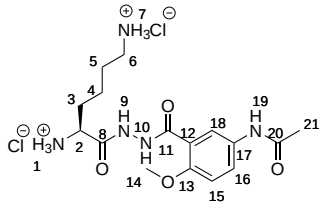

Compound **NT05** (100 mg, 0.17 mmol, 1.0 eq.) was dissolved in MeOH (4.0 mL) and 10 % Pd/C (20 mg) was added. The reaction was kept 2 hours under stirring in hydrogen atmosphere at room temperature. The catalyst was then removed over a celite pad and the solvent evaporated under vacuum. Successively, the resulting product was dissolved in dioxane (2.0 mL) and a 4 N solution of HCl in dioxane (1.7 mL, 40.0 eq.) was added. The reaction was kept 2 hours under stirring at room temperature. After this time, product **41** was isolated as hydrochloride salt by precipitation in diethyl ether. The crude was purified by crystallization in MeOH and diethyl ether to afford the pure compound **4.1** (65 mg, 0.15 mmol, yield 90 %) as a white powder.

Molecular weight = 424.32 g mol^{-1}

$R_f = 0$ (EtOAc)

HRMS: Calcd. for $[C_{16}H_{25}N_5O_4 + H]^+$: M/z 352.1985, found: 352.1985

^{1}H NMR (DMSO – d_6, 400 MHz): δ 10.86 (1H, s, NH9); 10.14 (1H, s, NH19); 10.05 (1H, s, NH10); 8.51 (3H, s, NH1); 8.13 (3H, s, NH7); 7.98 (1H, s, H18); 7.74 (1H, bp, H16); 7.09 (1H, bp, H15); 3.92 (1H, m, H2); 3.85 (3H, s, H14); 2.76 (2H, m, H6); 2.01 (3H, s, H21); 1.86 (2H, m, H3); 1.63 (2H, m, H5); 1.52 (2H, m, H4) ppm

^{13}C NMR (DMSO – d_6, 100 MHz): δ 168.0 (C20); 166.8 (C8); 163.4 (C11); 152.5 (C13); 132.5 (C12); 123.5 (C16); 121.1 (C18); 120.7 (C17); 112.4 (C15); 56.2 (C14); 50.6 (C2); 38.1 (C6); 30.1 (C3); 26.0 (C5); 23.6 (C21); 20.7 (C4) ppm

Melting point = 211–213 °C

IR: 2928 bp (N-H stretch, C-H stretch); 1647 (C=O stretch); 1546, 1492 (N-H bend); 1254 (C-O-C stretch) cm^{-1}

HPLC purity (SUNFIRE C18, 3.5 µm, H_2O + 0.1 % form. ac./MeOH, gradient 1–100 % in 20 min): t_R = 1.32 min, 95 %

(S)-6-(2-(5-benzamido-3-fluoro-2-hydroxybenzoyl)hydrazinyl)-6-oxohexane-1,5-diaminium chloride (**4.2**)

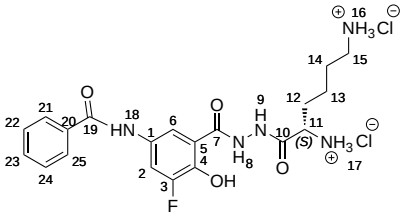

Compound **4.24** (50 mg, 0.07 mmol, 1.0 eq.) was dissolved in MeOH (4.0 mL) and 10 % Pd/C (10 mg) was added. The reaction was kept 2 hours under stirring in hydrogen atmosphere at room temperature. The catalyst was then removed over a celite pad and the solvent evaporated under vacuum. The resulting product was successively dissolved in dioxane (2.0 mL) in the presence of a 4 N solution of HCl in dioxane (0.7 mL, 40.0 eq.). The reaction was kept 2 hours under stirring at room temperature. After this time, product **4.24** (8 mg, 0.02 mmol, Yield 29 %) was isolated as hydrochloride salt by precipitation in diethyl ether.

Molecular weight = 490.36 g mol^{-1}

$R_f = 0$ (Cyclo/EtOAc 4:6)

HRMS: Calcd. for $[C_{20}H_{24}N_5O_4F + H]^+$: M/z 418.1891, found: 418.1900

^{1}H NMR (DMSO – d_6, 400 MHz): δ nd (NH9); 10.37 (1H, s, NH8); 9.45 (1H, s, NH18); 7.84 (3H, bp, H17); 7.23 (3H, bp, H16); 7.98, 7.60, 7.53 (5H, m, H21, H22, H23, H24, H25); 6.85 (1H, s, H2); 6.70 (1H, s, H6); 4.07 (1H,

bp, OH); 3.75 (1H, m, H11); 2.78 (2H, m, H15); 1.84 (2H, m, H12); 1.62 (2H, m, H13); 1.49 (2H, m, H14) ppm

^{13}C NMR (DMSO – d_6, 100 MHz): δ 170.0 (C10); 165.4 (C19); 165.2 (C7); 155.2 (C3); 136.7 (C1); 134.4 (C20); 131.6, 128.1, 127.3 (C21, C22, C23, C24, C25); 133.9 (C5); 129.7 (C2); 122.6 (C4); 118.0 (C6); 52.3 (C11); 38.0 (C15); 30.6 (C12); 26.2 (C13); 20.8 (C14) ppm

HPLC purity (XBridge C18, 3.5 µm, H_2O + 0.1 % form. ac./ACN, gradient 5–100 % in 20 min): t_R = 8.06 min, 84 %

(S)-1-((3R,4R)-1-((S)-2-((S)-2-(((benzyloxy)carbonyl)amino)propanamido)-3-methylbutanoyl)-4-(4-methylphenylsulfonamido)piperidin-3-yl)pyrrolidine-2--carboxylic acid (**4.4**)

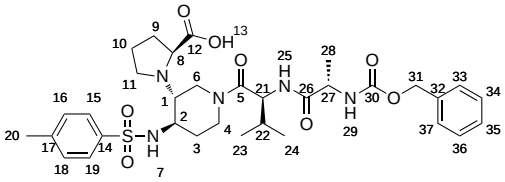

Compound **4.26** (150 mg, 0.22 mmol, 1.0 eq.) was dissolved in MeOH (8.0 mL) and NaOH 2 M (0.6 mL, 1.1 mmol, 5.0 eq.) was added dropwise to the solution. The reaction was stirred at 60° C for 2 h. The solvent was evaporated and the solid obtained was solubilized in water. The mixture was acidified with 10 % solution of $KHSO_4$ until pH = 2-3. A part of the product was extracted from the water phase with EtOAc and an another part of the desired compound was recuperated by solving an solid residue of the water phase with MeOH. The two combined organic phases were dried over Na_2SO_4 and concentrated under vacuum to yield compound **4.4** (134 mg, 0.20 mmol, Yield 91 %) as a white solid.

Molecular weight = 671.80 g mol^{-1}

R_f = 0 (Cyclo/EtOAc 6:4)

HRMS: Calcd. for $[C_{33}H_{45}N_5O_8S + H]^+$: M/z 672.3067, found: 672.3065

^{1}H NMR (DMSO – d_6, 400 MHz): δ (OH13 not detected); 7.75 (1H, bp, NH25); 7.72 (2H, m, H15, H19); 7.41 (2H, m, H16, H18); 7.35, 7.23 (5H, m, H33, H34, H35, H36, H37); 7.23 (1H, bp, NH29); 7.02 (1H, bp, NH7); 5.01 (2H, s, H31); 4.48 (1H, m, H21); 4.24 (1H, m, H6); 4.07 (1H, m, H27); 4.03 (1H, m, H4); 3.42 (1H, m, H8); 3.10 (1H, m, H4); 3.01 (1H, m, H2); 2.75 (1H, m, H6); 2.40 (1H, m, H11); 2.38 (3H, s, H20); 2.26 (1H, m, H1); 2.12 (1H, m, H9); 2.03 (1H, m, H3); 1.92 (1H, m, H22); 1.89 (1H, m, H11); 1.74 (1H, m, H3); 1.50 (1H, m, H10); 1.30 (1H, m, H9); 1.24 (1H, m, H10); 1.15 (3H, s, H28); 0.81, 0.78 (6H, m, H23, H24) ppm

^{13}C NMR (DMSO – d_6, 100 MHz): δ 176.6 (C12); 172.2 (C26); 171.9 (C5); 155.6 (C30); 142.6 (C17); 137.1 (C14); 136.9 (C32); 129.2 (C16, C18); 127.7,

126.3 (C33, C34, C35, C36, C37); 126.4 (C15, C19); 65.1 (C31); 61.8 (C8); 58.3 (C1); 52.7 (C21); 52.3 (C2); 49.7 (C27); 44.4 (C11); 43.8 (C4); 39.5 (C6); 32.5 (C9); 29.9 (C22); 29.3 (C3); 23.6 (C10); 20.7 (C20); 19.2; 17.8 (C23, C24); 18.1 (C28) ppm

Melting point = 163–165 °C

IR: 3302 (N-H stretch; O-H stretch); 2962, 2927, 2874 (C-H stretch); 1712, 1631 (C=O stretch); 1524 (N-H bend); 1452 (C=C stretch); 1331, 1226 (C-O-H bend, C-O stretch); 1185 (C-N stretch) cm^{-1}

3-fluoro-2-hydroxy-5-nitrobenzaldehyde (**4.14**)

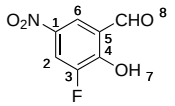

3-fluoro-2-hydroxybenzaldehyde (1.18 g, 8.4 mmol, 1.0 eq.) was dissolved in concentrated H_2SO_4 (20 mL) and the solution was kept at 0°C. Then, NH_4NO_3 (740 mg 9.2 mmol, 1.1 eq.) was added at 0°C and the reaction was let stirring at 0°C for 2h. At completion of the reaction, ice was added and the reaction mixture was poured in distilled water. A white precipitate was formed and filtered (1.28 g, 6.9 mmol). Yield 82 %

Molecular weight = 185.11 g mol^{-1}

R_f = 0.40 (EtOAc/MeOH 9:1 + 10 µL AcOH)

HRMS: Calcd. for $[C_7H_3NO_4F - H]^-$: M/z 184.0046, found: 184.0042

^{1}H NMR ($CDCl_3$, 300 MHz): δ 11.63 (1H, s, OH7); 10.03 (1H, d, J = 1.7 Hz, H8); 8.42 (1H, dd, J = 2.6, 1.5 Hz, H6); 8.25 (1H, dd, J = 9.9, 2.6 Hz, H2) ppm

^{13}C NMR ($CDCl_3$, 75 MHz): δ 195.14(C8); 155.23 (J = 12.6 Hz, C4); 152.19 (C3); 148.80 (C1); 124.21 (C5); 120.55 (C6); 117.62 (J = 22.0 Hz, C2) ppm

^{19}F NMR ($CDCl_3$, 188 MHz): -130.83 δ ppm

Melting point = 89–91 °C

IR: 3098-3052 (C-H aromatic and CHO stretching + broad peak for OH stretching); 1667 (C=O stretching); 1517 (NO2 stretching); 1472, 1447 (aromatic double bond stretching), 1396 (OH bending); 1366 (C-H Bending of CHO), 1342 (NO2 stretching) cm^{-1}

2-(benzyloxy)-3-fluoro-5-nitrobenzaldehyde (**4.15**)

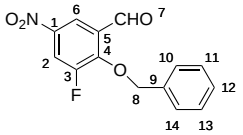

To a solution of **4.14** (1.26 g, 6.81 mmol, 1.0 eq.) in DMF, Cs_2CO_3 (3.54 g, 10.9 mmol, 1.6 eq.) and benzyl bromide (1.71 mL, 14.30 mmol, 2.1 eq.) were successively added. Then, the reaction mixture was stirred overnight at room temperature. After concentration under vacuum, the resulting residue was taken up with EtOAc and successively washed twice with water and brine, dried over Na_2SO_4, filtered and concentrated to obtain a yellow solid. The crude product was purified by column chromatography on a silica gel using Cyclohexane/EtOAc 9:1 and finally 8:2 as eluent to yield compound **4.15** as a white solid (1.67 g, 6.07 mmol). Yield 89 %.

Molecular weight = 275.23 g mol^{-1}

R_f = 0.30 (Cyclo/EtOAc 9:1)

HRMS: Calcd. for $[C_{14}H_9NO_4F - H]^-$: M/z 274.0516, found: 274.0511

^{1}H NMR ($CDCl_3$, 300 MHz): δ 10.26 (1H, s, H7); 8.47 (1H, dd, J = 2.8, 1.4 Hz, H6); 8.22 (1H, dd, J = 11.5, 2.8 Hz, H2); 7.40 (5H, s, H10, H11, H12, H13, H14); 5.48 (2H, d, J = 2.2 Hz, H8) ppm

^{13}C NMR ($CDCl_3$, 75 MHz): δ 186.66 (C7); 155.67 (C4); 152.30 (C3); 142.54 (C1); 134.63 (C9); 129.73 (C5); 129.4, 129.00, 128.57 (C10, C11, C12, C13, C14); 119.30 (C6); 117.64 (J = 24.8 Hz, C2); 77.43 (C8) ppm

^{19}F NMR ($CDCl_3$, 188 MHz): -123.32 δ ppm

Melting point = 97–99 °C

IR: 3098-2870 (C-H aromatic and CHO stretching); 1686 (C=O stretching); 1613-1600 (C=C aromatic stretching); 1527 (NO2 stretching); 1498-1452 (aromatic double bond stretching); 1340 (NO2 stretching) cm^{-1}

2-(benzyloxy)-3-fluoro-5-nitrobenzoic acid (**4.16**)

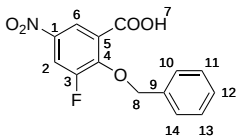

Micklatcher ML et al.; Synthesis 1999, 11, 1878–1880.

$NaClO_2$ (705 mg, 7.8 mmol, 1.3 eq.) was dissolved in water (5 mL) and set aside. During this time, compound **4.15** (1.65 g, 6.0 mmol, 1.0 eq.) was dissolved in 1,4-dioxane (15 mL) and water (5 mL). Sulfamic acid (874 mg, 9.0 mmol, 1.5 eq.) and $NaH_2PO_4 \cdot H_2O$ (2.81 g, 23.4 mmol, 3.9 eq.) were

added to the stirring reaction mixture. The mixture was cooled at 0° C for 15 min, and the $NaClO_2$ solution then was added dropwise to the mixture. Once addition was complete, the solution was stirred for an additional 15 min. Na_2SO_4 (906 mg, 7.2 mmol, 1.2 eq.) was added in one portion, and stirring was continued for an additional 15 min. The solution was then acidified to pH 1 by dropwise addition of concentrated HCl. After concentration under vacuum the crude residue obtained was taken up in 5 % aqueous NaOH solution, and concentrated HCl was added dropwise to the solution until pH 1 was reached. The solid formed was collected by filtration on a Buchner funnel and was allowed to dry overnight in the open air yielding **4.16** as a white solid (1.76 g, 6.0 mmol). Yield 100 %.

Molecular weight = 291.23 g mol^{-1}

$R_f = 0$ (Cyclo/EtOAc 8:2)

HRMS: Calcd. for $[C_{14}H_9NO_5F - H]^-$: M/z 290.0465, found: 290.0463; Calcd. for $[C_{14}H_{10}NO_5F + Na]^+$: M/z 314.0441, found: 314.0448

^{1}H NMR ($CDCl_3$, 300 MHz): δ 8.71 (1H, dd, J = 2.8, 1.6 Hz, H6); 8.21 (1H, dd, J = 11.0, 2.8 Hz, H2); 7.43 (6H, m, H7, H10, H11, H12, H13, H14); 5.45 (2H, d, J = 2.1 Hz, H8) ppm

^{13}C NMR ($CDCl_3$, 75 MHz): δ 164.62 (C7); 156.08 (C4); 152.72 (C3); 142.53 (C1); 134.19 (C9); 129.73 (C5); 129.19, 129.00, 128.83 (C10, C11, C12, C13, C14); 123.41 (C6); 116.80 (J = 24.8 Hz, C2); 77.96 (C8) ppm

^{19}F NMR ($CDCl_3$, 188 MHz): -122.30 δ ppm

Melting point = 100–102 °C

IR: 3431 (O-H stretching); 3095, 2890 (C-H aromatic stretching); 1682 (C=O stretching); 1616 (C=C aromatic stretching); 1525 (NO2 stretching); 1454-1410 (O-H bending); 1345 (C-O stretching), 1266 (NO2 stretching) cm^{-1}

tert-butyl 2-(2-(benzyloxy)-3-fluoro-5-nitrobenzoyl)hydrazinecarboxylate (**4.17**)

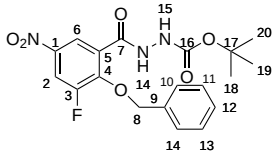

Compound **4.16** (1.05 g, 3.62 mmol, 1.0 eq.) was dissolved in 15 mL of DMF under argon atmosphere. Then, tert-butyl carbazate (526 mg, 3.98 mmol, 1.1 eq.), HBTU (1.51 g, 3.98 mmol, 1.1 eq.), HOBt (540 mg, 3.98 mmol, 1.1 eq.) and DIPEA (1.25 mL, 7.23 mmol, 2.0 eq.) were added at the same time to the stirring solution at 0° C. The reaction mixture was let stirring overnight at room temperature. After concentration under vacuum, the crude residue obtained was taken up with EtOAc and successively washed with

citric acid (100 % aqueous solution), water, K_2CO_3 (100 % aqueous solution) , and brine. The organic phase was then dried over Na_2SO_4, filtered and concentrated under vacuum. The resulting crude product was purified by column chromatography on silica gel using Cyclohexane/EtOAc 9:1 then 8:2 as eluent to afford compound **4.17** as a pale yellow solid (734 mg, 1.81 mmol, Yield 50 %).

Molecular weight = 405.38 g mol^{-1}

R_f = 0.30 (Cyclo/EtOAc 8:2)

HRMS: Calcd. for $[C_{19}H_{20}N_3O_6F+Na]^+$: M/z 428.1234, found: 428.1231

^{1}H NMR ($CDCl_3$, 300 MHz): δ 9.29 (1H, bp, NH14); 8.82 (1H, dd, J = 2.8, 1.6 Hz, H6); 8.14 (1H, dd, J = 11.0, 2.8 Hz, H2); 7.41 (5H, m, H10, H11, H12, H13, H14); 6.81 (1H, bp, NH15); 5.45 (2H, dd, J = 1.9 Hz, H8); 1.48 (9H, s, H18, H19, H20) ppm

^{13}C NMR ($CDCl_3$, 75 MHz): δ 161.44 (C7); 155.85 (C16); 154.70 (C3); 152.49 (C4); 142.91 (C1); 134.07 (C9); 129.67, 129.29, 129.05 (C10, C11, C12, C13, C14); 126.08 (C5); 122.93 (C6); 115.65 (J = 15.9 Hz, C2); 82.18 (C17); 77.96 (C8); 28.13 (C18, C19, C20) ppm

^{19}F NMR ($CDCl_3$, 188 MHz): -122.58 δ ppm

Melting point = 120–122 °C

IR: 3390, 3258 (N-H stretching); 3072, 2988 (C-H stretching); 1717, 1682 (C=O stretching); 1615 (C=C aromatic stretching); 1536 (NO2 stretching); 1498-1458 (N-H bending); 1395-1302 (C-O stretching), 1279 (NO2 stretching) cm^{-1}

tert-butyl 2-(5-amino-3-fluoro-2-hydroxybenzoyl)hydrazinecarboxylate (**4.22**)

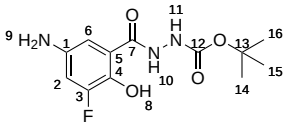

Compound **4.17** (520 mg, 1.28 mmol, 1.0 eq.) was dissolved in MeOH (15 mL) and Pd/C (104 mg, 20 % mass) was added under argon atmosphere. The reaction was let stirring one hour under hydrogen atmosphere and the solution was then filtered on a pad of Celite. The filtrate was evaporated under vacuum to afford compound **4.22** as a purple solid (370 mg, 1.28 mmol, Yield 100 %).

Molecular weight = 285.27 g mol^{-1}

R_f = 0 (Cyclo/EtOAc 8:2)

HRMS: Calcd. for $[C_{12}H_{16}N_3O_4F+Na]^+$: M/z 308.1023, found: 308.1020

^{1}H NMR (DMSO – d_6, 300 MHz): δ 10.80 (1H, bp, OH8); 10.20 (1H, s, NH10); 9.00 (1H, s, NH11); 6.82 (1H, s, H6); 6.67 (1H, d, J = 12.8 Hz, H2); 4.94 (2H, bp, NH9); 1.30 (9H, s, H14, H15, H16) ppm

^{13}C NMR (DMSO – d_6, 75 MHz): δ 168.19 (C7); 155.62 (C12); 153.59-150.42 (J = 239.4 Hz, C3); 141.40 (C1); 137.55 (C4); 118.12 (C5); 107.95 (C6); 107.13 (J = 20.4 Hz, C2); 79.90 (C13); 28.52 (C14, C15, C16) ppm

^{19}F NMR (DMSO – d_6, 188 MHz): -133.58 δ ppm

Melting point = 197–199 °C

IR: 3455 (N-H stretching); 3300 (broad peak for OH stretching); 2976 (C-H stretching); 1735 (C=O stretching); 1625 (C=C aromatic stretching); 1590-1497 (N-H bending); 1385-1307 (C-O stretching), 1270-1214 (C-N stretching) cm^{-1}

tert-butyl 2-(5-benzamido-2-(benzoyloxy)-3-fluorobenzoyl)hydrazinecarboxylate (**4.23**)

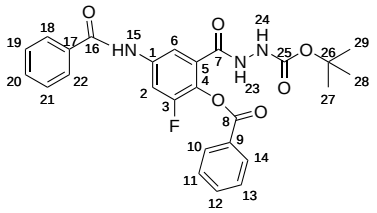

Compound **4.22** (346 mg, 1.21 mmol, 1.0 eq.) was dissolved in pyridine (15 mL) under argon atmosphere and phenyl chloroformate (563 µL, 4.85 mmol, 4.0 eq.) was slowly added at 0°C. The reaction was let stirring at room temperature for three hours. After removing pyridine under vacuum, the crude product was taken up with EtOAc and successively washed with citric acid (10 % aqueous solution), water, K_2CO_3 (10 % aqueous solution) , brine, dried over Na_2SO_4 filtered and concentrated under vacuum. The crude residue afforded was purified by column chromatography on silica gel using Cyclohexane/EtOAc 1:1 to yield compound **4.23** as a white solid (568 mg, 1.15 mmol, Yield 95 %).

Molecular weight = 493.48 g mol^{-1}

R_f = 0.50 (Cyclo/EtOAc 1:1)

HRMS: Calcd. for $[C_{26}H_{24}N_3O_6F + H]^+$: M/z 494.172, found: 494.1732; Calcd. for $[C_{26}H_{24}N_3O_6F + Na]^+$: M/z 516.1547, found: 516.1547

^{1}H NMR (DMSO – d_6, 300 MHz): δ 10.67 (1H, s, NH15); 10.18 (1H, s, NH23; 8.98 (1H, s, NH24); 8.10 (1H, d, H2); 7.83 (12H, m, H10, H11, H12, H13, H14, H15, H16, H17, H18, H19, H20, H21); 7.90 (1H, bp, H6); 1.38 (9H, s, H27, H28, H29) ppm

^{13}C NMR (DMSO – d_6, 75 MHz): δ 166.0 (C16); 164.0 (C7); 163.6 (C8); 154.8 (C25); 155.48 (C3); 152.40 (C9); 138.51, 138.37, 134.59 (C1, C5, C17); 134.3, 128.9, 130.2 (C10, C11, C12, C13, C14); 132.1, 125.6, 127.8 (C18, C19, C20, C21, C22); 128.40 (C4); 115.8 (C6); 109.8 (J = 23.4 Hz, C2); 79.3 (C26); 28.45 (C27, C28, C29) ppm

^{19}F NMR (DMSO – d_6, 188 MHz): -124.74 δ ppm

Melting point = 125–127 °C

IR: 3287 (N-H stretching); 2981 (C-H stretching); 1726 (C=O stretching); 1662 (C=C aromatic stretching); 1602-1541 (N-H bending); 1203-1157 (C-C(O)-C stretching) cm^{-1}

(S)-4-benzamido-2-(2-(6-(((benzyloxy)carbonyl)amino)-2-((tert-butoxycarbonyl)-amino)hexanoyl)hydrazinecarbonyl)-6-fluorophenyl benzoate (**4.24**)

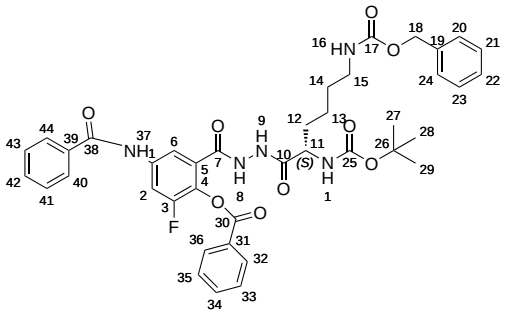

Compound **4.23** (100 mg, 0.20 mmol, 1.0 eq.) was dissolved in dioxane (5 mL) under argon atmosphere. HCl 4M in dioxane (1.5 mL, 6 mmol, 30.0 eq.) was added at 0° C and the reaction was let stirring 4 h at room temperature. The solvent was removed under vacuum and the Boc deprotected compound was used for the coupling reaction step without further purification. Precisely, It was dissolved in 5 mL of DMF under argon atmosphere then BocNH-Lys(Z)-OH (84 mg, 0.22 mmol, 1.1 eq.), DMTMM (61 mg, 0.22 mmol, 1.1 eq.) and NMM (44 µL, 0.40 mmol, 2.0 eq.) were added at the same time to the stirring solution at 0° C. The reaction mixture was let stirring overnight at room temperature. After concentration under vacuum, the crude residue obtained was taken up with EtOAc and successively washed with citric acid (10 % aqueous solution), water, K_2CO_3 (10 % aqueous solution), and brine. The organic phase was then dried over Na_2SO_4, filtered and concentrated under vacuum. The crude product obtained was purified by column chromatography on silica gel using EtOAc/Cyclohexane 6:4 then 100 % EtOAc as eluent to afford compound **4.23** as a white solid (67 mg, 0.09 mmol, Yield 45 %).

Molecular weight = 755.79 g mol^{-1}

R_f = 0.40 (Cyclo/EtOAc 4:6)

HRMS: Calcd. for $[C_{40}H_{42}N_5O_9F+Na]^+$: M/z 778.2864, found: 778.2866

^{1}H NMR (DMSO – d_6, 300 MHz): δ 10.68 (1H, s, NH37); 10.41 (1H, s, NH8); 10.0 (1H, s, NH9); 8.11 (1H, d, J = 7.6 Hz, H2); 7.92 (1H, d, J = 7.6 Hz, H6); 7.99, 7.64, 7.60 (5H, m, H40, H41, H42, H43, H44); 8.15, 7;76, 7.64 (5H, m, H32, H33, H34, H35, H36); 7.76, 7.57, 7.34 (5H, m, H20, H21, H22,

H23, H24); 7.20 (1H, s, NH16); 6.84 (1H, d, J = 8.2 Hz, NH1); 4.99 (2H, s, H18); 3.95 (1H, m, H11); 2.94 (2H, m, H17); 1.53 (2H, m, H12); (1.36 (9H, s, H27, H28, H29); 1.32 (2H, m, H14); 1.24 (2H, m, H13) ppm

^{13}C NMR (DMSO – d_6, 75 MHz): δ 171.2 (C10); 165.7 (C38); 163.4 (C30); 162.9 (C7); 155.9 (C17); 155.2 (C25); 154.5 (C3); 152.16 (C31); 138.0 (C39); 137.9 (C4); 137.1 (C19); 132.0, 128.6, 127.7 (C40, C41, C42, C43, C44); 134.2, 131.9, 130.0 (C32, C33, C34, C35, C36); 134.1, 128.5, 127.8 (C20, C21, C22, C23, C24); 130.8 (C1); 127.5 (C5); 115.8 (C6); 109.7 (C2); 77.8 (C26); 64.9 (C18); 52.6 (C11); 39.9 (C15); 30.7 (C12); 28.8 (C13); 22.6 (C14); 28.1 (C27, C28, C29) ppm

^{19}F NMR (DMSO – d_6, 188 MHz): -121.55 δ ppm

Melting point = 117–119 °C

IR: 3303 (N-H stretching); 2933 (C-H stretching); 1752-1672 (C=O stretching); 1529-1495 (N-H bending); 1259-1175 (C-C(O)-C stretching) cm^{-1}

HPLC purity (XBridge C18, 3.5 µm, H_2O + 0.1 % form. ac./ACN, gradient 5–100 % in 20 min): t_R = 18.88 min, 94 %

(S)-methyl 1-((3R,4R)-1-((S)-2-((((9H-fluoren-9-yl)methoxy)carbonyl)amino)-
-3-methylbutanoyl)-4-(4-methylphenylsulfonamido)piperidin-3-yl)pyrrolidine-
2-carboxylate (**4.25**)

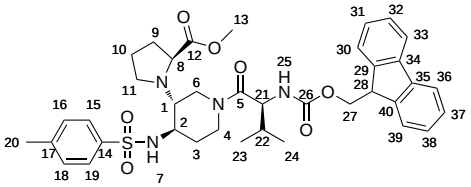

Compound **2.11** (500 mg, 1.31 mmol, 1.0 eq.) was dissolved in DMF (7.0 mL) under a nitrogen atmosphere and DIPEA (0.91 mL, 5.24 mmol, 4.0 eq) was added. This solution was let aside and meanwhile FmocNH-Val-OH (889 mg, 2.62 mmol, 2.0 eq.) was dissolved in DMF (10.0 mL) under a nitrogen atmosphere and the solution was cooled at 0°C. At this moment, HBTU (994 mg, 2.62 mmol, 2.0 eq.) and HOBt (354 mg, 2.62 mmol, 2.0 eq.) were then added at 0°C. The reaction was let stirring at 0°C for 1 h. Finally, the previous solution of compound **2.11** was added dropwise. The reaction was stirred at room temperature overnight. After concentration of the solvent under vacuum, the residue was taken up with EtOAc, washed successively with water, saturated aqueous $NaHCO_3$, brine, dried over Na_2SO_4 and the solvent evaporated under reduced pressure. The crude product obtained was purified by column chromatography on silica gel, using Cyclo/EtOAc 6:4 as eluent to afford compound **4.25** (493 mg, 0.70 mmol, Yield 53 %) as a white solid.

Molecular weight = 702.86 g mol^{-1}

$R_f = 0.35$ (Cyclo/EtOAc 6:4)

HRMS: Calcd. for $[C_{38}H_{46}N_4O_7S + H]^+$: M/z 703.3165, found: 703.3170

^{1}H NMR (DMSO – d_6, 400 MHz): δ 7.88 (4H, m, H15, H19, H33, H36); 7.72 (2H, m, H16, H18); 7.69 (2H, m, H30, H39); 7.67 (1H, bp, NH25); 7.39 (2H, m, H32, H37); 7.32 (2H, m, H31, H38); 7.00 (1H, bp, NH7); 4.18 (2H, m, H27); 4.16 (1H, m, H4); 4.14 (1H, m, H21); 4.11 (1H, m, H28); 4.08 (1H, m, H6); 3.80 (1H, m, H2); 3.66 (1H, m, H8); 3.48 (3H, s, H13); 3.05 (1H, m, H6); 2.92 (1H, m, H1); 2.75 (1H, m, H4); 2.37 (3H, s, H20); 2.34 (1H, m, H11); 2.17 (1H, m, H9); 2.02 (1H, m, H3); 1.92 (1H, m, H22); 1.70 (1H, m, H3); 1.64 (1H, m, H11); 1.48 (1H, m, H10); 1.23 (1H, m, H10); 1.13 (1H, m, H9); 0.85, 0.75 (6H, m, H23, H24) ppm

^{13}C NMR (DMSO – d_6, 100 MHz): δ 176.5 (C12); 175.8 (C5); 170.0 (C26); 143.8 (C29, C40); 142.6 (C17); 140.7 (C14); 140.6 (C34, C35); 127.6 (C32, C37); 127.1 (C31, C38); 125.5 (C16, C18); 125.4 (C30, C39); 120.2 (C15, C19, C33, C36); 65.5 (C27); 60.6 (C2); 55.4 (C21); 55.3 (C28); 52.8 (C1); 51.9 (C8); 51.8 (C13); 44.2 (C6); 44.1 (C11); 39.9 (C4); 32.7 (C9); 29.8 (C22); 29.3 (C3); 24.0 (C10); 21.0 (C20); 19.2, 18.5 (C23, C24) ppm

Melting point = 113–115 °C

IR: 3200 (N-H stretch); 2959, 2926, 2872 (C-H stretch); 1721, 1634 (C=O stretch); 1524 (N-H bend); 1449 (C=C stretch);); 1220 (C-C(O)-C stretch); 1164 (C-N stretch) cm^{-1}

(S)-methyl 1-((3R,4R)-1-((S)-2-((S)-2-(((benzyloxy)carbonyl)amino)propanamido)-3-methylbutanoyl)-4-(4-methylphenylsulfonamido)piperidin-3-yl)pyrrolidine-2-carboxylate (**4.26**)

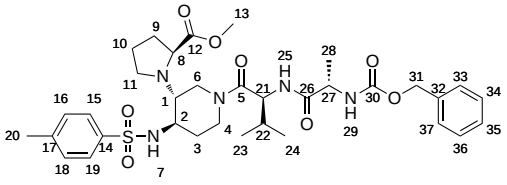

The N-protected compound **4.25** (880 mg, 1.25 mmol, 1.0 eq.) was dissolved in a 20 % solution of piperidine in DMF (10 mL) and the reaction mixture was let stirring at room temperature for 2 h. The solvent was evaporated under vacuum to give the Fmoc deprotected amine that was used for the next coupling reaction without any further purification.

The N-deprotected compound was dissolved in DMF (7.0 mL) under a nitrogen atmosphere and DIPEA (0.87 mL, 5.0 mmol, 4.0 eq) was added. This solution was let aside. Meanwhile CbzNH-Ala-OH (558 mg, 2.50 mmol, 2.0 eq.) was dissolved in DMF (10.0 mL) under a nitrogen atmosphere and the solution was cooled at 0°C. At this moment, HBTU (948 mg, 2.50 mmol, 2.0 eq.) and HOBt (338 mg, 2.50 mmol, 2.0 eq.) were then added

at 0°C. The reaction was let stirring at 0°C for 1 h. Finally, the previous solution of compound **4.25** was added dropwise. The reaction was stirred at room temperature overnight. After concentration of the solvent under vacuum, the residue was taken up with EtOAc, washed successively with water, saturated aqueous $NaHCO_3$, brine, dried over Na_2SO_4 and the solvent evaporated under reduced pressure. The crude product obtained was purified by column chromatography on silica gel using Cyclo/EtOAc 1:1 as eluent to afford compound **4.26** (656 mg, 0.96 mmol, Yield 77 %) as a white solid.

Molecular weight = 685.83 g mol^{-1}

$R_f = 0.15$ (Cyclo/EtOAc 6:4)

HRMS: Calcd. for $[C_{34}H_{47}N_5O_8S + H]^+$: M/z 686.3224, found: 686.3221

^{1}H NMR (DMSO – d_6, 400 MHz): δ 7.91 (1H, bp, NH25); 7.70 (2H, m, H15, H19); 7.44 (1H, bp, NH29); 7.41 (2H, m, H16, H18); 7.36, 7.27 (5H, m, H33, H34, H35, H36, H37); 7.18 (1H, bp, NH7); 5.01 (2H, s, H31); 4.45 (1H, m, H21); 4.24 (1H, m, H6); 4.06 (1H, m, H27); 4.05 (1H, m, H4); 3.83 (1H, m, H8); 3.64 (3H, s, H13); 3.07 (1H, m, H4); 3.01 (1H, m, H2); 2.52 (1H, m, H6); 2.38 (3H, s, H20); 2.37 (1H, m, H11); 2.35 (1H, m, H1); 2.15 (1H, m, H9); 2.03 (1H, m, H3); 1.92 (1H, m, H22); 1.73 (1H, m, H3); 1.65 (1H, m, H11); 1.50 (1H, m, H10); 1.24 (1H, m, H10); 1.14 (3H, s, H28); 1.13 (1H, m, H9); 0.81, 0.76 (6H, m, H23, H24) ppm

^{13}C NMR (DMSO – d_6, 100 MHz): δ 175.6 (C12); 172.3 (C26); 169.4 (C5); 155.5 (C30); 142.8 (C17); 136.9 (C14); 136.8 (C32); 129.6 (C16, C18); 127.7 (C33, C34, C35, C36, C37); 126.6 (C15, C19); 65.2 (C31); 60.3 (C8); 58.1 (C1); 52.7 (C21); 51.9 (C2); 51.6 (C13); 49.8 (C27); 43.8 (C11); 43.7 (C4); 39.5 (C6); 32.4 (C9); 29.7 (C22); 29.1 (C3); 23.6 (C10); 20.8 (C20); 18.2 (C23, C24); 17.7 (C28) ppm

Melting point = 123–125 °C

IR: 3294 (N-H stretch); 2963, 2929, 2874 (C-H stretch); 1720, 1665, 1625 (C=O stretch); 1519 (N-H bend); 1452 (C=C stretch);); 1220 (C-C(O)-C stretch); 1184 (C-N stretch) cm^{-1}

(S)-tert-butyl 2-(2-((1-amino-1-oxo-3-phenylpropan-2-yl)carbamoyl)hydrazinecarbonyl)-2-(4-(((benzyloxy)carbonyl)amino)butyl)hydrazinecarboxylate (**5.1**)

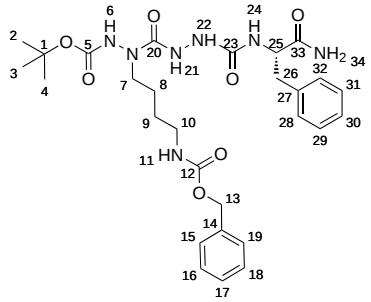

To a solution of **5.11** (360 mg, 0.7 mmol) and L-Phenylalaninamide hydrochloride (160.5 mg, 0.8 mmol; 1.1 eq.) in CH_3CN (10 mL), was added under argon atmosphere $N(Et)_3$ (0.6 mL, 4.2 mmol, 6.0 eq.). The clear solution obtained was stirred at room temperature for three days and evaporated under vaccum to give a residue which was purified by chromatography on silica gel eluting with a mixture EtOAc /MeOH 95/5 to afford compound **5.1** (143 mg, 0.25 mmol) as a white solid in Yield 35 % of yield.

Molecular weight = 585.65 g mol^{-1}

R_f = 0.70 (EtOAc/MeOH 95:5)

HRMS: Calcd. for $[C_{28}H_{39}N_7O_7 + Na]^+$: M/z 608.2809, found: 608.2808

^{1}H NMR (DMF – d_6, 400 MHz): δ 9.14 (1H, NH6); 8.65 (1H, NH22); 7.75 (3H, bp, NH21, NH34); 7.35 (5H, H28, H29, H30, H31, H32); 7.17-7.23 (5H, H15, H16, H17, H18, H19); 7.10 (1H, NH11); 6.18 (1H, NH24); 5.01 (2H, H13); 4.26 (1H, H25); 3.35 (2H, H7); 3.00 (2H, H10); 2.76, 3.06 (2H, H26); 1.43 (2H, H8); 1.42 (11H, H2, H3, H4, H9) ppm

^{13}C NMR (DMF – d_6, 100 MHz): δ 173.7(C33); 158.6 (C20); 157.9 (C5); 156.1 (C12); 155.0 (C23); 138.1, 129.1, 128.0, 126.1 (C27, C28, C29, C30, C31, C32); 137.3, 128.3, 127.7 (C14, C15, C16, C17, C18, C10); 80.1 (C1); 65.1 (C13); 54.4 (C25); 47.8 (C7); 40.1 (C10); 37.8 (C26); 28.1 (C2, C3, C4); 26.6 (C8); 24.0 (C9) ppm

Melting point = 136–138 °C

IR: 3292 (N-H stretch); 2935 (C-H stretch); 1661 (C=O stretch); 1524 (N-H bend); 1454-1368 (C=C stretch and C-N stretch); 1249-1156 (C-C stretch) cm^{-1}

Elemental analysis: Calcd. for $C_{17}H_{27}N_3O_4 \cdot 0.75\,H_2O$: C 56.12, H 6.83, N 16.37; found: C 56.33, H 6.95, N 16.03

HPLC purity (XBridge C18, 3.5 µm, H_2O + 0.1 % form. ac./ACN, gradient 5–100 % in 20 min): t_R = 14.72 min, 98 %

(S)-tert-butyl 2-(2-((1-amino-3-methyl-1-oxobutan-2-yl)carbamoyl)-2-methylhydrazinecarbonyl)-2-isopropylhydrazinecarboxylate (**5.2**)

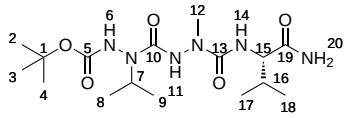

To a solution of L-Valinamide hydrochloride (68.7 mg, 0.45 mmol; 1.1 eq.) in DMF (5 mL), were added under argon atmosphere DIPEA (0.16 mL, 0.90 mmol, 2.2 eq.) and p-nitrophenyl chloroformate (90.7 mg, 0.45 mmol, 1.1 eq.). The clear solution obtained was stirred at room temperature. After formation of the activated intermediate, a solution of compound **5.15a** (100 mg, 0.41 mmol) and DMAP (20.1 mg, 0.41 mmol, 1.0eq.) was added to the reaction mixture and the reaction was stirred overnight at room temperature. Then, the solvent was evaporated under vacuum to give a residue which was purified by chromatography on silica gel eluting with a mixture EtOAc /MeOH 90/10 to afford compound **5.2** (95 mg, 0.24 mmol) as a white solid. Yield 60 %.

Molecular weight = 388.46 g mol^{-1}

R_f = 0.30 (EtOAc/MeOH 90:10)

HRMS: Calcd. for $[C_{16}H_{32}N_6O_5 + H]^+$: M/z 389.2512, found: 389.2505

^{1}H NMR (DMSO – d_6, 400 MHz): δ 8.90 (2H, bp, NH); 7.14 (2H, bp, NH2); 5.96 (1H, bp, NH); 4.36 (1H, m, H7); 3.89 (1H, m, H15); 2.92 (3H, s, H12); 2.05 (1H, m, H16); 1.44 (9H, s, H2, H3, H4); 1.03 (6H, m, H8, H9); 0.84 (6H, m, H17, H18) ppm

^{13}C NMR (DMSO – d_6, 100 MHz): δ 174.22, 158.31, 156.63, 156.05 (C5, C10, C13, C19); 80.47 (C1); 59.16 (C15); 48.86 (C7); 36.06 (C12); 29.89 (C16); 28.48 (C2, C3, C4); 19.86, 19.73, 19.20, 17.90 (C8, C9, C17, C18) ppm

Melting point = 283–285 °C

IR: 3417-3197 (N-H stretch); 2978 (C-H stretch); 1710-1653 (C=O stretch); 1533 (N-H bend); 1393-1333 (CH3 bend); 1275-1157 (C-N stretch) cm^{-1}

Elemental analysis: Calcd. for $C_{16}H_{32}N_6O_5$: C 49.47, H 8.30, N 21.63; found: C 50.39, H 8.31, N 21.01

HPLC purity (XBridge C18, 3.5 µm, H_2O + 0.1 % form. ac./ACN, gradient 5–100 % in 20 min): t_R = 11.78 min, 100 %

(S)-tert-butyl 2-(2-((1-(benzyloxy)-3-methyl-1-oxobutan-2-yl)carbamoyl)-2-methylhydrazinecarbonyl)-2-isopropylhydrazinecarboxylate (**5.3**)

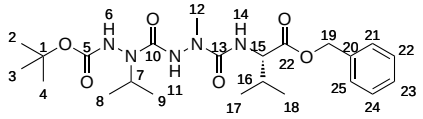

To a solution of H-L-Val-OBn hydrochloride (110 mg, 0.45 mmol; 1.1 eq.) in DMF (5 mL), were added under argon atmosphere DIPEA (0.16 mL, 0.90 mmol, 2.2 eq.) and p-nitrophenyl chloroformate (90.7 mg, 0.45 mmol, 1.1 eq.). The clear solution obtained was stirred at room temperature. After formation of the activated intermediate, a solution of compound **5.18** (100 mg, 0.41 mmol) and DMAP (20.1 mg, 0.41 mmol, 1.0eq.) was added to the reaction mixture and the reaction was stirred overnight at room temperature. After evaporation of the solvent under vacuum, the oily residue obtained was purified by chromatography on silica gel eluting with a mixture EtOAc 100 % to afford compound **5.3** (130 mg, 0.27 mmol) as a white solid. Yield 66 %.

Molecular weight = 479.57 g mol^{-1}

$R_f = 0.53$ (EtOAc)

HRMS: Calcd. for $[C_{23}H_{37}N_5O_6 + H]^+$: M/z 480.2822, found: 480.2823

^{1}H NMR (DMSO–d_6, 400 MHz): δ 7.33 (5H, m, H21, H22, H23, H24, H25); 7.18 (1H, bp, NH11); 6.35 (1H, bp, NH6); 6.19 (1H, bp, NH14); 5.16 (2H, dd, H19); 4.66 (1H, m, H7); 4.42 (1H, m, H15); 3.14 (3H, s, H12); 2.09 (1H, m, H16); 1.49 (9H, s, H2, H3, H4); 1.12 (6H, d + d, J = 6.4 Hz, H8, H9).0.93 (6H, m, H17, H18) ppm

^{13}C NMR (DMSO–d_6, 100 MHz): δ 173.0 (C22); 158.6 (C13); 151.9 (C10); 144.5 (C5); 135.9 (C20); 128.6, 128.3 (C21, C22, C23, C24, C25); 82.9 (C1); 66.5 (C19); 58.7 (C15); 48.9 (C7); 36.2 (C12); 31.1 (C16); 28.1 (C2, C3, C4); 19.2 (C8, C9); 18.9 (C17, C18) ppm

Melting point = 174–176 °C

IR: 3391, 3296 (N-H stretch); 2975 (C-H stretch); 1740, 1725, 1673, 1643 (C=O stretch); 1536, 1494 (N-H bend); 1272, 1243 (C-N stretch); 1179 (C-C(O)-C stretch) cm^{-1}

HPLC purity (XBridge C18, 3.5 µm, H_2O + 0.1 % form. ac./ACN, gradient 5–100 % in 20 min): t_R = 17.63 min, 97 %

Carbamic acid, N-(4,4-diethoxybutyl)-, phenylmethyl ester (**5.6**)

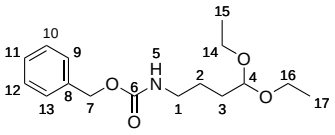

Noel P. McLaughlin and Paul Evans; J. Org. Chem. 2010, 75, 518–521.

To a solution of 4-aminobutyraldehyde diethylacetal (1.0 g, 6.2 mmol, 1.1 mL) and TEA (1.72 mL, 12.4 mmol, 2.0 eq.) in DCM (10 mL), was added dropwise at 0° C benzyl chloroformate (1.75 mL, 12.4 mmol, 2.0 eq.). The resulting mixture was stirred at room temperature overnight. The reaction mixture was then washed successively with a saturated solution of NH_4Cl , brine, dried over Na_2SO_4 and filtered. After evaporation of the solvent under vacuum, the crude product was purified by flash column chromatography on silica gel (c-Hex/EtOAc 3:1) to yield the title compound **5.6** (1.06 g 6.2 mmol) as a colourless oil. Yield 58 %.

Molecular weight = 295.37 g mol^{-1}

$R_f = 0.50$ (Cyclo/EtOAc 3:1)

HRMS: Calcd. for $[C_{16}H_{25}NO_4 + Na]^+$: M/z 318.1681, found: 318.1678

^{1}H NMR ($CDCl_3$, 300 MHz): δ 7.12 (5H, m, H9, H10, H11, H12, H13); 4.96 (3H, m, H7, NH); 4.49 (1H, t, J = 7.8 Hz, H4); 3.49 (4H, q, J = 7.0 Hz, H14, H16); 3.33 (2H, m, H1); 1.66 (4H, m, H2, H3); 1.02 (6H, t, J=7.0 Hz, H15, H17) ppm

Benzyl 2-hydroxypyrrolidine-1-carboxylate (**5.7**)

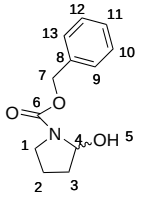

Noam S. Freeman et al.; Tetrahedron 2009, 65, 1737–1745 Xiang Y.G. et al.; Chemical Communications 2009, 45, 7045–7047.

A solution of CbZ protected 4-amino butyraldehyde diethyl acetal **5.6** in AcOH/water 2:1 v/v was stirred at room temperature overnight . After treatment, a colourless oil was obtained and immediately used without further purification in the next step. Yield 94 %.

Molecular weight = 221.25 g mol^{-1}

HRMS: Calcd. for $[C_{16}H_{25}NO_4 + Na]^+$: M/z 244.0950, found: 244.0942

^{1}H NMR (DMSO – d_6, 300 MHz): δ 7.36 (6H, m, H9, H10, H11, H12, H13, OH); 5.08 (2H, m, H7); 4.51 (1H, m, H4); 3.38 (2H, m, H1); 1.84 (4H, m, H2, H3) ppm

Tert-butyl 2-(4-(((benzyloxy)carbonyl)amino)butyl)hydrazinecarboxylate (**5.8**)

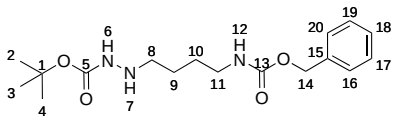

Noam S. Freeman et al.; Tetrahedron 2009, 65, 1737–1745.

A solution of tert-butyl carbazate (450 mg, 3.4 mmol, 1.0 eq.) and **5.7** (750 mg, 3.4 mmol, 1.0 eq.) in dry THF (0.65M) was stirred overnight at rt with 0.9 eq. of APTS (186 mg, 3.1 mmol, 0.9 eq.). Then, it was concentrated under vacuum to obtain the corresponding hydrazine, which was subsequently used without further purification. The hydrazine was dissolved in dry THF (0.15M) and treated with $NaBH_3CN$ (320 mg, 5.1 mmol, 1.5 eq.) under vigourous stirring. At this moment, acetic acid (408mg, 6.8 mmol, 0.4 mL, 2.0 eq.) was added and the reaction was stirred overnight at rt. It was noteworthy that additional $NaBH_3CN$ could be added if necessary to ensure completion of the reaction monitored by TLC (PE/EA 1:1). After evaporation of the solvent under vacuum the resulting residue was portioned between EtOAc and brine. The organic layer was successively washed with saturated aqueous $NaHCO_3$, brine, dried over Na_2SO_4 and concentrated under reduced pressure. The crude residue was then dissolved in MeOH , treated with 1M NaOH (163.2 mg, 4.08 mmol, 1.2 eq.) and stirred for 1h at rt. After removing the solvent under vaccum the residue was dissolved in EtOAc, washed with brine, dried over Na_2SO_4 and concentrated under vacuum to provide the desired compound. Purification by flash chromatography on silica gel using EtOAc/hexane 6:4 as eluent gave a white solid (562 mg, 1.67 mmol). Yield 49 %.

Molecular weight = 337.41 g mol^{-1}

R_f = 0.40 (EtOAc/hexane 6:4)

HRMS: Calcd. for $[C_{17}H_{27}N_3O_4 + Na]^+$: M/z 244.0950, found: 244.0942

^{1}H NMR ($CDCl_3$, 300 MHz): δ 7.31 (5H, m, H16, H17, H18, H19, H20); 5.74 (1H, bp, NH); 5.21 (1H, bp, NH); 5.07 (2H, s, H14); 3.44 (1H, bp, NH); 3.18 (2H, dd, J = 5.8 Hz, H8); 2.87 (2H, t, J = 6.5 Hz, H11); 1.51 (4H, m, H9, H10); 1.44 (9H, s, H2, H3, H4) ppm

^{13}C NMR ($CDCl_3$, 75 MHz): δ 203.5, 156,6 (C5, C13); 136.6 (C15); 128.5, 128.1 (C16, C17, C18, C19, C20); 84.0 (C1); 66.7 (C14); 51.1 (C8); 40.3 (C11); 28.1 (C2, C3, C4); 26.7 (C9); 21.5 (C10) ppm

Melting point = 67–69 °C

IR: 3350-3299 (N-H stretch); 2934-2866 (C-H stretch); 1687 (C=O stretch); 1532 (N-H bend); 1456 (C=C stretch aromatic) cm^{-1}

2-tert-butyl 1-(4-nitrophenyl) 1-(4-(((benzyloxy)carbonyl)amino)butyl)hydrazine-1,2-dicarboxylate (**5.9**)

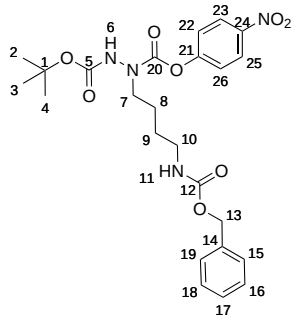

To a solution of **5.8** (443.1 mg, 1.31 mmol) in dry DCM (4 mL), pyridine (0.23 mL, 2.88 mmol, 2.2 eq.) was added at 0°C under argon atmosphere. After 10 minutes, a solution of p-nitro phenyl chloroformate (290.5 mg, 1.44 mmol, 1.1 eq.) in dry DCM was introduced dropwise and the reaction was stirred at 0°C for 40 minutes then at room temperature overnight. After evaporation of the solvent, the residue obtained was diluted in EtOAc. The organic phase was successively washed with 10 % citric acid, distilled water, 10 % aqueous K_2CO_3 and finally brine and dried over Na_2SO_4, filtered and concentrated. The white solid (560.2 mg, 1.12 mmol) obtained was sufficiently pure to be used in the next step. Yield 85 %.

Molecular weight = 502.52 g mol^{-1}

R_f = 0.85 (EtOAc/hexane 6:4)

HRMS: Calcd. for $[C_{24}H_{30}N_4O_8 + Na]^+$: M/z 525.1961, found: 525.1964

^{1}H NMR ($CDCl_3$, 300 MHz): δ 8.24 (2H, d, , J = 9.0 Hz, H23, H25); 7.32 (7H, m, H15, H16, H17, H18, H19, H22, H26); 6.83 (1H, bp, NH); 5.13 (2H, s, H13); 4.92 (1H, bp, NH); 3.71 (2H, m, H7); 3.24 (2H, s, H10); 1.68 (4H, m, H8, H9); 1.46 (9H, s, H2, H3, H4) ppm

^{13}C NMR ($CDCl_3$, 75 MHz): δ 156.44, 155.28, 154.90, 153,81, 145.20 (C5, C12, C20,C21, C24); 136.50 (C21); 128.51, 128.12 (C15, C16, C17, C18, C19); 125.16 (C23, C25); 122.30, 122.15 (C22, C26); 81.97 (C1); 66.72 (C13); 50.07 (C7); 40.50 (C10); 28.14 (C2, C3, C4); 27.01 (C8); 23.94 (C9) ppm

Melting point = 96–98 °C

IR: 3320 (N-H stretch); 2946-2872 (C-H stretch); 1744-1687 (C=O stretch); 1520-1496 (-NO2 aromatic); 1348 (-NO2 aromatic) cm^{-1}

Tert-butyl 2-(4-(((benzyloxy)carbonyl)amino)butyl)-2-(hydrazinecarbonyl)-hydrazinecarboxylate (**5.10**)

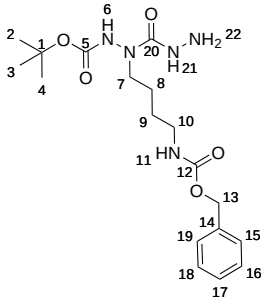

To a solution of **5.9** (200 mg, 0.4 mmol) in MeOH (4 mL), hydrazine monohydrate (0.12 mL, 2.4 mmol, 6.0 eq.) was added. The reaction was stirred overnight at room temperature (25°C). After evaporation of the solvent under vacuum, the residue was purified by flash chromatography on silica gel using EtOAc/MeOH 9:1 as eluent to afford compound **5.10** as a white solid (130 mg, 0.33 mmol). Yield 82 %.

Molecular weight = 395.45 g mol^{-1}

R_f = 0.60 (EtOAc/MeOH 9:1)

HRMS: Calcd. for $[C_{18}H_{29}N_5O_5 + H]^+$: M/z 396.2247, found: 396.2248

^{1}H NMR (Acetone–d_6, 300 MHz): δ 8.52 (2H, bp, NH); 7.31 (5H, m, H15, H16, H17, H18, H19); 6.37 (1H, bp, NH); 5.01 (2H, s, H13); 3.43 (2H, m, H7); 3.12 (2H, m, H10); 2.83 (2H, bp, NH2); 1.58 (4H, m, H8, H9); 1.44 (9H, s, H2, H3, H4) ppm

^{13}C NMR (Acetone–d_6, 75 MHz): δ 204.93, 155.89, 155.45 (C5, C12, C20); 137.65 (C14); 128.26, 127.61 (C15, C16, C17, C18, C19); 80.52 (C1); 65.44 (C13); 47.29 (C7); 40.18 (C10); 27.49 (C2, C3, C4); 26.94 (C8); 24.37 (C9) ppm

Melting point = 42–44 °C (hygroscopic solid)

IR: 3303 (N-H stretch); 2977-2934 (C-H stretch); 1699 (C=O stretch); 1515-1455 (C=C stretch); 1247-1157 (C-C stretch) cm^{-1}

Phenyl 5-((tert-butoxycarbonyl)amino)-4,11-dioxo-13-phenyl-12-oxa-2,3,5,10--tetraazatridecan-1-oate (**5.11**)

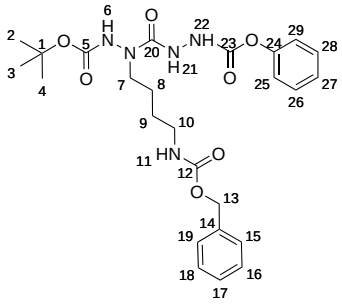

To a solution of **5.10** (128 mg; 0.32 mmol) in dry THF (100 mL) was added under argon atmosphere pyridine (64 L; 0.8 mmol; 2.5 eq.) and the mixture was stirred until a homogeneous solution was obtained. At this moment, phenyl chloroformate (44 µL; 0.35 mmol, 1.1 eq.) was introduced to the solution cooled to 0 ºC. After stirring for 15 min at rt, the solvent was evaporated under reduced pressure and the residue was dissolved in EtOAc (100 mL). The organic layer was washed successively with 10 % aqueous citric acid, distilled water, 10 % aqueous K_2CO_3, brine, dried over Na_2SO_4, filtered and concentrated under vacuum. The residue obtained was purified by flash chromatography on silica gel using EtOAc/Cyclohexane 6:4 as eluent to yield compound **5.11** as a white solid (158 mg, 0.31 mmol). Yield 96 %.

Molecular weight = 515.56 g mol^{-1}

R_f = 0.35 (EtOAc/Cyclohexane 6:4)

HRMS: Calcd. for $[C_{25}H_{33}N_5O_7 + Na]^+$: M/z 538.2278, found: 538.2277

^{1}H NMR ($CDCl_3$, 300 MHz): δ 7.48 (2H, bp, NH); 7.26 (10H, m, H15, H16, H17, H18, H19, H25, H26, H27, H28, H29); 5.31 (1H, bp, NH); 5.08 (2H, s, H13); 3.68 (2H, m, H7); 3.14 (2H, m, H10); 2.53 (1H, bp, NH); 1.33 (13H, s, H2, H3, H4, H8, H9) ppm

^{13}C NMR ($CDCl_3$, 75 MHz): δ 157.94, 156.80, 155.71, 154.78 (C5, C12, C20, C23); 150.65, 136.65 (C14, C24); 129.30, 128.45, 128.00, 125.66, 121.42 (C15, C16, C17, C18, C19, C25, C26, C27, C28, C29); 82.39 (C1); 65.58 (C13); 48.30 (C7); 40.59 (C10); 28.13 (C2, C3, C4); 26.72 (C8); 23.94 (C9) ppm

Melting point = 65–67 °C

IR: 3285 (N-H stretch); 2933 (C-H stretch); 1697 (C=O stretch); 1593 (N-H bend); 1518-1456 (C=C stretch); 1248-1158 (C-C stretch) cm^{-1}

Tert-butyl 2-isopropylhydrazinecarboxylate (**5.12**)

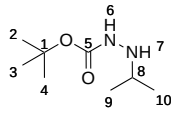

To a solution of tert-butyl carbazate (2.0 g, 15.1 mmol) and acetone (3.3 mL, 45.3 mmol, 3.0 eq.) in dry THF (0.65 M, 20 mL), was adding a catalytic amount of acetic acid (0.78 mL, 13.6 mmol, 0.9 eq.). The mixture was stirred overnight at room temperature. After concentration under vacuum the crude imine obtained was used without further purification. The imine was dissolved in dry THF (0.15 M, 100 mL) and treated with $NaBH_3CN$ (1.42 g, 22.7 mmol, 1.5 eq.) under vigorous stirring. A few granules of bromocresol green were introduced and the resulting blue solution was treated dropwise with p-toluenesulfonic acid monohydrate (2.86 g, 16.6 mmol, 1.1 eq.) in THF (4mL). Every addition of the acid solution was performed after indicator toning to maintain the reaction pH between 3.5 and 5. After the yellowish color persisted for 1 hour, the solvent was removed under reduced pressure and the residue was portioned between EtOAc and brine. The aqueous phase was extracted with EtOAc three times. The combined organic layers were successively washed with saturated aqueous $NaHCO_3$, brine, dried over $MgSO_4$ and concentrated under reduced pressure. The residue obtained was dissolved in MeOH (10 mL), treated with 1 M NaOH (18 mL, 18.1 mmol, 1.2 eq.) and stirred for 1 hour at room temperature. The solvent was removed under reduced pressure and the resulting residue was dissolved in EtOAc, washed with brine, dried over $MgSO_4$ and concentrated under vacuum to provide the desired compound that was purified by flash chromatography on silica gel using DCM/MeOH 98:2 as eluent. The product **5.12** (2.1 g, 12.1 mmol) was afforded as white solid. Yield 80 %.

Molecular weight = 174.24 g mol^{-1}

R_f = 0.50 (DCM/MeOH 98:2)

HRMS: Calcd. for $[C_8H_{18}N_2O_2 + Na]^+$: M/z 197.1266, found: 197.1266; Calcd. for $[C_{16}H_{37}N_4O_4 + Na]^+$: $2M/z$ 349.2815, found: 349.2816

^{1}H NMR ($CDCl_3$, 300 MHz): δ 5.31 (2H, bp, NH); 3.28 (1H, dt, J = 12.26, 6.3 Hz, H8); 1.47 (9H, s, H2, H3, H4); 1.12 (6H, d, J = 6.4 Hz, H9, H10) ppm

^{13}C NMR ($CDCl_3$, 75 MHz): δ 156.85 (C5); 80.34 (C1); 50.75 (C8); 28.33 (C2, C3, C4); 20.56 (C9, C10) ppm

Melting point = 89–91 °C

IR: 3278 (N-H stretch); 2973 (C-H stretch); 1701 (C=O stretch); 1474 (N-H bend); 1383-1365 (CH3 bend); 1149 (C-N stretch) cm^{-1}

Benzyl 2-(2-(tert-butoxycarbonyl)-1-isopropylhydrazinecarbonyl)-1-methylhydrazinecarboxylate (**5.15b**)

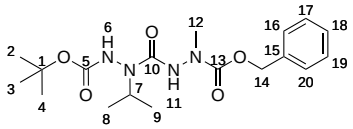

To a solution of **5.17** (800 mg, 2.32 mmol) in dry DCM (20 mL), compound **5.16** (404.2 mg, 2.32 mmol, 1.0 eq.) and DMAP (283.4 mg, 2.32 mmol, 1.0 eq.) were added. The reaction was stirred overnight at room temperature. After evaporation of the solvent under vacuum, the residue was purified by flash chromatography on silica gel using EtOAc/Cyclohexane 1:1 as eluent to afford compound **5.15b** (777,5 mg, 2.04 mmol) as a white solid. Yield 88 %.

Molecular weight = 380.44 g mol^{-1}

R_f = 0.55 (EtOAc/Cyclohexane 1:1)

HRMS: Calcd. for $[C_{18}H_{28}N_4O_5 + Na]^+$: M/z 403.1957, found: 403.1958

^{1}H NMR ($CDCl_3$, 300 MHz): δ 7.33 (5H, s, H16, H17, H18, H19, H20); 6.58 (1H, bp, NH); 6.12 (1H, bp, NH); 5.15 (2H, s, H14); 4.58 (1H, m, J = 13.3, 6.6 Hz, H7); 3.21 (3H, s, H12); 1.47 (9H, s, H2, H3, H4); 1.13 (6H, bp, H8, H9) ppm

^{13}C NMR ($CDCl_3$, 75 MHz): δ 163.29, 157.14, 155.32 (C5, C10, C13); 135.99 (C15); 128.48, 128.12, 127.86 (C16, C17, C18, C19, C20); 82.21 (C1); 68.08 (C14); 48.90 (C7); 38.56 (C12); 28.09 (C2, C3, C4); 19.52, 19.09 (C8, C9) ppm

Melting point = 49–51 °C

IR: 3283 (N-H stretch); 2979 (C-H stretch); 1695 (C=O stretch); 1499 (N-H bend); 1392-1336 (CH3 bend); 1155 (C-N stretch) cm^{-1}

Benzyl 1-methylhydrazinecarboxylate (**5.16**)

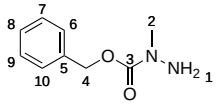

Malachowski W.P. et al.; J. Org. Chem. 2002, 67, 8962–8969.

Methyl hydrazine (2.0 mL, 38.0 mmol, 1.0 eq.) was dissolved in DCM (20 mL) and cooled at 0°C. An aqueous solution of NaOH (30.4 mL, 30.4 mmol, 0.8 eq.) was added slowly and the biphasic mixture was stirred rapidly for 5 min. At this moment, benzyl chloroformate (4.3 mL, 30.4 mmol, 0.8 eq.) was added dropwise and the reaction was slowly warmed to room temperature and stirred for 4 h. Then, the biphasic mixture was separated and the organic

layer was successively washed with water, brine, dried over Na_2SO_4, filtered and concentrated under vacuum. Purification of the crude oil by distillation (bp 104-134 °C, 0.2 mmHg) provided pure product as colourless oil (2.56 g, 14.2 mmol). Yield 47 %.

Molecular weight = 180.20 g mol^{-1}

HRMS: Calcd. for $[C_9H_{12}N_2O_2 + H]^+$: M/z 181.0977, found: 181.0974; Calcd. for $[C_9H_{12}N_2O_2 + Na]^+$: M/z 203.0796, found: 203.0798

^{1}H NMR ($CDCl_3$, 300 MHz): δ 7.33 (5H, m, H6, H7, H8, H9, H10); 5.12 (2H, s, H4); 4.38 (2H, s, NH2); 3.13 (3H, s, H2) ppm

^{13}C NMR ($CDCl_3$, 75 MHz): δ 136.45 (C5); 128.54, 128.18, 128.02 (C6, C7, C8, C9, C10); 67.66 (C4); 38.40 (C2) ppm

IR: 3332 (N-H stretch); 2953 (C-H stretch); 1694 (C=O stretch); 1498-1454 (N-H bend); 1392-1350 (CH3 bend); 1159 (C-N stretch) cm^{-1}

1-benzyl 2-(4-nitrophenyl) 1-methylhydrazine-1,2-dicarboxylate (**5.17**)

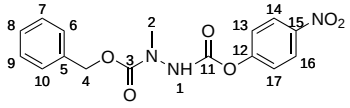

To a solution of **5.16** (500 mg, 2.77 mmol) in dry DCM (5 mL), pyridine (0.5 mL, 6.09 mmol, 2.2 eq.) was added at 0°C under argon atmosphere. After 10 minutes, a solution of p-nitro phenyl chloroformate (614.2 mg, 3.05 mmol, 1.1 eq.) in dry DCM was introduced dropwise and the reaction was stirred at 0°C for 40 minutes and at room temperature overnight. After evaporation of the solvent, the residue obtained was diluted in EtOAc. The organic phase was successively washed with 10 % citric acid, distilled water, 10 % aqueous K_2CO_3, brine, dried over Na_2SO_4, filtered and concentrated. The pale yellow oil (886.3 mg, 2.57 mmol) obtained was sufficiently pure to be used for the next step. Yield 93 %.

Molecular weight = 345.31 g mol^{-1}

R_f = 0.40 (Cyclo/EtOAc 6:4)

HRMS: Calcd. for $[C_{16}H_{15}N_3O_6 + Na]^+$: M/z 368.0859, found: 368.0852

^{1}H NMR ($CDCl_3$, 300 MHz): δ 8.23 (2H, d, J= 7.9 Hz, H14, H16); 7.32 (8H, m + bp, H6, H7, H8, H9, H10, H13, H17, NH); 5.21 (2H, s, H4); 3.29 (3H, s, H2) ppm

^{13}C NMR ($CDCl_3$, 75 MHz): δ 155.1 (C17); 145.2 (C15); 135.6 (C5); 128.6, 125.2, 121.9 (C6, C7, C8, C9, C10); 128.5, 128.1 (C13, C14, C16, C17); 68.6 (C4); 38.1 (C2) ppm

IR: 3287 (N-H stretch); 3084-2955 (C-H stretch); 1765-1709 (C=O stretch); 1616-1594 (-NO2 aromatic); 1522-1424 (N-H bend); 1345 (CH3 bend); 1212-1157 (C-N stretch) cm^{-1}

Tert-butyl 2-isopropyl-2-(2-methylhydrazinecarbonyl)hydrazinecarboxylate (**5.15a**)

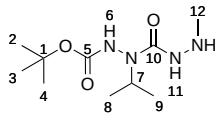

Compound **5.15b** (720 mg, 1.89 mmol, 1.0 eq.) was dissolved in MeOH (15 mL). Pd/C 10 % (144 mg, 20 % mass) was added and the reaction mixture was stirred overnight at room temperature under hydrogen atmosphere. The reaction mixture was filtered through a pad of Celite and after washing the pad of Celite several times with MeOH, the filtrate was evaporated under vacuum to afford compound **5.15a** (441 mg, 1.79 mmol) as white solid. Yield 95 %.

Molecular weight = 246.31 g mol^{-1}

$R_f = 0$ (EtOAc/Cyclohexane 1:1)

HRMS: Calcd. for $[C_{10}H_{22}N_4O_3 + H]^+$: M/z 257.1770, found: 257.1775; Calcd. for $[C_{10}H_{22}N_4O_3 + Na]^+$: M/z 269.1590, found: 269.1602

^{1}H NMR ($CDCl_3$, 300 MHz): δ 6.79 (2H, bp, NH); 4.57 (1H, m, J = 13.4, 6.7 Hz, H7); 4.35 (1H, bp, NH); 2.58 (3H, s, H12); 1.45 (9H, s, H2, H3, H4); 1.09 (6H, bp, H8, H9) ppm

^{13}C NMR ($CDCl_3$, 75 MHz): δ 158.22, 158.15 (C5, C10); 81.90 (C1); 48.46 (C7); 39.67 (C12); 28.10 (C2, C3, C4); 19.44, 19.25 (C8, C9) ppm

Melting point = 47–49 °C

IR: 3248 (N-H stretch); 2978 (C-H stretch); 1713-1643 (C=O stretch); 1469 (N-H bend); 1391-1314 (CH3 bend); 1239-1159 (C-N stretch) cm^{-1}

(S)-methyl 2-((S)-2-((tert-butoxycarbonyl)amino)-3-methylbutanamido)propanoate (**ValAla**)

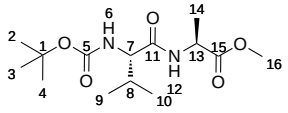

Boc-NH-Val-OH (500 mg, 2.3 mmol, 1.0 eq.) was dissolved in DMF (10.0 mL) under a nitrogen atmosphere and the solution was cooled at 0°C. At this moment, HOBt (387 mg, 2.5 mmol, 1.1 eq.) and HBTU (960 mg, 2.5 mmol, 1.1 eq.) were added. The solution was stirred at 0°C between 30 min and 1h and then the solution of alanine methyl ester hydrochloride (321 mg, 2.3 mmol, 1.0 eq.) and DIPEA (1.2 mL, 6.9 mmol, 3.0 eq.) in DMF (10.0 mL) was added. The reaction was stirred at room temperature overnight. After evaporation of the solvent under vacuum, the oily residue was taken

up with EtOAc and successively washed with 10 % aqueous citric solution, water, 10 % aqueous K_2CO_3 solution, brine, dried over Na_2SO_4, filtered and evaporated under reduced pressure to afford a residue which was purified by column chromatography on silica gel using Cyclohexane/EtOAc 7:3 as eluent to afford compound **ValAla** (564 mg, 1.87 mmol) as a white solid. Yield 81 %.

Molecular weight = 302.37 g mol^{-1}

R_f = 0.35 (Cyclohexane /EtOAc 7:3)

HRMS: Calcd. for $[C_{14}H_{26}N_2O_5 + Na]^+$: M/z 325.1739, found: 325.1746

^{1}H NMR (DMSO – d_6, 300 MHz): δ 8.29 (1H, d, J = 6.5 Hz, NH12); 6.61 (1H, d, J = 9.0 Hz, NH6); 4.25 (1H, m, H13); 3.78 (1H, m, H7); 3.60 (3H, s, H16); 1.92 (1H, m, H8); 1.37 (9H, s, H2, H3, H4); 1.27 (3H, d, J = 7.3 Hz, H14); 0.88 (3H, d, J = 6.7 Hz, H9); 0.86 (3H, d, J = 6.7 Hz, H10) ppm

^{13}C NMR (DMSO – d_6, 75 MHz): δ 172.9 (C15); 171.3 (C11); 155.4 (C5); 78.0 (C1); 59.1 (C7); 51.8 (C16); 47.5 (C13); 30.6 (C8); 28.2 (C2, C3, C4); 19.1, 18.0 (C9, C10); 16.9 (C14) ppm

Melting point = 142–144 °C

IR: 3310 (N-H stretch); 2976 (C-H stretch); 1751, 1682, 1649 (C=O stretch); 1557, 1524 (N-H bend); 1160 (C-C(O)-C stretch) cm^{-1}

(S)-2-((S)-2-((tert-butoxycarbonyl)amino)-3-methylbutanamido)propanoic acid (**ValAlaOH**)

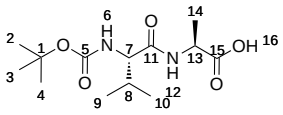

Compound **ValAla** (495 mg, 1.64 mmol, 1.0 eq.) was dissolved in MeOH (20.0 mL) and an aqueous solution of NaOH 2 M (4.1 mL, 8.19 mmol, 5.0 eq.) was added dropwise to the solution. The reaction was stirred at 60° C for 1 h. The solvents were evaporated and the solid obtained was solubilized in water. The mixture was acidified with 10 % aqueous $KHSO_4$ solution until pH = 2-3. At this moment, the product was extracted from the water phase with DCM. The organic phase was dried over Na_2SO_4 and evaporated under vacuum to afford compound **ValAlaOH** (435 mg, 1.51 mmol) as a white solid. Yield 92 %.

Molecular weight = 288.34 g mol^{-1}

R_f = 0 (Cyclohexane /EtOAc 7:3)

HRMS: Calcd. for $[C_{13}H_{24}N_2O_5 + H]^+$: M/z 289.1763, found: 289.1765; Calcd. for $[C_{13}H_{24}N_2O_5 + Na]^+$: M/z 311.1583, found: 311.1583

^{1}H NMR (DMSO – d_6, 300 MHz): δ 12.55 (1H, bp, H16); 8.10 (1H, d, J = 6.9 Hz, NH12); 6.61 (1H, d, J = 9.0 Hz, NH6); 4.17 (1H, dd, J = 14.2, 7.1

Hz, H13); 3.82 (1H, m, H7); 1.94 (1H, m, H8); 1.37 (9H, s, H2, H3, H4); 1.26 (3H, d, J = 7.3 Hz, H14); 0.84 (3H, d, J = 6.7 Hz, H9); 0.83 (3H, d, J = 6.7 Hz, H10) ppm

^{13}C NMR (DMSO – d_6, 75 MHz): δ 174.0 (C15); 171.0 (C11); 155.4 (C5); 78.0 (C1); 59.2 (C7); 47.4 (C13); 30.6 (C8); 28.2 (C2, C3, C4); 19.2, 18.0 (C9, C10); 17.2 (C14) ppm

Melting point = 92–94 °C

IR: 3307 (N-H stretch, O-H stretch); 2971, 2934 (C-H stretch); 1723, 1682, 1649 (C=O stretch); 1525 (N-H bend); 1160 (C-C(O)-C stretch) cm^{-1}

tert-butyl ((S)-1-(((S)-1-(((S)-1-amino-3-methyl-1-oxobutan-2-yl)amino)-1-oxopropan-2-yl)amino)-3-methyl-1-oxobutan-2-yl)carbamate (**ValAlaVal**)

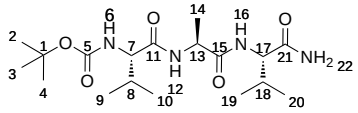

Compound **ValAlaOH** (417 mg, 1.45 mmol, 1.0 eq.) was dissolved in DMF (10.0 mL) under a nitrogen atmosphere and the solution was cooled at 0°C. At this moment, HOBt (245 mg, 1.6 mmol, 1.1 eq.) and HBTU (607 mg, 1.6 mmol, 1.1 eq.) were added. The solution was stirred at 0°C between 30 min and 1h and then the solution of valinamide hydrochloride (221 mg, 1.45 mmol, 1.0 eq.) and DIPEA (0.74 mL, 4.35 mmol, 3.0 eq.) in DMF (10.0 mL) was added. The reaction was stirred at room temperature overnight. After evaporation of the solvent under vacuum, the oily residue obtained was taken up with EtOAc. After a few minutes a white solid precipitated which after filtration afforded compound **ValAlaVal** (440 mg, 1.14 mmol) as a white solid. Yield 79 %.

Molecular weight = 386.49 g mol^{-1}

HRMS: Calcd. for $[C_{18}H_{34}N_4O_5 + H]^+$: M/z 387.2607, found: 387.2602; Calcd. for $[C_{18}H_{34}N_4O_5 + Na]^+$: M/z 409.2427, found: 409.2427

^{1}H NMR (DMSO – d_6, 400 MHz): δ 7.92 (1H, d, J = 7.2 Hz, H12); 7.69 (1H, d, J = 8.9 Hz, NH16); 7.36 (1H, s, NH22); 7.01 (1H, s, NH22); 6.71 (1H, d, J = 8.9 Hz, NH6); 4.38 (1H, m, H13); 4.09 (1H, dd, J = 8.8, 6.5 Hz, H17); 3.80 (1H, m, H7); 1.94 (2H, m, H8, H18); 1.37 (9H, s, H2, H3, H4); 1.19 (3H, d, J = 6.9 Hz, H14); 0.82 (12H, m, H9, H10, H19, H20) ppm

^{13}C NMR (DMSO – d_6, 100 MHz): δ 172.7 (C21); 171.8 (C15); 170.9 (C11); 155.4 (C5); 78.0 (C1); 59.5 (C7); 57.2 (C17); 48.0 (C13); 30.5, 30.3 (C8, C18); 28.2 (C2, C3, C4); 19.2, 17.9, 17.8 (C9, C10, C19, C20); 18.1 (C14) ppm

Melting point = 266–270 °C

IR: 3293 (N-H stretch); 2960 (C-H stretch); 1671, 1626 (C=O stretch); 1529 (N-H bend) cm^{-1}
Elemental analysis: Calcd. for $C_{18}H_{34}N_4O_5 \cdot 1.5\,H_2O$: C 52.28, H 9.04, N 13.55; found: C 52.37, H 8.24, N 13.60
HPLC purity (XBridge C18, 3.5 µm, H_2O + 0.2 % form. ac./ACN, gradient 5–100 % in 20 min): t_R = 11.90 min, 100 %

(S)-tert-butyl 2-(2-((1-amino-3-methyl-1-oxobutan-2-yl)carbamoyl)hydrazinecarbonyl)hydrazinecarboxylate (**aGlyaGlyVal**)

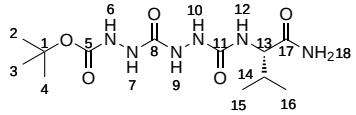

To a solution of L-Valinamide hydrochloride (270 mg, 1.77 mmol; 1.1 eq.) in CH_3CN (10 mL), were added under argon atmosphere TEA (1.35 mL, 9.66 mmol, 6.0 eq.) and compound **LVP14** (500 mg, 1.61 mmol, 1.0 eq.). The clear solution obtained was stirred at room temperature for three days. Then, the solvent was evaporated under reduced pressure to give a residue which was purified by chromatography on silica gel eluting with a mixture EtOAc /MeOH 90/10 to afford compound **aGlyaGlyVal** (328 mg, 0.99 mmol) as a white solid. Yield 60 %.

Molecular weight = 332.36 g mol^{-1}

R_f = 0.24 (EtOAc/MeOH 90:10)

HRMS: Calcd. for $[C_{12}H_{24}N_6O_5 + Na]^+$: M/z 355.1706, found: 355.1699

^{1}H NMR (DMSO–d_6, 400 MHz): δ 8.57 (1H, bp, NH6); 8.10 (2H, bp, NH7, NH9); 7.73 (1H, s, NH10); 7.32 (1H, bp, NH18); 7.03 (1H, s, NH18); 6.03 (1H, d, J = 8.7 Hz, NH12); 3.98 (1H, dd, J = 8.7, 5.4 Hz, H13); 1.98 (1H, m, H14); 1.39 (9H, s, H2, H3, H4); 0.84 (3H, d, J = 6.8 Hz, H15); 0.83 (3H, d, J = 6.8 Hz, H16) ppm

^{13}C NMR (DMSO–d_6, 100 MHz): δ 173.5 (C17); 158.5 (C8); 158.1 (C11); 155.9 (C5); 79.0 (C1); 57.5 (C13); 30.6 (C14); 28.1 (C2, C3, C4); 19.3, 17.4 (C15, C16) ppm

Melting point = 194–196 °C

IR: 3290 (N-H stretch); 2972 (C-H stretch); 1658 (C=O stretch); 1531 (N-H bend) cm^{-1}
Elemental analysis: Calcd. for $C_{12}H_{24}N_6O_5 \cdot 1.5\,H_2O$: C 40.10, H 7.59, N 23.39; found: C 40.29, H 6.77, N 23.25
HPLC purity (XBridge C18, 3.5 µm, H_2O + 0.2 % form. ac./ACN, gradient 5–100 % in 20 min): t_R = 8.88 min, 100 %

Bibliography

[1] Christian B. Anfinsen. "Principles that Govern the Folding of Protein Chains". In: *Science* 181.4096 (July 20, 1973), pp. 223–230.

[2] G. N. Ramachandran, C. Ramakrishnan, and V. Sasisekharan. "Stereochemistry of polypeptide chain configurations". In: *Journal of Molecular Biology* 7.1 (July 1, 1963), pp. 95–99.

[3] Linus Pauling and Robert B. Corey. "Two Rippled-Sheet Configurations of Polypeptide Chains, and a Note about the Pleated Sheets". In: *Proceedings of the National Academy of Sciences* 39.4 (Jan. 4, 1953), pp. 253–256.

[4] Faisal A. Syud et al. "Influence of Strand Number on Antiparallel beta-Sheet Stability in Designed Three- and Four-stranded beta-Sheets". In: *Journal of Molecular Biology* 326.2 (Feb. 14, 2003), pp. 553–568.

[5] W. F. DeGrado and J. D. Lear. "Induction of peptide conformation at apolar water interfaces. 1. A study with model peptides of defined hydrophobic periodicity". In: *Journal of the American Chemical Society* 107.25 (Dec. 1, 1985), pp. 7684–7689.

[6] Massimo Stefani and Christopher M. Dobson. "Protein aggregation and aggregate toxicity: new insights into protein folding, misfolding diseases and biological evolution". In: *Journal of Molecular Medicine* 81.11 (Aug. 27, 2003), pp. 678–699.

[7] Yvonne S. Eisele et al. "Targeting protein aggregation for the treatment of degenerative diseases". In: *Nature Reviews Drug Discovery* 14.11 (Nov. 2015), pp. 759–780.

[8] David Eisenberg and Mathias Jucker. "The Amyloid State of Proteins in Human Diseases". In: *Cell* 148.6 (Mar. 16, 2012), pp. 1188–1203.

[9] Julian D. Gillmore and Philip N. Hawkins. "Pathophysiology and treatment of systemic amyloidosis". In: *Nat Rev Nephrol* 9.10 (Oct. 2013), pp. 574–586.

[10] Christopher A. Ross and Michelle A. Poirier. "Protein aggregation and neurodegenerative disease". In: *, Published online: 01 July 2004; | doi:10.1038/nm1066* 10 (July 1, 2004), S10–S17.

[11] Fabrizio Chiti and Christopher M. Dobson. “Protein Misfolding, Functional Amyloid, and Human Disease”. In: *Annual Review of Biochemistry* 75.1 (2006), pp. 333–366.

[12] Adriano Aguzzi and Tracy O’Connor. “Protein aggregation diseases: pathogenicity and therapeutic perspectives”. In: *Nature Reviews Drug Discovery* 9.3 (Mar. 2010), pp. 237–248.

[13] Jean D. Sipe et al. “Amyloid fibril protein nomenclature: 2012 recommendations from the Nomenclature Committee of the International Society of Amyloidosis”. In: *Amyloid: The International Journal of Experimental and Clinical Investigation: The Official Journal of the International Society of Amyloidosis* 19.4 (Dec. 2012), pp. 167–170.

[14] V. N. Uversky. “Protein folding revisited. A polypeptide chain at the folding – misfolding – nonfolding cross-roads: which way to go?” In: *Cellular and Molecular Life Sciences CMLS* 60.9 (Sept. 2003), pp. 1852–1871.

[15] Geoff Clarke et al. “A one-hit model of cell death in inherited neuronal degenerations”. In: *Nature* 406.6792 (July 13, 2000), pp. 195–199.

[16] Andrew Singleton, Amanda Myers, and John Hardy. “The law of mass action applied to neurodegenerative disease: a hypothesis concerning the etiology and pathogenesis of complex diseases”. In: *Human Molecular Genetics* 13 (suppl 1 Jan. 4, 2004), R123–R126.

[17] Wilfredo Colon and Jeffery W. Kelly. “Partial denaturation of transthyretin is sufficient for amyloid fibril formation in vitro”. In: *Biochemistry* 31.36 (Sept. 1, 1992), pp. 8654–8660.

[18] H. Jane Dyson and Peter E. Wright. “Intrinsically unstructured proteins and their functions”. In: *Nature Reviews Molecular Cell Biology* 6.3 (Mar. 2005), pp. 197–208.

[19] K. S. Kosik, C. L. Joachim, and D. J. Selkoe. “Microtubule-associated protein tau (tau) is a major antigenic component of paired helical filaments in Alzheimer disease”. In: *Proceedings of the National Academy of Sciences* 83.11 (Jan. 6, 1986), pp. 4044–4048.

[20] Mihael H. Polymeropoulos et al. “Mutation in the alpha-Synuclein Gene Identified in Families with Parkinson’s Disease”. In: *Science* 276.5321 (June 27, 1997), pp. 2045–2047.

[21] Michael S. Wolfe. “Tau Mutations in Neurodegenerative Diseases”. In: *Journal of Biological Chemistry* 284.10 (June 3, 2009), pp. 6021–6025.

[22] T. R. Serio et al. “Nucleated conformational conversion and the replication of conformational information by a prion determinant”. In: *Science (New York, N.Y.)* 289.5483 (Aug. 25, 2000), pp. 1317–1321.

[23] Amy R. Hurshman et al. “Transthyretin aggregation under partially denaturing conditions is a downhill polymerization”. In: *Biochemistry* 43.23 (June 15, 2004), pp. 7365–7381.

[24] Brandon B. Holmes et al. “Heparan sulfate proteoglycans mediate internalization and propagation of specific proteopathic seeds”. In: *Proceedings of the National Academy of Sciences* 110.33 (Aug. 13, 2013), E3138–E3147.

[25] Maria Udan-Johns et al. “Prion-like nuclear aggregation of TDP-43 during heat shock is regulated by HSP40/70 chaperones”. In: *Human Molecular Genetics* 23.1 (Jan. 1, 2014), pp. 157–170.

[26] Kiran Yanamandra et al. “Anti-Tau Antibodies that Block Tau Aggregate Seeding In Vitro Markedly Decrease Pathology and Improve Cognition In Vivo”. In: *Neuron* 80.2 (Oct. 16, 2013), pp. 402–414.

[27] Per Westermark. “Aspects on human amyloid forms and their fibril polypeptides”. In: *FEBS Journal* 272.23 (Dec. 1, 2005), pp. 5942–5949.

[28] Beate Winner et al. “In vivo demonstration that alpha-synuclein oligomers are toxic”. In: *Proceedings of the National Academy of Sciences* 108.10 (Aug. 3, 2011), pp. 4194–4199.

[29] Kenjiro Ono, Margaret M. Condron, and David B. Teplow. “Structure–neurotoxicity relationships of amyloid beta-protein oligomers”. In: *Proceedings of the National Academy of Sciences* 106.35 (Jan. 9, 2009), pp. 14745–14750.

[30] Michel Goedert and Maria Grazia Spillantini. “A Century of Alzheimer’s Disease”. In: *Science* 314.5800 (Nov. 3, 2006), pp. 777–781.

[31] Mark P. Mattson. “Pathways towards and away from Alzheimer’s disease”. In: *Nature* 430.7000 (Aug. 5, 2004), pp. 631–639.

[32] Paul T. Francis et al. “The cholinergic hypothesis of Alzheimer’s disease: a review of progress”. In: *Journal of Neurology, Neurosurgery & Psychiatry* 66.2 (Jan. 2, 1999), pp. 137–147.

[33] Tim Scholz and Eckhard Mandelkow. “Transport and diffusion of Tau protein in neurons”. In: *Cellular and Molecular Life Sciences* 71.16 (Apr. 1, 2014), pp. 3139–3150.

[34] Hans Zempel and Eckhard Mandelkow. “Lost after translation: missorting of Tau protein and consequences for Alzheimer disease”. In: *Trends in Neurosciences* 37.12 (Dec. 1, 2014), pp. 721–732.

[35] Bahareh Eftekharzadeh, Bradley T. Hyman, and Susanne Wegmann. “Structural studies on the mechanism of protein aggregation in age related neurodegenerative diseases”. In: *Mechanisms of Ageing and Development* 156 (June 2016), pp. 1–13.

[36] K. Iqbal and I. Grundke-Iqbal. "Inhibition of Neurofibrillary Degeneration: A Promising Approach to Alzheimers Disease and Other Tauopathies". In: *Current Drug Targets* 5.6 (Aug. 1, 2004), pp. 495–502.

[37] Bin Zhang et al. "The Microtubule-Stabilizing Agent, Epothilone D, Reduces Axonal Dysfunction, Neurotoxicity, Cognitive Deficits, and Alzheimer-Like Pathology in an Interventional Study with Aged Tau Transgenic Mice". In: *The Journal of Neuroscience* 32.11 (Mar. 14, 2012), pp. 3601–3611.

[38] Elias Akoury et al. "Mechanistic Basis of Phenothiazine-Driven Inhibition of Tau Aggregation". In: *Angewandte Chemie International Edition* 52.12 (Mar. 18, 2013), pp. 3511–3515.

[39] Allal Boutajangout et al. "Passive immunization targeting pathological phospho-tau protein in a mouse model reduces functional decline and clears tau aggregates from the brain". In: *Journal of Neurochemistry* 118.4 (Aug. 1, 2011), pp. 658–667.

[40] Roger N. Rosenberg. "Metal Chelation Therapy for Alzheimer Disease". In: *Archives of Neurology* 60.12 (Dec. 1, 2003), pp. 1678–1679.

[41] Muralidhar L. Hegde et al. "Challenges Associated with Metal Chelation Therapy in Alzheimer's Disease". In: *Journal of Alzheimer's Disease* 17.3 (Jan. 1, 2009), pp. 457–468.

[42] Luiza M. F. Gomes et al. "8-Hydroxyquinoline Schiff-base compounds as antioxidants and modulators of copper-mediated Abeta peptide aggregation". In: *Journal of Inorganic Biochemistry* 139 (Oct. 2014), pp. 106–116.

[43] Akiko Kochi et al. "A novel hybrid of 6-chlorotacrine and metal–amyloid-beta modulator for inhibition of acetylcholinesterase and metal-induced amyloid-beta aggregation". In: *Chemical Science* 4.11 (Sept. 30, 2013), pp. 4137–4145.

[44] Hugh A. Pearson and Chris Peers. "Physiological roles for amyloid beta peptides". In: *The Journal of Physiology* 575.1 (Aug. 15, 2006), pp. 5–10.

[45] Ulrike C. Müller and Hui Zheng. "Physiological Functions of APP Family Proteins". In: *Cold Spring Harbor Perspectives in Medicine* 2.2 (Jan. 2, 2012), a006288.

[46] Gopal Thinakaran and Edward H. Koo. "Amyloid Precursor Protein Trafficking, Processing, and Function". In: *Journal of Biological Chemistry* 283.44 (Oct. 31, 2008), pp. 29615–29619.

[47] A. Güntert, H. Döbeli, and B. Bohrmann. "High sensitivity analysis of amyloid-beta peptide composition in amyloid deposits from human and PS2APP mouse brain". In: *Neuroscience* 143.2 (Dec. 1, 2006), pp. 461–475.

[48] Dennis J. Selkoe. "Alzheimer's Disease: Genes, Proteins, and Therapy". In: *Physiological Reviews* 81.2 (Apr. 1, 2001), pp. 741–766.

[49] Eileen McGowan et al. "Abeta42 Is Essential for Parenchymal and Vascular Amyloid Deposition in Mice". In: *Neuron* 47.2 (July 21, 2005), pp. 191–199.

[50] Woojin Kim and Michael H. Hecht. "Sequence Determinants of Enhanced Amyloidogenicity of Alzheimer Abeta42 Peptide Relative to Abeta40". In: *Journal of Biological Chemistry* 280.41 (Oct. 14, 2005), pp. 35069–35076.

[51] Tsuyoshi Takahashi and Hisakazu Mihara. "Peptide and Protein Mimetics Inhibiting Amyloid beta-Peptide Aggregation". In: *Accounts of Chemical Research* 41.10 (Oct. 21, 2008), pp. 1309–1318.

[52] Samuel I. A. Cohen et al. "Proliferation of amyloid-beta42 aggregates occurs through a secondary nucleation mechanism". In: *Proceedings of the National Academy of Sciences* 110.24 (Nov. 6, 2013), pp. 9758–9763.

[53] Satoko Matsumura et al. "Two Distinct Amyloid beta-Protein (Abeta) Assembly Pathways Leading to Oligomers and Fibrils Identified by Combined Fluorescence Correlation Spectroscopy, Morphology, and Toxicity Analyses". In: *Journal of Biological Chemistry* 286.13 (Jan. 4, 2011), pp. 11555–11562.

[54] Jae Sun Jeong et al. "Novel Mechanistic Insight into the Molecular Basis of Amyloid Polymorphism and Secondary Nucleation during Amyloid Formation". In: *Journal of Molecular Biology* 425.10 (May 27, 2013), pp. 1765–1781.

[55] Thomas Gurry and Collin M. Stultz. "Mechanism of Amyloid-beta Fibril Elongation". In: *Biochemistry* 53.44 (Nov. 11, 2014), pp. 6981–6991.

[56] Louise C Serpell. "Alzheimer's amyloid fibrils: structure and assembly". In: *Biochimica et Biophysica Acta (BBA) - Molecular Basis of Disease* 1502.1 (July 26, 2000), pp. 16–30.

[57] Rui Zhang et al. "Interprotofilament interactions between Alzheimer's Abeta1–42 peptides in amyloid fibrils revealed by cryoEM". In: *Proceedings of the National Academy of Sciences* 106.12 (Mar. 24, 2009), pp. 4653–4658.

[58] K. Rajasekhar, Malabika Chakrabarti, and T. Govindaraju. "Function and toxicity of amyloid beta and recent therapeutic interventions targeting amyloid beta in Alzheimer's disease". In: *Chemical Communications* 51.70 (Aug. 18, 2015), pp. 13434–13450.

[59] Marcus Fändrich, Matthias Schmidt, and Nikolaus Grigorieff. "Recent progress in understanding Alzheimer's beta-amyloid structures". In: *Trends in biochemical sciences* 36.6 (June 2011), pp. 338–345.

[60] Matthias Schmidt et al. "Comparison of Alzheimer Abeta(1–40) and Abeta(1–42) amyloid fibrils reveals similar protofilament structures". In: *Proceedings of the National Academy of Sciences* 106.47 (Nov. 24, 2009), pp. 19813–19818.

[61] Risto Cukalevski et al. "The Abeta40 and Abeta42 peptides self-assemble into separate homomolecular fibrils in binary mixtures but cross-react during primary nucleation". In: *Chemical Science* 6.7 (June 15, 2015), pp. 4215–4233.

[62] Thorsten Lührs et al. "3D structure of Alzheimer's amyloid-beta(1–42) fibrils". In: *Proceedings of the National Academy of Sciences of the United States of America* 102.48 (Nov. 29, 2005), pp. 17342–17347.

[63] William M. Tay et al. "The Alzheimer's Amyloid-beta(1–42) Peptide Forms Off-Pathway Oligomers and Fibrils That Are Distinguished Structurally by Intermolecular Organization". In: *Journal of Molecular Biology* 425.14 (July 24, 2013), pp. 2494–2508.

[64] Mahiuddin Ahmed et al. "Structural conversion of neurotoxic amyloid-beta(1–42) oligomers to fibrils". In: *Nature structural & molecular biology* 17.5 (May 2010), pp. 561–567.

[65] Verena H. Finder et al. "The Recombinant Amyloid-beta Peptide Abeta1–42 Aggregates Faster and Is More Neurotoxic than Synthetic Abeta1–42". In: *Journal of Molecular Biology* 396.1 (Feb. 12, 2010), pp. 9–18.

[66] Georg Meisl et al. "Differences in nucleation behavior underlie the contrasting aggregation kinetics of the Abeta40 and Abeta42 peptides". In: *Proceedings of the National Academy of Sciences* 111.26 (Jan. 7, 2014), pp. 9384–9389.

[67] Liping Yu et al. "Structural Characterization of a Soluble Amyloid beta-Peptide Oligomer". In: *Biochemistry* 48.9 (Mar. 10, 2009), pp. 1870–1877.

[68] Arthur Laganowsky et al. "Atomic view of a toxic amyloid small oligomer". In: *Science (New York, N.Y.)* 335.6073 (Mar. 9, 2012), pp. 1228–1231.

[69] Danting Huang et al. "Antiparallel beta-Sheet Structure within the C-Terminal Region of 42-Residue Alzheimer's Amyloid-beta Peptides When They Form 150-kDa Oligomers". In: *Journal of Molecular Biology* 427.13 (July 3, 2015), pp. 2319–2328.

[70] D. Allan Butterfield, Aaron M. Swomley, and Rukhsana Sultana. "Amyloid beta-Peptide (1–42)-Induced Oxidative Stress in Alzheimer Disease: Importance in Disease Pathogenesis and Progression". In: *Antioxidants & Redox Signaling* 19.8 (Dec. 18, 2012), pp. 823–835.

[71] Christian Haass and Dennis J. Selkoe. "Soluble protein oligomers in neurodegeneration: lessons from the Alzheimer's amyloid beta-peptide". In: *Nature Reviews Molecular Cell Biology* 8.2 (Feb. 2007), pp. 101–112.

[72] Paulius Cizas et al. "Size-dependent neurotoxicity of beta-amyloid oligomers". In: *Archives of Biochemistry and Biophysics* 496.2 (Apr. 15, 2010), pp. 84–92.

[73] Panchika Prangkio et al. "Multivariate Analyses of Amyloid-Beta Oligomer Populations Indicate a Connection between Pore Formation and Cytotoxicity". In: *PLOS ONE* 7.10 (Oct. 15, 2012), e47261.

[74] Ganesh M. Shankar et al. "Amyloid beta-Protein Dimers Isolated Directly from Alzheimer Brains Impair Synaptic Plasticity and Memory". In: *Nature medicine* 14.8 (Aug. 2008), pp. 837–842.

[75] Karie N. Dahlgren et al. "Oligomeric and Fibrillar Species of Amyloid-beta Peptides Differentially Affect Neuronal Viability". In: *Journal of Biological Chemistry* 277.35 (Aug. 30, 2002), pp. 32046–32053.

[76] Florentina Tofoleanu and Nicolae-Viorel Buchete. "Alzheimer Abeta peptide interactions with lipid membranes". In: *Prion* 6.4 (Sept. 1, 2012), pp. 339–345.

[77] Jiasi Wang et al. "New Insights in Amyloid Beta Interactions with Human Telomerase". In: *Journal of the American Chemical Society* 137.3 (Jan. 28, 2015), pp. 1213–1219.

[78] Chun Shi et al. "Intromitochondrial IB/NF-B signaling pathway is involved in amyloid beta peptide-induced mitochondrial dysfunction". In: *Journal of Bioenergetics and Biomembranes* 46.5 (July 23, 2014), pp. 371–376.

[79] Ali Reza A. Ladiwala et al. "Conformational Differences between Two Amyloid beta Oligomers of Similar Size and Dissimilar Toxicity". In: *Journal of Biological Chemistry* 287.29 (July 13, 2012), pp. 24765–24773.

[80] Kirsten L. Viola and William L. Klein. "Amyloid beta oligomers in Alzheimer's disease pathogenesis, treatment, and diagnosis". In: *Acta Neuropathologica* 129.2 (Jan. 22, 2015), pp. 183–206.

[81] Fernanda G. De Felice et al. “Protection of synapses against Alzheimer’s-linked toxins: Insulin signaling prevents the pathogenic binding of Abeta oligomers”. In: *Proceedings of the National Academy of Sciences* 106.6 (Oct. 2, 2009), pp. 1971–1976.

[82] Dimitra G. Georganopoulou et al. “Nanoparticle-based detection in cerebral spinal fluid of a soluble pathogenic biomarker for Alzheimer’s disease”. In: *Proceedings of the National Academy of Sciences of the United States of America* 102.7 (Feb. 15, 2005), pp. 2273–2276.

[83] Gunnar K. Gouras et al. “Intraneuronal beta-amyloid accumulation and synapse pathology in Alzheimer’s disease”. In: *Acta Neuropathologica* 119.5 (Mar. 31, 2010), pp. 523–541.

[84] Vanessa Schmidt, Anne-Sophie Carlo, and Thomas E. Willnow. “Apolipoprotein E receptor pathways in Alzheimer disease”. In: *Wiley Interdisciplinary Reviews: Systems Biology and Medicine* 6.3 (May 1, 2014), pp. 255–270.

[85] Susann Cattepoel et al. “Chronic Intranasal Treatment with an Anti-Abeta 30-42 scFv Antibody Ameliorates Amyloid Pathology in a Transgenic Mouse Model of Alzheimer’s Disease”. In: *PLOS ONE* 6.4 (Apr. 5, 2011), e18296.

[86] Ayumi Takamura et al. “Sortilin is required for toxic action of Abeta oligomers (AbetaOs): Extracellular AbetaOs trigger apoptosis, and intraneuronal AbetaOs impair degradation pathways”. In: *Life Sciences*. Contribution of Intraneuronal Amyloid beta Accumulation to Alzheimer’s Disease 91.23 (Dec. 10, 2012), pp. 1177–1186.

[87] Mary P. Lambert et al. “Vaccination with soluble Abeta oligomers generates toxicity-neutralizing antibodies”. In: *Journal of Neurochemistry* 79.3 (Nov. 1, 2001), pp. 595–605.

[88] Fernanda G. De Felice et al. “Alzheimer’s disease-type neuronal tau hyperphosphorylation induced by Abeta oligomers”. In: *Neurobiology of Aging* 29.9 (Sept. 1, 2008), pp. 1334–1347.

[89] Pascale N. Lacor et al. “Synaptic Targeting by Alzheimer’s-Related Amyloid beta Oligomers”. In: *The Journal of Neuroscience* 24.45 (Oct. 11, 2004), pp. 10191–10200.

[90] M. P. Lambert et al. “Diffusible, nonfibrillar ligands derived from Abeta1–42 are potent central nervous system neurotoxins”. In: *Proceedings of the National Academy of Sciences* 95.11 (May 26, 1998), pp. 6448–6453.

[91] N. Arispe. “Architecture of the Alzheimer’s AbetaP Ion Channel Pore”. In: *The Journal of Membrane Biology* 197.1 (Jan. 2004), pp. 33–48.

[92] Kelly Willemijn Menting and Jurgen A. H. R. Claassen. "beta-secretase inhibitor; a promising novel therapeutic drug in Alzheimer's disease". In: *Frontiers in Aging Neuroscience* 6 (2014), p. 165.

[93] Arun K. Ghosh and Heather L. Osswald. "BACE1 (beta-secretase) inhibitors for the treatment of Alzheimer's disease". In: *Chemical Society Reviews* 43.19 (Sept. 8, 2014), pp. 6765–6813.

[94] Najmeh Edraki et al. "N-(2-(Piperazin-1-yl)phenyl)arylamide Derivatives as beta-Secretase (BACE1) Inhibitors: Simple Synthesis by Ugi Four-Component Reaction and Biological Evaluation". In: *Archiv Der Pharmazie* 348.5 (May 2015), pp. 330–337.

[95] Kevin W. Hunt et al. "Spirocyclic beta-Site Amyloid Precursor Protein Cleaving Enzyme 1 (BACE1) Inhibitors: From Hit to Lowering of Cerebrospinal Fluid (CSF) Amyloid beta in a Higher Species". In: *Journal of Medicinal Chemistry* 56.8 (Apr. 25, 2013), pp. 3379–3403.

[96] Allen A. Thomas et al. "Discovery of 7-Tetrahydropyran-2-yl Chromans: beta-Site Amyloid Precursor Protein Cleaving Enzyme 1 (BACE1) Inhibitors That Reduce Amyloid beta-Protein (Abeta) in the Central Nervous System". In: *Journal of Medicinal Chemistry* 57.3 (Feb. 13, 2014), pp. 878–902.

[97] Hans Hilpert et al. "beta-Secretase (BACE1) Inhibitors with High in Vivo Efficacy Suitable for Clinical Evaluation in Alzheimer's Disease". In: *Journal of Medicinal Chemistry* 56.10 (May 23, 2013), pp. 3980–3995.

[98] Jian Jeffrey Chen et al. "Development of 2-aminooxazoline 3-azaxanthenes as orally efficacious beta-secretase inhibitors for the potential treatment of Alzheimer's disease". In: *Bioorganic & Medicinal Chemistry Letters* 25.4 (Feb. 15, 2015), pp. 767–774.

[99] Nima Razzaghi-Asl et al. "Design and synthesis of novel 3,5-bis-N-(aryl/heteroaryl) carbamoyl-4-aryl-1,4-dihydropyridines as small molecule BACE-1 inhibitors". In: *Bioorganic & Medicinal Chemistry* 21.22 (Nov. 15, 2013), pp. 6893–6909.

[100] Jin Hu et al. "The Resveratrol Trimer Miyabenol C Inhibits beta-Secretase Activity and beta-Amyloid Generation". In: *PLOS ONE* 10.1 (Jan. 28, 2015), e0115973.

[101] Biao Cheng et al. "Inhibiting toxic aggregation of amyloidogenic proteins: A therapeutic strategy for protein misfolding diseases". In: *Biochimica et Biophysica Acta (BBA) - General Subjects* 1830.10 (Oct. 2013), pp. 4860–4871.

[102] Martin Pettersson et al. "Discovery of indole-derived pyridopyrazine-1,6-dione -secretase modulators that target presenilin". In: *Bioorganic & Medicinal Chemistry Letters* 25.4 (Feb. 15, 2015), pp. 908–913.

[103] Adriana I. Velter et al. “Anilinotriazoles as potent gamma secretase modulators”. In: *Bioorganic & Medicinal Chemistry Letters* 24.24 (Dec. 15, 2014), pp. 5805–5813.

[104] Dale Schenk et al. “Immunization with amyloid-beta attenuates Alzheimer-disease-like pathology in the PDAPP mouse”. In: *Nature* 400.6740 (July 8, 1999), pp. 173–177.

[105] Frédérique Bard et al. “Peripherally administered antibodies against amyloid beta-peptide enter the central nervous system and reduce pathology in a mouse model of Alzheimer disease”. In: *Nature Medicine* 6.8 (Aug. 2000), pp. 916–919.

[106] J.-M. Orgogozo et al. “Subacute meningoencephalitis in a subset of patients with AD after Abeta42 immunization”. In: *Neurology* 61.1 (July 8, 2003), pp. 46–54.

[107] Grant Krafft et al. “ACU-193: A candidate therapeutic antibody that selectively targets soluble beta-amyloid oligomers”. In: *Alzheimer's & Dementia: The Journal of the Alzheimer's Association* 9.4 (July 1, 2013), P326.

[108] Laurent Pradier et al. “SAR228810: An antiprotofibrillar beta-amyloid antibody designed to reduce risk of amyloid-related imaging abnormalities (ARIA)”. In: *Alzheimer's & Dementia: The Journal of the Alzheimer's Association* 9.4 (July 1, 2013), P808–P809.

[109] Paige E. Cramer et al. “ApoE-Directed Therapeutics Rapidly Clear beta-Amyloid and Reverse Deficits in AD Mouse Models”. In: *Science* 335.6075 (Mar. 23, 2012), pp. 1503–1506.

[110] Rashid Deane, Zhenhua Wu, and Berislav V. Zlokovic. “RAGE (yin) versus LRP (yang) balance regulates alzheimer amyloid beta-peptide clearance through transport across the blood-brain barrier”. In: *Stroke; a Journal of Cerebral Circulation* 35.11 (Nov. 2004), pp. 2628–2631.

[111] Robert A. Marr and Daniel M. Hafez. “Amyloid-beta and Alzheimer's disease: the role of neprilysin-2 in amyloid-beta clearance”. In: *Frontiers in Aging Neuroscience* 6 (2014), p. 187.

[112] Angeleen Fleming et al. “Chemical modulators of autophagy as biological probes and potential therapeutics”. In: *Nature Chemical Biology* 7.1 (Jan. 2011), pp. 9–17.

[113] Ismael Santa-Maria et al. “Tramiprosate, a drug of potential interest for the treatment of Alzheimer's disease, promotes an abnormal aggregation of tau”. In: *Molecular Neurodegeneration* 2 (Sept. 6, 2007), p. 17.

[114] Liang Zhang et al. “Processing of Alzheimer’s Amyloid Precursor Protein during H2O2-Induced Apoptosis in Human Neuronal Cells”. In: *Biochemical and Biophysical Research Communications* 235.3 (June 27, 1997), pp. 845–848.

[115] Haiyan Xie et al. “Catechins and Procyanidins of Ginkgo biloba Show Potent Activities towards the Inhibition of beta-Amyloid Peptide Aggregation and Destabilization of Preformed Fibrils”. In: *Molecules* 19.4 (Apr. 22, 2014), pp. 5119–5134.

[116] Jan Bieschke et al. “EGCG remodels mature alpha-synuclein and amyloid-beta fibrils and reduces cellular toxicity”. In: *Proceedings of the National Academy of Sciences* 107.17 (Apr. 27, 2010), pp. 7710–7715.

[117] M. Ganguli et al. “Ten-year incidence of dementia in a rural elderly US community population The MoVIES Project”. In: *Neurology* 54.5 (Mar. 14, 2000), pp. 1109–1116.

[118] Daijiro Yanagisawa et al. “Curcumin derivative with the substitution at C-4 position, but not curcumin, is effective against amyloid pathology in APP/PS1 mice”. In: *Neurobiology of Aging* 36.1 (Jan. 1, 2015), pp. 201–210.

[119] Kenjiro Ono et al. “Effects of Grape Seed-derived Polyphenols on Amyloid beta-Protein Self-assembly and Cytotoxicity”. In: *Journal of Biological Chemistry* 283.47 (Nov. 21, 2008), pp. 32176–32187.

[120] Stefania Rigacci et al. “Aβ(1-42) Aggregates into Non-Toxic Amyloid Assemblies in the Presence of the Natural Polyphenol Oleuropein Aglycon”. In: *Current Alzheimer Research* 8.8 (Dec. 1, 2011), pp. 841–852.

[121] Sharmistha Sinha et al. “Lysine-Specific Molecular Tweezers Are Broad-Spectrum Inhibitors of Assembly and Toxicity of Amyloid Proteins”. In: *Journal of the American Chemical Society* 133.42 (Oct. 26, 2011), pp. 16958–16969.

[122] Yasuhiro Nakagami et al. “A novel beta-sheet breaker, RS-0406, reverses amyloid beta-induced cytotoxicity and impairment of long-term potentiation in vitro”. In: *British Journal of Pharmacology* 137.5 (Nov. 1, 2002), pp. 676–682.

[123] Tadamasa Arai et al. “Rational design and identification of a non-peptidic aggregation inhibitor of amyloid-beta based on a pharmacophore motif obtained from cyclo[-Lys-Leu-Val-Phe-Phe-]”. In: *Angewandte Chemie (International Ed. in English)* 53.31 (July 28, 2014), pp. 8236–8239.

[124] C. Soto et al. “Beta-sheet breaker peptides inhibit fibrillogenesis in a rat brain model of amyloidosis: implications for Alzheimer’s therapy”. In: *Nature Medicine* 4.7 (July 1998), pp. 822–826.

[125] Lars O. Tjernberg et al. “Arrest of -Amyloid Fibril Formation by a Pentapeptide Ligand”. In: *Journal of Biological Chemistry* 271.15 (Dec. 4, 1996), pp. 8545–8548.

[126] Céline Adessi et al. “Pharmacological Profiles of Peptide Drug Candidates for the Treatment of Alzheimer’s Disease”. In: *Journal of Biological Chemistry* 278.16 (Apr. 18, 2003), pp. 13905–13911.

[127] Cesare Giordano et al. “Synthesis and activity of fibrillogenesis peptide inhibitors related to the 17–21 beta-amyloid sequence”. In: *European Journal of Medicinal Chemistry* 44.1 (Jan. 2009), pp. 179–189.

[128] Mark A. Findeis et al. “Modified-Peptide Inhibitors of Amyloid beta-Peptide Polymerization”. In: *Biochemistry* 38.21 (May 1, 1999), pp. 6791–6800.

[129] S. Akikusa et al. “Practical assay and molecular mechanism of aggregation inhibitors of beta-amyloid”. In: *The Journal of Peptide Research: Official Journal of the American Peptide Society* 61.1 (Jan. 2003), pp. 1–6.

[130] Nicola Acerra, Neil M. Kad, and Jody M. Mason. “Combining intracellular selection with protein-fragment complementation to derive Abeta interacting peptides”. In: *Protein Engineering Design and Selection* 26.7 (Jan. 7, 2013), pp. 463–470.

[131] Ashim Paul et al. “Inhibition of Alzheimer’s amyloid-beta peptide aggregation and its disruption by a conformationally restricted alpha/beta hybrid peptide”. In: *Chemical Communications* 51.12 (Jan. 27, 2015), pp. 2245–2248.

[132] Tao L. Lowe et al. “Structure−Function Relationships for Inhibitors of beta-Amyloid Toxicity Containing the Recognition Sequence KLVFF”. In: *Biochemistry* 40.26 (July 1, 2001), pp. 7882–7889.

[133] Christopher W. Cairo et al. “Affinity-Based Inhibition of beta-Amyloid Toxicity”. In: *Biochemistry* 41.27 (July 1, 2002), pp. 8620–8629.

[134] Lívia Fülöp et al. “beta-Amyloid-derived pentapeptide RIIGLa inhibits Abeta1–42 aggregation and toxicity”. In: *Biochemical and Biophysical Research Communications* 324.1 (Nov. 5, 2004), pp. 64–69.

[135] Marcus A. Etienne et al. “Stoichiometric Inhibition of Amyloid beta-Protein Aggregation with Peptides Containing Alternating alpha,alpha-Disubstituted Amino Acids”. In: *Journal of the American Chemical Society* 128.11 (Mar. 1, 2006), pp. 3522–3523.

[136] Mark Taylor et al. “Development of a Proteolytically Stable Retro-Inverso Peptide Inhibitor of beta-Amyloid Oligomerization as a Potential Novel Treatment for Alzheimer’s Disease”. In: *Biochemistry* 49.15 (Apr. 20, 2010), pp. 3261–3272.

[137] Petra Rzepecki and Thomas Schrader. “beta-Sheet Ligands in Action: KLVFF Recognition by Aminopyrazole Hybrid Receptors in Water”. In: *Journal of the American Chemical Society* 127.9 (Mar. 1, 2005), pp. 3016–3025.

[138] Yu Zhou et al. “Structural Optimization and Biological Evaluation of Substituted Bisphenol A Derivatives as beta-Amyloid Peptide Aggregation Inhibitors”. In: *Journal of Medicinal Chemistry* 53.15 (Aug. 12, 2010), pp. 5449–5466.

[139] Krishna Chaitanya Nadimpally, Ashim Paul, and Bhubaneswar Mandal. “Reversal of Aggregation Using beta-Breaker Dipeptide Containing Peptides: Application to Abeta(1–40) Self-Assembly and Its Inhibition”. In: *ACS Chemical Neuroscience* 5.5 (May 21, 2014), pp. 400–408.

[140] Jitendra Kumar, Risa Namsechi, and Valerie L. Sim. “Structure-Based Peptide Design to Modulate Amyloid Beta Aggregation and Reduce Cytotoxicity”. In: *PLOS ONE* 10.6 (June 12, 2015), e0129087.

[141] Joana A. Loureiro et al. “Fluorinated beta-sheet breaker peptides”. In: *Journal of Materials Chemistry B* 2.16 (Mar. 27, 2014), pp. 2259–2264.

[142] Julia Kaffy et al. “Designed Glycopeptidomimetics Disrupt Protein–Protein Interactions Mediating Amyloid beta-Peptide Aggregation and Restore Neuroblastoma Cell Viability”. In: *Journal of Medicinal Chemistry* 59.5 (Mar. 10, 2016), pp. 2025–2040.

[143] Julia Kaffy et al. “Structure–activity relationships of sugar-based peptidomimetics as modulators of amyloid beta-peptide early oligomerization and fibrillization”. In: *European Journal of Medicinal Chemistry* 86 (Oct. 30, 2014), pp. 752–758.

[144] K. Rajasekhar et al. “Rationally Designed Peptidomimetic Modulators of Abeta Toxicity in Alzheimer’s Disease”. In: *Scientific Reports* 5 (Jan. 30, 2015), p. 8139.

[145] Yvonne Kallberg et al. “Prediction of Amyloid Fibril-forming Proteins”. In: *Journal of Biological Chemistry* 276.16 (Apr. 20, 2001), pp. 12945–12950.

[146] Katsumi Matsuzaki et al. “Design, synthesis, and biophysical properties of a helical Abeta1–42 analog: Inhibition of fibrillogenesis and cytotoxicity”. In: *Biochemical and Biophysical Research Communications* 371.4 (July 11, 2008), pp. 777–780.

[147] Enrico Brandenburg et al. “Inhibition of Amyloid Aggregation by Formation of Helical Assemblies”. In: *Chemistry – A European Journal* 17.38 (Sept. 12, 2011), pp. 10651–10661.

[148] C. Nerelius et al. “alpha-Helix targeting reduces amyloid-beta peptide toxicity”. In: *Proceedings of the National Academy of Sciences* 106.23 (Sept. 6, 2009), pp. 9191–9196.

[149] Mika Ito et al. “Effects of Ligands on Unfolding of the Amyloid beta-Peptide Central Helix: Mechanistic Insights from Molecular Dynamics Simulations”. In: *PLOS ONE* 7.1 (Jan. 23, 2012), e30510.

[150] Dmytro Honcharenko et al. “Synthesis and evaluation of antineurotoxicity properties of an amyloid-beta peptide targeting ligand containing a triamino acid”. In: *Organic & Biomolecular Chemistry* 12.34 (Aug. 6, 2014), pp. 6684–6693.

[151] Gilles Guichard and Ivan Huc. “Synthetic foldamers”. In: *Chemical Communications* 47.21 (May 16, 2011), pp. 5933–5941.

[152] Leila Vahdati et al. “Synthesis and conformational studies of a stable peptidomimetic beta-hairpin based on a bifunctional diketopiperazine turn inducer”. In: *New Journal of Chemistry* 39.5 (May 5, 2015), pp. 3250–3258.

[153] Lívia Fülöp et al. “A Foldamer-Dendrimer Conjugate Neutralizes Synaptotoxic beta-Amyloid Oligomers”. In: *PLOS ONE* 7.7 (July 30, 2012), e39485.

[154] J. Phillip Turner et al. “Rationally Designed Peptoids Modulate Aggregation of Amyloid-Beta 40”. In: *ACS Chemical Neuroscience* 5.7 (July 16, 2014), pp. 552–558.

[155] Yuan Luo et al. “Abeta42-Binding Peptoids as Amyloid Aggregation Inhibitors and Detection Ligands”. In: *ACS Chemical Neuroscience* 4.6 (June 19, 2013), pp. 952–962.

[156] Ghiam Yamin, Piotr Ruchala, and David B. Teplow. “A Peptide Hairpin Inhibitor of Amyloid beta-Protein Oligomerization and Fibrillogenesis”. In: *Biochemistry* 48.48 (Dec. 8, 2009), pp. 11329–11331.

[157] Kelly N. L. Huggins et al. “Designed Hairpin Peptides Interfere with Amyloidogenesis Pathways: Fibril Formation and Cytotoxicity Inhibition, Interception of the Preamyloid State”. In: *Biochemistry* 50.38 (Sept. 27, 2011), pp. 8202–8212.

[158] Gene Hopping et al. “Designed Trpzip-3 beta-Hairpin Inhibits Amyloid Formation in Two Different Amyloid Systems”. In: *ACS Medicinal Chemistry Letters* 4.9 (Sept. 12, 2013), pp. 824–828.

[159] James S. Nowick, Eric M. Smith, and Glenn Noronha. "Molecular Scaffolds. 3. An Artificial Parallel .beta.-Sheet". In: *The Journal of Organic Chemistry* 60.23 (Nov. 1, 1995), pp. 7386–7387.

[160] James S. Nowick et al. "An Artificial beta-Sheet Comprising a Molecular Scaffold, a beta-Strand Mimic, and a Peptide Strand1". In: *Journal of the American Chemical Society* 118.11 (Jan. 1, 1996), pp. 2764–2765.

[161] R. Jeremy Woods et al. "Cyclic Modular beta-Sheets". In: *Journal of the American Chemical Society* 129.9 (Mar. 1, 2007), pp. 2548–2558.

[162] Pin-Nan Cheng et al. "Amyloid beta-sheet mimics that antagonize protein aggregation and reduce amyloid toxicity". In: *Nature Chemistry* 4.11 (Nov. 2012), pp. 927–933.

[163] Jing Zheng et al. "Macrocyclic beta-Sheet Peptides That Inhibit the Aggregation of a Tau-Protein-Derived Hexapeptide". In: *Journal of the American Chemical Society* 133.9 (Mar. 9, 2011), pp. 3144–3157.

[164] Cong Liu et al. "Characteristics of Amyloid-Related Oligomers Revealed by Crystal Structures of Macrocyclic beta-Sheet Mimics". In: *Journal of the American Chemical Society* 133.17 (May 4, 2011), pp. 6736–6744.

[165] Jinghui Luo et al. "Inhibiting and Reversing Amyloid-beta Peptide (1–40) Fibril Formation with GramicidinS and Engineered Analogues". In: *Chemistry – A European Journal* 19.51 (Dec. 16, 2013), pp. 17338–17348.

[166] Yiling Xiao et al. "Abeta(1–42) Fibril Structure Illuminates Self-recognition and Replication of Amyloid in Alzheimer's". In: *Nature structural & molecular biology* 22.6 (June 2015), pp. 499–505.

[167] Bertrand Dorgeret et al. "Sugar-based peptidomimetics inhibit amyloid beta-peptide aggregation". In: *European Journal of Medicinal Chemistry* 46.12 (Dec. 2011), pp. 5959–5969.

[168] Manuela Bartolini and Vincenza Andrisano. "Strategies for the Inhibition of Protein Aggregation in Human Diseases". In: *ChemBioChem* 11.8 (May 17, 2010), pp. 1018–1035.

[169] Cliff I. Stains, Kalyani Mondal, and Indraneel Ghosh. "Molecules that Target beta-Amyloid". In: *ChemMedChem* 2.12 (Dec. 10, 2007), pp. 1674–1692.

[170] Sara Pellegrino et al. "Asymmetric Modular Synthesis of a Semirigid Dipeptide Mimetic by Cascade Cycloaddition/Ring Rearrangement and Borohydride Reduction". In: *The Journal of Organic Chemistry* 79.7 (Apr. 4, 2014), pp. 3094–3102.

[171] Meytal Landau et al. “Towards a Pharmacophore for Amyloid”. In: *PLOS Biol* 9.6 (June 14, 2011), e1001080.

[172] Alessandro Contini and Emanuela Erba. “Click-chemistry approach to azacycloalkene monosulfonyl diamines: synthesis and computational analysis of the reaction mechanism”. In: *RSC Advances* 2.28 (Oct. 15, 2012), pp. 10652–10660.

[173] Björn Eckhardt et al. “Structural characterization of a beta-turn mimic within a protein–protein interface”. In: *Proceedings of the National Academy of Sciences* 107.43 (Oct. 26, 2010), pp. 18336–18341.

[174] Sara Pellegrino et al. “Expedient chemical synthesis of 75mer DNA binding domain of MafA: an insight on its binding to insulin enhancer”. In: *Amino Acids* 43.5 (Apr. 4, 2012), pp. 1995–2003.

[175] David S. King, Cynthia G. Fields, and Gregg B. Fields. “A cleavage method which minimizes side reactions following Fmoc solid phase peptide synthesis”. In: *International Journal of Peptide and Protein Research* 36.3 (Sept. 1, 1990), pp. 255–266.

[176] Norma J. Greenfield. “Using circular dichroism spectra to estimate protein secondary structure”. In: *Nature protocols* 1.6 (2006), pp. 2876–2890.

[177] L. J. Smith et al. “Analysis of main chain torsion angles in proteins: prediction of NMR coupling constants for native and random coil conformations”. In: *Journal of Molecular Biology* 255.3 (Jan. 26, 1996), pp. 494–506.

[178] D. S. Wishart et al. “1H, 13C and 15N random coil NMR chemical shifts of the common amino acids. I. Investigations of nearest-neighbor effects”. In: *Journal of biomolecular NMR* 5.1 (Jan. 1995), pp. 67–81.

[179] Chad D. Tatko and Marcey L. Waters. “Selective Aromatic Interactions in beta-Hairpin Peptides”. In: *Journal of the American Chemical Society* 124.32 (Aug. 1, 2002), pp. 9372–9373.

[180] Lucia De Rosa et al. “Design, structural and biological characterization of a VEGF inhibitor beta-hairpin-constrained peptide”. In: *European Journal of Medicinal Chemistry* 73 (Feb. 12, 2014), pp. 210–216.

[181] Philippe Cuniasse et al. “Accounting for Conformational Variability in NMR Structure of Cyclopeptides: Ensemble Averaging of Interproton Distance and Coupling Constant Restraints”. In: *Journal of the American Chemical Society* 119.22 (June 1, 1997), pp. 5239–5248.

[182] Ana M. Fernández-Escamilla et al. “Design and NMR conformational study of a beta-sheet peptide based on Betanova and WW domains”. In: *Protein Science : A Publication of the Protein Society* 15.10 (Oct. 2006), pp. 2278–2289.

[183] Matthew Biancalana and Shohei Koide. "Molecular mechanism of Thioflavin-T binding to amyloid fibrils". In: *Biochimica Et Biophysica Acta* 1804.7 (July 2010), pp. 1405–1412.

[184] Anna I. Sulatskaya, Irina M. Kuznetsova, and Konstantin K. Turoverov. "Interaction of Thioflavin T with Amyloid Fibrils: Fluorescence Quantum Yield of Bound Dye". In: *The Journal of Physical Chemistry B* 116.8 (Mar. 1, 2012), pp. 2538–2544.

[185] Cristina Rodríguez-Rodríguez et al. "Crystal structure of thioflavin-T and its binding to amyloid fibrils: insights at the molecular level". In: *Chemical Communications (Cambridge, England)* 46.7 (Feb. 21, 2010), pp. 1156–1158.

[186] Nicoleta Kokkoni et al. "N-Methylated Peptide Inhibitors of beta-Amyloid Aggregation and Toxicity. Optimization of the Inhibitor Structure". In: *Biochemistry* 45.32 (Aug. 1, 2006), pp. 9906–9918.

[187] Sidhartha M. Chafekar et al. "Branched KLVFF Tetramers Strongly Potentiate Inhibition of beta-Amyloid Aggregation". In: *ChemBioChem* 8.15 (Oct. 15, 2007), pp. 1857–1864.

[188] Dimitri Brinet et al. "An improved capillary electrophoresis method for in vitro monitoring of the challenging early steps of Abeta1–42 peptide oligomerization: Application to anti-Alzheimer's drug discovery". In: *ELECTROPHORESIS* 35.23 (Dec. 1, 2014), pp. 3302–3309.

[189] Ying Feng et al. "Resveratrol inhibits beta-amyloid oligomeric cytotoxicity but does not prevent oligomer formation". In: *Neurotoxicology* 30.6 (Nov. 2009), pp. 986–995.

[190] Sharmistha Sinha et al. "Comparison of Three Amyloid Assembly Inhibitors: The Sugar scyllo-Inositol, the Polyphenol Epigallocatechin Gallate, and the Molecular Tweezer CLR01". In: *ACS Chemical Neuroscience* 3.6 (June 20, 2012), pp. 451–458.

[191] Suk-Joon Hyung et al. "Insights into antiamyloidogenic properties of the green tea extract (−)-epigallocatechin-3-gallate toward metal-associated amyloid-beta species". In: *Proceedings of the National Academy of Sciences* 110.10 (May 3, 2013), pp. 3743–3748.

[192] Jan Bieschke et al. "Small-molecule conversion of toxic oligomers to nontoxic beta-sheet–rich amyloid fibrils". In: *Nature Chemical Biology* 8.1 (Jan. 2012), pp. 93–101.

[193] James S. Nowick et al. "An Unnatural Amino Acid that Mimics a Tripeptide beta-Strand and Forms beta-Sheetlike Hydrogen-Bonded Dimers". In: *Journal of the American Chemical Society* 122.32 (Aug. 1, 2000), pp. 7654–7661.

[194] Ludovic Bannwarth et al. “Molecular Tongs Containing Amino Acid Mimetic Fragments: New Inhibitors of Wild-Type and Mutated HIV-1 Protease Dimerization”. In: *Journal of Medicinal Chemistry* 49.15 (July 1, 2006), pp. 4657–4664.

[195] Anamaria Vidu et al. “Toward the First Nonpeptidic Molecular Tong Inhibitor of Wild-Type and Mutated HIV-1 Protease Dimerization”. In: *ChemMedChem* 5.11 (Nov. 8, 2010), pp. 1899–1906.

[196] Fatemeh Tamaddon, Alireza Nasiri, and Somayeh Farokhi. “CsF–Celite as an efficient heterogeneous catalyst for sulfonylation and desulfonylation of heteroatoms”. In: *Catalysis Communications* 12.15 (Sept. 15, 2011), pp. 1477–1482.

[197] Joginder S. Bajwa et al. “Deprotection of N-tosylated indoles and related structures using cesium carbonate”. In: *Tetrahedron Letters* 47.36 (Sept. 4, 2006), pp. 6425–6427.

[198] Toshimasa Katagiri et al. “Preparation of Optically Pure alpha-Trifluoromethyl-alpha-amino Acids from N-Tosyl-2-trifluoromethyl-2-alkyloxycarbonyl Aziridine”. In: *The Journal of Organic Chemistry* 76.22 (Nov. 18, 2011), pp. 9305–9311.

[199] Vittoria Lupi et al. “Synthesis of 2,6-disubstituted morpholines through regioselective oxiranes ring opening by tosylamide under PTC conditions”. In: *Tetrahedron* 60.51 (Dec. 13, 2004), pp. 11709–11718.

[200] Tohru Fukuyama, Chung-Kuang Jow, and Mui Cheung. “2- and 4-Nitrobenzenesulfonamides: Exceptionally versatile means for preparation of secondary amines and protection of amines”. In: *Tetrahedron Letters* 36.36 (Sept. 4, 1995), pp. 6373–6374.

[201] Peter E. Maligres et al. “Nosylaziridines: Activated aziridine electrophiles”. In: *Tetrahedron Letters* 38.30 (July 28, 1997), pp. 5253–5256.

[202] Peter Wipf and Todd C. Henninger. “Solid-Phase Synthesis of Peptide Mimetics with (E)-Alkene Amide Bond Replacements Derived from Alkenylaziridines”. In: *The Journal of Organic Chemistry* 62.6 (Mar. 1, 1997), pp. 1586–1587.

[203] Stephen C. Miller and Thomas S. Scanlan. “Site-Selective N-Methylation of Peptides on Solid Support”. In: *Journal of the American Chemical Society* 119.9 (Mar. 1, 1997), pp. 2301–2302.

[204] Haoyun An and P. Dan Cook. “Solution phase combinatorial chemistry I. synthesis of polyazacyclophane scaffolds and tertiary amine libraries”. In: *Tetrahedron Letters* 37.40 (Sept. 30, 1996), pp. 7233–7236.

[205] Ulhas Bhatt et al. “Derivatized oxopiperazine rings from amino acids”. In: *Tetrahedron Letters* 38.21 (May 26, 1997), pp. 3679–3682.

[206] Haoyun An et al. "Solution Phase Combinatorial Chemistry. Synthesis of Novel Linear Pyridinopolyamine Libraries with Potent Antibacterial Activity". In: *The Journal of Organic Chemistry* 62.15 (July 1, 1997), pp. 5156–5164.

[207] Toshiro Ibuka et al. "A Thermodynamic Preference of Chiral N-Methanesulfonyl and N-Arenesulfonyl 2,3-cis-3-Alkyl-2-Vinylaziridines over Their 2,3-Trans-Isomers: Useful Palladium(0)-Catalyzed Equilibration Reactions for the Synthesis of (E)-Alkene Dipeptide Isosteres". In: *The Journal of Organic Chemistry* 62.4 (Feb. 1, 1997), pp. 999–1015.

[208] Christine Philippe et al. "Synthesis and evaluation of fluorinated analogues of monoamine reuptake inhibitors". In: *Journal of Fluorine Chemistry*. Special Issue: Fluorine Chemistry in France 134 (Feb. 2012), pp. 136–145.

[209] Andrew S. Kende, Kun Liu, and K. M. Jos Brands. "Total Synthesis of (-)-Altemicidin: A Novel Exploitation of the Potier-Polonovski Rearrangement". In: *Journal of the American Chemical Society* 117.42 (Oct. 1, 1995), pp. 10597–10598.

[210] Klaus Müller, Christoph Faeh, and François Diederich. "Fluorine in Pharmaceuticals: Looking Beyond Intuition". In: *Science* 317.5846 (Sept. 28, 2007), pp. 1881–1886.

[211] A. Bondi. "van der Waals Volumes and Radii". In: *The Journal of Physical Chemistry* 68.3 (Mar. 1, 1964), pp. 441–451.

[212] Eliane Schweizer et al. "A fluorine scan at the catalytic center of thrombin: C–F, C–OH, and C–OMe bioisosterism and fluorine effects on pKa and log D values". In: *ChemMedChem* 1.6 (June 2006), pp. 611–621.

[213] Kake Zhao et al. "Inhibition of dipeptidyl peptidase IV (DPP IV) by 2-(2-amino-1-fluoro-propylidene)-cyclopentanecarbonitrile, a fluoroolefin containing peptidomimetic". In: *Bioorganic & Medicinal Chemistry* 11.2 (Jan. 17, 2003), pp. 207–215.

[214] Attila E. Pavlath Miloš Hudlický. *Chemistry of organic fluorine compounds II: a critical review*. Washington, DC: American Chemical Society, 1995. 1296 pp.

[215] Ralph Paulini, Klaus Müller, and François Diederich. "Orthogonal multipolar interactions in structural chemistry and biology". In: *Angewandte Chemie (International Ed. in English)* 44.12 (Mar. 11, 2005), pp. 1788–1805.

[216] Kenneth L. Kirk. "Selective fluorination in drug design and development: an overview of biochemical rationales". In: *Current Topics in Medicinal Chemistry* 6.14 (2006), pp. 1447–1456.

[217] James S. Nowick et al. “An Extended beta-Strand Mimic for a Larger Artificial beta-Sheet”. In: *Journal of the American Chemical Society* 119.23 (June 1, 1997), pp. 5413–5424.

[218] James H. Tsai, Amy Sue Waldman, and James S. Nowick. “Two New beta-strand Mimics”. In: *Bioorganic & Medicinal Chemistry* 7.1 (Jan. 1999), pp. 29–38.

[219] Sandeep Kumar Mishra and N. Suryaprakash. “Intramolecular hydrogen bonds involving organic fluorine in the derivatives of hydrazides: an NMR investigation substantiated by DFT based theoretical calculations”. In: *Physical chemistry chemical physics: PCCP* 17.23 (June 21, 2015), pp. 15226–15235.

[220] Maria Luisa Gelmi et al. “3-demethoxy-3-glycosylaminothiocolchicines: Synthesis of a new class of putative muscle relaxant compounds”. In: *Journal of Medicinal Chemistry* 49.18 (Sept. 7, 2006), pp. 5571–5577.

[221] R. Fanelli et al. “Introduction of polar groups on the naphthalene scaffold of molecular tongs inhibiting wild-type and mutated HIV-1 protease dimerization”. In: *MedChemComm* 5.6 (May 28, 2014), pp. 719–727.

[222] Samir Messaoudi, Jean-Daniel Brion, and Mouâd Alami. “An Expeditious Copper-Catalyzed Access to 3-Aminoquinolinones, 3-Aminocoumarins and Anilines using Sodium Azide”. In: *Advanced Synthesis & Catalysis* 352.10 (July 5, 2010), pp. 1677–1687.

[223] Abdol R. Hajipour and Fatemeh Mohammadsaleh. “Synthesis of aryl azides from aryl halides promoted by Cu2O/tetraethylammonium prolinate”. In: *Tetrahedron Letters* 50.55 (2014), pp. 6799–6802.

[224] John T. Markiewicz, Olaf Wiest, and Paul Helquist. “Synthesis of primary aryl amines through a copper-assisted aromatic substitution reaction with sodium azide”. In: *The Journal of Organic Chemistry* 75.14 (July 16, 2010), pp. 4887–4890.

[225] Samantha Voth, Joshua W. Hollett, and J. Adam McCubbin. “Transition-metal-free access to primary anilines from boronic acids and a common (+)NH2 equivalent”. In: *The Journal of Organic Chemistry* 80.5 (Mar. 6, 2015), pp. 2545–2553.

[226] Kazuyuki Miyashita, Takayuki Sakai, and Takeshi Imanishi. “Total synthesis of (+/-)-spiroxin C”. In: *Organic Letters* 5.15 (July 24, 2003), pp. 2683–2686.

[227] F. D. Bellamy and K. Ou. “Selective reduction of aromatic nitro compounds with stannous chloride in non acidic and non aqueous medium”. In: *Tetrahedron Letters* 25.8 (Jan. 1, 1984), pp. 839–842.

[228] Celine Adessi and Claudio Soto. "Converting a Peptide into a Drug: Strategies to Improve Stability and Bioavailability". In: *Current Medicinal Chemistry* 9.9 (May 1, 2002), pp. 963–978.

[229] Senthil Kumar Ramanathan et al. "Modular Synthesis of Cyclic Peptidomimetics Inspired by -Turns". In: *Organic Letters* 7.6 (Mar. 1, 2005), pp. 1059–1062.

[230] Hyunsoo Han and Kim D. Janda. "Azatides: Solution and Liquid Phase Syntheses of a New Peptidomimetic". In: *Journal of the American Chemical Society* 118.11 (Jan. 1, 1996), pp. 2539–2544.

[231] Michael Thormann and Hans-Jörg Hofmann. "Conformational properties of azapeptides". In: *Journal of Molecular Structure: THEOCHEM* 469.1 (Sept. 1, 1999), pp. 63–76.

[232] Noam S. Freeman, Mattan Hurevich, and Chaim Gilon. "Synthesis of N-substituted Ddz-protected hydrazines and their application in solid phase synthesis of aza-peptides". In: *Tetrahedron* 65.8 (Feb. 21, 2009), pp. 1737–1745.

[233] Rosa E. Melendez and William D. Lubell. "Aza-Amino Acid Scan for Rapid Identification of Secondary Structure Based on the Application of N-Boc-Aza1-Dipeptides in Peptide Synthesis". In: *Journal of the American Chemical Society* 126.21 (June 1, 2004), pp. 6759–6764.

[234] Wei-Jun Zhang et al. "Impact of Azaproline on Amide Cis—Trans Isomerism: Conformational Analyses and NMR Studies of Model Peptides Including TRH Analogues". In: *Journal of the American Chemical Society* 125.5 (Feb. 1, 2003), pp. 1221–1235.

[235] Hans-Jurgen. Hess, Walter T. Moreland, and Gerald D. Laubach. "N-[2-Isopropyl-3-(L-aspartyl-L-arginyl)-carbazoyl]-L- tyrosyl-L-valyl-L-histidyl-L-prolyl-L-phenylalanine,1 an Isostere of Bovine Angiotensin II". In: *Journal of the American Chemical Society* 85.24 (Dec. 1, 1963), pp. 4040–4041.

[236] Hartmut Niedrich. "Hydrazinverbindungen als Heterobestandteile in Peptiden. XVI. Synthese von 9-Hydrazinoessigsäure-, 9-Azaglycin- und 5-alpha-Azaasparagin-Oxytocin". In: *Journal für Praktische Chemie* 314.5 (Jan. 1, 1972), pp. 769–779.

[237] P. Oehme et al. "[Pharmacology of hydrazino carbonic acids, hydrazino peptides and other hydrazine derivatives. IX. Studies on correlations between biological effect and structure of heterologeous eledoisinpenta, hexa and octapeptide sequences]". In: *Acta Biologica Et Medica Germanica* 28.1 (1972), pp. 121–131.

[238] Hyunsoo Han, Juyoung Yoon, and Kim D Janda. "Investigations of azapeptides as mimetics of Leu-enkephalin". In: *Bioorganic & Medicinal Chemistry Letters* 8.1 (Jan. 6, 1998), pp. 117–120.

[239] Anand S. Dutta et al. “Synthesis and biological activity of highly active .alpha.-aza analogs of luliberin”. In: *Journal of Medicinal Chemistry* 21.10 (Oct. 1, 1978), pp. 1018–1024.

[240] Jill M. Gassman and Joe Magrath. “An active-site titrant for chymotrypsin, and evidence that azapeptide esters are less susceptible to nucleophilic attack than ordinary esters”. In: *Bioorganic & Medicinal Chemistry Letters* 6.15 (Aug. 6, 1996), pp. 1771–1774.

[241] J. Edward Semple et al. “Synthesis and biological activity of P2–P4 azapeptidomimetic P1-argininal and P1-ketoargininamide derivatives: a novel class of serine protease inhibitors”. In: *Bioorganic & Medicinal Chemistry Letters* 7.3 (Feb. 4, 1997), pp. 315–320.

[242] Ruye Xing and Robert P. Hanzlik. “Azapeptides as Inhibitors and Active Site Titrants for Cysteine Proteinases”. In: *Journal of Medicinal Chemistry* 41.8 (Apr. 1, 1998), pp. 1344–1351.

[243] Todd L. Graybill et al. “Synthesis and evaluation of azapeptide-derived inhibitors of serine and cysteine proteases”. In: *Bioorganic & Medicinal Chemistry Letters* 2.11 (Nov. 1992), pp. 1375–1380.

[244] Todd L. Graybill et al. “Synthesis and evaluation of diacylhydrazines as inhibitors of the interleukin-1beta converting enzyme (ICE)”. In: *Bioorganic & Medicinal Chemistry Letters* 5.11 (June 8, 1995), pp. 1197–1202.

[245] Joe Magrath and Robert H. Abeles. “Cysteine protease inhibition by azapeptide esters”. In: *Journal of Medicinal Chemistry* 35.23 (Nov. 1, 1992), pp. 4279–4283.

[246] Nader E. Abo-Dya et al. “Benzotriazole-Mediated Synthesis of Azapeptides: En Route to an Aza-Leuenkephalin Analogue”. In: *The Journal of Organic Chemistry* 78.8 (Apr. 19, 2013), pp. 3541–3552.

[247] David Sabatino et al. “Structure–Activity Relationships of GHRP-6 Azapeptide Ligands of the CD36 Scavenger Receptor by Solid-Phase Submonomer Azapeptide Synthesis”. In: *Journal of the American Chemical Society* 133.32 (Aug. 17, 2011), pp. 12493–12506.

[248] Caroline Proulx and William D. Lubell. “Copper-Catalyzed N-Arylation of Semicarbazones for the Synthesis of Aza-Arylglycine-Containing Aza-Peptides”. In: *Organic Letters* 12.13 (July 2, 2010), pp. 2916–2919.

[249] Carine B. Bourguet et al. “Targeting the Prostaglandin F2alpha Receptor for Preventing Preterm Labor with Azapeptide Tocolytics”. In: *Journal of Medicinal Chemistry* 54.17 (Sept. 8, 2011), pp. 6085–6097.

[250] E. Wieczerzak et al. “Novel azapeptide inhibitors of cathepsins B and K. Structural background to increased specificity for cathepsin B”. In: *Journal of Peptide Research* 66.1 (Dec. 1, 2005), pp. 1–11.

[251] Murray D. Bailey et al. "Novel Azapeptide Inhibitors of Hepatitis C Virus Serine Protease". In: *Journal of Medicinal Chemistry* 47.15 (July 1, 2004), pp. 3788–3799.

[252] D. Boeglin et al. "Aza-scanning of the Potent Melanocortin Receptor Agonist Ac-His-d-Phe-Arg-Trp-NH2". In: *Chemical Biology & Drug Design* 67.4 (Apr. 1, 2006), pp. 275–283.

[253] Özlem Doğan Ekici et al. "Design, Synthesis, and Evaluation of Aza-Peptide Michael Acceptors as Selective and Potent Inhibitors of Caspases-2, -3, -6, -7, -8, -9, and -10". In: *Journal of Medicinal Chemistry* 49.19 (Sept. 1, 2006), pp. 5728–5749.

[254] Karen Ellis James et al. "Design, Synthesis, and Evaluation of Aza-Peptide Epoxides as Selective and Potent Inhibitors of Caspases-1, -3, -6, and -8". In: *Journal of Medicinal Chemistry* 47.6 (Mar. 1, 2004), pp. 1553–1574.

[255] Shridhar V. Andurkar et al. "Synthesis and Structural Studies of Aza Analogues of Functionalized Amino Acids: New Anticonvulsant Agents". In: *Journal of Medicinal Chemistry* 44.9 (Apr. 1, 2001), pp. 1475–1478.

[256] Richard D. Hill and John C. Vederas. "Azodicarboxamides: A New Class of Cysteine Proteinase Inhibitor for Hepatitis A Virus and Human Rhinovirus 3C Enzymes". In: *The Journal of Organic Chemistry* 64.26 (Dec. 1, 1999), pp. 9538–9546.

[257] Caroline Proulx et al. "Azapeptides and their therapeutic potential". In: *Future Medicinal Chemistry* 3.9 (July 2011), pp. 1139–1164.

[258] Ulf Ragnarsson. "Synthetic methodology for alkyl substituted hydrazines". In: *Chemical Society Reviews* 30.4 (Jan. 1, 2001), pp. 205–213.

[259] Anamarija Zega. "Azapeptides as Pharmacological Agents". In: *Current Medicinal Chemistry* 12.5 (Mar. 1, 2005), pp. 589–597.

[260] Damien Boeglin and William D. Lubell. "Aza-Amino Acid Scanning of Secondary Structure Suited for Solid-Phase Peptide Synthesis with Fmoc Chemistry and Aza-Amino Acids with Heteroatomic Side Chains". In: *Journal of Combinatorial Chemistry* 7.6 (Nov. 1, 2005), pp. 864–878.

[261] David Sabatino et al. "Exploring Side-Chain Diversity by Submonomer Solid-Phase Aza-Peptide Synthesis". In: *Organic Letters* 11.16 (Aug. 20, 2009), pp. 3650–3653.

[262] Olga Tsubrik and Uno Mäeorg. "Combination of tert-Butoxycarbonyl and Triphenylphosphonium Protecting Groups in the Synthesis of Substituted Hydrazines". In: *Organic Letters* 3.15 (July 1, 2001), pp. 2297–2299.

[263] Thomas Lebleu et al. “Selective monomethylation of primary amines with simple electrophiles”. In: *Chemical Communications* 50.15 (Jan. 23, 2014), pp. 1836–1838.

[264] William P. Malachowski et al. “The Synthesis of Azapeptidomimetic beta-Lactam Molecules as Potential Protease Inhibitors”. In: *The Journal of Organic Chemistry* 67.25 (Dec. 1, 2002), pp. 8962–8969.

[265] Laure Dufau et al. “Carbonylhydrazide-Based Molecular Tongs Inhibit Wild-Type and Mutated HIV-1 Protease Dimerization”. In: *Journal of Medicinal Chemistry* 55.15 (Aug. 9, 2012), pp. 6762–6775.

[266] Fabio Ramondo and Luigi Bencivenni. “Molecular conformation of isolated and hydrogen bonded N,N-diformohydrazide: an ab initio study”. In: *Journal of the Chemical Society, Perkin Transactions 2* 9 (Jan. 1, 1995), pp. 1797–1804.

[267] Charles H. Reynolds and Robert E. Hormann. “Theoretical Study of the Structure and Rotational Flexibility of Diacylhydrazines: Implications for the Structure of Nonsteroidal Ecdysone Agonists and Azapeptides”. In: *Journal of the American Chemical Society* 118.39 (Jan. 1, 1996), pp. 9395–9401.

[268] H. -J Lee et al. “The beta-turn preferential solution conformation of a tetrapeptide containing an azaamino acid residue”. In: *Journal of Molecular Structure* 569.1 (July 19, 2001), pp. 43–54.

[269] Ho-Jin Lee et al. “NBO approach to evaluate origin of rotational barrier of diformylhydrazine”. In: *Journal of Molecular Structure: THEOCHEM* 631.1 (Aug. 1, 2003), pp. 101–110.

[270] Vyacheslav S. Bryantsev, Timothy K. Firman, and Benjamin P. Hay. “Conformational Analysis and Rotational Barriers of Alkyl- and Phenyl-Substituted Urea Derivatives”. In: *The Journal of Physical Chemistry A* 109.5 (Feb. 1, 2005), pp. 832–842.

[271] Vincent Semetey et al. “Unexpected Stability of the Urea cis−trans Isomer in Urea-Containing Model Pseudopeptides”. In: *Organic Letters* 3.24 (Nov. 1, 2001), pp. 3843–3846.

[272] H. J. Lee et al. “Role of azaamino acid residue in beta-turn formation and stability in designed peptide”. In: *The Journal of Peptide Research: Official Journal of the American Peptide Society* 56.1 (July 2000), pp. 35–46.

[273] Ho-Jin Lee, Hyun-Mee Park, and Kang-Bong Lee. “The beta-turn scaffold of tripeptide containing an azaphenylalanine residue”. In: *Biophysical Chemistry* 125.1 (Jan. 2007), pp. 117–126.

[274] Cécile Abbas et al. “Original and efficient synthesis of 2:1-[alpha/aza]-oligomer precursors”. In: *Tetrahedron Letters* 50.28 (July 15, 2009), pp. 4158–4160.

[275] Zhou Zhou et al. "Synthesis and Structural Characterization of 2:1 [alpha/Aza]-oligomers". In: *European Journal of Organic Chemistry* 2014.34 (Dec. 1, 2014), pp. 7643–7650.

[276] Ho-Jin Lee et al. "A Theoretical Study of Conformational Properties of N-Methyl Azapeptide Derivatives". In: *Journal of the American Chemical Society* 124.40 (Oct. 1, 2002), pp. 11881–11893.

[277] Philipp A. Ottersbach, Gregor Schnakenburg, and Michael Gütschow. "Induction of chirality: experimental evidence of atropisomerism in azapeptides". In: *Chemical Communications* 48.46 (May 14, 2012), pp. 5772–5774.

[278] Philipp A. Ottersbach, Gregor Schnakenburg, and Michael Gütschow. "Atropisomerism in azadipeptides: evaluation of N1-methylation and thioamide introduction". In: *Tetrahedron Letters* 56.34 (Aug. 19, 2015), pp. 4889–4891.

[279] F. André et al. "Aza-peptides. II. X-ray structures of aza-alanine and aza-asparagine-containing peptides". In: *The Journal of Peptide Research: Official Journal of the American Peptide Society* 49.6 (June 1997), pp. 556–562.

[280] F. André et al. "Aza-peptides. III. Experimental structural analysis of aza-alanine and aza-asparagine-containing peptides". In: *The Journal of Peptide Research: Official Journal of the American Peptide Society* 50.5 (Nov. 1997), pp. 372–381.

[281] A. Lecoq et al. "Crystal state conformation of three azapeptides containing the Azaproline residue, a beta-turn regulator". In: *Biopolymers* 33.7 (July 1, 1993), pp. 1051–1059.

[282] M. Marraud and A. Aubry. "Crystal structures of peptides and modified peptides". In: *Biopolymers* 40.1 (1996), pp. 45–83.

[283] Z. Benatalah et al. "Evidence for a beta-turn in an azadipeptide sequence. Synthesis and crystal structure of ButCO-Pro-AzaAla-NHPri". In: *International Journal of Peptide and Protein Research* 38.6 (Dec. 1991), pp. 603–605.

[284] Joachim Gante et al. "Synthesis and properties of the first all-aza analogue of a biologically active peptide". In: *Journal of Peptide Science* 1.3 (May 1, 1995), pp. 201–206.

[285] Yitao Zhang, Roy M. Malamakal, and David M. Chenoweth. "Aza-Glycine Induces Collagen Hyperstability". In: *Journal of the American Chemical Society* 137.39 (Oct. 2015), pp. 12422–12425.

[286] Jay L. Banks et al. "Integrated Modeling Program, Applied Chemical Theory (IMPACT)". In: *Journal of Computational Chemistry* 26.16 (Dec. 1, 2005), pp. 1752–1780.

[287] W. Clark Still et al. “Semianalytical treatment of solvation for molecular mechanics and dynamics”. In: *Journal of the American Chemical Society* 112.16 (Aug. 1, 1990), pp. 6127–6129.

[288] George Chang, Wayne C. Guida, and W. Clark Still. “An internal-coordinate Monte Carlo method for searching conformational space”. In: *Journal of the American Chemical Society* 111.12 (June 1, 1989), pp. 4379–4386.

[289] Lawrence A. Kelley, Stephen P. Gardner, and Michael J. Sutcliffe. “An automated approach for clustering an ensemble of NMR-derived protein structures into conformationally related subfamilies”. In: *Protein Engineering* 9.11 (Jan. 11, 1996), pp. 1063–1065.

[290] W. Kohn and L. J. Sham. “Self-Consistent Equations Including Exchange and Correlation Effects”. In: *Physical Review* 140.4 (Nov. 15, 1965), A1133–A1138.

[291] P. Hohenberg and W. Kohn. “Inhomogeneous Electron Gas”. In: *Physical Review* 136.3 (Nov. 9, 1964), B864–B871.

[292] Axel D. Becke. “Density-functional thermochemistry. III. The role of exact exchange”. In: *The Journal of Chemical Physics* 98.7 (Apr. 1, 1993), pp. 5648–5652.

[293] Chengteh Lee, Weitao Yang, and Robert G. Parr. “Development of the Colle-Salvetti correlation-energy formula into a functional of the electron density”. In: *Physical Review B* 37.2 (Jan. 15, 1988), pp. 785–789.

[294] Warren J. Hehre et al. *Ab Initio Molecular Orbital Theory*. 1st ed. Wiley-Interscience, Mar. 10, 1986. 576 pp.

[295] Frisch, M. J. et al. *Gaussian 09, Revision A.02*. Wallingford CT, 2009.

[296] S. Miertuš, E. Scrocco, and J. Tomasi. “Electrostatic interaction of a solute with a continuum. A direct utilizaion of AB initio molecular potentials for the prevision of solvent effects”. In: *Chemical Physics* 55.1 (Feb. 1, 1981), pp. 117–129.

Annexes : X-Ray structures

Compound **5.2**

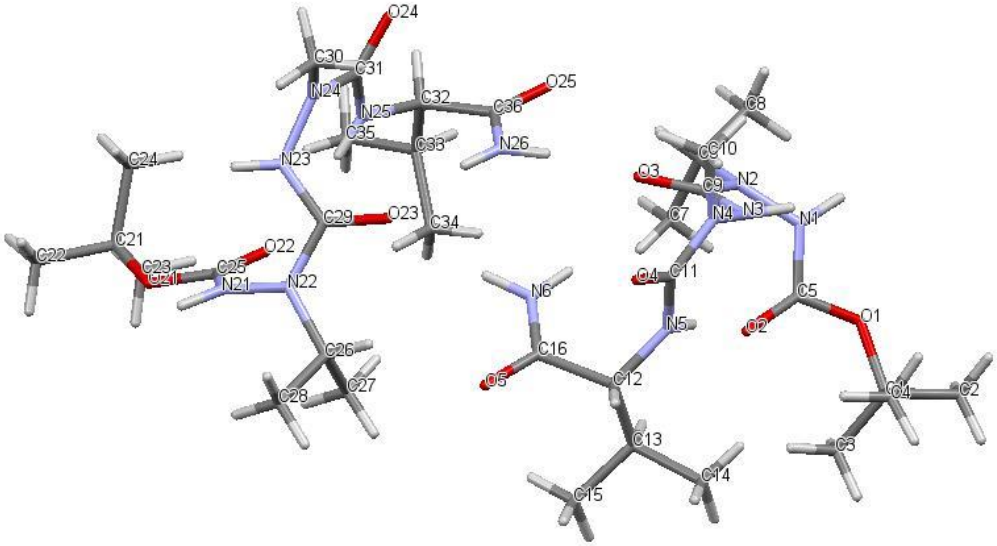

Space Group	P 2_1
Cell Lengths	**a** 10.4497(3) **b** 14.6303(4) **c** 15.2786(5)
Cell Angles	**α** 90 **β** 108.211(2) **γ** 90
Cell Volume	2218.83
Z, Z'	**Z**: 4 **Z'**: 0
R-Factor (%)	4

Label	Charge	SybylType	Xfrac + ESD	Yfrac + ESD	Zfrac + ESD
C1	0	C.3	0.7988(3)	-0.4020(2)	0.4371(2)
C2	0	C.3	0.9194(4)	-0.4439(3)	0.5089(3)
C3	0	C.3	0.8250(4)	-0.3864(3)	0.3456(3)
C4	0	C.3	0.6733(3)	-0.4579(3)	0.4258(2)
C5	0	C.2	0.6825(2)	-0.25791(19)	0.44130(14)
C6	0	C.3	0.6390(2)	-0.03893(18)	0.48121(17)
C7	0	C.3	0.7054(3)	-0.0348(2)	0.4066(2)
C8	0	C.3	0.7353(3)	-0.0151(2)	0.5751(2)

C9	0	C.2	0.4435(2)	-0.14353(17)	0.43632(13)
C10	0	C.3	0.1682(3)	-0.2192(2)	0.44865(17)
C11	0	C.2	0.2196(2)	-0.26497(16)	0.30935(13)
C12	0	C.3	0.2799(2)	-0.27166(17)	0.16811(13)
C13	0	C.3	0.4022(2)	-0.3031(2)	0.14071(15)
C14	0	C.3	0.4329(3)	-0.4031(2)	0.16809(19)
C15	0	C.3	0.3829(3)	-0.2907(3)	0.03807(17)
C16	0	C.2	0.2224(2)	-0.17944(17)	0.12704(13)
O1	0	O.3	0.78509(18)	-0.31415(15)	0.48070(12)
O2	0	O.2	0.61766(17)	-0.25403(15)	0.36053(10)
O3	0	O.2	0.37044(16)	-0.08435(12)	0.38823(10)
O4	0	O.2	0.09890(15)	-0.27399(14)	0.26681(10)
O5	0	O.2	0.14536(18)	-0.17479(13)	0.04749(10)
N1	0	N.am	0.66169(19)	-0.20403(15)	0.50793(11)
N2	0	N.am	0.57716(18)	-0.12884(14)	0.48425(12)
N3	0	N.am	0.39750(19)	-0.22953(14)	0.44453(11)
N4	0	N.am	0.26191(18)	-0.24852(15)	0.40207(11)
N5	0	N.am	0.31665(17)	-0.27211(14)	0.26818(11)
N6	0	N.am	0.2625(2)	-0.10581(15)	0.17828(13)
H1	0	H	0.7088	-0.21	0.5696
H2	0	H	0.4387	-0.2613	0.4931
H3	0	H	0.3963	-0.2665	0.3002
H4	0	H	0.2212	-0.0521	0.156
H5	0	H	0.3075	-0.1104	0.2365
H21	0	H	0.8993	-0.4524	0.565
H22	0	H	0.9401	-0.5013	0.4877
H23	0	H	0.9949	-0.4042	0.5197
H31	0	H	0.7472	-0.3605	0.3029
H32	0	H	0.8445	-0.4434	0.3227
H33	0	H	0.8992	-0.3464	0.3547
H41	0	H	0.5999	-0.431	0.381
H42	0	H	0.6877	-0.5184	0.4071
H43	0	H	0.6559	-0.4611	0.4833
H61	0	H	0.5687	0.0052	0.4666
H71	0	H	0.6417	-0.0498	0.3491
H72	0	H	0.7783	-0.0767	0.4205
H73	0	H	0.7384	0.0255	0.4039
H81	0	H	0.6892	-0.019	0.6198
H82	0	H	0.8084	-0.0573	0.5907
H83	0	H	0.7684	0.0449	0.5742
H101	0	H	0.2141	-0.2115	0.5122
H102	0	H	0.0999	-0.2648	0.4409
H103	0	H	0.1275	-0.1635	0.4227
H121	0	H	0.2109	-0.316	0.1457
H131	0	H	0.4776	-0.2674	0.1743
H141	0	H	0.5089	-0.4221	0.1512
H142	0	H	0.4524	-0.4089	0.2329

H143	0	H	0.3575	-0.4395	0.1375
H151	0	H	0.4611	-0.3109	0.025
H152	0	H	0.3072	-0.3251	0.0033
H153	0	H	0.368	-0.2277	0.0226
C21	0	C.3	0.2192(3)	0.4041(2)	-0.1267(2)
C22	0	C.3	0.1385(4)	0.4508(2)	-0.2152(2)
C23	0	C.3	0.3663(4)	0.4034(3)	-0.1159(4)
C24	0	C.3	0.1868(5)	0.4464(3)	-0.0449(3)
C25	0	C.2	0.1909(2)	0.25116(18)	-0.07044(14)
C26	0	C.3	0.1206(3)	0.02696(18)	-0.06093(16)
C27	0	C.3	0.2639(4)	0.0234(3)	-0.0627(3)
C28	0	C.3	0.0185(4)	0.0013(2)	-0.15264(18)
C29	0	C.2	0.0913(2)	0.13542(16)	0.05611(13)
C30	0	C.3	-0.0677(2)	0.2292(2)	0.18041(16)
C31	0	C.2	0.1746(2)	0.26065(16)	0.22788(13)
C32	0	C.3	0.4173(2)	0.24965(18)	0.27762(14)
C33	0	C.3	0.5389(2)	0.2588(2)	0.24220(18)
C34	0	C.3	0.5549(3)	0.1781(3)	0.1846(2)
C35	0	C.3	0.5392(4)	0.3495(3)	0.1956(3)
C36	0	C.2	0.4298(2)	0.16155(17)	0.33212(13)
O21	0	O.3	0.1658(2)	0.31152(14)	-0.13935(11)
O22	0	O.2	0.28820(16)	0.25025(14)	-0.00122(10)
O23	0	O.2	0.12481(16)	0.07701(12)	0.11740(9)
O24	0	O.2	0.17520(16)	0.27368(13)	0.30711(9)
O25	0	O.2	0.51905(18)	0.15579(13)	0.40769(10)
N21	0	N.am	0.08659(19)	0.19131(14)	-0.09050(11)
N22	0	N.am	0.08727(18)	0.11807(14)	-0.03270(11)
N23	0	N.am	0.05908(18)	0.22312(14)	0.07196(11)
N24	0	N.am	0.05597(17)	0.24679(15)	0.15937(11)
N25	0	N.am	0.28937(18)	0.25743(15)	0.20410(11)
N26	0	N.am	0.3494(2)	0.09238(15)	0.29625(13)
H6	0	H	0.0141	0.1975	-0.146
H7	0	H	0.0047	0.2544	0.0254
H8	0	H	0.28	0.2475	0.1483
H9	0	H	0.2869	0.0952	0.2463
H10	0	H	0.3622	0.0406	0.3308
H221	0	H	0.0457	0.4502	-0.2199
H222	0	H	0.1681	0.5125	-0.2145
H223	0	H	0.1515	0.4198	-0.2661
H231	0	H	0.4138	0.3737	-0.0596
H232	0	H	0.398	0.4646	-0.1143
H233	0	H	0.3813	0.3719	-0.1659
H241	0	H	0.2379	0.4164	0.01
H242	0	H	0.2093	0.5095	-0.041
H243	0	H	0.0936	0.4395	-0.0529
H261	0	H	0.1123	-0.0158	-0.0161
H271	0	H	0.3232	0.0397	-0.0036

H272	0	H	0.2748	0.0643	-0.1075
H273	0	H	0.284	-0.0373	-0.077
H281	0	H	-0.0696	0.0048	-0.1478
H282	0	H	0.0264	0.0421	-0.199
H283	0	H	0.0356	-0.0594	-0.1684
H301	0	H	-0.1396	0.2218	0.125
H302	0	H	-0.0863	0.2797	0.2141
H303	0	H	-0.0576	0.1756	0.2167
H321	0	H	0.4213	0.299	0.3192
H331	0	H	0.6165	0.259	0.2954
H341	0	H	0.6313	0.1873	0.1645
H342	0	H	0.5664	0.1239	0.2203
H343	0	H	0.4766	0.1726	0.1323
H351	0	H	0.6156	0.3526	0.1747
H352	0	H	0.5426	0.3973	0.238
H353	0	H	0.4594	0.3545	0.1446

Compound **3.11**

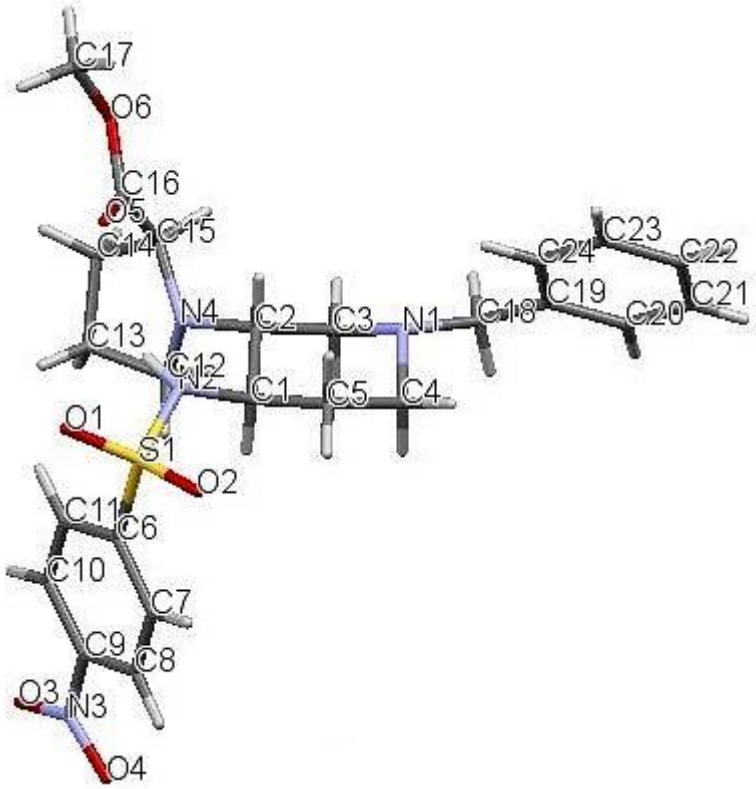

Space Group	P 2_1
Cell Lengths	**a** 12.4747(3) **b** 7.0633(2) **c** 17.6651(5)
Cell Angles	**α** 90 **β** 91.782(1) **γ** 90
Cell Volume	1555.76

Label	Charge	SybylType	Xfrac + ESD	Yfrac + ESD	Zfrac + ESD
S1	0	S.o2	0.565972	0.029108	0.140088
O1	0	O.2	0.53769	-0.040997	0.066266
O2	0	O.2	0.621666	-0.090314	0.193358
O3	0	O.2	0.79766	0.848768	0.063716
O4	0	O.2	0.910073	0.738808	0.146494
O5	0	O.2	0.229197	0.130893	0.096503
O6	0	O.3	0.068871	0.272919	0.100369
N1	0	N.3	0.342031	0.256735	0.387294
N2	0	N.3	0.455784	0.100462	0.176017
H2A	0	H	0.411961	0.142921	0.144854
N3	0	N.3	0.828872	0.727271	0.107391
N4	0	N.3	0.323325	0.414292	0.183068
C1	0	C.3	0.453355	0.205393	0.24765

H1	0	H	0.50965	0.30621	0.248076
C2	0	C.3	0.342531	0.297305	0.250157
H2	0	H	0.288955	0.192044	0.247203
C3	0	C.3	0.328736	0.394444	0.326631
H3A	0	H	0.38263	0.49644	0.333335
H3B	0	H	0.256513	0.452122	0.328241
C4	0	C.3	0.451437	0.182781	0.389012
H4A	0	H	0.461914	0.095948	0.432608
H4B	0	H	0.503174	0.288387	0.395067
C5	0	C.3	0.471198	0.077485	0.315752
H5A	0	H	0.545742	0.029263	0.31663
H5B	0	H	0.422153	-0.032453	0.311503
C6	0	C.3	0.647094	0.233081	0.129184
C7	0	C.2	0.74534	0.244832	0.166622
H7	0	H	0.77112	0.142993	0.197236
C8	0	C.2	0.806104	0.407988	0.158889
H8	0	H	0.873949	0.420145	0.184363
C9	0	C.2	0.76614	0.551933	0.113567
C10	0	C.2	0.669796	0.539629	0.074393
H10	0	H	0.645295	0.640099	0.042562
C11	0	C.2	0.609146	0.377356	0.082351
H11	0	H	0.542015	0.364832	0.05594
C12	0	C.3	0.374161	0.601323	0.177743
H12A	0	H	0.453278	0.590734	0.177389
H12B	0	H	0.353731	0.684695	0.219974
C13	0	C.3	0.32908	0.672487	0.102937
H13A	0	H	0.365833	0.613417	0.060041
H13B	0	H	0.335484	0.811854	0.099195
C14	0	C.3	0.212497	0.611756	0.104494
H14A	0	H	0.18496	0.579053	0.052978
H14B	0	H	0.167546	0.713953	0.125055
C15	0	C.3	0.212332	0.436275	0.156702
H15	0	H	0.165844	0.460636	0.20077
C16	0	C.2	0.173822	0.261529	0.114893
C17	0	C.3	0.020204	0.117504	0.059287
H17A	0	H	0.053825	0.104345	0.010158
H17B	0	H	-0.056651	0.141946	0.051326
H17C	0	H	0.030313	0.000433	0.088415
C18	0	C.3	0.314704	0.336616	0.460683
H18A	0	H	0.245802	0.405522	0.455114
H18B	0	H	0.370599	0.428961	0.476773
C19	0	C.2	0.305204	0.187193	0.521296
C20	0	C.2	0.324009	0.232161	0.597389
H20	0	H	0.347331	0.356212	0.610585
C21	0	C.2	0.309605	0.101169	0.653885
H21	0	H	0.322411	0.135716	0.705348
C22	0	C.2	0.276891	-0.0786	0.636037

H22	0	H	0.266856	-0.168532	0.675173
C23	0	C.2	0.25835	-0.129985	0.561168
H23	0	H	0.236006	-0.254977	0.548609
C24	0	C.2	0.272777	0.003148	0.504711
H24	0	H	0.260166	-0.032363	0.453334
C25	0	C.3	1.02588	0.738524	0.321217
H25A	0	H	0.958221	0.721811	0.29117
H25B	0	H	1.06775	0.61989	0.318017
C26	0	C.3	1.08946	0.900808	0.288845
H26A	0	H	1.16024	0.907999	0.315631
H26B	0	H	1.1019	0.875556	0.234697
C27	0	C.3	1.03424	1.08356	0.295882
H27A	0	H	0.965827	1.08092	0.265953
H27B	0	H	1.07942	1.18586	0.275651
C28	0	C.3	1.01188	1.123	0.379187
H28A	0	H	1.08056	1.14685	0.407148
H28B	0	H	0.96729	1.23843	0.382709
C29	0	C.3	0.955526	0.961559	0.415134
H29A	0	H	0.954661	0.984372	0.470407
H29B	0	H	0.88012	0.960521	0.395934
C30	0	C.3	1.00086	0.777698	0.402642
H30A	0	H	0.950055	0.680374	0.419984
H30B	0	H	1.06771	0.765545	0.433951
C25B	0	C.3	1.07362	0.741115	0.36579
H25C	0	H	1.09249	0.608372	0.354109
H25D	0	H	1.11029	0.778028	0.41406
C26B	0	C.3	1.10573	0.873945	0.301221
H26C	0	H	1.1836	0.861467	0.293198
H26D	0	H	1.06712	0.83601	0.253811
C27B	0	C.3	1.08027	1.075	0.318567
H27C	0	H	1.10668	1.15813	0.278059
H27D	0	H	1.11631	1.11252	0.366986
C28B	0	C.3	0.96218	1.09689	0.324157
H28C	0	H	0.927289	1.07807	0.273615
H28D	0	H	0.945495	1.22666	0.341379
C29B	0	C.3	0.91901	0.955722	0.378805
H29C	0	H	0.937423	0.999142	0.430886
H29D	0	H	0.839819	0.954915	0.37303
C30B	0	C.3	0.957321	0.762768	0.370698
H30C	0	H	0.922924	0.707611	0.3245
H30D	0	H	0.933306	0.688011	0.414442

université PARIS-SACLAY | ÉCOLE DOCTORALE Innovation thérapeutique : du fondamental à l'appliqué

Title : Synthetic mimics of beta-sheets: design, synthesis and evaluation of their ability to modulate the aggregation of the beta-amyloid 1-42 peptide.

Keywords : peptidomimetic, beta-sheet, beta-hairpin, beta-amyloid 1-42 peptide, azatide, capillary electrophoresis.

Abstract : Amyloidosis is the generic word to name a group of diseases that are caused by the misfolding and extracellular accumulation of various proteins. Alzheimer's disease (AD) is a neurodegenerative disorder linked to oligomerization and fibrillization of amyloid β peptides, with Aβ 1-42 being the most aggregative and neurotoxic one. To date, the exactly cause of the Alzheimer's disease is not still known and so there is no effective treatment of the disease.

An attractive strategy for treating AD could be the inhibition of the oligomerization of soluble Aβ monomers, by stabilizing the native unstructured conformation of the peptide, using compounds able to prevent the formation of β-sheets. Aβ fibrils present a cross-β structure in which the individual β-strands are oriented perpendicular to the fibril axis. Indeed, few structural studies of oligomeric species and fibrils revealed that the aggregation involves β-sheet structures.

A large number of small molecules have been proposed for their ability to inhibit or modulate Aβ1-42 aggregation and toxicity. However, the aggregation process is highly complex, and extremely difficult to control. Recent studies indicate that soluble transient oligomers preceding fibril formation are highly toxic species. Thus, the development of inhibitors targeting both oligomerization and fibrillization remains challenging despite its therapeutic significance. Peptides are today reasonable alternatives to small molecule pharmaceuticals. In particular, inhibition of Aβ-aggregation has been targeted using self-recognition elements (SREs), which are key amino acid sequences involved in the different aggregated species. To our knowledge, the use of small acyclic β-hairpins has been very rarely explored as β-sheet binders and inhibitors of aggregation. As Aβ-aggregation is a dynamic and complex process, we hypothesized that flexible β-hairpins could adapt themselves in the interaction with the different Aβ1-42 conformations present during the aggregation process, and in particular in the early stages of oligomerization. We designed acyclic β-hairpin mimics based on a piperidine-pyrrolidine semi-rigid scaffold developed recently as a flexible β-turn inducer, and on different SREs of Aβ1-42. The choice of the SREs was based on oligomer and fibril structures. The ability of all compounds to influence the Aβ 1-42 fibrillization process was evaluated by thioflavin-T fluorescence spectroscopy, used as an evaluation tool to define the inhibitory activity. The obtained results were successively supplemented by transmission electron microscopy. The most promising compounds were also studied by Capillary Electrophoresis (CE) using a method we recently proposed to monitor the very early steps of the oligomerization process overtime. The best inhibitors were investigated to determine their ability to reduce the toxicity of aggregated Aβ1-42 to SH-SY5Y neuroblastoma cells. Together with the evaluation of these molecules, we report in this thesis the conformational studies performed by NMR. These structure investigations were performed to investigate and confirm the β-hairpin conformational preference of the compounds in solution. Finally, we performed a practical synthetic pathway to obtain new peptidomimetic chains composed by aza-amino acid residues. In the literature only peptide sequence, with just one aza-amino acid residue in the middle, are known, but the hydrogen-bonding properties of 2:1 [Aza/α]-tripeptides have not yet, to our knowledge, been exploited in the design of the inhibition of protein-protein interactions. We present in this thesis the conformational studies of the 2:1 [Aza/α]-tripeptide sequence by NMR analyses, X-ray crystallography and molecular modelling. In conclusion, the structural elements made in this thesis provide valuable insights in the understanding of the aggregation process of Aβ 1-42 peptide and to explore the design of novel acyclic β-hairpin targeting amyloid-forming proteins.

université PARIS-SACLAY | ÉCOLE DOCTORALE Innovation thérapeutique : du fondamental à l'appliqué

Titre : Mimes synthétiques de feuillets bêta: conception, synthèse et évaluation de leur capacité à moduler l'agrégation du peptide bêta-amyloïde 1-42.

Mots clés : peptidomimétique, feuillets bêta, bêta-hairpin, peptide beta-amyloïde 1-42, azatide, électrophorèse capillaire.

Résumé : La maladie d'Alzheimer (MA) est une maladie neurodégénérative liée à l'oligomérisation et à la fibrillation du peptide β amyloïde, avec Aβ 1-42 étant le plus agrégeant et neurotoxique. La cause exacte de la maladie d'Alzheimer n'est pas encore connue et donc il n'y a pas de traitement efficace contre cette maladie. Une stratégie prometteuse pourrait être l'inhibition de l'oligomérisation de monomères solubles d'Aβ, en stabilisant la conformation non structurée native du peptide, à travers l'utilisation de composés capables d'empêcher la formation de feuillets β. En effet, les peu d'études structurales des espèces oligomériques et des fibrilles ont révélé que l'agrégation implique des structures en feuillet β. De nombreuses petites molécules ont été proposées pour leur capacité à inhiber ou moduler l'agrégation de Aβ 1-42 et sa toxicité. Cependant, le processus d'agrégation est très complexe et difficile à contrôler. Des études récentes indiquent que les oligomères solubles transitoires précédant la formation de fibrilles sont les espèces les plus toxiques. Ainsi, le développement d'inhibiteurs ciblant à la fois l'oligomérisation et la fibrillation reste difficile en dépit de son importance thérapeutique. Les peptides sont des alternatives raisonnables aux autres produits pharmaceutiques chimiques. En particulier, l'inhibition de l'agrégation de Aβ a été ciblée en utilisant des éléments d'auto-reconnaissance (SRE), qui sont des séquences d'acides aminés clés impliqués dans les différentes espèces agrégées.. À notre connaissance, l'utilisation de petites « β-hairpins » acycliques a été très rarement explorée comme ligands de feuillets-β et comme inhibiteurs de l'agrégation. Comme l'agrégation de Aβ est un processus dynamique et complexe, nous avons supposé que les « β-hairpins » flexibles pourraient mieux s'adapter dans l'interaction avec les différentes conformations de Aβ 1-42 présents pendant le processus d'agrégation, et en particulier dans les premiers stades de l'oligomérisation. Nous avons conçu des mimes de feuillets β acycliques basés sur un squelette semi-rigide de type pipéridine-pyrrolidine comme inducteur flexible de coude β, et sur différents SREs de Aβ 1-42. Le choix des SREs a été basée sur les structures d'oligomères et fibrilles. La capacité de tous les composés a été évaluée par spectroscopie de fluorescence à la thioflavine-T pour déterminer l'activité inhibitrice. Les résultats obtenus ont été complétés par microscopie à transmission électronique. Les composés les plus prometteurs ont également été étudiés par électrophorèse capillaire (EC) pour suivre les étapes très précoces du processus d'oligomérisation. Les meilleurs inhibiteurs ont été étudiés afin de déterminer leur capacité à réduire la toxicité de Aβ 1-42 sur des cellules de neuroblastome SH-SY5Y. Nous rapportons également dans cette thèse les études conformationnelles, effectuées par RMN et réalisées pour étudier et confirmer la capacité de composés de se structurer en solution comme des « β-hairpins ». Enfin, nous avons développé une voie de synthèse pour obtenir de nouvelles chaînes peptidomimétiques composées par des résidus aza-aminoacides. Dans la littérature, seules des séquences peptidiques comportant un seul résidu aza-aminoacide au milieu, sont connues, mais les propriétés de liaison hydrogène d'un 2:1 [aza/α] -tripeptide ne sont pas encore, à notre connaissance, étudiées ni exploitées dans la conception d'inhibiteurs des interactions protéine-protéine. Nous présentons dans cette thèse les études conformationelles réalisées par RMN, cristallographie aux rayons X et modélisation moléculaire.
On peut conclure que les éléments structurels décrits dans cette thèse fournissent des indications précieuses dans la compréhension du processus d'agrégation du peptide Aβ 1-42 et dans la conception de nouveaux « β-hairpins » acycliques ciblant des protéines amyloïdes.